## 2.5    GEOLOGY, SEISMOLOGY, AND GEOTECHNICAL ENGINEERING

{This section of the U.S. EPR FSAR is incorporated by reference with the following departure(s) and/or supplement(s).

This section presents information on the geological, seismological, and geotechnical engineering properties of the {CCNPP3} site. Section 2.5.1 describes basic geological and seismologic data, {focusing on those data developed since the publication of the Final Safety Analysis Report (FSAR) for licensing CCNPP Units 1 and 2.} Section 2.5.2 describes the vibratory ground motion at the site, including an updated seismicity catalog, description of seismic sources, and development of the Safe Shutdown Earthquake and Operating Basis Earthquake ground motions. Section 2.5.3 describes the potential for surface faulting in the site area, and Section 2.5.4 and Section 2.5.5 describe the stability of surface materials at the site.

Appendix D of Regulatory Guide 1.165, "Geological, Seismological and Geophysical Investigations to Characterize Seismic Sources," (NRC, 1997) provides guidance for the recommended level of investigation at different distances from a proposed site for a nuclear facility.

- ♦ The site region is that area within 200 mi (322 km) of the site location (Figure 2.5-1).

- ♦ The site vicinity is that area within 25 mi (40 km) of the site location (Figure 2.5-2).

- ♦ The site area is that area within 5 mi (8 km) of the site location (Figure 2.5-3).

- ♦ The site is that area within 0.6 mi (1 km) of the site location (Figure 2.5-4).

These terms, site region, site vicinity, site area, and site, are used in Sections 2.5.1 through 2.5.3 to describe these specific areas of investigation. These terms are not applicable to other sections of the FSAR.

The geological and seismological information presented in this section was developed from a review of previous reports prepared for the existing units, published geologic literature, interpretation of aerial photography, and a subsurface investigation and field and aerial reconnaissance conducted for preparation of this application. {Previous site-specific reports reviewed include the Preliminary Safety Analysis Report (BGE, 1968) and the Independent Spent Fuel Storage Installation Safety Analysis Report (CEG, 2005).} A review of published geologic literature was used to supplement and update the existing geological and seismological information. In addition, relevant unpublished geologic literature, studies, and projects were identified by contacting the U.S. Geological Survey (USGS), State geological surveys and universities. The list of references used to compile the geological and seismological information is presented in the applicable section.

{Field reconnaissance of the site and within a 25 mi (40 km) radius of the site was conducted by geologists in teams of two or more. Two field reconnaissance visits in late summer and autumn 2006 focused on exposed portions of the Calvert Cliffs, other cliff exposures along the west shore of Chesapeake Bay, and roads traversing the site and a 5 mi (8 km) radius of the CCNPP site. Key observations and discussion items were documented in field notebooks and photographs. Field locations were logged by hand on detailed topographic base maps and with hand-held Global Positioning System (GPS) receivers.

Aerial reconnaissance within a 25 mi (40 km) radius of the site was conducted by two geologists in a top-wing Cessna aircraft on January 3, 2007. The aerial reconnaissance investigated the

geomorphology of the Chesapeake Bay area and targeted numerous previously mapped geologic features and potential seismic sources within a 200 mi (322 km) radius of the CCNPP site (e.g., Mountain Run fault zone, Stafford fault system, Brandywine fault zone, Port Royal fault zone, and Skinkers Neck anticline). The flight crossed over the CCNPP site briefly but did not circle or approach the site closely in order to comply with restrictions imposed by the Federal Aviation Administration. Key observations and discussion items were documented in field notebooks and photographs. The flight path, photograph locations, and locations of key observations were logged with hand-held GPS receivers.

The investigations of regional and site physiographic provinces and geomorphic process, geologic history, and stratigraphy were conducted by Bechtel Power Corporation. The investigations of regional and site tectonics and structural geology were conducted by William Lettis and Associates.}

This section is intended to demonstrate compliance with the requirements of paragraph c of 10 CFR 100.23, "Geologic and Seismic Siting Criteria" (CFR, 2007).}

## 2.5.1    BASIC GEOLOGIC AND SEISMIC INFORMATION

The U.S EPR FSAR includes the following COL Item in Section 2.5.1:

> A COL applicant that references the U.S. EPR design certification will use site-specific information to investigate and provide data concerning geological, seismic, geophysical, and geotechnical information.

TheThis COL Item is addressed as follows:

{This section presents information on the geological and seismological characteristics of the site region (200 mi (322 km) radius), site vicinity (25 mi (40 km) radius), site area (5 mi (8 km) radius) and site (0.6 mi (1 km) radius). Section 2.5.1.1 describes the geologic and tectonic characteristics of the site region. Section 2.5.1.2 describes the geologic and tectonic characteristics of the site vicinity and location. The geological and seismological information was developed in accordance with the following NRC guidance documents:

- ♦ Regulatory Guide 1.70, Section 2.5.1, "Basic Geologic and Seismic Information," (NRC, 1978)

- ♦ Regulatory Guide 1.206, Section 2.5.1, "Basic Geologic and Seismic Information," (NRC, 2007) and

- ♦ Regulatory Guide 1.165, "Identification and Characterization of Seismic Sources and Determination of Safe Shutdown Earthquake Ground Motion," (NRC, 1997).

### 2.5.1.1    Regional Geology (200 mi (322 km) radius)

The U.S. EPR FSAR includes the following COL Item in Section 2.5.1.1:

> Regional geology is site specific and will be addressed by the COL applicant.

This COL Item is addressed as follows:

This section discusses the physiography, geologic history, stratigraphy, and tectonic setting within a 200 mi (322 km) radius of the site. The regional geologic map and explanation as

shown in Figure 2.5-5 and Figure 2.5-6 contain information on the geology, stratigraphy, and tectonic setting of the region surrounding the {CCNPP site (Schruben, 1994)}.  Summaries of these aspects of regional geology are presented to provide the framework for evaluation of the geologic and seismologic hazards presented in the succeeding sections.

{Sections 2.5.1.1.1 through 2.5.1.1.4 are added as a supplement to the U.S. EPR FSAR.

### 2.5.1.1.1      Regional Physiography and Geomorphology

The CCNPP site lies within the Coastal Plain Physiographic Province as shown in Figure 2.5-1 (Fenneman, 1946).  The area within a 200 mi (322 km) radius of the site encompasses parts of five other physiographic provinces.  These are: the Continental Shelf Physiographic Province, which is located east of the Coastal Plain Province, and the Piedmont, Blue Ridge, Valley and Ridge and Appalachian Plateau physiographic provinces, which are located successively west and northwest of the Piedmont Province (Thelin, 1991).

Each of these physiographic provinces is briefly described in the following sections.  The physiographic provinces in the site region are shown on Figure 2.5-1 (Fenneman, 1946).  A map showing the physiographic provinces of Maryland, as depicted by the Maryland Geological Survey (MGS), is shown on Figure 2.5-7.

### 2.5.1.1.1.1      Coastal Plain Physiographic Province

The Coastal Plain Physiographic Province extends eastward from the Fall Line (the physiographic and structural boundary between the Coastal Plain Province and the Piedmont Province) to the coastline as shown in Figure 2.5-1.  The Coastal Plain Province is a low-lying, gently-rolling terrain developed on a wedge-shaped, eastward-dipping mass of Cretaceous, Tertiary, and Quaternary age as shown in Figure 2.5-5 and Figure 2.5-6, which are unconsolidated and semi-consolidated sediments (gravels, sands, silts, and clays), that thicken toward the coast.  This wedge of sediments attains a thickness of more than 8,000 ft (2,430 m) along the coast of Maryland (MGS, 2007).  In general, the Coastal Plain Province is an area of lower topographic relief than the Piedmont Province to the west.  Elevations in the Coastal Plain Province of Maryland range from near sea level to 290 ft (88 m) above sea level near the District of Columbia - Prince Georges County line (Otton, 1955).

Four main periods of continental glaciation occurred in the site region during the Pleistocene. Glaciers advanced only as far south as northeastern Pennsylvania and central New Jersey as shown in Figure 2.5-5 and Figure 2.5-6.  However, continental glaciation affected sea level and both coastal and fluvial geomorphic processes, resulting in the landforms that dominate the Coastal Plain Province.

In Maryland, the MGS subdivides the Coastal Plain Physiographic Province into the Western Shore Uplands and Lowlands regions, the Embayment occupied by the Chesapeake Estuary system, and the Delmarva Peninsula Region on the Eastern Shore of the Chesapeake Bay as shown in Figure 2.5-7.  In the site region and vicinity, geomorphic surface expression is a useful criterion for mapping the contacts between Pliocene and Quaternary units as shown in Figure 2.5-5 and Figure 2.5-6 Constructional surface deposits define the tops of estuarine and fluvial terraces and erosional scarps correspond with the sides of old estuaries (McCartan, 1989a) (McCartan, 1989b).  In some areas, the physiographic expression of terraces that might have formed in response to alternate deposition and erosion during successive glacial stages is poorly defined (Glaser, 1994) (Glaser, 2003c).  Sea levels were relatively lower during glacial stages than present-day, and relatively higher than present-day during interglacial stages. Deposition and erosion during periods of higher sea levels led to the formation of several

discontinuous Quaternary-age stream terraces that are difficult to correlate (McCartan, 1989a). The distribution of Quaternary surficial deposits in the CCNPP site area and site location is discussed in Section 2.5.1.2.  Northeast of the Chesapeake Bay, the Western Shore Uplands Region consists of extensive areas of relatively little topographic relief, less than 100 ft (30 m). The Western Shore Lowlands Region located along the west shore of Chesapeake Bay and north of the Western Shore Uplands Region as shown in Figure 2.5-7 is underlain by interbedded quartz-rich gravels and sands of the Cretaceous Potomac Group and gravel, sand, silt and clay of the Quaternary Lowland deposits.  During glacial retreats, large volumes of glacial melt-waters formed broad, high energy streams such as the ancestral Delaware, Susquehanna, and Potomac Rivers that incised deep canyons into the continental shelf. Southwest of the Chesapeake Bay, marine and fluvial terraces developed during the Pliocene and Pleistocene.  As a result of post-Pleistocene sea level rise, the outline of the present day coastline is controlled by the configuration of drowned valleys, typified by the deeply recessed Chesapeake Bay and Delaware Bay.  Exposed headlands and shorelines have been modified by the development of barrier islands and extensive lagoons (PSEG, 2002).

### 2.5.1.1.1.2    Continental Shelf Physiographic Province

The Continental Shelf Physiographic Province is the submerged continuation of the Coastal Plain Province and extends from the shoreline to the continental slope as shown in Figure 2.5-1. The shelf is characterized by a shallow gradient of approximately 10 ft/mi to the southeast (Schmidt, 1992) and many shallow water features that are relicts of lower sea levels.  The shelf extends eastward for about 75 to 80 mi (121 to 129 km) , where sediments reach a maximum thickness of about 40,000 ft (12.2 km) (Edwards, 1981).  The eastward margin of the continental shelf is marked by the distinct break in slope to the continental rise with a gradient of approximately 400 ft/mi (Schmidt, 1992).

### 2.5.1.1.1.3    Piedmont Physiographic Province

The Piedmont Physiographic Province extends southwest from New York to Alabama and lies west of, and adjacent to, the Coastal Plain Physiographic Province as shown in Figure 2.5-1.  The Piedmont is a rolling to hilly province that extends from the Fall Line in the east to the foot of the Blue Ridge Mountains in the west as shown in Figure 2.5-1.  The Fall Line is a low east-facing topographic scarp that separates crystalline rocks of the Piedmont Province to the west from less resistant sediments of the Coastal Plain Province to the east (Otton, 1955) (Vigil, 2000).  The Piedmont Province is about 40 mi (64 km) wide in southern Maryland and narrows northward to about 10 mi (16 km) wide in southeastern New York.

Within the site region, the Piedmont Province is generally characterized by deeply weathered bedrock and a relative paucity of solid rock outcrop (Hunt, 1972).  Residual soil (saprolite) covers the bedrock to varying depths.  On hill slopes, the saprolite is capped locally by colluvium (Hunt, 1972).

In Maryland, the Piedmont Province is divided into the Piedmont Upland section to the east and the Piedmont Lowland section to the west, which is referred to as a sub-province in some publications as shown in Figure 2.5-7.  The Piedmont Upland section is underlain by metamorphosed sedimentary and crystalline rocks of Precambrian to Paleozoic age.  These lithologies are relatively resistant and their erosion has resulted in a moderately irregular surface.  Topographically higher terrain is underlain by Precambrian crystalline rocks and Paleozoic quartzite and igneous intrusive rocks.  The Piedmont Lowland section is a less rugged terrain containing fault-bounded basins filled with sedimentary and igneous rocks of Triassic and Early Jurassic age.

### 2.5.1.1.1.4      Blue Ridge Physiographic Province

The Blue Ridge Physiographic Province is bounded on the east by the Piedmont Province and on the west by the Valley and Ridge Province as shown in Figure 2.5-1. The Blue Ridge Province, aligned in a northeast-southwest direction, extends from Pennsylvania to northern Georgia. It varies in approximate width from 5 mi (8 km) to more than 50 mi (80 km) (Hunt, 1967). This province corresponds with the core of the Appalachians and is underlain chiefly by more resistant granites and granitic gneisses, other crystalline rocks, metabasalts (greenstones), phyllites, and quartzite along its crest and eastern slopes.

### 2.5.1.1.1.5      Valley and Ridge Physiographic Province

The Valley and Ridge Physiographic Province lies west of the Blue Ridge Province and east of the Appalachian Plateau Province as shown in Figure 2.5-1. This is designated as the Valley and Ridge Province in Maryland as shown in Figure 2.5-7. Valleys and ridges are aligned in a northeast-southwest direction in this province, which is between 25 and 50 mi (40 and 80 km) wide. The sedimentary rocks underlying the Valley and Ridge Province are tightly folded and, in some locations, faulted. Sandstone units that are more resistant to weathering are the ridge formers. Less resistant shales and limestones underlie most of the valleys as shown in Figure 2.5-5 and Figure 2.5-6. The Great Valley Section of the province as shown in Figure 2.5-7, to the east, is divided into many distinct lowlands by ridges or knobs, the largest lowland being the Shenandoah Valley in Virginia. This broad valley is underlain by shales and by limestones that are prone to dissolution, resulting in the formation of sinkholes and caves. Elevations within the Shenandoah Valley typically range between 500 and 1,200 ft (152 and 366 m) msl. The western portion of the Valley and Ridge Province is characterized by a series of roughly parallel ridges and valleys, some of which are long and narrow (Lane, 1983). Elevations within the ridges and valleys range from about 1,000 to 4,500 ft (305 to 1,372 m) msl (Bailey, 1999).

### 2.5.1.1.1.6      Appalachian Plateau Physiographic Province

Located west of the Valley and Ridge Province, the Appalachian Plateau Physiographic Province includes the western part of the Appalachian Mountains, stretching from New York to Alabama as shown in Figure 2.5-1. The Allegheny Front is the topographic and structural boundary between the Appalachian Plateau and the Valley and Ridge Province (Clark, 1992). It is a bold, high escarpment, underlain primarily by clastic sedimentary rocks capped by sandstone and conglomerates. In eastern West Virginia, elevations along this escarpment reach 4,790 ft (1,460 m) (Hack, 1989). West of the Allegheny Front, the Appalachian Plateau's topographic surface slopes gently to the northwest and merges imperceptibly into the Interior Low Plateaus. Only a small portion of this province lies within 200 mi (322 km) of the CCNPP site as shown in Figure 2.5-1.

The Appalachian Plateau Physiographic Province is underlain by sedimentary rocks such as sandstone, shale, and coal of Cambrian to Permian age as shown in Figure 2.5-5 and Figure 2.5-6. These strata are generally subhorizontal to gently folded into broad synclines and anticlines and exhibit relatively little deformation. These sedimentary rocks differ significantly from each other with respect to resistance to weathering. Sandstone units tend to be more resistant to weathering and form topographic ridges. The relatively less resistant shales and siltstones weather preferentially and underlie most valleys. The Appalachian Plateau is deeply dissected by streams into a maze of deep, narrow valleys and high narrow ridges (Lane, 1983). Limestone dissolution and sinkholes occur where limestone units with high karst susceptibility occur at or near the ground surface.

## 2.5.1.1.2     Regional Geologic History

The geologic and tectonic setting of the CCNPP site region is the product of a long, complex history of continental and island arc collisions and rifting, which spanned a period of over one billion years and formed the Appalachian Mountains (Appalachian Orogen) extended continental crust and coastal plain as shown in Figure 2.5-8.  This history of deformation imparts a pre-existing structural grain in the crust that is important for understanding the current seismotectonic setting of the region.  Episodes of continental collisions have produced a series of accreted terranes separated, in part, by low angle detachment faults.  Sources of seismicity may occur in the overlying, exposed, or buried terranes or may occur along structures within the North American basement buried beneath the accreted terranes or overthrust plates.  That is, regional seismicity may not be related to any known surface structure. Intervening episodes of continental rifting have produced high angle normal or transtensional faults that either sole downward into detachment faults or penetrate entirely through the accreted terranes and upper crust.  Understanding the history of the evolution and the geometry of these crustal faults, therefore, is important for identifying potentially active faults and evaluating the distribution of historical seismicity within the tectonic context of the site region.

Major tectonic events in the site region include five compressional orogenies and two extensional episodes (Faill, 1997a). While direct evidence of these deformational events is visible in the Blue Ridge and Piedmont provinces, it is buried beneath the coastal plain sediments in the site region but is inferred from geophysical data, as described in Section 2.5.1.1.4.3, and borehole data as described in Section 2.5.1.1.3.  The site region is located currently on the passive, divergent trailing margin of the North American plate following the last episode of continental extension and rifting.  Each of these tectonic events is described in the following paragraphs.

### 2.5.1.1.2.1     Grenville Orogeny

The earliest of the compressional deformational events (orogenies) recorded in the rocks of North America is the Grenville orogeny that occurred during Middle to Late Precambrian (Proterozoic) time, approximately one billion years ago, as a result of the convergence of the ancestral North American and African tectonic plates.  During this orogeny, various terranes were accreted onto the edge of the ancestral North American plate, forming the Grenville Mountains (Faill, 1997a), which were likely the size of the present day Himalayas (Fichter, 2000). The Grenville orogeny was followed by several hundred million years of tectonic quiescence, during which time the Grenville Mountains were eroded and their basement rocks exposed.  In Virginia and Maryland, the Grenville basement rocks are exposed in the Blue Ridge Province and portions of the Piedmont Province (Fichter, 2000).  This appears to be represented in Maryland by the Middletown Valley biotite granite gneiss in the Blue Ridge Province and the Baltimore Gneiss in the eastern Piedmont Province.

### 2.5.1.1.2.2     Late Precambrian Rifting

Following the Grenville orogeny, crustal extension and rifting began during Late Precambrian time, which caused the separation of the North America and African plates and created the proto-Atlantic Ocean (Iapetus Ocean).  Rifting is interpreted to have occurred over a relatively large area, sub-parallel to the present day Appalachian mountain range (Faill, 1997a) (Wheeler, 1996).  This period of crustal extension is documented by the metavolcanics of the Catoctin, Swift Run, and Sams Creek formations (Schmidt, 1992).  During rifting, the newly formed continental margin began to subside and accumulate sediment. Initial sedimentation resulted in an eastward thickening wedge of clastic sediments consisting of graywackes, arkoses, and shales deposited unconformably on the Grenville basement rocks.  In the Blue Ridge and

western Piedmont, the Weverton and Sugarloaf Mountain quartzites represent late Precambrian to early Cambrian fluvial and beach deposits. Subsequent sedimentation included a transgressive sequence of additional clastic sediments followed by a thick and extensive sequence of carbonate sediments.  Remnants of the rocks formed from these sediments can be found within the Valley and Ridge Province and Piedmont Province (Fichter, 2000).  In the western Piedmont, the sandy Antietam Formation was deposited in a shallow sea.  In the Valley and Ridge Province, a carbonate bank provided the environment of deposition for the thick carbonates ranging from the Cambrian Tomstown Dolomite through the Ordovician Chambersburg Formation. In the eastern Piedmont, the Setters Formation (quartzite and interbedded mica schist) and the Cockeysville Marble have been interpreted as metamorphosed beach and carbonate bank deposits that can be correlated from Connecticut to Virginia.   Accumulation of this eastward thickening wedge of clastic and carbonate sediments is thought to have occurred from the Middle to Late Cambrian into Ordovician time (PSEG, 2002).

### 2.5.1.1.2.3    Late Precambrian to Early Cambrian Orogenies (Potomac/Penobscot Orogency)

Fossil fauna, detailed geologic mapping, petrologic investigations, and radiometric age dates indicate that the Virgilina orogeny is a Late Proterozoic-earliest Cambrian compressional deformation event that may have involved the accretion of a crustally juvenile Carolina zone to a more crustally evolved Goochland zone in the Carolinas and southern Virginia (Hibbard, 1995) as shown in Figure 2.5-8.  Island arc rifting in the Carolina zone might have been associated with the Virgilina orogeny.  It is possible that the Virgilina orogeny deformed the Mather Gorge Formation in the central Piedmont of Maryland and northern Virginia.  The Sykesville Formation in the same area contains olistoliths of Mather Gorge phyllonite (Drake, 1999).  Because the Sykesville Formation was folded prior to the emplacement of the Early Ordovician Falls Church Intrusive Suite and Occoquan Granite, that folding, originally interpreted as a result of the Penobscot orogeny, is now believed to have formed as a result of the Cambrian to earliest Ordovician Potomac orogeny.  The deformation, metamorphism and west-directed thrusting affected the western portion of the Piedmont in the Potomac River Valley (Hibbard, 1995) (Drake, 1999).

During Late Cambrian time, as the now tectonically stable continental margin continued to subside, micro-continents and volcanic arcs, characteristic of an intra-oceanic island-arc terrane, began to develop in the proto-Atlantic Ocean as a result of east-directed oceanic subduction and initial closing of the proto-Atlantic.  The Penobscot orogeny (documented in the Maritime Provinces of Canada) is thought to have been caused by crustal convergence and accretion of these volcanic arcs thrust over micro-continents along the North American plate margin as shown in Figure 2.5-8.  This orogeny is considered to represent the beginning of the convergent phase in the closing of the proto-Atlantic Ocean (Fichter, 2000).  Subsequent convergent phases in the closing of the proto-Atlantic include the Taconic and Acadian orogenies and the Allegheny orogeny that finally closed the proto-Atlantic in the Permian.

### 2.5.1.1.2.4    Taconic Orogeny

The Taconic orogeny occurred during Middle to Late Ordovician time and was caused by continued collision of micro-continents and volcanic arcs with eastern North America along an eastward dipping subduction zone during progressive closure of the proto-Atlantic Ocean as shown in Figure 2.5-8.  Taconic terranes are preserved today in the Piedmont in a series of belts representing island-arcs and micro-continents.  They include the Chopawamsic belt, the Carolina Slate belt, the Eastern Slate belt, the Goochland-Raleigh belt as shown in Figure 2.5-9 (Bledsoe, 1980) (Fichter, 2000), and the Sussex Terrane, directly west of the CCNPP site. These

Taconic terranes are considered to have collided with, and accreted to, eastern North America at different times during the orogeny (Fichter and Baedke, 2000).  Closer to the CCNPP site, the central Piedmont in Northern Virginia, Maryland, and Pennsylvania contains several belts of rocks whose age is unknown and/or whose relation to the pre- or synorogenic rocks of the Taconic Orogen is uncertain (Drake, 1999).  These stratigraphic units include the Wissahickon Formation, which is now recognized in the Potomac Valley as three distinct lithotectonic assemblages (Drake, 1999).  Other stratigraphic units, whose ages range from Late Proterozoic to Late Ordovician and contain indications of Taconic deformation, include various units in the Ijamsville Belt, the Glenarm Group Belt, which includes the Baltimore Gneiss, the Potomac terrane that was thrust over the Glenarm Group belt, and the Baltimore mafic complex to the east as shown in Figure 2.5-9 (Horton, 1989) (Bledsoe, 1980) (Fichter, 2000).  Additional details on the complex stratigraphy of the Taconic orogen in the Piedmont are contained in Drake (Drake, 1999).

Accretion of the island-arcs and micro-continents to the eastern margin of North America created a mountain system, the Taconic Mountains, that became a major barrier between the proto-Atlantic to the east and the carbonate platform to the west.  The growth of this barrier transformed the area underlain by carbonate sediments to the west into a vast, elongate sedimentary basin, the Appalachian Basin.  The present day Appalachian Basin extends from the Canadian Shield in southern Quebec and Ontario Provinces, Canada, southwestward to central Alabama, approximately parallel to the Atlantic coastline (Colton, 1970).  The formation of the Appalachian Basin is one of the most significant consequences of the Taconic orogeny in the region defined by the Valley and Ridge Province and Appalachian Plateau Province.  The Taconic mountain system was the source of most of the siliclastic sediment that accumulated in the Appalachian Basin during Late Ordovician and Early Silurian time. Many of these units are preserved closest to the CCNPP site in the Valley and Ridge Province.  A continent-wide transgression in Early Silurian time brought marine shales and carbonate sedimentation eastward over much of the basin, and a series of transgressions and regressions thereafter repeatedly shifted the shoreline and shallow marine facies.  Carbonate deposition continued in the eastern part of the basin into Early Devonian time (Faill, 1997b).

### 2.5.1.1.2.5    Acadian Orogeny

The Acadian orogeny (Figure 2.5-8) was caused by the collision of the micro-continent Avalon with eastern North America during the Middle to Late Devonian Period.  At its peak, the orogeny produced a continuous chain of mountains along the east coast of North America and brought with it associated volcanism and metamorphism. Remnants of the Avalon terrane (the Acadian Mountains) can be found in the Piedmont Province within the pre-existing Taconic Goochland belt, Carolina Slate belt, and the Chopawamsic belt (Fichter, 2000).  The Acadian orogeny ended the largely quiescent environment that dominated the Appalachian Basin during the Silurian, as vast amounts of terrigenous sediment from the Acadian Mountains were introduced into the basin and formed the Catskill clastic wedge in Pennsylvania and New York as shown in Figure 2.5-5, Figure 2.5-6, and Figure 2.5-8.  Thick accumulations of clastic sediments belonging to the Catskill Formation are spread throughout the Valley and Ridge Province (Faill, 1997b).  During the Mississippian Period, the Acadian Mountains were completely eroded, and the basement rocks of the Avalon terrane were exposed (Fichter, 2000).

### 2.5.1.1.2.6    Allegheny Orogeny

The Allegheny orogeny occurred during the Late Carboniferous Period and extended into the Permian Period. The orogeny represents the final convergent phase in the closing of the proto-Atlantic Ocean in the Paleozoic Era (Figure 2.5-8). Metamorphism and magmatism were significant events during the early part of the Allegheny orogeny. The Allegheny orogeny was

caused by the collision of the North American and African plates, and it produced the Allegheny Mountains. As the African continent was thrust westward over North America, the Taconic and Acadian terranes became detached and also were thrust westward over Grenville basement rocks (Fichter, 2000). The northwest movement of the displaced rock mass above the thrust was progressively converted into the deformation of the rock mass, primarily in the form of thrust faults and fold-and-thrust structures, as seen in the Blue Ridge and Piedmont Plateau Provinces. The youngest manifestation of the Allegheny orogeny was northeast-trending strike-slip faults and shear zones in the Piedmont Province. The extensive, thick, and undeformed Appalachian Basin and its underlying sequence of carbonate sediments were deformed and a fold-and-thrust array of structures, long considered the classic Appalachian structure, was impressed upon the basin. The tectonism produced the Allegheny Mountains and a vast alluvial plain to the northwest. The Allegheny Front along the eastern margin of the Appalachian Plateau Province is thought to represent the westernmost extent of the Allegheny orogeny. Rocks throughout the Valley and Ridge Province are thrust faulted and folded up to this front, whereupon they become relatively flat and only slightly folded west of the Allegheny Front (Faill, 1998).

### 2.5.1.1.2.7 Early Mesozoic Extensional Episode (Triassic Rifting)

Crustal extension during Early Mesozoic time (Late Triassic and Early Jurassic) marked the opening of the Atlantic Ocean (Figure 2.5-8). This extensional episode produced numerous local, closed basins ("Triassic basins") along eastern North America (Faill, 1998). The elongate basins generally trend northeast, parallel to the pre-existing Paleozoic structures (Figure 2.5-10). The basins range in length from less than 20 mi (32 km) to over 100 mi (161 km) and in width from less than 5 mi (8 km) to over 50 mi (80 km) . The basins are exposed in the Piedmont Lowland of Maryland and Northern Virginia (Gettysburg and Culpeper Basins) and are also buried beneath sediments of the Coastal Plain. The closest exposed basin to the site, the Gettysburg Basin, extends northeast from the Frederick Valley at the south end of the basin into Pennsylvania. Valleys in these Mesozoic basins are developed on sandstone and shale units and trend northeast-southwest, parallel to the strike of the bedrock. Generally, the basins are asymmetric half-grabens with principal faults located along the western margin of the basins. Triassic and Jurassic rocks that fill the basins primarily consist of conglomerates, sandstones, and shales interbedded with basaltic lava flows. At several locations, these rocks are cross-cut by basaltic dikes. The basaltic rocks are generally more resistant to erosion and form local topographically higher landforms. In the Frederick Valley, the younger Mesozoic units are deposited on Ordovician age limestone units subject to dissolution and karst development. Areas in the Fredrick Valley underlain by limestone subject to dissolution have relatively low relief compared to the higher and more rugged terrain underlain by intrusive and extrusive rocks consisting predominantly of diabase and basalt (Brezinski, 2004).

### 2.5.1.1.2.8 Cenozoic History

The Early Mesozoic extensional episode gave rise to the Cenozoic Mid-Atlantic spreading center. The Atlantic seaboard presently represents the trailing passive margin related to the spreading at the Mid-Atlantic ridge. Ridge push forces resulting from the Mid-Atlantic spreading center are believed to be responsible for the northeast-southwest directed horizontal compressive stress presently observed along the Atlantic seaboard.

During Cenozoic time, as the Atlantic Ocean opened, the newly formed continental margin cooled and subsided, leading to the present day passive trailing divergent continental margin. As the continental margin developed, continued erosion of the Appalachian Mountains produced extensive sedimentation within the Coastal Plain. The Cenozoic history of the Atlantic continental margin, therefore, is preserved in the sediments of the Coastal Plain

Province, and under water along the continental shelf. The geologic record consists of a gently east-dipping, seaward-thickening wedge of sediments, caused by both subsidence of the continental margin and fluctuations in sea level. Sediments of the Coastal Plain Province cover igneous and metamorphic basement rocks and Triassic basin rift deposits.

During the Quaternary Period much of the northern United States experienced multiple glaciations interspersed with warm interglacial episodes.  The last (Wisconsinan) Laurentide ice sheet advanced over much of North America during the Pleistocene.  The southern limit of glaciation extended into parts of northern Pennsylvania and New Jersey, but did not cover the CCNPP site vicinity (Figure 2.5-5 and Figure 2.5-6).  South of the ice sheet, periglacial environments persisted throughout the site region (Conners, 1986).  Present-day Holocene landscapes, therefore, are partially the result of geomorphic processes, responding to isostatic uplift, eustatic sea level change, and alternating periglacial and humid to temperate climatic conditions (Cleaves, 2000).

### 2.5.1.1.3        Regional Stratigraphy

This section contains information on the regional stratigraphy within each of the physiographic provinces. The regional geology and generalized stratigraphy within a 200 mi (322 km) radius of the CCNPP site is shown on Figure 2.5-5 and Figure 2.5-6.

### 2.5.1.1.3.1        Coastal Plain Physiographic Province

### 2.5.1.1.3.1.1 Pre-Cretaceous Basement Rock

As described in the subsection on Cenozoic History (Section 2.5.1.1.2.7), early Mesozoic rifting and opening of the Atlantic Ocean was followed by the sea floor spreading and the continued opening of the Atlantic Ocean during the Cenozoic time.  Continued erosion of the Appalachian Mountains and the exposed Piedmont produced extensive sedimentation within the Coastal Plain Province that includes the CCNPP site region.

The non-marine and marine sediments deposited in the Coastal Plain Physiographic Province overlie what are most likely foliated metamorphic or granitic rocks, similar to those cropping out in the Piedmont approximately 50 mi (80 km) to the northwest (Figure 2.5-5 and Figure 2.5-6).  The Pre-Cretaceous basement bedrock is only encountered in the Coastal Plain Province by borings designed to characterize deep aquifers above the underlying basement rock.  The closest borehole to the CCNPP site that penetrates the basement rock is located in St. Mary's County about 13 mi (21 km) south of the site (Figure 2.5-11).  It has been indicated (Hansen, 1986) that most of the borings that penetrate coastal plain sediments and extend to the underlying basement have encountered metamorphic or igneous rocks.  For example, well DO-CE 88 in Dorchester, County located approximately 24 mi (39 km) east of the CCNPP site was drilled into gneissic basement rock at 3,304 ft (1,007 m) in depth (Figure 2.5-11).  Well QA-EB 110, in Queen Anne's County, located 38 mi (61 km) north of the CCNPP site, was drilled to explore for deep freshwater aquifers.  This well was drilled into basement at a depth of 2,518 ft (767 m).  The basement rock was only sampled in the drill cuttings and suggests a gneiss/schist from the mineralogy present, (i.e., biotite, chlorite, and clear quartz).

Regional geophysical and scattered borehole data indicate that a Mesozoic basin might be present in the site vicinity, buried beneath Coastal Plain sediments.  Triassic clastic deposits, indicative of a possible rift basin, were penetrated in Charles County (well CH-CE 37), located over 20 mi (32 km) west of the site, for an interval of 99 ft (30 m), returning samples of weathered brick red clay and shale.

Diabase was cored in the closest deep boring (SM-DF 84) to the CCNPP site that penetrated the Pre-Cretaceous basement.  The boring is located in Lexington Park, St. Mary's County, about 13 mi (21 km) south of the CCNPP site (Hansen, 1984) (Figure 2.5-11).  A statement regarding the presence of the diabase was made (Hansen, 1984):

> As no other basement lithologies were encountered, it is presently not known whether the diabase is from a sill or dike associated with the rift-basin sediments or whether it is cross-cutting the crystalline rocks.  The diabase is apparently a one-pyroxene (augite) rock, which Fisher (1964, p. 14) suggests is evidence of rapid, undifferentiated crystallization in a relatively thin intrusive body, such as a dike.

The occurrence of Mesozoic rift-basin rocks in St. Mary's and Prince George's County are further discussed (Hansen, 1986): "The basins that occur in Maryland are all half-grabens with near-vertical border faults along the western sides.  The strata generally strike north-easterly, but, in places, particularly in the vicinity of cross-faults, strike may diverge greatly from the average."

Because of the depth of Coastal Plain sediments, the basement rock type beneath the CCNPP site must be inferred based on surrounding borings and geophysical data.  The presence and character of basement rock beneath the CCNPP site is discussed further in Section 2.5.1.2.

### 2.5.1.1.3.1.2 Cretaceous Stratigraphic Units

Regionally, coastal plain deposits lap onto portions of the eastern Piedmont. In Stafford, Prince William, and Fairfax counties in Virginia Lower Cretaceous Potomac Formation sediments were deposited unconformably on a narrow belt of Ordovician Quantico Slate and on the Cambrian Chopawamsic Formation (Mixon, 2000).  The Potomac Formation occurs on Proterozoic to Cambrian metamorphic and igneous rocks in the Washington DC area (McCartan, 1990).

The Lower Cretaceous Potomac Group overlies a complex suite of basement rocks that includes strata as young as Triassic.  Jurassic units appear to be missing north of the Norfolk Arch (Hansen, 1978) (Figure 2.5-12). The undulatory and east-dipping basement surface that underlies the Coastal Plain resulted from a combination of downwarping, erosion, and faulting. This has led to local variations in the slope of the bedrock surface.  The Coastal Plain sediments deposited east of the Fall Line, range from Early Cretaceous to Quaternary in age and consist of interbedded silty clays, sands, and gravels that were deposited in both marine and non-marine environments.  These sediments dip and thicken toward the southeast.  Whereas the basement surface dips southeast at about 100 ft/mi in Charles County, west of the CCNPP site, a marker bed in the middle of the Cretaceous Potomac Group dips southeast at about 50 ft per mile (McCartan, 1989a).  This wedge of unlithified sediments consists of Early Cretaceous terrestrial sediments and an overlying sequence of well-defined, Late Cretaceous, marine stratigraphic units. These units from oldest to youngest are summarized in the following paragraphs.

The Lower Cretaceous strata of the Potomac Group consists of a thick succession of variegated red, brown, maroon, yellow, and gray silts and clays with interstratified beds of fine to coarse gray and tan sand. In the Baltimore-Washington area, the Potomac Group is subdivided from oldest to youngest into the Patuxent, Arundel, and Patapsco Formations.  This subdivision is recognizable in the greater Washington-Baltimore area where the clayey Arundel Formation is easily recognized and separates the two dominantly sandy formations (Hansen, 1984).  This distinction is less pronounced to the east and southeast where the Potomac Group is divided into the Arundel/Patuxent formations (undivided) and the overlying Patapsco Formation.  At Lexington Park, Maryland, the clayey beds that dominate the formation below a depth of 1,797 ft (548 m) are assigned to the Arundel/Patuxent Formations (undivided) (Hansen, 1984).

At the Lexington Park well, located about 13 mi (21 km) south of the CCNPP site (Figure 2.5-11), about 30 ft (9 m) of a denser, acoustically faster, light gray, fine to medium clayey sand occurs at the base of the Potomac Group and might represent an early Cretaceous, pre-Patuxent Formation.  These sediments might correlate with the Waste Gate Formation encountered east of Chesapeake Bay in the DOE Crisfield No. 1 well (Hansen, 1984).

The Patapsco Formation contains interbedded sands, silts, and clays, but it contains more sand than the overlying Arundel/Patuxent Formations (undivided).  The contact is marked by an interval dominated by thicker clay deposits.  The Arundel/Patuxent Formations (undivided) are marked by the absence of marine deposits.  The Mattaponi Formation was proposed (Cederstrom, 1957) for the stratigraphic interval immediately above the Patapsco Formation.  An identified interval (Hansen, 1984) as the Mattaponi (?) is now recognized as part of the upper Patapsco Formation.  In general, it appears that downwarping associated with the Salisbury Embayment (Figure 2.5-12) began early in the Cretaceous and continued intermittently throughout the Cretaceous and Tertiary periods.  Deposition apparently kept pace, resulting in a fluvial-deltaic environment.  Biostratigraphic data from test wells on the west side of Chesapeake Bay indicate that Upper Cretaceous sediments reach maximum thickness in Anne Arundel County and show progressive thinning to the south.  This appears to reflect deposition within the downwarping, northwest-trending Salisbury Embayment during the Cretaceous (Hansen, 1978).  In southern Calvert County, the Upper Cretaceous Aquia Formation rests unconformably on Lower Cretaceous sediments (Figure 2.5-13).  Thinning and overlapping within the Upper Cretaceous interval suggests that the northern flank of the Norfolk Arch was tectonically active during late Cretaceous time (Hansen, 1978) (Figure 2.5-12).

The Upper Cretaceous Magothy Formation is approximately 200 ft (61 m) thick in northern Calvert County but becomes considerably thinner southward at the CCNPP site and pinches out south of the site and north of wells in Solomons and Lexington Park, Maryland (Hansen, 1996) (Achmad, 1997) (Figure 2.5-13).  This pattern also appears to reflect thicker deposition in the Salisbury Embayment.  The Magothy Formation is intermittently exposed near Severna Park, Maryland, and in the interstream area between the Severn and Magothy Rivers.  This outcrop belt becomes thinner to the south in Prince Georges County.  The Magothy consists mainly of lignitic or carbonaceous light gray to yellowish quartz sand interbedded with clay layers.  The sand is commonly coarse and arkosic and in many places is cross bedded or laminar.  Pyrite and glauconite occur locally (Otton, 1955).

The upper Cretaceous Matawan and Monmouth formations are exposed in Anne Arundel County, Maryland. While the Matawan is absent in Prince Georges County, the Monmouth crops out in a narrow belt near Bowie, Maryland.  Exposures of these formations have not been identified in Charles County.  These formations are inseparable in sample cuttings and drillers' logs and are undifferentiated in southern Maryland (Otton 1955) (Hansen, 1996).  They consist mainly of gray to grayish-black micaceous sandy clay and weather to a grayish brown. Glauconite is common in both formations and fossils include fish remains, gastropods, pelecypods, foraminifera, and ostracods.  The presence of glauconite and this fossil fauna indicate that the Matawan and Monmouth are the oldest in a sequence of marine formations. These formations range in thickness from a few feet or less in their outcrop area to more than 130 ft (40 m) at the Annapolis Water Works (Otton, 1955).  The formations thin to the west and average about 45 ft (14 m) in Prince Georges County.  The combined formations along with the Brightseat Formation form the Lower Confining Beds (Section 2.4.12) that become progressively thinner from southern Anne Arundel County through Calvert County to St. Mary's County where this hydrostratigraphic unit appears to consist mainly of the Brightseat Formation (Hansen, 1996).

### 2.5.1.1.3.1.3 Tertiary Stratigraphic Units

The Brightseat Formation is exposed in a few localities in Prince Georges County and contains foraminifera of Paleocene age.  This unit is relatively thin (up to about 25 ft (8m)) but occurs widely in Calvert and St. Mary's counties.  It is generally  medium and olive gray to black, clayey, very fine to fine sand that is commonly micaceous and /or phosphatic (Otton, 1955) (Hansen, 1996).  It can be distinguished from the overlying Aquia Formation by the absence or sparse occurrence of glauconite. It generally contains less fragmental carbonaceous material than the underlying Cretaceous sediments (Otton, 1955).  The Brightseat Formation is bounded by unconformities with a distinct gamma log signature that is useful for stratigraphic correlation (Hansen, 1996).

The Late Paleocene Aquia Formation was formerly identified as a greensand due to the ubiquitous occurrence of glauconite.  This formation is a poorly to well sorted, variably shelly, and glauconitic quartz sand that contains calcareous cemented sandstone and shell beds.  The Aquia Formation was deposited on a shoaling marine shelf that resulted in a coarsening upward lithology.  This unit has been identified in the Virginia Coastal Plain and underlies all of Calvert County and most of St. Mary's County, Maryland (Hansen, 1996).  The Aquia Formation forms an important aquifer as discussed in Section 2.4.12.

The Late Paleocene Marlboro Clay was formerly considered to be a lower part of the early Eocene Nanjemoy Formation but is now recognized as a widely distributed formation.  The Marlboro Clay extends approximately 120 mi (193 km) in a northeast-southwest direction from the Chesapeake Bay near Annapolis, Maryland to the James River in Virginia.  Micropaleontological data indicate a late Paleocene age although the Eocene-Paleocene boundary may occur within the unit (Hansen, 1996).  The Marlboro Clay is one of the most distinctive stratigraphic markers of the Coastal Plain in Maryland and Virginia.  It consists chiefly of reddish brown or pink soft clay that changes to a gray color in the subsurface of southern St. Mary's and Calvert Counties.  Its thickness ranges from 40 ft (12 m) in Charles County to about 2 ft (60 cm) in St. Mary's County (Otton, 1955).  However, the thickness is relatively constant from Anne Arundel County south through the CCNPP site to Solomons and Lexington Park, Maryland (Figure 2.5-13).  The apparent localized thickening in Charles County might represent a local depocenter rather than a broader downwarping of the Salisbury Embayment relative to the Norfolk Arch (Figure 2.5-12).

The lower part of the overlying Early Eocene Nanjemoy Formation is predominantly a pale-gray to greenish gray, glauconitic very fine muddy sand to sandy clay.  This formation becomes coarser upward from dominantly sandy silts and clays to dominantly clayey sands.  The gradational contact between the two parts of the Nanjemoy is defined on the basis of geophysical log correlations (Hansen, 1996).  In southern Maryland the Nanjemoy Formation ranges in thickness from several ft in its outcrop belt to as much as 240 ft (73 m) in the subsurface in St Mary's County (Otton, 1955) (Figure 2.5-13).

The Middle Eocene Piney Point Formation was recognized (Otton, 1955) as a sequence of shelly glauconitic sands underlying the Calvert Formation in southern Calvert County.  The contact with the underlying Nanjemoy Formation is relatively sharp on geophysical logs, implying a depositional hiatus or unconformity (Hansen, 1996).  The Piney Point Formation ranges in thickness from 0 ft (0 m) in central Calvert County to about 90 ft (27 m) at Point Lookout at the confluence of the Potomac River and Chesapeake Bay (Hansen, 1996).  The Piney Point Formation contains distinctive carbonate-cemented interbeds of sand and shelly sand that range up to about 5 ft (1.5 m) in thickness (Hansen, 1996) and a characteristic fauna belonging to the Middle Eocene Jackson Stage (Otton, 1955).  This unit is recognizable in the subsurface in Charles, Calvert, St. Marys, Dorchester, and Somerset Counties in Maryland and in

Northumberland and Westmoreland Counties in Virginia but has not been recognized at the surface (Otton, 1955).

The work of several investigators were summarized (Hansen, 1996) who identified a 1 to 4 ft (30 to 122 cm) thick interval of clayey, slightly glauconitic, fossiliferous olive-gray, coarse sand containing fine pebbles of phosphate. This thin interval of late Oligocene (?) age occurs near the top of the Piney Point Formation and appears to correlate with the Old Church Formation in Virginia. This formation appears to thicken downdip between Piney Point and Point Lookout (Hansen, 1996). The absence of middle Oligocene deposits in most of the CCNPP site region indicates possible emergence or non-deposition during this time interval. Erosion or non-deposition during this relatively long interval of time produced an unconformity on the top of the Piney Point Formation that is mapped as a southeast dipping surface in the CCNPP site vicinity (Figure 2.5-14).

Renewed downwarping within the Salisbury Embayment resulted in marine transgression across older Cretaceous and Eocene deposits in Southern Maryland. The resulting Miocene-age Chesapeake Group consists of three marine formations; from oldest to youngest these are the Calvert, Choptank and St. Marys Formations. The basal member of the group, the Calvert Formation, is exposed in Anne Arundel, Calvert, Prince Georges, St. Mary's and Charles Counties. Although these formations were originally defined using biostratigraphic data, they are difficult to differentiate in well logs (Hansen, 1996) (Glaser, 2003a). The basal sandy beds are generally 10 to 20 ft (3 to 6 m) thick and consist of yellowish green to greenish light gray, slightly glauconitic fine to medium, quartz sand. The basal beds unconformably overlie older Oligocene and Eocene units and represent a major early Miocene marine transgression (Hansen, 1996). The overlying Choptank and St. Marys formations are described in greater detail in Section 2.5.1.2.3.

The Upper Miocene Eastover Formation and the Lower to Upper Pliocene Yorktown Formation occur in St. Mary's County and to the south in Virginia (McCartan, 1989b) (Ward, 2004). These units appear to have not been deposited to the north of St. Mary's County and that portion of the Salisbury Embayment may have been emergent (Ward, 2004).

### 2.5.1.1.3.1.4 Plio-Pleistocene and Quaternary Deposits

Surficial deposits in the Coastal Plain consist, in general, of two informal stratigraphic units: the Pliocene-age Upland deposits and the Pleistocene to Holocene Lowland deposits. These deposits are mapped (Mc Cartan, 1989a) (MaCartan, 1989b) as two units of Upper Pliocene fluvial Upland Gravels. It was recognized (McCartan, 1989b) that an Upper Pliocene sand with gravel cobbles and boulders that blankets topographically high areas in the southeast third of St. Mary's County. The Upland Deposits are areally more extensive in St. Mary's County than in Calvert County (Glaser, 1971). The map pattern has a dendritic pattern and since it caps the higher interfluvial divides, this unit is interpreted as a highly dissected sediment sheet whose base slopes toward the southwest (Glaser, 1971) (Hansen, 1996). This erosion might have occurred due to differential uplift during the Pliocene or down cutting in response to lower base levels when sea level was lower during period of Pleistocene glaciation.

McCartan (1989b) differentiates three Upper Pleistocene estuarine deposits, Quaternary stream terraces, Holocene alluvial deposits and colluvium in St. Mary's County. The Lowland deposits in southern Maryland were laid down in fluvial to estuarine environments (Hansen, 1996) and are generally found along the Patuxent and Potomac River valleys and Chesapeake Bay. These deposits occur in only a few places along the eastern shore of Chesapeake Bay. The Lowland deposits extend beneath Chesapeake Bay and the Potomac River filling deep, ancestral river channels with 200 ft (61 m) or more of fluvial or estuarine sediments (Hansen, 1996). These

deep channels and erosion on the continental slope probably occurred during periods of glacial advances and lower sea levels. Deposition most likely occurred as the glaciers retreated and melt waters filled the broader ancestral Susquehanna and Potomac Rivers.

### 2.5.1.1.3.2 Piedmont Physiographic Province

There are two distinct divisions to the rocks of the Piedmont Physiographic Province. The first is a set of predominantly Late Precambrian and Paleozoic age crystalline rocks and the second is a set of Early Mesozoic (Triassic) age sedimentary rocks deposited locally in down-faulted basins within the crystalline rocks (Section 2.5.1.1.1) (Fichter, 2000) (Figure 2.5-5, Figure 2.5-6, and Figure 2.5-10).

### 2.5.1.1.3.2.1 Crystalline Rocks (Late Precambrian and Paleozoic)

Crystalline rocks of the Piedmont Province primarily occur within the Piedmont Upland section. The crystalline rocks consist of deformed and metamorphosed meta-sedimentary, meta-igneous, and meta-volcanic rocks intruded by mafic dikes and granitic plutons (Markewich, 1990). The rocks belong to a number of northeast-trending belts that are defined on the basis of rock type, structure and metamorphic grade (Bledsoe, 1980) and are interpreted to have formed along and offshore of ancestral North America (Pavlides, 1994). From east to west the main lithotectonic belts are: the Goochland-Raleigh belt; the Carolina and Eastern slate belts; the Chopawamsic and Milton belts; and the Western/Inner Piedmont belt (Bledsoe, 1980) (Fichter, 2000) (Figure 2.5-9). The stratigraphy of the crystalline rock in these lithotectonic belts are discussed in the following paragraphs.

#### 2.5.1.1.3.2.1.1 Goochland-Raleigh Belt

The Goochland-Raleigh belt stretches southward from Fredericksburg, Virginia, to the North Carolina state line east of the Spotsylvania fault (presented in Section 2.5.1.1.4.4.2) (Frye, 1986) (Figure 2.5-9). The Goochland belt (Virginia) is composed predominantly of granulite facies (high grade) metamorphic rocks and the Raleigh belt (North Carolina) is composed of sillimanite (very high grade) metamorphic rocks (Fichter, 2000). The Goochland-Raleigh belt is interpreted to be a microcontinent that was accreted to ancestral North America during the Taconic orogeny. Some geologists believe that the micro-continent was rifted from ancestral North America during the proto-Atlantic rifting while others believe that it formed outbound of ancestral North America (exotic or suspect terrane). Rocks of the Goochland-Raleigh belt are considered to be the oldest rocks of the Piedmont Province and bear many similarities to the Grenville age rocks of the Blue Ridge Province (Spears, 2002).

The Po River Metamorphic Suite and the Goochland terrane, that lie southeast of the Spotsylvania fault, make up the easternmost part of the Goochland-Raleigh belt. The Po River Metamorphic Suite was named after the Po River in the Fredericksburg area and comprises amphibolite grade (high grade) metamorphic rocks, predominantly biotite gneiss and lesser amounts of hornblende gneiss and amphibolite (Pavlides, 1989). The age of this unit is uncertain, but it has been assigned a provisional age of Precambrian to Early Paleozoic (Pavlides, 1980). The Goochland terrane was first studied along the James River west of Richmond, Virginia, and contains the only dated Precambrian rocks east of the Spotsylvania fault. It is a Precambrian granulite facies (high grade) metamorphic terrane.

#### 2.5.1.1.3.2.1.2 Carolina Slate and Eastern Slate Belts

The Carolina Slate belt extends southward from southern Virginia to central Georgia, while the Eastern Slate belt is located predominantly in North Carolina, east of the Goochland-Raleigh belt (Figure 2.5-9). Both the Carolina and Eastern Slate belts are composed of greenschist facies (low grade) metamorphic rocks (Fichter, 2000), including meta-graywacke, tuffaceous argillites,

quartzites, and meta-siltstones (Bledsoe, 1980).  The Carolina and Eastern Slate belts are interpreted to be island-arcs that were accreted to ancestral North America during the Taconic orogeny.  The island-arcs are interpreted to have been transported from somewhere in the proto-Atlantic Ocean, and are therefore considered to be exotic or suspect terranes.  Rocks of the Carolina and Eastern Slate belts generally are considered to be Early Paleozoic in age.  Granitic and gabbro-rich plutons that intrude the belts generally are considered to be Middle to Late Paleozoic in age (Bledsoe, 1980).

### 2.5.1.1.3.2.1.3 Chopawamsic Belt, including Milton and Charlotte Belts

The Chopawamsic belt, and its southeastward extensions, the Milton and Charlotte belts comprise a broad central part of the Piedmont Province from Virginia to Georgia (Figure 2.5-9).  The belt is interpreted to be part of an island-arc and consist predominantly of meta-sedimentary and meta-volcanic rocks.

The Chopawamsic belt, also referred to as the "Chopawamsic Volcanic Belt" (Bailey, 1999) and the "Central Virginia Volcanic-Plutonic Belt (Rader, 1993) takes its name from exposures along Chopawamsic Creek in northern Virginia. The belt trends northeastward from the North Carolina state line, crosses the James River between Richmond and Charlottesville and continues northeastward to south of Washington D.C., where it is covered by Coastal Plain deposits.  The Chopawamsic belt is bounded on the west by the Chopawamsic fault and on the east by the Spotsylvania fault (Section 2.5.1.1.4).  The Chopawamsic belt is interpreted to be an island-arc that was accreted to ancestral North America during the Taconic orogeny (Figure 2.5-8).  The Chopawamsic belt is regarded as an exotic or suspect terrain. Rocks in the Chopawamsic belt are Early Paleozoic in age. Recent U-Pb studies consistently yield Ordovician ages for Chopawamsic volcanic rocks and Rb-Sr and U-Pb dating of granite rocks give late Ordovician ages (Spears, 2002).

The Chopawamsic belt is comprised of the Chopawamsic Formation and the Ta River Metamorphic Suite. The Chopawamsic Formation and the Ta River Metamorphic Suite are interpreted to have formed as an island-arc.  The Chopawamsic Formation is interpreted to have formed as the continent-ward side of the island-arc and the Ta River Metamorphic Suite as the ocean-ward side (Pavlides, 2000).  The Chopawamsic Formation consists of a sequence of felsic, intermediate and mafic meta-volcanic rocks with subordinate meta-sedimentary rocks.  The Ta River Metamorphic Suite consists of a sequence of amphibolites and amphibole-bearing gneisses with subordinate ferruginous quartzites and biotite gneiss.  Rocks of the Ta River Metamorphic Suite are generally thought to be more mafic and to have experienced higher-grade regional metamorphism than the rocks of the Chopawamsic Formation (Spears, 2002).

The Chopawamsic Formation and Ta River Metamorphic Suite are unconformably overlain by the Quantico and Arvonia Formations.  The Quantico and Arvonia Formations consist of meta-sedimentary rocks including slates, phyllites, schists, and quartzites.  These meta-sedimentary rocks are considered to have been deposited in successor basins after the subjacent terranes were eroded and formed depositional troughs.  Rocks of the Arvonia Formation are exposed in the Arvonia and Long Island synclines, while rocks of the Quantico Formation are exposed in the Quantico syncline. Rocks of the Arvonia, Long Island, and Quantico synclines form three belts across the central Virginia Piedmont, the Quantico synclines to the southeast and the Arvonia and Long Island synclines to the north (Spears, 2002).

The Chopawamsic Formation and the Ta River Metamorphic Suite are intruded by a number of granite plutons.  The number of plutons and their relation to one another, however, remains

uncertain (Spears, 2002). Rocks of the Falmouth Intrusive Suite intrude the Ta River Metamorphic Suite and Quantico Formation in the form of dikes, sills, and small irregular intrusions (Pavlides, 1980).

### 2.5.1.1.3.2.1.4 Western/Inner Piedmont Belt/Baltimore Terrane

The Western Piedmont belt, referred to as the Inner Piedmont belt in some publications, extends southward from Pennsylvania, where it has been designated as part of the Baltimore Gneiss and Glenarm Group (Baltimore terrane) through North Carolina and into Georgia (Figure 2.5-9). It is composed of greenschist facies (low grade) and amphibolite facies (high grade) meta-sedimentary rocks.  These meta-sedimentary rocks enclose blocks of meta-basalt, ultramafic rocks, granite and other quasi-exotic lithologies and are called mélanges (Pavlides, 2000).  These mélanges are interpreted to have formed in a Cambrian-Ordovician back-arc or marginal basin that lay on the continent-ward side of an island-arc terrane (Pavlides, 1989).  The Baltimore terrane, a Middle Proterozoic metamorphosed sequence of felsic to intermediate rocks (Horton, 1989), consists of the Baltimore Gneiss and its cover sequence, the Glenarm Group, which consists of the basal Setters Formation, the Cockeysville Marble and the pelitic Loch Raven Schist.  Mineral assemblages within the Glenarm Group indicate that it was metamorphosed during the Paleozoic (Horton, 1989).  The Potomac terrane (not shown on Figure 2.5-9 due to scale) was thrust upon the Baltimore terrane during the Taconic orogeny.

Two distinct types of mélange deposits occur within a collage of thrust slices in the Western Piedmont belt.  The first type is a block-in-phyllite mélange that constitutes the Mine Run Complex of Virginia. It consists of a variety of meta-plutonic, meta-volcanic, mafic, and ultramafic blocks enclosed within a matrix of phyllite or schist and meta-sandstones of feldspathic or quartz meta-graywacke.  The Mine Run complex is interpreted to consist of four imbricated thrust slices, each with its own distinctive exotic block content (Pavlides, 1989).

The second mélange type within the Western Piedmont belt is a meta-diamictite and contains a less extensive variety of exotic blocks, the most common being mafic and ultramafic blocks. The exotic blocks are enclosed in a micaceous quartzofeldspathic matrix, which has contemporaneously deposited schist and quartz-lump fragments as its characterizing features. Several varieties of meta-diamictite have been recognized in Virginia and described as the Lunga Reservoir and Purcell Branch Formations (Pavlides, 1989).

The mélanges of the Western Piedmont are overlain unconformably by Ordovician age meta-sedimentary rocks and are intruded by Ordovician age and Late Ordovician or Early Silurian age felsic plutons, such as the Lahore and Ellisville plutons (Pavlides, 1989).

### 2.5.1.1.3.2.1.5 Ijamsville Belt/Westminster Terrane

The Ijamsville-Pretty Boy-Octoraro terrane is more currently known as the Westminster terrane (Horton, 1989).  This belt consists of pelitic schist or phyllite characterized by albite porphyroblasts and a green and purple phyllite unit.  Rocks of the Ijamsville/Westminster terrane were interpreted to comprise a tectonic assemblage of undated rocks of the rise and slope deepwater deposits of the Iapetus Ocean that were thrust onto the Grenville-age Blue Ridge Province along the Martic overthrust during the Taconic orogeny (Drake, 1989) (Horton, 1989).

### 2.5.1.1.3.2.2 Sedimentary Rocks (Early Mesozoic)

Mesozoic sedimentary rocks of the Piedmont Province occur primarily within the Piedmont Lowland section (Figure 2.5-10). The sediments were deposited in a series of northeast-trending basins described below in Section 2.5.1.1.4.4.3.  Sediments filling the basins include intermontane fanglomerates, fresh-water limestone, mudstones, siltstones and

sandstones, and basic igneous intrusive dikes and sills and lava flows (Markewich, 1990). The Lower Mesozoic sediments deposited in these basins usually are referred to as Triassic basin deposits, although the basins are now known to also contain Lower Jurassic rocks.

### 2.5.1.1.3.2.3 Surficial Sediments (Cenozoic)

Surficial sediments in the Piedmont Province consist of residual and transported material. The residual soils have developed in place from weathering of the underlying rocks, while the transported material – alluvium and colluvium – has been moved by water or gravity and deposited as unconsolidated deposits of clay, silt, sand, and gravel (Carter, 1976). Surficial sediments in the Piedmont Upland section are interpreted to be the product of Cenozoic weathering, Quaternary periglacial erosion and deposition, and recent anthropogenic activity (Sevon, 2000).

Residual soil in the Piedmont Province consists of completely decomposed rock and saprolite. Residual soils occur almost everywhere, except where erosion has exposed the bedrock on ridges and in valley bottoms. Saprolite comprises the bulk of residual soil in the Piedmont Province and is defined as an earthy material in which the major rock-forming minerals (other than quartz) have been altered to clay but the material retains most of the textural and structural characteristics of the parent rock. The saprolite forms by chemical weathering, its thickness and mineralogy being dependent on topography, parent rock lithology and the presence of surface and/or ground water (Cleaves, 2000).

Relief affects the formation of soils by causing differences in internal drainage, runoff, soil temperatures, and geologic erosion. In steep areas where there is rapid runoff, little percolation of water through the soil and little movement of clay, erosion is severe and removes soil as rapidly as it forms. Gently sloping areas, on the other hand, are well drained and geologic erosion in these areas is generally slight. The characteristics of the underlying rock strongly influence the kind of changes that take place during weathering. Because of differences in these characteristics, the rate of weathering varies for different rock types. The igneous, metamorphic and sedimentary rocks of the Piedmont Province are all sources of parent material for the soils.

Colluvium in the Piedmont Province occurs discontinuously on hilltops and side slopes, while thicker colluvium occurs in small valleys lacking perennial streams. Alluvium is present in all valleys with perennial streams (Sevon, 2000).

### 2.5.1.1.3.3    Blue Ridge Physiographic Province

The Blue Ridge Physiographic Province is underlain by a broad, northeast-trending, structurally complex metamorphic terrane (Mixon, 2000). In the site region, the Blue Ridge occurs southward from south-central Pennsylvania through Virginia (Figure 2.5-1). The Blue Ridge terrain consists of stratified meta-sedimentary rocks and meta-basalts of Early Paleozoic and Late Precambrian age and an underlying gneissic and granitic basement-rock complex of Middle to Late Precambrian age (Figure 2.5-5 and Figure 2.5-6).

### 2.5.1.1.3.4    Valley and Ridge Physiographic Province

The Valley and Ridge Physiographic Province is underlain primarily by layered sedimentary rock that has been intensely folded and locally thrust faulted. The sedimentary rocks range in age from Cambrian to Pennsylvanian. The valley areas within the Great Valley (Figure 2.5-7) are underlain predominantly by thick sequences of limestone, dolomite and shale. The upland areas of the Valley and Ridge Province (Appalachian Mountains) to the west are underlain predominantly by resistant sandstones and conglomerates, while the lowland areas are

underlain predominantly by less resistant shale, siltstone, sandstone and limestone (Colton, 1970) (Figure 2.5-5 and Figure 2.5-6).

### 2.5.1.1.3.5    Appalachian Plateau Physiographic Province

The Appalachian Plateau Physiographic Province is underlain by rocks that are continuous with those of the Valley and Ridge Province, but in the Appalachian Plateau the layered rocks are nearly flat-lying or gently tilted and warped, rather than being intensely folded and faulted. Rocks of the Allegheny Front along the eastern margin of the province consist of thick sequences of sandstone and conglomerate, interbedded with shale, ranging in age from Devonian to Pennsylvanian. Rocks of the Appalachian Plateau west of the Allegheny Front are less resistant and consist of Permian age sandstone, shale and coal (Lane, 1983) (Hack, 1989) (Figure 2.5-5 and Figure 2.5-6).

### 2.5.1.1.4    Regional Tectonic Setting

In 1986, the Electric Power Research Institute (EPRI) developed a seismic source model for the Central and Eastern United States (CEUS), which included the CCNPP site region (EPRI, 1986). The CEUS is a stable continental region (SCR) characterized by low rates of crustal deformation and no active plate boundary conditions.  The EPRI source model included the independent interpretations of six Earth Science Teams and reflected the general state of knowledge of the geoscience community as of 1986.  The seismic source models developed by each of the six teams were based on the tectonic setting and the occurrence, rates, and distribution of historical seismicity.  The original seismic sources identified by EPRI (1986) are thoroughly described in the EPRI study reports (EPRI, 1986) and are summarized in Section 2.5.2.2.

Since 1986, additional geological, seismological, and geophysical studies have been completed in the CEUS and in the CCNPP site region.  The purpose of this section is to summarize the current state of knowledge on the tectonic setting and tectonic structures in the site region and to highlight new information acquired since 1986 that is relevant to the assessment of seismic sources.

A global review of earthquakes in SCRs shows that areas of Mesozoic and Cenozoic extended crust are positively correlated with large SCR earthquakes.  Nearly 70% of SCR earthquakes with M 6 occurred in areas of Mesozoic and Cenozoic extended crust (Johnston, 1994).  Additional evidence shows an association between Late Proterozoic rifts and modern seismicity in eastern North America (Johnston, 1994) (Wheeler, 1995) (Ebel, 2002).  Paleozoic and Mesozoic extended crust underlies the entire 200 mi (322 km) CCNPP site region (Figure 2.5-15). However, as discussed in this section, there is no evidence for late Cenozoic seismogenic activity of any tectonic feature or structure in the site region (Crone, 2000) (Wheeler, 2005). Although recent characterization of several tectonic features has modified our understanding of the tectonic evolution and processes of the mid-Atlantic margin, no structures or features have been identified in the site region since 1986 that show clear evidence of seismogenic potential greater than what was recognized and incorporated in the EPRI study (EPRI, 1986) seismic source model.

The following sections describe the tectonic setting of the site region by discussing the: (1) plate tectonic evolution of eastern North America at the latitude of the site, (2) origin and orientation of tectonic stress, (3) gravity and magnetic data and anomalies, (4) principal tectonic features, and (5) seismic sources defined by regional seismicity. Historical seismicity occurring in the site region is described in Section 2.5.2.1.  The geologic history of the site region was discussed in Section 2.5.1.1.2.

### 2.5.1.1.4.1    Plate Tectonic Evolution of the Atlantic Margin

The Late Precambrian to Recent plate tectonic evolution of the site region is summarized in Section 2.5.1.1.2 and in Figure 2.5-8.  Most of the present-day understanding of the plate tectonic evolution comes from research performed prior to the 1986 EPRI report (EPRI, 1986).  Fundamental understanding about the timing and architecture of major orogenic events was clear by the early 1980's, after a decade or more of widespread application of plate tectonic theory to the evolution of the Appalachian orogenic belt (e.g., (Rodgers, 1970) (Williams, 1983)).  Major advances in understanding of the plate tectonic history of the Atlantic continental margin since the EPRI study report (EPRI, 1986) include the organization of lithostratigraphic units and how they relate to the timing and kinematics of Paleozoic events (e.g., Hatcher, 1989) (Hibbard, 2006) (Hibbard, 2007) and the refinement of the crustal architecture of the orogen and passive margin (e.g., (Hatcher, 1989) (Glover, 1995b) (Klitgord, 1995)).

The following subsections divide the regional plate tectonic history into: (1) Late Proterozoic and Paleozoic tectonics and assembly of North American continental crust, (2) Mesozoic rifting and passive margin formation, and (3) Cenozoic vertical tectonics associated with exhumation, deposition, and flexure.

### 2.5.1.1.4.1.1 Late Proterozoic and Paleozoic Plate Tectonic History

Although details about the kinematics, provenance, and histories of lithostratigraphic units within the Appalachian orogenic belt continue to be debated and reclassified (e.g., (Hatcher, 1989) (Horton, 1991) (Glover, 1995b) (Hibbard, 2006)), it is well accepted that plate boundary deformation has occurred repeatedly in the site region since late Precambrian time.  Suturing events that mark the welding of continents to form supercontinents and rifting events that mark the breakup of supercontinents to form ocean basins have each occurred twice during this interval.  Foreland strata, deformation structures, and metamorphism associated with the Grenville (Middle Proterozoic) and Allegheny (Late Paleozoic) orogenies record the closing of ocean basins and welding of continents to form the supercontinents Rodinia and Pangaea, respectively (Figure 2.5-8).  Synrift basins, normal faults, and postrift strata associated with the opening of the Iapetus (Late Proterozoic to Early Cambrian) and Atlantic (Early Mesozoic) Ocean basins record the break-up of the supercontinents.  The principal structures that formed during the major events are salient to the current seismic hazards in that: (1) they penetrate the seismogenic crust, (2) they subdivide different crustal elements that may have contrasting seismogenic potential, and (3) their associated lithostratigraphic units make up the North American continental crust that underlies most of the site region.  Many of the principal structures are inherited faults that have been reactivated repeatedly through time.  Some are spatially associated with current zones of concentrated seismic activity and historical large earthquakes.  For example, the 1811-1812 New Madrid earthquake sequence ruptured a failed Late Proterozoic rift that also may have been active in the Mesozoic (Ervin, 1975).

During the interval between opening of the Iapetus Ocean and opening of the Atlantic Ocean, the eastern margin of the ancestral North America continent was alternately (1) an active rift margin accommodating lithospheric extension with crustal rift basins and synrift strata and volcanism; (2) a passive continental margin accumulating terrestrial and shallow marine facies strata; and (3) an active collisional margin with accretion of microcontinents, island arcs, and eventually the African continent.  Major Paleozoic mountain building episodes associated with the collision and accretion events included the Taconic, Acadian, and Allegheny Orogenies.  More localized collisional events in the site region include the Avalon, Virgilina and Potomac (Penobscot) orogenies (Hatcher, 1987) (Hatcher, 1989) (Glover, 1995b) (Hibbard, 1995) (Drake, 1999) (Figure 2.5-8).  The geologic histories of these orogenies are described in Section 2.5.1.1.2.

Tectonic structures developed during the interval between the Late Proterozoic and Triassic Periods are variable in sense of slip and geometry. Late Proterozoic and early Cambrian rifting associated with the breakup of Rodinia and development of the Iapetus Ocean formed east-dipping normal faults through Laurentian (proto-North American) crust (Figure 2.5-16 and Figure 2.5-17). Late Proterozoic extended crust of the Iapetan margin probably underlies the Appalachian fold belt southeastward to beneath much of the Piedmont Province (Wheeler, 1996). Paleozoic compressional events associated with the Taconic, Acadian, and Allegheny orogenies formed predominantly west-vergent structures that include (1) Valley and Ridge Province shallow folding and thrusting within predominantly passive margin strata, (2) Blue Ridge Province nappes of Laurentian crust overlain by Iapetan continental margin deposits, (3) Piedmont Province thrust-bounded exotic and suspect terranes including island arc and accretionary complexes interpreted to originate in the Iapetan Ocean, and (4) Piedmont Province and sub-Coastal Plain Province east-dipping thrust, oblique, and reverse fault zones that collectively are interpreted to penetrate much of the crust and represent major sutures that juxtapose crustal elements (Hatcher, 1987) (Horton, 1991) (Glover, 1995b) (Hibbard, 2006) (Figure 2.5-16 and Figure 2.5-17). Many investigators recognize significant transpressional components to major faults bounding lithostratigraphic units (Hatcher, 1987) (Glover, 1995b) (Hibbard, 2006) (Figure 2.5-8 and Figure 2.5-16).

### 2.5.1.1.4.1.2 Mesozoic and Cenozoic Passive Margin Evolution

At the time of the EPRI (1986) study much was published about the structure and crustal elements of the Mesozoic to Cenozoic Atlantic passive margin (e.g., (Klitgord, 1979)). However, it was not until the Geological Society of America's Decade of North American Geology (DNAG) volume on the U.S. Atlantic continental margin (Sheridan, 1988), seminal papers within it (e.g., (Klitgord, 1988)), and later summary publications (e.g., (Klitgord, 1995) (Withjack, 1998)) that the current understanding of the margin structure and tectonic history was formulated comprehensively.

The current Atlantic passive continental margin has evolved since rifting initiated in the Early Triassic. The progression from active continental rifting to sea-floor spreading and a passive continental margin included: (1) initial rifting and hot-spot plume development, (2) thinning of warm, buoyant crust with northwest-southeast extension, normal faulting and deposition of synrift sedimentary and volcanic rocks, and (3) cooling and subsidence of thinned crust and deposition of postrift sediments on the coastal plain and continental shelf, slope, and rise (Klitgord, 1988) (Klitgord, 1995). The transition between the second (rifting) and third (drifting) phases during the Early Jurassic marked the initiation of a passive margin setting in the site region, in which active spreading migrated east away from the margin. As the thinned crust of the continental margin cooled and migrated away from the warm, buoyant crust at the mid-Atlantic spreading center, horizontal northwest-southeast tension changed to horizontal compression as gravitational potential energy from the spreading ridge exerted a lateral "ridge push" force on the oceanic crust. Northwest-southeast-directed postrift shortening, manifested in Mesozoic basin inversion structures, provides the clearest indication of this change in stress regime (Withjack, 1998). The present-day direction of maximum horizontal compression—east-northeast to west-southwest—is rotated from this hypothesized initial postrift direction.

The crustal structure of the passive continental margin includes areas of continental crust, (Iapetan-extended crust (Wheeler, 1996)), rifted continental crust, rift-stage (transitional) crust, marginal oceanic crust, and oceanic crust (Klitgord, 1995) (Figure 2.5-18 and Figure 2.5-19). Rifted continental crust is crust that has been extended, faulted, and thinned slightly. In the site region, rifted-continental crust extends from the western border faults of the exposed synrift Danville, Scottsville, Culpeper, Gettysburg, and Newark basins to the basement hinge

zone, approximately coincident with the seaward edge of the continental shelf (Klitgord, 1995) (Figure 2.5-12 and Figure 2.5-19). Rifted crust also includes exposed and buried Upper Triassic to Lower Jurassic basins within the eastern Piedmont and Coastal Plain Provinces, including the Richmond, Taylorsville, and Norfolk basins (Figure 2.5-10). Several additional basins with poorly defined extent also underlie the Coastal Plain and Continental Shelf and are shown directly east and northeast of the site (Figure 2.5-10). Buried synrift basins are delineated based on sparse drillhole data, magnetic and gravity anomalies, and seismic reflection data (e.g., (Benson, 1992)). Figure 2.5-19 shows east-dipping basin-bounding faults that penetrate the seismogenic crust and have listric geometries at depth. Many of the synrift normal faults are interpreted as Paleozoic thrust faults reactivated during Mesozoic rifting. The Mesozoic basins are discussed further in Section 2.5.1.1.4.4.3 as well as the hypothesized Queen Anne basin shown as lying beneath the site (Figure 2.5-10).

Rift-stage (transitional) crust is extended continental crust intruded by mafic magmatic material during rifting. In the site region, this crustal type coincides with the basement hinge zone and postrift Baltimore Canyon Trough (Klitgord, 1995) (Figure 2.5-12). The basement hinge zone is defined where pre-Late Jurassic basement abruptly deepens seaward from about 1 to 2.5 mi (1.6 to 4 km) to more than 5 mi (8 km) . Overlying this lower crustal unit seaward of the basement hinge zone is the Jurassic volcanic wedge, representing a period of excess volcanism and is greater than 65 mi (105 km) wide and 1 to 5 mi (1.5 to 8 km) thick. The wedge is identified on seismic reflection lines as a prominent sequence of seaward-dipping reflectors. The East Coast magnetic anomaly (ECMA) coincides with the seaward edge of the wedge (Figure 2.5-18) (Section 2.5.1.1.4.3.2).

The last transitional crustal unit between continental and oceanic crust is marginal oceanic crust (Klitgord, 1995) (Figure 2.5-18). Marginal oceanic crust is located east of the ECMA where the Jurassic volcanic wedge merges with the landward edge of oceanic crust. Here, the transition from rifting to sea-floor spreading created a thicker than normal oceanic crust with possible magmatic underplating.

A postrift unconformity separates synrift from postrift deposits and represents the change in tectonic regime in the Middle Jurassic from continental rifting to the establishment of the passive margin ("drifting"). Sedimentary rocks below the unconformity are cut by numerous faults. In contrast, the rocks and strata above the unconformity accumulated within the environment of a broadly subsiding passive margin and are sparsely faulted. Sediments shed from the faulted blocks of the rifting phase and from the core of the Allegheny orogen accumulated on the coastal plain, continental shelf, slope, and rise above the postrift unconformity and contributed to subsidence of the cooling postrift crust by tectonic loading.

Postrift deformation is recorded in synrift basins and within postrift strata as normal faults seaward of the basement hinge zone and as contractional features landward of the basement hinge zone. Extensive normal faulting penetrates the postrift strata (and upper strata of the volcanic wedge) of the marginal basin overlying the volcanic wedge (Figure 2.5-18 and Figure 2.5-19). This set of faults is thought to have been caused by sediment loading on the outer edge of the margin due to differential compaction of the slope-rise deposits relative to adjacent carbonate platform deposits (Poag, 1991) (Klitgord, 1995). These faults are interpreted as margin-parallel structures that bound large mega-slump blocks and are not considered active tectonic features (Poag, 1991).

Schlische (2003) summarizes evidence for postrift shortening and positive basin inversion (defined as extension within basins followed by contraction) in several Atlantic margin basins, including the Newark, Taylorsville, and Richmond basins in the site region (Figure 2.5-10).

Contractional postrift deformation is interpreted to record the change in stress regime from horizontal maximum extension during rifting to horizontal maximum compression during passive margin drifting. The hypothesis that the change in stress regime following rifting was recorded in reverse and strike slip faulting and folding was known prior to the 1986 EPRI study (e.g., (Sanders, 1963) (Swanson, 1982) (Wentworth, 1983)), but significant advances in the documentation and characterization of the rift to drift transition and postrift deformation has occurred since the mid-1980s (Withjack, 1998) (Schlische, 2003). Based on structural analysis and age control of basaltic dikes and faulting, much of the site region was under a state of northwest-southeast maximum compression by earliest Jurassic time (Withjack, 1998). This deformation regime may have persisted locally into the Cenozoic based on the recognized early Cenozoic contractional growth faulting associated with the northeast-striking Brandywine fault system (Jacobeen, 1972) (Wilson, 1990), Port Royal fault zone (Mixon, 1984) (Mixon, 2000) and Skinkers Neck anticline (Mixon, 1984) (Mixon, 2000) (Section 2.5.1.1.4.4.4). The present-day stress field of east-northeast to west-southwest maximum horizontal compression (Zoback, 1989a) is rotated from the hypothesized Jurassic and Cretaceous northwest-southeast orientation. The east-northeast to west-southwest maximum horizontal stress direction is consistent with resolved dextral transpressive slip locally documented on the northeast-striking Stafford fault system (Mixon, 2000), a recognized Tertiary tectonic feature (Section 2.5.1.1.4.4.4.1).

### 2.5.1.1.4.1.3 Cenozoic Passive Margin Flexural Tectonics

Tectonic processes along the Atlantic passive continental margin in the Cenozoic Era include vertical tectonics associated with lithospheric flexure. Vertical tectonics are dominated by: (1) cooling of the extended continental, transitional, and oceanic crust as the spreading center migrates eastward, and (2) the transfer of mass from the Appalachian core to the Coastal Plain and Continental Shelf, Slope, and Rise via erosion. Erosion and exhumation of the Allegheny crustal root of the Piedmont, Blue Ridge, Valley and Ridge, and Appalachian Plateau Provinces has been balanced by deposition on and loading of the Coastal Plain and offshore provinces by fluvial, fluvial-deltaic, and marine sediment transport. Margin-parallel variations in the amount of uplift and subsidence have created arches (e.g. South New Jersey and Norfolk Arches) and basins or embayments (e.g. Salisbury Embayment) along the Coastal Plain and Continental Shelf (Figure 2.5-12).

Flexural zones show both passive-margin-normal and passive-margin-parallel trends. Flexure normal to the passive margin is clearly recorded in the basement hinge zone (Figure 2.5-19). The vertical relief across the offshore basement hinge zone accounts for a change in postrift sediment thickness from 1 to 2.5 mi (1.6 to 4 km) to over 5 mi (8 km) and indicates lateral changes in tectonic loading (Klitgord, 1995). It has been proposed that the downwarping of the margin in the vicinity of the main depocenter of the Baltimore Canyon Trough led to the flexural uplift of the Coastal Plain units to the west (Watts, 1982). However, more recent studies show that sea-level variations since the Cretaceous are compatible with the present elevations of exposed Coastal Plain strata and thus do not support flexural uplift of the Coastal Plain (e.g., (Pazzaglia, 1993)).

A simple elastic model of Cenozoic flexural deformation across the Atlantic passive margin has been used to approximate the response of rifted continental crust to surface erosion of the Piedmont and deposition on the Coastal Plain and Continental Shelf (Pazzaglia, 1994) (Figure 2.5-12 and Figure 2.5-19). The boundary between areas of net Cenozoic erosion and deposition, the Fall Line, marks the flexural hinge between uplift and downwarping. Geologic correlation and longitudinal profiles of Miocene to Quaternary river terraces on the Piedmont with deltaic and marine equivalent strata on the Coastal Plain provide data for model validation (Pazzaglia, 1993). A one-dimensional elastic plate model replicates the form of the profiles and

maintenance of the Fall Line with flexure driven by exhumation of the Piedmont and adjacent Appalachian provinces coupled with sediment loading in the Salisbury Embayment and Baltimore Canyon Trough (Pazzaglia, 1994). Model results suggest a long-term denudation rate of approximately 33 ft (10 m) per million years and about 115 to 426 ft (35 to 130 m) of upwarping of the Piedmont in the last 15 million years.

The flexural hinge zones (Fall Line and basement hinge zone) do not appear to be seismogenic. The spatial association between the Fall Line and observed Cenozoic faults such as the Stafford and Brandywine fault systems is commonly attributed to the fact that those faults are recognizable where Cenozoic cover is thin and there is greater exposure of bedrock compared to areas farther east toward the coast (e.g., (Wentworth, 1983)). It is suggested (Pazzaglia, 1994) that low rates of contractional deformation on or near the hinge zone documented on Cenozoic faults may be a second-order response to vertical flexure and horizontal compressive stresses. Neither the Fall Line nor basement hinge zone was considered a potential tectonic feature by EPRI (1986). They were considered zones where ground amplification could be affected. It is also suggested (Weems, 1998) that multiple fall lines (i.e., alignments of anomalously steep river gradients) located near or within the Fall Line may be of neo-tectonic origin. Subsequent studies performed during the North Anna ESP study demonstrates that the fall lines (Weems, 1998) are erosional features and not capable tectonic sources (NRC, 2005) (Section 2.5.1.1.4.4.5.1) Post-EPRI seismicity also shows no spatial patterns suggestive of seismicity aligned with either the basement hinge zone or Fall Line. Crone and Wheeler (Crone, 2000) and Wheeler (Wheeler, 2005) (Wheeler, 2006) also do not list these as potentially Quaternary active features. Accordingly, it is concluded that these features are not capable tectonic sources. Post-EPRI seismicity also shows no spatial patterns suggestive of seismicity aligned with either the basement hinge zone or Fall Line (Section 2.5.2).

Along-strike variations in the amount of epeirogenic movement along the Atlantic continental margin has resulted in a series of arches and embayments identified based on variations in thickness of Coastal Plain strata from Late Cretaceous through Pleistocene time. The Salisbury Embayment is a prominent, broad depocenter in the site region, and coincides with Chesapeake Bay and Delaware Bay (Figure 2.5-12). At the margins of the Salisbury Embayment are the South New Jersey Arch to the northeast and the Norfolk Arch to the south. Both arches are broad anticlinal warps reflected in the top of basement and overlying sediments. The processes that form and maintain the arches and embayments are poorly understood, and there has been little advancement in the thinking about these features since publication of the EPRI study report (EPRI, 1986). Poag (2004), however, uses new basement data obtained from seismic reflection profiles and exploratory boreholes in the region of the main Chesapeake Bay impact crater to show that the Norfolk Arch is not as well expressed as originally interpreted by earlier authors (Brown, 1972) using limited data. Previous elevation differences cited as evidence for the basement arch appear to be due to subsidence differential between the impact crater and the adjacent deposits (Poag, 2004) (Section 2.5.1.1.4.4.4). Regardless, no published hypothesis was found suggesting causality between epeirogenic processes maintaining these specific arches and the embayment and potentially seismogenic structures, and there is no spatial association of seismicity with the basement arches. Thus, it is concluded that these features are not capable tectonic sources.

### 2.5.1.1.4.2    Tectonic Stress in the Mid-Continent Region

Expert teams that participated in the 1986 EPRI evaluation of intra-plate stress generally concluded that tectonic stress in the CEUS region is characterized by northeast-southwest-directed horizontal compression. In general, the expert teams concluded that the most likely source of tectonic stress in the mid-continent region was ridge-push force associated with the Mid-Atlantic ridge, transmitted to the interior of the North American plate

by the elastic strength of the lithosphere. Other potential forces acting on the North American plate were judged to be less significant in contributing to the magnitude and orientation of the maximum compressive principal stress. Some of the expert teams noted that deviations from the regional northeast-southwest trend of principal stress may be present along the east coast of North America and in the New Madrid region. They assessed the quality of stress indicator data and discussed various hypotheses to account for what were interpreted as variations in the regional stress trajectories.

Since 1986, an international effort to collate and evaluate stress indicator data has resulted in publication of a new world stress map (Zoback, 1989a) (Zoback, 1989b). Data for this map are ranked in terms of quality, and plate-scale trends in the orientations of principal stresses are assessed qualitatively based on analysis of high-quality data (Zoback, 1992). Subsequent statistical analyses of stress indicators confirmed that the trajectory of the maximum compressive principal stress is uniform across broad continental regions at a high level of statistical confidence. In particular, the northeast-southwest orientation of principal stress in the CEUS inferred by the EPRI experts is statistically robust, and is consistent with the theoretical trend of compressive forces acting on the North American plate from the mid-Atlantic ridge (Coblentz and Richardson, 1995).

More recent assessments of lithospheric stress do not support inferences by some EPRI expert teams that the orientation of the principal stress may be locally perturbed in the New England area, along the east coast of the United States, or in the New Madrid region. A variety of data was summarized (Zoback, 1989a), including well-bore breakouts, results of hydraulic fracturing studies, and newly calculated focal mechanisms, which indicate that the New England and eastern seaboard regions of the U.S. are characterized by horizontal northeast-southwest to east-west compression. Similar trends are present in the expanded set of stress indicators for the New Madrid region. Zoback and Zoback (Zoback, 1989a) grouped all of these regions, along with a large area of eastern Canada, with the CEUS in an expanded "Mid-Plate" stress province characterized by northeast-southwest directed horizontal compression.

In addition to better documenting the orientation of stress, research conducted since 1986 has addressed quantitatively the relative contributions of various forces that may be acting on the North American plate to the total stress within the plate. Richardson and Reding (Richardson, 1991) performed numerical modeling of stress in the continental U.S. interior, and considered the contribution to total tectonic stress to be from three classes of forces:

- ◆ Horizontal stresses that arise from gravitational body forces acting on lateral variations in lithospheric density. These forces commonly are called buoyancy forces. Richardson and Reding emphasize that what is commonly called ridge-push force is an example of this class of force. Rather than a line-force that acts outwardly from the axis of a spreading ridge, ridge-push arises from the pressure exerted by positively buoyant, young oceanic lithosphere near the ridge against older, cooler, denser, less buoyant lithosphere in the deeper ocean basins (Turcotte, 2002). The force is an integrated effect over oceanic lithosphere ranging in age from about 0 to 100 million years (Dahlen, 1981). The ridge-push force is transmitted as stress to the interior of continents by the elastic strength of the lithosphere.

- ◆ Shear and compressive stresses transmitted across major plate boundaries (strike-slip faults and subduction zones).

- ◆ Shear tractions acting on the base of the lithosphere from relative flow of the underlying asthenospheric mantle.

Richardson and Reding (Richardson, 1991) concluded that the observed northeast-southwest trend of principal stress in the CEUS dominantly reflects ridge-push body forces. They estimated the magnitude of these forces to be about 2 to 3 X $10^{12}$ N/m (i.e., the total vertically integrated force acting on a column of lithosphere 1 m wide), which corresponds to average equivalent stresses of about 40 to 60 MPa distributed across a 30 mi (50 km) thick elastic plate. The fit of the model stress trajectories to data was improved by the addition of compressive stress (about 5 to 10 MPa) acting on the San Andreas Fault and Caribbean plate boundary structures. The fit of the modeled stresses to the data further suggested that shear stresses acting on these plate boundary structures is in the range of 5 to 10 MPa.

Richardson and Reding (Richardson, 1991) noted that the general northeast-southwest orientation of principal stress in the CEUS also could be reproduced in numerical models that assume a shear stress, or traction, acting on the base of the North American plate. Richardson and Reding (Richardson, 1991) and Zoback and Zoback (Zoback, 1989) do not favor this as a significant contributor to total stress in the mid-continent region.  A basal traction predicts or requires that the horizontal compressive stress in the lithosphere increases by an order of magnitude moving east to west, from the eastern seaboard to the Great Plains.  Zoback and Zoback (Zoback, 1989) noted that the state of stress in the southern Great Plains is characterized by north-northeast to south-southwest extension, which is contrary to this prediction.  They further observed that the level of background seismic activity is generally higher in the eastern United States than in the Great Plains, which is not consistent with the prediction of the basal traction model that compressive stresses (and presumably rates of seismic activity) should be higher in the middle parts of the continent than along the eastern margin.

To summarize, analyses of regional tectonic stress in the CEUS since EPRI (1986) have not significantly altered the characterization of the northeast-southwest orientation of the maximum compressive principal stress.  The orientation of a planar tectonic structure relative to the principal stress direction determines the magnitude of shear stress resolved onto the structure.  Given that the current interpretation of the orientation of principal stress is similar to that adopted in EPRI (1986), a new evaluation of the seismic potential of tectonic features based on a favorable or unfavorable orientation to the stress field would yield similar results. Thus, there is no significant change in the understanding of the static stress in the CEUS since the publication of the EPRI source models in 1986, and there are no significant implications for existing characterizations of potential activity of tectonic structures.

### 2.5.1.1.4.3      Gravity and Magnetic Data and Features of the Site Region and Site Vicinity

Gravity and magnetic anomaly datasets of the site region have been published following the 1986 EPRI study.  Significant datasets include regional maps of the gravity and magnetic fields in North America by the Geological Society of America (GSA), as part of the Society's DNAG project (Tanner, 1987) (Hinze, 1987).  The DNAG datasets are widely available in digital form via the internet (Hittelman, 1994).  A magnetic anomaly map of North America was published in 2002 that featured improved reprocessing of existing data and compilation of a new and more complete database (Bankey, 2002) (Figure 2.5-20).

These maps present the potential field data at 1:5,000,000-scale, and thus are useful for identifying and assessing gravity and magnetic anomalies with wavelengths on the order of tens of kilometers or greater (Bankey, 2000) (Hittelman, 1994).  Regional gravity anomaly maps are based on Bouguer gravity anomalies onshore and free-air gravity anomalies offshore.  The primary sources of magnetic data reviewed for this CCNPP Unit 3 study are from aeromagnetic

surveys onshore and offshore (Bankey, 2002), and the DNAG datasets available digitally from the internet (Hittelman, 1994).

Most of the contributed gravity and magnetic data that went into the regional compilations were collected prior to the 1986 EPRI study; thus, most of the basic data were available for interpretation at local and regional scales. Large-scale compilations (1:2,500,000-scale) of the free-air anomalies offshore and Bouguer anomalies onshore were published in 1982 by the Society of Exploration Geophysicists (Lyons, 1982) (Sheridan, 1988). The DNAG magnetic anomaly maps were based on a prior analog map of magnetic anomalies of the U.S. published in the early 1980's (Zietz, 1982) (Behrendt, 1983) (Sheridan, 1988).

In addition, the DNAG Continent-Ocean transect program published a synthesis of gravity and magnetic data with seismic and geologic data (Klitgord, 1995). Transect E-3, which crosses the site region, is presented in Figure 2.5-16 and Figure 2.5-17. Much of the seismic and geophysical data through the Piedmont region was reanalyzed from a geophysical survey conducted along Interstate I-64 in Virginia that was published prior to release of the 1986 EPRI study (e.g., (Harris, 1982)).

In summary, the gravity and magnetic data published since 1986 do not reveal any new anomalies related to geologic structures that were not identified prior to the 1986 EPRI study. Rather, post-EPRI publications have refined the characteristics and tectonic interpretation of the anomalies. Discussion of the gravity and magnetic anomalies is presented in the following sections.

### 2.5.1.1.4.3.1 Gravity Data and Features

Gravity data compiled at 1:5,000,000-scale for the DNAG project provide documentation of previous observations that the gravity field in the site region is characterized by a long-wavelength, east-to-west gradient in the Bouguer gravity anomaly over the continental margin (Harris, 1982) (Hittelman, 1994) (Figure 2.5-21). The free-air gravity anomaly shows broad gravity lows over offshore oceanic crust near the continental margin and over the broad marginal embayments. Offshore marginal platforms are marked by shorter-wavelength, higher-amplitude gravity highs and lows. The present shelf edge is marked by a prominent free-air gravity anomaly that also corresponds to the continent-ocean boundary (Sheridan, 1988) (Klitgord, 1995).

Bouguer gravity values increase eastward from about -80 milligals (mgal) in the Valley and Ridge Province of western Virginia to about +10 mgal in the Coastal Plain Province, corresponding to an approximately 90 mgal regional anomaly across the Appalachian Orogen (Figure 2.5-17 and Figure 2.5-21). This regional gradient is called the "Piedmont gravity gradient" (Harris, 1982), and is interpreted to reflect the eastward thinning of the North American continental crust and the associated positive relief on the Moho discontinuity with proximity to the Atlantic margin.

The Piedmont gravity gradient is punctuated by several smaller positive anomalies with wavelengths ranging from about 15 to 50 mi (25 to 80 km) , and amplitudes of about 10 to 20 mgal. Most of these anomalies are associated with accreted Taconic terranes such as the Carolina/Chopawamsic terrane (Figure 2.5-17). Collectively, they form a gravity high superimposed on the regional Piedmont gradient that can be traced northeast-southwest on the 1:5,000,000-scale DNAG map relatively continuously along the trend of the Appalachian orogenic belt through North Carolina, Virginia, and Maryland (Figure 2.5-21). The continuity of this positive anomaly diminishes to the southwest in South Carolina, and the trend of the anomaly is deflected eastward in Maryland, Pennsylvania, and Delaware.

The short-wavelength anomalies and possible associations with upper crustal structure are illustrated by combining gravity profiles with seismic reflection data and geologic data (Harris, 1982) (Glover, 1995b).  In some cases, short-wavelength positive anomalies are associated with antiformal culminations in Appalachian thrust sheets.  For example, there is a positive anomaly associated with an anticline at the western edge of the Blue Ridge nappe along the Interstate I-64 transect (Harris, 1982) (Figure 2.5-17).  The anomaly is presumably due to the presence of denser rocks transported from depth and thickened by antiformal folding in the hanging wall of the thrust.

The Salisbury geophysical anomaly (SGA) is a paired Bouguer gravity anomaly and magnetic high that is located along the west side of the Salisbury Embayment (Klitgord, 1995) (Figure 2.5-17, Figure 2.5-18, Figure 2.5-20, and Figure 2.5-21).  The SGA is located about 10 mi (16 km) west of the CCNPP site (Figure 2.5-22).  The anomaly is expressed most clearly as a magnetic lineation that separates a zone of short-wavelength, high-amplitude magnetic lineations to the west from a zone of low-amplitude, long-wavelength anomalies to the east. The gravity data show the SGA to form the western margin of a broad gravity low that extends seaward to the basement hinge zone.  The anomaly takes the form of a north-northeast-trending gravity high having about 30 mgal relief (Johnson, 1973).  The anomaly has also been named the Sussex-Curioman Bay trend (Levan, 1963) or the Sussex-Leonardtown anomaly (Daniels, 1985), and is believed to reflect an east-dipping mafic rock body associated with a suture zone buried beneath coastal plain sediments (Figure 2.5-17).  The SGA is interpreted (Klitgord, 1995) to mark the likely location of the Taconic suture that separates the Goochland terrane on the west from a zone of island arc and oceanic metavolcanics formed in the Iapetus Ocean on the east.  The SGA is shown (Horton, 1991) to be associated with the buried Sussex terrane is a probable mafic mélange that was interpreted by Lefort and Max (Lefort, 1989) to mark the Alleghenian "Chesapeake Bay suture" (Figure 2.5-16).

The offshore portions of the site region contain a prominent, long-wavelength free-air gravity anomaly associated with the transition from continental to oceanic crust (Sheridan, 1988) (Klitgord, 1995) (Figure 2.5-19).  This anomaly is large (75 to 150 mgal peak to trough) and is 45 to 80 mi (72 to 129 km) wide.  Variations in the amplitude and shape of the anomaly along the Atlantic margin are due to seafloor relief, horizontal density variations in the crust, and relief on the crust-mantle boundary (Sheridan, 1988) (Klitgord, 1995).

In summary, gravity data published since the mid-1980s confirm and provide additional documentation of previous observations of a gradual "piedmont gravity gradient" across the Blue Ridge and Piedmont Provinces of Virginia and a prominent gravity anomaly at the seaward margin of the continental shelf. Shorter-wavelength anomalies such as the SGA also are recognized in the data.  All anomalies were known at the time of the 1986 EPRI study. The "piedmont gravity gradient" is interpreted to reflect eastward thinning of the North American crust and lithosphere.  The free-air anomaly at the outer shelf edge is interpreted as reflecting the transition between continental and oceanic crust.  Second-order features in the regional field, such as the Salisbury geophysical anomaly and the short discontinuous northeast-trending anomaly east of the site, primarily reflect density variations in the upper crust associated with the boundaries and geometries of Appalachian thrust sheets and accreted terranes.

### 2.5.1.1.4.3.2 Magnetic Data and Features

Magnetic data compiled for the 2002 Magnetic Anomaly Map of North America reveal numerous northeast-southwest-trending magnetic anomalies, generally parallel to the structural features of the Appalachian orogenic belt (Bankey, 2002) (Figure 2.5-20).  Unlike the gravity field, the magnetic field is not characterized by a regional, long-wavelength gradient

that spans the east-west extent of the site region. A magnetic profile along Interstate-64 published to accompany a seismic reflection profile (Harris, 1982) shows anomalies with wavelengths of about 6 to 30 mi (10 to 48 km). It has been concluded (Harris, 1982) that anomalies in the magnetic field primarily are associated with upper-crustal variations in magnetic susceptibility and, unlike the gravity data, do not provide information on crustal-scale features in the lithosphere.

Prominent north- to northeast-trending magnetic anomalies in the CCNPP site region include the interior New York-Alabama, Ocoee, and Clingman lineaments, the Coastal Plain Salisbury geophysical anomaly and near shore Brunswick magnetic anomaly, and the offshore East Coast magnetic anomaly (King, 1978) (Klitgord, 1988) (Klitgord, 1995) (Bankey, 2002) (Figure 2.5-20). The offshore Blake Spur magnetic anomaly is outside the site region.

King and Zietz (1978) identified a 1,000 mi (1,600 km) long lineament in aeromagnetic maps of the eastern U.S. that they referred to as the "New York-Alabama lineament" (NYAL) (Figure 2.5-20). The NYAL primarily is defined by a series of northeast-southwest-trending linear magnetic anomalies in the Valley and Ridge province of the Appalachian fold belt that systematically intersect and truncate other magnetic anomalies. The NYAL is located about 160 mi (257 km) northwest of the CCNPP site.

The Clingman lineament is an approximately 750 mi (1,200 km) long, northeast-trending aeromagnetic lineament that passes through parts of the Blue Ridge and eastern Valley and Ridge provinces from Alabama to Pennsylvania (Nelson, 1981). The Ocoee lineament splays southwest from the Clingman lineament at about latitude 36°N (Johnston, 1985a). The Clingman-Ocoee lineaments are sub-parallel to and located about 30 to 60 mi (48 to 97 km) east of the NYAL. These lineaments are located about 60 mi northwest of the CCNPP site.

King and Zietz (King, 1978) interpreted the NYAL to be a major strike-slip fault in the Precambrian basement beneath the thin-skinned fold-and-thrust structures of the Valley and Ridge province, and suggested that it may separate rocks on the northwest that acted as a mechanical buttress from the intensely deformed Appalachian fold belt to the southeast. Shumaker (Shumaker, 2000) interpreted the NYAL to be a right-lateral strike-slip fault that formed during an initial phase of Late Proterozoic continental rifting that eventually led to the opening of the Iapetus Ocean.

The Clingman lineament also is interpreted to arise from a source or sources in the Precambrian basement beneath the accreted and transported Appalachian terranes (Nelson, 1981). Johnston (Johnston, 1985a) observed that the "preponderance of southern Appalachian seismicity" occurs within the "Ocoee block", a Precambrian basement block bounded by the NYAL and Clingman-Ocoee lineaments (the Ocoee block was previously defined by (Johnston, 1985b)). Based on the orientations of nodal planes from focal mechanisms of small earthquakes, it was noted (Johnston, 1985) that most events within the Ocoee block occurred by strike-slip displacement on north-south and east-west striking faults, Johnston (Johnston, 1985a) did not favor the interpretation of seismicity occurring on a single, through-going northeast-southwest-trending structure parallel to the Ocoee block boundaries.

The Ocoee block lies within a zone defined by Wheeler (Wheeler, 1995) (Wheeler, 1996) as extended continental crust of the Late Proterozoic to Cambrian Iapetan terrane. Synthesizing geologic and geophysical data, Wheeler (Wheeler, 1995) mapped the northwest extent of the Iapetan normal faults in the subsurface below the Appalachian detachment, and proposed that earthquakes within the region defined by Johnston and Reinbold (Johnston, 1985b) as the

Ocoee block may be the result of reactivation of Iapetan normal faults as reverse or strike-slip faults in the modern tectonic setting.

The East Coast magnetic anomaly (ECMA) is a prominent, linear, segmented magnetic high that extends the length of the Atlantic continental margin from the Carolinas to New England (Figure 2.5-20). The anomaly is about 65 mi (105 mi) wide and has an amplitude of about 500 nT. This anomaly approximately coincides with the seaward edge of the continental shelf, and has been considered to mark the transition from continental to oceanic crust. Klitgord et al. (1995) note that the anomaly is situated above the seaward edge of the thick Jurassic volcanic wedge and lower crustal zone of magmatic under plating along the boundary between rift-stage and marginal oceanic crust (Figure 2.5-18 and Figure 2.5-19). The ECMA is not directly associated with a fault or tectonic feature, and thus is not a potential seismic source.

The Brunswick magnetic anomaly (BMA) is located along the basement hinge zone offshore of the Carolinas, at the southern portion of the site region about 200 mi (322 km) from the CCNPP site (Figure 2.5-20). The lineament is narrower and has less amplitude than the ECMA (Klitgord, 1995). The BMA may continue northward along the hinge zone of the Baltimore Canyon Trough, but the magnetic field there is much lower in amplitude and the lineament is diffuse. The BMA is not directly related to a fault or other tectonic structure, and thus is not a potential seismic source.

The Blake Spur magnetic anomaly (BSMA) is located east of the site region above oceanic crust, about 290 mi (465 km) from the CCNPP site (Figure 2.5-20). The BSMA is a low-amplitude magnetic anomaly that lies subparallel to the East Coast magnetic anomaly (Klitgord et al., 1995). The BSMA probably formed during the Middle Jurassic as the midocean ridge spreading center shifted to the east. The BSMA coincides with a fault-bounded, west-side-down scarp in oceanic basement. Since its formation, the BSMA has been a passive feature in the Atlantic crust, and thus is not a potential seismic source.

The Salisbury geophysical anomaly (SGA), as mentioned above, is a paired Bouguer gravity and magnetic anomaly along the west side of the Salisbury embayment that is located about 10 mi (16 km) of the CCNPP site (Figure 2.5-22). The anomaly is expressed in the magnetic data as a lineament separating short-wavelength, high-amplitude magnetic lineations to the west from a zone of low-amplitude, long-wavelength anomalies to the east. The contrast in magnetic signature is related to the juxtaposition of terranes of contrasting affinity beneath coastal plain sediments, and in particular the mafic to ultramafic rocks and mélange termed the Sussex terrane by Horton et al. (1991) and believed to represent alternatively a Taconic (Glover, 1995b) or Alleghenian (Lefort, 1989) suture (Figure 2.5-16). Lower intensities to the west are associated with the Goochland terrane, which represents continental basement (Figure 2.5-17).

Discrete magnetic lows associated with the Richmond and Culpeper basins are discernible on the 2002 North America magnetic anomaly map (Bankey, 2002) (Figure 2.5-22). Basaltic and diabase dikes and sills are a component of the synrift fill of the exposed basins in the Piedmont and of the Taylorsville basin (Schlische, 2003) (Klitgord, 1995). The distinctive, elongate magnetic anomalies associated with these igneous bodies within the synrift basins of the Piedmont are also used beneath the Coastal Plain to delineate the Taylorsville, Queen Anne, and other synrift basins (e.g., (Benson, 1992)). The elongate magnetic anomalies are less prevalent in the magnetic field east of the Salisbury geophysical anomaly. Either the eastern rift basins do not contain as much volcanic material as the western set of rift basins or the depth to this volcanic material is considerably greater (Klitgord, 1995). Small, circular magnetic highs across the coastal plain have been interpreted as intrusive bodies (Horton, 1991) (Klitgord, 1995).

Approximately 5 to 7 mi (8 to 11 km) east of the CCNPP site is an unnamed short, discontinuous weak to moderate northeast-trending magnetic anomaly that aligns subparallel to the SGA (Figure 2.5-22).  Similar features to the south have been interpreted as granitic intrusive anomalies, whereas Benson (1992) interprets the feature as being bound by a Mesozoic basin (Figure 2.5-10).  A deep borehole (SM-DF-84, Figure 2.5-11) drilled near the southern margin of this feature encountered Jurassic (?) volcanic rocks (dated at $169 \pm 8$ million years old) related to Mesozoic rifting, or perhaps basic metavolcanic rocks accreted to North America as part of the Brunswick Terrane (Hansen, 1986).

A magnetic profile along an approximately west-northwest to east-southeast transect through central Pennsylvania (Glover, 1995b) (Figure 2.5-17) indicates that paired high and low magnetic anomalies are associated with the western margins of crustal units truncated by thrust faults. Many of these anomalies have very high amplitudes and short wavelengths. For example, there is a 400-600 nT anomaly associated with the western margin of the Blue Ridge thrust nappe. Similarly, along a continuing transect line through Virginia, Glover and Klitgord (Glover, 1995a) show a 1500-2000 nT anomaly associated with the western edge of the Potomac mélange.  This transect crosses the Salisbury geophysical anomaly where it is expressed as an 600 nT anomaly (Figure 2.5-17).  In summary, magnetic data published since the mid-1980's confirm and provide additional documentation of previous observations (i.e., pre-EPRI) across this region of eastern North America, and do not reveal any new anomalies related to geologic structures previously unknown to EPRI (EPRI, 1986).

### 2.5.1.1.4.4     Principal Tectonic Structures

Research since the EPRI study (EPRI, 1986) has advanced the understanding of the character and timing of the crustal architecture and tectonic history of the Atlantic continental margin. The research has explained the significance of many geophysical anomalies and has clarified the timing and kinematics of tectonic processes from the Late Precambrian through the Cenozoic. Since the EPRI study (EPRI, 1986) was completed, new Cenozoic tectonic features have been proposed and described in the site region, and previously described features have since been characterized in more detail.  New features identified since the EPRI study (EPRI, 1986) in the CCNPP site region area include gentle folds and a  hypothesized minor fault on the western shore of Chesapeake Bay directly south of the CCNPP site (Kidwell, 1997).  Also, new geologic data collected since 1986 has clarified the geometry and location of the Port Royal fault zone and Skinkers Neck anticline, and tectonic features representing the southern continuation of the Brandywine fault system, all of which are discussed further in the following sections.  Tectonic features suggested by poorly constrained data include an unnamed fault underlying the upper Chesapeake Bay inferred by Pazzaglia (Pazzaglia, 1993), a series of warps beneath the lower Patuxent River and Chesapeake Bay near the CCNPP site hypothesized by McCartan (McCartan, 1995), and a hypothesized Stafford fault system by Marple and Talwani (Marple, 2004b) that is significantly longer and more active than previously recognized (Mixon, 2000).  An additional geologic feature discovered since EPRI (1986) in the site region is the Eocene Chesapeake Bay impact crater (Figure 2.5-5 and Figure 2.5-6) (King, 1974) (Schruben, 1994).  Based on the absence of published literature documenting Quaternary tectonic deformation and spatially associated with seismicity, we conclude that this feature is not a capable tectonic source (Section 2.5.1.1.4.4.4).

In the sections below, specific tectonic features and their evidence for activity published since the EPRI (1986) study are discussed.  We find that no new information has been published since 1986 on any tectonic feature within the CCNPP site region that would cause a significant change in the EPRI seismic source model.

We divide principal tectonic structures within the 200 mi (322 km) CCNPP site region into five categories based on their age of formation or most recent reactivation. These categories include Late Proterozoic, Paleozoic, Mesozoic, Tertiary, and Quaternary. Late Proterozoic, Paleozoic, and Mesozoic structures are related to major plate tectonic events and generally are mapped regionally on the basis of geological and/or geophysical data. Late Proterozoic structures include normal faults active during post-Grenville orogeny rifting and formation of the Iapetan passive margin. Paleozoic structures include thrust and reverse faults active during Taconic, Acadian, Alleghenian, and other contractional orogenic events. Mesozoic structures include normal faults active during break-up of Pangaea and formation of the Atlantic passive margin.

Tertiary and Quaternary structures within the CCNPP site region are related to the tectonic environment of the Atlantic passive margin. This passive margin environment is characterized by southwest- to northeast-oriented, horizontal principal compressive stress, and vertical crustal motions. The vertical crustal motions associated with loading of the coastal plain and offshore sedimentary basins and erosion and exhumation of the Piedmont and westward provinces of the Appalachians. Commonly, these structures are localized, and represent reactivated portions of older bedrock structures. Zones of seismicity not clearly associated with a tectonic feature are discussed separately in Section 2.5.1.1.4.5.

### 2.5.1.1.4.4.1 Late Proterozoic Tectonic Structures

Extensional structures related to Late Proterozoic-Early Cambrian rifting of the former supercontinent Rhodinia and formation of the Iapetan Ocean basin are located along a northeast-trending belt between Alabama and Labrador, Canada, and along east-west-trending branches cratonward (Wheeler, 1995) (Johnston, 1994) (Figure 2.5-23). Major structures along this northeast-trending belt include the Reelfoot rift, the causative tectonic feature of the 1811-1812 New Madrid earthquake sequence. Within the 200 mi (322 km) site region, a discrete Late Proterozoic feature includes the New York-Alabama lineament (King, 1978) (Shumaker, 2000). The Rome Trough (Ervin and McGinnis, 1975) is located directly outside the 200-mile (322 km) site region. Extended crust of the Iapetan passive margin extends eastward beneath the Appalachian thrust front approximately to the eastern edge of Mesozoic extended crust within the eastern Piedmont physiographic province (Wheeler, 1996) (Figure 2.5-15). This marks the western boundary of major Paleozoic sutures that juxtapose Laurentian crust against exotic crust amalgamated during the Paleozoic orogenies (Wheeler, 1996) (Figure 2.5-16 and Figure 2.5-17). At its closest approach, the area of extended Iapetan crust is located about 70 mi (113 km) northwest of the CCNPP site (Figure 2.5-23).

The earthquake potential of Iapetan normal faults was recognized by the EPRI team members due to the association between the Reelfoot rift and the 1811 to 1812 New Madrid earthquake sequence (EPRI, 1986). Seismic zones in eastern North America spatially associated with Iapetan normal faults include the Giles County seismic zone of western Virginia, and the Charlevoix, Quebec seismic zone, both of which are located outside the CCNPP site region (Wheeler, 1995) (Figure 2.5-23). Because the Iapetan structures are buried beneath Paleozoic thrust sheets and/or strata, their dimensions are poorly known except in isolated, well studied cases.

Although published literature since the EPRI study (EPRI, 1986) has made major advances in showing the association between local seismic sources and Late Proterozoic structures (Wheeler, 1992) (Wheeler, 1995) and has highlighted the extent of extended Iapetan passive margin crust (Wheeler, 1995) (Wheeler, 1996), no new information has been published since

1986 on any Late Proterozoic feature within the CCNPP site region that would cause a significant change in the EPRI study (EPRI, 1986) seismic source model.

### 2.5.1.1.4.4.2 Paleozoic Tectonic Structures

The central and western portions of the CCNPP site region encompass portions of the Piedmont, Blue Ridge, Valley and Ridge, and Appalachian Plateau physiographic provinces (Figure 2.5-1). Structures within these provinces are associated with thrust sheets, shear zones, and sutures that formed during convergent and transpressional Appalachian orogenic events of the Paleozoic Era. Tectonic structures of this affinity exist beneath the sedimentary cover of the Coastal Plain and Continental Shelf Provinces. Paleozoic structures shown on Figure 2.5-23 include: 1) sutures juxtaposing allochthonous (tectonically transported) rocks against proto-North American crust, 2) regionally extensive Appalachian thrust faults and oblique-slip shear zones, and 3) a multitude of smaller structures that accommodated Paleozoic deformation within individual blocks or terranes (Figure 2.5-16, Figure 2.5-17, and Figure 2.5-18). The majority of these structures dip eastward and sole into one or more levels of low angle, basal Appalachian decollement (Figure 2.5-17). Below the decollement are rocks that form the North American basement complex (Grenville or Laurentian crust).

Researchers have observed that much of the sparse seismicity in eastern North America occurs within the North American basement below the basal decollement. Therefore, seismicity within the Appalachians may be unrelated to the abundant, shallow thrust sheets mapped at the surface (Wheeler, 1995). For example, seismicity in the Giles County seismic zone, located in the Valley and Ridge Province, is occurring at depths ranging from 3 to 16 mi (5 to 25 km) (Chapman, 1994), which is generally below the Appalachian thrust sheets and basal decollement (Bollinger, 1988).

### 2.5.1.1.4.4.2.1 Appalachian Structures

Paleozoic faults within 200 mi (322 km) of the CCNPP site and catalog seismicity are shown on Figure 2.5-23 and Figure 2.5-24 (see section 2.5.2 for a complete discussion on seismicity). Paleozoic faults with tectonostratigraphic units are shown on Figure 2.5-16, Figure 2.5-17, and Figure 2.5-18.  Faults mapped within the Appalachian provinces (Piedmont, Blue Ridge, Valley and Ridge) are discussed in this section along with postulated Paleozoic faults in the Coastal Plain that are buried by Cenozoic strata.  No new information has been published since 1986 on any Paleozoic fault in the site region that would cause a significant change in the EPRI study (EPRI, 1986) seismic source model.  Paleozoic faults are discussed below from west to east across the CCNPP site region.

Major Paleozoic tectonic structures of the Appalachian Mountains within 200 mi (322 km) of the site include the Little North Mountain-Yellow Breeches fault zone, the Hylas shear zone, the Mountain Run–Pleasant Grove fault system, the Brookneal shear zone, and the Central Piedmont shear zone (including the Spotsylvania fault) (Figure 2.5-23).  These structures bound lithotectonic units as defined in recent literature (Horton, 1991) (Glover, 1995b) (Hibbard, 2006) (Hibbard, 2007).

The northeast-striking Little North Mountain fault zone is located within the eastern Valley and Ridge Physiographic Province of western Virginia, eastern Maryland, and southern Pennsylvania (Figure 2.5-16 and Figure 2.5-23).  The fault zone forms the tip of an upper level thrust sheet that attenuated Paleozoic shelf deposits of the Laurentian continental margin during the Alleghenian Orogeny (Hibbard, 2006).  The east-dipping Little North Mountain thrust sheet soles into a decollement shown as a couple miles deep (Figure 2.5-17).  This decollement represents an upper-level detachment above a deeper decollement about 5 mi (8 km) deep (Glover, 1995b) (Figure 2.5-17).  The Little North Mountain fault and Yellow

Breeches fault to the northeast mark the approximate location of the westernmost thrusts that daylight within the Valley and Ridge Province (Figure 2.5-23). Farther west, thrust ramps branching from the deeper decollement rarely break the surface and overlying fault-related folds control the morphology of the Valley and Ridge Province.

The Little North Mountain-Yellow Breeches fault zone is not considered a capable tectonic source. The decollement associated with the Little North Mountain thrust is within a couple miles of the surface, suggesting the fault probably does not penetrate to seismogenic depths. No seismicity is attributed to the Little North Mountain-Yellow Breeches fault zone and published literature does not indicate that it offsets late Cenozoic deposits or exhibits geomorphic expression indicative of Quaternary deformation. Therefore, this Paleozoic fault is not considered to be a capable tectonic source.

The Hylas shear zone, active between 330 and 220 million years ago, comprises a 1.5 mi (2.4 km) wide zone of ductile shear fabric and mylonites located 71 mi (115 km) southwest of the site (Bobyarchick, 1979). The Hylas shear zone also locally borders the Mesozoic Richmond basin and appears to have been reactivated during Mesozoic extension to accommodate growth of the basin (Figure 2.5-10). Based on review of published literature and historical seismicity, there is no reported geomorphic expression, historical seismicity, or Quaternary deformation along the Hylas shear zone, thus this feature is not considered to be a capable tectonic source.

The Mountain Run-Pleasant Grove fault system is located within the Piedmont Physiographic Province in Virginia and Maryland and may extend to near Newark, New Jersey (Hibbard et al., 1995) (Figure 2.5-17 and Figure 2.5-23). This fault system extends across the entire site region and juxtaposes multiple-tectonized, allochthonous rocks and terranes to the east against the passive margin rocks of North American affinity to the west. The fault zone exhibits mylonitic textures, indicative of the ductile conditions in which it formed during the Paleozoic Era. Locally the allochthonous rocks are the Potomac composite terrane (Horton et al., 1991), which consists of a stack of thrust sheets containing tectonic mélange deposits that include ophiolites, volcanic arc rocks, and turbidites. This east-dipping thrust probably shallows to a decollement a couple miles below ground surface, and is shown to be truncated by the Brookneal shear zone (Figure 2.5-17) (Glover, 1995b). In the site region, the Mesozoic Culpeper basin overlies the Mountain Run-Pleasant Grove fault system, suggesting that portions of the Paleozoic thrust fault system may have been reactivated as normal faults in the Triassic (Figure 2.5-10). In northern Virginia, about 70 mi (113 km) west of the site, the Everona fault was identified within Tertiary, and possibly early Quaternary, debris flow deposits (Pavlides, 1983) (Pavlides, 1986). Subsequent studies performed during the North Anna ESP (Dominion, 2004a) on the activity of the Everona-Mountain Run fault system indicate that this fault system is not a capable tectonic source (Section 2.5.1.1.4.4.5.2).

The Brookneal shear zone is located within the Piedmont in Virginia and probably extends beneath the Coastal Plain across Virginia and Maryland to within about 50 mi (80 km) of the site (Figure 2.5-16 and Figure 2.5-23). The dextral-reverse shear zone is the northern continuation of the Brevard zone, a major terrane boundary extending from Alabama to North Carolina (Hibbard, 2002). The Brookneal shear zone juxtaposes magmatic and volcaniclastic rocks of the Chopawamsic volcanic arc to the east against the Potomac mélange to the west. This east-dipping thrust possibly truncates the Mountain Run fault at about 2.5 mi (4 km) depth, then flattens to a decollement at about 4 to 5 mi (6 to 8 km) depth that dips gently eastward beneath the surface trace of the Spotsylvania fault (Figure 2.5-17) (Glover, 1995b). Southwest of the site region, the Mesozoic Danville basin locally coincides with the Brookneal shear zone, suggesting that portions of the Paleozoic fault may have been reactivated as normal faults in

the Triassic Period. The Brookneal shear zone is not considered a capable tectonic source. No seismicity is attributed to it and published literature does not indicate that it offsets late Cenozoic deposits or exhibits geomorphic expression indicative of Quaternary deformation. Therefore, this Paleozoic fault is not considered to be capable tectonic source.

The northeast-striking Central Piedmont shear zone - Spotsylvania fault has been mapped in the Virginia piedmont as far north as Fredericksburg and beneath the Coastal Plain in eastern Virginia and Maryland (Hibbard, 2006) (Horton, 1991) (Glover, 1995b) (Figure 2.5-16, Figure 2.5-17 and Figure 2.5-23). At its closest approach, the fault is about 40 mi (64 km) northwest of the site (Figure 2.5-16) The Spotsylvania fault is a dextral-reverse fault that is part of the Central Piedmont shear zone (Hibbard, 2006). The fault juxtaposes terranes of different affinity, placing continental rocks of the Goochland terrane to the east against volcanic arc rocks of the Chopawamsic terrane to the west. The east-dipping fault likely penetrates the crust at gentle to intermediate angles, and truncates the basal Appalachian decollement and higher decollement of the Brookneal shear zone (Figure 2.5-17) (Glover, 1995b).

The Spotsylvania fault is not considered a capable tectonic source. Specific studies of this feature by Dames and Moore (DM, 1977b) demonstrate that the Spotsylvania thrust fault exhibits negligible vertical deformation of a pre- to early-Cretaceous erosion surface and is not related to Tertiary faulting along the younger Stafford fault zone (Section 2.5.1.1.4.4.4). The fault was determined by the NRC (AEC) to be not capable within the definition of 10 CFR 100, Appendix A (CFR, 2006). No subsequent evidence has been published since the Dames and Moore (DM, 1977b) study to indicate potential Quaternary activity on the fault.

### 2.5.1.1.4.4.2.2 Coastal Plain Structures

Major Paleozoic tectonic structures beneath the Coastal Plain in the 25 mi (40 km) CCNPP site vicinity include faults bounding the Sussex terrane west of the site and unnamed faults mapped seaward of the CCNPP site by Glover and Klitgord (Glover, 1995a) (Figure 2.5-16, Figure 2.5-17 and Figure 2.5-23). These fault zones, cited here as the western and eastern zones, are interpreted to dip steeply east, penetrate the crust, and juxtapose lithostratigraphic terranes.

The western fault zone coincides with the margins of the Sussex Terrane of Horton (Horton, 1991) (Figure 2.5-16 and Figure 2.5-17). The narrow Sussex Terrane and potential bounding faults are delimited in part by the Salisbury geophysical anomaly, a positive gravity and magnetic high described in Section 2.5.1.1.4.3. The eastern fault zone is shown to extend from coastal North Carolina to southern Delaware, trending north along the eastern part of southern Chesapeake Bay before branching into two splays that trend northeast across the Delmarva Peninsula (Figure 2.5-16 and Figure 2.5-23). The regional crustal cross section shows the fault zone as dipping east at moderate to steep angles (Figure 2.5-17).

No seismicity is attributed to the buried Paleozoic faults and published literature does not indicate that these faults offset late Cenozoic deposits or exhibit geomorphic expression indicative of Quaternary deformation. Therefore, the Paleozoic structures (faults bounding the Sussex terrane west of the site and unnamed faults mapped seaward of the CCNPP site by Glover and Klitgord (Glover, 1995a) in the site vicinity are not considered to be capable tectonic sources.

Other Paleozoic faults mapped by Hibbard (Hibbard, 2006) within the 200 mi (322 km) site region are smaller features that typically are associated with larger Paleozoic structures and accommodate internal deformation within the intervening structural blocks (Figure 2.5-23). No seismicity is attributed to these faults and published literature does not indicate that any of

these faults offset late Cenozoic deposits or exhibit geomorphic expression indicative of Quaternary deformation.  Therefore, these Paleozoic structures in the site region are not considered to be capable tectonic sources

### 2.5.1.1.4.4.3 Mesozoic Tectonic Structures

Mesozoic basins have long been considered potential sources for earthquakes along the eastern seaboard and were considered by most of the EPRI teams in their definition of seismic sources (EPRI, 1986). A series of elongate rift basins of early Mesozoic age are exposed in a belt extending from Nova Scotia to South Carolina and define the area of extended Mesozoic crust (Figure 2.5-10). These Mesozoic rift basins, also commonly referred to as Triassic basins, exhibit a high degree of parallelism with the surrounding structural grain of the Appalachian orogenic belt. The parallelism generally reflects reactivation of pre-existing Paleozoic structures (Ratcliffe, 1986). The rift basins formed during extension and thinning of the crust as Africa and North America rifted apart to form the modern Atlantic Ocean (Section 2.5.1.1.4.1.2).

Generally, the rift basins are asymmetric half-grabens with the primary rift-bounding faults on the western margin of the basin (Figure 2.5-10, Figure 2.5-18 and Figure 2.5-19) (Withjack, 1998).  Within the 200 mi (322 km) CCNPP site region, rift basins with rift-bounding faults on the western margin include the exposed Danville, Richmond, Culpeper, Gettysburg, and Newark basins, and the buried Taylorsville, Norfolk, and other smaller basins (Figure 2.5-10).  In most of the above-mentioned basins, the basin-bounding normal fault is located in close proximity to a Paleozoic thrust or reverse fault (e.g., the Culpeper basin and the Paleozoic Mountain Run fault zone; the Richmond basin and the Paleozoic Hylas shear zone) (Figure 2.5-10 and Figure 2.5-23).  The rift-bounding normal faults are interpreted by some authors to be listric at depth and merge into Paleozoic low angle basal décollement (Manspeizer, 1989).  Other authors interpret rift-bounding faults to penetrate deep into the crust following deep crustal fault zones (Figure 2.5-19).

The geometry and continuity of buried rift basins beneath the Coastal Plain and Continental Shelf is not clear, but the recognition and interpretation of these basins have expanded since the EPRI (1986) study.  In addition to the identification of new basins since 1986, several alternative geometries have been proposed for the site region (Figure 2.5-10 and Figure 2.5-16) (Horton, 1991) (Benson, 1992) (Klitgord, 1995) (Withjack, 1998) (LeTourneau, 2003).  Interpretations are constrained loosely based on sparse borehole, seismic, and aeromagnetic anomaly data (Benson, 1992).  Some authors show the Queen Anne basin located beneath the CCNPP site (e.g., in Figure 2.5-10(Benson, 1992) and in Figure 2.5-16 (Horton, 1991)).  More recent compilations of rift basins do not show the CCNPP site overlying a Mesozoic basin (e.g., in Figure 2.5-10 (Withjack, 1998) and in Figure 2.5-16 (Glover, 1995b)).

Reactivation of faults bordering or within Triassic basins in the Cenozoic as reverse faults is recognized in several basins within the site region and is discussed in Section 2.5.1.1.4.1.2. (e.g., (Schlische, 2003)).  For example, the buried Taylorsville basin coincides with numerous postrift contractional structures of Cretaceous and Tertiary age including the Brandywine, Port Royal, Skinkers Neck, and Hillville faults (Section 2.5.1.1.4.4.4).

Aside from the global finding of Johnston et al. (1994) that areas of Mesozoic extended crust are correlated with large magnitude earthquakes within stable continental regions (i.e., New Madrid seismic zone), there are no specific Mesozoic basin-bounding faults that have demonstrable associated seismic activity or evidence for recent fault activity (Figure 2.5-10 and Figure 2.5-24).  The major postulated basins closest to the site (Taylorsville and Queen Anne) were considered during the 1980s to exist and several were incorporated into seismic sources by the different EPRI teams. Seismicity potentially associated with reactivation of faults

bordering or beneath the Mesozoic basins is captured in the existing EPRI seismic source model.  No new data have been developed to demonstrate that any of the Mesozoic basins are currently active, and Crone and Wheeler (Crone, 2000), Wheeler (Wheeler, 2005) and Wheeler (Wheeler, 2006) do not recognize any basin-margin faults that have been reactivated during the Quaternary in the site region.  No Mesozoic basin in the site region is associated with a known capable tectonic source, and no new information has been developed since 1986 that would require a significant revision to the EPRI seismic source model.

### 2.5.1.1.4.4.4 Tertiary Tectonic Structures

Several faults were active during the Tertiary Period within the 200 mi (322 km) CCNPP site region (Figure 2.5-25). These faults have been recognized in the western part of the Coastal Plain Province where Tertiary strata crop out in river valleys and where the faults have bee investigated using seismic and borehole data.  These faults include the relatively well characterized Stafford fault system in Virginia, the Brandywine fault system in Maryland, and the National Zoo/Rock Creek faults in Washington, D.C.  Additional faults and fault-related folds defined by seismic and borehole data include the Port Royal fault zone and Skinkers Neck anticline in Virginia, and the Hillville fault in Maryland.  Tertiary structures that have been proposed but are poorly constrained by data include east-facing monoclines along the western shore of Chesapeake Bay (McCartan, 1995) and a northeast-striking fault in the upper Chesapeake Bay (Pazzaglia, 1993).  In addition, Kidwell (Kidwell, 1997) uses detailed stratigraphic analysis of the Calvert Cliffs area to postulate the existence of several broad folds developed in Miocene strata as well as a poorly constrained postulated fault.  All of these structures are located within about 50 mi (80 km) of the site, and the proposed east-facing monoclines of McCartan (McCartan, 1995) are within a few miles of the CCNPP site.  Within 25 mi (40 km) of the site, the only fault with documented Tertiary displacement is the Hillville fault (Hansen, 1978) (Hansen, 1986) (Figure 2.5-25).

Several faults associated with the Eocene Chesapeake Bay impact crater have been identified near the mouth of the Chesapeake Bay about 60 mi (97 km) south of the site (Powars, 1999) (Figure 2.5-5).  The impact crater formed on a paleo-continental shelf when the Eocene sea in this location was approximately 1,000 ft (305 m) deep.  The Chesapeake Bay impact crater was discovered in 1993, and thus post-dates the EPRI study (EPRI, 1986).  The 35-million year old Chesapeake Bay impact crater is a 56 mi (90 km) wide, complex peak-ring structure defined by a series of inner and outer ring faults, some of which penetrate the Proterozoic and Paleozoic crystalline basement rocks (Powars, 1999). These faults and others within the outer and inner ring include normal-faulted slump blocks and compaction faults that extend up-section into upper Miocene and possibly younger deposits. Published literature does not indicate that any faults related to the impact crater are seismogenic or offset Quaternary deposits.

Multiple, fault-bounded secondary craters of Eocene age also have been interpreted from multichannel seismic profiles previously collected by Texaco along the Potomac River and Chesapeake Bay 20 and 40 mi (32 and 64 km) north and northwest of the main Chesapeake Bay impact crater (Poag, 2004).  The secondary impact craters have diameters ranging from 0.25 to 2.9 mi (0.4 to 4.7 km).  Faults associated with the secondary craters occasionally penetrate Proterozoic and Paleozoic crystalline basement rocks (Poag, 2004).  Primarily middle Miocene to Quaternary sediments thicken and sag into the primary and secondary craters.  Faults associated with the impact crater are not considered capable tectonic sources and are not discussed further in this section.

Faults and folds mapped within the 200 mi (322 km) CCNPP site region that displace Tertiary Coastal Plain deposits are described below.  These structures include the Stafford fault system, Brandywine fault system, National Zoo/Rock Creek faults, Port Royal fault zone, Skinkers Neck

anticline, and the Hillville fault.  Additional hypothesized Tertiary structures for which compelling geologic or geophysical evidence is lacking are then described.  These structures include hypothesized east-facing monoclines along the western shore of Chesapeake Bay near the CCNPP site described by McCartan (McCartan, 1995), a hypothesized fault in the upper Chesapeake Bay mapped by Pazzaglia (Pazzaglia, 1993), and structures interpreted in Calvert Cliffs by Kidwell (Kidwell, 1997).

*2.5.1.1.4.4.4.1 Stafford Fault of Mixon,et al.*

The Stafford fault (#10 on Figure 2.5-31) approaches within 47 mi (76 km) southwest of the site (Figure 2.5-25).  The 42 mi (68 km) long fault system strikes approximately N35°E (Newell, 1976). The fault system consists of several northeast-striking, northwest-dipping, high-angle reverse to reverse oblique faults including, from north to south, the Dumfries, Fall Hill, Brooke, Tank Creek, Hazel Run, and an unnamed fault (Mixon et al., 2000). Two additional northeast-striking, southeast-side-down faults, the Ladysmith and the Acadia faults, are included here as part of the Stafford fault system.  These individual faults are 10 to 25 mi (16 to 40 km) long and are separated by 1.2 to 3 mi (2 to 5 km) wide en echelon, left step-overs. The left-stepping pattern and horizontal slickensides found on the Dumfries fault suggest a component of dextral shear on the fault system (Mixon, 2000).

Locally, the Stafford fault system coincides with the Fall Line and a northeast-trending portion of the Potomac River (Figure 2.5-25).  Mixon and Newell (Mixon, 1977) suggest that the Fall Line and river deflection may be tectonically controlled.  Detailed drilling, trenching, and mapping in the Fredericksburg region by Dames and Moore (DM, 1973) showed that the youngest identifiable fault movement on any of the four primary faults comprising the Stafford fault system was pre-middle Miocene in age.

Subsequent studies of the Stafford fault system better document the timing of displacement. Mesozoic and Tertiary movement is documented by displacement of Ordovician bedrock over lower Cretaceous strata along the Dumfries fault and abrupt thinning of the Paleocene Aquia Formation across multiple strands of the fault system (Mixon, 2000).  Minor late Tertiary activity of the fault system is documented by an 11-inch displacement by the Fall Hill fault of a Pliocene terrace deposit along the Rappahannock River (Mixon, 1978) (Mixon, 2000) and an 18 in (46 cm) displacement by the Hazel Run fault of upland gravels of Miocene or Pliocene age (Mixon, 1978).  Both offsets suggest southeast-side-down displacement (Mixon, 1978).

Recent geologic and geomorphic analysis of the Stafford fault system for the application of North Anna Early Site Permit (ESP) to the NRC provides additional constraints on the age of deformation (Dominion, 2004a).  Geomorphic analyses (structure contour maps and topographic profiles) of upland surfaces capped by Neogene marine deposits and topographic profiles of Pliocene and Quaternary fluvial terraces of the Rappahannock River near Fredericksburg, Virginia, indicate that these surfaces are not visibly deformed across the Stafford fault system (Dominion, 2004a).   In addition, field and aerial reconnaissance of these features during the North Anna ESP, and as part of this CCNPP Unit 3 study, indicate that there are no distinct scarps or anomalous breaks in topography on the terrace surfaces associated with the mapped fault traces.  The NRC (2005) agreed with the findings of the subsequent study for the North Anna ESP, and stated:  "Based on the evidence cited by the applicant, in particular the applicant's examination of the topography profiles that cross the fault system, the staff concludes that the applicant accurately characterized the Stafford fault system as being inactive during the Quaternary Period."  Collectively, this information indicates that the Stafford fault system is not a capable tectonic source as defined in Appendix A of Regulatory Guide 1.165 (NRC, 1997).

Marple (Marple, 2004a) recently proposed a significantly longer Stafford fault system that extends from Fredericksburg, Virginia to New York City as part of a northeastern extension of the postulated East Coast fault system (ECFS), (Figure 2.5-31) (Section 2.5.1.1.4.4.5.15). The proposed northern extension of the Stafford fault system is based on: (1) aligned apparent right-lateral deflections of the Potomac (22 mi (35 km) deflection), Susquehanna (31 mi (50 km) deflection) and Delaware Rivers (65 mi (105 km) deflection) (collectively these are named the "river bend trend"), (2) upstream incision along the Fall Line directly west of the deflections, and (3) limited geophysical and geomorphic data. Marple and Talwani (Marple, 2004b) proposed that the expanded Stafford fault system of Marple (Marple, 2004a) was a northeast extension of the ECFS of Marple and Talwani (Marple, 2000). Marple and Talwani (Marple, 2004b) further speculate that the ECFS and the Stafford fault system were once a laterally continuous and through-going fault, but subsequently were decoupled to the northwest and southeast, respectively, during events associated with the Appalachian orogeny.

Data supporting the extended Stafford fault system of Marple (Marple, 2004a) is limited. Marple and Talwani (Marple, 2004b) suggest that poorly located historical earthquakes that occurred in the early 1870's and 1970's lie close to the southwestern bend in the Delaware River and concluded an association between historical seismicity and the postulated northern extension of the Stafford fault system. Review of seismicity data available both before and after the EPRI study (EPRI, 1986) indicates a poor correlation in detail between earthquake epicenters and the expanded Stafford fault system (Figure 2.5-25). Geophysical, borehole and trench data collected by McLaughlin (McLaughlin, 2002), near the Delaware River across the trace of the postulated expanded Stafford fault system of Marple (Marple, 2004a), provide direct evidence for the absence of Quaternary deformation. Collectively, there is little geologic and seismologic evidence to support this extension of the fault system beyond that mapped by Mixon (Mixon, 2000).

In summary, all significant information on timing of displacement for the Stafford fault system was available prior to 1986 and incorporated into the EPRI (1986) seismic source models. New significant information published since 1986 regarding the activity of the Stafford fault system includes the geomorphic and geologic analysis performed for the North Anna ESP that concluded the fault system was not active (Dominion, 2004a). Field and aerial reconnaissance performed for the North Anna ESP and this CCNPP COL application also did not reveal any geologic or geomorphic features indicative of potential Quaternary activity along the fault system. Therefore, on the basis of a review of existing geologic literature, the Stafford fault system is not considered a capable tectonic source, and there is no new information that would require a significant revision to the EPRI (1986) seismic source model.

### 2.5.1.1.4.4.4.2 Brandywine Fault System

The Brandywine fault system is located approximately 30 mi (48 km) west of the site and north of the Potomac River (Figure 2.5-25). The 12 to 30 mi (19 to 48 km) long Brandywine fault system consists of a series of en echelon northeast-trending, southeast-dipping reverse faults with east-side-up vertical displacement. Jacobeen (Jacobeen, 1972) and Dames and Moore (DM, 1973) first described the fault system from Vibroseis™ profiles and a compilation of borehole data as part of a study for a proposed nuclear power plant at Douglas Point along the Potomac River. The fault system is composed of the Cheltenham and Danville faults, which are 4 mi and 8 mi (6 to 13 km) long, respectively. These two faults are separated by a 0.6 to 1 mi (1 to 1.6 km) wide left step-over (Jacobeen, 1972). Later work by Wilson and Fleck (Wilson, 1990) interpret one continuous 20 to 30 mi (32 to 48 km) long fault that transitions into a west-dipping flexure to the south near the Potomac River. The mapped trace of the Brandywine fault system coincides with the western margin of the Taylorsville basin (Mixon, 1977) (Hansen, 1986) (Wilson, 1990). This observation lead Mixon and Newell (Mixon, 1977) to

speculate the origin of the Brandywine fault system may be related to the reversal of a pre-existing zone of crustal weakness (i.e., Taylorsville Basin border fault).

The Brandywine fault system was active in the Early Mesozoic and reactivated during late Eocene and possibly middle Miocene time (Jacobeen, 1972) (Wilson, 1990).  Basement rocks have a maximum vertical displacement of approximately 250 ft (76 m) across the fault (Jacobeen, 1972).  Also, the Cretaceous Potomac Formation is 150 ft (46 m) thinner on the east (up-thrown) side of the fault indicating syndepositional activity of the fault.  The faulting is interpreted to extend upward into the Eocene Nanjemoy Formation (70 ft (21 m) offset) (Wilson, 1990), and die out as a subtle flexure developed within the Miocene Calvert Formation (8 ft (2.4 km) flexure) (Jacobeen, 1972).

Wilson and Fleck (Wilson, 1990) speculate that the fault system continues northeast toward the previously mapped Upper Marlboro faults, near Marlboro, Maryland (Figure 2.5-25).  Dryden (Dryden, 1932) reported several feet of reverse faulting in Pliocene Upland deposits in a railroad cut near Upper Marlboro, Maryland (Prowell, 1983).  However, these faults are not observed beyond this exposure.  Wheeler (Wheeler, 2006) suggests that the Upper Marlboro faults have a surficial origin (i.e., landsliding) based on the presence of very low dips and geometric relations inconsistent with tectonic faulting.  Field reconnaissance conducted as part of this CCNPP Unit 3 study used outcrop location descriptions from Prowell (Prowell, 1983) but failed to identify any relevant exposures associated with the faults of Dryden (Dryden, 1932).  Wheeler's (Wheeler, 2006) assessment of the Upper Marlboro fault appears to be consistent with the outcrop described by Dryden (Dryden, 1932) as not being associated with the Brandywine fault system.

Geologic information indicates that the Brandywine fault system was last active during the Miocene.  All geologic information on the timing of displacement on the Brandywine fault system was available and incorporated into the EPRI seismic source models in 1986.  The post-EPRI study by Wilson and Fleck (Wilson, 1990) extended the fault north and south as an anticline, but offers no new information about the timing of the deformation.  There is no pre-EPRI or post-EPRI seismicity associated with this fault system.  This fault system is identified only in the subsurface and geologic mapping along the surface projection of the fault zone does not show a fault (DM, 1973) (McCartan, 1989a) (McCartan, 1989b).  Field and aerial reconnaissance performed as part of this CCNPP Unit 3 study, coupled with interpretation of Light Detection and Ranging (LiDAR) data (see Section 2.5.3.1 for additional information regarding the general methodology), revealed no anomalous geomorphic features indicative of potential Quaternary activity.  The Brandywine fault system, therefore, is not a capable tectonic source and there is no new information developed since 1986 that would require a significant revision to the EPRI seismic source model.

### 2.5.1.1.4.4.4.3 Port Royal Fault Zone and Skinkers Neck Anticline

The Port Royal fault zone and Skinkers Neck anticline are located about 32 mi (51 km) west of the CCNPP site, south of the Potomac River (Figure 2.5-25).  First described by Mixon and Powars (Mixon, 1984), these structures have been identified within the subsurface by: (1) contouring the top of the Paleocene Potomac Formation, (2) developing isopach maps of the Lower Eocene Nanjemoy Formation, and (3) interpreting seismic lines collected in northern Virginia (Milici, 1991) (Mixon, 1992) (Mixon, 2000).  The fault and anticline are not exposed in surface outcrop.  The Port Royal fault zone is located about 4 to 6 mi (6 to 10 km) east and strikes subparallel to the Skinkers Neck anticline and the Brandywine fault system. In our discussion, we consider the Skinkers Neck anticline to consist of a combined anticline and fault zone, following previous authors.

Mixon and Newell (Mixon, 1977) first hypothesized that a buried fault zone existed beneath Coastal Plain sediments and connected the Taylorsville basin in the north to the Richmond basin in the south along a fault zone coincident with the Brandywine fault zone of Jacobeen (Jacobeen, 1972). The inferred fault of Mixon and Newell (Mixon, 1977) coincides with a gravity gradient used to target exploration studies that led to the discovery of the Port Royal fault and Skinkers Neck anticline in 1984 (Mixon, 1984) (Mixon, 1992).

The Port Royal fault zone consists of a 32 mi (51 km) long, north to northeast-striking fault zone that delineates a shallow graben structure that trends parallel to a listric normal fault bounding the Taylorsville basin (Mixon, 2000) (Milici, 1991). In map view, the fault zone makes a short left-step to the Brandywine fault system (Figure 2.5-25). Along the northern part of the fault zone, near the town of Port Royal, Virginia, the fault is expressed in the subsurface as a 3 mi (5 km) wide zone of warping with a west-side-up sense of displacement. Water well and seismic reflection data show an apparent west-side-up vertical component for the southwestern part of the structure also (Mixon, 1992) (Mixon, 2000) (Milici, 1991).

The Skinkers Neck anticline is located directly west of the Port Royal fault zone and southwest of the mapped terminus of the Brandywine fault system (Figure 2.5-25). The north- to northeast-striking structure is 30-mi (48 km) long and 3 to 5 mi (5 to 8 km) wide, and is defined as an asymmetric, low-amplitude, north-plunging anticline with a west-bounding fault (Mixon, 2000). Locally, Mixon (Mixon, 2000) map the feature as two separate, closely-spaced anticlines. Along the west side of the structure, a fault zone strikes north-to-northeast and is interpreted as a fault-bounded, down-dropped block. The Skinkers Neck anticline is not mapped north of the Potomac River by Mixon (Mixon, 1992) (Mixon, 2000). However, McCartan (McCartan, 1989a) shows two folds north of the Potomac River, west of the Brandywine fault system, and along trend with the Skinkers Neck anticline as mapped by Mixon (Mixon, 2000).

The Port Royal fault zone and Skinkers Neck anticline likely are associated with Paleozoic structures that were reactivated in the Early Mesozoic, Paleocene, and possibly middle Miocene (Mixon, 1992) (Mixon, 2000) (McCartan, 1989c). Similar to the Brandywine fault system, these structures closely coincide with the Mesozoic Taylorsville basin (Mixon, 1992) (Milici, 1991). This apparent coincidence with a Mesozoic basin suggests that the Port Royal fault zone and the Skinkers Neck anticline represent possible pre-existing zones of crustal weakness. Post-Mesozoic deformation includes as much as 30 to 33 ft (9 to 10 km) of Paleocene offset, and less than 25 ft (7.6 m) of displacement across the basal Eocene Nanjemoy Formation. Deformation on the order of 5 to 10 ft (1.5 to 3 m) is interpreted to extend upward into the Middle Miocene Calvert and Choptank Formations (Mixon, 1992). The overlying Late Miocene Eastover Formation is undeformed across both the Port Royal fault zone and Skinkers Neck anticline, constraining the timing of most recent activity (Mixon, 1992) (Mixon, 2000).

Although the Port Royal fault zone and Skinkers Neck anticline where characterized after the EPRI study (EPRI, 1986), geological information available to the EPRI teams regarding the pre-Quaternary activity of the structures was available (Mixon, 1984). Both of these structures are mapped in the subsurface as offsetting Tertiary or older geologic units (Mixon, 2000). Field and aerial (inspection by plane) reconnaissance, coupled with interpretation of aerial photography (review and inspection of features preserved in aerial photos) and LiDAR data (see Section 2.5.3.1 for additional information regarding the general methodology), conducted during this CCNPP Unit 3 study shows that there are no geomorphic features indicative of potential Quaternary activity along the surface-projection of the fault zone (i.e., along the northern banks of the Potomac River and directly northeast of the fault zone). Also, there is no pre-EPRI or post-EPRI (EPRI, 1986) seismicity spatially associated with the Port Royal fault zone or the Skinkers Neck anticline. In summary, the Port Royal fault zone and Skinkers Neck

anticline are not considered capable tectonic sources, there is no new information developed since 1986 that would require revision to the EPRI seismic source model regarding these features.

*2.5.1.1.4.4.4.4 National Zoo Faults*

The National Zoo faults in Washington D.C. approach to within 47 mi (76 km) of the site (Figure 2.5-25).  The National Zoo faults are primarily low-angle to high-angle, northwest-striking, southwest-dipping thrust faults that occur within a 1.0 to 1.5 mi (1.6 to 2.4 km) long, north to northeast-trending fault zone (Prowell, 1983) (McCartan, 1990) (Fleming, 1994) (Froelich, 1975).  The mapped surface traces of these faults range from 500 to 2000 ft (152 to 610 km) with up to 20 ft (6 m) of post-Cretaceous reverse displacement visible in outcrops at the National Zoo (Fleming, 1994).  The faults were first identified by Darton (Darton, 1950) in exposures along Rock Creek in historic excavations between the National Zoo and Massachusetts Avenue in Washington D.C.

The National Zoo faults were active during the Early Mesozoic with probable reactivation during the Pliocene (Darton, 1950) (McCartan, 1990) (Fleming, 1994).  This fault zone is coincident with the mapped trace of the Early Paleozoic Rock Creek shear zone, which led several researches to infer that the National Zoo faults are related to reversal of a pre-existing zone of crustal weakness (McCartan, 1990) (Fleming, 1994).  Combined with the Rock Creek fault zone, the National Zoo faults could be up to 16 mi (26 km) long.  Differential offset across basement and Potomac Group contacts also suggests Paleozoic fault reactivation (Fleming, 1994).  The Cretaceous Potomac formation offsets are primarily less than 50 ft (15 m) and isopach maps show a thickening of Coastal Plain sediments east of these faults (Fleming, 1994) (Darton, 1950).  The youngest two faults juxtapose basement rocks over Pliocene Upland gravels (Fleming, 1994) (McCartan, 1990).  One exposure of these two faults is still preserved along Adams Mill road as a special monument (Prowell, 1983).  Based on our field reconnaissance with USGS researchers, future additional investigations are planned by the USGS to further investigate the age of the gravels and lateral continuity of the National Zoo faults.

All information on timing of displacement of the National Zoo faults was available and incorporated into the EPRI seismic source models in 1986.  Although later detailed mapping of these thrust faults with the Rock Creek shear zone was published after completion of the EPRI study (EPRI, 1986), Darton (Darton, 1950) and Prowell (Prowell, 1983) identified these faults as active during Cenozoic time.  In addition, there is no pre-EPRI or post-EPRI seismicity spatially associated with this fault zone.  Therefore, the conclusion is that the National Zoo faults are not a capable tectonic source.  There also is no new published geologic information developed since 1986 that would require a significant revision to the EPRI seismic source model.

*2.5.1.1.4.4.4.5 Hillville Fault Zone*

The Hillville fault zone of Hansen (1978) approaches to within 5 mi (8 km) of the site in the subsurface (Figure 2.5-25, Figure 2.5-26, and Figure 2.5-27).  The 26 mi (42 km) long, northeast-striking fault zone is composed of steep southeast-dipping reverse faults that align with the east side of the north-to northeast-trending Sussex-Currioman Bay aeromagnetic anomaly (i.e. SGA, Figure 2.5-22).  Based on seismic reflection data, collected about 9 mi (15 km) west-southwest of the site, the fault zone consists of a narrow zone of discontinuities that vertically separate basement by as much as 250 ft (76 m) (Hansen, 1978).

The Hillville fault zone delineates a possible Paleozoic suture zone reactivated in the Mesozoic and Early Tertiary.  The fault zone is interpreted as a lithotectonic terrane boundary that separates basement rocks associated with Triassic rift basins on the west from low-grade

metamorphic basement on the east (i.e., Sussex Terrane/Taconic suture of Glover and Klitgord, (Glover, 1995a) (Figure 2.5-17) (Hansen, 1986). The apparent juxtaposition of the Hillville fault zone with the Sussex-Currioman Bay aeromagnetic anomaly suggests that the south flank of the Salisbury Embayment may be a zone of crustal instability that was reactivated during the Mesozoic and Tertiary. Cretaceous activity is inferred by Hansen (Hansen, 1978) who extends the fault up into the Cretaceous Potomac Group. The resolution of the geophysical data does not allow an interpretation for the upward projection of the fault into younger overlying Coastal Plain deposits (Hansen, 1978). Hansen (Hansen, 1978), however, used stratigraphic correlations of Coastal Plain deposits from borehole data to speculate that the Hillville fault may have been active during the Early Paleocene.

There is no geologic data to suggest that the Hillville fault is a capable tectonic source. Field and aerial reconnaissance, coupled with interpretation of aerial photography and LiDAR data (see Section 2.5.3.1 for additional information regarding the general methodology), conducted during this COL study shows that there are no geomorphic features indicative of potential Quaternary activity along the surface-projection of the Hillville fault zone. A review of geologic cross sections (McCartan, 1989a) (McCartan, 1989b) (Glaser, 2003b) (Glaser, 2003c) show south-dipping Lower to Middle Miocene Calvert Formation and no faulting along projection with the Hillville fault zone. Furthermore Quaternary terraces mapped by McCartan (McCartan, 1989b) and Glaser (Glaser, 2003b) (Glaser, 2003c) bordering the Patuxent and Potomac Rivers were evaluated for features suggestive of tectonic deformation by interpreting LiDAR data and aerial reconnaissance (Figure 2.5-26 and Figure 2.5-27). No northeast-trending linear features coincident with the zone of faulting were observed where the surface projection of the fault intersects these Quaternary surfaces. Aerial reconnaissance of this fault zone also demonstrated the absence of linear features coincident or aligned with the fault zone. Lastly, interpretation of the detailed stratigraphic profiles collected along Calvert Cliffs and the western side of Chesapeake Bay provide geologic evidence for no expression of the fault where the projected fault would intersect the Miocene-aged deposits (Kidwell, 1997; see Section 2.5.3 for further explanation). Therefore, we conclude that the Hillville fault zone is not a capable tectonic source, and there is no new information developed since 1986 that would require a significant revision to the EPRI model.

### 2.5.1.1.4.4.4.6 Unnamed Fault beneath Northern Chesapeake Bay, Cecil County, Maryland

Pazzaglia (1993) proposed a fault in northern Chesapeake Bay that comes to within 70 mi (113 km) north of the site (Figure 2.5-25). On the basis of geologic data and assuming that the bay is structurally controlled, Pazzaglia (1993) infers a 14 mi (23 km) long, northeast-striking fault with a southwest-side up sense of displacement. Near the mouth of the Susquehanna River, in Maryland, the unnamed fault is interpreted to vertically separate Pleistocene Turkey Point gravels of the Quaternary Pennsauken Formation on the east at elevations higher than a similar gravel deposit mapped on the west side of the Chesapeake Bay. The amount of apparent vertical separation is unconstrained because the base of the gravel unit is not exposed west of the bay; however, estimates of the exposed section provide a minimum of 26 ft (8 m) of vertical separation of the Pleistocene Turkey Point gravels (Pazzaglia, 1993).

This fault is unconfirmed based on the lack of direct supporting evidence. First, the fault has not been observed as a local discontinuity on land. Second, the correlation of gravels is permissible based on the data, but has not been confirmed by detailed stratigraphic or chronologic studies. Geologic mapping of the area (Higgins, 1986) shows Miocene Upland gravels along the northeast mouth of the Susquehanna River where Pazzaglia (Pazzaglia, 1993) maps the Quaternary Pennsauken Formation.

There is no geologic data to suggest that this unnamed fault zone is a capable tectonic source. There is no pre-EPRI or post-EPRI seismicity spatially associated with this fault zone. Field and aerial reconnaissance conducted to support CCNPP Unit 3 shows that there are no geomorphic features indicative of potential Quaternary activity along the surface-projection of the unnamed fault; therefore, this fault is not a capable tectonic source.

*2.5.1.1.4.4.4.7 Unnamed Monocline beneath Chesapeake Bay*

McCartan (McCartan, 1995) show east-facing monoclinal structures bounding the western margin of Chesapeake Bay 1.8 and 10 mi (2.9 and 16 km) east and southeast, respectively, of the site (Figure 2.5-25). Also, McCartan (McCartan, 1995) interprets an east-facing monocline about 10 mi (16 km) west of the site. The three monoclinal structures are depicted on two cross sections as warping Lower Paleocene to Upper Miocene strata with approximately 60 to 300 ft (18 to 91 m) of relief. The monoclines exhibit a west-side up sense of structural relief that projects upward into the Miocene Choptank Formation (McCartan, 1995). The overlying Late Miocene St. Marys Formation is not shown as warped. Boreholes shown with the cross sections accompanying the McCartan (MaCartan, 1995) map provide the only direct control on cross section construction. The boreholes are widely spaced and do not appear to provide a constraint on the existence and location of the warps. No borehole data is available directly west of the cliffs and within the bay to substantiate the presence of the warp. No surface trace or surface projection of the warps is indicated on the accompanying geologic map. Based on text accompanying the map and cross sections, we infer that the cross sections imply two approximately north- to northeast-striking, west-side up structures, of presumed tectonic origin.

McCartan (McCartan, 1995) interpret the existence of the monocline based on three observations in the local landscape. Firstly, the north to northeast-trending western shore of Chesapeake Bay within Calvert County is somewhat linear and is suggestive of structural control (McCartan, 1995). Secondly, land elevation differences west and east of Chesapeake Bay are on the order of 90 ft (27 m), with the west side being significantly higher in elevation, more fluvially dissected, and composed of older material compared to the east side of Chesapeake Bay. On the west side of the bay, the landscape has surface elevations of 100 to 130 ft (30 to 40 m) msl and drainages are incised into the Pliocene Upland Deposits and Miocene-aged deposits of the St. Mary's, Choptank, and Calvert Formations. Along the eastern shoreline of the Delmarva Peninsula, surface elevations are less than 20 to 30 ft (6 to 9 m) msl and the surface exhibits minor incision and a more flat-lying topographic surface. These eastern shore deposits are mapped as Quaternary estuarine and deltaic deposits. Thirdly, variations in unit thickness within Tertiary deposits between Calvert Cliffs and Delmarva Peninsula are used to infer the presence of a warp. Based on these physiographic, geomorphic and geologic observations, McCartan (McCartan, 1995) infer the presence of a fold along the western shore of Chesapeake Bay (Figure 2.5-25).

Based on the paucity of geologic data constraining the cross sections of McCartan (McCartan, 1995), the existence of the monocline is speculative. The borehole data that constrain the location of the monocline are approximately 18 to 21 mi (29 to 34 km) apart and permit, but do not require the existence of a monocline. McCartan (McCartan, 1995) do not present additional data that are inconsistent with the interpretation of flat-lying, gently east-dipping Miocene strata shown in prior published cross sections north and south of this portion of Chesapeake Bay (Cleaves et al., 1968; Milici, et al., 1995) and within Charles and St. Mary's Counties, Maryland (McCartan, 1989a) (McCartan, 1989b) (DM, 1973). No geophysical data are presented as supporting evidence for this feature. In contrast, shallow, high-resolution geophysical data collected along the length of Chesapeake Bay to evaluate the ancient courses of the submerged and buried Susquehanna River provide limited evidence strongly indicating that

Tertiary strata are flat lying and undeformed along the western shore of Chesapeake Bay (Colman, 1990) (Figure 2.5-29).

Alternatively, the change in physiographic elevation and geomorphic surfaces between the western and eastern shores of Chesapeake Bay can be explained by erosional processes directly related to the former course of the Susquehanna River, coupled with eustatic sea level fluctuations during the Quaternary (Colman, 1990) (Owens, 1979). Colman and Halka (Colman, 1989) also provide a submarine geologic map of Chesapeake Bay at and near the site which depicts Tertiary and Pleistocene deposits interpreted from high-resolution geophysical profiles. No folding or warping or faulting is depicted on the Colman and Halka (Colman, 1989) map which encompasses the warp of McCartan (McCartan, 1995). Colman (Colman, 1990) utilize the same geophysical data to track the former courses of the Susquehanna River between northern Chesapeake Bay and the southern Delmarva Peninsula. Paleo-river profiles developed from the geophysical surveys that imaged the depth and width of the paleochannels show that the Eastville (150 ka) and Exmore (200 to 400 ka) paleochannels show no distinct elevation changes within the region of the Hillville fault and McCartan (McCartan, 1995) features.

Field reconnaissance along much of the western shoreline shows that the north- to northeast-trending linear coastline could be controlled locally, in part, by a weak, poorly-developed, sub-vertical joint set oriented subparallel to the coast (Section 2.5.1.2.4). The observation that the west side of Chesapeake Bay is elevated and dissected, and that approximately 37 ka estuarine deposits are approximately 6 feet above sea level is compelling evidence for recent (late Quaternary) uplift. Similar elevated, dissected topography and approximately 37 ka estuarine deposits are observed over broad portions of the Coastal Plain along the eastern seaboard east and west of Chesapeake Bay. These surfaces of apparent anomalous elevations have recently been attributed to the presence of a glacial fore-bulge developed outboard of the Laurentide ice sheet (Scott, 2006).

There is no geologic data to suggest that the postulated monocline along the western margin of Chesapeake Bay of McCartan (McCartan, 1995), if present, is a capable tectonic source. Field and aerial reconnaissance, coupled with interpretation of aerial photography and LiDAR data (see Section 2.5.3.1 for additional information regarding the general methodology), conducted during this COL study, shows that there are no geomorphic features indicative of folding directly along the western shores of Chesapeake Bay. There is no pre-EPRI or post-EPRI seismicity spatially associated with this structure. These data indicate that the McCartan (McCartan, 1995) warps, if present, most likely do not deform Pliocene to Quaternary deposits, and thus are not capable tectonic sources that would require a revision to the EPRI (1986) seismic source model.

*2.5.1.1.4.4.4.8 Unnamed Folds and Postulated Fault within Calvert Cliffs, Western Chesapeake Bay, Calvert County, Maryland*

The Calvert Cliffs along the west side of Chesapeake Bay provide a 25 mile (40 km) long nearly continuous exposure of Miocene, Pliocene and Quaternary deposits (Figure 2.5-26). Kidwell (1988 and 1997) prepared over 300 comprehensive lithostratigraphic columns along a 25 mi (40 km) long stretch of Calvert Cliffs (Figure 2.5-30). Because of the orientation of the western shore of Chesapeake Bay, the cliffs intersect any previously potential structures (i.e., Hillville fault) trending northeast or subparallel to the overall structural trend of the Appalachians. The cliff exposures provide a 230 ft (70 m) thick section of Cenozoic deposits that span at least 10 million years of geologic time.

On the basis of the stratigraphic profiles, Kidwell (Kidwell, 1997) develops a chronostratigraphic sequence of the exposed Coastal Plain deposits and provides information on regional dip and

lateral continuity.  The Miocene Choptank Formation is subdivided into two units and is unconformably overlain by the St .Marys Formation.  The St. Marys Formation is subdivided into three subunits each of which is bound by a disconformity.  The youngest subunit is unconformably overlain by the Pliocene Brandywine Formation (i.e., Pliocene Upland gravels). The exposed Coastal Plain deposits strike northeast and dip south-southeast between 1 and 2 degrees.  The southerly dip of the strata is disrupted occasionally by several low amplitude broad undulations in the Choptank Formation, and decrease in amplitude upward into the St Marys Formation (Figure 2.5-30).  Kidwell (Kidwell, 1997) interprets the undulations as monoclines and asymmetrical anticlines.  The undulations typically represent erosional contacts that have wavelengths on the order of 2.5 to 5 mi (4 to 8 km) and amplitudes of 10 to 11 ft (about 3 m). Any inferred folding of the overlying Pliocene and Quaternary fluvial strata is very poorly constrained or obscured because of highly undulatory unconformities within these younger sand and gravel deposits.  For instance, the inferred folding of the overlying Pliocene and Quaternary channelized sedimentary deposits consist of intertidal sand and mud-flats, tidal channels and tidally-influenced rivers exhibit as much as 40 ft (12 m) of erosional elevation change (Figure 2.5-30).

Near Moran Landing, about 1.2 mi (1.9 km) south of the site, Kidwell (Kidwell, 1997) interprets an apparent 6 to 10 ft (2 to 3 m) elevation change in Miocene strata, and a 3 to 12 ft (1 to 3.6 m) elevation change in Pliocene and Quaternary(?) fluvial material (Figure 2.5-26 and Figure 2.5-30).  Kidwell (1997) infers the presence of a fault to explain the difference in elevation of strata across Moran Landing.  The postulated fault is not shown on the Kidwell (Kidwell, 1997) section, or any published geologic map; however, the inferred location is approximately 1.2 mi (1.9 km) south of the CCNPP site.  The hypothesized fault is not exposed in the cliff face and is based entirely on a change in elevation and bedding dip of Miocene stratigraphic boundaries projected across the fluvial valley of Moran Landing.  Kidwell (Kidwell, 1997) postulates that the fault strikes northeast and exhibits a north-side down sense of separation across all the geologic units (Miocene through Quaternary).  With regard to the apparent elevation changes for the Pliocene and Quaternary unconformities, these can be readily explained by channeling and highly irregular erosional surfaces (Figure 2.5-30).

LiDAR data was reviewed for the possible presence of northeast-striking lineaments in the region of Moran Landing and to the southeast along the Patuxent River. Field and aerial reconnaissance, coupled with interpretation of aerial photography and LiDAR data (see Section 2.5.3.1 for additional information regarding the general methodology), conducted during the CCNPP Unit 3 investigation shows that there are no geomorphic features indicative of potential Quaternary activity developed in the Pliocene-Quaternary surfaces along a southeast projection from Chesapeake Bay across the Patuxent and Potomac Rivers (Figure 2.5-26).  The features also do not coincide with magnetic and gravity anomalies, and thus are not rooted, and more likely are surficial in origin.  There is no pre-EPRI or post-EPRI (1986) seismicity spatially associated with the Kidwell (Kidwell, 1997) features, nor are there direct geologic data to indicate that the features proposed by Kidwell (Kidwell, 1997) are capable tectonic sources (Section 2.5.3.2.3)

### 2.5.1.1.4.4.5 Quaternary Tectonic Features

In an effort to provide a comprehensive database of Quaternary tectonic features, Crone and Wheeler (Crone, 2000), Wheeler (Wheeler, 2005), and Wheeler (Wheeler, 2006) compiled geological information on Quaternary faults, liquefaction features, and possible tectonic features in the CEUS.  Crone and Wheeler (Crone, 2000) and Wheeler (Wheeler, 2005) evaluated and classified these features into one of four categories (Classes A, B, C, and D; see Table 2.5-1 for definitions (Crone, 2000) (Wheeler, 2005)) based on strength of evidence for Quaternary activity.

Within a 200 mi (322 km) radius of the CCNPP site, Crone and Wheeler (Crone, 2000), Wheeler (Wheeler, 2005) and Wheeler (Wheeler, 2006) identified 17 potential Quaternary features (Figure 2.5-31).  Work performed as part of the CCNPP Unit 3 investigation, including literature review, interviews with experts, and geologic reconnaissance, did not identify any additional potential Quaternary tectonic features within the CCNPP site region, other than those previously mentioned (McCartan, 1995) (Kidwell, 1997).  Within approximately 200 mi (322 km) of the site, Crone and Wheeler (Crone, 2000) found only one feature described in the literature that exhibited potential evidence for Quaternary activity (Figure 2.5-31).  This feature (shown as number 12) is the paleo-liquefaction features within the Central Virginia seismic zone.

The following sections provide descriptions of 15 of the 17 potential Quaternary features identified by Crone and Wheeler (Crone, 2000), Wheeler (Wheeler, 2005) (Wheeler, 2006), and of the postulated East Coast fault system of Marple and Talwani (Marple, 2004).  Note that the Central Virgina and Lancaster seismic zones are discussed in Section 2.5.1.1.4.5 and Section 2.5.2.  Out of the 17 features evaluated for this CCNPP Unit 3 study, nearly all are classified as Class C features, with the exception of the Central Virginia seismic zone (Class A).

The features are labeled with the reference numbers utilized in Figure 2.5-31:

1.   Fall lines of Weems (1998) (Class C)

2.   Ramapo fault system (Class C)

3.   Kingston fault (Class C)

4.   New York Bight fault (offshore) (Class C)

5.   Cacoosing Valley earthquake (Class C)

6.   Lancaster seismic zone (Class C)

7.   New Castle County faults (Class C)

8.   Upper Marlboro faults (Class C)

9.   Everona-Mountain Run fault zone (Class C)

10.  Stafford fault of Mixon et al. (Class C)

11.  Lebanon Church fault (Class C)

12.  Central Virginia seismic zone (Class A)

13.  Hopewell fault (Class C)

14.  Old Hickory faults (Class C)

15.  Stanleytown-Villa Heights faults (Class C)

16.  (The Stafford fault system of Marple is included in (17), i.e. the East Coast fault system)

17.  East Coast fault system (Class C)

The Everona-Mountain Run fault zone and Stafford fault of Mixon (Mixon, 2000) also are discussed in detail in previous Section 2.5.1.1.4.4.2 and Section 2.5.1.1.4.4.4.1.

### 2.5.1.1.4.4.5.1 Fall Lines of Weems (1998)

In 1998, Weems defined seven fall lines across the Piedmont and Blue Ridge Provinces of North Carolina and Virginia (Figure 2.5-31). The eastern fall line is located approximately 47 mi (76 km) west of the CCNPP site. The fall lines, not to be confused with the Fall Line separating the Piedmont and Coastal Plain provinces, are based on the alignment of short stream segments with anomalously steep gradients. Weems (1998) explores possible ages and origins (rock hardness, climatic, and tectonic) of the fall lines and "based on limited available evidence favors a neo-tectonic origin" for these geomorphic features during the Quaternary. Weems (1998) interprets longitudinal profiles for major drainages flowing primarily southeast and northwest across the Piedmont and Blue Ridge Provinces to assess the presence and origin of the "fall zones".

A critical evaluation of Weems' (1998) study, as part of the North Anna ESP, demonstrates that there are inconsistencies and ambiguities in Weems' (1998) correlations and alignment of steep reaches of streams used to define continuous fall lines (Dominion, 2004b). The North Anna ESP study concludes that that the individual fall zones of Weems (1998) may not be as laterally continuous as previously interpreted. For instance, stratigraphic, structural and geomorphic relations across and adjacent to the Weems (1998) fall zones can be readily explained by differential erosion due to variable bedrock hardness rather than Quaternary tectonism (Dominion, 2004b). Furthermore, there is no geomorphic expression of recent tectonism, such as the presence of escarpments, along the trend of the fall lines between drainages where one would expect to find better preservation of tectonic geomorphic features. Similarly, Wheeler (2005) notes that the Weems (1998) fall zones are not reproducible and are subjective, thus tectonic faulting is not yet demonstrated as an origin, and the fall lines are designated as a Class C feature. In the Safety Evaluation Report for the North Anna ESP site study, the NRC staff agrees with the assessment that the fall lines of Weems (1998) are nontectonic features (NRC, 2005). In summary, based on review of published literature, field reconnaissance, and geologic and geomorphic analysis performed previously for the North Anna ESP application, the fall lines of Weems (1998) are erosional features related to contrasting erosional resistances of adjacent rock types, and are not tectonic in origin, and thus are not capable tectonic sources.

### 2.5.1.1.4.4.5.2 Everona-Mountain Run Fault Zone

The Mountain Run fault zone is located along the eastern margin of the Culpeper Basin and lies approximately 71 mi (114 km) southwest of the site (Figure 2.5-17 and Figure 2.5-31). The 75 mi (121 m) long, northeast-striking fault zone is mapped from the eastern margin of the Triassic Culpeper Basin near the Rappahannock River southwestward to near Charlottesville, in the western Piedmont of Virginia (Pavlides, 1986). The fault zone consists of a broad zone of sheared rocks, mylonites, breccias, and phyllites of variable width.

The Mountain Run fault zone is interpreted to have formed initially as a thrust fault upon which back-arc basin rocks (mélange deposits) of the Mine Run Complex were accreted onto ancestral North America at the end of the Ordovician (Pavlides, 1989). This major suture separates the Blue Ridge and Piedmont terranes (Pavlides, 1983) (Figure 2.5-17). Subsequent reactivation of the fault during the Paleozoic and/or Mesozoic produced strike-slip and dip-slip movements. Horizontal slickensides found in borehole samples and at several places near the base of the Mountain Run scarp suggest strike-slip movement, whereas small-scale folds in the uplands near the scarp suggest an oblique dextral sense of slip (Pavlides, 2000). The timing of the reverse and strike-slip histories of the fault zone, and associated mylonitization and brecciation,

is constrained to be pre-Early Jurassic, based on the presence of undeformed Early Jurassic diabase dikes that cut rocks of the Mountain Run fault zone (Pavlides, 2000).

The northeast-striking Mountain Run fault zone is moderately to well-expressed geomorphically (Pavlides, 2000). Two northwest-facing scarps occur along the fault zone, including: (1) the 1 mi (1.6 km) long Kelly's Ford scarp located directly northeast of the Rappahannock River and; (2) the 7 mi (11 km) long Mountain Run scarp located along the southeast margin of the linear Mountain Run drainage. Conspicuous bedrock scarps in the Piedmont, an area characterized by deep weathering and subdued topography, has led some experts to suggest that the fault has experienced a Late Cenozoic phase of movement (Pavlides, 2000) (Pavlides, 1983).

Near Everona, Virginia, a small reverse fault, found in an excavation, vertically displaces "probable Late Tertiary" gravels by 5 ft (1.5 m) (Pavlides, 1983). The fault strikes northeast, dips 20 degrees northwest, and based on kinematic indicators is an oblique strike-slip fault. More recently others have estimated that the offset colluvial gravels are Pleistocene age (Manspeizer et. al, 1989). The Everona fault is located about 0.5 mi (0.8 km) west of the Mountain Run fault zone. Due to the close proximity of these two faults and their shared similar orientation and sense of slip, the Everona and Mountain Run faults are considered to be part of the same fault zone, hence the Everona-Mountain Run fault zone (Crone, 2000). Crone and Wheeler (Crone, 2000) assessed that the faulting at Everona is likely to be of Quaternary age, but because the likelihood has not been tested by detailed paleo-seismological or other investigations, this feature was assigned to Class C.

Field and aerial reconnaissance, and geomorphic analysis of deposits and features associated with the fault zone, recently performed for the North Anna ESP provide new information on the absence of Quaternary faulting along the Everona-Mountain Run fault zone (Dominion, 2004a). In response to NRC comments for the North Anna ESP, geologic cross sections and topographic profiles were prepared along the Mountain Run fault zone to further evaluate the inferred tectonic geomorphology coincident with the fault zone. The results of the additional analysis were presented in the response to an NRC Request for Additional Information (RAI) (Dominion, 2004a) and are summarized below:

♦   There is no consistent expression of a scarp along the Mountain Run fault in the vicinity of the Rappahannock River. The northwest-facing Kelly's Ford scarp is similar to a northwest-facing scarp along the southeastern valley margin of Mountain Run; both scarps were formed by streams that preferentially undercut the southeastern valley walls, creating asymmetric valley profiles.

♦   There is no northwest-facing scarp associated with the Mountain Run fault zone between the Rappahannock and Rapidan Rivers. Undeformed late Neogene colluvial deposits bury the Mountain Run fault zone in this region, demonstrating the absence of Quaternary fault activity.

♦   The northwest-facing "Mountain Run" scarp southwest of the Rappahannock River alternates with a southeast-facing scarp on the opposite side of Mountain Run valley; both sets of scarps have formed by the stream impinging on the edge of the valley.

All of the information on timing of displacement of the Mountain Run fault zone and associated faults was available and incorporated into the EPRI seismic source models in 1986. Significant new information developed since 1986 includes the work performed for the North Ana ESP that shows the Mountain Run fault zone has not been active during the Quaternary. In addition, the

NRC staff agrees that the scarps along the Mountain Run Fault zone were not produced by Cenozoic fault activity (NRC, 2005). Similarly, Crone and Wheeler (Crone, 2000) do not show the Mountain Run fault zone as a known Quaternary structure in their compilation of active tectonic features in the CEUS, having assigned it to Class C. Based on the findings of the previous studies performed for the North Anna ESP and approval by the Nuclear Regulatory Commission (NRC, 2005), it is concluded that the Everona-Mountain Run fault zone is not a capable tectonic source. No new information has been developed since 1986 that would require a significant revision to the EPRI seismic source model.

### 2.5.1.1.4.4.5.3 Stafford Fault of Mixon, et al.

The Stafford fault (#10 on Figure 2.5-31) approaches within 47 mi southwest of the site (Figure 2.5-25). The Stafford fault (Mixon, 2000) is discussed in more detail in Section 2.5.1.1.4.4.4.1 (Stafford Fault System). The northern extension of the Stafford fault system as proposed by Marple (#16 on Figure 2.5-31) is discussed in Section 2.5.1.1.4.4.5.15. The 42 mile (68 km) long fault system strikes approximately N35°E and was identified and described first by Newell (Newell, 1976). The fault system consists of a series of five northeast-striking, northwest-dipping, high-angle reverse faults including, from north to south, the Dumfries, Fall Hill, Hazel Run, and Brooke faults, and an unnamed fault. The Brooke fault also includes the Tank Creek fault located northeast of the Brooke fault (Mixon, 2000).

No new significant information has been developed since 1986 regarding the activity of the Stafford fault system with the exception of the response to an NRC RAI for the North Anna ESP (Dominion, 2004a). Field reconnaissance performed for the CCNPP Unit 3 study also did not reveal any geologic or geomorphic features indicative of potential Quaternary activity along the fault system. In addition, near the site and along the portion of the Stafford fault mapped by Mixon et al. (2000) no seismicity is attributed to the Stafford fault. Similarly, Wheeler (Wheeler, 2005) does not show the Stafford fault system as a Quaternary structure in his compilation of active tectonic features in the CEUS. The NRC (NRC, 2005) agreed with the findings of the subsequent study for the North Anna ESP, and stated: "Based on the evidence cited by the applicant, in particular the applicant's examination of the topography profiles that cross the fault system, the staff concludes that the applicant accurately characterized the Stafford fault system as being inactive during the Quaternary Period." Based on a review of existing information for the Stafford fault system, including the response to the NRC RAI for the North Anna ESP, the Stafford fault system is not a capable tectonic source and there is no new information developed since 1986 that would require a significant revision to the EPRI seismic source model.

### 2.5.1.1.4.4.5.4 Ramapo Fault System

The Ramapo fault system is located in northern New Jersey and southern New York State, approximately 130 mi (209 km) north-northeast of the CCNPP site (Figure 2.5-31). This fault system consists of northeast-striking, southeast-dipping, normal faults that bound the northwest side of the Mesozoic Newark basin that to the northeast become a single 40 mi (64 km) long northeast-striking fault (Ratcliffe, 1971) (Schlische, 1992) (Drake, 1996) (Figure 2.5-10). Bedrock mapping by Drake (Drake, 1996) shows primarily northwest-dipping Lower Jurassic and Upper Triassic Newark Supergroup rocks in the hanging wall and tightly folded and faulted Paleozoic basement rocks in the footwall of the fault. The Ramapo fault splays into several fault strands southwest of Bernardsville and merges with the Flemington Fault zone. This fault zone also splays into several northeast- to east-trending faults in Rockland and Westchester Counties, New York.

The Ramapo fault system has been considered a potentially active tectonic feature because the fault: (1) exhibits repeated reactivation during the Paleozoic, (2) bounds the Mesozoic Newark

basin (i.e. the region is composed of extended crust), and (3) aligns with earthquake epicenters (Wheeler, 2006) (Aggarwal, 1978).  In cross section and map view, the seismicity data and focal mechanisms illustrate a 60° to 65° southeast-dipping fault zone that projects upward to the mapped trace of the Ramapo fault.  In addition, 14 focal mechanism solutions have orientations that are consistent with the present-day stress field and suggest reverse reactivation of the Ramapo fault.  Collectively, these data led Aggarwal and Sykes (Aggarwal, 1978) to conclude that the Ramapo fault is likely active.

Many of the assumptions and conclusions made by Aggarwal and Sykes (Aggarwal, 1978) were later reevaluated with alternative interpretations suggesting the fault probably has not been active during the Quaternary.  Subsequent fault activity studies included several types of geophysical and geologic techniques.  First, a modified velocity model and a carefully re-evaluated earthquake catalog refined the location of the earthquakes previously inferred as aligned with the Ramapo fault, and demonstrated that approximately half of the reported earthquakes occur near the margins of the Newark Basin, far from the Ramapo fault, but still within the Ramapo fault system proper (Kafka, 1985) (Thurber, 1985) (Wheeler, 2006).  In addition, a reassessment of the eastern U.S. stress field demonstrated that the present-day stress field is oriented east-southeast (Zoback, 1989a), which would be inconsistent with the previously inferred reverse reactivation of the fault.  Kinematic analysis of fault zone samples collected from deep exploratory boreholes provides evidence that the latest style of deformation probably included extensional faulting during the Mesozoic (Ratcliffe, 1980) (Ratcliffe, 1982) (Burton, 1985) (Ratcliffe, 1990).  The borehole data also confirm that the dip of the Ramapo fault is 10° to 15° shallower than inferred by Aggarwal and Sykes (Aggarwal, 1978).

In summary, several papers infer that evidence for Quaternary deformation exists near the Ramapo fault zone (Nelson, 1980) (Newman, 1983) (Newman, 1987) (Kafka, 1989); however, Crone and Wheeler (Crone, 2000) and Wheeler (Wheeler, 2006) argue convincingly that none of the data used to infer seismic slip can be used to differentiate seismic from asesimic slip. Additionally, trenches excavated across the up-dip projection of the fault zone revealed no evidence for Quaternary faulting (Stone, 1984) (Ratcliffe, 1990).  Besides the presence of microseismicity within the vicinity of the Ramapo fault zone, there is no clear evidence of Quaternary tectonic faulting (Crone, 2000) (Wheeler, 2006), thus the Ramapo fault system is assigned a Class C designation by Crone and Wheeler (Crone, 2000).  The Ramapo fault zone was a known structure for the EPRI study (EPRI, 1986).  Based on the review of post-EPRI literature and seismicity, there is no new information developed since 1986 that would require a significant change to the EPRI seismic source model.

### 2.5.1.1.4.4.5.5 Kingston Fault

The Kingston fault is located in central New Jersey, approximately 175 mi (282 km) northeast of the CCNPP site (Figure 2.5-31).  The Kingston fault is a 7 mi (11 km) long north to northeast-striking fault that offsets Mesozoic basement and is overlain by Coastal Plain sediments (Owens, 1998).  Stanford (Stanford, 1995) use borehole and geophysical data to interpret a thickening of as much as 80 ft (24 m) of Pliocene Pennauken Formation across the surface projection of the Kingston fault.  Stanford (Stanford, 1995) interprets the thickening of the Pennauken Formation gravel as a result of faulting rather than fluvial processes.  Geologic cross sections prepared by Stanford (Stanford, 2002) do not show that the bedrock-Pennauken contact is vertically offset across the Kingston fault.  Therefore, it seems reasonable to conclude that faulting of the Pennauken Formation is not required and that apparent thickening of the Pliocene gravels may represent a channel-fill from an ancient pre-Pliocene channel. Furthermore, Pleistocene glaciofluvial gravels that overlie the fault trace are not offset, thus indicating the fault is not a capable tectonic source (Stanford, 1995).  Wheeler (Wheeler, 2006) reports that the available geologic evidence does not exclusively support a fault versus a fluvial

origin for the apparent thickening of the Pennauken Formation. Wheeler (Wheeler, 2005) assigns the Kingston fault as a Class C feature based on a lack of evidence for Quaternary deformation. Given the absence of evidence for Quaternary faulting and the presence of undeformed Pleistocene glaciofluvial gravels overlying the fault trace, we conclude that the fault is not a capable tectonic feature.

### 2.5.1.1.4.4.5.6 New York Bight Fault

On the basis of seismic surveys, the New York Bight fault is characterized as an approximately 31 mile (50 km) long, north-northeast-striking fault, located offshore of Long Island, New York (Schwab, 1997a) (Schwab, 1997b) (Figure 2.5-31). The fault is located about 208 mi (335 km) northeast of the CCNPP site. Seismic reflection profiles indicate that the fault originated during the Cretaceous and continued intermittently with activity until at least the Eocene. The sense of displacement is northwest-side down and displaces bedrock as much as 280 ft (85 m), and Upper Cretaceous deposits about 150 ft (46 m) (PSEG, 2002). High-resolution seismic reflection profiles that intersect the surface projection of the fault indicate that middle and late Quaternary sediments are undeformed within a resolution of 3 ft (1 m) (Schwab, 1997a) (Schwab, 1997b). Only a few, poorly located earthquakes are spatially assoiciated within the vicinity of the New York Bight fault (Wheeler, 2006). Wheeler (Wheeler, 2006) defines the fault as a feature having insufficient evidence to demonstrate that faulting is Quaternary and assigns the New York Bight fault as a Class C feature. Based on the seismic reflection surveys of Schwab (Schwab, 1997a) (Schwab, 1997b) and the absence of Quaternary deformation, we conclude that the New York Bight fault is not a capable tectonic source.

### 2.5.1.1.4.4.5.7 Cacoosing Valley Earthquake Sequence

The 1993 to 1997 Cacoosing Valley earthquake sequence occurred along the eastern margin of the Lancaster seismic zone with the main shock occurring on January 16, 1994, near Reading, Pennsylvania, about 135 mi (217 km) north of the CCNPP site (Seeber, 1998) (Figure 2.5-31). This earthquake sequence also is discussed as part of the Lancaster seismic zone discussion (Section 2.5.1.1.4.5.2). The maximum magnitude earthquake associated with this sequence is an event of mbLg 4.6 (Seeber, 1998). Focal mechanisms associated with the main shock and aftershocks define a shallow subsurface rupture plane confined to the upper 1.5 mi (2.4 km) of the crust. It appears that the earthquakes occurred on a pre-existing structure striking N45°W in contrast to the typical north-trending alignment of microseismicity that delineates the Lancaster seismic zone. Seeber (Seeber, 1998) use the seismicity data, as well as the shallow depth of focal mechanisms, to demonstrate that the Cacoosing Valley earthquakes likely were caused by anthropogenic changes to a large rock quarry. Wheeler (Wheeler, 2006) defines the fault as a feature having insufficient evidence to demonstrate that faulting is Quaternary and assigns the Cacoosing Valley earthquake sequence as a Class C feature. Based on the findings of Seeber (Seeber, 1998), we interpret this earthquake sequence to be unrelated to a capable tectonic source.

### 2.5.1.1.4.4.5.8 New Castle County Faults

The New Castle faults are characterized as 3 to 4 mi (4.8 to 6.4 km) long buried north and northeast-striking faults that displace an unconformable contact between Precambrian to Paleozoic bedrock and overlying Cretaceous deposits. The faults are located in northern Delaware, near New Castle, about 97 mi (156 km) northeast of the CCNPP site (Figure 2.5-31). Spoljaric (Spoljaric, 1972) (Spoljaric, 1973) interprets the presence of the New Castle County faults using structural contours for the top of basement. On the basis of geophysical and borehole data, coupled with Vibroseis™ profiles, Spolijaric (Spolijaric, 1973) (Spolojaric, 1974) interprets a 1 mi (1.6 km) wide, N25°E-trending graben in basement rock. The graben is bounded by faults having displacements on the order of 32 to 98 ft (10 to 30 m) across the basement-Cretaceous boundary (Spoljaric, 1972). Also, there is a suggestion that the overlying

Cretaceous deposits are tilted in a direction consistent with fault deformation; however, there is no direct evidence to indicate that these sediments are displaced.  Sbar (Sbar, 1975) evaluates a 1973 M3.8 earthquake and its associated aftershocks, and note that the microseismicity defines a causal fault striking northeast and parallel to the northeast-striking graben of Spoljaric (Spoljaric, 1973).  Subsequently, subsurface exploration by the Delaware Geological Survey (McLaughlin, 2002), that included acquisition of high resolution seismic reflection profiles, borehole transects, and paleoseismic trenching, provides evidence for the absence of Quaternary faulting on the New Castle faults.  Wheeler (Wheeler, 2005) characterizes the New Castle County faults as a Class C feature.  Based on McLaughlin (McLaughlin, 2002) there is strong evidence to suggest that the New Castle County faults as mapped by Spolijaric (Spolijaric, 1972) are not a capable tectonic source.

### 2.5.1.1.4.4.5.9 Upper Marlboro Faults

The Upper Marlboro faults are located in Prince George's County, Maryland, approximately 36 mi (58 km) northwest of the CCNPP site (Figure 2.5-31).  These faults were first shown by Dryden (Dryden, 1932) as a series of faults offsetting Coastal Plain sediments.  The faults were apparently exposed in a road cut on Crain Highway at 3.3 mi (5.3 km) south of the railroad crossing in Upper Marlboro, Maryland (Prowell, 1983).  Two faults displace Miocene and Eocene sediments and a third fault is shown offsetting a Pleistocene unit.  These faults are not observed beyond this exposure.  No geomorphic expression has been reported or was noticed during field reconnaissance for the CCNPP Unit 3 study.  Based on a critical review of available literature, Wheeler (Wheeler, 2006) re-interprets the Upper Marlboro faults as likely related to surficial landsliding because of the very low dips and concavity of the fault planes.  The Marlboro faults are classified by Crone and Wheeler (Crone, 2000) and Wheeler (Wheeler, 2006), as a Class C feature based on a lack of evidence for Quaternary faulting.  Given the absence of seismicity along the fault, lack of published literature documenting Quaternary faulting, coupled with the interpretation of Crone and Wheeler (Crone, 2000) and Wheeler (Wheeler, 2006), we conclude that the Upper Marlboro faults are not a capable tectonic source.

### 2.5.1.1.4.4.5.10 Lebanon Church Fault

The Lebanon Church fault is a poorly-known northeast-striking reverse fault located in the Appalachian Mountains of Virginia, near Waynesboro, about 119 mi (192 km) southwest of the CCNPP site (Prowell, 1983) (Figure 2.5-31).  The fault is exposed in a single road cut along U.S. Route 250 as a small reverse fault that offsets Miocene-Pliocene terrace gravels up to as about 5 ft (1.5 m) (Prowell, 1983).  The terrace gravels overlie Precambrian metamorphic rocks of the Blue Ridge Province.  An early author (Nelson, 1962) considered the gravels to be Pleistocene, whereas Prowell (1983) interprets the gravel to be Miocene to Pliocene.  Wheeler (Wheeler, 2006) classifies the Lebanon Church fault as a Class C feature having insufficient evidence to demonstrate that faulting is Quaternary.  As part of this CCNPP Unit 3 study, inquiries with representatives with the Virginia Geological Survey and United States Geological Survey indicate that there is no new additional geologic information on this fault.  Based on literature review, discussion with representatives with Virginia Geological Survey, as well as the absence of seismicity spatially associated with the feature, we conclude that the Lebanon Church fault is not a capable tectonic source.

### 2.5.1.1.4.4.5.11 Hopewell Fault

The Hopewell fault is located in central Virginia, approximately 89 mi (143 km) southwest of the CCNPP site (Figure 2.5-31).  The Hopewell fault is a 30 mi (48 km) long, north-striking, steeply east-dipping reverse fault (Mixon, 1989) (Dischinger, 1987).  The fault was originally named the Dutch Gap fault by Dischinger (Dischinger, 1987), and was renamed the Hopewell fault by Mixon (Mixon, 1989).  The fault displaces a Paleocene-Cretaceous contact and is inferred to offset the Pliocene Yorktown Formation (Dischinger, 1987).  Mixon (Mixon, 1989) extend the

mapping of Dischinger (Dischinger, 1987), but include conflicting data regarding fault activity. For instance, a cross section presented by Mixon (Mixon, 1989) shows the Hopewell fault displacing undivided upper Tertiary and Quaternary units, whereas the geologic map used to produce the section depicts the fault buried beneath these units.  A written communication from Newell (Wheeler, 2006) explains that the Hopewell fault was not observed offsetting Quaternary deposits and the representation of the fault in the Mixon (Mixon, 1989) cross section is an error.  Thus, the Hopewell fault zone is assigned as a Class C feature because no evidence is available to demonstrate Quaternary surface deformation.  Based on the written communication of Newell (Wheeler, 2006), an absence of published literature documenting Quaternary faulting, and an absence of seismicity spatially associated with the feature, we conclude that the Hopewell fault is not a capable tectonic source.

### 2.5.1.1.4.4.5.12 Old Hickory Faults

The Old Hickory faults are located near the Fall Line in southeastern Virginia, approximately 115 mi (185 km) south-southwest of the CCNPP site (Figure 2.5-31).  Based on mining exposures of the Old Hickory Heavy Mineral deposit, the Old Hickory faults consist of a series of five northwest-striking reverse faults that offset Paleozoic basement and Pliocene Coastal Plain sediments. The northwest-striking reverse faults juxtapose Paleozoic Eastern Slate Belt diorite over the Pliocene Yorktown Formation (Berquist, 1999).  Strike lengths range between 330 to 490 ft (100 to 150 m) and are spaced about 164 ft (50 m) apart.  Berquist and Bailey (Berquist, 1999) report up to 20 ft (6 m) of oblique dip-slip movement on individual faults, and suggest that the faults may be reactivated Mesozoic structures.  There is no stratigraphic or geomorphic evidence of Quaternary or Holocene activity of the Old Hickory faults (Berquist, 1999).  Crone and Wheeler (Crone, 2000) and Wheeler (Wheeler, 2006) conclude that "no Quaternary fault is documented" and assign a Class C designation to the Old Hickory faults.  Based on the absence of published literature documenting the presence of Quaternary deformation, and the absence of seismicity spatially associated with this feature, we conclude that the Old Hickory faults are not a capable tectonic source.

### 2.5.1.1.4.4.5.13 Stanleytown-Villa Heights Faults

The postulated Stanleytown-Villa Heights faults are located in the Piedmont of southern Virginia, approximately 223 mi (359 km) southwest of the CCNPP site (Figure 2.5-31).  The approximately 660 ft long (201 m long) faults juxtapose Quaternary alluvium against rocks of Cambrian age, and reflect an east-side-down sense of displacement (Crone, 2000).  No other faults are mapped nearby (Crone, 2000).  Geologic and geomorphic evidence suggests the "faults" are likely the result of landsliding.  Crone and Wheeler (Crone, 2000) classify the Stanleytown-Villa Heights faults as a Class C feature based on lack of evidence for Quaternary faulting.  Based on the absence of published literature documenting the presence of Quaternary faulting, and the absence of seismicity spatially associated with this feature, we conclude that the Stanleytown-Villa Heights faults are not a capable tectonic source.

### 2.5.1.1.4.4.5.14 East Coast Fault System

The postulated East Coast fault system (ECFS) of Marple and Talwani (2000) trends N34°E and is located approximately 70 mi (113 km) southwest of the site (Figure 2.5-31). The 370 mi (595 km) long fault system consists of three approximately 125 mi (201 km) long segments extending from the Charleston area in South Carolina northeastward to near the James River in Virginia (Figure 2.5-31).  The three segments were initially referred to as the southern, central, and northern zones of river anomalies (ZRA-S, ZRA-C, ZRA-N) and are herein referred to as the southern, central and northern segments of the ECFS.  The southern segment is located in South Carolina; the central segment is located primarily in North Carolina.  The northern segment, buried beneath Coastal Plain deposits, extends from northeastern North Carolina to southeastern Virginia, about 70 mi (113 km) southwest of the CCNPP site.  Marple and Talwani

(Marple, 2000) map the northern terminus of the ECFS between the Blackwater River and James River, southeast of Richmond.  Identification of the ECFS is based on the alignment of geomorphic features along Coastal Plain rivers, areas suggestive of uplift, and regions of local faulting.  The right-stepping character of the three segments, coupled with the northeast orientation of the fault system relative to the present day stress field, suggests a right-lateral strike-slip motion for the postulated ECFS (Marple and Talwani, 2000).

The southern segment of the fault system, first identified by Marple and Talwani (1993) as an approximately 125 mi (201 km) long and 6 to 9 mi (10 to 14.5 km) wide zone of river anomalies, has been attributed to the presence of a buried fault zone.  The southern end of this segment is associated with the Woodstock fault, a structure defined by fault-plane solutions of microearthquakes and thought to be the causative source of the 1886 Charleston earthquake (Marple, 2000). The southern segment is geomorphically the most well-defined segment of the fault system and is associated with micro-seismicity at its southern end.  This segment was included as an alternative geometry to the areal source for the 1886 Charleston earthquake in the 2002 USGS hazard model (Section 2.5.2) for the National Seismic Hazard Mapping Project (Frankel, 2002).

Crone and Wheeler (Crone, 2000) do not include the central and northern segments of the ECFS in their compilation of potentially active Quaternary faults.  The segments also were not presented in workshops or included in models for the Trial Implementation Project (TIP), a study that characterized seismic sources and ground motion attenuation models at two nuclear power plant sites in the southeastern United States (Savy, 2002).  As a member of both the USGS and TIP workshops, Talwani did not propose the northern and central segments of the fault system for consideration as a potential source of seismic activity.  There is no pre-EPRI or post-EPRI seismicity spatially associated with the northern and central segments of the fault system.

Recent geologic and geomorphic analysis of stream profiles across sections of the ECFS, and critical evaluation of Marple and Talwani (Marple, 2000) for the North Anna ESP, provides compelling evidence that the northern segment of the ECFS, which lies nearest to the CCNPP site, has a very low probability of existence (Dominion, 2004b).  Wheeler (Wheeler, 2005) states that although the evidence for a southern section of the ECFS is good, there is less evidence supporting Quaternary tectonism along the more northerly sections of the ECFS, and designates the northern portion of the fault system as a Class C feature.

In the Safety Evaluation Report for the North Anna ESP site, the NRC staff agreed with the assessment of the northern segment of the East Coast Fault System (ECFS-N) presented by the North Anna applicant (NRC, 2005).  Based on their independent review, the NRC staff concluded that:

- ♦ "Geologic, seismologic, and geomorphic evidence presented by Marple and Talwani is questionable."

- ♦ "The majority of the geologic data cited by Marple and Talwani in support of their postulated ECFS apply only to the central and southern segments."

- ♦ There are "no Cenozoic faults or structure contour maps indicating uplift along the ECFS-N."

- ♦ "The existence and recent activity of the northern segment of the ECFS is low."

Despite the statements above, the NRC concluded that the ECFS-N could still be a contributor to the seismic hazard at the North Anna site and should be included in the ground motion modeling to determine the Safe Shutdown Earthquake. The NRC agreed with the 10% probability of existence and activity proposed in the North Anna ESP application. The results of the revised ground motion calculations indicate that the ECFS-N does not contribute to the seismic hazard at the North Anna ESP site. The CCNPP site is approximately 70 mi (113 km) northeast of the ECFS-N, or 7 mi (11 km) further away than the North Anna site is from the ECFS-N. Based on the above discussion and the large distance between the site and the ECFS-N, this fault is not considered a contributing seismic source and need not be included in the seismic hazard calculations for the CCNPP site.

Marple and Talwani (Marple, 2004) suggest a northeast extension of the ECFS of Marple and Talwani (Marple, 2000), based on existing limited geologic, geophysical and geomorphic data. Marple and Talwani (Marple, 2004) postulate that the northern ECFS may step left (northwest) to the Stafford fault system near northern Virginia and southern Maryland (Figure 2.5-31) and thus extending the ECFS along the Stafford fault up to New York. As stated in Section 2.5.1.1.4.4.4.1, the NRC (NRC, 2005) agreed with an analysis of the Stafford fault performed as part of the North Anna ESP application and states: "Based on the evidence cited by the applicant, in particular the applicant's examination of the topography profiles that cross the fault system, the staff concludes that the applicant accurately characterized the Stafford fault system as being inactive during the Quaternary Period."

In summary, the ECFS in its entirety represents a new postulated tectonic feature that was not known to the EPRI Earth Science Teams in 1986. The 1986 EPRI models include areal sources to model the Charleston seismic source; therefore, the southern segment of the East Coast fault system is in essence covered by the different Charleston sources zone geometries. A review of the seismic sources that contribute 99% of the seismic hazard to the CCNPP shows that the Charleston source is not a contributor. The central and northern segments of the ECFS represent a new tectonic feature in the Coastal Plain that postdates the EPRI studies. The closest approach of the northern segment to the site is approximately 77 mi (124 km) as described above. Although the postulated ECFS represents a potentially new tectonic feature in the Coastal Plain of Virginia and North Carolina (Marple, 2000), current interpretations of the ECFS based on existing data indicate that the fault zone probably does not exist (especially the northern segment) and, if it does exists, has a very low probability of activity and does not contribute to hazard at the site.

### 2.5.1.1.4.5    Seismic Sources Defined by Regional Seismicity

Within 200 mi (322 km) of the CCNP site, two potential seismic sources are defined by a concentration of small to moderate earthquakes. These two seismic sources include the Central Virginia seismic zone in Virginia and the Lancaster seismic zone in southeast Pennsylvania, both of which are discussed below (Figure 2.5-31).

### 2.5.1.1.4.5.1 Central Virginia Seismic Zone

The Central Virginia seismic zone is an area of persistent, low level seismicity in the Piedmont Province (Figure 2.5-24 and Figure 2.5-31). The zone extends about 75 mi (121 km) in a north-south direction and about 90 mi (145 km) in an east-west direction from Richmond to Lynchburg and is coincident with the James River (Bollinger, 1985). The CCNPP site is located 47 to 62 mi (76 to 100 km) northeast of the northern boundary of the Central Virginia seismic zone. The largest historical earthquake to occur in the Central Virginia seismic zone was the body-wave magnitude (mb) 5.0 Goochland County event on December 23, 1875 (Bollinger, 1985). The maximum intensity estimated for this event was Modified Mercalli Intensity (MMI) VII in the epicentral region. More recently, an mb 4.5 earthquake (two closely-spaced events

that when combined = Mw 4.1) occurred on December 9, 2003 within the Central Virginia seismic zone (Kim and Chapman, 2005). The December 9, 2003 earthquake occurred close to the Spotsylvania fault, but due to the uncertainty in the location of the epicenter (3.7 to 5 mi (6 to 8 km) ), no attempt could be made to locate the epicenter with a specific fault or geologic lineament in the CVSZ (Kim, 2005).

Seismicity in the Central Virginia seismic zone ranges in depth from about 2 to 8 mi (3 to 13 km) (Wheeler, 1992). It is suggested (Coruh, 1988) that seismicity in the central and western parts of the zone may be associated with west-dipping reflectors that form the roof of a detached antiform, while seismicity in the eastern part of the zone near Richmond may be related to a near-vertical diabase dike swarm of Mesozoic age. However, given the depth distribution of 2 to 8 mi (3 to 13 km) (Wheeler, 1992) and broad spatial distribution, it is difficult to uniquely attribute the seismicity to any known geologic structure and it appears that the seismicity extends both above and below the Appalachian detachment.

No capable tectonic sources have been identified within the Central Virginia seismic zone, but two paleo-liquefaction sites have been identified within the seismic zone (Crone, 2000) (Obermier, 1998). The presence of these paleo-liquefaction features on the James and Rivanna Rivers shows that the Central Virginia seismic zone reflects both an area of paleo-seismicity as well as observed historical seismicity. Based on the absence of widespread paleo-liquefaction, however, it was concluded (Obermier, 1998) that an earthquake of magnitude 7 or larger has not occurred within the seismic zone in the last 2,000 to 3,000 years, or in the eastern portion of the seismic zone for the last 5,000 years. It was also conclude that the geologic record of one or more magnitude 6 or 7 earthquakes might be concealed between streams, but that such events could not have been abundant in the seismic zone. In addition, these isolated locations of paleo-liquefaction may have been produced by local shallow moderate magnitude earthquakes of M 5 to 6.

The paleo-liquefaction sites reflect pre-historical occurrences of seismicity within the Central Virginia seismic zone, and do not indicate the presence of a capable tectonic source. Recently, Wheeler (Wheeler, 2006) hypothesizes that there may be two causative faults for the small dikes of Obermier and McNulty (Obermier, 1998), and that earthquakes larger than those represented by historic seismicity are possible; whereas Marple and Talwani (Marple, 2004) interpret seismicity data to infer the presence of a hypothesized northwest-trending basement fault (Shenandoah fault) that coincides with the Norfolk fracture zone (Marple, 2004). However, no definitive causative fault or faults have been identified within the Central Virginia seismic zone (Wheeler, 2006).

The 1986 EPRI source model includes various source geometries and parameters to capture the seismicity of the Central Virginia seismic zone. Subsequent hazard studies have used maximum magnitude (Mmax) values that are within the range of maximum magnitudes used by the six EPRI models. Collectively, upper-bound maximum values of Mmax used by the EPRI teams range from mb 6.6 to 7.2 (Section 2.5.2.2). More recently, Bollinger (Bollonger, 1992) has estimated a Mmax of mb 6.4 for the Central Virginia seismic source. Chapman and Krimgold (Chapman, 1994) have used a Mmax of mb 7.25 for the Central Virginia seismic source and most other sources in their seismic hazard analysis of Virginia. This more recent estimate of Mmax is similar to the Mmax values used in the 1986 EPRI studies. Similarly, the distribution and rate of seismicity in the Central Virginia seismic source have not changed since the 1986 EPRI study (Section 2.5.2.2.8). Thus, there is no change to the source geometry or rate of seismicity. In 2005, the NRC agreed with the findings of the North Anna ESP application's assessment of the Central Virginia seismic zone (NRC, 2005). Therefore, the conclusion is that no new information

has been developed since 1986 that would require a significant revision to the EPRI seismic source model.

### 2.5.1.1.4.5.2 Lancaster Seismic Zone

The Lancaster seismic zone, as defined by Armbruster and Seeber (Armbruster, 1987), of southeast Pennsylvania has been a persistent source of seismicity for at least two centuries. The seismic zone is about 80 mi (129 km) long and 80 mi (129 km) wide and spans a belt of allochthonous Appalachian crystalline rocks between the Great Valley and Martic Line about 111 mi (179 km) northwest of the CCNPP site (Figure 2.5-31).  The Lancaster seismic zone crosses exposed Piedmont rocks that include thrust faults and folds associated with Paleozoic collisional orogenies.  It also crosses the Newark-Gettysburg Triassic rift basin which consists of extensional faults associated with Mesozoic rifting. Most well-located epicenters in the Lancaster seismic zone lie directly outside the Gettysburg-Newark basin (Scharnberger, 2006). The epicenters of 11 events with magnitudes 3.04 to 4.61 rmb from 1889 to 1994 from the western part of Lancaster seismic zone define a north-south trend that intersects the juncture between the Gettysburg and Newark sub-basins.  This juncture is a hinge around which the two sub-basins subsided, resulting in east-west oriented tensile stress.  Numerous north-south trending fractures and diabase dikes are consistent with this hypothesis.  It is likely that seismicity in at least the western part of the Lancaster seismic zone is due to present-day northeast-southwest compressional stress which is activating the Mesozoic fractures, with dikes perhaps serving as stress concentrators (Armbruster, 1987).

It also is probable that some recent earthquakes in the Lancaster seismic zone have been triggered by surface mining.  For instance, the 16 January 1994 Cacoosing earthquake (mb 4.6) is the largest instrumented earthquake occurring in the Lancaster seismic zone (Section 2.5.1.1.4.4.5.7).  This event was part of a shallow (depths generally less than 1.5 mi (2.4 km)) earthquake sequence linked to quarry activity (Seeber, 1998).  The earthquake sequence that culminated in the January 16 event initiated after a quarry was shut down and the quarry began to fill with water.  Seeber (Seeber, 1998) interprets the reverse-left lateral oblique earthquake sequence to be due to a decrease in normal stress caused by quarrying followed by an increase in pore fluid pressure (and decrease in effective normal stress) when the pumps were turned off and the water level increased.

Prior to the Cacoosing earthquake sequence, the 23 April 1984 Martic earthquake (mb 4.1) was the largest instrumented earthquake in the seismic zone and resembles pre-instrumental historical events dating back to the middle 18th century.  The 1984 earthquake sequence appears centered at about 2.8 mi (4.5 km) in depth and may have ruptured a steeply east-dipping, north-to northeast-striking fault aligned subparallel to Jurassic dikes with a reverse-right lateral oblique movement, consistent with east-northeast horizontal maximum compression.  These dikes are associated with many brittle faults and large planes of weakness suggesting that they too have an effect on the amount of seismicity in the Lancaster seismic zone. Most of the seismicity in the Lancaster seismic zone is occurring on secondary faults at high angles to the main structures of the Appalachians.  The EPRI study (EPRI, 1986) source models do not identify the Lancaster seismic zone as a separate seismic source.  However, the 5.3 to 7.2 Mb maximum magnitude distributions of EPRI source zones are significantly greater than any reported earthquake in this Lancaster seismic zone.  Thus, the EPRI study (EPRI, 1986) models adequately characterized this region and no significant update is required.}

### 2.5.1.2　　Site Geology

The U.S. EPR FSAR includes the following COL Item in Section 2.5.1.2:

Site-specific geology information will be addressed by the COL applicant.

This COL Item is addressed as follows:

{Sections 2.5.1.2.1 through 2.5.1.2.6 are added as a supplement to the U.S. EPR FSAR.

### 2.5.1.2.1　　Site Area Physiography and Geomorphology

The CCNPP site area is located within the Western Shore Uplands of the Atlantic Coastal Plain Physiographic Province and is bordered by the Chesapeake Bay to the east and the Patuxent River to the west (Figure 2.5-4 and Figure 2.5-7).

The site vicinity geologic map (Figure 2.5-27 and Figure 2.5-28), compiled from the work of several investigators, indicates that the counties due east from the CCNPP site across Chesapeake Bay are underlain by Pleistocene to Recent sands. Most of the site vicinity is underlain by Tertiary Coastal Plain deposits. Quaternary to Recent alluvium beach deposits and terrace deposits are mapped along streams and estuaries. Quaternary terrace and Lowland deposits are shown in greater detail on the scale of the site area geologic map (Figure 2.5-32). Geologic cross sections in the site area indicate that the Tertiary Upland deposits are underlain by gently dipping Tertiary Coastal Plain deposits described in Section 2.5.1.2.2 (Figure 2.5-33).

The topography within 5 mi (8 km) of the site consists of gently rolling hills with elevations ranging from about sea level to nearly 130 ft (40 m) msl (Figure 2.5-4). The site is well-drained by short, ephemeral streams that form a principally dendritic drainage pattern with many streams oriented in a northwest-southeast direction (Figure 2.5-5). As shown on the site area and site topographic and geological maps, the ground surface above approximately 100 ft (30 m) msl is capped by the Upper Miocene-Pliocene Upland deposits (Figure 2.5-4, Figure 2.5-5, Figure 2.5-32, and Figure 2.5-33). These deposits occupy dissected upland areas of the Cove Point quadrangle in which the CCNPP site is located (Figure 2.5-32 and Figure 2.5-33) (Glaser, 2003a). The longest stream near the site is Johns Creek, which is approximately 3.5 mi (5.6 km) long before it drains into St. Leonard Creek (Figure 2.5-4 and Figure 2.5-34). The ephemeral stream channels near the CCNPP site are either tributary to Johns Creek or flow directly to the Chesapeake Bay. These stream channels maintain their dendritic pattern as they cut down into the underlying Choptank and St. Marys Formations (Figure 2.5-27, Figure 2.5-32 and Figure 2.5-33).

The Chesapeake Bay shoreline forms the eastern boundary of the CCNPP site and generally consists of steep cliffs with narrow beach at their base. The cliffs reach elevations of about 100 ft (30 m) msl along the eastern portion of the site's shoreline. Narrow beaches whose width depends upon tidal fluctuations generally occur at the base of the cliffs. Field observations indicate that these steep slopes fail along nearly vertical irregular surfaces. The slope failure appears to be caused by shoreline erosion along the base of the cliffs. Shoreline processes and slope failure along Chesapeake Bay are discussed in Section 2.4.9. Approximately 2500 ft (762 m) of the shoreline from the existing CCNPP Units 1 and 2 intake structure southward to the existing barge jetty is stabilized against shoreline erosion (Figure 2.4-50). The CCNPP Unit 3 will be constructed at a final grade elevation of approximately 85 ft (26 km) msl and will be set back approximately 1,000 ft (305 m) from the Chesapeake Bay shoreline.

As described in Section 2.5.1.1.1, the Chesapeake Bay was formed toward the end of the Wisconsinan glacial stage, which marked the end of the Pleistocene epoch.  As the glaciers retreated, the huge volumes of melting ice fed the ancestral Susquehanna and Potomac Rivers, which eroded older Coastal Plain deposits forming a broad river valley.  The rising sea level covered the Continental Shelf and reached the mouth of the Bay about 10,000 years ago.  Sea level continued to rise, eventually submerging the area now known as the Susquehanna River Valley prior to sea level dropping to the current elevation.  The Bay assumed its present dimensions about 3000 years ago (Section 2.4.9).

### 2.5.1.2.2      Site Area Geologic History

The site area geologic history prior to the early Cretaceous is inferred from scattered borehole data, geophysical surveys and a synthesis of published information.  Sparse geophysical and borehole data indicate that the basement rock beneath the site may consist of exotic crystalline magmatic arc material (Glover, 1995b).  Although the basement has not been penetrated directly beneath the site with drill holes, regional geologic cross sections developed from geophysical, gravity and aeromagnetic, as well as limited deep borehole stratigraphic data beyond the site area, suggest Precambrian and Paleozoic crystalline rocks are most likely present at a depth of about 2,600 ft (792 m)  beneath the site (Section 2.5.1.2.3 and Section 2.5.1.2.4).  Tectonic models discussed in Section 2.5.1.2.4 hypothesize that the crystalline basement was accreted to the pre-Taconic North American margin during  the Paleozoic along a suture that lies about 10 mi (16 km) west of the site (Figure 2.5-17 and Figure 2.5-23).  Therefore, the crystalline basement beneath the Coastal Plain sediments in the site area might consist of an accreted nappe-like block of Carolina-Chopawamsic magmatic arc terrane with windows of Laurentian Grenville basement (Figure 2.5-16 and Figure 2.5-17) (Klitgord, 1995).

As discussed in Section 2.5.1.1.2 and Section 2.5.1.2.4, Mesozoic rift basins are exposed in the Piedmont Physiographic Province and are buried beneath Coastal Plain sediments.  The Queen Anne Basin was originally postulated by Hansen (1988) and was considered to underlie the site (Horton, 1991).  However, this interpretation does not appear to be supported by most of the borehole data and current interpretations (Section 2.5.1.2.4).

During the early Cretaceous, sands, clays, sandy clays, and arkosic sands of the Arundel/Patuxent Formations (undivided) were deposited on the crystalline basement in a continental and fluviatile environment.  Individual beds of sand or silt grade rapidly into sediments with different compositions or gradations, both vertically and horizontally, which suggests they were deposited in alluvial fan or deltaic environments.  Clay layers containing carbonized logs, stumps and other plant remains indicate the existence of quiet-water, swamp environments between irregularly distributed stream channels.  Thicker clays near the top of this unit in St Mary's County are interpreted to indicate longer periods of interfluvial quiet water deposition (Hansen, 1984).

The overlying beds of the Patapsco Formation are similar to the deposits in the Arundel/Patuxent (undivided) formations and consist chiefly of materials derived from the eroded crystalline rocks of the exposed Piedmont to the west and reworked Lower Cretaceous sediments.  These sediments were deposited in deltaic and estuarine environments with relatively low relief.  The Upper Cretaceous Raritan Formation appears to be missing from the site area due either to non-deposition or erosion on the northern flank of the structurally positive Norfolk Arch.

The Magothy Formation represents deposits from streams flowing from the Piedmont and depositing sediments in the coastal margins of the Upper Cretaceous sea.  Subsequent uplift and tilting of the Coastal Plain sediments mark the end of continental deposition and the

beginning of a marine transgression of the region. This contact is a regional unconformity marked in places by a basal layer of phosphatic clasts in the overlying Brightseat Formation.

During the Early Paleocene Epoch, the Brightseat Formation marks a marine advance in the Salisbury embayment (Ward, 2004). Uplift or sea level retreat is indicated by the burrowed contact (unconformity) of the Brightseat Formation with the overlying Aquia Formation. The marine Aquia Formation which is noted for its high glauconite content and shell beds was deposited in a shoaling marine environment indicated by a generally coarsening upward lithology (Hansen, 1996). A mix of light-colored quartz grains and greenish to blackish glauconite grains and iron staining indicated the change to a sandbank facies in the upper Aquia formation (Hansen, 1996). A marine transgression during the Late Paleocene/Early Eocene into the central portion of the Salisbury Embayment deposited the Marlboro Clay (Ward, 2004). During the Early Eocene, a moderately extensive marine transgression deposited the Potopaco Member of the Nanjemoy Formation. A subsequent transgression deposited the Woodstock Member of the Nanjemoy Formation (Ward, 2004). The most extensive marine transgression during the middle Eocene resulted in the deposition of the Piney Point Formation (Ward, 2004). The site area may have been emergent during the Oligocene as the Late Oligocene Old Church Formation indicates sea level rise and submergence to the north and south of the site area (Ward, 2004). A brief regression was followed by nearly continuous sedimentation in the Salisbury Embayment punctuated by short breaks, resulting in a series of thin, unconformity-bounded beds (Ward, 2004). A series of marine transgressions into the Salisbury Embayment during the Miocene produced the Calvert, Choptank and St. Marys Formations. Pliocene and Quaternary geologic history is discussed in Section 2.5.1.2.1.

### 2.5.1.2.3     Site Area Stratigraphy

Site specific information on the stratigraphy underlying the CCNPP site is limited by the total depths of the various borings advanced by site investigators over the years. Only a few scattered borings have been advanced below the Aquia Formation (Hansen, 1986). The deepest boring known to have been advanced at the site is CA-Ed 22 which was drilled to a total depth of 789 ft (240 m) and completed as a water supply well in 1968 (Hansen, 1996). This boring penetrates the full Tertiary stratigraphic section and intersects the contact between the Tertiary and the Cretaceous section at the base of the Aquia Formation. The closest boring which advances to pre-Cretaceous bedrock is approximately 13 mi (21 km) south of the site at Lexington Park in St. Mary's County, (Figure 2.5-11) (Hansen, 1986). This boring cored a diabase dike in the pre-Cretaceous basement (Section 2.5.1.1.3). The few borings that have reached basement rock in the site area are widely scattered (Figure 2.5-11) but the majority indicates that the basement rock beneath the site is likely to be similar to the schists and gneisses found in the Piedmont Physiographic Province approximately 50 mi (80 km) to the west (Figure 2.5-1). Alternatively, this crystalline basement might have been accreted to the exposed Piedmont as a result of continental collision during a Paleozoic orogeny (Section 2.5.1.1.1.4 and Section 2.5.1.2.2). Figure 2.5-35 shows the locations of the various borings at the site and identifies those completed as either water supply wells or observation wells. Many of these borings were drilled to 200 ft (61 m) in total depth; six were advanced to a total depth of 400 ft (122 m). Figure 2.5-36 is a site-specific stratigraphic column based on correlations by Hansen (Hansen, 1996), Achmad and Hansen (Achmad, 1997) and Ward and Powars (Ward, 2004).

The CCNPP site is located on Coastal Plain sediments ranging in age from Lower Cretaceous to Recent, which, in turn, were deposited on the pre-Cretaceous basement rock. The Cretaceous section shown on the site stratigraphic column is projected to the site from proximal borings which intersect the pre-Cretaceous basement (Figure 2.5-13).

Coastal Plain sediments were deposited in a broad basement depression known as the Salisbury Embayment extending from eastern Virginia to southern New Jersey (Figure 2.5-12) (Ward, 2004).  These sediments were deposited during periods of marine transgression/ regression and exhibit lateral and vertical variation in both lithology and texture.

### 2.5.1.2.3.1     Lower Cretaceous Potomac Group and pre-Potomac sediments

As discussed in Section 2.5.1.1.3, Hansen and Wilson (Hansen, 1984) assign the lowermost 30 ft (9 m) of the Lexington Park well (SM-Df 84), 13 mi (21 km) south of the CCNPP site (Figure 2.5-11) (Hansen, 1986), to the Waste Gate formation.  These sediments are described as gray silts and clays, interbedded with fine to medium silty fine to medium sands.  Although these sediments might correlate with the Waste Gate Formation identified in a well in Crisfield, Maryland (Do-CE 88), east of the Chesapeake Bay (Figure 2.5-11), there is no direct evidence indicating whether this unit occurs beneath the CCNPP site.

The Potomac Group is comprised of a sequence of interbedded sands and silty to fine sandy clays.  Because this formation was not encountered by any borings drilled at the CCNPP site, the description of these units is based on published data (Hansen, 1984) (Achmad, 1997).  Regionally, the Potomac Group consists of, from oldest to youngest, the Patuxent Formation, the Arundel Formation and the Patapsco Formation.  These units are considered continental in origin and are in unconformable contact with each other.

The Lower Cretaceous Patuxent Formation consists of a sequence of variegated sands and clays which form a major aquifer in the Baltimore area, approximately 50 mi (80 km) up-dip from the site, but which have not been tested in the vicinity of the site.  The nearest well intercepting the Patuxent is approximately 13 mi (21 km) south of the site and here the formation contains much less sand than is found in the upper part of the Potomac Group. The Patuxent is approximately 600 to 700 ft (182 m to 213 m) thick and is overlain by the Arundel/ Patapsco formations (undivided)

In the Baltimore area, the Arundel Formation consists of clays which are brick red near the Fall Line.  Further down-dip toward the southeast, the color changes to gray and this unit is difficult to separate in the subsurface from those clays present in the underlying Patuxent and overlying Patapsco formations. Consequently, the Arundel and the Patuxent are often undivided (Hansen, 1984) in the literature and referred as the Arundel/Patuxent formations (undivided). Hansen and Wilson (Hansen, 1984) describe the upper portion of the Arundel/Patuxent formations (undivided) as variegated silty clay with thin very fine sand and silt interbeds that may be as thick as 150 to 200 ft (46 to 61 m) beneath the CCNPP site (Figure 2.5-13).  The Arundel Formation is not recognized in southern Maryland (Hansen, 1996).

### 2.5.1.2.3.2     Upper Cretaceous Formations

The Patapsco formation is the uppermost unit in the Potomac Group and consists of gray, brown and red variegated silts and clays interbedded with lenticular, cross-bedded clayey sands and minor gravels.  This formation is a major aquifer near the Fall Line in the Baltimore area, but the Patapsco is untested near the CCNPP site.  The thickness of the Patapsco Formation based on regional correlations is 1,000 to 1,100 ft thick beneath the CCNPP site.

The Mattaponi (?) formation described as overlying the Potomac group in Hansen and Wilson (Hansen, 1984) is no longer recognized by the Maryland Geological Survey.  The section formerly assigned to the Mattaponi (?) has been included within the Patapsco Formation.

The Magothy Formation unconformably overlies the Patapsco Formation beneath the site. The Magothy is comprised chiefly of pebbly, medium coarse sand, although there are clayey portions in the upper part (Achmad, 1997).  This formation is much thinner at the site than further north in Calvert County and pinches out within a few mi to the south (Achmad, 1997). The Monmouth and Matawan formations have not been differentiated from the Magothy Formation in the site area.

### 2.5.1.2.3.3        Tertiary Formations

The earliest Tertiary sediments beneath the site are assigned to the Lower Paleocene Brightseat Formation, a thin dark gray sandy clay identified in the deepest boring (CA-Ed 22) at the site as the Lower Confining Unit (Figure 2.5-13).  The Brightseat Formation is identified in the gamma log as a higher than normal gamma response below the Aquia sand.  According to Ward and Powars (Ward, 2004) the Brightseat Formation marks a marine advance in the Salisbury Embayment and occurs principally in the northeastern portion of the Embayment.  This stratigraphic unit was reached by the water supply well CA-Ed 22 in 1968 (Figure 2.5-13). Achmad and Hansen (Achmad, 1997) describe the Brightseat Formation as approximately 10 ft (3 m) thick consisting mainly of very fine sand and clay with a bioturbated fabric. The absence of a bioturbated contact with the underlying beds suggests an unconformable contact.

The Aquia Formation unconformably overlies the Brightseat Formation and consists of clayey, silty, very shelly glauconitic sand (Ward, 2004).  Microfossil study has placed the Aquia in the upper Paleocene.  In the type section, the Aquia Formation is divided into two members, the Piscataway Creek and the Paspotansa, but at the CCNPP site, these members are not differentiated.  Achmad and Hansen (Achmed, 1997) describe the Aquia Formation as approximately 150 ft (46 m) thick. The sand becomes fine-grained in the lower 50 ft (15 m) of the formation.

The Marlboro clay is a silvery-gray to pale-red plastic clay interbedded with yellowish-gray to reddish silt occurring at the base of the Nanjemoy Formation (Ward, 2004).  Achmad and Hansen (1997) describe approximately 10 ft (3 m) of clay with thin, indistinct laminae of differing colored silt.  Its contact with the underlying Aquia Formation is somewhat gradational while the contact between the Marlboro and the overlying Nanjemoy appears to be sharp indicating that the Nanjemoy unconformably overlies the Marlboro.  Microfossil studies indicate the presence of a mixture of very late Paleocene and very early Eocene flora.  Based on geophysical logs from CA-Ed 22, the Marlboro clay appears to be approximately 15 ft (4.6 m) thick beneath the CCNPP site (Figure 2.5-13).

At the CCNPP site, the Nanjemoy Formation is divided into the Potapaco and Woodstock members between the overlying Piney Point Formation and the underlying Marlboro clay.  The Nanjemoy Formation is described as olive black, very fine grained, well-sorted silty glauconitic sands (Ward, 2004).  Based on electric log data, the thickness of the Nanjemoy Formation beneath the CCNPP site is approximately 180 ft (55 m).  About 80 ft (24 m) of this unit was penetrated by CCNPP Unit 3 borings, B-301 and B-401 (Figure 2.5-37 and Figure 2.5-38), drilled during the subsurface investigation.

The Piney Point Formation is a thin glauconitic sand and clay unit unconformably overlying the Nanjemoy formation. According to Achmad and Hansen (Achmad, 1997), the Piney Point is approximately 20 ft (6 m) thick at the CCNPP site and extends from about the middle of Calvert County, north of the CCNPP site, toward the south to beyond the Potomac River; increasing in thickness to approximately 130 ft (40 m) at Point Lookout at the confluence of the Potomac River and Chesapeake Bay.  Formerly considered late Eocene in age, the Piney Point is assigned

to the middle Eocene (Achmad, 1997) (Ward, 2004). The unit has a distinctive natural gamma signature associated with the presence of glauconite and is a useful marker bed.

This distinctive natural gamma signature is present in boring B-301 at a depth of 302 ft (92 m) (205 ft (62 m) msl). This interval is described as dark greenish gray, dense clayey sand grading to very dense silty sands in their bottom 25 ft (8 m). Boring B-401 encountered the Piney Point Formation at a depth of 278 ft (85 m) (-181 ft (-55 m) msl).

According to Hansen (Hansen, 1996), the top of the Piney Point Formation occurs at an approximate elevation of -200 ft (-61 m) msl in the CCNPP site area (Figure 2.5-14). The absence of late Eocene and early Miocene sediments indicate the absence of deposition or erosion for millions of years. A structure contour map of the top of the Piney Point Formation shows an erosion surface that dips gently toward the southeast (Figure 2.5-14).

The Chesapeake Group at the CCNPP site is divided into three marine formations which are, from oldest to youngest, the Calvert Formation, the Choptank Formation and the St. Marys Formation. These units are difficult to distinguish in the subsurface due to similar sediment types and are undivided at the CCNPP site (Glaser, 2003c). Achmad and Hansen (Achmad, 1997) indicate that the Chesapeake Group is approximately 245 ft (75 m) thick beneath the CCNPP site, based on boring CA-Ed 22 data. Kidwell (Kidwell, 1997) states that the stratigraphic relations within this group are highly complex. Based on cross sections presented in Kidwell (Kidwell, 1997), the contact between the St. Marys Formation and the underlying Choptank is estimated to be approximately 22 ft (7 m) deep in boring B-301 and at 10 ft (3 m) deep in B-401. The thickness of the Chesapeake Group (undifferentiated) is 280 ft in boring B-301 and 268 ft in B-401. The difference in these thicknesses and that in CA-Ed 22 is attributed to the geophysical log of the latter boring not continuing to the top of the boring and/or difference in the chosen top of the St. Marys Formation.

Although the formational contacts within the Chesapeake Group are difficult to impossible to identify, there are several strata which are encountered in most of the CCNPP Unit 3 investigation borings. The most persistent of these is the calcite-cemented sand shown in Figure 2.5-42 and probably is one of the units Kidwell (Kidwell, 1997) interprets as the Choptank Formation.

About 20 ft below the base of this cemented sand unit as a second, but much thinner cemented sand which is identified primarily by "N" values (the sum of the blow counts for the intervals 6 to 12 in (15 to 30 cm) and 12 to 18 in (30 to 46 cm) sample intervals in a standard SPT) higher than those immediately above and below.

The base of the Chesapeake Group (Piney Point Formation) is clearly identified in the geophysical log (Figure 2.5-37 and Figure 2.5-38) by the characteristic gamma curve response. Based on the boring log, this gamma curve response appears to be related to calcite-cemented sand.

The surficial deposits consist of two informal stratigraphic units: the Pliocene-age Upland deposits and Pleistocene to Holocene Lowland deposits. The Upland deposits consist of two units deposited in a fluviatile environment. The Upland deposits are areally more extensive in St. Mary's County than in Calvert County (Glaser, 1971). The outcrop distribution has a dendritic pattern and since it caps the higher interfluvial divides, this unit is interpreted as a highly dissected sediment sheet whose base slopes toward the southwest (Glaser, 1971) (Hansen, 1996). This erosion might have occurred due to differential uplift during the Pliocene or down

cutting in response to lower base levels when sea level was lower during periods of Pleistocene glaciation.

### 2.5.1.2.3.4      Quarternary Formations

The Lowland deposits are considered to consist of three lithologic units.  The basal unit is estimated to be 10 to 20 ft (3 to 6 m) thick and is often described as cobbly sand and gravel.  This unit may represent high energy stream deposits in an alluvial environment near the base of eroding highlands to the west.  The basal unit is overlain by as much as 90 ft (27 m) of bluish gray to dark brown clay that may be silty or sandy (Glaser, 1971)  The uppermost of the three units consists of 10 to 30 ft (3 to 9 m) of pale gray, fairly well sorted, medium to coarse sand (Glaser, 1971).  The Lowland deposits were laid down in fluvial to estuarine environments (Hansen, 1996) and are generally found along the Patuxent and Potomac River valleys and the Chesapeake Bay.  These deposits occur in only a few places along the east shore of Chesapeake Bay.

Sands overlying the Chesapeake Group at the CCNPP site are mapped by Glaser (2003c) as Upland Deposits.  Within the CCNPP Unit 3 power block these sands range in thickness from a feather edge in borings on the southern edge, to more than 50 ft in B-405.

Boring B-301 intersected 22 ft (7 m) of silty sand above the contact with the Chesapeake Group, while B-401 has 10 ft (3 m) of silty sand (Figure 2.5-37 and Figure 2.5-38).  The sand in both borings grades into a coarser sand unit just above the contact.  These sands are attributed to the Upland deposits previously mapped (Glaser, 2003c).

Terrace deposits in the CCNPP site area (Figure 2.5-32 and Figure 2.5-34) consist of interbedded light gray to gray silty sands and clay with occasional reddish brown pockets and are approximately 50 ft (15 m) thick. These units are Pliocene to Holocene in age.

Holocene deposits, mapped as Qal on the site Geologic Map, includes heterogeneous sediments underlying floodplains and beach sands composed of loose sand.

### 2.5.1.2.4      Site Area Structural Geology

The local structural geology of the CCNPP site described in this section is based primarily on a summary of published geologic mapping (Cleaves, 1968) (Glaser, 1994) (McCartan, 1995) (Achmad, 1997) (Glaser, 2003b) (Glaser, 2003c), aeromagnetic and gravity surveys (Hansen, 1978) (Hittelman, 1994) (Milici, 1995) (Bankey, 2002), detailed lithostratigraphic profiles along Calvert Cliffs (Kidwell, 1988) (Kidwell, 1997), results of earlier investigations performed at the CCNPP site (BGE, 1968) (CEG, 2005), as well as CCNPP site reconnaissance and subsurface exploration performed for this CCNPP Unit 3 study.  Sparse geophysical and borehole data indicate that the basement likely consists of exotic crystalline magmatic arc material (Hansen, 1986) (Glover, 1995b).  Although the basement beneath the site has not been penetrated with drill holes, regional geologic cross sections developed from geophysical, gravity and aeromagnetic, as well as limited deep borehole data from outside of the CCNPP site area, suggest that Precambrian and Paleozoic crystalline rocks and, less likely, Mesozoic rift-basin deposits are present at about 2,500 ft (762 m) msl (Section 2.5.1.2.2).

Tectonic models hypothesize that the crystalline basement underlying the site was accreted to a pre-Taconic North American margin in the Paleozoic along a suture that lies about 10 mi (16 km) west of the site (Figure 2.5-17 and Figure 2.5-23).  The plate-scale suture is defined by a distinct north-northeast-trending magnetic anomaly that dips easterly between 35 and 45 degrees and lies about 7.5 to 9 mi (12 to 14.5 m) beneath the CCNPP site (Glover, 1995b)

(Figure 2.5-17).  Directly west of the suture lies the north to northeast-trending Taylorsville Basin and to the east, the postulated Queen Anne Mesozoic rift basin (Figure 2.5.1-9).  These Mesozoic basins are delineated from geophysical data and a limited number of deep boreholes that penetrate the crust, and generally are considered approximately located where buried beneath the Coastal Plain (Jacobeen, 1972) (Hansen, 1986) (Benson, 1992) (LeTourneau, 2003).  Most authors interpret Mesozoic basins directly west or east of the site; however, because the available geologic information used to constrain the basin locations is sparse, some depict the CCNPP site area to be underlain by a Mesozoic basin (Benson, 1992) (Figure 2.5-10).  However, on the basis of a review of existing published geologic literature, site-specific data, and field reconnaissance, suggests there is no known basin-related fault or geologic evidence of basin-related faulting in the basement directly beneath the CCNPP site area.

Recent 1:24,000-scale mapping (Glaser, 2003b) (Glaser, 2003c) for Calvert County and St. Mary's County shows the stratigraphy at the CCNPP site area consisting of nearly flat-lying Cenozoic Coastal Plain sediments that have accumulated within the west-central part of the Salisbury Embayment (Figure 2.5-32 and Figure 2.5-33).  The Salisbury Embayment is defined as a regional depocenter that has undergone slow crustal and regional downwarping as a result of sediment overburden during the Early Cretaceous and much of the Tertiary.  The Coastal Plain deposits within this region of the Salisbury Embayment generally strike northeast-southwest and have a gentle dip to the southeast at angles close to or less than one to two degrees (Figure 2.5-32 and Figure 2.5-33).  The gentle southerly dip of the sediments result in a surface outcrop pattern in which the strata become successively younger in a southeast direction across the embayment.  The gentle-dipping to flat-lying Miocene Coastal Plain deposits are exposed in the steep cliffs along the western shoreline of Chesapeake Bay and provide excellent exposures to assess the presence or absence of tectonic-related structures.

Local geologic cross sections of the site area depict unfaulted, southeast-dipping Eocene-Miocene Coastal Plain sediments in an unconformable contact with overlying Pliocene Upland deposits (Glaser, 1994) (Achmad, 1997) (Glaser, 2003b) (Glaser, 2003c) (Figure 2.5-13, Figure 2.5-32, and Figure 2.5-33).  No faults or folds are depicted on these geologic cross sections.  A review of an Early Site Review report (BGE, 1977), i.e. Perryman site, and a review of the Preliminary Safety Analysis Report for the Douglas Point site (Potomac Electric Power Company, 1973), located along the eastern shore of the Potomac River about 45 mi (72 km) west-southwest of the CCNPP site, also reported no faults or folds within a 5 mi (8 km) radius of the CCNPP site.  The Updated Final Safety Analysis Report for the Hope Creek site, located in New Jersey along the northern shore of Delaware Bay, also was reviewed for tectonic features previously identified within 5 mi (8 km) of the CCNPP site, yet none were identified (PSEG, 2002).  Review of a seismic source characterization study (URS, 2000) for a liquidefied natural gas plant at Cove Point, about 3 mi (5 km) southeast of the site, also identified no faults or folds projecting toward or underlying the CCNPP site area.

On the basis of literature review, and aerial and field reconnaissance, the only potential structural features at and within the CCNPP site area consist of a hypothetical buried northeast-trending fault (Hansen, 1986), two inferred east-facing monoclines developed within Mesozoic and Tertiary deposits along the western shore of Chesapeake Bay (McCartan, 1995), and multiple subtle folds or inflections in Miocene strata and a postulated fault directly south of the site (Kidwell, 1997) (Figure 2.5-25).  The Hillville fault of Hansen and Edwards (Hansen, 1986) and inferred fold of McCartan (McCartan, 1995) and Kidwell (Kidwell, 1997) are described in Sections 2.5.1.1.4.4.4 and Section 2.5.3.  As previously discussed in Section 2.5.1.1.4.4.4, none of these features are considered capable tectonic sources, as defined in RG 1.165, Appendix A.  Each of these features is discussed briefly below.  Only the Hillville fault has been mapped

within or directly at the 5 mi (8 km) radius of the CCNPP site area (Figure 2.5-27, Figure 2.5-28, and Figure 2.5-32).

Hillville fault of Hansen and Edwards (Hansen, 1986): The 26 mile long Hillville fault approaches to within 5 mi (8 km) of the CCNPP site (Figure 2.5-32). The fault consists of a northeast-striking zone of steep southeast-dipping reverse faults that coincide with the Sussex-Currioman Bay aeromagnetic anomaly. The style and location of faulting are based on seismic reflection data collected about 9 mi (14 km) west-southwest of the site. A seismic line imaged a narrow zone of discontinuities that vertically separate basement by as much as 250 ft (76 m) (Hansen, 1978). Hansen and Edwards (Hansen, 1986) interpret this offset as part of a larger lithotectonic terrane boundary that separates basement rocks associated with Triassic rift basins on the west and low-grade metamorphic basement on the east. The Hillville fault may represent a Paleozoic suture zone that was reactivated in the Mesozoic and Early Tertiary. Based on stratigraphic correlation between boreholes within Tertiary Coastal Plain deposits, Hansen and Edwards (Hansen, 1986) speculate that the Hillville fault was last active in the Early Paleocene. There is no pre-EPRI and post-EPRI (1986) seismicity spatially associated with this feature (Figure 2.5-25) nor is there any geomorphic evidence of Quaternary deformation. The Hillville fault is not considered a capable tectonic source.

In addition, two speculative and poorly constrained east-facing monoclines along the western margin of Chesapeake Bay are mapped within the 5 mi (8 km) radius of the CCNPP site area. East-facing monoclines (McCartan, 1995): The unnamed monoclines are not depicted on any geologic maps of the area, including those by the authors, but they are shown on geologic cross sections that trend northwest-southeast across the existing site and south of the CCNPP site near the Patuxent River (McCartan, 1995) (Figure 2.5-25). East-facing monoclines are inferred beneath Chesapeake Bay at about 2 and 10 mi (3.2 to 16 km) east and southeast, respectively, from the CCNPP site. Along a northerly trench, the two monoclines delineate a continuous north-trending, east-facing monocline. As mapped in cross section and inferred in plan view, the monoclines trend approximately north along the western shore of Chesapeake Bay. The monoclines exhibit a west-side up sense of structural relief that projects into the Miocene Choptank Formation (McCartan, 1995). The overlying Late Miocene St. Marys Formation is not shown as warped. Although no published geologic data are available to substantiate the existence of the monoclines, McCartan (McCartan, 1995) believes the distinct elevation change across Chesapeake Bay and the apparent linear nature of Calvert Cliffs are tectonically controlled. CCNPP site and aerial reconnaissance, coupled with literature review, for the CCNPP Unit 3 study strongly support a non-tectonic origin for the physiographic differences across the Chesapeake Bay (Section 2.5.1.1.4.4.4). There is no pre-EPRI or post-EPRI (1986) seismicity spatially associated with this feature, nor is there geologic data to suggest that the monocline proposed by McCartan (McCartan, 1995) is a capable tectonic source.

Multiple subtle folds or inflections developed in Miocene Coastal Plain strata including a postulated fault are mapped in the cliff exposures along the west side of Chesapeake Bay. Kidwell's (Kidwell, 1997) postulated folds and fault: Kidwell (Kidwell, 1988) (Kidwell, 1997) prepared over 300 lithostratigraphic columns along a 25 mi (40 km) long stretch of Calvert Cliffs that intersect much of the CCNPP site (Figure 2.5-30). When these stratigraphic columns are compiled into a cross section, they collectively provide a 25 mi (40 km) long nearly continuous exposure of Miocene, Pliocene and Quaternary deposits. Kidwell's (Kidwell, 1997) stratigraphic analysis indicates that the Miocene Coastal Plain deposits strike northeast and dip very shallow between 1 and 2 degrees to the south-southeast, which is consistent with the findings of others (McCartan, 1995) (Glaser 2003b) (Glaser, 2003c). The regional southeast-dipping strata are disrupted occasionally by several low amplitude broad undulations developed within Miocene Coastal Plain deposits (Figure 2.5-30). The stratigraphic undulations are interpreted as

monoclines and asymmetrical anticlines by Kidwell (Kidwell, 1997).  In general, the undulatory stratigraphic contacts coincide with basal unconformities having wavelengths of 2.5 to 5 mi (4 to 8 km) and amplitudes of 10 to 11 ft (approximately 3 meters).  Based on prominent stratigraphic truncations, the inferred warping decreases upsection into the overlying upper Miocene St. Marys Formation.  Any inferred folding of the overlying Pliocene and Quaternary fluvial deposits is poorly constrained and can be readily explained by highly variable undulating unconformities.

Near Moran Landing, about 1.2 mi (1.9 km) south of the site, Kidwell (Kidwell, 1997) interprets an apparent 6 to 10 ft (2 to 3 m) elevation change in Miocene strata, and a 3 to 12 (0.9 to 3.7 m) ft elevation change in Pliocene and Quaternary (?) fluvial material (Figure 2.5-25 and Figure 2.5-30).  Kidwell (Kidwell, 1997) infers the presence of a fault to explain the difference in elevation of strata across Moran Landing.  The postulated fault is not shown on the Kidwell (Kidwell, 1997) section, or any published geologic map, however the inferred location is approximately 1.2 mi (1.9 m) south of the CCNPP site.  The hypothesized fault is not exposed in the cliff face, but Kidwell (Kidwell, 1997) postulates the presence of a fault, and is based entirely on a change in elevation and bedding dip of Miocene stratigraphic boundaries projected across the fluvial valley of Moran Landing.  Kidwell (Kidwell, 1997) postulates that the fault strikes northeast and exhibits a north-side down sense of separation across all the geologic units (Miocene through Quaternary).  With regard to the apparent elevation changes for the Pliocene and Quaternary unconformities, these can be readily explained by channeling and highly irregular erosional surfaces.  Field and aerial reconnaissance, coupled with interpretation of aerial photography and LiDAR data (Section 2.5.3.1 for additional information regarding the general methodology) conducted as part of this CCNPP Unit 3 study revealed no features suggestive of tectonic deformation developed in the surrounding Pliocene and Quaternary surfaces.

There is no pre-EPRI or post-EPRI study (EPRI, 1986) seismicity spatially associated with the Kidwell (Kidwell, 1997) features, the hypothetical features are not aligned or associated with gravity and magnetic anomalies, nor is there data to indicate that the features proposed by Kidwell (Kidwell, 1997) are capable tectonic sources.

The most detailed subsurface exploration of the site was performed by Dames & Moore as part of the original PSAR (BGE, 1968) for the existing CCNPP foundation and supporting structures.  The PSAR study included drilling as many as 85 geotechnical boreholes, collecting downhole geophysical data, and acquiring seismic refraction data across the site.  Dames and Moore (BGE, 1968) developed geologic cross sections extending from Highway 2/4 northwest of the site to Camp Conoy on the southeast which provide valuable subsurface information on the lateral continuity of Miocene Coastal Plain sediments and Pliocene Upland deposits (Figure 2.5-32 and Figure 2.5-34).  Cross sections C-C' and D-D' pre-date site development and intersect the existing and proposed CCNPP site for structures trending north-northeast, parallel to the regional structural grain.  These sections depict a nearly flat-lying, undeformed geologic contact between the Middle Miocene Piney Point Formation and the overlying Middle Miocene Calvert Formation at about –200 ft (-61 m) msl (Figure 2.5-41 and Figure 2.5-42).

Geologic sections developed from geotechnical borehole data collected as part of the CCNPP Unit 3 study also provide additional detailed sedimentological and structural relations for the upper approximately 400 ft (122 m) of strata directly beneath the footprint of the site.  Similar to the previous cross sections prepared for the site, new geologic borehole data support the interpretation of flat-lying and unfaulted Miocene and Pliocene stratigraphy at the CCNPP site (Figure 2.5-39 and Figure 2.5-43).  A cross section prepared oblique to previously mapped northeast-trending structures (i.e., Hillville fault), inferred folds (McCartan, 1995) (Kidwell,

1997), and the fault of Kidwell (Kidwell, 1997) shows nearly flat-lying Miocene and Pliocene stratigraphy directly below the CCNPP site. Multiple key stratigraphic markers provide evidence for the absence of Miocene-Pliocene faulting and folding beneath the site. Minor perturbations are present across the Miocene-Pliocene stratigraphic boundary, as well as other Miocene-related boundaries, however these minor elevation changes are most likely related to the irregular nature of the fluvial unconformities and are not tectonic-related.

Numerous investigations of the Calvert Cliffs coastline over many decades by government researchers, stratigraphers, and by consultants for Baltimore Gas and Electric, as well as investigations for the CCNPP Unit 3, have reported no visible signs of tectonic deformation within the exposed Miocene deposits near the site, with the only exception being that of Kidwell (Kidwell, 1997) (Figure 2.5-44). Collectively, the majority of published and unpublished geologic cross sections compiled for much of the site area and site, coupled with regional sections (Achmad, 1997) (Glaser, 2003b) (Glaser, 2003c) and site and aerial reconnaissance, indicate the absence of Pliocene and younger faulting and folding. A review and interpretation of aerial photography, digital elevation models, and LiDAR data of the CCNPP site area, coupled with aerial reconnaissance, identified few discontinuous north to northeast-striking lineaments. None of these lineaments were interpreted as fault-related, nor coincident with the Hillville fault or the other previously inferred Miocene-Pliocene structures mapped by McCartan (McCartan, 1995) and Kidwell (Kidwell, 1997) (Section 2.5.3). A review of regional geologic sections and interpretation of LiDAR data suggest that the features postulated by Kidwell (Kidwell, 1997), if present, are not moderate or prominent structures, and do not deform Pliocene and Quaternary strata. In summary, on the basis of regional and site geologic and geomorphic data, there are no known faults within the site area, with the exception of the poorly constrained Hillville fault that lies along the northwestern perimeter of the 5 mi (8 km) radius of the site (Hansen, 1986).

### 2.5.1.2.5    Site Area Geologic Hazard Evaluation

No geologic hazards have been identified within the CCNPP site area. No geologic units at the site are subject to dissolution. No deformation zones were encountered in the exploration or excavation for CCNPP Units 1 and 2 and none have been encountered in the site investigation for CCNPP Unit 3. Because the CCNPP Unit 3 plant site is located at an elevation of approximately 85 ft (26 m) msl and approximately 1,000 ft (305 m) from the Chesapeake Bay shoreline, it is unlikely that shoreline erosion or flooding will impact the CCNPP site.

### 2.5.1.2.6    Site Engineering Geology Evaluation

### 2.5.1.2.6.1    Engineering Soil Properties and Behavior of Foundation Materials

Engineering soil properties, including index properties, static and dynamic strength, and compressibility are discussed in Section 2.5.4. Variability and distribution of properties for the foundation bearing soils will be evaluated and mapped as the excavation is completed.

Settlement monitoring will based on analyses performed for the final design.

### 2.5.1.2.6.2    Zones of Alteration, Weathering, and Structural Weakness

No unusual weathering profiles have been encountered during the site investigation. No dissolution is expected to affect foundations. Any noted desiccation, weathering zones, joints or fractures will be mapped during excavation and evaluated.

### 2.5.1.2.6.3    Deformational Zones

No deformation zones were encountered in the exploration or excavation for CCNPP Units 1 and 2 and none have been encountered in the site investigation for CCNPP Unit 3.  Excavation mapping is required during construction and any noted deformational zones will be evaluated. No capable tectonic sources as defined by Regulatory Guide 1.165 (NRC, 1997) exist in the CCNPP site region.

### 2.5.1.2.6.4    Prior Earthquake Effects

Outcrops are rare within the CCNPP site area.  Studies of the CCNPP Unit 1 and 2 excavation, available outcrops, and extensive exposures along the western shore of Chesapeake Bay have not indicated any evidence for earthquake activity that affected the Miocene deposits.  There is no evidence of earthquake-induced liquefaction in the State of Maryland (Crone, 2000) (Wheeler, 2005).

### 2.5.1.2.6.5    Effects of Human Activities

No mining operations, excessive extraction or injection of ground water or impoundment of water has occurred within the site area that can affect geologic conditions.

### 2.5.1.2.6.6    Site Ground Water Conditions

A detailed discussion of ground water conditions is provided in Section 2.4.12.

### 2.5.1.3    References

{This section is added as a supplement to the U.S. EPR FSAR.

**Achmad, 1997.** Hydrogeology, model simulation, and water-supply potential of the Aquia and Piney Point-Nanjemoy Aquifers in Calvert and St. Mary's Counties, Maryland, Department of Natural Resources, Maryland Geological Survey Report of Investigations No. 64, 197 p., G. Achmad and H. Hansen, 1997.

**Aggarwal, 1978.**  Earthquakes, Faults, and Nuclear Power Plants in Southern New York and Northern New Jersey, Science, Volume 200, p 425-429, Y. Aggarwal, and L. Sykes, 1978.

**Armbruster, 1987.** The 23 April 1984 Martic Earthquake and The Lancaster Seismic Zone In Eastern Pennsylvania, Bulletin of the Seismological Society of America, Volume 77, Number 2, p 877-890, J. Armbruster, and L. Seeber, 1987.

**Bailey, 1999.** The Geology of Virginia: Generalized Geologic Terrane Map of the Virginia Peidmont and Blue Ridge, Physiographic Map of Virginia, College of William and Mary, Department of Geology, C. Bailey, 1999, Website: www.wm.edu/geology/virginia/phys_regions.html, Date accessed: June 25, 2007.

**BGE, 1968.**  Preliminary Safety Analysis Report Calvert Cliffs Nuclear Power Plant Units 1 and 2, Volume 1, Docket 50-317 and 50-318, Baltimore Gas and Electric, 1968.

**BGE, 1977.**  Limited Early Site Review Perryman Site Suitability-Site Safety Report, Volume III, Baltimore Gas and Electric, July 1977.

**Bankey, 2002.**  Magnetic Anomaly Map of North America, U.S. Geological Survey, 1 sheet, scale 1:10,000,000, V. Bankey, A. Cuevas, D. Daniels, C. Finn, I. Hernandez, P. Hill, R. Kucks, W. Miles, M. Pilkington, C. Roberts, W. Roest, V. Rystrom, S. Shearer, S. Snyder, R. Sweeney, and J. Velez, 2002.

**Behrendt, 1983.** Structural elements of the U.S. Atlantic margin delineated by the second vertical derivative of the aeromagnetic data, U.S. Geological Survey Geophysical Investigation Map GP-956, scale 1:2,500,000, J. Behrendt and M. Grim, 1983.

**Benson, 1992.** Map of Exposed and Buried Early Mesozoic Rift Basins/Synrift Rocks of the U.S. Middle Atlantic Continental Margin, Delaware Geological Survey Miscellaneous Map Series No. 5, R. Benson, 1992.

**Berquist, 1999.** Late Cenozoic Reverse Faulting in the Fall Zone, Southeastern Virginia, The Journal of Geology, Volume 107, p 727-732, C. Berquist, Jr and C. Bailey, 1999.

**Bledsoe, 1980.** Executive Summary, Review of Potential Host Rocks for Radioactive Waste Disposal in the Southeastern United States, prepared by E.I. du Pont de Nemours and Company for the U.S. Department of the Energy, DP-1559, H. Bledsoe and I. Marine, October 1980.

**Bobyarchick, 1979.** Deformation and Metamorphism in the Hylas Zone and Adjacent Parts of the Eastern Piedmont in Virginia, Geological Society of America Bulletin, Volume 90, p 739–752, A. Bobyarchick and L. Glover, 1979.

**Bollinger, 1985.** Seismicity, Seismic Reflection Studies, Gravity and Geology of the Central Virginia Seismic Zone: Part I. Seismicity, Geological Society of America Bulletin, Volume 96, 49–57, G. Bollinger and M. Sibol, January 1985.

**Bollinger, 1988.** The Giles County, Virginia, Seismic Zone – Seismological Results and Geological Interpretations, U.S. Geological Survey Professional Paper 1355, G. Bollinger and R. Wheeler, 1988.

**Bollinger, 1992.** Specification of Source Zones, Recurrence Rates, Focal Depths, and Maximum Magnitudes for Earthquakes Affecting the Savannah River Site in South Carolina, U.S. Geological Survey Bulletin 2017, G. Bollinger, 1992.

**Brezinski, 2004.** Stratigraphy of the Frederick Valley and its Relationship to Karst Development, Maryland Geological Survey, Report of Investigations Number 75, D. Brezinski, 2004

**Brown, 1972.** Structural and stratigraphic framework and spatial distribution of permeability of the Atlantic Coastal Plain, North Carolina to New York, U.S. Geological Survey Professional Paper 796, p 79, P. Brown, J. Miller, and F. Swain, 1972.

**Burton, 1985.** Attitude, movement history, and structure of cataclastic rocks of the Flemington fault—Results of core drilling near Oldwick, New Jersey, U.S. Geological Survey Miscellaneous Field Studies, Map MF-1781, 1 sheet, W. Burton and N. Ratcliffe, 1985.

**Carter, 1976.** Soil Survey of Louisa County, Virginia, U.S. Department of Agriculture, Soil Conservation Service, J. Carter, March 1976.

**Cederstrom, 1957**. Structural Geology of Southeastern Virginia, American Association of Petroleum Geologists Bulletin, Volume 29, D. Cederstrom, 1957.

**CFR, 2007.** Geologic and Seismic Siting Criteria, Title 10, Code of Federal Regulations, Part 100.23, 2007.

**Chapman, 1994.**  Seismic Hazard Assessment for Virginia, Virginia Tech Seismological Observatory, Department of Geological Sciences, M. Chapman and F. Krimgold, February 1994.

**Clark, 1992.**  Central Appalachian Periglacial Geomorphology, A Field Excursion Guidebook under the auspices of the 27th International Geographical Congress, Commission on Frost Action Environments, Agronomy Series Number 120, G. Clark,  R. Behling, D. Braun, E. Ciolkosz, J. Kite, and B. Marsh, August 1992.

**Cleaves, 1968.** Geologic Map of Maryland, Maryland Geologic Survey, 1 sheet, scale 1:250,000, E. Cleaves, J. Edwards, Jr, and J. Glaser, 1968.

**Cleaves, 2000.** Regoliths of the Middle-Atlantic Piedmont and Evolution of a Polymorphic Landscape, Southeastern Geology, Volume 39, Numbers 3 and 4, p 199-122, E. Cleaves, October 2000.

**Coblentz.** Statistical Trends in the Intraplate Stress Field, Journal of Geophysical Research, Volume 100, 20,245–20, 255, D. Coblentz, and R. Richardson, 1995.

**Colman, 1989.**  Quaternary Geology of the Southern Maryland Part of the Chesapeake Bay, U.S Geological Survey, MF-1948-C, Scale 1:125,000, 3 plates, S. Colman, and J. Halka, 1989.

**Colman, 1990.**  Ancient channels of the Susquehanna River beneath Chesapeake Bay and the Delmarva Peninsula, Geological Society of America Bulletin, Volume 102, p 1268-1279, S. Colman, J. Halka, C. Hobbs, R. Mixon, and D. Foster, 1990.

**Colton, 1970.**  The Appalachian Basin – Its Depositional Sequences and Their Geologic Relationships, Chapter 2 in Studies of Appalachian Geology: Central and Southern by G. Fisher, F. Pettijohn, J. Reed, Jr, and K. Weaver, Interscience Publishers, G. Colton, 1970.

**Conners, 1986.**  Quaternary Geomorphic Processes in Virginia, in The Quaternary of Virginia – A Symposium Volume, edited by J. McDonald and S. Bird, Virginia Division of Mineral Resources, Publication 75, J. Conners, 1986.

**CEG, 2005.** Calvert Cliffs Independent Spent Fuel Storage Installation, Updated Environmental Report, Volume 3, Revision 7, Constellation Energy Group, 2005.

**Coruh, 1988.**  Seismogenic Structures in the Central Virginia Seismic Zone, Geology, Volume 16, p 748-751, C.Coruh, G. Bollinger, and J. Costain, August 1988.

**Crone, 2000.**  Data for Quaternary Faults, Liquefaction Features, and Possible Tectonic Features in the Central and Eastern United States, east of the Rocky Mountain front, U.S. Geological Survey Open-File Report 00-260, A. Crone and R. Wheeler, 2000.

**Dahlen, 1981.**  Isostacy and Ambient State of Stress in the Oceanic Lithosphere, Journal of Geophysical Research, Volume 86, p 7801–7807, F. Dahlen, 1981.

**DM, 1973.**  Supplemental Geologic Data, North Anna Power Station, Louisa County, Virginia, Virginia Electric and Power Company Report, , Dames and Moore, August 17, 1973.

**DM, 1977a.**  A Seismic Monitoring Program at the North Anna Site in Central Virginia, January 24, 1974 through August 1, 1977, for Virginia Electric and Power Company, Dames and Moore, September 13, 1977.

**DM, 1977b.** Lateral Continuity of a Pre- or Early Cretaceous Erosion Surface Across Neuschel's Lineament Northern Virginia, for Virginia Electric and Power Company, Dames and Moore, April 1977.

**Daniels, 1985.** Geologic Interpretation of Basement Rocks of the Atlantic Coastal Plain, United States Department of Interior Geological Survey Open-File Report 85-655, D. Daniels and G. Leo, 1985.

**Darton, 1950.** Configuration of the Bedrock Surface of the District of Columbia and Vicinity, Maryland Geological Survey, 4 sheets, scale 1:31,680, N. Darton, 1950.

**Dischinger, 1987.** Late Mesozoic and Cenozoic Stratigraphic and Structural Framework near Hopewell, Virginia, U.S. Geological Survey Bulletin 1567, p 48, J. Dischinger, 1987.

**Dominion, 2004a.** Response to 6/1/04 RAI 2.5.1-5, 2.5.1-6, 2.5.3-2, and 2.5.1-5, Letter No. 5, U.S. Nuclear Regulatory Committee, Serial No. 04-347, and Docket No. 52-008, Dominion, 2004.

**Dominion, 2004b.** Response to 4/15/04 RAI 2.5.1-1 to 2.5.1-4, 2.5.2-2 to 2.5.2-4, and 2.5.3-1, Letter No. 3, U.S. Nuclear Regulatory Committee, Serial No. 04-270, and Docket No. 52-008, Dominion, 2004.

**Drake, 1989.** The Taconic Orogen, in Hatcher, R.D. William T., and Viele, G.W., eds., The Appalachian –Ouachita Orogen in the United States, DNAG, Volume F-2, p 101-177, A. Drake Jr, A. Sinha, J. Laird, and R. Guy, 1989.

**Drake, 1999.** Geologic map of the Seneca quadrangle, Montgomery County, Maryland, and Fairfax and Loudon Counties, Virginia, U.S. Geological Survey, Geologic Quadrangle Map GQ-1802, A. Drake Jr, S. Southworth, and K. Lee, 1999.

**Drake, 1996.** Bedrock Geological Map of Northern New Jersey, U.S. Geological Survey, 2 sheets, scale 1:100,000, A. Drake Jr, R. Volkert, D. Monteverde, G. Herman, H. Houghton, R. Parker, and R. Dalton, 1996.

**Dryden, 1932.** Faults and joints in the Costal Plain of Maryland, Journal of the Washington Academy of Sciences, Volume 22, p 469-472, A. Dryden Jr, 1932.

**Ebel, 2002.** Earthquakes in the Eastern Great Lakes Basin from a regional perspective, Tectonophysics, p 17-30, J. Ebel and M. Tuttle, 2002.

**Edwards, 1981.** A Brief Description of the Geology of Maryland, Maryland Geological Survey, Pamphlet Series, J. Edwards Jr, 1981, Website: www.mgs.md.gov/esic/brochures/mdgeology.html, Date accessed: June 25, 2007.

**EPRI, 1986.** Seismic Hazard Methodology for the Central and Eastern United States, EPRI Report NP-4726, Electric Power Research Institute, July 1986.

**Ervin, 1975.** Reelfoot Ridft: reactivated precursor to the Mississippi Embayment, Geological Society of America Bulletin, Volume 86, Number 9, p 1287-1295, C. Ervin and L. McGinnis, 1975.

**Faill, 1997a.** A Geologic History of the North-Central Appalachians, Part 1, Orogenesis from the Mesoproterozoic through the Taconic Orogeny, Journal of Science, Volume 297, p 551–619, R. Faill, 1997.

**Faill, 1997b.** A Geologic History of the North-Central Appalachians, Part 2, The Appalachian basin from the Silurian through the Carboniferous, Journal of Science, Volume 297, p 729-761, R. Faill, 1997.

**Faill, 1998.** A Geologic History of the North-Central Appalachians, Part 3, The Allegheny Orogeny, American Journal of Science, Volume 298, p 131–179, R. Faill, February 1998.

**Fenneman, 1946.** Physical Divisions of the United States, U.S. Geological Survey, 1:7,000,000-scale map, N. Fenneman and D. Johnson, 1946.

**Fichter, 2000.** The Geological Evolution of Virginia and the Mid-Atlantic Region: Chronology of Events in the Geologic History of Virginia, Stages A through M, James Madison University, L. Fichter and S. Baedke, September 2000, Website: geollab.jmu.edu/vageol/vahist.html, Date accessed: June 25, 2007.

**Fisher, 1964.** Triassic Rocks of Montgomery County in Geology of Howard and Montgomery Counties, Maryland Geological Survey, p 10-17, G. Fisher, 1964.

**Fleming, 1994.** Geologic Map of the Washington West Quadrangle, District of Columbia, Montgomery and Prince Georges Counties, Maryland, and Arlington and Fairfax Counties, Virginia, U.S. Geological Survey, 1 sheet, scale 1:24,000, A. Fleming, A. Drake Jr, and L. McCartan, 1994.

**Frankel, 2002.** Documentation for the 2002 Update of the National Seismic Hazard Maps: U.S. Geological Survey Open-File Report 02-420, A. Frankel, M. Petersen, C. Mueller, K. Haller, R. Wheeler, E. Leyendecker, R. Wesson, S. Harmsen, C. Cramer, D. Perkins, and K. Rukstales, 2002.

**Froelich, 1975.** Preliminary Geologic Map, District of Columbia, U.S. Geological Survey, 1 sheet, scale 1: 24,000, A. Froelich and J. Hack, 1975.

**Frye, 1986.** Roadside Geology of Virginia, Mountain Press Publishing Company, K. Frye, 1986.

**Glaser, 1971.** Geology and mineral resources of Southern Maryland: Maryland Geological Survey Report of Investigations No 15, 85 p., J. Glaser, 1971.

**Glaser, 1994.** Geologic Map of Calvert County, Department of Natural Resources Maryland Geological Survey, scale 1:62,500, J. Glaser, 1994.

**Glaser, 2003a.** Geologic Map of Prince George's County, Maryland, Maryland Geological Survey, 1 sheet, scale 1:62,500, J. Glaser, 2003.

**Glaser, 2003b.** Geologic Map of the Broomers Island Quadrangle, Calvert and St. Mary's Counties, Maryland, Maryland Geological Survey, 1 sheet, scale 1: 24,000, J. Glaser, 2003.

**Glaser, 2003c.** Geologic Map of the Cove Point Quadrangle, Calvert County, Maryland, Maryland Geological Survey, 1:24,000 scale, J. Glaser, 2003c.

**Glover, 1995a.** E-3 Southwestern Pennsylvania to Baltimore Canyon Trough, Geological Society of America Centennial Continent/Ocean Transect #19, L. Glover III, and K. Klitgord, 1995.

**Glover, 1995b.** Chapter 1, Tectonics of the central Appalachian orogen in the vicinity of corridor E-3, with implications for tectonics of the southern Appalachians, in L. Glover III and K.

Klitgord, Chief Compilers, E-3 Southwestern Pennsylvania to Baltimore Canyon Trough, Geological Society of America Continent/Ocean Transect #19, Explanatory Pamphlet, p 2–49, L. Glover III, J. Costain, and C. Coruh, 1995.

**Hack, 1989.** Geomorphology of the Appalachian Highlands, R. Hatcher Jr, W. Thomas, and G. Viele, eds., The Geology of North America, Volume F-2, The Appalachian-Ouachita Orogen in the United States, Geological Society of America, J. Hack, 1989.

**Hansen, 1978.** Upper Cretaceous (Senonian) and Paleocene (Danian) Pinchouts on the South Flank of the Salisbury Embayment, Maryland and their relationship to antecedent basement structures, Department of Natural Resources Maryland Geological Survey Report of Investigations No. 29, p 36, H. Hansen, 1978.

**Hansen, 1984.** Summary of Hydrogeologic Data from a Deep (2678 ft.) Well at Lexington Park, St. Mary's County, Maryland, Maryland Geological Survey Open File Report No. 84-02-1, H. Hansen and J. Wilson, 1984.

**Hansen, 1986.** The Lithology and Distribution of Pre-Cretaceous basement rocks beneath the Maryland Coastal Plain, Department of Natural Resources Maryland Geological Survey Report of Investigations No. 44, p 27, H. Hansen and J. Edwards Jr, 1986.

**Hansen, 1988.** Buried rift basin underlying coastal plain sediments, central Delmarva Peninsula, Maryland, Geology, Volume 49, p 779-782, H. Hansen, September 1988.

**Hansen, 1996.** Hydrostratigraphic Framework of the Piney Point-Nanjemoy Aquifer and Aquia Aquifer in Calvert and St. Mary's Counties, Maryland, Maryland Geological Survey, Open-File Report No 96-02-8, p 45, H. Hansen, 1996.

**Harris, 1982.** Interpretive seismic profile along Interstate I-64 from the Valley and Ridge to the Coastal Plain in central Virginia, United States Geological Survey Oil and Gas Investigations Chart OC-123, L. Harris, W. deWitt Jr, and K. Bayer, 1982.

**Hatcher, 1987.** Tectonics of the southern and central Appalachian internides, Annual Reviews of Earth and Planetary Science, Volume 15, p 337–362, R. Hatcher Jr, 1987.

**Hatcher, 1989.** Alleghenian Orogen, in Hatcher, R.D., William, A., Viele, G., eds., The Appalachian-Ouachita Orogen in the United States, Geological Society of America DNAG, Volume F-2, p 233-318, R. Hatcher, W. Thomas, P. Geiser, A. Snoke, S. Mosher, and D. Wiltschko, 1989.

**Hibbard, 1995.** Orogenesis exotic to the Iapetan cycle in the Southern Appalachians, J. Hibbard, C. van Staal, and P. Cawood, eds., Current Perspectives in the Appalachian-Caledonian Orogen, Special Paper - Geological Association of Canada, Volume 41, p 191-206, J. Hibbard and S. Samson, 1995.

**Hibbard, 2002.** The Carolina Zone: overview of Neoproterozoic to early Paleozoic per-Gondwanan terranes along the eastern flank of the southern Appalachians, Earth Science Reviews, Volume 57, p 299-399, J. Hibbard, E. Stoddard, D. Secor, and A. Dennis, 2002.

**Hibbard, 2007.** A Comparative Analysis of Pre-Silurian Crustal Building Blocks of the Northern and the Southern Appalachian Orogen, American Journal of Science, Volume 307, p 23, J. Hibbard, C. van Staal, and D. Rankin, 2007.

**Hibbard, 2006.** Lithotectonic map of the Appalachian orogen, Canada – United States of America, Geological Survey of Canada Map 02096A, 2 sheets, Scale1:1,500,000, J. Hibbard, C. van Staal, D. Rankin, and H. Williams, 2006

**Higgins, 1986.** Geologic Map of Cecil County, State of Maryland, U.S. Geological Survey, 1 sheet, Scale 1:62500, M. Higgins and L. Conant, 1986.

**Hinze, 1987.** Magnetic Anomaly map of North America, Decade of North American Geology (DNAG), Geological Society of America, Scale 1:5,000,000, 5 plates, W. Hinze and P. Hood, 1987.

**Hittelman, 1994.** Geophysics of North America, National Oceanic and Atmospheric Administration, A. Hittelman, J. Kinsfather, and H. Meyers, 1994.

**Horton, 1989.** Tectonostratigraphic terranes and their Paleozoic boundaries in the central and southern Appalachians. Geological Society of America, Special paper 230, p 213-245, J. Horton, A. Drake, and D. Rankin, 1989.

**Horton, 1991.** Preliminary Tectonostratigraphic Terrane Map of the Central and Southern Appalachians, U.S. Geological Survey Miscellaneous Investigations Series Map I-2163, J. Horton, A. Drake, D. Rankin, and R. Dallmeyer, 1991.

**Hunt, 1967.** Physiography of the United States, W.H. Freeman and Company, p 480, C. Hunt, 1967.

**Hunt, 1972.** Geology of Soils; Their Evolution, Classification, and Uses, W.H. Freeman and Company, p 344, C. Hunt, 1972.

**Jacobeen, 1972.** Seismic Evidence for High Angle Reverse Faulting in the Coastal Plain of Prince Georges and Charles County, Maryland, Maryland Geological Survey, Information Circular No. 13, F. Jacobeen Jr, 1972.

**Johnson, 1973.** Bouguer gravity of northeastern Virginia and the Eastern Shore Peninsula, Virginia Division of Mineral Resources Report of Investigations 32, p 48, S. Johnson, 1973.

**Johnston, 1985a.** Seismotectonics of the Southern Appalachians, Bulletin of the Seismological Society of America, Volume 75, Number 1, p 291-312, A. Johnston, D. Reinbold, and S. Brewer, 1985.

**Johnston, 1985b.** A basement block model for Southern Appalachian seismicity, Geological Society of America - Abstracts with Programs, Volume 17, Number 2, p 97, A. Johnston, and D. Reinbold, 1985.

**Johnston, 1994.** The Earthquakes of Stable Continental Regions: Volume 1 - Assessment of Large Earthquake Potential, EPRI, TR-102261-V1, A. Johnston, K. Coppersmith, L. Kanter, and C. Cornell, 1994.

**Kafka, 1985.** Earthquake Activity in the Greater New York City Area: Magnitudes, Seismicity, and Geologic Structures, Bulletin of the Seismological Society of America, Volume 75, Number 5, p 1285-1300, A. Kafka, E. Schlesinger-Miller, and N. Barstow, 1985.

**Kafka, 1989.** Earthquake activity in the greater New York City area—A faultfinder's guide, in Weiss, D., ed. Field trip guidebook: New York State Geological Association, 61st Annual Meeting,

Middletown, New York, October 13-15, 1989, Guidebook, p 177-203, A. Kafka, M. Winslow, and N. Barstow, 1989.

**Kidwell, 1988.** Reciprocal sedimentation and noncorrelative hiatuses in marine-paralic siliciclastics: Miocene outcrop evidence, Geology, Volume 16, p 609-612, S. Kidwell, 1988.

**Kidwell, 1997.** Anatomy of Extremely Thin Marine Sequences Landward of a Passive-Margin Hinge Zone: Neogene Calvert Cliffs Succession, Maryland, Journal of Sedimentary Research, Volume 67, Number 2, p 322-340, S. Kidwell, 1997.

**Kim, 2005.** The 9 December 2003 Central Virginia Earthquake Sequence: A Compound Earthquake in the Central Virginia Seismic Zone: Bulletin of the Seismological Society of America, Volume 95, Number 6, p 2428-2445, W. Kim and M. Chapman, 2005.

**King, 1978.** The new York-Alabama lineament: geophysical evidence for a major crustal break in the basement beneath the Appalachian basin, Geology, Volume 6, p 312-318, E. King and I. Zietz,  1978.

**Klitgord, 1979.** Basin structure of the U.S. Atlantic margin, J. Watkins, L. Montadert, and P. Dickerson, eds, Geological and geophysical investigations of continental margins: American Association of Petroleum Geologists Memoir 29, p 85-112, K. Klitgord and J. Behrendt, 1979.

**Klitgord, 1988.** U.S. Atlantic continental margin; Structural and tectonic framework, R. Sheridan and J. Grow, eds., The Atlantic Continental Margin, U.S., Geological Society of America, The Geology of North America, Volume I-2, p 19-55, K. Klitgord, D. Hutchinson, and H. Schouten, 1988.

**Klitgord, 1995.** Mid-Atlantic Continental Margin: The Mesozoic-Cenozoic Continent-Ocean Boundary, in L. Glover III, and K. Klitgord, Chief Compilers, E-3 Southwestern Pennsylvania to Baltimore Canyon Trough, Geological Society of America Continent/Ocean Transect #19, Explanatory Pamphlet, K. Klitgord, C. Poag, L. Glover, R. Sheridan, D. Hutchinson, R. Mixon, and R. Benson, 1995.

**Lane, 1983.** Physiographic Provinces of Virginia, Virginia Geographer, Volume XV, Fall-Winter, C. Lane, 1983.

**Lefort, 1989.** Is there an Archean crust beneath Chesapeake Bay (abs): Abstracts, 28th International Geological Congress, p 2-227, J. Lefort and M. Max, July 1989.

**LeTourneau, 2003.** Tectonic and climatic controls on the stratigraphic architecture of the Late Triassic Taylorsville Basin, Virginia and Maryland, P. Olsen, eds., The great rift valleys of Pangea in eastern North America, Sedimentology, Stratigraphy and Paleontology, Volume 2, p 12-58, P. LeTourneau, 2003.

**LeVan, 1963.** A magnetic survey of the Coastal Plain in Virginia, Virginia Division of Mineral Resources Report of Investigations 4, p 17, D. LeVan and R. Pharr, 1963.

**Lyons, 1982.** Gravity anomaly map of the United States, Society of Exploration Geophysicists, scale 1:2,500,000, sheets, P. Lyons, N. O'Hara, 1982.

**Manspeizer, 1989.** Post-Paleozoic Activity, Geology of North America, Volume F-2, The Appalachian-Ouachita Orogen in the United States, Geological Society of America, W.

Manspeizer, J. DeBoer, J. Costain, A. Froelich, C. Coruh, P. Olsen, G. McHone, J. Puffer, and D. Prowell, 1989.

**Markewich, 1990.** Contrasting Soils and Landscapes of the Piedmont and Coastal Plain, Eastern United States, Geomorphology, Volume 3, p 417–447, H. Markewich, M. Pavich, and G. Buell, 1990.

**Marple, 1993.** Evidence for Possible Tectonic Upwarping Along the South Carolina Coastal Plain from an Examination of River Morphology and Elevation Data, Geology, Volume 21, p 651–654, R. Marple and P. Talwani, 1993.

**Marple, 2000.** Evidence for a Buried Fault System in the Coastal Plain of the Carolinas and Virginia - Implications for Neotectonics in the Southeastern United Sates, Geological Society of America Bulletin, Volume 112, Number 2, p 200–220, R. Marple and P. Talwani, February 2000.

**Marple, 2004a.** Relationship of the Stafford fault zone to the right-stepping bends of the Potomac, Susquehanna, and Delaware Rivers and related upstream incision along the U.S. Mid-Atlantic fall line; in Southeastern Geology, Volume 42, Number 3, p 123-144, R. Marple, 2004.

**Marple, 2004b.** Proposed Shenandoah Fault and East Coast-Stafford Fault System and Their Implications for Eastern U.S. Tectonics, Southeastern Geology, Volume 43, Number 2, p 57-80, R. Marple and P. Talwani, 2004.

**MGS, 2007.** Physiographic Provinces and their Subdivisions in Maryland, Maryland Geological Survey, 2007, Website: http://www.mgs.md.gov, Date accessed: June 25, 2007.

**McCartan, 1989a.** Geologic Map of Charles County, Maryland, Maryland Geological Survey, 1 sheet, Scale 1:62,500, L. McCartan, 1989.

**McCartan, 1989b.** Geologic Map of St. Mary's County, Maryland: Maryland Geological Survey map, Scale 1:62,500, L. McCartan, 1989.

**McCartan, 1989c.** Atlantic Coastal Plain Sedimentation and Basement Tectonics Southeast of Washington, D.C., Field Trip Guide Book T214, 28th International Geological Congress, July 13, L. McCartan, 1989.

**McCartan, 1990.** Geologic Map of the Coastal Plain and Upland Deposits, Washington, D.C., Maryland, and Virginia, U.S. Geological Survey, 1 sheet, Scale 1:24,000, L. McCartan, 1990.

**McCartan, 1995.** Geologic Map and Cross Sections of the Leonardtown 30 X 60 minute quadrangle, Maryland and Virginia. U.S. Geological Survey Open-file report OFR 95-665, p 38, 1 plate, L. McCartan, W. Newell, J. Owens and G. Bradford, 1995.

**McLaughlin, 2002.** Results of Trenching Investigations along the New Castle Railroad Survey-1 Seismic Line, New Castle, Delaware, Delaware Geological Survey, Open File Report 43, p 17, P. McLaughlin, S. Baxter, K. Ramsey, T. McKenna, S. Strohmeier, 2002.

**Milici, 1991.** Preliminary geologic section across the buried part of the Taylorsville basin, Essex and Caroline Counties, Virginia: Virginia Division of Mineral resources Open File Report 91-1, p 31, R. Milici, K. Bayer, P. Pappano, J. Costain, C. Coruh, J. Cahit, 1991

**Milici, 1995.** Structural Section Across the Atlantic Coastal Plain, Virginia and Southeasternmost Maryland, Virginia Division of Mineral Resources, Publication 140, 2 plates, R. Milici, J. Costain, C. Coruh, and P. Pappano, 1995.

**Mixon, 1977**. Stafford Fault System: Structures Documenting Cretaceous and Tertiary Deformation Along the Fall Line in Northeastern Virginia, Geology, Volume 5, p 437–440, R. Mixon and W. Newell, 1977.

**Mixon, 1978.** The Faulted Coastal Plain Margin at Fredericksburg, Virginia, Tenth Annual Virginia Geology Field Conference, R. Mixon and W. Newell, October 1978.

**Mixon, 1984.** Folds and faults in the Inner Coastal Plain of Virginia and Maryland – Their effects on distribution and thickness of Tertiary rock units and local geomorphic history, in Frederiksen, N.O., and Krafft, K., eds., Cretaceous and Tertiary stratigraphy, paleontology, and structure, southwestern Maryland and northeastern Virginia: Field trip volume and guidebook (for field trip held October 17, 1984), Reston, Va. American Association of Stratigraphic Palynologists, p 112-122, R. Mixon and D. Powars, 1984.

**Mixon, 1989.** Geologic Map and Generalized Cross Sections of the Coastal Plain and Adjacent Parts of the Piedmont, Virginia, U.S. Geological Survey, Miscellaneous Investigations Series Map I-2033, 2 sheets, Scale 1:250,000, R. Mixon, C. Berquist, W. Newell, G. Johnson, D. Powers, J. Schindler, and E. Rader, 1989.

**Mixon, 1992.** Nature and Timing of Deformation of Upper Mesozoic and Cenozoic Deposits in the Inner Atlantic Coastal Plain, Virginia and Maryland, U.S. Geological Survey Circular C1059, p 65-73, R. Mixon, D. Powars, and D. Daniels, 1992.

**Mixon, 2000.** Geologic Map of the Fredericksburg 30' x 60' Quadrangle, Virginia and Maryland, U.S. Geological Survey, Geologic Investigations Series Map I-2607, R. Mixon, L. Pavlides, D. Powars, A. Froelich, R. Weems, J. Schindler, W. Newell, L. Edwards, and L. Ward, 2000.

**Nelson, 1962.** Geology and Mineral resources of Albermarle County, Virginia Division of Mineral Resources Bulletin 77, 92 p., 1 folded map, Scale 1:62,500, W. Nelson, 1962.

**Nelson, 1980.** Determination of Holocene fault movement along the Ramapo fault in southeastern New York using pollen stratigraphy, Geological Society of America Abstracts with Programs, Volume 12, Number 2, p 75, S. Nelson, 1980.

**Nelson, 1981.** The Clingman Lineament; Aeromagnetic Evidence for a Major Discontinuity in the North American Basement, Geological Society of America, Southeastern Section, Abstracts with Programs, Volume 13, Number 1, p 31, A. Nelson and I. Zietz, January 1981.

**Newell, 1976.** Detailed Investigation of a Coastal Plain-Piedmont Fault Contact in Northeastern Virginia, U.S. Geological Survey Open-File Report 76-329, W. Newell, D. Prowell, and R. Mixon, 1976.

**Newman, 1983.** Holocene neotectonics of the lower Hudson Valley: Geological Society of America Abstracts with Programs, Volume 15, Number 3, p 148, W. Newman, L. Cinquemani, J. Sperling, L. Marcus, and R. Pardi, 1983.

**NRC, 1978.** Standard Format and Content of Safety Analysis Reports for Nuclear Power Plants, LWR Edition, Regulatory Guide 1.70, Revision 3, U.S. Nuclear Regulatory Commission, November 1978.

**NRC, 1997.** Identification and Characterization of Seismic Sources and Determination of Safe Shutdown Earthquake Ground Motion, U.S. Nuclear Regulatory Commission, Regulatory Guide 1.165, March 1997.

**NRC, 2005.** Safety Evaluation Report for an Early Site Permit (ESP) at the North Anna ESP Site – NUREG-1835, Nuclear Regulatory Commission, September 2005.

**NRC, 2007.** Basis Geologic and Seismic Information, Regulatory Guide 1.206, Section 2.5.1, U.S. Nuclear Regulatory Commission, June, 2007.

**Obermier, 1998.** Paleoliquefaction Evidence for Seismic Quiescence in Central Virginia During the Late and Middle Holocene Time (abs), Eos Transactions of the American Geophysical Union, Volume 79, Number 17, p S342, S. Obermier and W. McNulty, 1998.

**Otton, 1955.** Ground-Water Resources of the Southern Maryland Coastal Plain, Maryland Department of Geology, Mines and Water Resources, Bulletin 15, p 347, E. Otton, 1955.

**Owens, 1979.** Upper Cenozoic Sediments of the Lower Delaware Valley and the Northern Delmarva Peninsula, New Jersey, Pennsylvania, Delaware, and Maryland, Geological Survey Professional Paper 1067-D, U.S. Geological Survey, J. Owens and J. Minard, 1979

**Owens, 1998.** Bedrock geologic map of central and southern New Jersey, U.S. Geological Survey M.I. Series Map I-2540-B, 4 sheets, Scale 1:100,000, J. Owens, P. Sugarman, N. Sohl, R. Parker, H. Houghton, R. Volkert, Jr., and R. Orndoff, 1998

**Pavlides, 1980.** Revised Nomenclature and Stratigraphic Relationships of the Fredericksburg Complex and Quantico Formation of the Virginia Piedmont, U.S. Geological Survey Professional Paper 1146, L. Pavlides, 1980.

**Pavlides, 1983.** Late Cenozoic faulting along the Mountain Run Fault Zone, central Virginia Piedmont, GSA Abstracts with Programs, Volume 15, Number 2, L. Pavlides, 1983.

**Pavlides, 1986.** Mountain Run Fault Zone of Virginia, U.S. Geological Survey Open-File Report 87-93, 93–94, L. Pavlides, 1986.

**Pavlides, 1989.** Early Paleozoic Composite Mélange Terrane, Central Appalachian Piedmont, Virginia and Maryland: Its Origin and Tectonic History, Geological Society of America Special Paper 228, p 135–193, L. Pavlides, 1989.

**Pavlides, 1994.** Early Paleozoic Alkalic and Calc-Alkalic Plutonism and Associated Contact Metamorphism, Central Virginia Piedmont, U.S. Geological Survey Professional Paper 1529, L. Pavlides, J. Arth, J. Sutter, T. Stern, and H. Cortesini Jr, 1994.

**Pavlides, 2000.** Geology of the Piedmont and Blue Ridge Provinces, Chapter II of the pamphlet to accompany the U.S. Geological Survey, Geologic Investigations Series Map I-2607, L. Pavlides, 2000.

**Pazzaglia, 1993.** Stratigraphy, petrography, and correlation of late Cenozoic middle Atlantic Coastal Plain deposits: Implications for late-stage passive-margin geologic evolution, Geological Society of America Bulletin, Volume 105, p 1617-1634, F. Pazzaglia, 1993.

**Pazzaglia, 1993.** Fluvial terraces of the lower Susquehanna River, Geomorphology, Volume 8, p 83-113, F. Pazzaglia and T. Gardner, 1993.

**Pazzaglia, 1994.** Late Cenozoic flexural deformation of the middle U.S. Atlantic passive margin, Journal of Geophysical Research, Volume 99, Number B6, p 12, 143-12, 157, F. Pazzaglia and T. Gardner, 1994.

**Poag, 1991.** Rise and demise of the Bahama-Grand Banks gigaplatform, northern margin of the Jurassic proto-Atlantic seaway, Marine Geology, Volume 102, p 63-130, C. Poag, 1991.

**Poag, 2004.** The Chesapeake Bay Crater; geology geophysics of a late Eocene submarine impact structure, Springer-Verland: Berlin, p 522, W. Poag, C. Koeberl, and W. Reimold, 2004.

**PEPC, 1973.** Preliminary safety analysis report, Douglas Point Nuclear Generating Station, Units 1 and 2, Volume 2, Dames and Moore for the Potomac Electric Power Company, Docket Number 50448-2 and 50449-2, 1973.

**Powars, 1999.** The effects of the Chesapeake Bay Impact Crater on the Geological Framework and Correlation of Hydrogeologic Units of the Lower York-James Peninsula, Virginia, U.S. Geological Survey Professional Paper 1612, p 82, 9 plates, D. Powars and T. Bruce, 1999.

**Prowell, 1983**. Index of Faults of Cretaceous and Cenozoic Age in the Eastern United States, U.S. Geological Survey Miscellaneous Field Studies Map MF-1269, D. Prowell, 1983.

**PSEG, 2002**. Section 2.5, Geology, Seismology, and Geotechnical Engineering, Updated Final Safety Analysis Report, Revision 12, Hope Creek Generating Station, submitted to the NRC (LR-N02-0179), 2002.

**Rader, 1993.** Geologic map of the Virginia – expanded explanation: Virginia Division of Mineral Resources, E. Rader and N. Evans, eds., 1993.

**Ratcliffe, 1971.** The Ramapo fault system in New York and Adjacent Northern New Jersey—A case of tectonic heredity, Geological Society of America Bulletin, Volume 82, p 125-142, N. Ratcliffe, 1971.

**Ratcliffe, 1980.** Brittle faults (Ramapo fault) and phyllonitic ductile shear zones in the basement rocks of the Ramapo seismic zones New York and New Jersey, and their relationship to current seismicity, in Manspeizer, W., ed., Field studies of New Jersey geology and guide to field trips Newark, New Jersey, Rutgers University, Geology Department, U.S., New York State Geological Association, 52nd annual meeting, October 10, 1980, Guidebook, p 278-312, N. Ratcliffe, 1980.

**Ratcliffe, 1982.** Results of core drilling of the Ramapo fault at Sky Meadow Road, Rockland County, New York, and assessment of evidence for reactivation to produce current seismicity, U.S. Geological Survey Miscellaneous Investigations, Map I-1401, 1 sheet, N. Ratcliffe, 1982.

**Ratcliffe, 1986.** Seismic Reflection Geometry of the Newark Basin Margin in Eastern Pennsylvania, NUREG/CR-4676, N. Ratcliffe, W. Burton, R. D' Angelo, and J. Costain, 1986.

**Ratcliffe, 1990.** Orientation, movement history, and cataclastic rocks of Ramapo fault based on core drilling and trenching along the western margin of the Newark basin near Bernardsville, New Jersey, U.S., Geological Survey Miscellaneous Investigations, Map I-1982, 1 sheet, N. Ratcliffe, W. Burton, and M. Pavich, 1990.

**Richardson, 1991.** North American Plate Dynamics, Journal of Geophysical Research, Volume 96, R. Richardson and L. Reding, 1991.

**Rodgers, 1970.** The tectonics of the Appalachians, Wiley-Interscience: New York, NY, p 271, J. Rodgers, 1970.

**Sanders, 1963.** Late Triassic tectonic history of northeaster United States, American Journal of Science 261, p 501-524, J. Sanders, 1963.

**Savy, 2002.** Guidance for Performing Probabilistic Seismic Hazard Analysis for a Nuclear Plant Site: Example Application to the Southeastern United States, Nuclear Regulatory Commission, NUREG-CR/6607, J. Savy, W. Foxall, N. Abrahamson, and D. Bernreuter, 2002.

**Sbar, 1975.** The Delaware-New Jersey earthquake of February 28, 1973, Bulletin of the Seismological Society of America, Volume 65, p 85-92, M. Sbar, R. Jordan, C. Stephens, T. Pickett, K. Woodruff, and C. Sammis, 1975.

**Scharnberger, 2006.** The Lancaster Seismic Zone of southeast Pennsylvania in relation to the Gettysburg-Newark basin, Geological Society of America Abstracts with Programs, Volume 38, Number 2, p 83, C. Scharnberger, 2006

**Schlische, 1992.** Structural and Stratigraphic Development of the Newark Extension Basin, Eastern North America: Evidence for the Growth of the Basin and its Bounding Structures, Geological Society of America Bulletin, Volume 104, p 1246-1263, R. Schlische, October 1992.

**Schlische, 2003.** Progress in Understanding the Structural Geology, Basin Evolution, and Tectonic History of the Eastern North America Rift System, P. LeTourneau and P. Olsen, eds., The Great Rift Valleys of Pangea in Eastern North America, Volume 1, R. Schlische, 2003.

**Schmidt, 1992.** Maryland's Geology, Tidewater Publishers, Centreville, Maryland, p 164, M. Schmidt Jr, 1992.

**Schruben, 1994.** Geology of the conterminous United States at 1:250,000, 000 scale; a digital representation of the 1974 P. B. King and H. M. Beikman map, U.S. Geological Survey Digital Data Series DDS-0011, P. Schruben, R. Arndt, W. Bawiec, and R. Ambroziak, 1994.

**Schwab, 1997a.** Initial results of high-resolution sea-floor mapping offshore of the New York–New Jersey metropolitan area using sidescan sonar, Northeastern Geology and Environmental Sciences Volume 9, Number 4, p 243–262, W. Schwab, M. Allison, W. Corso, L. Lotto, B. Butman, M. Bucholtz ten Brink, J. Denny, W. Danforth, and D. Foster, 1997.

**Schwab, 1997b.** Mapping the sea floor offshore of the New York–New Jersey metropolitan area using sidescan sonar—preliminary report, U.S. Geological Survey Open-File Report 97-61, 3 sheets, W. Schwab, W. Corso, M. Allison, B. Butman, J. Denny, L. Lotto, W. Danforth, D. Foster, T. O'Brien, D. Nichols, B. Irwin, and K. Parolski, 1997.

**Scott, 2006.** Correlating Late Pleistocene Deposits on the Coastal Plain of Virginia with the Glacial-Eustatic sea-level curve (MS Thesis), Old Dominion University, p 112, T. Scott, May 2006.

**Seeber, 1998.** The 1994 Cacoosing Valley earthquakes near Reading, Pennsylvania: A shallow rupture triggered by quarry unloading, Journal of Geophysical Research, Volume 103, Number B10, p 24, 505-24, 521, L. Seeber, J. Armbruster, W. Kim, N. Barstow, and C. Scharnberger, 1998.

**Sevon, 2000.** Regolith in the Piedmont Upland section, Piedmont Province, York, Lancaster, and Chester Counties, Southeastern Pennsylvania, Southeastern Geology, Volume 39, Number 3 and 4, p 223–241, W. Sevon, October 2000.

**Sheridan, 1988.** The Atlantic Continental Margin, U.S.Geological Society of America, The Geology of North America, Volume 1-2, p 610, R. Sheridan and J. Grow, 1988.

**Sheridan, 1988.** Geophysical Data, R. Sheridan and J. Grow, eds., The Atlantic Continental Margin, U.S. Geological Society of America, The Geology of North America, Volume 1, p 177-196, R. Sheridan, J. Grow, and K. Klitgord, 1988.

**Shumaker, 2000.** The New York-Alabama Lineament; An Early Iapetian Wrench Fault?, American Association of Petroleum Geologists Bulletin, Volume 84, Number 9, p 1393, R. Shumaker, September 2000.

**Spears, 2002.** Geology of the central Virginia Piedmont between the Arvonia syncline and the Spotsylvania high-strain zone, Thirty-Second Annual Virginia Geological Conference, Charlottesville, Virginia, October 11-13, D. Spears and C. Bailey, 2002.

**Spoljaric, 1972.** Geology of the Fall Zone in Delaware, Delaware Geological Survey, p 30, N. Spoljaric, March 1972.

**Spoljaric, 1973.** Normal Faults in Basement Rocks of the Northern Coastal Plain, Delaware, Geological Society of America Bulletin, Volume 84, p 2781-2783, N. Spoljaric, 1973.

**Stanford, 1995.** Possible Pliocene-Pleistocene Movement on a Reactivated Mesozoic Fault In Central New Jersey, Geological Society of America Abstracts with Programs, Volume 27, Number 1, p 83, S. Stanford, D. Jagel, and D. Hall, 1995.

**Stanford, 2002.** Surficial Geology of the Monmouth Junction Quadrangle, Somerset, Middlesex, and Mercer Counties, New Jersey, Department of Environment Protection New Jersey Geological Survey Open-File Map OFM 47, 1 plate, Scale 1: 24,000, S. Stanford, 2002.

**Stone, 1984.** Faults in Pleistocene sediments at trace of Ramapo fault in Geological Survey research, fiscal year 1981, U.S. Geological Survey, Professional Paper 1375, p. 49, B. Stone and N. Ratcliffe, 1984.

**Swanson, 1982.** Preliminary model for early transform history in central Atlantic rifting, Geology, 10:317-320, M. Swanson, 1982.

**Tanner, 1987.** Gravity Anomaly map of North America, Decade of North American Geology (DNAG), Geological Society of America, Scale 1:5,000,000, 5 plates, J. Tanner, 1987.

**Thelin, 1991.** Landforms of the Conterminous United States–A Digital Shaded-Relief Portrayal, U.S. Geological Survey, pamphlet to accompany Geological Investigation Series Map I-2206, G. Thelin and R. Pike, April 17 1991.

**Thurber, 1985.** Crustal structure along the Ramapo fault zone, New York State, Earthquake Notes, Volume 56, p 145-152, C. Thurber and T. Caruso, 1985.

**Turcotte, 2002.** Geodynamics, Cambridge University Press, p 456, D. Turcotte and G. Schubert, 2002.

**URS, 2000.** Seismic Characterization study for the expansion of the Williams Gas Pipeline – Transco LNG facility, Cove Point, Maryland, URS Corporation, October 2000.

**Vigil, 2000.** A Tapestry of Time and Terrain, U.S. Geological Survey, pamphlet to accompany U.S. Geological Survey, Geological Investigation Series Map I-2720, J. Vigil, R. Pike, and D. Howell, February 24, 2000.

**Ward, 2004.** Tertiary Lithology and Paleontology, in Southworth, S. and Burton, W., eds., Geology of the National Capital Region- Field Trip Guidebook: U.S. Geological Survey Circular 1264, p 263-279, L. Ward and D. Powars, 2004.

**Watts, 1982.** Tectonic Subsidence, Flexure, and Global Changes of Sea Level, Nature, Volume 297, p 469-474, A. Watts, 1982.

**Weems, 1998.** Newly Recognized En Echelon Fall Lines in the Piedmont and Blue Ridge Provinces of North Carolina and Virginia, With a Discussion of Their Possible Ages and Origins, U.S. Geological Survey Open-File Report 98-374, R. Weems,1998.

**Wentworth, 1983,** Regenerate Faults of Small Cenozoic Offset - Probable Earthquake Sources in the Southeastern United States, U.S. Geological Survey, Professional Paper 1313-S, C. Wentworth and M. Mergner-Keefer, 1983.

**Wheeler, 1992.** Geologic Implications of Earthquake Source Parameters in Central and Eastern North America, Seismological Research Letters, Volume 63, Number 4, p 491–505, R. Wheeler and A. Johnston, 1992.

**Wheeler, 1995.** Earthquakes and the Cratonward Limit of Iapetan Faulting in Eastern North America, Geology, Volume 23, 105–108, R. Wheeler, 1995.

**Wheeler, 1996.** Earthquakes and the Southeastern Boundary of the Intact Iapetan margin in Eastern North America, Seismological Research letters, Volume 67, Number 5, p 77-83, R. Wheeler, 1996.

**Wheeler, 2005.** Known or Suggested Quaternary Tectonic Faulting, Central and Eastern United States – New and Updated Assessments for 2005, U.S. Geological Survey, Open File Report 2005-1336, p 37, R. Wheeler, 2005.

**Wheeler, 2006.** Quaternary tectonic faulting in the Eastern United States, Engineering Geology, Volume 82, p 165-186, R. Wheeler, 2006.

**Williams, 1983.** Appalachian suspect terranes, R. Hatcher Jr, H. Williams and I. Zietz, eds., Contributions to the Tectonics and Geophysics of Mountain Chains, Geological Society of America Memoir 159, p 33-53, H. Williams and R. Hatcher, 1983.

**Wilson, 1990.** Geology and Hydrologic Assessment of Coastal Plain Aquifiers in the Waldorf Area, Charles County, Maryland, Maryland Geological Survey, Report of Investigations No. 53,138 p., 8 plates, J. Wilson and W. Fleck, 1990.

**Withjack, 1998.** Diachronous rifting drifting, and inversion on the passive margin of eastern North America: An analog for other passive margins, American Association of Petroleum Geologist Bulletin, Volume 82, p 817-835, M. Withjack, R. Schlische, and P. Olsen, 1998.

**Zietz, 1982.** Composite magnetic anomaly map of the United States, Part A: Conterminous United States, U.S. Geological Survey Map GP-54923, Scale 1:2,500,000, I. Zietz, 1982.

**Zoback, 1989a.** Tectonic Stress Field of the Coterminous United States, in L. C. Pakiser and M. D. Mooney, eds., Geophysical Framework of the Continental United States, Geological Society of America Memoir 172, p 523–539, M. Zoback and M. Zoback, 1989.

**Zoback, 1989b.** Global patterns of tectonic stress, Nature, Volume 341, p 291-296, M. Zoback, M. Zoback, J. Adams, M. Assumpcao, S. Bell, E. Bergman, P. Blumling, N. Brereton, D. Denham, J. Ding, K. Fuchs, N. Gay, S. Gregersen, H. Gupta, A. Gvishiani, K. Jacob, R. Klein, P. Knoll, M. Magee, J. Mercier, B. Muller, C. Paquin, K. Rajendran, O. Stephansson, G. Suarez, M. Suter, A. Udias, Z. Xu, and M. Zhizhin,. 1989.

**Zoback, 1992.** Stress Field Constraints on Intraplate Seismicity in Eastern North America, Journal of Geophysical Research, Volume 97, p 11,761–11,782, M. Zoback, 1992.}

## 2.5.2    VIBRATORY GROUND MOTION

The U.S. EPR FSAR includes the following COL Items for Section 2.5.2:

A COL applicant that references the U.S. EPR design certification will review and investigate site-specific details of the seismic, geophysical, geological, and geotechnical information to determine the safe shutdown earthquake (SSE) ground motion for the site and compare site-specific ground motion to the Certified  Seismic Design Response Spectra (CSDRS) for the U.S. EPR.

This COL Item is addressed as follows:

{This section provides a detailed description of the vibratory ground motion assessment that was carried out for the {CCNPP Unit 3} site, resulting in the development of the {CCNPP Unit 3} site Safe Shutdown Earthquake (SSE) ground motion response spectra. {The starting point for this site assessment is the EPRI-SOG probabilistic seismic hazard analysis (PSHA) methodology outlined in EPRI NP-4726-A 1988 (EPRI, 1988) and tectonic interpretations in EPRI NP-4726 1986 (EPRI, 1986).

Nuclear Regulatory Commission (NRC) Regulatory Guide 1.165, "Identification And Characterization of Seismic Sources and Determination of Safe Shutdown Earthquake Ground Motion," March, 1997, (NRC, 1997a) states in Section B, Discussion:

"The CEUS is considered to be that part of the United States east of the Rocky Mountain front, or east of Longitude 105 West (Refs. 4, 5).  To determine the SSE in the CEUS, an accepted PSHA methodology with a range of credible alternative input interpretations should be used.  For sites in the CEUS, the seismic hazard methods, the data developed, and seismic sources identified by Lawrence Livermore National Laboratory (LLNL) (Refs. 4-6) and the Electric Power Research Institute (EPRI) (Ref. 7) have been reviewed and accepted by the staff."

Reference 7 is Electric Power Research Institute, "Probabilistic Seismic Hazard Evaluations at Nuclear Power Plant Sites in the Central and Eastern United States," NP-4726, All Volumes, 1989-1991.  The title and number of the referenced document are not in agreement.  The title of EPRI-4726 is "Seismic Hazard Methodology for the Central and Eastern United States."  No document could be found that had the title provided by the NRC.

In lieu of the reference 7, i.e., EPRI document, NP-4726, All Volumes, 1989-1991, Section 2.5.2 will implement EPRI NP-4726, "Seismic Hazard Methodology for the Central and Eastern United States," 1986 and EPRI-4726-A, "Seismic Hazard Methodology for the Central and Eastern United States,"1988.  EPRI NP-4726-1986 and EPRI-4726-A, 1988 have been determined to be acceptable as described below.

Additionally, the PSHA methodology used for the CCNPP 3 site is described in EPRI NP-6395-D-1989 (EPRI, 1989a).  EPRI NP-6395-D (EPRI, 1989a) has been determined to be an acceptable PSHA methodology by the NRC is also described below.

The NRC has accepted the use of the following, which were included in the North Anna Early Site Permit Application by Dominion Nuclear North Anna, LLC, which was approved in NUREG-1835, Safety Evaluation Report for an Early Site Permit (ESP) at the North Anna Site, 2005. (NRC, 2005)

♦   EPRI 4726, 1986, "Seismic Hazard Methodology for the Central and Easter United States" was included in the Early Site Permit Application as reference 120. It is also specifically included as a reference in Section C of NUREG-1835.

♦   EPRI-NP-6395-D, 1989, "Probabilistic seismic hazard evaluation at nuclear plant sites in the central and eastern United States, Resolution of the Charleston Earthquake Issue."

a.   Early Site Permit Application as reference 115.

b.   Generic Letter 88-20, "Individual Plant Examinations of External Events (IPEEE) for Severe Accident Vulnerabilities" (NRC, 1991)

The NRC has accepted the use of the EPRI NP-4726-A, 1988 in the letter dated Oct 31, 2005, T. Mundy, Exelon to NRC, Subject: Response Supplemental Draft Safety Evaluation Report (DSER) Item, page 16 of 112 and page 54 of 112, (Adams Accession No. ML053120131) (Exelon, 2005).

The EPRI-SOG tectonic interpretations in EPRI NP-4726 1986 (EPRI, 1986). were updated with more recent geological, seismological, and geophysical data under the guidance of NRC Regulatory Guide 1.165, (NRC, 1997a). Sections 2.5.2.1 through 2.5.2.3 document this review and update, as needed, of the EPRI-SOG seismicity, seismic source, and ground motion models.

Section 2.5.2.4 develops PSHA parameters at the site assuming the very hard rock foundation conditions implied by currently accepted ground motion attenuation models.

Section 2.5.2.5 summarizes information about the seismic wave transmission characteristics of the CCNPP Unit 3 site with reference to more detailed discussion of all engineering aspects of the subsurface in Section 2.5.4.

Section 2.5.2.6 describes the development of the horizontal SSE ground motion for the CCNPP Unit 3 site. The selected SSE ground motion is based on the risk-consistent/performance-based approach of Regulatory Guide 1.208, A Performance-Based Approach to Define the Site-Specific Earthquake Ground Motion (NRC, 2007a), with reference to NUREG/CR-6728 (NRC, 2001), NUREG/CR-6769 (NRC, 2002b), and ASCE/SEI 43-05 (ASCE 2005). Horizontal ground motion amplification factors are developed using site-specific data and estimates of near-surface soil and rock properties. These amplification factors are then used to scale the hard rock spectra to develop Uniform Hazard Spectra accounting for site-specific conditions using Approach 2A of NUREG/CR-6728 (NRC, 2001) and NUREG/CR-6769 (NRC, 2002). Horizontal SSE spectra are developed from these soil Uniform Hazard Spectra using the performance-based approach of ASCE/SEI 43-05 (ASCE 2005), as implemented in Regulatory Guide 1.208 (NRC, 2007a). The SSE motion is defined at the free ground surface of a hypothetical outcrop at the base of the nuclear island foundation. See Sections 2.5.4 and 2.5.2.5 for further discussion of the subsurface conditions.

Section 2.5.2.6 also describes vertical SSE spectra, which are developed by scaling the horizontal SSE by a frequency-dependent vertical-to-horizontal (V:H) factor.

The SSE spectra that are described in this section are considered performance goal-based (risk-informed) site specific safe shutdown earthquake response spectra. The SSE spectra, and its specific location at a free ground surface, reflect the seismic hazard in terms of a PSHA and geologic characteristics of the site and represent the site-specific ground motion response spectrum (GMRS) of Regulatory Guide 1.208 (NRC, 2007a). These spectra are expected to be modified as appropriate to develop ground motion for design considerations.

The SSE developed in this section meets the requirements of paragraph (d) of 10 CFR 100.23 (CFR, 2007).}

### 2.5.2.1    Seismicity

The U.S. EPR FSAR includes the following COL Item in Section 2.5.2.1:

   Seismicity is site specific and will be addressed by the COL applicant.

This COL Item is addressed as follows:

{The seismic hazard analysis conducted by EPRI as delineated in NP-6395-D 1989 (EPRI, 1989a) relied, in part, on an analysis of historical seismicity in the central and eastern United States (CEUS) to estimate seismicity parameters (rates of activity and Richter b-values) for individual seismic sources.  The historical earthquake catalog used in the EPRI analysis was complete through 1984.  The earthquake data for the site region that has occurred since 1984 was reviewed and used to update the EPRI catalog (EPRI, 1988).

Geologic evidence for prehistoric seismicity in the site region is discussed in Section 2.5.2.2.1.7.

{Sections 2.5.2.1.1 and 2.5.2.1.2 are added as a supplement to the U.S. EPR FSAR.

### 2.5.2.1.1    Regional Seismicity Catalog Used for 1989 Seismic Hazard Analysis Study

Many seismic networks record earthquakes in the CEUS.  A large effort was made during the EPRI seismic hazard analysis study to combine available data on historical earthquakes and to develop a homogeneous earthquake catalog that contained all recorded earthquakes for the region.  "Homogeneous" means that estimates of body-wave magnitude, $m_b$, for all earthquakes are consistent, that duplicate earthquakes have been eliminated, that non-earthquakes (e.g., mine blasts and sonic booms) have been eliminated, and that significant events in the historical record have not been missed.  Thus, the EPRI catalog (EPRI, 1988) forms a strong basis on which to estimate seismicity parameters.

### 2.5.2.1.2    Updated Seismicity Data

Regulatory Guide 1.165 (NRC, 1997a) specifies that earthquakes of a Modified Mercalli Intensity (MMI) greater than or equal to IV or of a magnitude greater than or equal to 3.0 should be listed for seismic sources, "any part of which is within a radius of 200 mi (320 km) of the site (the site region)."  While updating the EPRI catalog (EPRI, 1988) for this evaluation of vibratory ground motion a latitude-longitude window of 35° to 43° N, 71° to 83° W was used.  This window incorporates the 200 mi (320 km) radius "site region" and seismic sources contributing significantly to CCNPP Unit 3 site earthquake hazard. Figure 2.5-1 shows the CCNPP Unit 3 site and its associated site region. Figure 2.5-45 through Figure 2.5-50 show this site region and the defined latitude-longitude window.

The updated catalog was compiled from the following sub-catalogs:

♦   EPRI Catalog (EPRI, 1988).  The various data fields of the EPRI catalog are described in EPRI NP-4726-A 1988 (EPRI, 1988).

♦   Southeastern US Seismic Network (SEUSSN) Catalog.  The SEUSSN catalog is available from the Virginia Tech Seismological Observatory web site (SEUSSN, 2006).  On the date of September 8, 2006, the SEUSSN catalog had 1223 records dating from March 1568 to

December 2004 within the site region latitude-longitude window. Of these, 230 records occurred in 1985 or later.

♦ Advanced National Seismic System (ANSS) Catalog. The ANSS catalog (ANSS 2006) was searched on September 8, 2006, for all records within the site region latitude-longitude window, resulting in 570 records from 1964 to July 11, 2006. Of these, 402 records occurred in 1985 or later.

♦ Canada On-line Bulletin (Canada). The Canadian catalog is available from the Natural Resources Canada online earthquake database site (Canada, 2006). On the date of the catalog update, September 13, 2006, the Canadian catalog had 189 records dating from April 25, 1969 to July 11, 2006 within the site region latitude-longitude window. Of these, 160 records occurred in 1985 or later.

♦ Ohio Seismic Network Catalog (Ohio). The Ohio catalog is available from the Ohio Department of Natural Resources website (Ohio, 2006). On the date of the catalog update, September 8, 2006, the Ohio catalog had 92 records dating from December 3, 1951 to July 1, 2006 within the site region latitude-longitude window. Of these, 83 records occurred in 1985 or later.

An examination of the eastern US seismic networks indicated that no single network has complete coverage over the full project region. The large, reputable networks that have partial coverage of the project region include: Lamont-Doherty Seismic Network, Weston Observatory, ANSS (ANSS, 2006), SEUSSN (SEUSSN, 2006), Canada On-line Bulletin (Canada, 2006) and Ohio Seismic Network (Ohio, 2006). A search of the available information from each network was made to determine what data were available and what combination of catalogs would provide the best coverage of the project region.

The SEUSSN, and ANSS catalogs (SEUSSN, 2006) (ANSS, 2006) were determined to be the best seismicity catalogs to be used for a temporal update (1985 to present) of the EPRI catalog (EPRI, 1988) in the CCNPP Unit 3 site region. As a national catalog, the ANSS catalog (ANSS, 2006) compiles data from several regional networks, including SEUSSN. Where these catalogs spatially overlap, the more primary SEUSSN catalog (SEUSSN, 2006) was preferred, though there are some events uniquely listed in the ANSS catalog and these are retained in the updated catalog presented here as Table 2.5-2. The SEUSSN (SEUSSN, 2006) catalog has consistent coverage over the southern and central portions of the project region. The ANSS (ANSS, 2006) catalog was used for coverage in the remaining northern portion of the project region. There appears, however, diminished coverage of the ANSS (ANSS, 2006) catalog in the very northwest portion of the project region near and along the border of Canada. Given the apparent diminished coverage, additional regional catalogs with northern coverage are evaluated.

It was found that the Weston Observatory and Lamont-Doherty Seismic Networks contribute their information to ANSS, so that further independent information from these seismic networks in the Northeast was not sought.

The Canada (Canada, 2006) and Ohio (Ohio, 2006) catalogs both have coverage in the northern and northwestern portion of the project region and were included as supplemental material to the SEUSSN and ANSS catalogs (SEUSSN, 2006) (ANSS 2006). The ranking order used in creating a composite catalog was: EPRI, SEUSSN, ANSS, Canada and Ohio (EPRI, 1988)(SEUSSSN, 2006) (ANSS, 2006)(Canada, 2006)(Ohio, 2006).

The magnitudes given in these catalogs were converted to best or expected estimate of $m_b$ magnitude ($E(m_b)$, also called Emb), using the conversion factors given as Eq. 4-1 and Table 4-1 in EPRI NP-4726-A 1988 (EPRI, 1988):

$$Emb = 0.253 + 0.907 \cdot Md \qquad\qquad \text{Eq. 2.5.2-1}$$

$$Emb = 0.655 + 0.812 \cdot ML \qquad\qquad \text{Eq. 2.5.2-2}$$

where $Md$ is duration or coda magnitude and $ML$ is "local" magnitude.

The EPRI-SOG methodology modifies the Emb values to develop unbiased estimates of seismicity recurrence parameters. The modified Emb magnitudes are designated $m_b^*$ (or Rmb). Eq. 4-2 of NP-4726-A 1988 (EPRI, 1988) indicates that the equation from which $m_b^*$, or Rmb, is estimated from the best estimate of magnitude $E(m_b)$, or Emb, and the variance of $m_b$, $\sigma^2_{mb}$, or $Smb^2$ is:

$$m_b^* = E(m_b) + (1/2) \cdot ln(10) \cdot b \cdot \sigma^2_{mb} \qquad\qquad \text{Eq. 2.5.2-3}$$

where $b = 1.0$

Values for $\sigma^2_{mb}$ or $Smb$ were estimated for the four catalogs (EPRI, 1988)(SEUSSSN, 2006) (ANSS, 2006)(Canada, 2006)(Ohio, 2006), and an $m_b^*$ (Rmb) was assigned to each event added to the updated catalog in Table 2.5-2.

The result of the above process was a catalog of 113 earthquakes listed in Table 2.5-2 as the update of the EPRI NP-4726-A (EPRI, 1988) seismicity catalog recommended for the site region.

Regulatory Guide 1.206 (NRC, 2007c) provides for a discussion of each earthquake, provide information, whenever available, on the epicenter coordinates, depth of focus, date, origin time, highest intensity, magnitude, seismic moment, source mechanism, source dimensions, distance from the site, and any strong-motion recordings. Additionally it request an identification of the sources of the information. It also requests that that application identifies all magnitude designations such as mb, ML, Ms, or Mw.

The data/information was not available in all cases; however, in those cases where the requested information was available, it has been included in the discussion and in appropriate tables. Specifically, date, origin time, location, depth (when available), epicentral distance, and intensity (when available) are included in the discussion and applicable tables and/or figures. All available magnitudes were considered in development of Emb, in analogy with the EPRI-SOG catalog NP-4726-A (EPRI, 1988) being updated. Other information, such as seismic moment, source mechanism, source dimensions, and any strong motion readings, was not found. For the purpose of recurrence analysis, all earthquakes in Table 2.5-2 are considered independent events.

The 113 events in the 35° to 43° N, 71° to 83° W latitude-longitude window, incorporating the 200 mi (320 km) radius site region, from 1985 to July 11, 2006 with Emb magnitude 2.8 or greater have been incorporated into a number of figures, including figures presenting tectonic features, as discussed in Section 2.5.1, and presenting seismic sources in Section 2.5.2.2 (e.g., Figure 2.5-45 through Figure 2.5-50).

The EPRI PSHA study (EPRI, 1989a) expressed maximum magnitude ($M_{max}$) values in terms of body-wave magnitude ($m_b$), whereas most modern seismic hazard analyses describe $M_{max}$ in

terms of moment magnitude (**M**).  To provide a consistent comparison between magnitude scales, this study relates body-wave magnitude to moment magnitude using the arithmetic average of three equations, or their inversions, presented by Atkinson (Atkinson, 1995) and by Frankel (USGS, 1996), and in EPRI TR-102293 (EPRI,1993).  The conversion relations are very consistent for magnitudes 4.5 and greater and begin to show divergence at lower magnitudes. (Table 2.5-3 lists $m_b$ and **M** equivalences developed from these relations over the range of interest for this study.)  Throughout the discussion below in Sections 2.5.2.2 and 2.5.2.3, the largest assigned values of $M_{max}$ distributions assigned by the Earth Science Teams described in EPRI NP-4726 1986 (EPRI, 1986) to seismic sources are presented for both magnitude scales ($m_b$ and **M**) to give perspective on the maximum earthquakes that were considered possible in each seismic source.  For example, EPRI $m_b$ values of $M_{max}$ are followed by the equivalent **M** value.  A table of conversion values from $m_b$ to **M** and **M** to $m_b$ is provided in Table 2.5-3.}

### 2.5.2.2     Geologic and Tectonic Characteristics of Site and Region

The U.S. EPR FSAR includes the following COL Item in Section 2.5.2.2:

Geologic and tectonic characteristics are site specific and will be addressed by the COL applicant.

This COL Item is addressed as follows:

{As described in Section 2.5.1, a comprehensive review of available geological, seismological, and geophysical data has been performed for the CCNPP Unit 3 site region and adjoining areas. As discussed in Section 2.5.1.2.6, excavation mapping is required during construction and any noted deformational zones will be evaluated and NRC notified when excavations are open for inspection.  The following sections summarize the seismic source interpretations (EPRI,1986) from the 1989 EPRI PSHA study (EPRI, 1989a), relevant post-EPRI seismic source characterization studies, and updated interpretations of new and existing sources provided by the more recent data.  Based on evaluation of this information, no new information was found that would suggest potentially significant modifications to the EPRI seismic source model (EPRI, 1989a), with the following two exceptions:

♦ The East Coast fault system (ECFS) represents a new postulated seismic source along the Atlantic Seaboard, as described previously in Section 2.5.1.1.4.4.  The hypothesized ECFS is separated into a southern, central, and northern segment.  The southern segment of the ECFS has been proposed by Marple (Marple, 2000) as being the source for the 1886 Charleston earthquake.

♦ The average recurrence interval for large magnitude earthquakes in the Charleston seismic source zone, located 465 mi (748 km) from the CCNPP Unit 3 site, is currently believed to be 550 years based on paleoliquefaction data, rather than several thousand years based on seismicity used in the EPRI seismic source mode (EPRI, 1989a).  The Charleston source geometry also has been modified to include the possibility that the 1886 Charleston earthquake occurred on the southern segment of the ECFS.

Although the Charleston source lies outside the site region (200-mi radius), a preliminary sensitivity analysis performed for the CCNPP Unit 3 site shows that this source is a significant contributor of low frequency (1 Hz) ground motion, and thus the Charleston source has been included in the PSHA study for the site.  Since publication of the EPRI seismic source model (EPRI, 1989a), significant new information has been developed for assessing the earthquake source that produced the 1886 Charleston earthquake.  Paleoliquefaction features and other new information published since the 1986 EPRI project (EPRI,1986) have significant

implications regarding the geometry, $M_{max}$, and recurrence of $M_{max}$ in the Charleston seismic source.  A summary of the Updated Charleston Seismic Source (UCSS) model prepared by Bechtel (Bechtel, 2006) and incorporated into the PSHA study for the CCNPP Unit 3 site is presented below in Section 2.5.2.2.2.7.  As for the high frequency seismic ground motion hazard at the site, it is captured by the existing EPRI NP-6395-D (EPRI, 1989a) study, and therefore, no modifications are recommended.  The following sections present a summary of the EPRI NP-4726 (EPRI, 1986) seismic sources (Section 2.5.2.2.1) and post-EPRI seismic source characterization studies (Section 2.5.2.2.2).

Sections 2.5.2.2.1 and 2.5.2.2.2 are added as a supplement to the U.S. EPR FSAR.

### 2.5.2.2.1　　Summary of EPRI Seismic Sources

Summarized in this section are the seismic sources and parameters used in the 1989 EPRI project EPRI NP-6452-D (EPRI, 1989b).  The following description of seismic sources is limited to those sources within 200 mi (320 km) of the CCNPP Unit 3 site (the "site region") followed by those at distances greater than 200 mi (320 km) (i.e., Charleston) (Section 2.5.2.2.2) that appear to impact the hazard at the CCNPP Unit 3 site.

In the 1986 EPRI project (EPRI, 1986), six independent Earth Science Teams (ESTs) evaluated geological, geophysical, and seismological data to develop seismic sources in the CEUS.  These sources were used to model the occurrence of future earthquakes and evaluate earthquake hazards at nuclear power plant sites across the CEUS.  The six ESTs involved in the EPRI project were Bechtel Group, Dames & Moore, Law Engineering, Rondout Associates, Weston Geophysical Corporation, and Woodward-Clyde Consultants.  Each team produced a report which was included in EPRI NP-4726, 1986 (EPRI, 1986) that provides detailed descriptions of how they identified and defined seismic sources.  The results were implemented into a probabilistic seismic hazard analysis (PSHA) reported in EPRI NP-6395-D (EPRI, 1989a).  EPRI NP-6452-D (EPRI,1989b) summarized the parameters used in the final PSHA calculations and this reference is the primary source for the seismicity parameters used in this current CCNPP Unit 3 COL application.  For the computation of hazard in the 1989 study (EPRI, 1989a) a few of the seismic source parameters were modified or simplified from the original parameters determined by the six ESTs as discussed in EPRI NP-6452-D (EPRI, 1989b).

The seismic source models developed for each of the six EST teams are shown on Figure 2.5-45 through Figure 2.5-50.  The sources that contributed 99 percent of the CCNPP Unit 3 site hazard are shown and labeled on the figures.  For the 1989 EPRI seismic hazard calculations, a screening criterion was implemented to identify those sources whose combined hazard exceeded 99 percent of the total hazard from all sources for two ground motions measurements (EPRI, 1989).  These sources are identified in the descriptions below as "primary" seismic sources.  Other sources, which together contributed less than one percent of the total hazard from all sources for the two ground motion measures, are identified in the descriptions below as "additional" seismic sources.  Earthquakes with $m_b > 3.0$ are also shown in Figure 2.5-45 through Figure 2.5-50 to show the spatial relationships between seismicity and seismic sources.  Earthquake epicenters include events from both the EPRI earthquake catalog (EPRI, 1988) and for the period between 1985 and June 2006, as described in Section 2.5.2.1.2.

Earthquake epicenters from the EPRI earthquake catalog include events from the period between 1627 and 1984, updated with seismicity in the CEUS from the period between 1985 and 2006, as described in Section 2.5.2.1.2 (Table 2.5-2). The maximum magnitude, the closest distance to the CCNPP Unit 3 site, and the probability of activity of each EST's seismic sources are summarized in Table 2.5-4 through Table 2.5-9.  These tables present the parameters assigned to each source and specify whether or not the source contributed to 99 percent of the

site hazard in the original EPRI seismic hazard analyses.  The tables also indicate whether new information has been identified that would lead to a significant revision of the source's geometry, maximum earthquake magnitude, or recurrence parameters.  The seismicity recurrence parameters (a- and b-values) used in the EPRI seismic hazard study were computed for each one-degree latitude and longitude cell that intersects any portion of a seismic source.

Each EST used separate nomenclature to describe the seismic sources in the CEUS and the CCNPP Unit 3 site region.  A number of different names may have been used by the EPRI teams to describe the same or similar tectonic features or sources, or one team may describe seismic sources that another team does not.  For example, the Woodward-Clyde team identified their source that covers the seismicity of central Virginia as the "State Farm Complex," whereas most of the other teams named their source as the Central Virginia Seismic Zone (CVSZ).  Each team's source names, data, and rationale are included in their team-specific documentation (EPRI, 1986).  Brief descriptions of the seismic sources that contribute 99 percent of the site seismic hazard are described in the following sections.

As indicated in this section, the EPRI PSHA study (EPRI, 1989a) expressed maximum magnitude ($M_{max}$) values in terms of body-wave magnitude ($m_b$), whereas most modern seismic hazard analyses describe $M_{max}$ in terms of moment magnitude (**M**).  To provide a consistent comparison between magnitude scales, this study relates body-wave magnitude to moment magnitude using the arithmetic average of three equations, or their inversions, presented by Atkinson (Atkinson, 1995) and by Frankel (USGS, 1996) and in EPRI TR-102293 (EPRI, 1993).  The conversion relations are very consistent for magnitudes 4.5 and greater and begin to show divergence at lower magnitudes.  Throughout this section, the largest assigned values of $M_{max}$ distributions assigned by the ESTs to seismic sources are presented for both magnitude scales ($m_b$ and **M**) to give perspective on the maximum earthquakes that were considered possible in each seismic source.  For example, EPRI $m_b$ values of $M_{max}$ are followed by the equivalent **M** value.

The most significant EPRI sources for each of the six ESTs, with respect to the CCNPP Unit 3 site, are described below.  For each team, the listed sources contributed to 99 percent of the total seismic hazard for that team at the CCNPP Unit 3 site.  The assessment of these and other EPRI sources within the site region has found that the EPRI source parameters (maximum magnitude, geometry, recurrence rate) are sufficient to capture the current understanding of the seismic hazard in the site region.

Except for the two specific cases described earlier, no new seismological, geological, or geophysical information in the literature published since the 1986 EPRI source model (EPRI, 1986) suggests that these sources should be modified for the CCNPP Unit 3 site.  The two cases where new information suggests modification of the EPRI source characterizations is the addition of the postulated northern segment of the ECFS (ECFS-N) and the new recurrence rates and geometry parameters for the existing Charleston source.  The ECFS-N segment, as discussed in Section 2.5.1.1.4.4, is a hypothesized fault with a very low probability of exisistence and activity.  A sensitivity analysis performed for the Dominion North Anna site (Dominion, 2005) demonstrates that the postulated ECFS-N has a negligible affect on ground motions at the North Anna site.  Because the CCNPP Unit 3 site is approximately 70 mi (113 km) northeast of the ECFS-N, or 7 mi (11 km) further away than the North Anna site is from the ECFS-N, and based on the sensitivity analysis performed for the Dominion North Anna site, this postulated fault is not considered a contributing seismic source and does not need to be included in the seismic hazard calculations for the CCNPP Unit 3 site.  Furthermore, several features used to define the postulated ECFS-N segment have been shown to be non-tectonic features or inactive (see Section 2.5.1.1.4.4).

Each EST's characterization of the Charleston seismic source was replaced by four alternative source geometries. For each geometry, large earthquake occurrences (**M** 6.7 to 7.5) were modeled with a range of mean recurrence rates, and smaller earthquakes ($m_b$ from 5.0 to 6.7) were modeled with an exponential magnitude distribution, with rates and b-values determined from historical seismicity. Also, all surrounding sources for each team were redrawn so that the new Charleston source geometries were accurately represented as a "hole" in the surrounding source, and seismic activity rates and b-values were recalculated for the modified surrounding sources, based on historical seismicity. Further details and the results of sensitivity analyses performed on the modified seismic sources are presented in Section 2.5.2.4.

### 2.5.2.2.1.1    Sources Used for EPRI PSHA – Bechtel Group

Bechtel Group identified and characterized three seismic sources that contribute to 99 percent of the hazard at the CCNPP Unit 3 site. All three of these sources are within the site region and include the:

♦ Southern Appalachians Region (BZ5)

♦ Central Virginia (E)

♦ Atlantic Coastal Region (BZ4)

Also identified within the site region are five other seismic sources that do not contribute to 99 percent of the hazard at the site. These sources include the:

♦ Stafford Fault (17)

♦ Eastern Mesozoic Basins (13)

♦ Bristol Trends (24)

♦ Lebanon Trend (23)

♦ New York-Alabama Lineament (25)

Seismic sources identified by the Bechtel Group team within the site region are listed in Table 2.5-4. A map showing the locations and geometries of the Bechtel Group seismic sources contributing 99% of the seismic hazard is provided in Figure 2.5-45. The seismic source identified by the Bechtel Group that contributes most to the site hazard at 1 Hz and 10-4 mean annual frequency of exceedance is the Atlantic Coastal Region (source BZ4). The following is a brief discussion of each of the seismic sources that contribute to 99 percent of the site hazard.

### Southern Appalachians Region (BZ5)

The CCNPP Unit 3 site is located within the Southern Appalachians Region background source (BZ5). It is a large background source that extends from New York to Alabama and encompasses a majority of the site region. The largest $M_{max}$ assigned by the Bechtel Group to this zone is $m_b$ 6.6 (**M** 6.5).

### Central Virginia (E)

The CCNPP Unit 3 site is located approximately 49 mi (79 km) (northwest of the Central Virginia Seismic Zone (E). The source is defined exclusively on the basis of seismicity in the central Virginia region. No tectonic features were identified within the source. The largest maximum

earthquake magnitude ($M_{max}$) that the Bechtel Group assigned to this zone is body-wave magnitude ($m_b$) 6.6 (**M** 6.5).

**Atlantic Coastal Region (BZ4)**

The Atlantic Coastal Region background source (BZ4) is located about 65 mi (105 km) southeast and east of the CCNPP Unit 3 site. This source is a large background zone that extends from offshore New England to Alabama and encompasses the easternmost portion of the site region. The largest $M_{max}$ assigned by the Bechtel Group to this zone is $m_b$ 7.4 (**M** 7.9), reflecting its assumption that there is a small probability that a Charleston-type earthquake could occur within this region.

### 2.5.2.2.1.2    Sources Used for EPRI PHSA – Dames & Moore

Dames & Moore identified and characterized seven seismic sources that contribute to 99 percent of the hazard at the CCNPP Unit 3 site. These sources include:

- Connecticut Basin (47)

- Southern Appalachian Mobile Belt (53)

- Southern Cratonic Margin "Default Zone 10" (41)

- Newark-Gettysburg Basin (42)

- Central Virginia Seismic Zone (40)

- Appalachian Fold Belt (4)

- Kink in Fold Belt "1" (4A)

All of these source zones are within the site region except the Kink in Fold Belt (4A), which is 416 mi (669 km) away from the CCNPP Unit 3 site. Twelve (12) other seismic sources were identified within the site region that did not contribute to 99 percent of the hazard. These less significant sources include the:

- Stafford Fault Zone (44)

- Combination Zone 4-4A-4B-4C-4D (C01)

- Kink in Fold Belt (4C)

- Hopewell Fault Zone (45)

- Buried Triassic Basins (48)

- Dan River Basin (46)

- East Marginal Basin (8)

- Combination Zone 8-9 (C02)

- Kink in Fold Belt (Giles Co. Area) (4B)

♦   Kink in Fold Belt (4D)

♦   Jonesboro Basin (49)

♦   Ramapo Fault (43)

Seismic sources identified by Dames & Moore within the site region are listed in Table 2.5-5.  A map showing the locations and geometries of the Dames & Moore seismic sources contributing 99% of the seismic hazard is provided in Figure 2.5-46.  The seismic source identified by the Dames & Moore that contributes most to the site hazard at 1 Hz and 10-4 mean annual frequency of exceedance is the Central Virginina Seismic Zone (source 40).  The following is a brief discussion of each of the seismic sources that contribute to 99 percent of the hazard at the CCNPP Unit 3 site.

### Connecticut Basin (47)

The CCNPP Unit 3 site is located within the Connecticut Basin (47) source.  Similar to the Newark-Gettysburg Basin (42), this source is defined based on the presence of a Triassic basin and the assumption that the bounding Mesozoic rift structures could be reactivated. The largest earthquake $M_{max}$ assigned by the Dames & Moore team to this zone is $m_b$ 7.2 (**M** 7.5).

### Southern Appalachian Mobile Belt (53)

The CCNPP Unit 3 site is located within the Southern Appalachian Mobile Belt default zone (53). This default source comprises crustal rocks that have undergone several periods of divergence and convergence.  The source is bounded on the east by the East Coast magnetic anomaly and on the west by the westernmost boundary of the Appalachian gravity gradient.  The largest $M_{max}$ assigned by the Dames & Moore team to this zone is $m_b$ 7.2 (**M** 7.5).

### Southern Cratonic Margin "Default Zone 10" (41)

The CCNPP Unit 3 site is located 40 mi (64 km) east of the Southern Cratonic Margin default zone (41).  This large default background zone is located between the Appalachian Fold Belt (4) and the Southern Appalachian Mobile Belt (53) and includes the region of continental margin deformed during Mesozoic rifting.  Located within this default zone are many Triassic basins and border faults. The largest $M_{max}$ assigned by the Dames & Moore team to this zone is $m_b$ 7.2 (**M** 7.5).

### Newark-Gettysburg Basin (42)

The Newark-Gettysburg Basin source (42) is about 57 mi (92 km) northwest of the CCNPP Unit 3 site.  This source incorporates the Newark, Gettysburg, and Culpeper Triassic basins that formed during Mesozoic rifting.  The largest $M_{max}$ assigned by the Dames & Moore team to this zone is $m_b$ 7.2 (**M** 7.5).

### Central Virginia Seismic Zone  (40)

The Central Virginia Seismic Zone (40) is about 68 mi (109 km) southwest of the CCNPP Unit 3 site.  This source is defined based on the pattern of clustered seismicity in the central Virginia area.  No known tectonic features were associated with this seismic activity.  The largest $M_{max}$ assigned by the Dames & Moore team to this zone is $m_b$ 7.2 (**M** 7.5).

### Appalachian Fold Belts (4)

The Appalachian Fold Belts source (4) is about 86 mi (138 km) west of the CCNPP Unit 3 site. This source extends from New York to Alabama and consists of the Appalachian folded

mountain belt of Paleozoic age.  The largest $M_{max}$ assigned by the Dames & Moore team to this zone is $m_b$ 7.2 (**M** 7.5).

**Kink in Fold Belt "1" (4a)**

The Kink in Fold Belt source (4a) is about 416 mi (669 km) west of the CCNPP Unit 3 site and is a contributing source outside the site region.  Kinks in Paleozoic fold belts were defined based on bends of the fold belts and areas of greater seismicity.  The largest $M_{max}$ assigned by the Dames & Moore team to this zone is $m_b$ 7.2 (**M** 7.5).

### 2.5.2.2.1.3      Sources Used for EPRI PSHA – Law Engineering

Law Engineering identified and characterized 12 seismic sources that contribute to 99 percent of the hazard at the CCNPP Unit 3 site.  These sources include:

- Combination Zone 22-35 (C11)

- Reactivated Eastern Seaboard Normal (22)

- Combination Zone 8-35 (C10)

- Mesozoic Basins (8-bridged) (C09)

- Eastern Piedmont (107)

- Eastern Basement (17)

- Six individual mafic plutons (M16, M17, M18, M19, M20, M21)

Law Engineering also characterized 15 other seismic sources within the site region that do not contribute to 99 percent of the hazard.  These less significant sources include the:

- Combination Zone 22 -24-35 (C13)

- Mesozoic Basins-16 (8-16)

- Eastern Basement Background (217)

- Mafic Pluton (M25)

- Mafic Pluton (M22)

- Mafic Pluton (M26)

- Mafic Pluton (M23)

- Mafic Pluton (M24)

- Mesozoic Basins – 12 (8-12)

- Western New England (101)

- Mafic Pluton (M29)

♦   Mafic Pluton (M27)

♦   Mafic Pluton (M30)

♦   Ohio-Pennsylvania Block (112)

♦   Mafic Pluton (M28)

Note that half of these sources are mafic pluton seismic sources.  Seismic sources identified by Law Engineering within the site region are listed in Table 2.5-6.  A map showing the locations and geometries of the Law Engineering seismic sources contributing 99% of the seismic hazard is provided in Figure 2.5-47.  The seismic source identified by the Law Engineering that contributes most to the site hazard at 1 Hz and 10-4 mean annual frequency of exceedance is the Eastern Basement (source 17).  The following is a brief discussion of each of the seismic sources that contribute to 99 percent of the site hazard.

### Combination Source 22-35 (C11)

The CCNPP Unit 3 site is located within the C11 combination source.  The C11 combination zone has the same geometry as the Reactivated Eastern Seaboard Normal (22) source zone, excluding the Charleston seismic source zone (35).  The largest $M_{max}$ assigned by the Law Engineering team to this combination zone is $m_b$ 6.8 (**M** 6.8).

### Reactivated Eastern Seaboard Normal (22)

The CCNPP Unit 3 site is located within the Reactivated Eastern Seaboard Normal (22) source.  This source is characterized as a region along the eastern seaboard in which Mesozoic normal faults are reactivated as high-angle reverse faults.  Law Engineering assigned a single $M_{max}$ of $m_b$ 6.8 (**M** 6.8) to this zone.

### Combination Sources 8-35 (C10)

The CCNPP Unit 3 site is located approximately 5 mi (8 km) southeast of the C10 combination zone.  The C10 combination source zone has the same geometry as the Mesozoic Basins combination zone (C09), excluding the Charleston region (35).  The largest $M_{max}$ assigned by the Law Engineering team to both combination sources is $m_b$ 6.8 (**M** 6.8).

### Mesozoic Basins (8-bridged) (C09)

The Mesozoic basins (C09) source includes eight bridged basins, the closest of which is about 5 mi northwest from the CCNPP Unit 3 site.  This source was defined based on northeast-trending, sediment-filled troughs in basement rock bounded by normal faults.  The largest $M_{max}$ assigned by the Law Engineering team to this zone was $m_b$ 6.8 (**M** 6.8).

### Eastern Piedmont (107)

The Eastern Piedmont (107) is about 5 mi (8 km) west of the CCNPP Unit 3 site. This source is characterized as a seismotectonic region having a positive Bouguer gravity anomaly field and a pattern of short wavelength magnetic anomalies.  Law Engineering interprets this source to represent a crustal block underlain by mafic or transitional crust east of the relict North American continental margin.  The largest $M_{max}$ assigned by the Law Engineering team to this zone is $m_b$ 5.7 (**M** 5.3).

### Eastern Basement (17)

The CCNPP Unit 3 site is located 44 mi (71 km) southeast of the Eastern Basement source (17).  This source is defined as an area containing pre-Cambrian and Cambrian normal faults, which

developed during the opening of the Iapetus Ocean, in the basement rocks beneath the Appalachian decollement.  The Giles County and eastern Tennessee zones of seismicity are included in this source and are located approximately 230 mi and 415 mi, respectively, from the CCNPP Unit 3 site.  The largest $M_{max}$ assigned by the Law Engineering team to this zone is $m_b$ 6.8 (**M** 6.8).

**Six Individual Mafic Plutons (M16, M17, M18, M19, M20, and M21)**

The six significant mafic pluton sources (M16, M17, M18, M19, M20, and M21) are located between 52 mi (and 116 mi from the CCNPP Unit 3 site. Mafic pluton M21 is located 52 mi west of the site.  Law Engineering considers pre- and post-metamorphic mafic plutons in the Appalachians to be stress concentrators and, therefore, earthquake sources.  Law Engineering does not define a seismic source in central Virginia, but the plutons, of small areal extent, capture a majority of the seismicity of central Virginia, due to the method in which 70 percent of the seismicity from the surrounding one degree square area 69 mi by 69 mi (111 km x 111 km) is assigned to each pluton.  A single $M_{max}$ of $m_b$ 6.8 (**M** 6.8) is assigned by the Law Engineering team to all mafic pluton sources.

### 2.5.2.2.1.4     Sources Used for EPRI PSHA – Rondout Associates

Rondout identified and characterized four seismic sources that contribute to 99 percent of the hazard at the CCNPP Unit 3 site.  All four sources are within the site region and include:

- Background 49 (C01)

- Shenandoah (30)

- Central Virginia (29)

- Quakers (31)

Rondout also identified seven other seismic sources within the site region that did not contribute to 99 percent of the hazard at the site.  These sources include:

- Combination Zone 49 + 32 (C09)

- Appalachian Basement 3 and 4 (49-03 and 49-04)

- Norfolk Fracture Zone (32)

- Combination Zone 50 (02) + 12 (C07)

- Grenville Province 2 (50-02)

- Giles County (28)

Seismic sources identified by Rondout within the site region are listed in Table 2.5-7.  A map showing the locations and geometries of the Rondout seismic sources contributing 99% of the seismic hazard is provided in Figure 2.5-48.  The seismic source identified by the Rondout that contributes most to the site hazard at 1 Hz and $10^{-4}$ mean annual frequency of exceedance is the Central Virginia source (source 107).  The following is a discussion of each of the seismic sources that contribute to 99 percent of the hazard at the CCNPP Unit 3 site.

### Background 49 (C01)

The CCNPP Unit 3 site is located within the Background 49 source.  This background source contains Paleozoic or younger crust that is east of the Precambrian cratonic margin.  Rondout assigned a $M_{max}$ of $m_b$ 5.8 (**M** 5.4) to this source.

### Shenandoah (30)

The CCNPP Unit 3 site is located 13 mi (21 km) east of the Shenandoah source.  This Shenandoah source is defined based on geophysical and geologic features.  The source includes the intersection of the Pittsburg-Washington lineament and the strong gravity gradient associated with the edge of the ancient Paleozoic craton.  It also includes both the post-Cretaceous Brandywine and Stafford fault zones.  Rondout assigned a $M_{max}$ of $m_b$ 6.5 (**M** 6.3) to this source.

### Central Virginia (29)

The CCNPP Unit 3 site is located 55 mi (89 km) northeast of the Central Virginia source.  This source is defined based on seismicity and the possible intersection of the extension of the Norfolk fault zone and a northeast-trending linear zone defined by aeromagnetic, gravity, and volcanic-plutonic rocks.  The largest $M_{max}$ assigned by Rondout to this source is $m_b$ 7.0 (**M** 7.2).

### Quakers (31)

The CCNPP Unit 3 site is located 70 mi (113 km) south of the Quakers source. This source contains the old buried Paleozoic cratonic edge, which was mapped using gravity data.  This region was reactivated multiple times during the opening and closing of the Iapetus Ocean and during Mesozoic rifting.  Rondout assigned a $M_{max}$ of $m_b$ 6.8 (**M** 6.8) to this source.

### 2.5.2.2.1.5    Sources Used for EPRI PSHA – Weston Geophysical

Weston Geophysical identified and characterized 11 seismic sources that contributed to 99 percent of the hazard at the CCNPP Unit 3 site.  All 11 of these sources are within the site region and include:

- Combination Zone 104 – 22–26 (C23)

- Combination Zone 104 – 25 (C21)

- Combination Zone 104 – 22–25 (C24)

- Combination Zone 104 – 28BCDE – 22 – 25 (C27)

- Combination Zone 104 – 28BCDE – 22 – 26 (C28)

- Combination Zone 104 – 28BE – 26 (C34)

- Combination Zone 104 – 28BE – 25 (C35)

- Zone of Mesozoic Basins (28E)

- Central Virginia Seismic Zone (22)

- Combination Zone 103 – 23 – 24 (C19)

- Combination Zone 21 –19 (C07)

Weston Geophysical also identified 17 seismic sources within the site region that do not contribute to 99 percent of the hazard at the site. These less significant sources include the:

- ◆ Combination Zone 104-26 (C22)

- ◆ Combination Zone 104-28BCDE (C25)

- ◆ Combination Zone 104-28BCDE-22 (C26)

- ◆ Southern Coastal Plain (104)

- ◆ Combination Zone 28A thru E (C01)

- ◆ Zone of Mesozoic Basin (28B)

- ◆ Southern Appalachians (103)

- ◆ Combination Zone 103-23 (C17)

- ◆ Combination Zone 103-24 (C18)

- ◆ New York Nexus (21)

- ◆ Combination Zone 21-19-10A (C08)

- ◆ Mesozoic Basin (or intersection of Sources 28 and 21) (28A)

- ◆ Zone of Mesozoic Basin (28D)

- ◆ Combination Zone 21-19-10A -28A (C09)

- ◆ Combination Zone 21-19-28A (C10)

- ◆ Zone of Mesozoic Basin (28C)

- ◆ Appalachian Plateau (102)

The majority of these sources are combination zones. Seismic sources identified by Weston Geophysical within the site region are listed in Table 2.5-8. A map showing the locations and geometries of the Weston Geophysical seismic sources contributing 99% of the seismic hazard is provided in Figure 2.5-49. The seismic source identified by the Weston Geophysical that contributes most to the site hazard at 1 Hz and $10^{-4}$ mean annual frequency of exceedance is the Central Virginia Seismic Zone (source 22). The following is a discussion of each of the seismic sources that contribute to 99 percent of the hazard at the site.

**Seven Combination Zones 104-25 (C21); 104-22-26 (C23); 104-22-25 (C24); 104-28BCDE-22-25 (C27); 104-28BCDE-22-26 (C28); 104-28BE-26 (C34); 104-28BE-25 (C35))**

Weston Geophysical specified a seven combination seismic source zones that encompass the CCNPP Unit 3 and contribute to the 99 percent seismic hazard. These seven combination zones all represent the combination of different seismic sources within a large South Coastal Plain Background zone (104). Although not shown on Figure 2.5-49, the South Coastal Plain

Background zone (104) has the same perimeter as the seven combination zones described here. The largest $M_{max}$ assigned by the Weston team to each of these seven combination sources is $m_b$ 6.6 (**M** 6.5).

### Zone of Mesozoic Basins (28E)

The CCNPP Unit 3 site is located 4 mi (6 km) east of the Zone of Mesozoic Basins source (28E). This source surrounds three northeast-trending elongated zones of Mesozoic basins that extend from South Carolina to southern New Jersey. The largest $M_{max}$ value assigned by Weston to this zone is $m_b$ 6.6 (**M** 6.5).

### Central Virginia Seismic Zone (22)

The CCNPP Unit 3 site is located 45 mi (72 km) northeast of the CVSZ (22) source. This source is defined based on a northwest trending alignment of seismicity that extends from Richmond to Waynesboro, Virginia. The largest Mmax value assigned by Weston Geophysical to this zone is mb 6.6 (**M** 6.5).

### Two Combination Zones 21-19 (C07) and 103-23-24 (C19)

Two additional combination sources, 21 – 19 (C07) and 103 – 23 – 24 (C19), are located 113 mi (182 km) and 73 (117 km) mi from the CCNPP Unit 3 site, respectively. Combination zone 21-19 is the New York Nexus source zone minus the Moodus (19) source zone. Combination zone 103-23-24 is the Southern Appalachinas (103) source zone minus the Giles County (23) and New York Alabama-Clingman (24) source zones. The largest $M_{max}$ assigned by the Weston team to each of these two combination sources is $m_b$ 6.6 (**M** 6.5).

### 2.5.2.2.1.6    Sources Used for EPRI PSHA – Woodward-Clyde Consultants

Woodward-Clyde Consultants identified and characterized seven seismic sources that contributed to 99 percent of the hazard at the CCNPP Unit 3 site. All seven of these sources are within the site region and include:

♦ Calvert Cliffs Background (B20)

♦ Tyrone-Mt. Union Lineament (61)

♦ New Jersey Isostatic Gravity Saddle (21)

♦ Pittsburg-Washington Lineament (63)

♦ Central Virginia Gravity Saddle (26)

♦ State Farm Complex (27)

♦ Newark Basin Perimeter (23)

Woodward-Clyde Consultants also identified eight seismic sources within the site region that do not contribute to 99 percent of the hazard at the site. These sources include:

♦ New Jersey Isostatic Gravity Saddle No. 2 (Combo c2) (21A)

♦ Richmond Basin (28)

♦ Continental Shelf Int. (02)

- ◆ Southeast NY/NJ/PA NOTA Zone (53)

- ◆ Continental Shelf (01)

- ◆ Newark Basin (22)

- ◆ Ramapo Fault (24)

- ◆ Hudson Valley (25)

Seismic sources identified by Woodward-Clyde within the site region are listed in Table 2.5-9. A map showing the locations and geometries of the Woodward-Clyde seismic sources contributing 99% of the seismic hazard is provided in Figure 2.5-50. The seismic source identified by Woodward-Clyde that contributes most to the site hazard at 1 Hz and $10^{-4}$ mean annual frequency of exceedance is the Calvert Cliffs Background source (B20). Following is a brief discussion of each of the seismic sources that contributed to 99 percent of the site hazard.

### Calvert Cliffs Background (B20)

The CCNPP Unit 3 site is located within the Woodward-Clyde Consultants Calvert Cliffs Background source, a large, rectangular background source that is centered on the site. T his source is not based on any geological, geophysical, or seismological features. The largest $M_{max}$ assigned by Woodward-Clyde Consultants to this zone is $m_b$ 6.6 (**M** 6.5).

### Tyrone-Mt. Union Lineament (61)

The CCNPP Unit 3 site is located within the Tyrone-Mt. Union Lineament source. This source is based on a northwest-trending lineament, inferred to be a deep crustal fracture, mapped using geologic and geophysical data. The 435 mi (700 km) long and 62 mi (100 km) wide source surrounds the lineament. The largest $M_{max}$ assigned to this source is $m_b$ 7.1 (**M 7.3**).

### New Jersey Isostatic Gravity Saddle (21)

The New Jersey Isostatic Gravity Saddle is located 48 mi (77 lm) northeast of the CCNPP Unit 3 site. This source is based on a gravity saddle mapped using isostatic gravity from coastal New Jersey to south of New York City and surrounds a region of concentrated historical earthquakes. The largest $M_{max}$ assigned to this source is $m_b$ 6.9 (**M** 7.0).

### Pittsburg-Washington Lineament (63)

The Pittsburg-Washington Lineament source is located 52 mi (84 km) northeast of the CCNPP Unit 3 site. This northwest-trending lineament is based on offset features in gravity and magnetic data. The 435 mi (700 km) long and 62 mi (100 km) wide source surrounds the lineament. The largest $M_{max}$ assigned to this source is $m_b$ 7.1 (**M 7.3**).

### Central Virginia Gravity Saddle (26)

The Central Virginia Gravity Saddle source is about 67 mi (108 km) southwest of the CCNPP Unit 3 site. This source was defined based on a saddle in the northeast-trending gravity high associated with the Appalachians. Central Virginia seismicity is located along the south and southwest margin of the gravity saddle. This source is an alternative interpretation of the seismicity in the central Virginia area. The largest $M_{max}$ assigned by Woodward-Clyde Consultants to this zone is $m_b$ 7.0 (**M** 7.2).

---

**State Farm Complex (27)**

The State Farm Complex source is about 69 mi (111 km) southwest of the CCNPP Unit 3 site. This source was defined based on pre-Cambrian gneissic terrain located in central Virginia and bounded on the east by the Richmond Basin and on the west by Goochland fault. There is a strong concentration of seismicity on either side of the feature, which is centered in the CVSZ. The largest $M_{max}$ assigned by Woodward-Clyde Consultants to this source is $m_b$ 6.9 (**M** 7.0).

**Newark Basin Perimeter (23)**

The Newark Basin Perimeter source is located 103 mi (165 km) northeast of the CCNPP Unit 3 site. This source is based on a northeast-trending Triassic basin, named the Newark basin, that extends from New Jersey to New York. The largest $M_{max}$ assigned to this source was $m_b$ 6.8 (**M 6.8**).

### 2.5.2.2.1.7    Characterization of the Central Virginia Seismic Zone

In the 1989 EPRI seismic hazard study (EPRI, 1989a), the CVSZ represented an important contributor to seismic hazard for the CCNPP Unit 3 site, particularly for low structural frequencies (see Section 2.5.2.6.1 below). The EPRI study (EPRI, 1989a) is designed to incorporate multiple expert opinions into one PSHA to capture the epistemic uncertainty related to lack of knowledge regarding seismic sources in the CEUS. Each EST characterized the CVSZ differently, as shown on Figure 2.5-51 and listed in Table 2.5-10. In spite of these different interpretations, the central portion of each source represents the densest cluster of earthquake activity in the region. The largest $M_{max}$ for these different characterizations of the CVSZ range from $m_b$ 6.6 to $m_b$ 7.2 (**M** 6.5 to 7.5), as listed in Table 2.5-10.

With the exception of Law Engineering, all of the ESTs identified a source representing the CVSZ. Law Engineering instead identified multiple mafic plutons in the region. The seismicity parameters for these mafic plutons were calculated from a large region surrounding each pluton, which effectively captures the majority of seismicity in central Virginia. Thus, the mafic plutons indirectly represent a local seismic source for Law Engineering as provided in EPRI Report NP-4726, 1986, Volume 7) (EPRI, 1986).

Seismicity in the CVSZ ranges in depth from about 2 mi (3 km) to 8 mi (13 km) (Wheeler, 1992). Coruh (Coruh, 1988) suggest that seismicity in the central and western parts of the zone may be associated with west-dipping reflectors that form the roof of a detached antiform, while seismicity in the eastern part of the zone near Richmond may be related to a near-vertical diabase dike swarm of Mesozoic age. However, given the depth distribution of 2 mi (3 km) to 8 mi (13 km) (Wheeler, 1992) and broad spatial distribution, it is difficult to uniquely attribute the seismicity to any known geologic structure and it appears that the seismicity extends both above and below the Appalachian detachment.

Since the EPRI study (EPRI, 1989a), two liquefaction features have been found within the CVSZ (Obermeier, 1998). As described in Section 2.5.1.1.4.5, these new observations are consistent with the $M_{max}$ values and recurrence parameters assigned by the EPRI teams. The lack of widespread liquefaction features in the 186 mi (300 km) of stream exposures searched within the CVSZ, despite the presence of mid- to late-Holocene potentially liquefiable deposits, has led some researchers (Obermeier, 1998) to conclude that it is unlikely that an earthquake of magnitude 7 or larger has occurred within the seismic zone in the last 2,000 to 3,000 years, or in the eastern portion of the seismic zone for the last 5,000 years.

Within the CCNPP Unit 3 site region, the paleo-liquefaction features found within the Central Virginia seismic zone are only two recorded occurrences of Quaternary earthquake-induced

geologic failure. Within the CCNPP Unit 3 site region, the literature review conducted for the development of this section, which included compilations of potential Quaternary features by Crone and Wheeler (Crone, 2000), Wheeler (Wheeler, 2005), and Wheeler (Wheeler, 2006), found no other documented evidence of Quaternary earthquake-induced geologic failure, such as earthquake-induced liquefaction, landsliding, land spreading, or lurching. Outside of the CCNPP Unit 3 site region, widespread liquefaction is recorded near Charleston, South Carolina. These data are incorporated in the Updated Charleston Seismic Source Model presented in Section 2.5.2.2.2.7.

The 1986 EPRI source model (EPRI, 1986) includes various source geometries and parameters to capture the seismicity of the Central Virginia seismic zone (Figure 2.5-51). Subsequent hazard studies have used maximum magnitude ($M_{max}$) values that are within the range of maximum magnitudes used by the six EPRI models. Collectively, upper-bound maximum values of $M_{max}$ used by the EPRI teams range from $m_b$ 6.6 to 7.2 (**M** 6.5 to 7.5) (Table 2.5-10). More recently, Bollinger (USGS, 1992) has estimated a $M_{max}$ of $m_b$ 6.4 (**M** 6.2) for the Central Virginia seismic source. Chapman (Chapman, 1994) has used a $M_{max}$ of $m_b$ 7.25 (**M** 7.6) for the Central Virginia seismic source and most other sources in their seismic hazard analysis of Virginia. This more recent estimate of $M_{max}$ is similar to the $M_{max}$ values used in the 1986 EPRI studies (EPRI, 1986). Similarly, the distribution and rate of seismicity in the Central Virginia seismic source has not changed since the 1986 EPRI study (EPRI, 1986). Thus, there is no change to the source geometry or rate of seismicity. In addition the NRC agreed with these findings as part of a review of Dominion Nuclear North Anna LLC's ESP application and assessment of the Central Virginia seismic zone as documented in NUREG-1835, Safety Evaluation Report for an Early Site Permit (ESP) at the North Anna ESP Site, (NRC, 2005). This supports the conclusion that no new information has been developed since 1986 that would require a significant revision to the EPRI seismic source model (EPRI, 1986).

### 2.5.2.2.2        Post-EPRI Seismic Source Characterization Studies

Since the EPRI seismic hazard project (EPRI, 1989), seven studies have been performed to characterize seismic sources relevant to the CCNPP Unit 3 site probabilistic seismic hazard analysis. Four of these studies characterize seismic sources within the CCNPP Unit 3 site region and include the following:

♦   Sources and parameters for the Savannah River nuclear site in South Carolina (USGS, 1992)

♦   Seismic hazard of Virginia (Chapman, 1994)

♦   United States Geological Survey's National Seismic Hazard Mapping Project (USGS, 1996) (USGS, 2002)

♦    North Anna ESP Application (Dominion, 2005)

These four studies are described below in Sections 2.5.2.2.2.1 through 2.5.2.2.2.4.

Three additional studies centered outside the CCNPP Unit 3 site area have been performed to characterize seismic sources in the southeastern United States. These studies include the following:

♦   South Carolina Department of Transportation's seismic hazard mapping project (Chapman, 2002)

♦ The Nuclear Regulatory Commission's Trial Implementation Project (TIP) study (NRC, 2002a)

♦ The Southern Nuclear Company's ESP application for Vogtle Units 2 and 3 that included the Updated Charleston Seismic Source model (Bechtel, 2006).

These studies are described below in Sections 2.5.2.2.2.5 through 2.5.2.2.2.7.

Based on review of these recent studies that lie outside of the site region, it was determined that an update of the Charleston seismic source for the EPRI (EPRI, 1986) (EPRI, 1989a) seismic hazard project was required to assess the seismic hazard at the CCNPP Unit 3 site (Figure 2.5-52).  For example, a preliminary sensitivity analysis of the Charleston source zone that included the postulated East Coast Fault system (Section 2.5.1.1.4.4) indicates that, at low frequencies (1 Hz), the Charleston source is a significant contributor to the seismic hazard at the CCNPP Unit 3 site.  Thus, new PSHA models that have been developed to address the Charleston source are summarized in the following sections.  In particular, the PSHA for the CCNPP Unit 3 site incorporates the Updated Charleston Seismic Source (UCSS) model developed by Bechtel (Bechtel, 2006) for the Vogtle nuclear power plant in Georgia.  The UCSS (Bechtel, 2006) is presented in Section 2.5.2.2.2.7.

In addition, located in the CCNPP Unit 3 site region is the Lancaster seismic zone of Pennsylvania, 120 mi (193 km) North of the CCNPP Unit 3 site (Figure 2.5-52).  The significance of the Lancaster seismic zone with respect to the CCNPP Unit 3 site seismic hazard is discussed in Section 2.5.2.2.2.8.  In addition, several small earthquake clusters that post-date EPRI (EPRI, 1989a) include the Howard County earthquake sequence of Maryland (Reger, 1994).  The Howard County earthquake swarm is discussed in Section 2.5.2.2.2.9.

### 2.5.2.2.2.1    Seismic Sources and Parameters for the Savannah River Nuclear Site

USGS (USGS, 1992) specified sources, recurrence rates, focal depths, and maximum magnitudes for earthquake sources in the southeastern United States to be used in probabilistic seismic hazard analyses at the Savannah River nuclear site in South Carolina (Table 2.5-11). Bollinger's approach to seismic zonation in the Eastern United States was based primarily on the historical record of earthquake activity.  Maximum magnitudes were derived from a combination of three different estimates based on the 1000 year earthquake, the maximum historical earthquake plus one magnitude unit, and the calculated values from various published relationships between magnitude and fault rupture area.  Bollinger identified two seismic sources within the CCNPP Unit 3 site region (200 mi radius).  These sources are the CVSZ (RZ6) and a complementary background zone (CZ1) (Table 2.5-11).  The CVSZ was defined by Bollinger as a rectangular zone centered on the majority of the seismicity in the central Virginia area.  The maximum magnitude earthquake value estimated for this source was $m_b$ 6.4 (**M** 6.2) (USGS, 1992).  For the complimentary background zone a $M_{max}$ value of $m_b$ 5.75 (**M** 5.36) was used.  The $M_{max}$ values for the Central Virginia and complementary background sources in the USGS (USGS, 1992) study are lower than the largest $M_{max}$ values assigned by most of the EPRI teams (Table 2.5-10).

### 2.5.2.2.2.2    Seismic Hazard of Virginia

In 1994, a seismic hazard assessment of Virginia was performed to examine the seismic hazard within Virginia on a county-by-county basis (Chapman, 1994).  Seismic sources and earthquake frequency-magnitude recurrence relationships were defined using the results of network monitoring by the Seismological Observatory at Virginia Polytechnic Institute and State University and published geologic and geophysical investigations.  The study defined a total of

10 seismic sources (Table 2.5-12). Within the CCNPP Unit 3 site region, Chapman (Chapman, 1994) defined six contiguous, non-overlapping sources that were based primarily on patterns of seismicity. The most prominent area of historical seismicity within the site region is defined as the Central Virginia Seismic Zone. An $M_{max}$ value of **M** 7.53 ($m_b$ 7.22) was assigned to all sources in their model, with the exception of New Madrid. Chapman (Chapman, 1994) assumed that a Charleston-size event was capable of occurring in any of the sources within the CCNPP Unit 3 site region.

Subsequent to the Chapman and Krimgold study, Johnston (Johnston, 1996) reduced his magnitude estimate of the Charleston earthquake to **M** 7.3 from the prior estimate of **M** 7.53 as cited in Chapman (Chapman, 1994). Using the magnitude conversion described in Section 2.5.2.2.1, **M** = 7.3 converts to $m_b$ = 7.1, which is within the range of largest $M_{max}$ values ($m_b$ 6.6 to 7.2) assigned by the EPRI teams to the Central Virginia seismic zone. These later studies, therefore, are consistent with the interpretations of the EPRI EST teams.

### 2.5.2.2.2.3 United States Geological Survey (USGS) Model

In 2002, the USGS produced updated seismic hazard maps for the conterminous United States based on new seismological, geophysical, and geological information (USGS, 2002). The 2002 maps reflect changes to the source model used to construct the previous version of the national seismic hazard maps (USGS, 1996). The most significant modifications to the CEUS portion of the source model include changes in the recurrence, $M_{max}$, and geometry of the Charleston and New Madrid sources. Unlike the EPRI models that incorporate many local sources, the USGS source model in the CCNPP Unit 3 site region (200 mi (320 km) radius) includes only three sources that are important to the site hazard: the Extended Margin background, Stable Craton background, and the New Madrid (Table 2.5-13). Except for the Charleston and New Madrid zones, where earthquake recurrence is modeled by paleoliquefaction data, the hazard for the large background or "maximum magnitude" zones is largely based on historical seismicity and the variation of that seismicity.

As part of the 2002 update of the National Seismic Hazard Maps, the USGS developed a model of the Charleston source that incorporates available data regarding recurrence, $M_{max}$, and geometry of the source zone. The USGS model uses two equally weighted source geometries: a) an areal source enveloping most of the tectonic features and liquefaction data in the greater Charleston area, and b) a north-northeast-trending elongated areal source enveloping the southern half of the southern segment of the proposed East Coast fault system (ECFS) (Table 2.5-13 and Figure 2.5-53). The USGS (USGS, 2002) report does not specify why the entire southern segment of the ECFS is not contained in the source geometry. For $M_{max}$, the study defines a distribution of magnitudes and weights for Charleston of **M** 6.8 (0.20), 7.1 (0.20), 7.3 (0.45), 7.5 (.15). For recurrence, USGS (USGS, 2002) adopt a mean paleoliquefaction-based recurrence interval of 550 years and represent the uncertainty with a continuous lognormal distribution.

### 2.5.2.2.2.4 North Anna ESP Application

A seismic source characterization study was performed as part of an Early Site Permit application for the North Anna nuclear power plant, located in central Virginia, by Dominion Nuclear North Anna LLC (Dominion, 2005). Aspects of the study have been summarized previously in Sections 2.5.1.1.4.4 and 2.5.1.1.4.4. In particular, Dominion Nuclear North Anna LLC (Dominion, 2004a) (Dominion, 2004b) performed additional studies and/or addressed Requests for Additional Information (RAI) associated with several potential seismic sources, including the fall lines of Weems (USGS, 1998), Everona-Mountain Run Fault Zone, Stafford Fault System, postulated East Coast Fault System (ECFS) (Marple, 2000), and CVSZ. All of these

features have been discussed previously in Section 2.5.1.  With the exception of the southern segment of the postulated East Coast fault system, the presence of these features does not warrant modification to the EPRI (EPRI, 1989a) PSHA study (see Section 2.5.1.1.4.4).  The ECFS-south is included in the updated Charleston Source Study Bechtel (Bechtel, 2006) presented below in Section 2.5.2.2.2.7.

### 2.5.2.2.2.5      South Carolina Department of Transportation Model

Chapman (Chapman, 2002) created probabilistic seismic hazard maps for the South Carolina Department of Transportation (SCDOT).  In the SCDOT model, treatment of the 1886 Charleston, South Carolina, earthquake and similar events dominates estimates of hazard statewide.  The SCDOT model employs a combination of line and area sources to characterize Charleston-type earthquakes in three separate geometries and uses a slightly different $M_{max}$ range (**M** 7.1 to 7.5) than the Chapman (Chapman, 2002) model (Table 2.5-14 and Figure 2.5-54).  Three equally-weighted seismic sources defined for this study include:

- ♦  a larger Coastal South Carolina zone called the Charleston area source that includes most of the paleoliquefaction sites

- ♦  a line source capturing the intersection of the Woodstock and Ashley River faults, that is modeled as three parallel line sources

- ♦  a southern ECFS line source called the ZRA fault source

The respective magnitude distributions and weights used for all sources for $M_{max}$ are **M** 7.1 (0.20), 7.3 0(0.60), 7.5 (0.20).  The mean recurrence interval used in the SCDOT study is 550 years, based on the paleoliquefaction record.

### 2.5.2.2.2.6      The Trial Implementation Project Study

The Lawrence Livermore National Laboratory Trial Implementation Project (TIP) (NRC, 2002a) study focuses on seismic zonation and earthquake recurrence models for two nuclear plant sites in the southeastern U.S. i.e., the Vogtle site in Georgia and the Watts Bar site in Tennessee.  The TIP study (NRC, 2002a) uses an expert elicitation process to characterize the Charleston seismic source, considering published data through 1996.  The TIP study (NRC, 2002a) identifies multiple alternative zones for the Charleston source and for the South Carolina–Georgia seismic zone, as well as alternative background seismicity zones for the Charleston region.  However, the TIP study (NRC, 2002a) focuses primarily on implementing the Senior Seismic Hazard Advisory Committee (SSHAC) PSHA methodology (NRC, 1997b) and was designed to be as much of a test of the methodology as a real estimate of seismic hazard.  As a result, its findings are not included explicitly in this report for the CCNPP Unit 3 site.

### 2.5.2.2.2.7      Updated Charleston Seismic Source (UCSS) Model

It has been nearly 20 years since the six EPRI ESTs evaluated hypotheses for earthquake causes and tectonic features and assessed seismic sources in the CEUS (EPRI, 1986).  The EPRI Charleston source zones developed by each EST are shown in Figure 2.5-55 and summarized in Table 2.5-15.  Several studies that post-date the 1986 EPRI EST assessments have demonstrated that the source parameters for geometry, $M_{max}$, and recurrence of $M_{max}$ in the Charleston seismic source require an update to capture a more current understanding for both the 1886 Charleston earthquake and the seismic source that produced this earthquake.  In addition, recent PSHA studies of the South Carolina region (NRC, 2002a) (Chapman, 2002), southeastern United States (USGS, 2002), and for the Vogtle site (Bechtel, 2006) have developed models of the Charleston seismic source that differ significantly from the earlier EPRI characterizations.

The Updated Charleston Seismic Source model of Bechtel (Bechtel, 2006) was included in the PSHA study for the CCNPP Unit 3 site.

The UCSS model prepared by Bechtel (Bechtel, 2006) is summarized below.  Methods used to update the Charleston seismic source follow guidelines provided in Regulatory Guide 1.165 (NRC, 1997a).  Bechtel (Bechtel, 2006) performed a SSHAC Level 2 study to incorporate current literature and data and the understanding of experts into an update of the Charleston seismic source model.  This level of effort is outlined in the NUREG/CR-6372 (NRC,1997b) report, which provides guidance on incorporating uncertainty and the use of experts in PSHA studies.

The UCSS model also incorporates new information to re-characterize geometry, $M_{max}$, and recurrence for the Charleston seismic source.  These components are summarized in the following sections.  Paleoliquefaction data imply that the Charleston earthquake process is defined by repeated, relatively frequent, large earthquakes located in the vicinity of Charleston, indicating that the Charleston source behaves differently from the rest of the eastern seaboard.

### UCSS Geometry

The UCSS model includes four mutually exclusive source zone geometries (A, B, B', and C; Figure 2.5-56).  The latitude and longitude coordinates that define these four source zones are presented in Table 2.5-16.  Details regarding each source geometry are given below.  The four geometries of the UCSS are defined based on the following: current understanding of geologic and tectonic features in the 1886 Charleston earthquake epicentral region; the 1886 Charleston earthquake shaking intensity; distribution of seismicity; and geographic distribution, age, and density of liquefaction features associated with both the 1886 and prehistoric earthquakes. These features, shown in Figure 2.5-57 and Figure 2.5-58, strongly suggest that the majority of evidence for the Charleston source is concentrated in the Charleston area and is not widely distributed throughout South Carolina. Table 2.5-17 provides a subset of the Charleston tectonic features differentiated by pre- and post-EPRI (EPRI, 1986) information.  In addition, pre- and post-1986 instrumental seismicity, $m_b$ 3, are shown on Figure 2.5-57 and Figure 2.5-58. Seismicity continues to be concentrated in the Charleston region in the Middleton Place–Summerville seismic zone (MPSSZ), which has been used to define the intersection of the Woodstock and Ashley River faults (SSA, 1981) (SSA, 1993).  In addition, two earthquakes in 2002 ($m_b$ 3.5 and 4.4) are located offshore of South Carolina along the Helena Banks fault zone in an area previously devoid of seismicity of $m_b > 3$.  A compilation of the EPRI ESTs Charleston source zones is provided in Figure 2.5-55 as a comparison to the UCSS geometries shown in Figure 2.5-56.

### Geometry A – Charleston

Geometry A is an approximately 62 mi x 31 mi (100 km x 50 km), northeast-oriented area centered on the 1886 Charleston meizoseismal area (Figure 2.5-56).  Geometry A is intended to represent a localized source area that generally confines the Charleston source to the 1886 meizoseismal area (i.e., a stationary source in time and space).  Geometry A completely incorporates the 1886 earthquake MMI X isoseismal (Bollinger, 1977), the majority of identified Charleston-area tectonic features and inferred fault intersections, and the majority of reported 1886 liquefaction features.  Geometry A excludes the northern extension of the southern segment of the East Coast fault system because this system extends well north of the meizoseismal zone and is included in its own source geometry (Geometry C).  Geometry A also excludes outlying liquefaction features, because liquefaction occurs as a result of strong ground shaking that may extend well beyond the areal extend of the tectonic source. Geometry A also envelopes instrumentally located earthquakes spatially associated with the MPSSZ (SSA, 1981) (USGS, 1983b) (SSA, 1993).

The preponderance of evidence strongly supports the conclusion that the seismic source for the 1886 Charleston earthquake is located in a relatively restricted area defined by Geometry A. Geometry A envelopes (a) the meizoseismal area of the 1886 earthquake, (b) the area containing the majority of local tectonic features (although many have large uncertainties associated with their existence and activity, as described earlier), (c) the area of ongoing concentrated seismicity, and (d) the area of greatest density of 1886 liquefaction and prehistoric liquefaction. These observations show that future earthquakes with magnitudes comparable to the Charleston earthquake of 1886 will most likely occur within the area defined by Geometry A. A weight of 0.70 is assigned to Geometry A (Figure 2.5-59). To confine the rupture dimension to within the source area and to maintain a preferred northeast fault orientation, Geometry A is represented in the model by a series of closely spaced, northeast-trending faults parallel to the long axis of the zone.

### Geometries B, B′, and C

While the preponderance of evidence supports the assessment that the 1886 Charleston meizoseismal area and Geometry A define the area where future events will most likely be centered, it is possible that the tectonic feature responsible for the 1886 earthquake either extends beyond or lies outside Geometry A. Therefore, the remaining three geometries (B, B′, and C) are assessed to capture the uncertainty that future events may not be restricted to Geometry A. The distribution of liquefaction features along the entire coast of South Carolina and observations from the paleoliquefaction record that a few events were localized (moderate earthquakes to the northeast and southwest of Charleston), suggest that the Charleston source could extend well beyond Charleston proper. Geometries B and B′ are assessed to represent a larger source zone, while Geometry C represents the southern segment of the hypothesized East Coast fault system as a possible source zone. The combined geometries of B and B′ are assigned a weight of 0.20, and Geometry C is assigned a weight of 0.10. Geometry B′ a subset of B, formally defines the onshore coastal area as a source (similar to the SCDOT coastal source zone) that would restrict earthquakes to the onshore region. Geometry B, which includes the onshore and offshore regions, and Geometry B′ are mutually exclusive and given equal weight in the UCSS model. Therefore, the resulting weights are 0.10 for Geometries B and B′.

### Geometry B – Coastal and Offshore Zone

Geometry B is a coast-parallel, approximately 162 mi x 62 mi (260 km x 100 km) source area that a) incorporates all of Geometry A, b) is elongated to the northeast and southwest to capture other, more distant liquefaction features in coastal South Carolina (Amick, 1990a) (Amick, 1990b) (NRC, 1990) (Talwani, 2001), and c) extends to the southeast to include the offshore Helena Banks fault zone (Behrendt, 1987; Figure 2.5-56 and Figure 2.5-58). The elongation and orientation of Geometry B is roughly parallel to the regional structural grain as well as roughly parallel to the elongation of 1886 isoseismals. The northeastern and southwestern extents of Geometry B are controlled by the mapped extent of paleoliquefaction features (Amick, 1990a) (Amick, 1990b) (NRC, 1990) (Talwani, 2001).

The location and timing of paleoliquefaction features in the Georgetown and Bluffton areas to the northeast and southwest of Charleston have suggested to some researchers that the earthquake source may not be restricted to the Charleston area (Obermeier, 1989) (NRC, 1990) (Talwani, 2001). A primary reason for defining Geometry B is to account for the possibility that there may be an elongated source or multiple sources along the South Carolina coast. Paleoliquefaction features in the Georgetown and Bluffton areas may be explained by an earthquake source both northeast and southwest of Charleston, as well as possibly offshore.

Geometry B extends southeast to include an offshore area and the Helena Banks fault zone. The Helena Banks fault zone is clearly shown by multiple seismic reflection profiles and has

demonstrable late Miocene offset (Behrendt, 1987). Offshore earthquakes in 2002 ($m_b$ 3.5 and 4.4) suggest a possible spatial association of seismicity with the mapped trace of the Helena Banks fault system (Figure 2.5-56 and Figure 2.5-58). Whereas these two events in the vicinity of the Helena Banks fault system do not provide a positive correlation with seismicity or demonstrate recent fault activity, these small earthquakes are considered new data since the EPRI studies. The EPRI earthquake catalog (EPRI, 1988) was devoid of any events ($m_b$ > 3.0) offshore from Charleston. The recent offshore seismicity also post-dates the development of the USGS and SCDOT source models that exclude any offshore Charleston source geometries.

A low weight of 0.10 is assigned to Geometry B (Figure 2.5-59), because the preponderance of evidence indicates that the seismic source that produced the 1886 earthquake lies onshore in the Charleston meizoseismal area and not in the offshore region. To confine the rupture dimension to within the source area and to maintain a preferred northeast fault orientation, Geometry B is represented in the model by a series of closely spaced, northeast-trending faults parallel to the long axis of the zone.

### Geometry B' – Coastal Zone

Geometry B' is a coast-parallel, approximately 162 mi x 31 mi (260 km x 50 km source area that incorporates all of Geometry A, as well as the majority of reported paleoliquefaction features (Amick, 1990a) (Amick, 1990b) (NRC, 1990) (Talwani, 2001). Unlike Geometry B, however, Geometry B' (Figure 2.5-55) does not include the offshore Helena Banks Fault Zone (Figure 2.5-58).

The Helena Banks fault system is excluded from Geometry B' to recognize that the preponderance of the data and evaluations support the assessment that the fault system is not active. It is also excluded because most evidence strongly suggests that the 1886 Charleston earthquake occurred onshore in the 1886 meizoseismal area and not on an offshore fault. Whereas there is little uncertainty regarding the existence of the Helena Banks fault, there is a lack of evidence that this feature is still active. Isoseismal maps documenting shaking intensity in 1886 indicate an onshore meizoseismal area (the closed bull's eye centered onshore north of downtown Charleston, Figure 2.5-58). An onshore source for the 1886 earthquake as well as the prehistoric events is supported by the instrumentally recorded seismicity in the MPSSZ and the corresponding high density cluster of 1886 and prehistoric liquefaction features.

Similar to Geometry B above, a weight of 0.10 is assigned to Geometry B' and reflects the assessment that Geometry B' has a much lower probability of being the source zone for Charleston-type earthquakes than Geometry A (Figure 2.5-59). To confine the rupture dimension to within the source area and to maintain a preferred northeast fault orientation, Geometry B' is represented in the model by a series of closely spaced, northeast-trending faults parallel to the long axis of the zone.

### Geometry C – East Coast Fault System – South (ECFS-s)

Geometry C is an approximately 123 mi x 19 mi (200 km x 30 km), north-northeast-oriented source area enveloping the southern segment of the proposed East Coast fault system (ECFS-s) shown inFigure 3 of Marple (Marple, 2000) (Figure 2.5-56 and Figure 2.5-60). The USGS hazard model (USGS, 2002) (Figure 2.5-53) incorporates the postulated ECFS-S as a distinct source geometry (also known as the zone of river anomalies (ZRA) depicted in Figure 2.5-60); however, as described earlier, the USGS model truncates the northeastern extent of the proposed fault segment. The South Carolina Department of Transportation hazard model (Chapman, 2002) also incorporates the ECFS-S as a distinct source geometry; however, this model extends the southern segment of the proposed East Coast fault system farther to the south than originally

postulated by Marple (Marple, 2000) to include, in part, the distribution of liquefaction in southeastern South Carolina (Figure 2.5-56).

In this CCNPP Unit 3 site evaluation, the area of Geometry C is restricted to envelope the original depiction of the proposed ECFS-S by Marple (Marple, 2000).  Truncation of the zone to the northeast as shown by the 2002 USGS model is not supported by available data, and the presence of liquefaction in southeastern South Carolina is best captured in Geometries B and B', rather than extending the ECFS-S farther to the south than defined by the data of Marple (Marple, 2000).

A low weight of 0.10 is assigned to Geometry C to reflect the assessment that Geometries B, B', and C all have equal, but relatively low, likelihood of producing Charleston-type earthquakes (Figure 2.5-59).  As with the other UCSS geometries, Geometry C is represented as a series of parallel, vertical faults oriented northeast-southwest and parallel to the long axis of the narrow rectangular zone.  The faults and extent of earthquake ruptures are confined within the rectangle depicting Geometry C.

### UCSS Model Parameters

Based on studies by Bollinger (Bollinger, 1985) (Bollinger,1991) (USGS, 1992), a 20-km-thick seismogenic crust is assumed for the UCSS.  To model the occurrence of earthquakes in the characteristic part of the Charleston distribution ($\mathbf{M} > 6.7$), the model uses a series of closely-spaced, vertical faults parallel to the long axis of each of the four source zones (A, B, B', and C).  Faults and earthquake ruptures are limited to within each respective source zone and are not allowed to extend beyond the zone boundaries, and ruptures are constrained to occur within the depth range of 0 mi to 12.5 mi (0 km to 20 km).  Modeled fault rupture areas are assumed to have a width-to-length aspect ratio of 0.5, conditional on the assumed maximum fault width of 0 mi to 12.5 mi (0 km to 20 km).  To obtain $M_{max}$ earthquake rupture lengths from magnitude, the empirical relationship reported in Wells (SSA, 1994) between surface rupture length and $\mathbf{M}$ for earthquakes of all slip types is used.  To maintain as much similarity as possible with the original EPRI model, the UCSS model treats earthquakes in the exponential part of the distribution ($\mathbf{M} < 6.7$) as point sources uniformly distributed within the source area (full smoothing), with a constant depth fixed at 10 km.

### UCSS Maximum Magnitude

The six EPRI ESTs developed a distribution of weighted $M_{max}$ values and weights to characterize the largest earthquakes that could occur on Charleston seismic sources (Table 2.5-15).  On the low end, the Law Engineering team assessed a single $M_{max}$ of $m_b$ 6.8 to seismic sources it considered capable of producing earthquakes comparable in magnitude to the 1886 Charleston earthquake.  On the high end, four teams defined $M_{max}$ upper bounds ranging between $m_b$ 7.2 and $m_b$ 7.5.  For the CCNPP Unit 3 PSHA, the $m_b$ magnitude values have been converted to moment magnitude ($\mathbf{M}$), as described previously.  The $m_b$ value and converted moment magnitude value for each team are shown below.  The range in $\mathbf{M}$ for the six ESTs is 6.5 to 8.0.

| Team | Charleston $M_{max}$ range |
|---|---|
| Bechtel Group | $m_b$ 6.8 to 7.4 ($\mathbf{M}$ 6.8 to 7.9) |
| Dames & Moore | $m_b$ 6.6 to 7.2 ($\mathbf{M}$ 6.5 to 7.5) |
| Law Engineering | $m_b$ 6.8 ($\mathbf{M}$ 6.8) |
| Rondout | $m_b$ 6.6 to 7.0 ($\mathbf{M}$ 6.5 to 7.2) |
| Weston Geophysical | $m_b$ 6.6 to 7.2 ($\mathbf{M}$ 6.5 to 7.5) |
| Woodward-Clyde Consultants | $m_b$ 6.7 to 7.5 ($\mathbf{M}$ 6.7 to 8.0) |

The **M** equivalents of EPRI $m_b$ estimates for Charleston $M_{max}$ earthquakes show that the upper bound values are similar to, and in two cases exceed, the largest modern estimate of **M** 7.3 ± 0.26 (Johnston, 1996) for the 1886 earthquake. The upper bound values for five of the six ESTs also exceed the preferred estimate of **M** 6.9 by Bakun (Bakun, 2004) for the Charleston event. The EPRI $M_{max}$ estimates are more heavily weighted toward the lower magnitudes, with the upper bound magnitudes given relatively low weights by several ESTs (Table 2.5-3 through Table 2.5-8). Therefore, updating the $M_{max}$ range and weights to reflect the current range of technical interpretations is warranted for the UCSS.

Based on assessment of the currently available data and interpretations regarding the range of modern $M_{max}$ estimates (Table 2.5-18), the UCSS model modifies the USGS magnitude distribution (USGS, 2002) to include a total of five discrete magnitude values, each separated by 0.2 **M** units (Figure 2.5-59). The UCSS $M_{max}$ distribution includes a discrete value of **M** 6.9 to represent the Bakun best estimate of the 1886 Charleston earthquake magnitude, as well as a lower value of **M** 6.7 to capture a low probability that the 1886 earthquake was smaller than the Bakun mean estimate of **M** 6.9. Bakun did not explicitly report a 1-sigma range in magnitude estimate of the 1886 earthquake, but do provide a 2-sigma range of **M** 6.4 to **M** 7.2 (Bakun, 2004).

The UCSS magnitudes and weights are as follows:

| M | Weight | |
|---|---|---|
| 6.7 | 0.10 | |
| 6.9 | 0.25 | (Bakun ,2004) mean |
| 7.1 | 0.30 | |
| 7.3 | 0.25 | (Johnston, 1996) mean |
| 7.5 | 0.10 | |

This results in a weighted $M_{max}$ mean magnitude of **M** 7.1 for the UCSS, which is slightly lower than the mean magnitude of **M** 7.2 in the USGS model (USGS, 2002).

**UCSS Recurrence Model**

In the 1989 EPRI study (EPRI, 1989a), the six EPRI ESTs used an exponential magnitude distribution to represent earthquake sizes for their Charleston sources. Parameters of the exponential magnitude distribution were estimated from historical seismicity in the respective source areas. This resulted in recurrence intervals for $M_{max}$ earthquakes (at the upper end of the exponential distribution) of several thousand years.

The current model for earthquake recurrence is a composite model consisting of two distributions. The first is an exponential magnitude distribution used to estimate recurrence between the lower-bound magnitude used for hazard calculations and $m_b$ 6.7. The parameters of this distribution are estimated from the earthquake catalog, as they were for the 1989 EPRI study (EPRI, 1989a). This is the standard procedure for smaller magnitudes and is the model used, for example, by the USGS 2002 national hazard maps (USGS, 2002). In the second distribution, $M_{max}$ earthquakes (**M** > 6.7) are treated according to a characteristic model, with discrete magnitudes and mean recurrence intervals estimated through analysis of geologic data, including paleoliquefaction studies. In this document, $M_{max}$ is used to describe the range of largest earthquakes in both the characteristic portion of the UCSS recurrence model and the EPRI exponential recurrence model.

This composite model achieves consistency between the occurrence of earthquakes with **M** < 6.7 and the earthquake catalog and between the occurrence of large earthquakes (**M** > 6.7) with paleoliquefaction evidence.  It is a type of "characteristic earthquake" model, in which the recurrence rate of large events is higher than what would be estimated from an exponential distribution inferred from the historical seismic record.

### $M_{max}$ Recurrrence Intervals

This section describes how the UCSS model determines mean recurrence intervals for $M_{max}$ earthquakes.  The UCSS model incorporates geologic data to characterize the recurrence intervals for $M_{max}$ earthquakes.  As described earlier, identifying and dating paleoliquefaction features provides a basis for estimating the recurrence of large Charleston area earthquakes.  Most of the available geologic data pertaining to the recurrence of large earthquakes in the Charleston area were published after 1990 and, therefore, were not available to the six EPRI ESTs.  In the absence of geologic data, the six EPRI EST estimates of recurrence for large, Charleston-type earthquakes were based on a truncated exponential model using historical seismicity (EPRI, 1986) (EPRI, 1989a).  The truncated exponential model also provided the relative frequency of all earthquakes greater than $m_b$ 5.0 up to $M_{max}$ in the EPRI PSHA (EPRI, 1989a).  The recurrence interval of $M_{max}$ earthquakes in the EPRI models was on the order of several thousand years, which is significantly greater than more recently published estimates of about 500 to 600 years, based on paleoliquefaction data (Talwani, 2001).

### Paleoliquefaction Data

Strong ground shaking during the 1886 Charleston earthquake produced extensive liquefaction, and liquefaction features from the 1886 event are preserved in geologic deposits at numerous locations in the region.  Documentation of older liquefaction-related features in geologic deposits provides evidence for prior strong ground motions during prehistoric large earthquakes.  Estimates of the recurrence of large earthquakes in the UCSS are based on dating paleoliquefaction features.  Many potential sources of ambiguity and/or error are associated with dating and interpreting paleoliquefaction features.  This assessment does not reevaluate field interpretations and data; rather, it reevaluates criteria used to define individual paleoearthquakes in the published literature.  In particular, the UCSS reevaluates the paleoearthquake record interpreted by Talwani and Shaeffer (Talwani, 2001) based on that study's compilation of sites with paleoliquefaction features.

Talwani and Schaeffer compiled radiocarbon ages from paleoliquefaction features along the coast of South Carolina.  These data include ages that provide contemporary, minimum, and maximum limiting ages for liquefaction events.  Radiocarbon ages were corrected for past variability in atmospheric $^{14}$C using well established calibration curves and converted to "calibrated" (approximately calendric) ages.  From the compilation of calibrated radiocarbon ages from various geographic locations, they correlated individual earthquake episodes.  They identified an individual earthquake episode based on samples with a "contemporary" age constraint that had overlapping calibrated radiocarbon ages at approximately 1-sigma confidence interval.  The estimated age of each earthquake was "calculated from the weighted averages of overlapping contemporary ages"  They defined as many as eight events from the paleoliquefaction record (named 1886, A, B, C, D, E, F, and G, in order of increasing age), and offered two scenarios to explain the distribution and timing of paleoliquefaction features (Table 2.5-19). (Talwani, 2001)

The two scenario paleoearthquake records proposed by Talwani and Schaeffer (Talwani, 2001), Scenario 1 and Scenario 2, have different interpretations for the size and location of prehistoric events (Table 2.5-19).  In Scenario 1, the four prehistoric events that produced widespread liquefaction features similar to the large 1886 Charleston earthquake (A, B, E, and G) are

---

interpreted to be large, Charleston-type events. Three events, C, D, and F, are defined by paleoliquefaction features that are more limited in geographic extent than other events and are interpreted to be smaller, moderate-magnitude events (approximately M 6). Events C and F are defined by features found north of Charleston in the Georgetown region, and Event D is defined by sites south of Charleston in the Bluffton area. In Scenario 2, all events are interpreted as large, Charleston-type events. Furthermore, Events C and D are combined into a large Event C'. Talwani and Schaeffer (Talwani, 2001) justify the grouping of the two events based on the observation that the calibrated radiocarbon ages that constrain the timing of Events C and D are indistinguishable at the 95 percent (2-sigma) confidence interval.

The length and completeness of the paleoearthquake record based on paleoliquefaction features is a source of epistemic uncertainty in the UCSS. The paleoliquefaction record along the South Carolina coast extends from 1886 to the mid-Holocene. The consensus of the scientists who have evaluated these data is that the paleoliquefaction record of earthquakes is complete only for the most recent ~2000 years and that it is possible that liquefaction events are missing from the older portions of the record. The suggested incompleteness of the paleoseismic record is based on the argument that past fluctuations in sea level have produced time intervals of low water table conditions (and thus low liquefaction susceptibility), during which large earthquake events may not have been recorded in the paleoliquefaction record. While this assertion may be true, it cannot be ruled out that the paleoliquefaction record is complete back to the mid-Holocene. (Talwani, 2001)

**2-Sigma Analysis of Event Ages**

Analysis of the coastal South Carolina paleoliquefaction record is based on the Talwani and Schaeffer data compilation. As described above, Talwani and Schaeffer use calibrated radiocarbon ages with 1-sigma error bands to define the timing of past liquefaction episodes in coastal South Carolina. The standard in paleoseimology, however, is to use calibrated ages with 2-sigma (95.4 percent confidence interval) error bands (e.g., (Sieh, 1989) (Grant, 1994)). Likewise, in paleoliquefaction studies, to more accurately reflect the uncertainties in radiocarbon dating, the use of calibrated radiocarbon dates with 2-sigma error bands (as opposed to narrower 1-sigma error bands) is advisable (Tuttle, 2001). The Talwani and Schaeffer use of 1-sigma error bands may lead to over-interpretation of the paleoliquefaction record such that more episodes are interpreted than actually occurred. In recognition of this possibility, the conventional radiocarbon ages presented in Talwani and Schaeffer have been recalibrated and reported with 2-sigma error bands. The recalibration of individual radiocarbon samples and estimation of age ranges for paleoliquefaction events show broader age ranges with 2-sigma error bands which are used to obtain broader age ranges for paleoliquefaction events in the Charleston area. (Talwani, 2001)

Event ages based on overlapping 2-sigma ages of paleoliquefaction features are presented in Table 2.5-19. Paleoearthquakes have been distinguished based on grouping paleoliquefaction features that have contemporary radiocarbon samples with overlapping calibrated ages. Event ages have then been defined by selecting the age range common to each of the samples. For example, an event defined by overlapping 2-sigma sample ages of 100–200 cal. yr. BP (before present) and 50–150 cal. yr. BP would have an event age of 50–150 cal. yr. BP. The UCSS study considers the "trimmed" ages to represent the approximately 95 percent confidence interval, with a "best estimate" event age as the midpoint of the approximately 95 percent age range.

The 2-sigma analysis identified six distinct paleoearthquakes in the data presented by Talwani and Schaeffer. As noted by that study, Events C and D are indistinguishable at the 95 percent confidence interval, and in the UCSS, those samples define Event C' (Table 2.5-19). Additionally, the UCSS 2-sigma analysis suggests that Talwani and Schaeffer Events F and G may have been a

single, large event, defined in the UCSS as F′.  One important difference between the UCSS result and that of Talwani and Schaeffer is that the three Events C, D, and F in their Scenario 1, which are inferred to be smaller, moderate-magnitude events, are grouped into more regionally extensive Events C′ and F′ (Table 2.5-19).  Therefore, in the UCSS, all earthquakes in the 2-sigma analysis have been interpreted to represent large, Charleston-type events.  Analysis suggests that there have been four large earthquakes in the most-recent, ~2000-year, portion of the record (1886 and Events A, B, and C′).  In the entire ~5000-year paleoliquefaction record, there is evidence for six large, Charleston-type earthquakes (1886, A, B, C′, E, and F′) (Table 2.5-19). (Talwani, 2001).

Recurrence intervals developed from the earthquakes recorded by paleoliquefaction features assume that these features were produced by large $M_{max}$ events and that both the ~2000-year and ~5000-year records are complete.  However, the UCSS mentions at least two concerns regarding the use of the paleoliquefaction record to characterize the recurrence of past $M_{max}$ events.  First, it is possible that the paleoliquefaction features associated with one or more of these pre-1886 events were produced by multiple moderate-sized events closely spaced in time.  If this were the case, then the calculated recurrence interval would yield artificially short recurrence for $M_{max}$, because it was calculated using repeat times of both large ($M_{max}$) events and smaller earthquakes.  Limitations of radiocarbon dating and limitations in the stratigraphic record often preclude identifying individual events in the paleoseismologic record that are closely spaced in time (i.e., separated by only a few years to a few decades).  Several seismic sources have demonstrated tightly clustered earthquake activity in space and time that are indistinguishable in the radiocarbon and paleoseismic record:

- ♦ New Madrid (December 1811, January 1812, February 1812)

- ♦ North Anatolian Fault (August 1999 and November 1999)

- ♦ San Andreas Fault (1812 and 1857)

Therefore, the UCSS acknowledges the distinct possibility that $M_{max}$ occurs less frequently than what is calculated from the paleoliquefaction record.

A second concern is that the recurrence behavior of the $M_{max}$ event may be highly variable through time.  For example, the UCSS considers it unlikely that **M** 6.7 to **M** 7.5 events have occurred on a Charleston source at an average repeat time of about 500 to 600 years (Talwani, 2001) throughout the Holocene Epoch.  Such a moment release rate would likely produce tectonic landforms with clear geomorphic expression, such as are present in regions of the world with comparably high rates of moderate to large earthquakes (for example, faults in the Eastern California shear zone with sub-millimeter per year slip rates and recurrence intervals on the order of about 5000 years have clear geomorphic expression (SSA, 2000).  Perhaps it is more likely that the Charleston source has a recurrence behavior that is highly variable through time, such that a sequence of events spaced about 500 years apart is followed by quiescent intervals of thousands of years or longer.  This sort of variability in inter-event time may be represented by the entire mid-Holocene record, in which both short inter-event times (e.g., about 400 years between Events A and B) are included in a record with long inter-event times (e.g., about 1900 years between Events C' and E).

**Recurrence Rates**

The UCSS model calculates two average recurrence intervals covering two different time intervals, which are used as two recurrence branches on the logic tree (Figure 2.5-59).  The first average recurrence interval is based on the four events that occurred within the past ~2000

years.  This time period is considered to represent a complete portion of the paleoseismic record based on published literature e.g., (Talwani, 2001)) and feedback from those researchers questioned (Talwani , 2001).  These events include 1886, A, B, and C' (Table 2.5-19).  The average recurrence interval calculated for the most recent portion of the paleoliquefaction record (four events over the past ~2000 years) is given 0.80 weight on the logic tree (Figure 2.5-59).

The second average recurrence interval is based on events that occurred within the past ~5000 years.  This time period represents the entire paleoseismic record based on paleoliquefaction data (Talwani, 2001).  These events include 1886, A, B, C', E, and F', as listed in Table 2.5-19.  As mentioned previously, published papers and researchers questioned suggest that the older part of the record (older than ~2000 years ago) may be incomplete.  Whereas this assertion may be true, it is also possible that the older record, which exhibits longer inter-event times, is complete.  The average recurrence interval calculated for the ~5000-year record (six events) is given 0.20 weight on the logic tree (Figure 2.5-59).  The 0.80 and 0.20 weighting of the ~2000-year and ~5000-year paleoliquefaction records, respectively, reflect incomplete knowledge of both the current short-term recurrence behavior and the long-term recurrence behavior of the Charleston source.

The mean recurrence intervals for the most-recent ~2000-year and past ~5000-year records represent the average time interval between earthquakes attributed to the Charleston seismic source.  The mean recurrence intervals and their parametric uncertainties were calculated according to the methods outlined by Savage (SSA, 1991) and Cramer (Cramer, 2001).  The methods provide a description of mean recurrence interval, with a best estimate mean Tave and an uncertainty described as a lognormal distribution with median T0.5 and parametric lognormal shape factor $\sigma$ 0.5.

The lognormal distribution is one of several distributions, including the Weibull, Double Exponential, and Gaussian, among others, used to characterize earthquake recurrence (Ellsworth, 1999).  Ellsworth (Ellsworth,1999) and Matthews (SSA, 2002) propose a Brownian-passage time model to represent earthquake recurrence, arguing that it more closely simulates the physical process of strain build-up and release.  This Brownian-passage time model is currently used to calculate earthquake probabilities in the greater San Francisco Bay region (USGS, 2003).  Analyses show that the lognormal distribution is very similar to the Brownian-passage time model of earthquake recurrence for cases where the time elapsed since the most recent earthquake is less than the mean recurrence interval (Cornell, 1988) (Ellsworth, 1999).  This is the case for Charleston, where 120 years have elapsed since the 1886 earthquake and the mean recurrence interval determined over the past ~2000 years is about 548 years. The UCSS study has calculated average recurrence interval using a lognormal distribution because its statistics are well known (NIST, 2006) and it has been used in numerous studies (e.g., those performed by Savage (SSA, 1991), Working Group on California Earthquake Probabilities (WGCEP, 1995), and Cramer (Cramer 2001).

The average interval between earthquakes is expressed as two continuous lognormal distributions.  The average recurrence interval for the ~2000-year record, based on the three most recent inter-event times (1886-A, A-B, and B-C'), has a best estimate mean value of 548 years and an uncertainty distribution described by a median value of 531 years and a lognormal shape factor of 0.25.  The average recurrence interval for the ~5000-year record, based on five inter-event times (1886-A, A-B, B-C', C'-E, and E-F'), has a best estimate mean value of 958 years and an uncertainty distribution described by a median value of 841 years and a lognormal shape factor of 0.51.  At one standard deviation, the average recurrence interval for the ~2000-year record is between 409 and 690 years; for the ~5000-year record, it is between 452 and 1,564 years.  Combining these mean values of 548 and 958 years with their respective

logic tree weights of 0.8 and 0.2 results in a weighted mean of 630 years for Charleston $M_{max}$ recurrence.

The mean recurrence interval values used in the UCSS model are similar to those determined by earlier studies. Talwani and Schaeffer consider two possible scenarios to explain the distribution in time and space of paleoliquefaction features. In Scenario 1, large earthquakes have occurred with an average recurrence of $454 \pm 21$ years over about the past ~2000 years; in Scenario 2, large earthquakes have occurred with an average recurrence of $523 \pm 100$ years over the past ~2,000 years. Talwani and Schaeffer state that, "In anticipation of additional data we suggest a recurrence rate between 500 and 600 years for **M** 7+ earthquakes at Charleston." For the ~2000-year record, the 1-standard-deviation range of 409 to 690 years completely encompasses the range of average recurrence interval reported by Talwani and Schaeffer. The best-estimate mean recurrence interval value of 548 years is comparable to the midpoint of the Talwani and Schaeffer best-estimate range of 500 to 600 years. The best estimate mean recurrence interval value from the ~5000-year paleoseismic record of 958 years is outside the age ranges reported by Talwani and Schaeffer, although they did not determine an average recurrence interval based on the longer record (Talwani, 2001).

In the updated seismic hazard maps for the conterminous United States, Frankel (USGS, 2002) used a mean recurrence value of 550 years for characteristic earthquakes in the Charleston region. This value is based on the above-quoted 500–600 year estimate from Talwani and Schaeffer (Talwani, 2001). Frankel (USGS, 2002) did not incorporate uncertainty in mean recurrence interval in their calculations.

For computation of seismic hazard, discrete values of activity rate (inverse of recurrence interval) are required as input to the PSHA code (SSA, 1968). To evaluate PSHA based on mean hazard, the mean recurrence interval and its uncertainty distribution should be converted to mean activity rate with associated uncertainty. The final discretized activity rates used to model the UCSS in the PSHA reflect a mean recurrence of 548 years and 958 years for the ~2000-year and ~5000-year branches of the logic tree, respectively. Lognormal uncertainty distributions in activity rate are obtained by the following steps: (1) invert the mean recurrence intervals to get mean activity rates; (2) calculate median activity rates using the mean rates and lognormal shape factors of 0.25 and 0.51 established for the ~2000-year and ~5000-year records, respectively; and (3) determine the lognormal distributions based on the calculated median rate and shape factors. The lognormal distributions of activity rate can then be discredited to obtain individual activity rates with corresponding weights.

### Characterization of Lancaster Seismic Zone

The Lancaster Seismic Zone (LSZ) of southeastern Pennsylvania is identified as a post-EPRI seismic zone located about 111 mi (179 km) northwest of the CCNPP Unit 3 site (Figure 2.5-52). This region of seismicity in the Appalachian mountains of Pennsylvania is described in Section 2.5.1.1.4.5 and includes roughly two centuries of seismicity. Despite its moderate rate of activity, the largest known earthquake was magnitude mbLg 4.1 **(**SSA, 1987). One larger event has been attributed to anthropogenic causes (i.e. Cacoosing Valley Earthquake mbLg 4.6; (Seeber, 1998). No evidence of larger prehistoric earthquakes, such as paleoliquefaction features, has been discovered (Wheeler, 2006). While the lack of large earthquakes in the relatively short historical record cannot preclude the future occurrence of large events, there is a much higher degree of uncertainty associated with the assignment of $M_{max}$ for the LSZ than other CEUS seismic source zones, such as New Madrid and Charleston, where large historical earthquakes are known to have occurred.

Although the Lancaster seismic zone is not explicitly included in the original EPRI source model (EPRI, 1986), various EPRI source geometries and parameters provide conservative $M_{max}$ distributions for the LSZ. A wide range of $M_{max}$ values and associated probabilities were assigned to these EPRI sources to reflect the uncertainty of multiple experts from each EST. The body-wave magnitude ($m_b$) $M_{max}$ values assigned by the ESTs for source geometries that envelop the LSZ range from $m_b$ 5.3 to 7.2 (**M** 4.88 to 7.5). The Dames & Moore sources that envelop the LSZ include an upper-bound $M_{max}$ value of $m_b$ 7.2 (**M** 7.5). Sources from the Woodward-Clyde and Rondout teams that envelop the LSZ were also assigned large upper-bound $M_{max}$ values of $m_b$ 6.8 to 7.1 (**M** 6.8 to 7.33). Thus, the maximum magnitude distributions of EPRI source zones are significantly greater than the largest reported earthquake in the LSZ.

Despite the identification of the LSZ by Armbruster and Seeber (SSA, 1987), subsequent post-EPRI seismic source characterizations studies (Chapman, 1994) (USGS, 1992) (USGS, 2002) do not identify the zone as a seismic source zone. The $M_{max}$ distribution assigned to the seismic source zones that cover, but do not define, the LSZ are $m_b$ 7.2 (**M** 7.5) (Chapman, 1994), $m_b$ 5.78 (**M** 5.4) (Bollinger, 1992), and $m_b$ 7.2 (**M** 7.5) (USGS, 1996) (USGS, 2002). Like the EPRI models, these magnitude distributions are larger than any instrumented or pre-instrumental historical events dating back to the 18th century (SSA, 1987). However, all of the post-EPRI (EPRI, 1986) background sources zones that encompass the LSZ effectively capture the EPRI background zones for the LSZ. Based on the available seismological and geologic evidence and available published literature for the LSZ, the existing EPRI seismic source model does not require a significant change. Therefore, it is concluded that no new information has been developed since 1986 that would require a significant revision to the EPRI seismic source model.

### Earthquake Swarm of Howard County, Maryland

Howard County of Maryland, located about 12 mi (19 km) southwest of Baltimore, experienced 21 confirmed and probable shallow (approximately 1650 ft t(503 m) to 1980 ft (604 m) deep) earthquakes between March and November 1993 (Reger, 1994). The largest events recorded are mbLg 2.5 and mbLg 2.7 and occurred early in the sequence. Some minor cosmetic damage was reported near the epicenters (e.g., plaster cracked; light objects fell from shelves; bicycles fell over); however, there were no reports of structural damage. Analyses of seismicity data define a short (1000 ft (305 m) long) northwest-striking reverse fault with a minor component of left-lateral slip. Researchers speculate that the earthquakes may be associated with a diabase dike either aligned with the inferred reverse fault or offset by the inferred reverse fault; however, the cause of the earthquake swarm remains unknown. Field examination by the Maryland Geological Survey did not find any evidence for surface fault rupture in the region of the inferred surface projection of the fault (Reger, 1994). This earthquake swarm occurred in a region that historically has been aseismic and post-dates the EPRI source model (EPRI, 1986). Based on the small size of the maximum earthquakes and shallow depth, as well as the absence of a well-defined geologic structure aligned with the microseismicity, the Howard County earthquake swarm is not interpreted as a capable tectonic source. In summary, the EPRI model (EPRI, 1986) does not need to be revised to accommodate this minor earthquake swarm.}

### 2.5.2.3    Correlation of Earthquake Activity with Seismic Sources

The U.S. EPR FSAR includes the following COL Item in Section 2.5.2.3:

> Correlation of earthquake activity with seismic sources is site specific and will be addressed by the COL applicant, consistent with the guidance of RG 1.208 and RG 1.165, as appropriate.

This COL Item is addressed as follows:

{The updated EPRI seismicity catalog was reviewed in order to evaluate the spatial pattern of seismicity relative to the EPRI seismic source model (EPRI, 1986) and potential correlation of seismicity to possible geologic or tectonic structures.  The EPRI seismicity catalog covers earthquakes in the CEUS for the time period from 1627 to 1984, as described in Section 2.5.2.1. This catalog has been updated for this CCNPP Unit 3 site investigation for the time period from 1985 to 2006, as described in Section 2.5.2.1. Figure 2.5-45 through Figure 2.5-50 show the distribution of earthquake epicenters from both the EPRI (pre-1985) and updated (post-1984) earthquake catalogs in comparison to the seismic sources identified by each of the EPRI ESTs.

Comparison of the updated earthquake catalog to the EPRI earthquake catalog (EPRI, 1988) yields the following conclusions:

♦    The updated catalog does not show any earthquakes within the site region that can be associated with a known geologic or tectonic structure. As described in Section 2.5.1, the majority of seismicity in the CCNPP Unit 3 site region appears to be occurring at depth within the basement beneath the Appalachian decollement.

♦    The updated catalog does not show a unique cluster of seismicity that would suggest a new seismic source outside of the EPRI seismic source model (EPRI, 1986).

♦    The updated catalog does not show a pattern of seismicity that would require significant revision to the EPRI seismic source geometry.

♦    The updated catalog does not show or suggest any increase in $M_{max}$ for any of the EPRI seismic sources (EPRI, 1986).

♦    The updated catalog does not show any increase in seismicity parameters (rate of activity, b value) for any of the EPRI seismic sources (EPRI, 1986) (see Section 2.5.2.6.5).}

### 2.5.2.4    Probabilistic Seismic Hazard Analysis and Controlling Earthquake

The U.S. EPR FSAR includes the following COL Item in Section 2.5.2.4:

The probabilistic seismic hazard analysis is site specific and will be addressed by the COL applicant, consistent with the guidance of NUREG/CR-6372, RG 1.165 and RG 1.208, as appropriate.

This COL Item is addressed as follows:

{Sections 2.5.2.4.1 through 2.5.2.4.6 are added as a supplement to the U.S. EPR FSAR.

### 2.5.2.4.1    1989 EPRI Probabilistic Seismic Hazard Analysis

Following the recommendation of Regulator Guide 1.165 (NRC, 1997)), the 1989 EPRI study, EPRI NP-6395-D (EPRI, 1989a) forms a basis with which to start seismic hazard calculations.  The first step was to replicate the results published from the 1989 EPRI study (EPRI, 1989a), to verify that seismic sources were modeled correctly and that the current seismic hazard software could accurately reproduce the 1989 results.  The PSHA software used determines the annual frequency of exceedance as a function of minimum ground motion in an integration of hazard contribution of seismic sources - characterized by various parameters, including spatial extent and location, magnitude frequency recurrence, and tectonic environment - propagating the ground motion from the sources to the site through an appropriate attenuation relation.  This software and the manner in which it is used allows for the incorporation of numerous elements

of modeling and parametric variability, including alternative models and parametric distributions, as well as consideration of statistical uncertainties. This replication was made using the ground motion equations from the 1989 EPRI study, and it was made for rock hazard conditions in order to remove any effect that soil amplification might have on the comparison.

Table 2.5-20 compares the mean seismic hazard calculated for several amplitudes for peak ground acceleration (PGA) and for spectral velocity (SV) at 10 and 1 Hz. Spectral velocity was the response spectrum measure used in the 1989 EPRI study. For amplitudes corresponding to annual exceedance frequencies in the range $10^{-4}$ to $10^{-6}$, the 2006 calculations replicate the 1989 EPRI results (EPRI, 1989a) to an accuracy that is in the range of 3 percent to 12 percent, with the 2006 calculations indicating slightly higher hazard. This is acceptable agreement, given that independent software was used to perform these calculations. Comparisons were also made for the median hazard and the 85 percent hazard, and these comparisons showed somewhat larger differences, with the 2006 results generally (but not always) showing higher hazards than the EPRI results (EPRI, 1989a). These comparisons are of less importance and concern because the mean hazard will be used to derive recommended seismic design levels.

### 2.5.2.4.2    Effects of New Regional Earthquake Catalog

One of the important sensitivity studies examined the effect of earthquakes that have occurred since the 1989 EPRI study (EPRI, 1989a) was performed in order to determine if activity rates have changed. Seismicity rates in the EPRI study were based on an earthquake catalog that extended through 1984. This sensitivity study examined additional earthquakes that occurred during the period of 1985 to 2005 and calculated rates of activity in regions surrounding the CCNPP Unit 3 site.

Figure 2.5-61 shows historical seismicity in the region of the site, with three areas that were used to examine the effect of additional seismicity: a 124 mi (200 km) × 124 mi (200 km) square region centered on the site, a 249 mi (400 km) × 249 mi (400 km) square region centered on the site, and a Rondout source 29. The latter source was selected as a representative source for the Central Virginia seismic zone.

To examine the effect of additional seismicity, the EPRI software discussed in EPRI NP-6452-D 1989 (EPRI, 1989b) was run, first with the original earthquake catalog (through 1984) (EPRI, 1986), and then with the extended catalog (through 2005). This software calculates seismicity parameters (a- and b-values) from which annual rates of earthquake occurrence can be derived. For these calculations, the seismicity was assumed to be spatially homogeneous within each source.

Figure 2.5-62, Figure 2.5-63, and Figure 2.5-64 compare annual rates of earthquake occurrence verses magnitude for the three sources examined in this sensitivity study (the 124 mi (200 km) × 124 mi (200 km) square region centered on the site, the 249 mi (400 km) × 249 mi (400 km) square region centered on the site, and the Rondout source 29). All three plots are in terms of $m_b$ magnitude, which is the scale used in the original EPRI calculations. All three plots show that the additional seismicity from 1985-2005 indicates lower seismicity rates for the square sources surrounding the site and virtually the same seisicity rate in the Central Virginia Seismic Zone that was calculated using the original EPRI earthquake catalog (EPRI, 1986).

These comparisons indicate that the original seismicity rates that were calculated for seismic sources are adequate. These seismicity rates were developed during the 1989 EPRI study (EPRI, 1989a) for seismic sources developed by the six Earth Science Teams and do not need to be updated.

### 2.5.2.4.3    New Maximum Magnitude Information

As discussed above in Section 2.5.2.2, no new scientific information has been published that would lead to a change in the EPRI seismic source characterization or parameters, including the assessment of maximum magnitude.  The only exception is the Charleston source, which is addressed in the next subsection.  Therefore, the maximum magnitude distributions assigned by the EPRI EST teams to their sources have not been modified for the assessment of seismic hazard.

### 2.5.2.4.4    New Seismic Source Characterizations

As described above in Section 2.5.2.2.2.7, a new Charleston source model (the UCSS) has been developed to reflect updated estimates of the possible geometries of seismic sources in the Charleston region, the possible characteristics magnitudes that might occur, and the possible mean recurrence rates associated with those characteristic magnitudes.  There are four geometries:

- ♦    Geometry A, weight 0.7

- ♦    Geometry B, weight 0.1

- ♦    Geometry B', weight 0.1

- ♦    Geometry C, weight 0.1

The distribution of characteristic magnitudes for these sources is described in Section 2.5.2.2.7.2.  A discrete distribution with 5 values and weights is used.  The distribution of mean recurrence intervals is described in Section 2.5.2.2.7.3, and it is developed using two data periods for paleoliquefaction events.  Each data period has its own mean and uncertainty estimate for mean recurrence interval, and a discrete distribution with 5 values and weights is used to model each distribution, thus resulting in a total of 10 mean recurrence values (with weights) describing uncertainty in mean recurrence interval.

The above four geometries were represented with parallel faults oriented Northeast-Southwest and spaced at 6 mi (10 km) apart, and the activity rate of each geometry was distributed among the parallel faults.  A general rupture length equation was used (Wells and Coppersmith 1994) to model a finite rupture length for each earthquake.  The large distance between the CCNPP Unit 3 site and the Charleston seismic sources means that the exact details of the fault models and rupture lengths are not critical to the calculation of hazard from the Charleston source.

None of the six EPRI Earth Science Teams had a Charleston source that contributed to the 99 percent hazard in the original EPRI 1989 (EPRI, 1989a) calculations, in part because the implicit recurrence interval for large Charleston earthquakes was much longer than is now modeled (i.e., the activity rate was estimated to be lower).  To include possible re-occurrences of large earthquakes in the Charleston region, the UCSS was added to each EST's list of sources.

### 2.5.2.4.5    New Ground Motion Models

Since publication of the 1989 EPRI study (EPRI, 1989a), much work has been done to evaluate strong earthquake ground motion in the central and eastern United States.  This work was summarized EPRI TR-1009684 (EPRI, 2004) in the form of updated ground motion equations that estimate median spectral acceleration and uncertainty as a function of earthquake magnitude and distance.  Epistemic uncertainty is modeled using multiple ground motion equations and multiple estimates of aleatory uncertainty (sigma), all with associated weights.

Different sets of equations are recommended for sources that represent rifted verses non-rifted parts of the earth's crust.  Equations are available for spectral frequencies of 100 Hz (equivalent to PGA), 25 Hz, 10 Hz, 5 Hz, 2.5 Hz, 1 Hz, and 0.5 Hz, and these equations apply to hard rock conditions.

EPRI published an update, EPRI TR-1014381 (EPRI, 2006a) in 2006 to the estimates of aleatory uncertainty.  This update reflected the observation that the aleatory uncertainties in the original EPRI attenuation study (EPRI, 2004) were probably too large, resulting in over-estimates of seismic hazard.  The 2006 EPRI study (EPRI, 2006a) recommends a revised set of aleatory uncertainties (sigmas) with weights, that can be used to replace the original aleatory uncertainties published in the 2004 EPRI study (EPRI, 2004).

The ground motion model used in the seismic hazard calculations consisted of the median equations from the EPRI 2004 study (EPRI 2004), with the updates for the aleatory uncertainties (EPRI, 2006a).  EPRI TR-1014381 (EPRI, 2006a) was used in lieu of the Regulatory Guide 1.208 cited document, i.e. EPRI Report 1013105 (EPRI, 2006b).  EPRI Report 1013105 (EPRI, 2006b) was an Update Report while EPRI TR-1014381 (EPRI, 2006a) is the final report.  For the purposes of revised estimates of aleatory uncertainty in the central and eastern U.S., there is no technical difference between the documents.  The "Recommended CEUS Sigma" values and "Conclusions" of both reports are identical.

Additionally, Equation 7 of Regulatory Guide 1.208 (NRC, 2007a), Appendix D, Page D-5, was not used as written, in the determination mean distance of the controlling earthquake.

The deviation is described as follows:

Equation 7 is addressed in Appendix D, Step 3, Determining Controlling Earthquakes, as:

"The mean distance of the controlling earthquake is based on magnitude-distance bins greater than distances of 100 km (63 mi) as discussed in Step 5 and determined according to the following:

$$\text{Ln}\{D_C(1 - 2.5\text{Hz})\} = \sum_{d > 100} \text{Ln}(d)\sum_{m} P > 100(m, d)_2 \qquad \text{Equation 7}$$

where d is the centroid distance value for each distance bin."

The definition for the term "P" is provided in Appendix D, Step 1, Determining Controlling Earthquakes."

P is defined as: This distribution, P > 100 (m,d), is defined by the following:

$$P > 100(m, d)_1 = [P(m, d)_1] \div \left[\sum_{m} \sum_{d > 100} [P(m, d)_1]\right] \qquad \text{Equation 3}$$

As written Equation 7 is in error.  The specific error is that the term P > 100 (m,d)$_2$ in Equation 7 should be P> 100 (m,d)$_1$ as defined in Step 1, i.e., difference in subscript 2 in Step 3 versus subscript 1 in Step 1.

By the definition in Step 1, P > 100 (m,d)$_1$ refers to the probability of the fractional contribution of each magnitude and distance bin (beyond 100 km) to the total hazard for the average of 1 and 2.5 Hz, whereas P > 100 (m,d)$_2$ refers to of the fractional contribution of each magnitude and distance bin to the total hazard for the average of 5 and 10 Hz.  Step 3 explicitly refers to mean magnitude and distance of the controlling earthquakes associated with the ground motions determined in Regulatory Guide 1.208, Appendix D, Step 2 for the average of 1 and 2.5 Hz.

The corrected equation provides for evaluating the mean distance of the controlling earthquake for distances of 100 km or greater for the average of 1 and 2.5 Hz (NRC, 2007a).

### 2.5.2.4.6    Updated EPRI Probabilistic Seismic Hazard Analysis Deaggregation, and 1 Hz, 2.5 Hz, and 10 Hz Spectral Accelerations Incorporating Significant Increases Based on the Above Sensitivity Studies

With the above assumptions on seismic sources (the original EPRI EST teams sources, plus the Charleston sources) and the substitution of the updated ground motion model and aleatory uncertainty model, the seismic hazard was recalculated for the CCNPP Unit 3.  This calculation was first made for hard rock conditions, and these results were then modified (as described below) to account for local site conditions.

The calculation of seismic hazard consists of calculating annual frequencies of exceeding different amplitudes of ground motion, for all combinations of seismic sources, seismicity parameters, maximum magnitudes, ground motion equations, and ground motion aleatory uncertainties.  This calculation is made separately for each of the six EPRI EST teams and results in a family of seismic hazard curves.  The alternative assumptions on seismic sources, seismicity parameters, maximum magnitudes, ground motion equations, and ground motion aleatory uncertainties are weighted, resulting in a combined weight associated with each hazard curve.  From the family of hazard curves and their weights, the mean hazard (and the distribution of hazard) can be calculated.

Figure 2.5-95 through Figure 2.5-101 are plots of the resulting updated probabilistic seismic hazard hard rock curves for the seven spectral ordinates (100 Hz (equivalent to PGA), 25 Hz, 10 Hz, 5 Hz, 2.5 Hz, 1 Hz, and 0.5 Hz).  The mean and fractile (15%, 50% (median), and 85%) hazard curves are indicated.

Figure 2.5-65 shows mean and median uniform hazard spectra for $10^{-4}$ and $10^{-5}$ annual frequencies of exceedance from these calculations at the seven structural frequencies at which ground motion equations are available.  Numerical values of these spectra are documented in Table 2.5-24.

The seismic hazard was deaggregated for implementation of Regulatory Guide 1.208 (NRC, 2007a).  That is, the contributions by earthquake magnitude and distance to hazard at the $10^{-4}$, $10^{-5}$, and $10^{-6}$ ground motions were determined for 1 Hz, 2.5 Hz, 5 Hz, and 10 Hz.  The deaggregations for 1 Hz and 2.5 Hz were combined to produce a single mean low-frequency (LF) deaggregation, and the deaggregations for 5 Hz and 10 Hz were combined to produce a single mean high-frequency (HF) deaggregation.  These deaggregations were done for ground motions corresponding to mean $10^{-4}$, $10^{-5}$, and $10^{-6}$ annual frequencies of exceedance.  The resulting deaggregations by magnitude and distance are shown in Figure 2.5-66 through Figure 2.5-69, Figure 2.5-89, and Figure 2.5-90 for $10^{-4}$ (Figure 2.5-66 and Figure 2.5-67) $10^{-5}$ (Figure 2.5-68 and Figure 2.5-69) and $10^{-6}$ (Figure 2.5-89 and Figure 2.5-90).  These figures also show the contribution by ground motion epsilon, which is the number of standard deviations that the $10^{-4}$, $10^{-5}$, or $10^{-6}$ (log) ground motion is above or below the median (log) ground

motion. (This deaggregation is done in logarithmic space because ground motions are assumed to follow a lognormal distribution.) In Figure 2.5-66 through Figure 2.5-69, Figure 2.5-89, and Figure 2.5-90 earthquake magnitudes have been converted to the moment magnitude scale.

Figure 2.5-66 through Figure 2.5-69, Figure 2.5-89, and Figure 2.5-90 show that small, local earthquakes dominate the HF motion, but that a significant contribution to hazard (from 15 percent to 30 percent) occurs for LF motions from large, distant earthquakes in the Charleston SC region. Representative earthquake magnitudes and distances were developed for the $10^{-4}$ and $10^{-5}$ ground motions as these are used to develop the recommended ground motion response spectrum (GMRS).

A deviation was taken to the formulas presented in Regulatory Guide 1.208 (NRC, 2007a). Appendix D, Development of Seismic Hazard Information Base and Determination of Controlling Earthquakes for determination of the controlling earthquake for high frequencies (5-10 Hz). The procedure in Regulatory Guide 1.208 (NRC, 2007a), Appendix D specifies averaging the high frequency contributions to hazard across the entire magnitude-distance bins matrix to determine the overall mean magnitude and mean distance of the controlling earthquake.

Use of this process leads to a less accurate description of the magnitudes and distances contributing most significantly to the high frequency hazard than the alternative adopted.

The alternative was to select the mean magnitude and mean distance contributing to the high frequency ground motion from the $R < 100$ km results only. Use of all distances in the calculation of mean magnitude and distance controlling earthquake values of $\mathbf{M} = 5.5$ and $R = 97$ for the $10^{-4}$ event. It is clear from the total deaggregation results (see Figure 2.5-67 of the FSAR) that this is not the distance of the earthquake controlling high frequency motions. Use of the alternative method leads to the same mean magnitude but to the closer distance, $R$, of 35 km, in better agreement with the deaggregation results (again, as shown in the figure). The same method was followed for the $10^{-5}$ annual frequency of exceedance results.

This alternative process is acceptable as use of the procedure in Regulatory Guide 1.208 (NRC, 2007a), Appendix D would have resulted in a lesser representative controlling magnitude.

The deaggregation of seismic hazard at annual frequencies of exceedance of $10^{-4}$ and $10^{-5}$ was divided into two groups: those contributions for $R < 62$ mi) 100 km, and those contributions for $R > 62$ mi (100 km). Table 2.5-21 shows the mean magnitudes and distances for each group, as well as the mean magnitude and distance overall.

With these deggregations, the representative LF earthquake was selected using the $R > 62$ mi (100 km) mean magnitude and mean distance (the dark-shaded cells in Table 2.5-21). In order to accurately represent the magnitudes and distances contributing to the HF ground motion, the mean magnitude and mean distance was selected from the $R < 62$ mi (100 km) results (the light-shaded cells in Table 2.5-21). The alternative, selecting the overall mean magnitude and mean distance to represent the HF earthquake, would have meant using $\mathbf{M} = 5.5$ and $R = 97$ for the $10^{-4}$ HF event. From Figure 2.5-67 this has a lower contribution to hazard than the $\mathbf{M} = 5.5, R = 22$mi (35 km) result from the $R < 62$ mi (100 km) results. This method of selecting mean magnitude and mean distance was followed for the $10^{-5}$ annual frequency of exceedance results as well.

As an example of how individual seismic sources contribute to mean seismic hazard, Figure 2.5-91 and Figure 2.5-92 show the mean seismic hazard by source for the Rondout team. This team is selected as an example because they have the simplest interpretation of seismic sources among all EPRI EST teams.  For the Rondout team, the following sources were modeled:

- ◆ Source RND-29: central Virginia seismic zone

- ◆ Source RND-30: source in northern Virginia and central Maryland

- ◆ Source RND-31: source in eastern Pennsylvania, New Jersey, and southern New England

- ◆ Source RND-C01: background source for the eastern seaboard

- ◆ Sources Charleston: the UCSS source described above

These plots confirm the sensitivities described in the deaggregation plots.  That is, local sources, particularly the central Virginia seismic zone, tend to dominate the hazard, particularly for high frequency ground motions (10 Hz).  However, for low frequency ground motion (1 Hz) the Charleston source has an important contribution to hazard.

Figure 2.5-93 and Figure 2.5-94show the median seismic hazard by source for the Rondout team, for 10 Hz and 1 Hz, respectively.  Qualitatively these plots show the same effects as the plots for mean seismic hazard (Figure 2.5-91 and Figure 2.5-92).

Figure 2.5-65 shows mean and median uniform hazard response spectra (UHRS) for the CCNPP Unit 3 site for rock conditions, accounting for all seismic sources in the analysis.  Important factors affecting the analysis are the Charleston seismic source (as shown in Figure 2.5-66 through Figure 2.5-69, Figure 2.5-89, and Figure 2.5-90), the updated ground motions equations from EPRI TR-1009684 (EPRI, 2004) and the revised estimates of aleatory uncertainty provided by EPRI EPRI TR-1014381 (EPRI, 2006a).}

### 2.5.2.5     Seismic Wave Transmission Characteristics of the Site

The U.S. EPR FSAR includes the following COL Item in Section 2.5.2.5.

Seismic wave transmission characteristics are site specific and will be addressed by the COL applicant.

This COL Item is addressed as follows:

{The uniform hazard spectra described in the preceding section are defined on hard rock (shear-wave velocity of 9200 ft/sec (2804 m/sec)), which is located more than 2500 ft (762 m) below the current ground surface at the CCNPP Unit 3 site.  The seismic wave transmission effects of this thick soil column on hard rock ground motions are described in this section.

Section 2.5.2.5.1 is added as a supplement to the U.S. EPR FSAR.

### 2.5.2.5.1     Development of Site Amplification Functions

### 2.5.2.5.1.1     Methodology

The calculation of site amplification factors is performed in the following 4 steps:

1.  Develop a base-case soil and rock column in which mean low-strain shear wave velocities and material damping values, and strain-dependencies of these properties, are estimated for relevant layers from the hard rock horizon to the surface. At the CCNPP Unit 3 site, hard rock ($V_s$ = 9200 ft/sec (2804 m/sec) is at a depth of approximately 2600 ft (792 m).

2.  Develop a probabilistic model that describes the uncertainties in the above properties, locations of layer boundaries, and correlation between the velocities in adjacent layers, and generate a set of 60 artificial "randomized" profiles.

3.  Use the seismic hazard results at $10^{-4}$ and $10^{-5}$ annual frequencies of exceedance to generate smooth spectra, representing LF and HF earthquakes at the two annual frequencies, for input into dynamic response analysis.

4.  Use an equivalent-linear site-response formulation together with Random Vibration Theory (RVT) to calculate the dynamic response of the site for each of the 60 artificial profiles, and calculate the mean and standard deviation of site response. This step is repeated for each of the four input motions ($10^{-4}$ and $10^{-5}$ annual frequencies, HF and LF smooth spectra).

> RVT methods characterize the input rock motion using a Fourier amplitude spectrum instead of time domain earthquake input motions. This spectrum is propagated through the soil to the surface using frequency domain transfer functions and computing peak ground accelerations or spectral accelerations using extreme value statistics. The RVT analysis that was conducted accounted for the strain dependent soil properties.

These steps are described in the following subsections.

### 2.5.2.5.1.2    Base Case Soil/Rock CCNPP Unit 3 and Uncertainties

Development of a base case soil/rock column is described in detail in Section 2.5.4. Summaries of the low strain shear wave velocity, material damping, and strain-dependent properties of the base case materials are provided below in this section. These parameters are used in the site response analyses.

The geology at the CCNPP Unit 3 site consists of marine and fluvial deposits overlying bedrock. The upper 400± ft (122 m) of the site soils was investigated using test borings, cone penetration testing, test pits, and geophysical methods. Information on subsurface conditions below this depth was assembled from available geologic information from various resources and will be discussed later in this section.

Soils in the upper 400 ft (122 m) of the site can generally be divided into the following geotechnical strata:

♦   Stratum I: Terrace Sand, loose to dense

♦   Stratum IIa: Chesapeake Clay/Silt, firm to hard

♦   Stratum IIb: Chesapeake Cemented Sand, with other sand layers, medium to very dense

♦   Stratum IIc: Chesapeake Clay/Silt, stiff to hard

♦    Stratum IIIa: Nanjemoy Cemented Clay/Silt, stiff to hard

♦    Stratum IIIb: Nanjemoy Sand, dense to very dense

Two borings, B-301 and B-401 provide the deepest site-specific soils information collected during the geotechnical investigation for the CCNPP Unit 3 site, and they were also used to obtain the deepest suspension P-S velocity logging profile at the site. The P-S measurements provide shear and compressional wave velocities and Poisson's ratios in soils at 1.6 ft (0.5 m) intervals to a depth of about 400 ft (122 m).

Various available geologic records were reviewed and communications were made with staff at the Maryland Geological Survey, the United States Geological Survey, the Triassic-Jurassic Study Group, Lamont-Doherty Earth Observatory, and Columbia University to develop estimates of subsurface soil properties below 400 ft (122 m) depth. Further details, including associated references, are presented in Subsection 2.5.1. Soils below 400 ft (122 m) consist of Coastal Plain sediments of Eocene, Paleocene, and Cretaceous eras, extending to an estimated depth of about 2555 ft (779 km) below the ground surface. These soils contain sequences of sand, silt, and clay. Given their geologic age, they are expected to be competent soils, consolidated to at least the weight of the overlying soils.

Several available geologic records were reviewed to estimate bedrock characteristics below the site. Various bedrock types occur in the CCNPP Unit 3 site region, including Triassic red beds, Jurassic diabase, granite, schist, and gneiss. However, only granitoid rocks (metamorphic gneiss, schist, or igneous granitic rocks) similar to those exposed in the Piedmont, could be discerned as the potential regional rock underlying the CCNPP Unit 3 site. This rock type was assumed as the predominant rock type at the CCNPP Unit 3 site.

Two sonic profiles were found for wells in the area that penetrated the bedrock, one at Chester, Maryland (about 40 mi (64 km) north of the site) and another at Lexington Park, Maryland (about 10 mi (16 km) south of the site). These two profiles were digitized and converted to shear wave velocity, based on a range of assumed Poisson's ratios for soil and rock.

Unit weights for the soils beneath the site are in the range of about 115 to 120 pcf (pounds per cubic foot) (1765 kg/m$^3$ to 1929 kg/m$^3$). The bedrock unit weight was assigned a value of 160 pcf (2592 kg/m$^3$).

Generic EPRI curves from EPRI TR-102293 (EPRI, 1993) were adopted to describe the strain dependencies of shear modulus and damping for subsurface soils. The EPRI "sand" curves cover a depth range up to 1,000 ft (305 m). Since soils at the CCNPP Unit 3 site extend beyond 1,000 feet (305 m), similar curves were extrapolated from the EPRI curves, extending beyond the 1000 ft (305 m), to obtain data for deeper soils. EPRI curves for the upper 400 ft (122 m) of the site soils were based on available results from the site investigation. Below 400 ft (122 m), a site-specific geologic profile was used as a basis for the soil profiles, including engineering judgment to arrive at the selected EPRI curves. The damping curves for soils were truncated at 15 percent for the site response analysis.

Bedrock was assumed to behave elastically with a damping ratio of 1 percent.

### 2.5.2.5.1.3      Site Properties Representing Uncertainties and Correlations

To account for variations in shear-wave velocity across the site, 60 artificial profiles were generated using the stochastic model developed by Toro (Toro, 1996), with some modifications to account for conditions at the CCNPP Unit 3 site. These artificial profiles represent the soil

column from the top of bedrock (with a bedrock shear-wave velocity of 9,200 ft/s (2804 m/sec) to the ground surface.  This model uses as inputs the following quantities:

♦   The median shear-wave velocity profile, which is equal to the base-case soil and rock profiles described above

♦   The standard deviation of ln(Vs) (the natural logarithm of the shear-wave velocity) as a function of depth, which is developed using available site and regional data (refer to Section 2.5.4)

♦   The correlation coefficient between ln(Vs) in adjacent layers, which is taken from generic studies

♦   The probabilistic characterization of layer thickness as a function of depth, which is also taken from generic studies, and then modified to allow for sharp changes in the base-case velocity profile

♦   The depth to bedrock, which is randomized to account for epistemic uncertainty in the bedrock-depth data described in Section 2.5.4.

Figure Figure 2.5-72 shows the median $V_s$ value as a function of depth, and it also shows actual values obtained from boreholes B-301 and B-401 from the P-S velocity logging measurement, both as recorded and smoothed over a window of 9.8 ft (3 m).  The bottomFigure in Figure 2.5-72 shows the logarithmic standard deviations calculated from the smoothed data, which were used to generate multiple profiles.  Below 400 ft (122 m), data are available from two profiles from Chester and Lexington Park.  The shear-wave velocities from these two profiles, and the logarithmic standard deviation computed from them, are shown in Figure 2.5-73.

Values for the standard deviation of ln(Vs) as a function of depth were developed using Vs data from site boreholes B-301 and B-401 (for the top 400 ft of the profile), and from boreholes at Chester and Lexington Park (for greater depths).  Refer to Section 2.5.4 for more details on these data.

This study uses the inter-layer correlation model from Toro for category U.S. Geological Survey "C" as delineated in Toro.  (Toro, 1996)

The probabilistic characterization of layer thickness consists of a function that describes the rate of layer boundaries as a function of depth.  This study utilized a generic form of this function, taken from Toro (Toro, 1996), and then modified to allow for sharp changes in the adopted base-case velocity profile.

Section 2.5.4.7.2.2 indicates that the shear-wave velocity of 9,200 ft/s (2804 m/sec) (for bedrock) is estimated at a depth of approximately 2531 ft (771 m).  This value is taken as the base case or median depth.  This information on bedrock depth is based on boreholes located tens of miles away from the site where are discussed in Section 2.5.4.7.2.2.  The uncertainty associated with depth to bedrock is characterized by a uniform distribution over the interval of 2531 ft 771 m), plus or minus 50 ft (15 m) (the latter number is one half the contouring interval used to estimate the depth to bedrock).  Because bedrock occurs at a large depth, the specific details of modeling uncertainty in this depth are not critical to the calculation of site response.

Figure 2.5-74 illustrates the $V_S$ profiles generated for profiles 1 through 10, using the median, logarithmic standard deviation, and correlation model described. These profiles include uncertainty in depth to bedrock. In total, 60 profiles were generated. Figure 2.5-75 compares the median of these 60 $V_S$ profiles to the median $V_S$ profile described in the previous section, indicating excellent agreement. ThisFigure also shows the ±1 standard deviation values of the 60 profiles, reflecting the standard deviations indicated in Figure 2.5-72 and Figure 2.5-73.

Median values of shear stiffness ($G/G_{MAX}$) and damping for each geologic unit are described in Section 2.5.4. Uncertainties in the properties for each soil unit are characterized using the values obtained by Costantino (Constantino, 1996). Figure 2.5-76 and Figure 2.5-77 illustrate the shear stiffness and damping curves generated for one of the geologic units, the Chesapeake silt/clay that is present at the depth range from approximately 100 ft (30 m) to 280 ft (85 m).

This set of 60 profiles, consisting of $V_S$ versus depth, depth to bedrock, stiffness, and damping, are used to calculate and quantify site response and its uncertainty, as described in the following sections.

### 2.5.2.5.1.4    Development of Low-Frequency and High-Frequency Smooth Spectra

In order to derive smooth spectra corresponding to the $10^{-4}$ and $10^{-5}$ amplitudes, the mean magnitudes and distances summarized in Table 2.5-21 were used in the following way. The magnitudes and distances were applied to spectral shape equations from NUREG/CR-6728 (NRC, 2001) to determine realistic spectral shapes for the four representative earthquakes ($10^{-4}$ and $10^{-5}$, HF and LF events) – see Figure 2.5-70 and Figure 2.5-71. The HF shapes were scaled to the Uniform Hazard Spectra mean values for $10^{-4}$ or $10^{-5}$, as appropriate, from Table 2.5-24 for 5 Hz, 10 Hz, 25 Hz, and 100 Hz. The shapes were used to interpolate between these 4 structural frequencies. Below 5 Hz, the HF spectral shape was extrapolated from 5 Hz, without regard to Uniform Hazard Spectra amplitudes at lower frequencies. The LF shapes were scaled to the Uniform Hazard Spectra values for $10^{-4}$ or $10^{-5}$, as appropriate, from Table 2.5-24 for 0.5 Hz, 1 Hz, and 2.5 Hz. Below 0.5 Hz the spectral shape was extrapolated from 0.5 Hz. Above 2.5 Hz the spectral shape was extrapolated from 2.5 Hz, without regard to Uniform Hazard Spectra amplitudes at higher frequencies.

Creation of smoothed $10^{-4}$ and $10^{-5}$ spectra in this way ensures that the HF spectra match the $10^{-4}$ and $10^{-5}$ Uniform Hazard Spectra values at high frequencies (5 Hz and above), and ensures that the LF spectra match the $10^{-4}$ and $10^{-5}$ Uniform Hazard Spectra values at low frequencies (2.5 Hz and below). In between calculated values, the spectra have smooth and realistic shapes that reflect the magnitudes and distances dominating the seismic hazard, as reflected in Table 2.5-21.

### 2.5.2.5.1.5    Site Response Analysis

The site response analysis performed for the CCNPP Unit 3 site used Random Vibration Theory (RVT). The application of RVT to site response has been described by Schneider (Schneider, 1991), Stepp (Stepp, 1991), Silva (Silva, 1997), and Rathje (Rathje, 2006), and a theoretical description of the method will not be presented here. Given a site-specific soil column and the above studies, the fundamental assumptions are as follows:

♦ The site response can be modeled using horizontal soil layers and a one-dimensional analysis.

♦ Vertically-propagating shear waves are the dominant contributor to site response.

♦ An equivalent-linear formulation of soil nonlinearity is appropriate for the characterization of site response.

These are the same assumptions that are implemented in the SHAKE program (Idriss, 1992) and that constitute standard practice for site-response calculations.  In this respect, RVT and SHAKE are similar.  Both use an iterative, frequency-domain equivalent-linear calculation to determine site response, and the frequency-domain representation of wave propagation in the the layered medium is identical for both approaches.  The difference is that RVT works with ground-motion power spectrum (and its relation to the response spectrum and other peak-response quantities), thus representing an ensemble of ground motions, while SHAKE works with individual time histories and their Fourier transforms, thus representing one specific ground motion.  Starting from the same inputs (e.g. the site properties described in Section 2.5.2.5.1.3 and the same rock response spectrum), both procedures will lead to similar estimates of site response (see, for example, Rathje (Rathje, 2006)).

The RVT site-response analysis requires the estimation of an additional parameter, strong motion duration, which does not have a strong influence on the calculated site response.  Strong motion durations of the rock motions are calculated from the mean magnitudes and distances of the controlling earthquakes as taken from the deaggregation results (see Table 2.5-21).  Estimates of strong motion duration depend on crustal shear-wave velocity,  , and seismic stress drop, $\Delta\sigma$, as follows:

$$T = \frac{1}{f_c} + 0.05R$$

Eq. 2.5.2-1

where R is the distance of controlling earthquake and earthquake corner frequency $f_c$ is defined as:

$$fc = 4.9 \times 10^6 \beta \left(\frac{\Delta\sigma}{M_0}\right)^{1/3}$$

and

$$M_0 = 10^{(1.5\mathbf{M} + 16.05)}$$

where $M_0$ is the seismic moment and **M** is the magnitude of the controlling earthquake (Rathje, 2006).  A value of 3.5 km/s was used for $\beta$ and 120 bars for $\Delta\sigma$, reflecting eastern US conditions.

One parameter that is used by both the RVT method and SHAKE is the effective strain ratio.  This parameter is estimated using the expression (**M**-1)/10 (Idriss, 1992), where **M** is the magnitude of the controlling earthquake taken from the deaggregation analysis.  A value of 0.5, rather than 0.45, was used for the $10^{-4}$ and $10^{-5}$ HF runs to remain within the 0.5 - 0.7 range found empirically by Kramer (Kramer, 1996).  Values of 0.58 and 0.59, derived from Idriss  (Irdriss, 1992) formula, were used for the $10^{-4}$ and $10^{-5}$ LF runs.  As is the case for strong motion duration, computed site response is not very sensitive to estimates of effective strain ratio.

The RVT method starts with the response spectrum of rock motion (for example, the $10^{-4}$ HF spectrum).  It then generates a Fourier spectrum corresponding to that input response spectrum, using an estimate of strong motion duration (calculated as described above) as an additional input.  This step is denoted as the Inverse RVT (or IRVT) step.  An iterative procedure

(similar to that in SHAKE) is applied to calculate peak and effective shear strains in each layer using RVT, update the stiffness and damping in each layer using the calculated effective strains and the $G/G_{max}$ and damping curves for the layer, and repeat the process until it converges. The final (or strain-compatible) stiffness and damping are then used to calculate the strain-compatible site transfer function. This transfer function is then multipled by the Fourier spectrum of the input rock motion to obtain the Fourier spectrum of the motion at the top of soil (in this case at 41 ft depth for outcrop conditions), from which the 41 ft depth outcrop response spectrum is calculated using RVT.

This process is repeated multiple times, once for each set of simulated profile parameters. For sixty site profiles, sixty 41 ft depth outcrop response spectra are calculated, from which statistics of site response are obtained.

As an example, Figure 2.5-78 shows 60 site spectra (41 ft depth outcrop) calculated for the $10^{-4}$ HF input motion, along with the median spectrum (shown as the red curve). The heavy curve at the bottom shows the calculated logarithmic standard deviation from the 60 response spectra, plotted with values shown on the right axis of the figure. Across all frequencies, logarithmic standard deviations are in the range 0.15 to 0.30.

In addition, the above calculations are repeated multiple times, once for each input rock spectrum. Thus the site response is calculated separately for the $10^{-4}$ HF, $10^{-4}$ LF, $10^{-5}$ HF, $10^{-5}$ LF, $10^{-6}$ HF, and $10^{-6}$ LF spectra.

In comparison to the SHAKE approach, the RVT approach avoids the requirement of performing spectral matching on the input time histories to match an input rock spectrum, and avoids analyzing each individual time history with a site-response program.

The site amplification factor is defined as the 41 ft depth outcrop response spectral amplitude at each frequency divided by the input rock spectral amplitude. Figure 2.5-78 shows the logarithmic mean and standard deviation of site amplification factor at 41 ft depth from the 60 profiles for the $10^{-4}$ HF input motion. As would be expected by the large depth of sediments at the site, amplifications are largest at low frequencies, and de-amplification occurs at high frequencies because of soil damping. The maximum strains in the soil column are low for this motion, and this is shown in Figure 2.5-79, which plots the maximum strains calculated for the 60 profiles versus depth. Maximum strains are generally less than 0.01 percent, with some profiles having strains in shallow layers up to 0.03 percent.

Figure 2.5-80 and Figure 2.5-81 show similar plots of amplification factors and maximum strains for the 10-4 LF motion. The results are similar to those for the HF motion, with the soil column generally exhibiting maximum strains less than 0.01 percent.

Figure 2.5-82 through Figure 2.5-85 show comparable plots of amplification factors and maximum strains for the 10-5 input motion, both HF and LF. For this higher motion, larger maximum strains are observed, but they are still generally less than 0.03 percent. A few profiles exhibit maximum strains of about 0.1 percent at shallow depths. These strains are within the range for which the equivalent linear site response formulation has been validated.

Table 2.5-23 documents the mean amplification factors for $10^{-4}$ and $10^{-5}$ rock input motions, and for HF and LF spectra.}

### 2.5.2.6     Ground Motion Response Spectra

The U.S. EPR FSAR includes the following COL Item in Section 2.5.2.6:

A COL applicant that references the U.S. EPR design certification will verify that the site-specific seismic parameters are enveloped by the CSDRS (anchored at 0.3 g PGA) and the 10 generic soil profiles discussed in Section 2.5.2 and Section 3.7.1 and summarized in Table 3.7.1-6.

This COL Item is addressed as follows:

{This section and Section 3.7.1 describes the reconciliation of the site-specific parameters for CCNPP Unit 3 and demonstrates that these parameters are enveloped by the Certified Seismic Design Response Spectra (CSDRS), anchored at 0.3 g PGA, and the 10 generic soil profiles used in the design of the U.S. EPR.

Table 5.0-1 of the U.S. EPR FSAR identifies shear wave velocity as a required parameter to be enveloped, defined as "Minimum shear wave velocity of 1000 feet per second (Low strain best estimate average value at bottom of basemat)."

Figure 2.5-102 compares the 10 generic soil profile cases used for the U.S. EPR and the average shear wave velocity profile that was adopted for the CCNPP site (shown in Figure 2.5-67 and Figure 2.5-87.

The CCNPP Unit 3 Average Profile shown in the aboveFigure is for soils below El. +44 ft (bottom of the basemat). Soils such as Stratum I Terrace Sand will not be used for support of foundations of Category I structures. Therefore, shear wave velocity measurements in the CCNPP site soils above El. +44 ft. regardless of value, are excluded from this evaluation as they lie above the basemat. Results from the aboveFigure indicate that:

1.  The CCNPP Unit 3 Average Profile is bounded by the 10 generic profiles used for the U.S. EPR.

2.  The CCNPP Unit 3 Average Profile offers a shear wave velocity at the bottom of the basemat (approx. El. +44 ft (or depth = 0 in the above figure)) of 1,450 ft/sec.

3.  The minimum shear wave velocity from the CCNPP Unit 3 Average Profile is 1,130 ft/sec.

4.  The characteristic shear wave velocity of the soil column (weighted with respect to the 344 ft soil column) is 1,510 ft/sec.

On the basis of the above, the idealized CCNPP Unit 3 site shear wave velceoocity profile is bounded by the 10 generic soil profiles used for the U.S. EPR and meets the minimum 1,000 ft/sec criterion identified in the U.S. EPR FSAR.

GMRS was conducted in accordance with the performance-based approach described in Regulatory Position 5 of Regulatory Guide 1.208 (NRC, 2007a).

The Safe Shutdown Earthquake (SSE) ground motion was developed starting from the $10^{-4}$ and $10^{-5}$ rock Uniform Hazard Spectra. At high frequencies, the appropriate ($10^{-4}$ or $10^{-5}$) HF mean amplification factor was applied to the $10^{-4}$ and $10^{-5}$ rock spectrum, to calculate site spectral amplitudes for $10^{-4}$ and $10^{-5}$ annual frequencies of exceedance. At low frequencies, a similar technique was used with the LF mean amplification factors. At intermediate frequencies the larger of the HF and LF site spectral amplitudes was used.

Figure 2.5-86 illustrates the resulting site spectra.  At high frequencies the HF spectral amplitudes are always greater, and at low frequencies the LF spectral amplitudes are always greater.  The two sets of spectral amplitudes cross at 2-3 Hz.

This procedure corresponds to Approach 2A in NUREG/CR-6728 (NRC, 2001) and NUREG/CR-6769 (NRC, 2002b), wherein the rock Uniform Hazard Spectra (for example, at $10^{-4}$) is multiplied by a mean amplification factor at each frequency to estimate the $10^{-4}$ site Uniform Hazard Spectra.  Note that the amplification factors plotted in Figure 2.5-78, Figure 2.5-80, Figure 2.5-82, and Figure 2.5-84 are mean logarithmic amplification factors, which correspond approximately to the median.  The amplification factors used to prepare Figure 2.5-86 are arithmetic mean amplification factors, which are slightly higher than the median.

The low-frequency character of the spectra in Figure 2.5-86 reflects the low-frequency amplification of the site, as shown in the amplification factors of Figure 2.5-78, Figure 2.5-80, Figure 2.5-82, and Figure 2.5-84.  That is, there is a fundamental site resonance at about 0.22 Hz, with a dip in site response at about 0.4 Hz, and this dip occurs for all 60 of the site profiles that were used to characterize the site profile.  As a result, there is a dip in the site spectra for $10^{-4}$ and
$10^{-5}$ at 0.4 Hz that reflects the site characteristics.

The ASCE (ASCE, 2005) performance-based approach was used to derive an SSE from the $10^{-4}$ and $10^{-5}$ site spectra.  The SSE spectrum is derived at each structural frequency as follows:

$$A_R = SA(10^{-5})/SA(10^{-4})$$

$$DF = 0.6 \, A_R^{0.8}$$

$$SSE = max(SA(10^{-4}) \times max(1.0, DF), 0.45 \times SA(10^{-5}))$$

The last term in the above equation was not published in this form in ASCE (SCE, 2005) but is a supplemental modified form, as presented in NRC Regulatory Guide 1.208 (NRC, 2007a).  The resulting horizontal SSE spectrum is plotted in Figure 2.5-87.  This spectrum has been smoothed slightly, particularly around 1.5 Hz, to remove slight bumps and dips in the spectrum resulting from the site amplification calculations that are not statistically significant.  The average change in spectral amplitudes for the 5 frequencies that were smoothed was an increase of 1%, which is not significant.

A vertical SSE spectrum was calculated by deriving vertical-to-horizontal (V:H) ratios and applying them to the horizontal SSE.  As background and for comparison purposes, V:H ratios were obtained by the following methods:

1.  Rock V:H ratios for the central and eastern United States (CEUS) were calculated from NUREG-6728 (NRC, 2001), using the recommended ratios for *PGA* < 0.2g, which applies at this site (see Figure 2.5-88).

2.  Soil V:H ratios for the western United States (WUS) were calculated from two publications (Abrahamson, 1997) (Campbell, 1997) that have equations estimating both horizontal and vertical motions on soil.  Horizontal and vertical motions were predicted from these two references for **M** = 5.5 and *R* = 9 mi (15 km).  **M** = 5.5 was selected because earthquakes around this magnitude dominate the high frequency motions, and *R* = 9 mi (15 km) was selected because this distance resulted in a

horitontal PGA of approximately 0.1 g at the site, which is close to the PGA associated with the horizontal SSE.  For each reference, the V:H ratio was formed, and the average ratio (average from the two references) was then calculated.

3.  The WUS V/H ratios for soil were modified in an approximate way for CEUS conditions by shifting the frequency axis of the V:H ratios so that they more closely resemble what might be expected at a soil site.  This shifted the WUS peak V/H ratio from about 15 Hz to about 45 Hz.

Figure 2.5-88 shows these three V:H ratios plotted vs. structural frequency.  As a conservative choice, the envelope V/H ratio shown as a thick dashed line was selected because this envelops all three approaches.  The recommended V:H ratio is 1.0 for frequencies greater than 25 Hz, 0.75 for frequencies less than 5 Hz, and is interpolated (log-linear) between 5 and 25 Hz. Figure 2.5-87 plots the resulting vertical SSE, calculated in this manner from the horizontal SSE. Table 2.5-22 lists the horizontal and vertical SSE amplitudes.}

### 2.5.2.7    Conclusions

{This section is added as a supplement to the U.S. EPR FSAR.

Constellation Generation Group and UniStar Nuclear Operating Services used the seismic source and ground motion models published by the Electric Power Research Institute (EPRI) for the central and eastern United States (CEUS), Seismic Hazard Methodology for the Central and Eastern United States, (EPRI, 1986).  As such, FSAR Section 2.5.2 focuses on those data developed since publication of this 1986 EPRI report.  Regulatory Guide 1.165, Identification and Characterization of Seismic Sources and Determination of Safe Shutdown Earthquake Ground Motion, (NRC, 1997), indicates that applicants may use the seismic source interpretations developed by Lawrence Livermore National Laboratory (LLNL) in the "Eastern Seismic Hazard Characterization Update," published in 1993, or the EPRI document as inputs for a site-specific analysis.

Constellation Generation Group and UniStar Nuclear Operating Services also used the guidance of Regulatory Guide 1.208, A Performance–Based Approach to Define the Site-Specific Earthquake Ground Motion, (NRC, 2007a) to develop the Ground Motion Response Spectrum (GMRS) used for the development of the Safe Shutdown Earthquake (SSE).

Constellation Generation Group and UniStar Nuclear Operating Services has provided a characterization of the seismic sources surrounding the site, as required by 10 CFR 100.23. Constellation Generation Group and UniStar Nuclear Operating Services has adequately addressed the uncertainties inherent in the characterization of these seismic sources through a PSHA, and that this PSHA followed the guidance provided in Regulatory Guide 1.208 (NRC, 2007a).

The GMRS developed by UniStar Nuclear uses the performance-based approach described in Regulatory Guide 1.208 (NRC, 2007a), adequately representing the regional and local seismic hazards and accurately includes the effects of the local CCNPP Unit 3 subsurface properties.

The performance-based approach outlined in Regulatory Guide 1.208 (NRC, 2007a) is an advancement over the solely hazard-based reference probability approach recommended in Regulatory Guide 1.165 (NRC, 1997) and it was used where appropriate in the determination of the GMRS.  The performance-based approach uses not only the seismic hazard characterization of the site from the PSHA but also basic seismic fragility SSC modeling in order to obtain an SSE that directly targets a structural performance frequency value.  Constellation Generation Group

and UniStar Nuclear Operating Services conclude that the application for the CCNPP Unit 3 site is acceptable from a geologic and seismologic standpoint and meets the requirements of 10 CFR 100.23(d) (CFR, 2007).

Deviations from the NRC guidance in Regulatory Guide 1.165 (NRC, 1997), Regulatory Guide 1.208 (NRC, 2007a), or review criteria in Standard Review Plan 2.5.2 (NRC, 2007b) have been identified and acceptable alternatives, including technical justification, have been provided.}

### 2.5.2.8      References

{This section is added as a supplement to the U.S. EPR FSAR.

**Abrahamson, 1997**.  Empirical Response Spectral Attenuation Relations for Shallow Crustal Earthquakes.  N. A. Abrahamson and W. J. Silva, Seismological Research Letter,  Volume 68, Number 1, pp. 94-127, 1997.

**Amick 1990a**.  Paleoliquefaction Investigations Along the Atlantic Seaboard With Emphasis on the Prehistoric Earthquake Chronology of Coastal South Carolina, D. Amick, unpublished Ph.D. dissertation, University of South Carolina, selected pages, 1990.

**Amick, 1990b**.  Characteristics of Seismically Induced Liquefaction Sites and Features Located In the Vicinity of the 1886 Charleston, South Carolina Earthquake, D. Amick, G. Maurath, and R. Gelinas, Seismological Research Letter, Volume 61, Number 2, pp. 117-130, 1990.

**ANSS, 2006**.  Advanced National Seismic System catalog, catalog-search2_pl_search_090806.htm, obtained from the ANSS website on September 8, 2006.  Website: http://www.ncedc.org/anss/catalog-search.html, Date accessed:  September 8, 2006.

**ASCE, 2005**.  American Society of Civil Engineers, "Seismic Design Criteria for Structures, Systems, and Components in Nuclear Facilities," American Society for Civil Engineers/Structural Engineering Institute, Report ASCE/SEI 43-05, 2005.

**Atkinson, 1987**.  Stochastic prediction of ground motion and spectral response parameters at hard-rock sites in eastern North America, G. M. Atkinson and D. M. Boore, Seismological Society of America, Bulletin, Volume 77, Number 2, pp. 440-467, 1987.

**Atkinson, 1995**.  Ground-Motion Relations for Eastern North America, G. M. Atkinson and D. M. Boore, Seismological Society of America, Bulletin, Volume 85, Number 1, pp 17-30, 1995.

**Bakun, 2004**.  Magnitudes and Locations of the 1811-1812 New Madrid, Missouri, and the 1886 Charleston, South Carolina, Earthquakes, W. H. Bakun and M. G. Hopper, Seismological Society of America, Bulletin, Volume 94, Number 1, pp. 64-75, 2004

**Bechtel, 2006**.  Update of Charleston Seismic Source and Integration with EPRI Source Models, Bechtel engineering study report 25144-006-V14-CY06-00006, revision 001002, September 8, 2006.  S. C Lindvall and R. D. Hartleb.  Release was provided by letter AR-07-0883, dated April 19, 2007 from Charles Pierce, Southern Company to Rod Krich, Constellation.

**Behrendt, 1981**.  Cenozoic Faulting in the Vicinity of the Charleston, South Carolina, 1886 Earthquake: Geology, J. C. Behrendt, R. M. Hamilton, H. D. Ackermann, and V. J. Henry, Volume 9, Number 3, pp. 117-122, 1981.

**Behrendt, 1983**. Marine Multichannel Seismic-reflection Evidence for Cenozoic Faulting and Deep Crustal Structure Near Charleston, South Carolina, C. Behrendt, R. M. Hamilton, H. D. Ackermann, V. J. Henry, and K. C. Bayer, U. S. Geological Survey Professional Paper 1313-J, pp. J1-J29, 1983.

**Behrendt, 1987**. The Helena Banks Strike-slip (?) Fault Zone in the Charleston, South Carolina, Earthquake Area: Results From a Marine, High-resolution, Multichannel, Seismic-reflection Survey, J. C. Behrendt and A. Yuan, Geological Society of America, Bulletin, Volume 98, pp. 591-601, 1987.

**Bollinger, 1977.** Reinterpretation of the Intensity Data for the 1886 Charleston, South Carolina, Earthquake in Studies Related to the Charleston, South Carolina, Earthquake of 1886-A Preliminary Report, D. W. Rankin, edition, G. A. Bollinger, U. S. Geological Survey Professional Paper 1028, pp. 17-32, 1977.

**Bollinger, 1985**. An Analysis of Earthquake Focal Depths in the Southeastern U. S., G. A. Bollinger, M. C. Chapman, M. S. Sibol, and J. K. Costain, American Geophysical Union, Geophysical Research Letter, Volume 12, Number 11, pp. 785-788, 1985.

**Bollinger, 1989**. Magnitude recurrence relations for the Southeastern United States and its subdivisions, G. A. Bollinger, F. C. Davison Jr., M. S. Sibol, and J. B. Birch, Journal of Geophysical Research, Volume 94, Number B3, pp. 2857-2873, 1989.

**Bollinger, 1991**. Seismicity of the Southeastern United States; 1698-1986 in Neotectonics of North America, Decade Map Volume to Accompany the Neotectonic Maps, D. B. Slemmons, E. R. Engdahl, M. D. Zoback, and D. D. Blackwell G. A. Bollinger, A. C. Johnston, P. Talwani, L. T. Long, K. M. Shedlock, M. S. Sibol, and M. C. Chapman, pp. 291-308, 1991

**Campbell, 1997**. Empirical near-source attenuation relationships for horizontal and vertical components of peak ground acceleration, peak ground velocity, and pseudo-absolute acceleration response spectra, K. W. Campbell, Seismological Society Of America, Seismological Research Letter, Volume 68, Number 1, pp. 154-179, 1997.

**Canada, 2006**. Canadian catalog is searchable through the on-line bulletin from the Natural Resources Canada, Earthquake Search, Website: http://earthquakescanada.nrcan.gc.ca/stnsdata/nedb/bull_e.php, Date accessed: September 13, 2006.}

**CFR, 2007**. Geologic and Seismic Siting Factors, Title 10, Code of Federal Regulations, Part 100.23(d), 2007

**Chapman, 1994**. Seismic Hazard Assessment for Virginia, M. C. Chapman and F. Krimgold, Virginia Tech Seismological Observatory, Department of Geological Sciences, February 1994.

**Chapman, 2002**. Seismic Hazard Mapping for Bridge and Highway Design in South Carolina, M. C. Chapman and P. Talwani, South Carolina Department of Transportation Report, 2002.

**Cook, 1979**. Thin-skinned Tectonics in the Crystalline Southern Appalachians: COCORP Seismic Reflection Profiling of the Blue Ridge and Piedmont, F. A. Cook, A. Albaugh, D. S., Brown, L. D., Kaufman, S., Oliver, J. E., Hatcher, R. D. Jr., Geology, Volume 7, pp. 563-567, 1979.

**Cook, 1981**. COCORP Seismic Profiling of the Appalachian Orogen Beneath the Coastal Plain of Georgia, F. A. Cook, L. D. Brown, S. Kaufman, J. E. Oliver, and T. A. Petersen, Geological Society of America Bulletin, Volume 92, Number 10, pp. 738-748, 1981.

**Cornell, 1988**. Temporal and Magnitude Dependence in Earthquake Recurrence Models, C. A. Cornell and S. R. Winterstein, Seismological Society of America, Bulletin, Volume 79, pp. 1522-1537, 1988.

**Coruh, 1988**. Seismogenic structures in the central Virginia seismic zone, C. Coruh, G. A. Bollinger, and J. K Costain, Geology, Volume 16, pp. 748-751, 1988.

**Costantino, 1996.** Recommendations for Uncertainty Estimates in Shear Modulus Reduction and Hysteretic Damping Relationships, C. J. Costantino, (1996). Published as an appendix in "Description and validation of the stochastic ground motion model," W.J. Silva, N. Abrahamson, G. Toro and C. Costantino. (1997). Report Submitted to Brookhaven National Laboratory, Associated Universities, Inc. Upton, New York 11973, Contract No. 770573.

**Cramer, 2001**. A Seismic Hazard Uncertainty Analysis for the New Madrid Seismic Zone, C. H. Cramer, Engineering Geology, Volume 62, pp. 251-266, 2001.

**Crone, 2000.** Data for Quaternary Faults, Liquefaction Features, and Possible Tectonic Features in the Central and Eastern United States, east of the Rocky Mountain front, U.S. Geological Survey Open-File Report 00-260, A. J. Crone and R. L. Wheeler, 2000.

**Dominion, 2004a**. Dominion Nuclear North Anna LLC, Docket No. 52-008, Response to 6/1/04 RAI 2.5.1-5, 2.5.1-6, 2.5.3-2, and 2.5.1-5, Letter No. 5, U.S. Nuclear Regulatory Commission, Serial No. 04-347, 2004.

**Dominion, 2004b**. Dominion Nuclear North Anna LLC, Docket No. 52-008, Response to 4/15/04 RAI 2.5.1-1 to 2.5.1-4, 2.5.2-2 to 2.5.2-4, and 2.5.3-1, Letter No. 3, U.S. Nuclear Regulatory Committee, Serial No. 04-270, 2004.

**Dominion, 2005**. Dominion North Anna LLC, Docket No. 52-008, North Anna Early Site Permit Application, Revision 5, Adams Accession No. ML052150253, July 2005.

**Ellsworth, 1999**. A Physically-Based Earthquake Recurrence Model for Estimation of Long-Term Earthquake Probabilities, W. L. Ellsworth, M. V. Matthews, R. M. Nadeau, S. P. Nishenko, P. A. Reasenberg, and R. W. Simpson, U.S. Geological Survey Open-File Report 99-522, 1999.

**EPRI, 1986.** Seismic Hazard Methodology for the Central and Eastern United States, Tectonic Interpretations, Electric Power Research Institute, Report NP-4726, Volumes 5–10, July 1986.

**EPRI, 1988.** Seismic Hazard Methodology for the Central and Eastern United States, Electric Power Research Institute, Report NP-4726-A, Revision 1, Volume 1, Part 2, 1988.

**EPRI, 1989a**. Probabilistic Seismic Hazard Evaluations at Nuclear Power Plant Sites in the Central and Eastern United States: Resolution of the Charleston Earthquake Issue, Electric Power Research Institute, Report NP-6395-D, 1989.

**EPRI, 1989b**. EQHAZARD Primer, Electric Power Research Institute, Report NP-6452-D, June 1989.

**EPRI, 1992.** The stable continental region earthquake database: in Methods for assessing maximum earthquakes in the central and eastern U.S., Electric Power Research Institute, Report RP-2556-12, 1992.

**EPRI, 1993.** Guidelines for Determining Design Basis Ground Motions, Volume 5: Quantification of Seismic Source Effects, Electric Power Research Institute, Report TR-102293, November 1993.

**EPRI, 1994**. The earthquakes of stable continental regions, Volume I: Assessment of Large Earthquake Potential, Electric Power Research Institute, Final Report TR-102261-V1, 1994.

**EPRI, 2004.** CEUS Ground Motion Project Final Report, Electric Power Research Institute, TR-1009684 2004, December 2004.

**EPRI, 2006a**. Program on Technology Innovation: Truncation of the Lognormal Distribution and Value of the Standard Deviation for Ground Motion Models in the Central and Eastern United States, Electric Power Research Institute, Report TR-1014381, August 2006.

**EPRI, 2006b.** Program on Technology Innovation: Truncation of the Lognormal Distribution and Value of the Standard Deviation for Ground Motion Models in the Central and Eastern United States, Electric Power Research Institute, Technical Update 1013105, February 2006.

**Exelon, 2005**. Letter dated October 31, 2005, T. Mundy, Exelon to NRC, Subject: Response Supplemental Draft Safety Evaluation Report (DSER) Item, page 16 of 112 and page 54 of 112, (Adams Accession Number ML053120131), 2005.

**Fletcher, 1978**. Seismic Trends and Travel-time Residuals in Eastern North America and Their Tectonic Implications, J. B. Flectcher, M. L. Sbar, and L. R. Sykes, Geological Society of America Bulletin, Volume 89, pp. 1656-1676, 1978.

**Grant, 1994**. Paleoseismic Evidence of Clustered Earthquakes on the San Andreas Fault in the Carrizo Plain, California, L. B. Grant, and K. Sieh, Journal of Geophysical Research, Volume 99, Number B4, pp. 6819-6841, 1994.

**Idriss, 1992**. SHAKE91: A computer program for conducting equivalent linear seismic response analyses of horizontally layered soil deposits, I. M. Idriss, and J. I Sun, Department of Civil and Environmental Engineering, Center for Geotechnical Modeling, University of California, Davis, Calif., 1992

**Johnston, 1985**. Recurrence rates and probability estimates for the New Madrid seismic zone, A. C. Johnston and S. J. Nava, Journal of Geophysical Research, Volume 90, pp. 6737–6753, 1985.

**Johnston, 1996**. Seismic Moment Assessment of Earthquake in Stable Continental Regions – III. New Madrid 1811-1812, Charleston 1886 and Lisbon 1755, A. C. Johnston, Geophysical Journal International, Volume 126, pp. 314-344, 1996.

**Kramer, 1996.** Geotechnical Earthquake Engineering, S. L. Kramer, Prentice-Hall, 1996.

**Marple, 1990**. Field Investigations of the Woodstock Lineament, R. T. Marple and P. Talwani, Seismological Society of America, Seismological Research Letter, Volume 61, Number 3-4, p. 156, 1990.

**Marple, 1993**.  Evidence For Possible Tectonic Upwarping Along The South Carolina Coastal Plain From An Examination Of River Morphology And Elevation Data, R. T. Marple and P. Talwani, Geology, Volume 21, pp. 651-654, 1993.

**Marple, 2000**.  Evidence for a Buried Fault System in the Coastal Plain of the Carolinas and Virginia - Implications for Neotectonics in the Southeastern United Sates, R. T. Marple and P. Talwani, Geological Society of America Bulletin, Volume 112, Number 2., pp. 200-220, 2000.

**Marple, 2004**.  P., Proposed Shenandoah Fault and East Coast-Stafford Fault System and Their Implications for Eastern U. S. Tectonics, R. T. Marple and P. Talwani, Southeastern Geology, Volume 43, Number 2, pp. 57-80, 2004.

**Martin, 1994**.  G. W., Seismic Parameters from Liquefaction Evidence, J. R. Martin and G. W. Clough, Journal of Geotechnical Engineering, Volume 120, Number 8, pp. 1345-1361, 1994.

**NIST, 2006**. NIST/SEMATECH, e-Handbook of Statistical Methods, http://www.itl.nist.gov/div898/handbook/, accessed 11 January 2006, Chapter 1 downloaded in PDF form from http://www.itl.nist.gov/div898/handbook/toolaids/pff/1-eda.pdf.

**NRC, 1986**.  Identification of a Northwest Trending Seismogenic Graben Near Charleston, South Carolina, NUREG/CR-4075, U.S. Nuclear Regulatory Commission 1986.

**NRC, 1990.**  Paleoliquefaction Features Along the Atlantic Seaboard, NUREG/CR-5613, U. S. Nuclear Regulatory Commission, 1990

**NRC, 1991**.  Generic Letter 88-20, Individual Plant Examinations of External Events (IPEEE) for Severe Accident Vulnerabilities, U. S. Nuclear Regulatory Commission, 1991.

**NRC, 1997a**.  Identification and Characterization of Seismic Sources and Determination of Safe Shutdown Earthquake Ground Motion**,** Regulatory Guide 1.165, U. S. Nuclear Regulatory Commission, March 1997.

**NRC, 1997b**.  Recommendations for Probabilistic Seismic Hazard Analysis: Guidance on Uncertainty and Use of Experts, Prepared by Senior Seismic Hazard Analysis Committee (SSHAC), NUREG/CR-6372, U. S. Nuclear Regulatory Commission, 1997.

**NRC, 2001**.  Technical Basis for Revision of Regulatory Guidance on Design Ground Motions, Hazard- and Risk-Consistent Ground Motion Spectra Guidelines, NUREG/CR-6728, U. S. Nuclear Regulatory Commission, 2001.

**NRC, 2002a**.  Guidance for Performing Probabilistic Seismic Hazard Analysis for a Nuclear Plant Site: Example Application to the Southeastern United States, NUREG/CR-6607, U. S. Nuclear Regulatory Commission, 2002.

**NRC, 2002b**.  Technical Basis for Revision of Regulatory Guidance on Design Ground Motions: Development of Hazard- & Risk-Consistent Seismic Spectra for Two Sites, NUREG/CR-6769, U.S. Nuclear Regulatory Commission**,** 2002,

**NRC, 2005**.  Safety Evaluation Report for an Early Site Permit (ESP) at the North Anna ESP Site, NUREG-1835, U. S. Nuclear Regulatory Commission, September 2005

**NRC, 2007a**.  A Performance-Based Approach to Define the Site-Specific Earthquake Ground Motion, U. S. Nuclear Regulatory Commission, Regulatory Guide 1.208, March 2007.

**NRC, 2007b**.  Vibratory Ground Motion, Standard Review Plan, NUREG-0800, Section 2.5.2, Revision 4, U.S. Nuclear Regulatory Commission, March 2007.

**NRC, 2007c.**  Combined License Applications For Nuclear Power Plants (LWR Edition), Regulatory Guide 1.206, U.S. Nuclear Regulatory Commission, March 2007

**Obermeier, 1989**.  Liquefaction evidence for Repeated Holocene Earthquakes in the Coastal Region of South Carolina, S. F. Obermeier, R. E. Weems, R. B. Jacobson, and G. S. Gohn, Annals of the New York Academy of Sciences, Volume 558, pp. 183-195, 1989.

**Obermeier, 1998**.  Paleoliquefaction Evidence for Seismic Quiescence in Central Virginia During the Late and Middle Holocene Time (abs), S. F. Obermier and W. E. McNulty.  Eos Transactions, American Geophysical Union, Volume 79, No. 17, p S342, 1998.

**Ohio, 2006**.  Ohio Seismic Network catalog, "http://www.dnr.state.oh.us/OhioSeis, KEY TO COLUMN DATA.htm, Oh_eq_1950 to 1999.htm, and Oh_eq_2000_to_present.htm," Ohio Department of Natural Resources, September 8, 2006.  Website: http://www.dnr.state.oh.us/OhioSeis.

**Ramsey, 1995**.  Radiocarbon calibration and analysis of stratigraphy: the OxCal program, C. Bronk Ramsey, C., Radiocarbon, Volume 37, Number 2, pp. 425-430, 1995.

**Ramsey, 2001**.  Development of the radiocarbon program OxCal: Radiocarbon, C. Bronk Ramsey, Volume 43, Number 2A, pp. 355-363, 2001.

**Rathie, 2006**. Site-Specific Validation of Random Vibration Theory Based Seismic Site Response Analysis, Journal of Geotechnical and Geoenvironmental Engineering, American Society of Civil Engineers, Volume 132, No. 7, G. M. Rathie, C. Ozbey, July, 2006.

**Reger, 1994**.  Summary of the Howard County, Maryland, Earthquakes of 1993, Southeastern U.S. Seismic Network Bulletin No. 28, Appendix A.,  Website: http://www.geol.vt.edu/outreach/vtso/anonftp/catalog/bul28.list1, J. P. Reger, 1994.

**Schneider, 1991.** Estimation of Ground Motion at Close Distances Using the Band-Limited White Noise Model, Proceedings 4th International Conference on Seismic Zonation, Bol. 4, Earthquake Engineering Research Institute, J. F. Schneider, W. J. Silva, S. J. Chiou, and J. C. Stepp, Stanford, CA, pp 187-194, 1991.

**Seeber, 1981**.  The 1886 Charleston, South Carolina earthquake and the Appalachian detachment, L. Seeber and J. G. Armbruster, Journal of Geophysical Research, Volume 86, Number B9, pp. 7874-7894, 1981.

**Seeber, 1998**.  The 1994 Cacoosing Valley earthquakes near Reading, Pennsylvania: A shallow rupture triggered by quarry unloading, L. Seeber, J. G. Armbruster, W. Y. Kim, N. Barstow, C. Scharnberger, Journal of Geophysical Research, Volume 103, Number B10, pp. 24,505-24,521, 1998.

**SEUSSN, 2006**.  South Eastern United States Seismic Network catalog, "susn2004cat.txt," Virginia Tech Seismic Observatory, September 8, 2006.  Website: http://www.geol.vt.edu/outreach/vtso/.

**Sieh, 1989**.  Precise Chronology of Earthquakes Produced by the San Andreas fault in Southern California, K. Sieh, M. Stuiver, and D. A. Brillinger, Journal of Geophysical Research, Volume 94, Number B1, pp. 603-623, 1989.

**Silva, 1997.** Description and validation of the stochastic ground motion model, Final report, Brookhaven National Laboratory, Contract No. 770573, W. J. Silva, N. Abrahamson, G. Toro, C. Costantino, Associated Universities, Inc., Upton, N.Y., 1997

**Smith, 1985**.  Preliminary interpretation of a detailed gravity survey in the Bowman and Charleston, S.C. Seismogenic zones: Abstracts with Programs, W. A. Smith and P. Talwani, Geological Society of America southeastern section, Volume 17, Number 2, p. 137, 1985.

**SSA, 1968**.  Engineering Seismic Risk Analysis, Seismological Society of America, Bulletin, Volume 58, Number 5, pp. 1583-1606, C. A. Cornell, 1968.

**SSA, 1981**.  Results of recent South Carolina seismological studies, Seismological Society of America, Bulletin, Volume 71, Number 6, pp. 1883-1902, A. C. Tarr, P. Talwani, S. Rhea, D. Carver, and D. Amick, 1981.

**SSA, 1987**.  The 23 April 1984 Martic Earthquake and The Lancaster Seismic Zone In Eastern Pennsylvania, Bulletin of the Seismological Society of America, Vol. 77, No. 2, pp. 877-890, J. Armbruster and L. Seeber, 1987.

**SSA, 1991**.  Criticism of Some Forecasts of the National Earthquake Evaluation Council, Seismological Society of America, Bulletin, Volume 81, Number 3, pp. 862-881, J. C. Savage, 1991.

**SSA, 1993**.  Fault Plane Solutions and Relocations of Recent Earthquakes in Middleton Place-Summerville Seismic Zone near Charleston, South Carolina, Seismological Society of America, Bulletin, Volume 83, Number 5, pp. 1442-1466, S. Madabhushi and P. Talwani, 1993.

**SSA, 1994**.  New Empirical Relationships Among Magnitude, Rupture Length, Rupture Width, Rupture Area, and Surface Displacement, Seismological Society of America, Bulletin, Volume 84, Number 4, pp. 974-1002,  D. L. Wells and K. J Coppersmith, August 1994.

**SSA, 1995**.  Seismic Hazards in Southern California: Probable earthquakes, 1994 to 2024, Bulletin of the Seismological Society of America, Volume 85, pp. 379-439, Working Group on California Earthquake Probabilities, 1995.

**SSA, 2000**.  Paleoseismology of the Johnson Valley, Kickapoo, and Homestead Valley faults: clustering of earthquakes in the Eastern California shear zone, Seismological Society of America, Bulletin, Volume 90, Number 5, pp. 1200-1236, T. K. Rockwell, S. Lindvall, M. Herzberg, D. Murbach, T. Dawson, and G. Berger 2000.

**SSA, 2002**.  A Brownian model for recurrent earthquakes, Seismological Society of America, Bulletin, Volume 92, pp. 2233-2250, M. V. Matthews, W. L. Ellsworth, and P. A. Reasenberg, 2002.

**Stepp, 1991.** Site response evaluations based upon generic soil profiles using random vibration methodology. Proceedings 4th International Conference on Seismic Zonation, Vol. 4, Earthquake Engineering Research Institute, J.C. Stepp, W. J. Silva, H.B. Seed, I. M. Idriss, R. McGuire, J. Schneider, Stanford, Calif., pp. 739-746, 1991

**Sykes, 1978**. Intraplate Seismicity, Reactivation of Preexisting Zones of Weakness, Alkaline Magmatism, and Other Tectonism Postdating Continental Fragmentation, L. R. Sykes, Reviews of Geophysics, Volume 16, pp. 621-688, 1978.

**Talwani, 1982**. An internally consistent pattern of seismicity near Charleston, South Carolina, P. Talwani, Geology, Volume 10, pp. 655–658, 1982.

**Talwani, 1999**. Fault Geometry and Earthquakes in Continental Interiors, P. Talwani, Tectonophysics, Volume 305, pp. 371-379, 1999.

**Talwani, 2000**. Macroscopic Effects of the 1886 Charleston Earthquake, A Compendium of Field Trips of South Carolina Geology, P. Talwani, South Carolina Geological Survey, pp. 1-6, 2000.

**Talwani, 2001**. Recurrence Rates of Large Earthquakes in the South Carolina Coastal Plain Based on Paleoliquefaction Data, P. Talwani and W. T. Schaeffer, Journal of Geophysical Research, Volume 106, Number B4, pp. 6621-6642, 2001.

**Talwani, 2004**. Macroseismic effects of the 1886 Charleston earthquake, P. Talwani and M. Katunam, Carolina Geological Society field trip guidebook, p. 18, 2004.

**Toro, 1996**. Probabilistic Models of Site Velocity Profiles for Generic and Site-Specific Ground Motion Amplification Studies, G. R. Toro, Published as an appendix in W. J. Silva, N. Abrahamson, G. Toro and C. Costantino, (1997), Description and validation of the stochastic ground motion model, Report Submitted to Brookhaven National Laboratory, Associated Universities, Inc. Upton, New York 11973, Contract No. 770573, 1996.

**Tuttle, 2001**. The Use of Liquefaction Features in Paleoseismology: Lessons Learned in the New Madrid Seismic Zone, central United States, M. P. Tuttle, Journal of Seismology, Volume 5, pp. 361-380, 2001.

**USGS, 1983a**. Land multichannel seismic-reflection evidence for tectonic features near Charleston, South Carolina, Studies Related to the Charleston, South Carolina, Earthquake of 1886- Tectonics and Seismicity, U.S. Geologic Survey, Professional Paper 1313-I, pp. I1-I18, R. M. Hamilton, J.C. Behrendt, and H. D. Ackermann, 1983.

**USGS, 1983b**. Seismicity Near Charleston, South Carolina, March 1973 to December 1979 in Studies Related to the Charleston, South Carolina Earthquake of 1886: Tectonics and Seismicity, G. S. Gohn (ed.), U. S. Geological Survey, Professional Paper 1313, pp. R1-R17, A. C. Tarr and S. Rhea, 1983.

**USGS, 1983c**. Regenerate Faults of the Southeastern United States, in Studies Related to the Charleston, South Carolina, Earthquake of 1886: Tectonics and seismicity, Gohn, G. S. (ed.), C. M. Wentworth and M. Mergener-Keefer, US Geological Survey Professional Paper 1313, pp. S1-S20, 1983.

**USGS, 1992**.  Specification of Source Zones, Recurrence Rates, Focal Depths, and Maximum Magnitudes for Earthquakes Affecting the Savannah River Site in South Carolina, U.S. Geological Survey, Bulletin 2017, G. A. Bollinger, 1992.

**USGS, 1996**.  National seismic-hazard maps: documentation, U. S Geological Survey, Open-File Report 96-532, A. Frankel, T. Barnhard, D. Perkins, E. V. Leyendecker, N. Dickman, S. Hanson, and M. Hopper, 1996.

**USGS, 1997**.  Geology of the Pringletown, Ridgeville, Summerville, and Summerville Northwest 7.5-minute quadrangles, Berkeley, Charleston, and Dorchester counties, South Carolina: Miscellaneous Investigations Series, U. S. Geological Survey, R. E. Weems, E. M. Lemon, Jr. and M. S. Nelson, 1997.

**USGS, 1998**.  Newly Recognized En Echelon Fall Lines in the Piedmont and Blue Ridge Provinces of North Carolina and Virginia, With a Discussion of Their Possible Ages and Origins, U.S. Geological Survey, Open-File Report 98-374, R. E. Weems, 1998

**USGS, 2002**.  Documentation for the 2002 Update of the National Seismic Hazard Maps, U.S. Geological Survey Open-File Report 02-420, A. D. Frankel, M. D. Petersen, C. S. Mueller, K. M Haller, R. L. Wheeler, E. V. Leyendecker, R. L. Wesson, S. C. Harmsen, C. H. Cramer, D. M. Perkins, and K. S. Rukstales, 2002.

**USGS, 2003**.  Earthquake Probabilities in the San Francisco Bay region: 2002-2031, U. S. Geological Survey Open-File Report 03-2134, Working Group on California Earthquake Probabilities, 2003.

**Weems, 2002**.  Structural and tectonic setting of the Charleston, South Carolina, region; evidence from the Tertiary stratigraphic record, R. E. Weems and W. C. Lewis, Geological Society of America, Bulletin, Volume 114, Number 1, pp. 24-42, 2002.

**WGCEP, 1995.**  Working Group on California Earthquake Probabilities, Seismic Hazards in Southern California: Probable earthquakes, 1994 to 2024, Bulletin of the Seismological Society of America, Volume 85, pp. 379-439, 1995.

**Wheeler, 1992**.  Geologic Implications of Earthquake Source Parameters in Central and Eastern North America, Seismological Research Letters, R. L. Wheeler, and A. C. Johnston Volume 63, No. 4, pp. 491–505, 1992

**Wheeler, 2005**.  Known or Suggested Quaternary Tectonic Faulting, Central and Eastern United States – New and Updated Assessments for 2005, U.S. Geological Survey, Open File Report 2005-1336, R. L. Wheeler, 2005.

**Wheeler, 2006**.  Quaternary tectonic faulting in the Eastern United States, Engineering Geology, Volume 82, pp. 165-186, R. L. Wheeler, 2006.}

## 2.5.3    SURFACE FAULTING

The U.S. EPR FSAR includes the following COL Item in Section 2.5.3:

> A COL applicant that references the U.S. EPR design certification will investigate site-specific surface and subsurface geologic, seismic, geophysical, and geotechnical aspects within 25 miles around the site and evaluate any impact to the design.  The COL applicant will demonstrate that no capable faults exist at the site in accordance with the requirements of 10 CFR 100.23 and 10 CFR 50, Appendix S.  If non-capable surface faulting is present under foundations for safety-related structures, the COL applicant will demonstrate that the faults have no significant impact on the structural integrity of safety-related structures, systems or components.

This COL Item is addressed as follows:

{There is no potential for tectonic fault rupture and there are no capable tectonic sources within a 25 mi (40 km) radius of the CCNPP site.}  A capable tectonic source is a tectonic structure that can generate both vibratory ground motion and tectonic surface deformation, such as faulting or folding at or near the earth's surface in the present seismotectonic regime (NRC, 1997).  The following sections provide the data, observations, and references to support this conclusion. Information contained in these sections was developed in accordance with RG 1.165 (NRC, 1997), and is intended to satisfy 10 CFR 100.23, "Geologic and Seismic Siting Criteria" (CFR, 2007a) and 10 CFR 50, Appendix S, "Earthquake Engineering Criteria for Nuclear Power Plants" (CFR 2007b).

Sections 2.5.3.1 through 2.5.3.9 are added as a supplement to the U.S. EPR FSAR.

### 2.5.3.1    Geological, Seismological, and Geophysical Investigations

The following investigations were performed to assess the potential for surface fault rupture at and within a 25 mi (40 km) radius of the CCNPP Unit 3 site:

♦   Compile and review existing geologic and seismologic data

♦   Interpret aerial photography

♦   Interpret satellite and LiDAR imagery

♦   Field and aerial (inspection by plane) reconnaissance

♦   Review of pre-EPRI and post-EPRI (1989) seismicity (e.g. earthquake catalog used in EPRI (1989) ended in 1983.  Pre-EPRI catalog is 1500's through 1983; post-EPRI is 1983 through 2006)

♦   Discuss site area geology with researchers at the U.S. Geological Survey (USGS), Maryland Geological Survey (MGS), and academic institutions.

The geologic and geotechnical information available for the existing CCNPP Units 1 and 2 site, as well as the proposed CCNPP Unit 3 site, is contained in three principal sources:

1.   Work performed for the existing CCNPP Units 1 and 2 and complementary structures (BGE, 1968) (Constellation, 2005); and geotechnical foundation studies for adjacent parking lots (BPC, 1981).

2.  Published and unpublished geologic mapping performed primarily by the USGS and MGS.

3.  Seismicity data compiled and analyzed in published journal articles and, more recently, as part of Section 2.5.2.

Existing information was supplemented by aerial and field reconnaissance within a 25 mi (40 km) radius of the site, and interpretation of aerial photography along all known faults within the 5 mi (8 km) radius of the site.  In addition, Light Detection and Ranging (LiDAR) data acquired from surrounding counties (Charles County, St Mary's County and Calvert County), that covered all known faults within much of the approximately 25 mi (40 km) radius and the entire 5 mi (8 km) radius, was reviewed and interpreted with respect to published Quaternary geologic maps as shown in Figure 2.5-26.  Satellite imagery (raster imagery) of the CCNPP site region also was acquired for review and interpretation.  These field and office-based studies were performed to verify, where possible, the existence of mapped bedrock faults in the CCNPP site area and to assess the presence or absence of geomorphic features suggestive of potential Quaternary fault activity along the mapped faults, or previously undetected faults.  Features reviewed during the field reconnaissance and office-based analysis of aerial photography, satellite imagery, and LiDar data, were based on a compilation of existing regional geologic information, as well as discussions with experts at the USGS and MGS who have worked in the vicinity of the CCNPP site.

Field reconnaissance of the site and within a 25 mi (40 km) radius of the site was conducted by geologists in teams of two or more.  Two field reconnaissance visits in late summer and autumn, 2006 focused on exposed portions of the Calvert Cliffs, other cliff exposures along the west shore of Chesapeake Bay, and roads traversing the site and a 5 mi (8 km) radius of the site.  Key observations and discussion items were documented in field notebooks and photographs.  Field locations were logged by hand on detailed topographic base maps and with hand-held Global Positioning System (GPS) receivers.

Aerial reconnaissance within a 25 mi (40 km) radius of the site was conducted by two geologists in a top-wing Cessna aircraft on January 3, 2007.  The aerial reconnaissance investigated the geomorphology of the Chesapeake Bay area and targeted numerous previously mapped geologic features and potential seismic sources within a 200 mi (322 km) radius of the site (e.g., Mountain Run fault zone, Stafford fault system, Brandywine fault zone, Port Royal fault zone, and Skinkers Neck anticline).  The flight crossed over the CCNPP site briefly but did not circle or approach the site closely in order to comply with restrictions imposed by the Federal Aviation Administration.  Key observations and discussion items were documented in field notebooks and photographs.  The flight path, photograph locations, and locations of key observations were logged with hand-held GPS receivers.

The investigations of regional and site physiographic provinces and geomorphic process, geologic history, and stratigraphy were conducted by Bechtel Power Corporation.  The investigations of regional and site tectonics and structural geology were conducted by William Lettis and Associates.

### 2.5.3.1.1    Previous Site Investigations

Previous site investigations performed for the existing units are summarized in the CCNPP Units 1 and 2 Preliminary Safety Analysis Report (PSAR) (BGE, 1968) and Independent Spent Fuel Storage Installation (ISFSI) Safety Analysis Report (SAR) (CGG, 2005).  As cited in the CCNPP Units 1 and 2 PSAR and ISFSI SAR, these previous investigations provide the following results documenting the absence of Quaternary faults at and within the area of the CCNPP Unit 3 site:

♦     Interpretation of air photos and topographic maps. This interpretation revealed no evidence of surface rupture, surface warping, or offset of geomorphic features indicative of active faulting.

♦     Interviews with personnel from government agencies and private organizations. These interviews concluded that no known faults are present beneath the existing CCNPP Units 1 and 2 or CCNPP Unit 3 site areas.

♦     Seismicity Analysis -This analysis showed that: no microseismic activity has occurred in the site area; the site is located in a region that has experienced only infrequent minor earthquake activity; the closest epicentral location is greater than 25 mi (40 km) away. No earthquake within 50 mi (80 km) of the CCNPP site has been large enough to cause significant damage since the region has been populated over the past approximately 300 years. Section 2.5.2 provides a full discussion on the seismicity analysis for the CCNPP site.

♦     Approximately 85 exploratory boreholes were drilled at the CCNPP Units 1 and 2 site area. Borehole data have provided evidence for the lateral continuity of strata across the existing CCNPP Units 1 and 2 site area and the inspection of soil samples has revealed no adverse effects indicative of geologically recent or active faulting.

♦     Field reconnaissance of limited surface outcrops at the site and along the western shore of Chesapeake Bay, coupled with geophysical surveys, provided evidence for no faulting at the CCNPP site.

At the time of the original studies for the PSAR (BGE, 1968), there were no published maps showing bedrock faults within a 5 mi (8 km) radius of the CCNPP site. The closest significant bedrock faults mapped prior to 1968 were faults located about 50 mi (80 km) west of the CCNPP site in the Piedmont Province (BGE, 1968). The Geologic Map of Maryland (MGS, 1968) shows no faults within a 25 mi (40 km) radius of the CCNPP site.

### 2.5.3.1.2    Regional and Local Geological Studies

Since the late 1960's, extensive mapping of the CCNPP site region within the Coastal Plain Province by the MGS (MGS, 1971) (MGS, 1994) (MGS, 2003a) (MGS, 2003b) (MGS, 2003c) (MGS, 1986) and by the USGS (USGS, 1989c) (USGS, 1989d) (USGS, 1979a) (USGS, 1986), (USGS, 1979b) (USGS, 1995) (USGS, 2000b) has been performed to improve the industry's knowledge of the Coastal Plain stratigraphy and geologic structure within the region. Coastal Plain mapping includes geologic cross sections across the CCNPP site area (USGS, 2003b) (USGS, 2003c) and a developed geologic cross Section based on mapping and borehole data (Achmad, 1997). In addition, closely-spaced shallow-penetration seismic-reflection profiles in the Chesapeake Bay provide limited below-water information on the Tertiary-Quaternary history of Chesapeake Bay (USGS, 1989a) (USGS, 1989b) (GSA, 1990), as well as limited information on the absence of Middle Miocene faulting. This compilation of previous mapping and exploration studies, coupled with site-specific reconnaissance for CCNPP Unit 3, provides the principal basis for the few, if any, bedrock faults recognized within the site area.

In addition, the USGS recently completed a compilation of all Quaternary faults, liquefaction features, and possible tectonic features in the eastern U.S. (USGS, 2000a) (USGS, 2005) (Wheeler, 2006). These compilations do not show any Quaternary faults or features within a 25 mi (40 km) or 5 mi (8 km) radius of the site as shown in Figure 2.5-31. The nearest potential Quaternary features (USGS, 2000a) (USGS, 2005) (Wheeler, 2006) are the Stafford fault 47 mi (76 km) west-southwest, and the Upper Marlboro faults 36 mi (58 km) to the northeast, respectively, of

the CCNPP site as shown in Figure 2.5-31. Two documented paleo-liquefaction sites (Obermier, 1998) on the James and Rivanna Rivers within the Central Virginia seismic zone are both located over 25 mi (40 km) from the CCNPP site as shown in Figure 2.5-31.

Local geologic cross-sections oriented northwest-southeast within the site area (5 mi (8 km) radius) depict unfaulted southeast-dipping Eocene-Miocene Coastal Plain sediments that are unconformably overlain by Pliocene Upland deposits (MGS, 1994) (Achmad, 1997) (MGS, 2003b) (MGS, 2003c) as shown in Figure 2.5-13, Figure 2.5-32, and Figure 2.5-33. No faults or folds are depicted on these geologic cross-sections. A review of a PSAR for a proposed nuclear power plant along the eastern shore of the Potomac River (e.g., Douglas Point), located 45 mi (72 km) west-southwest of the CCNPP site, also reported no faults or folds within a 5 mi (8 km) radius of the CCNPP site (PEPCO, 1973). Lastly, review of a seismic source characterization study (URS, 2000) for a liquefied natural gas plant at Cove Point, about 3 mi (4.8 km) southeast of the CCNPP site, also mentions no faults or folds present in the Cove Point area that could project toward the CCNPP site.

The most detailed subsurface exploration of the CCNPP site was performed by Dames and Moore as part of the original PSAR (BGE, 1968) for the CCNPP Units 1 and 2 foundation and supporting structures. This PSAR study included drilling 85 geotechnical boreholes, collecting down-hole geophysical data, and acquiring seismic refraction data across the site. As summarized in the PSAR (BGE, 1968), geologic cross sections were developed extending from Highway 2/4 northwest of the CCNPP site to Camp Conoy on the southeast, which provide valuable subsurface information on the lateral continuity of Miocene Coastal Plain sediments and Pliocene Upland deposits as shown in Figure 2.5-32, Figure 2.5-41, and Figure 2.5-42. Cross-sections C-C' to D-D' pre-date site development in the Conoy Landing area, and shadow the existing CCNPP Units 1 and 2 site and the proposed CCNPP Unit 3 site for structures trending north-northeast, parallel to the regional structural grain. These sections depict a nearly flat-lying, undeformed geologic contact between the Eocene Piney Point Formation and the overlying Middle Miocene Calvert Formation at about -200 ft (-61 m) msl as shown in Figure 2.5-41 and Figure 2.5-42.

Geologic cross-sections developed from geotechnical data collected from approximately 85 boreholes as part of the CCNPP Unit 3 study also provide additional detailed information for the upper approximately 400 ft (123 km) of strata on the presence or absence of structures directly beneath the footprint of the site. Similar to the previous cross sections prepared for the site, the new geologic borehole data support an interpretation of gently-dipping to flat-lying and unfaulted Miocene and Pliocene stratigraphy at the CCNPP site as shown in Figure 2.5-34, Figure 2.5-39 and Figure 2.5-43. Cross Section E-E' prepared oblique to previously mapped northeast-trending structures (i.e., Hillville fault; inferred folds (USGS, 1995) (Kidwell, 1997) and postulated fault (Kidwell, 1997)) shows nearly flat-lying Miocene and Pliocene stratigraphy directly underling the CCNPP site as shown in Figure 2.5-39. Multiple key stratigraphic markers within the Chesapeake Group provide evidence for the absence of Miocene-Pliocene faulting and folding beneath the CCNPP site. Minor perturbations are present across the Miocene-Pliocene stratigraphic boundary, as well as other subunits within the Miocene Chesapeake Group. Although the stratigraphic contacts between the Calvert and Choptank Formations, as well as the Choptank and St. Marys Formation, cannot be readily delineated, there are several key lithologic contacts (i.e., cemented sand separated by uncemented sand layers) that exhibit flat-lying bedding and lateral continuity. The near-horizontal subunits provide evidence for the absence of surface-fault rupture beneath the CCNPP site as shown in Figure 2.5-39. A prominent geologic contact between the Piney Point and Calvert Formations, and Nanjemoy and Piney Point Formations, identified in exploratory boreholes B-303 and B-403

also provides evidence for a very low-gradient, nearly flat-lying Miocene deposit directly beneath the site as shown in Figure 2.5-39.

Geotechnical data collected directly to the south of the CCNPP site were compiled along sections E-E' and E'-E" and shown in Figure 2.5-39 and Figure 2.5-43. Although these geotechnical boreholes are limited in depth (from -325 ft to 37.5 ft (-99 to 11.4 m) msl), they provide additional evidence of the lateral continuity between the Pliocene Upland gravel deposits and Miocene St. Marys Formation, as well as a cemented sand unit in the upper part of the St. Marys Formation. The nearly flat-lying and undisrupted nature of these shallow Miocene-Pliocene deposits are consistent with sections E-E' and E'-E", and observations of the exposed Miocene and Pliocene strata along the western shore of Chesapeake Bay near the existing the CCNPP site as shown in Figure 2.5-44.

### 2.5.3.2    Geological Evidence, or Absence of Evidence, for Surface Deformation

As shown on Figure 2.5-32, only one inferred bedrock fault (i.e., Hillville fault) has been mapped at or near the 5 mi (8 km) radius of the CCNPP site (Hansen, 1978). In addition to the Hillville fault (Hansen, 1978), several other structures have been proposed within the 5 mi (8 km) radius of the site that have either shown in geologic cross-sections or published papers: (a) that two hypothesized east-facing monoclines are postulated beneath Chesapeake Bay (USGS, 1995) and (b) multiple stratigraphic undulations (inferred folds and warps) and a fault are postulated along the western margin of Chesapeake Bay (Kidwell, 1997). The Hillville fault (MGS, 1978) and inferred folds (USGS, 1995) (Kidwell, 1997) are described in Section 2.5.1 and below. None of these features are considered capable tectonic sources, as defined in Appendix A of Regulatory Guide 1.165 (NRC, 1997). Only the Hillville fault has been mapped within or near the 5 mi (8 km) radius of the CCNPP site, whereas the other features (USGS, 1995) (Kidwell, 1997) are only shown on cross sections as shown in Figure 2.5-25.

No deformation or geomorphic evidence indicative of potential Quaternary activity has been reported in the literature for the Hillville fault; whereas the features (USGS, 1995) (Kidwell, 1997) have been loosely inferred to have been active during the Quaternary. No evidence of Quaternary deformation along these inferred structures was identified during aerial and field reconnaissance, as well as during air photo and LiDAR interpretation undertaken for the CCNPP Unit 3 study. The Hillville fault is interpreted as a lithotectonic terrane boundary that coincides with the Sussex-Currioman Bay aeromagnetic anomaly (MGS, 1986), whereas the other postulated features have not been attributed to a known tectonic structure.

### 2.5.3.2.1    Hillville Fault Zone

The 26 mi (42 km) long Hillville fault (MGS, 1978) approaches to within 5 mi (8 km) of the CCNPP site as shown in Figure 2.5-32. The fault consists of a northeast-striking zone of steep southeast-dipping reverse faults that coincide with the Sussex-Currioman Bay aeromagnetic anomaly. The style and location of faulting are based on seismic reflection data collected about 9 mi (14.5 km) west-southwest of the CCNPP site. Seismic line St M-1 imaged a narrow zone of discontinuities that vertically separate basement by as much as 250 ft (76 m) (MGS, 1978) as shown in Figure 2.5-27. It has been interpreted (MGS, 1986) that this offset is part of a larger lithotectonic terrane boundary that separates basement rocks associated with Triassic rift basins on the west from low-grade metamorphic basement on the east. The Hillville fault may represent a Paleozoic suture zone that was reactivated in the Mesozoic and Early Tertiary similar to the Brandywine fault system located to the west of the CCNPP site. Based on stratigraphic correlation between boreholes within Tertiary Coastal Plain deposits, it is speculated (MGS, 1986) that the Hillville fault was last active in the Early Paleocene.

Field and aerial (inspection by plane) reconnaissance, coupled with interpretation of aerial photography (review and inspection of features preserved in aerial photos) and LiDAR data shows that there are no geomorphic features indicative of potential Quaternary activity along the surface-projection of the Hillville fault zone. Multiple Quaternary fluvial terraces of the Patuxent and Potomac Rivers previously mapped (USGS, 1989c) (USGS, 1989d) (MGS, 1994) (MGS, 2003b) (MGS, 2003c) were evaluated for features suggestive of tectonic deformation using the LiDAR data as shown in Figure 2.5-26. Furthermore, where the Hillville fault would intersect the steep cliffs of Chesapeake Bay, there is direct observation of no faulting in the exposed Miocene strata. This is consistent with cross sections (Kidwell, 1997) (Achmad, 1997) (MGS, 2003b) (MGS, 2003c) that trend oblique to and across the northeast strike of the Hillville fault and do not show a fault as shown in Figure 2.5-13, Figure 2.5-30, and Figure 2.5-33. There is no pre-Electric Power Research Institute (EPRI) or post-EPRI (EPRI, 1986) study of seismicity spatially associated with this feature, or any geomorphic evidence of Quaternary deformation as shown in Figure 2.5-25. Thus, based on the absence of geomorphic expression, seismicity, and offset of Miocene to Quaternary surficial deposits, it is concluded that the Hillville fault is not a surface-fault rupture hazard at the CCNPP site.

### 2.5.3.2.2    East Facing Monoclines

Two speculative and poorly constrained east-facing monoclines along the western margin of Chesapeake Bay are depicted in geologic cross sections (USGS, 1995) within the 5 mi (8 km) radius of the CCNPP site. East-facing monoclines are inferred beneath Chesapeake Bay at about 2 and 10 mi (3.2 and 16 km) east and southeast, respectively, of the CCNPP site as shown in Figure 2.5-25. The east-facing monoclines (USGS, 1995) are not depicted on any geologic maps of the area but they are shown on geologic cross-sections (USGS, 1995) that trend northwest-southeast across the CCNPP site and south of the site near the Patuxent River. A partial representation of cross sections A-A' and E-E' is provided in Figure 2.5-40 (USGS, 1995). As mapped in cross Section and inferred in plan view, the monoclines align with the western shore of Chesapeake Bay and by association define a north-trending structure beneath the Chesapeake Bay. The monoclines exhibit a west-side up sense of motion that projects into the Miocene Choptank Formation (USGS, 1995). The monoclines are shown deforming the Lower Paleocene to Upper Miocene strata with approximately 60 to 300 ft (18 to 91 m) of structural relief. The overlying Late Miocene St. Marys Formation is not shown as warped. Boreholes used to construct the Section are widely spaced and do not provide good constraint on the existence and location of the postulated monoclines (cross sections A-A' and E-E') (USGS, 1995). Although no published geologic data are available to substantiate the existence of the monoclines, it is inferred (USGS, 1995) that the distinct elevation change (about 100 ft (30 m)) between Calvert Cliffs and the Delmarva Peninsula to the east, and the apparent linear nature of the Calvert Cliffs, to be tectonically controlled.

Existing published geologic, aeromagnetic, and gravity data provide evidence for the absence of a prominent north-trending monocline directly underlying Chesapeake Bay. Regional aeromagnetic and gravity maps show that the overall trend of potential structures buried beneath the Coastal Plain and Chesapeake Bay near the site trend northeast or subparallel to mapped faults and folds in the Piedmont Province to the west of the CCNPP site as shown in Figure 2.5-20, Figure 2.5-21, and Figure 2.5-22. A structural contour map of the top of the Middle Eocene Piney Point and Nanjemoy contact shows a northeast-striking undeformed contact across the Chesapeake Bay, consistent with regional bedding, yet inconsistent with a postulated more north-trending structure approximately parallel to the western margin of the Chesapeake Bay as shown in Figure 2.5-14. Lastly, an east-west oriented cross-Section located about 30 mi (48 km) north of the CCNPP site also depicts nearly flat-lying Cretaceous and Paleocene stratigraphy across the Chesapeake Bay, and does not depict a fold or fault (MGS, 1978).

The change in physiographic elevation and geomorphic surfaces between the western and eastern shores of Chesapeake Bay can be explained by erosional processes directly related to the former course of the Susquehanna River, coupled with eustatic sea level fluctuations during the Quaternary (USGS, 1989a) (USGS, 1989b) (GSA, 1990) (USGS, 1979a) (USGS, 1979b). It is interpreted (GSA, 1990) by high resolution, shallow geophysical data to delineate several former river course(s) and provide geometrical constraints on the width and depth of the paleo-Susquehanna River between northern Chesapeake Bay and the southern Delmarva Peninsula as shown in Figure 2.5-29. Paleo-river profiles of the Eastville (150 ka) and Exmore (200 to 400 ka) Susquehanna paleochannels show no distinct elevation changes within the CCNPP site area and along projection features (USGS, 1995), as well as the Hillville fault (MGS, 1978). A submarine geologic map of Tertiary and Pleistocene deposits below the Chesapeake Bay at and near the CCNPP site developed from the shallow, high-resolution seismic reflection profiles has been developed (USGS, 1989a) (USGS, 1989b). No folds, warps or faults are depicted on these maps (USGS, 1989a) (USGS, 1989b) which encompass the hypothesized (USGS, 1995) east-facing monocline. Lastly, structure contour maps of the top of Tertiary deposits, developed from shallow seismic reflection data, show no geomorphic features that could be interpreted as fault or fold related (USGS, 1989b).

In summary, site and aerial reconnaissance, coupled with literature review, do not provide evidence for the existence of the hypothesized east-facing monocline (USGS, 1995). There also is no pre-EPRI or post-EPRI (EPRI, 1986) study of seismicity spatially associated with these features. If the feature does exist, the Miocene St. Marys Formation is not depicted (USGS, 1995) to be deformed. Therefore, the inferred monoclines (USGS, 1995) are older than Late Miocene in age and do not represent a surface-fault rupture or deformation hazard at the CCNPP site.

### 2.5.3.2.3    Stratigraphic Undulations and Hypothesized Fault

Multiple subtle folds or inflections and a postulated fault have been mapped (Kidwell, 1997) in cliff exposures of the Miocene Choptank and St Marys Formations along the west side of Chesapeake Bay. Based on structural relations, such as an apparent decrease in warping up-section through the exposed Miocene section, it is suggested (Kidwell, 1997) that the postulated deformation may reflect growth faulting, or the presence of other tensional structures at depth. Over 300 lithostratigraphic columns along an approximately 25 mi (40 km) long stretch of Calvert Cliffs between Chesapeake Beach and Little Cove Point were prepared (Kidwell, 1988) (Kidwell, 1997) as shown in Figure 2.5-30. When these stratigraphic columns are compiled into a cross section, they provide an approximately 25 mi (40 km) long nearly continuous log of Miocene, Pliocene and Quaternary deposits exposed in the cliffs directly east of the CCNPP site as shown in Figure 2.5-30. A stratigraphic analysis (Kidwell, 1997) indicates that the Miocene Coastal Plain deposits strike northeast and dip 1 to 2 degrees to the south consistent with the findings of others (USGS, 1995) (MGS, 2003b) (MGS, 2003c). However, the very low regional southerly dip is disrupted occasionally by several subtle low amplitude and broad undulations developed within the Miocene Coastal Plain deposits. The stratigraphic undulations (represented at 150 times vertical exaggeration in Figure 2.5-30) are interpreted (Kidwell, 1997) as monoclines and asymmetrical anticlines. The undulatory stratigraphic contacts of the Miocene deposits often coincide with basal unconformities having wavelengths typically on the order of 2.5 to 5 mi (4 to 8 km) and amplitudes of 10 to 11 ft (3 to 3.4 m). South of the CCNPP site, near Little Cove Point, the stratigraphic undulations within the Miocene St. Marys Formation decrease in wavelength (approaching one mile) and amplitude (approximately 9 ft (2.7 m) or less). Based on stratigraphic truncations, the inferred warping also appears to decrease up-Section into the overlying upper Miocene St. Marys Formation near the CCNPP site. Any inferred folding of the overlying Pliocene and Quaternary fluvial

strata is very poorly constrained or obscured, because of highly undulatory unconformities within these sand and gravel deposits.

Near Moran Landing, about 1.2 mi (1.9 km) south of the CCNPP site, an apparent 6 to 10 ft (1.8 to 3 m) elevation change in Miocene strata, and a 3 to 12 ft (0.9 to 3.7 km) elevation change in Pliocene and Quaternary (?) fluvial deposits has been interpreted (Kidwell, 1997) as shown in Figure 2.5-30. The presence of a fault to explain the difference in elevation of similar strata across Moran Landing has been inferred (Kidwell, 1997). The postulated fault is not shown on the Section or any published geologic map; however, the inferred location is approximately 1.2 mi (1.9 km) south of the CCNPP site. The hypothesized fault is not exposed in the cliff face and is based entirely on the change in elevation and bedding dip of Miocene stratigraphic boundaries across Moran Landing as shown in Figure 2.5-30. It is postulated (Kidwell, 1997) that the fault strikes northeast and exhibits a down-to-the-north sense of separation. The apparent elevation change of the Pliocene and Quaternary contacts, however, can be explained by fluvial processes (channeling and irregular erosional and depositional surfaces).

Field and aerial (inspection by plane) reconnaissance, coupled with interpretation of aerial photography (review and inspection of features preserved in aerial photos) and LiDAR data, conducted for this investigation shows that there are no geomorphic features indicative of potential Quaternary activity along trend with the postulated folds and fault interpreted by Kidwell (Kidwell, 1997). LiDAR data was reviewed for the presence of northeast-striking lineaments in the region of Moran Landing and to the southeast between the Patuxent and Potomac Rivers as shown in Figure 2.5-26. No features suggestive of tectonic deformation were interpreted in the Pliocene (Upland deposits) or Quaternary fluvial surfaces (USGS, 1989c) (USGS, 1989d) (MGS, 2003b) (MGS, 2003c), some of which approach approximately 450 ka in age. There is no pre-EPRI or post-EPRI (EPRI, 1986) study seismicity spatially associated with the Kidwell (Kidwell, 1997) features, nor is there geomorphic evidence to strongly suggest that these features, including the postulated fault, pose a surface-fault rupture hazard at the CCNPP site. The hypothesized fault also is not aligned with any magnetic or gravity anomaly previously interpreted by others, suggesting that the apparent elevation change across Moran Landing is surficial in origin.

In summary, with the exception of Kidwell (Kidwell, 1997), numerous investigations of the Chesapeake Bay coastline by government researchers, stratigraphers, and consultants for Baltimore Gas and Electric have reported no visibly distinct signs of tectonic deformation within the exposed Miocene deposits near the CCNPP site as shown in Figure 2.5-44. Collectively, the majority of published and unpublished geologic information for the CCNPP site area, coupled with regional geologic sections (Achmad, 1997) (MGS, 2003b) (MGS, 2003c) and site and aerial reconnaissance, indicate the absence of Late Miocene and younger faulting and folding. A review of regional geologic sections and interpretation of LiDAR data suggest that the features, if present, are not prominent structures and do not appear to be developed within the Pliocene to Quaternary landscape. In summary, on the basis of regional and site data, there are no known faults within the site area, with the exception of the poorly constrained Hillville fault that lies along the western perimeter of the 5 mi (8 km) radius of the site. The Hillville fault has been documented as being last active in the Paleocene epoch (MGS, 1986).

### 2.5.3.3     Correlation of Earthquakes with Capable Tectonic Sources

No reported historical earthquake epicenters have been associated with bedrock faults within the 25 mi (40 km) radius of the CCNPP site vicinity as shown in Figure 2.5-25.

## 2.5.3.4      Ages of Most Recent Deformations

As presented in Section 2.5.3.2, the Hillville fault and postulated folds and faults within 5 mi (8 km) of the CCNPP site do not exhibit evidence of Quaternary activity.  It is interpreted (MGS, 1978) that the Hillville fault formed during the Paleozoic Era as part of the regional Taconic orogeny, and locally may have been reactivated during the Paleozoic with the youngest deformation being Paleocene.  Based on a review of available published geologic literature, field and aerial (inspection by plane) reconnaissance, and interpretation of aerial photography (review and inspection of features preserved in aerial photos) and LiDAR data, the postulated structures (USGS, 1995) (Kidwell, 1997), if they exist, are constrained to the Miocene and do not appear to affect Pliocene and Quaternary deposits.

## 2.5.3.5      Relationship of Tectonic Structures in the Site Area to Regional Tectonic Structures

Of the three features evaluated within the 5 mi (8 km) radius of the CCNPP site, only the Hillville fault has been linked with a regional tectonic structure.  The Hillville fault zone delineates a possible Paleozoic suture zone reactive in the Mesozoic and Early Tertiary. Tectonic models hypothesize that the crystalline basement underlying the CCNPP site was accreted to a pre-Taconic North American margin in the Paleozoic along a suture that lies about 10 mi (16 km) west of the CCNPP site as shown in Figure 2.5-17 and Figure 2.5-23.  The lithosphere plate-scale suture is defined by a distinct north-northeast-trending magnetic anomaly that dips easterly between 35 and 45 degrees and lies about 8 to 9 mi (12.9 to 14.5 km) beneath the CCNPP site (GSA, 1995) as shown in Figure 2.5-17.  Directly west of the suture lies the north-to northeast-trending Taylorsville basin and to the east, the postulated Queen Anne Mesozoic rift basin as shown in Figure 2.5-10.  The fault zone is interpreted as a lithotectonic terrane boundary that separates basement rocks associated with Triassic rift basins on the west from low-grade metamorphic basement on the east (i.e., Sussex Terrane/Taconic suture (GSA, 1995); see Figure 2.5-17) (MGS, 1986).  The apparent juxtaposition of the Hillville fault zone with the Sussex-Currioman Bay aeromagnetic anomaly suggests that the south flank of the Salisbury Embayment may be a zone of crustal instability that was reactivated during the Mesozoic and Tertiary.  Cretaceous activity is inferred (MGS, 1978) and the fault extended up into the Cretaceous Potomac Group.  The resolution of the geophysical data does not permit an interpretation for the upward projection of the fault into the younger overlying Coastal Plain deposits.  Stratigraphic correlations of Coastal Plain deposits from borehole data were used (MGS, 1978) to speculate that the Hillville fault may have been active during the Early Paleocene.

## 2.5.3.6      Characterization of Capable Tectonic Sources

Based on previous discussions in Section 2.5.3.4, there are no capable tectonic sources within 5 mi (8 km) of the CCNPP site.

## 2.5.3.7      Designation of Zones of Quaternary Deformation Requiring Detailed Fault Investigation

There are no zones of Quaternary deformation requiring detailed investigation within the CCNPP site area.  A review and interpretation of aerial photography, digital elevation models, and LiDAR data of the site area, coupled with aerial reconnaissance, identified a few discontinuous north to northeast-striking lineaments.  None of these lineaments are interpreted as fault-related, or coincident with the Hillville fault or the other previously inferred Miocene-Pliocene structures.  Aerial and field reconnaissance of the western shoreline of Chesapeake Bay suggests that some of the lineaments along the western shoreline may be related to a weak to poorly developed, near-vertical, north to northeast-trending fracture or

joint set.  These fractures provide discontinuities by which large blocks of the St. Marys and Choptank Formations spall and form colluvial rubble at the base of the steep cliffs; however, these weak fractures do not represent a surface-fault rupture hazard at the site.

### 2.5.3.8     Potential for Tectonic or Non-Tectonic Deformation at the Site

The potential for tectonic deformation at the site is negligible. This is based on:

1. The nearly flat-lying Miocene stratigraphy beneath the site interpreted from both existing and new borehole data,

2. The absence of faulting in Miocene deposits exposed along the cliffs at the eastern boundary of the CCNPP site as shown in Figure 2.5-43,

3. The interpretation of aerial photography and LiDAR data.

Collectively, these data support the interpretation for the absence of any Quaternary surface faults or capable tectonic sources within the site area. In addition, there is no evidence of non-tectonic deformation at the site, such as glacially induced faulting, collapse structures, growth faults, salt migration, or volcanic intrusion.

### 2.5.3.9     References

**Achmad, 1997.**  Hydrogeology, model simulation, and water-supply potential of the Aquia and Piney Point-Nanjemoy Aquifers in Calvert and St. Marys Counties, Maryland, G. Achmad and H. Hansen, 1997.

**BPC, 1981.**  Subsurface Investigation and Foundation Report, North Parking Area, Calvert Cliffs Nuclear Power Plant, Lusby, Maryland, Bechtel Power Corporation, June 1981.

**BGE, 1968.**  Preliminary Safety Analysis Report Calvert Cliffs Nuclear Power Plant Units 1 and 2, Volume 1, Docket 50-317 and 50-318, Baltimore Gas and Electric Company, 1968.

**CFR, 2007a.** Geologic and Seismic Siting Criteria, Title 10, Code of Federal Regulations, Part 100.23, 2007.

**CFR, 2007b.** Earthquake Engineering Criteria for Nuclear Power Plants, Title 10, Code of Federal Regulations, Part 50, Appendix S, 2007.

**CEG, 2005.**  Calvert Cliffs Independent Spent Fuel Storage Installation, Updated Environmental Report, Volume 3, Revision 7, Constellation Energy, 2005.

**EPRI, 1986.**  Seismic Hazard Methodology for the Central and Eastern United States: EPRI NP-4726, Electric Power Research Institute, 1986.

**GSA, 1990.**  Ancient channels of the Susquehanna River beneath Chesapeake Bay and the Delmarva Peninsula, Geological Society of America Bulletin, Volume 102, p 1268-1279, S. Colman, J. Halka, C. Hobbs III, R. Mixon, D. Foster, 1990.

**GSA, 1995.**  E-3 Southwestern Pennsylvania to Baltimore Canyon Trough, Geological Society of America Centennial Continent/Ocean Transect #19, L. Glover III and K. Klitgord, 1995.

**Kidwell, 1988.** Reciprocal Sedimentation and Noncorrelative Hiatuses in Marine-Paralic Siliciclastics: Miocene Outcrop Evidence, Geology, Volume 16, p 609-612, S. Kidwell, 1988.

**Kidwell, 1997.** Anatomy of Extremely Thin Marine Sequences Landward of a Passive-Margin Hinge Zone: Neogene Calvert Cliffs Succession, Journal of Sedimentary Research, Volume 67, Number 2, p 322-340, S. Kidwell,1997.

**MGS, 1968.** Geologic Map of Maryland, Scale 1:250,000, Department of Natural Resources, Maryland Geological Survey, E. Cleaves, J. Edwards Jr., and J. Glaser, 1968.

**MGS, 1971.** Geology and mineral resources of Southern Maryland, Report of Investigations Number 15, p 85, Maryland Geological Survey, J. Glaser, 1971.

**MGS, 1978.** Upper Cretaceous (Senonian) and Paleocene (Danian) Pinchouts on the South Flank of the Salisbury Embayment, Maryland and their relationship to antecedent basement structures, Report of Investigations Number 29, p 36, Department of Natural Resources, Maryland Geological Survey, H. Hansen, 1978.

**MGS, 1986.** The Lithology and Distribution of Pre-Cretaceous basement rocks beneath the Maryland Coastal Plain, Report of Investigations Number 44, p 27, Department of Natural Resources, Maryland Geological Survey, H. Hansen and J. Edwards Jr., 1986.

**MGS, 1994.** Geologic Map of Calvert County, Department of Natural Resources, Maryland Geological Survey, Scale 1:62,500, J. Glaser, 1994.

**MGS, 2003a.** Geologic Map of Prince George's County, Maryland, Maryland Geological Survey, Scale 1:62,500, J. Glaser, 2003a.

**MGS, 2003b.** Geologic Map of the Broomers Island Quadrangle, Calvert and St. Marys Counties, Maryland, Maryland Geological Survey, Scale 1: 24,000, J. Glaser, 2003.

**MGS, 2003c.** Geologic Map of the Cove Point Quadrangle, Calvert County, Maryland, Maryland Geological Survey, Scale 1:24,000, J. Glaser, 2003c.

**NRC, 1997.** Identification and Characterization of Seismic Sources and Determination of Safe Shutdown Earthquake Ground Motion, Regulatory Guide 1.165, U.S. Nuclear Regulatory Commission, March 1997.

**Obermier, 1998.** Paleoliquifaction Evidence for Seismic Quiescence in Central Virginia During the Late and Middle Holocene Time (abs), Eos Transactions of the American Geophysical Union, Volume 79, Number 17, p S342, S. Obermier and W. McNulty, 1998.

**PEPCO, 1973.** Preliminary Safety Analysis Report, Douglas Point Nuclear Generating Station, Units 1 and 2, Volume 2, Docket Number 50448-2 and 50449-2, Potomac Electric Power Company, 1973.

**URS, 2000.** Seismic Characterization Study for the Expansion of the Williams Gas Pipeline-Tranco LNG Facility, Cove Point, Maryland, URS Corporation, October 2000.

**USGS, 1979a.** Upper Cenozoic Deposits of the Central Delmarva Peninsula, Maryland and Delaware, U.S. Geological Survey, Professional Paper 1067-A, J. Owens and C. Denny, 1979.

**USGS, 1979b.** Upper Cenozoic Sediments of the Lower Delaware Valley and the Northern Delmarva Peninsula, New Jersey, Pennsylvania, Delaware, and Maryland, U.S. Geological Survey, Professional Paper 1067-D, J. Owens and J. Minard, 1979.

**USGS, 1986.** Geologic Map of Dorchester County, Maryland, U.S. Geological Survey, Scale 1:62,500, J. Owens and C. Denny, 1986.

**USGS, 1989a.** Quaternary Geology of the Southern Maryland Part of the Chesapeake Bay, U.S. Geological Survey, Miscellaneous Field Studies Map MF-1948-C, Scale 1:125,000, S. Colman and J. Halka, 1989.

**USGS, 1989b.** Quaternary Geology of the Northern Maryland part of the Chesapeake Bay, U.S. Geological Survey, Miscellaneous Field Studies Map MF-1948-B, Scale 1:125,000, S. Colman and J. Halka, 1989.

**USGS, 1989c.** Geologic Map of Charles County, Maryland, U.S. Geological Survey, Scale 1:62,500, L. McCartan, 1989.

**USGS, 1989d.** Geologic Map of St. Marys County, Maryland, U.S. Geological Survey, Scale 1:62,500, L. McCartan, 1989.

**USGS, 1995.** Geologic Map and Cross Sections of the Leonardtown 30 X 60 minute quadrangle, Maryland and Virginia, U.S. Geological Survey, L.McCartan, W. Newell, J. Owens, and G. Bradford, 1995.

**USGS, 2000a.** Data for Quaternary Faults, Liquefaction Features, and Possible Tectonic Features in the Central and Eastern United States, East of the Rocky Mountain Front, Open-File Report 00-260, U.S. Geological Survey, A. Crone and R. Wheeler, 2000.

**USGS, 2000b.** Geologic Map of the Fredericksburg 30' x 60' Quadrangle, Virginia and Maryland, Geologic Investigations Series Map I-2607, U.S. Geological Survey, R. Mixon, L. Pavlides, D. Powars, A. Froelich, R. Weems, J. Schindler, W. Newell, L. Edwards, L. Ward, 2000.

**USGS, 2005.** Known or Suggested Quaternary Tectonic Faulting, Central and Eastern United States – New and Updated Assessments for 2005, Open File Report 2005-1336, U.S. Geological Survey, R. Wheeler, 2005.

**Wheeler, 2006.** Quaternary tectonic faulting in the Eastern United States, Engineering Geology, Volume 82, p 165-186, R. Wheeler, 2006.}

## 2.5.4    STABILITY OF SUBSURFACE MATERIALS AND FOUNDATIONS

The U.S. EPR FSAR includes the following COL Item for Section 2.5.4:

A COL aApplicant that references the U.S. EPR design certification will present site-specific information about the properties and stability of soils and rocks that may affect the nuclear power plant facilities, under both static and dynamic conditions including the vibratory ground motions associated with the CSDRS and the site-specific SSE.

This COL Item is addressed as follows:

{This section addresses site-specific subsurface materials and foundation conditions. It was prepared based on the guidance in relevant sections of NRC Regulatory Guide 1.206, Combined License Applications for Nuclear Power Plants (LWR Edition) (NRC, 2007).

{The information presented in this section is based on results of a subsurface investigation program implemented at the CCNPP Unit 3 site, and evaluation of the collected data, unless indicated otherwise.  The data are contained in Geotechnical Subsurface Investigation Data Report (Schnabel, 2007a) (Schnabel, 2007b).  The data is also presented as Appendix 2.5-A and Appendix 2.5-B.

The CCNPP Units 1 and 2 Updated Final Safety Analysis Report (UFSAR) (BGE, 1982) contains a summary of the geotechnical information collected previously for the construction of CCNPP Units 1 and 2.  The planned CCNPP Unit 3 is approximately 2,000 ft south of the existing units. CCNPP Units 1 and 2 UFSAR (BGE, 1982) contains mostly general information that is quantitatively limited in its extent and depth of exploration relative to the investigation performed for the CCNPP Unit 3.  Therefore, the comparison information was limited to those cases where comparable information was obtained from the CNNPP Unit 3 subsurface investigation (Schnabel, 2007a) was available in the CCNPP Units 1 and 2 UFSAR (BGE, 1982).

References to elevation values in this subsection are based on the National Geodetic Vertical Datum of 1929 (NGVD29), unless stated otherwise.}

### 2.5.4.1    Geologic Features

The U.S. EPR FSAR includes the following COL Item in Section 2.5.4.1:

Geologic features are site-specific and will be addressed by the COL applicant.

This COL Item is addressed as follows.

Section 2.5.1.1 addresses the regional geologic settings, including regional physiography and geomorphology, regional geologic history, regional stratigraphy, regional tectonic and non-tectonic conditions, and geologic hazards, as well as maps, cross-sections, and references. Section 2.5.1.2 addresses the geologic conditions specific to the site, including site structural geology, site physiography and geomorphology, site geologic history, site stratigraphy and lithology, site structural geology, seismic conditions, and site geologic hazard evaluation, accompanied by figures, maps, and references.  Pre-loading influences on soil deposits, including estimates of consolidation, pre-consolidation pressures, and methods used for their estimation are addressed in Section 2.5.4.2.  Related maps and stratigraphic profiles are also addressed in Section 2.5.4.2.

{In summary, the site is located in the Atlantic Coastal Plain physiographic province. The soils were formed by ancient rivers carrying large quantities of solids from the northern and western regions into the Atlantic Ocean. These deposits were placed under both freshwater (fluvial) and saltwater (marine) environments, and are about 2,500 feet thick at the site (BGE, 1982). The upper soils are Quaternary, Holocene- and/or Pleistocene-Age deposits formed as beaches or terraces. The lower soils are Miocene-, Eocene-, Paleocene-, and Cretaceous-Age deposits. The Miocene and Eocene soils belong to the Chesapeake and Nanjemoy groups. The Holocene, Pleistocene, Miocene, and Eocene soils were the subject of a detailed subsurface exploration for the COL investigation, as described below.}}

### 2.5.4.2    Properties of Subsurface Materials

The U.S. EPR FSAR includes the following COL Item in Section 2.5.4.2:

> A COL applicant that references the U.S. EPR design certification will reconcile the site-specific soil properties with those used for design of U.S. EPR Seismic Category I structures and foundations described in Section 3.8.

This COL Item is addressed as follows:

{All Seismic Category 1 structures at the CCNPP Unit 3 site are to be supported on, and confined with, compacted structural fill. Therefore, soil properties identified in the U.S. EPR FSAR sections are applicable to compacted structural fill.

Once the potential sources of structural fill have been identified, the material(s) are sampled and tested in the laboratory to establish their static and dynamic properties. Chemical tests are also performed on candidate backfill materials. The results are evaluated to verify that the candidate backfill materials meet the design requirements for structural fill. The structural fill for CCNPP Unit 3 shall be sound, durable, well graded sand or sand and gravel, with a maximum 25 percent fines content, and free of organic matter, trash, and other deleterious materials.

This section addresses the properties of subsurface materials. It is divided into several parts, as follows.

♦   Section 2.5.4.2.1.1 through 2.5.4.2.1.3 describe the subsurface conditions and properties of soils

♦   Section 2.5.4.2.1.4 describes the chemical properties of soils

♦   Section 2.5.4.2.1.5 addresses materials below a depth of 400 ft

♦   Section 2.5.4.2.1.6 provides a summary of the field investigation program

♦   Section 2.5.4.2.1.7 provides a summary of the laboratory testing program

♦   Section 2.5.4.2.1.8 provides a summary of the subsurface investigation

These sections are added as a supplement to the U.S. EPR FSAR.

### 2.5.4.2.1    Description of Subsurface Materials

The site geology is comprised of deep Coastal Plain sediments underlain by bedrock, which is about 2,500 ft below the ground surface for CCNPP Units 1 and 2 UFSAR (BGE, 1982). The site

soils consist of marine and fluvial deposits.  The upper approximately 400 ft of the site soils were the subject of the CCNPP Unit 3 subsurface investigation.  These soils can be divided into the following stratigraphic units.

- Stratum I: Terrace Sand

- Stratum IIa: Chesapeake Clay/Silt

- Stratum IIb: Chesapeake Cemented Sand

- Stratum IIc: Chesapeake Clay/Silt

- Stratum III: Nanjemoy Sand

Information on deeper soils (below 400 ft) was obtained from the available literature, and it will be discussed later in this subsection.  Identification of Strata I through III was based on their physical and engineering characteristics.  The characterization of the soils was based on a suite of tests performed on these soils, consisting of standard penetration tests (SPT) in soil borings including hammer energy measurements, cone penetration test (CPT) soundings, test pits, geophysical suspension P-S velocity logging, field electrical resistivity testing, and  observation wells, as well as extensive laboratory testing.  The extent of the field tests is summarized in Table 2.5-25.  Locations of these tests are shown in Figure 2.5-103 through Figure 2.5-105.  Subsurface profiles inferred from these tests are shown in Figure 2.5-107 through Figure 2.5-111, with a subsurface profile legend provided in Figure 2.5-106 .

The natural topography at the CCNPP site, at the time of the subsurface exploration, was gently rolling.  Site-wide, however, the relief could vary by as much as 100 ft.  In the area where CCNPP Unit 3 is planned, ground surface elevations at the time of the exploration ranged from approximately elevation 50 ft to elevation 120 ft, with an average of about elevation 88 ft.  The planned elevation (rough grade) in the powerblock area ranges from about elevation 75 ft to elevation 85 ft, with the centerline of Unit 3 at elevation 84.7 ft, or approximately elevation 85 ft.  The Powerblock includes the Reactor Building, Fuel Building, Safeguard Building, Emergency Power Generating Building, Nuclear Auxiliary Building, Access Building, Radioactive Waste Building, Turbine Building, and Ultimate Heat Sink.

The subsurface conditions were established from the information contained in the Geotechnical Subsurface Investigation Data Report (Schnabel, 2007a).  The subsurface profiles illustrate these conditions.  The maximum depth explored was about 400 ft beneath the ground surface at boring locations B-301 and B-401.  The maximum depth explored by CPT soundings was 142 ft beneath the ground surface at location C-407 (CPT soundings encountered repeated refusal and, therefore, could not be consistently extended to greater depths).  Field tests (borings, CPTs, etc.) identified as 300-series, e.g., B-301 or C-301, are located in Unit 3 area.  Tests identified as 400-series, e.g., B-401 or C-401, are located in an area adjacent to CCNPP Unit 3, hereafter referred to as Construction Laydown Area 1 (CLA1).  Field tests identified as 700 series, e.g., B-701 or C-701, are located outside of these two areas, and include the proposed cooling tower, switchyard, and intake/discharge piping locations.  Bedrock is too deep (about 2,500 ft below ground) to be of interest for earthwork and foundation design and construction.  Therefore, rock properties will not be addressed in similar detail as the overlying soils.  The major strata identified from the boring logs, as shown on the subsurface profiles (Strata I, II, and III), are described in detail in the next subsections.

### 2.5.4.2.1.1    Stratum I – Terrace Sand

The Terrace Sand stratum consists primarily of light-brown to brown sand with varying amounts of silt, clay, and/or gravel, sometimes with silt or clay interbeds.  This stratum was fully penetrated by boreholes installed within CCNPP Unit 3 Powerblock area and the adjoining CLA1 area (the 300 and 400 series borings) and by a majority of boreholes drilled outside of these two areas (the 700 series borings).  This stratum is not present in low lying areas.

The thickness of Stratum I soils was estimated from the boring logs.  In CCNPP Unit 3 area, its thickness with respect to the existing ground surface varies from about 2 ft to 51 ft, with an average thickness of about 21 ft.  The average bottom for Stratum I soils is about elevation 66 ft in CCNPP Unit 3 area.  The average thickness and bottom elevation for Stratum I soils for the combined CCNPP Unit 3 and CLA1 areas is about 27 ft and elevation 65 ft, respectively.  Additional information on thickness and termination elevation for this stratum at locations other than Unit 3, including site-wide, is presented in Table 2.5-26 and Table 2.5-27.  Based on site-wide information, the termination elevation for Stratum I was estimated at about elevation 61 ft.  An elevation of 60 ft was adopted for simplicity.

It should be noted that at isolated locations, sandy soils with an appearance similar to Stratum I soils were encountered.  These soils are suspected of being man-made fill. They were present at the ground surface, above Stratum I soils, and were encountered in 17 borings (B-309, B-336, B-340, B-341, B-406, B-409, B-412, B-415, B-419, B-420, B-438/A, B-439, B-440, B-701, B-710, B-713, and B-768).  Mainly, they were found in areas which had previously been developed at the site, such as Camp Conoy, roadways, and ball field areas.  Their thickness ranged from approximately 0.5 ft to 17 ft, with an average thickness of about 7 ft.

Soil samples were collected from the borings via SPT and tube samples.  Samples were collected more frequently in the upper portion of the borings than in the lower portion, e.g., typically 6 samples were obtained in the upper 15 ft.  Thereafter, samples were obtained at 5 ft intervals.  SPT N-values were measured during the sampling and recorded on the boring logs.  In CCNPP Unit 3 area, the SPT N-values in Stratum I soils ranged from 0 blows/ft (weight of hammer (WOH) or weight of rod (WOR)) to 70 blows/ft, with an average measured N-value of 10 blows/ft. Additional SPT information on this layer at locations other than Unit 3, including site-wide, is presented in Table 2.5-28.  The measured N-values versus elevation are presented in Figure 2.5-112.  It indicates that a majority of the SPT N-values are within a relatively uniform range of about 3 to 13 blows/ft, with occasional higher values between about elevation 70 ft and elevation 90 ft.

The WOH and WOR values were very infrequent in Stratum I soils.  A total of 5 WOH and WOR conditions were encountered in borings at CCNPP Unit 3 location, and a total of 5 were observed in all other borings.  At the CCNP Unit 3 location, three of these conditions were in boring B-309 in materials designated as "fill," which will be removed during construction.  The fourth episode was in boring B-314 at the ground surface which will also be removed during construction.  The fifth value was in boring B-322 at about elevation 70 ft, at the location of the Essential Service Water System (ESWS) Cooling Tower.  The cause of this low SPT value is likely due to sampling disturbance.  A review of the boring logs and stratigraphic profiles for the same soils at other locations do not indicate this to be the predominant situation.  Rather, the low SPT value is an isolated, infrequent situation, most likely caused by factors other than the natural condition of Stratum I soils.  Nonetheless, these soils will be removed during excavation for the ESWS Cooling Tower to at least elevation 60 ft.  In conclusion, at the CCNP Unit 3 location, the 5 WHO and WOR results are inconsequential to the stability of Stratum I soils.

Five drill rigs were used for the COL subsurface exploration.  SPT hammer energies were measured for each of the five drilling rigs utilized.  Energy measurements were made in 5 borings (B-401, B-403, B-404, B-409, and B-744).  Because the SPT N-value used in correlations with engineering properties is the value corresponding to 60 percent hammer efficiency, the measured SPT N-values were adjusted based on the energy measurements, in accordance with American Society for Testing and Materials (ASTM) D6066 (ASTM, 2004f)).  The average energy transfer ratio (ETR) obtained from hammer energy measurements for each drilling rig was applied to the measured SPT N-values.  The average ETR ranged from 78 percent to 87 percent, or an N-value adjustment factor ranging from 1.30 to 1.45.  A summary of the measured ETR values for each drill rig is shown in Table 2.5-29.  The measured SPT N-values from each boring were adjusted using the appropriate ETR value shown in Table 2.5-29 for the drill rig utilized.  The adjusted average field-measured N-value for Stratum I soils is 16 blows/ft.  A value of 15 blows/ft was conservatively adopted for engineering purposes, as shown in Table 2.5-30.  Based on corrected SPT N-values, Stratum I soils are considered medium dense on average.

CPT soundings were performed in Stratum I soils.  The cone tip resistance, $q_c$, in these soils ranged from about 2 to 570 tons per square ft (tsf), with an average of about 120 tsf.  The CPT tip resistance profile versus elevation is shown in Figure 2.5-113.  The results indicate the $q_c$ values in Stratum I soils to be typically limited to about 200 tsf, with values peaking much higher between elevation 80 ft to elevation 90 ft.  The CPT results also indicate the presence of clay zones within this stratum, at about elevation 115 ft, elevation 100 ft, and elevation 90 ft.  Estimated relative density from CPT data ranges from about 30 to near 100 percent, with an average of about 65 percent.

Laboratory index tests and testing for determination of engineering properties were performed on selected samples from Stratum I soils.  Laboratory test quantities are summarized in Table 2.5-31.  Sample selection for testing was primarily based on the observed soil uniformity from the field classification, or conversely, the variation in material description based on logging in the field, in order to obtain a quantitative measure of the uniformity, or the variation, respectively.  The following index tests were performed on Stratum I soils, with results as noted.

|  | No. of Tests | Min. Value | Max. Value | Average Value |
|---|---|---|---|---|
| Water Content (%) | 31 | 3 | 44 | 15 |
| Liquid Limit (LL)(%) | 31 | Non-Plastic (NP) | 75 | NP |
| Plastic Limit (PL)(%) | 31 | NP | 23 | NP |
| Plasticity Index (PI) | 31 | NP | 52 | NP |
| Fines Content (%) | 85 | 3 | 71 | 19 |
| Unit Weight (pcf) | 3 | 115 | 124 | 120 |

The test results are summarized in Table 2.5-32.  The water content and Atterberg limits are presented versus elevation in Figure 2.5-114.  They are also shown on a plasticity chart in Figure 2.5-115.  For engineering purposes, Stratum I soils were characterized, on average, as non-plastic with an average fines content (materials passing No. 200 Sieve) of 20 percent.  Grain size analyses indicated that these soils are primarily fine or fine-medium sands.  The Unified Soil Classification System (USCS) designations were poorly-graded sand/silty sand, silty sand, well-graded sand, clayey sand, clay of high plasticity, silt, clay, and silt with high plasticity, with the predominant classifications of SP-SM and SM.  The often plastic and fine-grained soil classifications are from the interbeds within this stratum.  Based on the laboratory results, an average unit weight of 120 pounds per cubic foot (pcf) was adopted for these soils.

The shear strength of Stratum I soils was evaluated based on laboratory testing and correlations with SPT N-values and CPT results. Initially, an angle of shearing resistance (or friction angle), $\phi'$, for the granular Terrace Sand was estimated from an empirical correlation with SPT N-values (Bowles, 1996). Using the SPT N-value adjusted for hammer efficiency, a $\phi'$ of about 34 degrees was obtained for N = 15 blows/ft and for medium-grained sand. A value of $\phi'$ = 33 degrees was considered appropriate. Friction angle values were also obtained from the CPT results, estimated using the method recommended in EPRI Report EL-6800 (EPRI, 1990). They are presented versus elevation in Figure 2.5-116. The values shown in Figure 2.5-116 range from about 29 to 49 degrees, with an average value of about 40 degrees. One direct shear test was performed on a sample of Stratum I soils designated as clay by USCS, resulting in $\phi'$ = 29.2 degrees and c' = 0.3 tsf. The laboratory strength results are given in Table 2.5-33. From the above interpretations, a summary of average $\phi'$ values for Stratum I soils is compiled as follows.

|  | SPT | CPT | Direct Shear |
|---|---|---|---|
| $\phi'$ (degrees) | 33 | 40 | 29* |

* c' = 0.3 tsf not shown

Based on the above, $\phi'$ = 32 degrees and c' = 0 is conservatively adopted for Stratum I soils.

Consolidation properties and stress history of Stratum I soils were evaluated via laboratory testing and evaluation of the CPT data. A summary of the laboratory consolidation test results is presented in Table 2.5-34. The results are also shown versus elevation in Figure 2.5-117. Results indicate that, on average, these soils are preconsolidated to 5 tsf, with an overconsolidation ratio (OCR) of at least 4. OCR derived from CPT data are shown in Figure 2.5-118. The CPT-interpreted results are scattered over a large range, from OCR = 0.6 to OCR = 10, with no unique trend. At best, an average OCR may be discerned from the CPT data, or an approximate average OCR of 4 to 5. Summary OCR values from CPT data are shown in Table 2.5-34. An average OCR = 4 and preconsolidation pressure (Pp') of 4 tsf were adopted for Stratum I soils based on available data.

Static (or high strain) elastic modulus, E, for coarse-grained soils can be evaluated using the following relationship (Davie, 1988).

$$E = 18\,N \text{ (in tsf)} \hfill \text{Eq. 2.5.4-1}$$

where N = SPT N-value in blows/ft. Substituting the previously established N-value for Stratum I soils (SPT N-value = 15), an elastic modulus of 270 tsf was estimated for these soils. Also, elastic modulus can be estimated based on shear wave velocity for sandy soils (Senapathy, 2001), as follows.

$$E = 2\,G\,(1 + \mu) \hfill \text{Eq. 2.5.4-2}$$

where,

$$G_{.0001\%} = \gamma/g\,(Vs)^2 \hfill \text{Eq. 2.5.4-3}$$
$$G_{.0001\%} / G_{.375\%} = 10 \quad \text{(for sands)} \hfill \text{Eq. 2.5.4-4}$$

In Eqs. 2.5.4-2 through 2.5.4-4, $G_{.0001\%}$ = small strain shear modulus (i.e., strain in the range of $10^{-4}$ percent), $G_{.375\%}$ = large strain (static) shear modulus (i.e., strains in the range of 0.25 percent to 0.5 percent), $\mu$ = Poisson's ratio, $\gamma$ = total soil density, g = acceleration of gravity, and Vs = shear wave velocity.

Using Vs = 790 ft/sec obtained from the measurements at the site (refer to Section 2.5.4.4 for discussions on this topic), $\gamma$ = 120 pcf, and taking $\mu$ = 0.3 for sand, a static (or high strain) modulus of elasticity of 302 tsf is estimated from Eq. 2.5.4-2. Using an average of the estimated values from SPT and shear wave velocity, an elastic modulus of 286 tsf is estimated. A value of 280 tsf was adopted for Stratum I soils. Values of E are shown in Table 2.5-35.

The static shear modulus, G, is related to the static modulus of elasticity by the following relationship:

$$G = E / (2 (1 + \mu))$$                                                 Eq. 2.5.4-5

Using $\mu$ = 0.3 for sandy soils, a shear modulus of 108 tsf was estimated for these soils based on E = 280 tsf. A value of 116 tsf was estimated using Eq. 2.5.4-3. A value of 110 tsf was conservatively adopted for Stratum I soils. Values of G are shown in Table 2.5-35.

The coefficient of subgrade reaction for 1-ft wide or 1-ft square footings, $k_1$, was obtained from "Evaluation of Coefficient of Subgrade Reaction" (Terzaghi, 1955). Based on material characterization for Stratum I soils, $k_1$ = 75 tons per cubic ft (tcf) was estimated and adopted.

Active, passive, and at-rest static earth pressure coefficients, $K_a$, $K_p$, and $K_0$, respectively, were estimated assuming frictionless vertical walls and horizontal backfill using Rankine's Theory and based of the following relationships (Lambe, 1969):

$$K_a = \tan^2(45 - \phi'/2)$$                                            Eq. 2.5.4-6
$$K_p = \tan^2(45 + \phi'/2)$$                                            Eq. 2.5.4-7
$$K_0 = 1 - \sin(\phi')$$                                                 Eq. 2.5.4-8

Substituting previously adopted $\phi'$ = 32 degrees for Stratum I soils, the following earth pressure coefficients were estimated; $K_a$ = 0.3, $K_p$ = 3.3, $K_0$ = 0.47. Values adopted for engineering purposes are $K_a$ = 0.3, $K_p$ = 3.3, and $K_0$ = 0.5.

The sliding coefficient is tangent $\delta$, where $\delta$ is the friction angle between the soil and the material it is bearing against, in this case concrete. Based on "Foundations & Earth Structures" (NFEC, 1986), tangent $\delta$ = 0.4 was adopted for Stratum I soils.

All of the material properties adopted for engineering purposes for Stratum I soils, as well as other relevant information, are summarized in Table 2.5-36.

### 2.5.4.2.1.2    Stratum II – Chesapeake Soils

The Chesapeake soils are the dominant materials in the upper 400 ft of the site, with a combined thickness of about 270 ft. They were subdivided into three layers, based on visual appearance and material properties, namely

- ♦ Stratum IIa - Chesapeake Clay/Silt

- ♦ Stratum IIb - Chesapeake Cemented Sand

- ♦ Stratum IIc - Chesapeake Clay/Silt

Each of these strata is described below.

**Stratum IIa – Chesapeake Clay/Silt**

The Chesapeake Clay/Silt stratum was encountered beneath the Terrace Sand in all boreholes, except in low lying areas where Stratum I soils had been eroded. Stratum IIa typically consists of light to dark gray clay and/or silt, although it is predominately clay, with varying amounts of sand.

The thickness of Stratum IIa soils was estimated from the boring logs. In CCNPP Unit 3 area, its thickness varies from about 4 ft to 35 ft, with an average thickness of about 20 ft. Additional information on thickness of this stratum at locations other than CCNPP Unit 3, including site-wide, is presented in Table 2.5-26.

The stratum thickness was based on estimating the termination elevations encountered for the layer at boring locations. In CCNPP Unit 3 area, the termination elevations of Stratum IIa soils were estimated to range from about elevation 56 ft to elevation 38 ft, with an average termination elevation 47 ft. In combined CCNPP Unit 3 and CLA1 areas, the termination elevations were from elevation 56 ft to elevation 27 ft, with an average elevation 46 ft. An elevation 45 ft was adopted for simplicity. Additional termination information on this layer at locations other than CCNPP Unit 3, including site-wide, is presented in Table 2.5-27. Only data from borings that fully penetrated the layer were considered for determination of termination elevations.

Soil samples were collected from the borings via SPT and tube sampling. SPT N-values were measured during the sampling and recorded on the boring logs. In the CCNPP Unit 3 area, the SPT N-values ranged from 1 blow/ft to 46 blows/ft, with an average uncorrected N-value of 9 blows/ft. Additional SPT information on this layer at locations other than CCNPP Unit 3, including site-wide, is presented in Table 2.5-28. The measured N-values versus elevation are presented in Figure 2.5-112. ThisFigure indicates the SPT N-values to be within a relatively narrow range, indicating uniformity in both depth and laterally, although some increase in SPT N-value with depth is evident in Figure 2.5-112.

The measured SPT N-values from each boring were adjusted using the appropriate ETR value shown in Table 2.5-29 for the drill rig utilized. The adjusted average field-measured N-value for Stratum IIa soils is 13 blows/ft. A value of 10 blows/ft was conservatively adopted for engineering purposes, as shown in Table 2.5-30. Based on adjusted SPT N-values, Stratum IIa soils are considered stiff on average.

CPT soundings were performed in Stratum IIa soils. The cone tip resistance values ranged from about 10 to 200 tsf, with an average value of about 50. A profile of $q_c$ versus elevation is shown in Figure 2.5-113. The results also indicate a mild increase in tip resistance with depth.

Index tests and testing for determination of engineering properties were performed on selected samples from Stratum IIa soils. Sample selection for testing was primarily based on the observed soil uniformity from the field classification, or conversely, the variation in material description based on logging in the field, in order to obtain a quantitative measure of the

uniformity, or the variation, respectively.  The following index tests were performed on Stratum IIa soils, with results as noted.

|  | No. of Tests | Min. Value | Max. Value | Average Value |
|---|---|---|---|---|
| Water Content (WC) (%) | 67 | 11 | 88 | 32 |
| Liquid Limit (LL) (%) | 67 | Non-Plastic (NP) | 86 | 57 |
| Plastic Limit (PL) (%) | 67 | NP | 22 | 22 |
| Plasticity Index (PI) | 67 | NP | 64 | 35 |
| Fines Content (%) | 72 | 29 | 99 | 77 |
| Unit Weight (pcf) | 40 | 103 | 124 | 116 |

The test results are summarized in Table 2.5-32.  The water content and Atterberg limits are presented versus elevation in Figure 2.5-114.  They are also shown on the plasticity chart in Figure 2.5-115.  For engineering purposes, Stratum IIa soils were characterized, on average, as medium-high plasticity clays, with an average PI = 35.  Their predominant USCS designation was clay of high plasticity and silt of high plasticity (CH and MH), however, sometimes with silty sand, silty sand to clayey sand, and organic clay.  The organic designation was based on laboratory (liquid limit) tests.  As visual indications to presence of organic soils were not noted during the field sampling, follow up laboratory organic contents tests were performed.  Results of 8 tests indicated organic contents in the range of 0.1 percent to 1.6 percent, with an average of 0.9 percent.  With less than 1 percent organic matter on average, and observations during sampling, these soils are not considered organic.  Also from the laboratory test results, an average unit weight of 115 pcf was adopted for these soils.

The shear strength of Stratum IIa soils was evaluated based on laboratory testing, and using correlations with SPT N-values and the CPT results.  The results are summarized in Table 2.5-37.

The undrained shear strength, $s_u$, was estimated from empirical correlations with SPT N-value (Lowe, 1975), using

$$s_u = N/16 \text{ (in tsf)} \hspace{4cm} \text{Eq. 2.5.4-9}$$

where N = SPT N-value in blows/ft.  Substituting the previously established N-value for Stratum IIa soils (SPT N-value = 10), $s_u$ = 0.63 tsf is estimated for these soils.  Undrained shear strength was also estimated using the CPT data, following a CPT-$s_u$ correlation from Robertson (Robertson, 1988) as follows.

$$s_u = (q_t - \sigma_v) / N_{kt} \hspace{4cm} \text{Eq. 2.5.4-10}$$

where, $q_t$ is the cone tip resistance, $\sigma_v$ is the total overburden stress, and $N_{kt}$ is cone factor that varies between 10 and 20.  A cone factor $N_{kt}$ = 15 was used as an average value for the analysis of the CPT data.  The shear strength values obtained from the CPT data indicate an average $s_u$ = 1.6 tsf.  Results of 43 laboratory unconsolidated undrained (UU) triaxial and unconfined compression (UC) tests on selected samples indicate an average $s_u$ = 1.1 tsf.  The laboratory shear strength test results are shown versus elevation in Figure 2.5-119.  The CPT-derived values are shown versus elevation in Figure 2.5-120.  Based on these results, an undrained shear strength of 1.0 tsf was conservatively adopted for Stratum IIa soil.

The angle of shearing resistance of these soils was evaluated from laboratory test results.  The results are shown in Table 2.5-33.  Eleven direct shear tests were performed on samples of Stratum IIa soils, mostly designated as CL and CH by the USCS soil classification system, resulting in an average $\phi'$ = 25 degrees and c' = 0.5 tsf. Strength parameters from 6 isotropically consolidated triaxial (CIU-bar) tests, indicated average (effective) $\phi'$ = 27 degrees and c' = 0.4 tsf

and average (total) $\phi$ = 14 degrees and c = 0.7 tsf. From the above, the following is a summary of average $\phi'$ and $\phi$ values for Stratum IIa soils based on various data and interpretation.

|  | Direct Shear | CIU-bar |
|---|---|---|
| $\phi'$ (degrees) | 25 | 27 |
| c' (tsf) | 0.5 | 0.4 |
| $\phi$ (degrees) | --- | 14 |
| c (tsf) | --- | 0.7 |

The direct shear and CIU-bar results are comparable. Based on the above, $\phi'$ = 26 degrees and c' = 0.4 tsf is adopted for Stratum IIa soils.

Consolidation properties and stress history of Stratum IIa soils were assessed via laboratory testing and evaluation of the CPT data. A summary of the laboratory consolidation test results is presented in Table 2.5-34. The results are also plotted versus elevation and shown in Figure 2.5-117. Results indicate that, on average, these soils are preconsolidated to about 9 tsf, with an OCR of at least 5. OCR data derived from CPT results are shown in Figure 2.5-118. The CPT-interpreted results are scattered over a large range, from OCR = 0.6 to OCR = 10, with no unique trend. At best, an average OCR may be discerned from the CPT data, or an approximate OCR of 5 to 6. Summary of OCR values from CPT data is shown in Table 2.5-34. An OCR = 4 and a preconsolidation pressure of 6 tsf were conservatively adopted for Stratum IIa soils.

Static modulus of elasticity for fine-grained soils was evaluated using the following relationship (Davie, 1988).

$$E = 600\ s_u \qquad \text{Eq. 2.5.4-11}$$

This relationship was modified for the CCNPP site soils based on their plasticity, as follows.

$$E = 450\ s_u \qquad \text{Eq. 2.5.4-12}$$

Substituting the previously established $s_u$ for Stratum IIa soils (i.,e., $s_u$ = 1 tsf), an elastic modulus of 450 tsf is estimated. Other relationships for static modulus of elasticity are also available for fine-grained soils (Senapathy, 2001), as follows.

$$G_{.0001\%}/G_{.375\%} = 21/\sqrt{PI} \text{ (for clays)} \qquad \text{Eq. 2.5.4-13}$$
$$G_{.375\%}/s_u = 200 \quad \text{(for clays)} \qquad \text{Eq. 2.5.4-14}$$

It is noted that Eq. 2.5.4-14 (Senapathy, 2001) was derived based on Eqs. 2.5.4-2 and 2.5.4-11 using a Poisson's ratio of 0.5, and therefore this equation has similarities with Eq. 2.5.4-12. Using Vs = 1,100 ft/sec obtained from the measurements at the site (refer to subsection 2.5.4.4 for discussions on this topic), $\gamma$ = 115 pcf, PI = 35, and using $\mu$ = 0.45 for clay, static (or high strain) modulus of elasticity of 1,766 tsf is estimated from Eqs. 2.5.4-2, 2.5.4-3, and 2.5.4-13. Using $s_u$ = 1.0 tsf, an elastic modulus of 580 tsf is estimated from Eqs. 2.5.4-2 and 2.5.4-14. Of the preceding estimates, the value based on PI appears high whereas the other two estimates are comparable, therefore, the PI-based value was omitted in selecting an average elastic modulus for Stratum IIa soils. Using an average of the estimated values from undrained strength and shear wave velocity correlated with $s_u$, an elastic modulus of 515 tsf is estimated (average of 450 and 580 tsf). A value of 510 tsf was conservatively adopted for Stratum IIa soils. The values are shown in Table 2.5-35.

The static shear modulus, G, was estimated using Eq. 2.5.4-5. Using $\mu$ = 0.45 for clay soils, a shear modulus of 176 tsf is estimated based on the corresponding E value. Values of 609 and

200 tsf were estimated using Eqs. 2.5.4-13 and 2.5.4.-14. The highest value was ignored for conservatism. An average of the two other values, 180 tsf, was conservatively adopted for Stratum IIa soils. The values are shown in Table 2.5-35.

The coefficient of subgrade reaction for 1-ft wide or 1-ft square footings, $k_1$, was obtained from Terzaghi (Terzaghi, 1955). Based on material characterization for Stratum IIa soils, $k_1 = 75$ tcf was estimated and adopted.

Active, passive, and at rest static earth pressure coefficients, $K_a$, $K_p$, and $K_0$, respectively, were estimated using Eqs. 2.5.4-6, 2.5.4-7, and 2.5.4-8. Substituting the previously adopted $\phi' = 26$ degrees for Stratum IIa soils, the following earth pressures coefficients are estimated; $K_a = 0.4$, $K_p = 2.6$, and $K_0 = 0.6$. Given the overconsolidated nature of the soils, and considering the adopted OCR value, the $K_0$ value was increased by 33 percent based on experience. The adopted values for engineering purposes are $K_a = 0.4$, $K_p = 2.6$, and $K_0 = 0.8$.

The sliding coefficient (tangent $\delta$) of 0.35 was adopted for Stratum IIa soils in contact with concrete (NFEC, 1986).

All of the material properties adopted for engineering purposes for Stratum IIa soils, as well as other useful information, are summarized in Table 2.5-36.

**Stratum IIb – Chesapeake Cemented Sand**

The Chesapeake Cemented Sand stratum was encountered beneath Stratum IIa in all the boreholes. This stratum includes interbedded layers of light to dark gray silty/clayey sands, sandy silts, and low to high plasticity clays, with varying amounts of shell fragments and with varying degrees of cementation. The predominant soils, however, are sandy.

The thickness of Stratum IIb soils was estimated from the boring logs. In the CCNPP Unit 3 area, its thickness varies from about 57 ft to 73 ft, with an average thickness of about 66 ft. Additional information on the thickness of this layer at locations other than CCNPP Unit 3, including site-wide, is presented in Table 2.5-26.

In CCNPP Unit 3 area, the termination elevations of Stratum IIb soils were estimated to range from about elevation 3 ft to elevation -31 ft, with an average termination elevation -19 ft. In combined CCNPP Unit 3 and CLA1 areas, the termination elevations were in the same range as in CCNPP Unit 3, however, with an average elevation -17 ft. An elevation of -15 ft was adopted for simplicity. Additional information on termination elevations for this layer at locations other than CCNPP Unit 3, including site-wide, is presented in Table 2.5-27. Only data from borings that fully penetrated the layer were considered for determination of termination elevations.

Soil samples were collected from the borings via SPT and tube samples. In the CCNPP Unit 3 area, the SPT N-values ranged from 4 blows/ft to greater than 100 blows/ft, with an average N-value of 45 blows/ft. Site-wide, an average SPT N-value of 41 blows/ft was estimated. SPT values exceeding 100 blows/ft were common in these soils, resulting in sampler refusal. Based on SPT N-values and penetration resistances observed, on average, Stratum IIb soils are considered very dense. The measured SPT N-values from each boring were adjusted using the appropriate ETR value shown in Table 2.5-29 for the drill rig utilized. The adjusted average field-measured N-value for Stratum IIb soils is 48 blows/ft when the adjusted values are "capped" at 100 blows/ft. When the adjusted values are not capped at 100 blows/ft, an average N-value of 56 blows/ft is obtained. For conservatism, a value of 45 blows/ft was adopted for engineering purposes, as shown in Table 2.5-30. Additional SPT information on this layer at locations other than Unit 3, including site-wide, is presented in Table 2.5-28. The measured

N-values versus elevation are presented in Figure 2.5-112. They indicate large variations in SPT N-value over the entire thickness of this stratum, due to varying degrees of cementation. Higher cementation in the top half and relatively lower cementation in the lower half is suggested by the SPT N-values. Laterally, the variation in cementation is rather uniform across both CCNPP Unit 3 powerblock and CLA1 areas.

CPT soundings were attempted in Stratum IIb soils. However, the soils could only be partly penetrated. All CPT soundings experienced refusal when encountering the highly cemented portions of these soils. The CPT soundings could only be advanced after predrilling through the highly cemented zones, and sometimes the predrilling had to be repeated due to the intermittent presence of hard zones at the same sounding. Values of $q_c$ from the soundings ranged from about 40 to over 600 tsf. The average $q_c$ value may range from 200 to 300 tsf. The results corroborate with the SPT N-values where the highest N-values were measured in zones that CPT soundings encountered refusal or could not penetrate these soils, approximately between elevation 20 and elevation 40 ft. The $q_c$ profile is shown in Figure 2.5-113.

Low SPT N-values and $q_c$ values are very infrequent in this stratum, given the influence of cementation. The low values are very likely the result of sampling disturbance, or in one case (at C-406, elevation ~30 ft, $q_c$~10 tsf) the low tip resistance is due to the relatively low overburden pressure at that location. They could also be influenced by ground water, given that the "confined" ground water level is roughly near the top of this stratum (refer to Section 2.5.4.6 for ground water information). The cementation in Stratum IIb soils varies, including zones that are highly cemented and others with little cementation. The degree of cementation was subjectively evaluated during the field exploration by observing the degree of shell fragmentation present and testing the soils with diluted hydrochloric acid, as noted on the boring logs. The cementation is affected by the presence of shells in these soils. The influence of iron oxide may also be a factor, although no specific test was performed on the samples for verification of iron contents. These soils, however, have been studied in the past by others, as follows.

Based on a study of soils near Calvert Cliffs (Rosen, 1986), dolomite or calcite, which is present in the local soils, is identified as the cementing agent. The absence of dolomite or calcite in certain parts may be due to low pH ground water. Abundant iron cement is also reported in some areas near Calvert Cliffs, with significant accumulation of shells that had dissolved. The degree of cementation is affected by the level of dolomitization in the sandy soils, a process that began in the Chesapeake Groups soils once they were covered by the clayey soils above.

The abundant shells in some zones within this stratum renders these zones very porous. In a few borings, loss of drilling fluid was noted, e.g., in borings B-302, B-406, B-414, B-426, B-703, and B-710. These porous zones were encountered either near the upper or the lower part of the stratum. Fluid loss was estimated to be in the range of 300 to 600 gallons at each of the 400-series borings. The loss was judged to be due to the nested accumulation of coarse materials, particularly shell fragments at these locations. The fluid loss in boring B-309, and in the upper portion of boring B-710, was in suspected fill materials.

Index tests and testing for the determination of engineering properties were performed on selected samples from Stratum IIb soils. Sample selection for testing was primarily based on the observed soil uniformity from the field classification, or conversely, the variation in material description based on logging in the field, in order to obtain a quantitative measure of the

uniformity, or the variation, respectively.  The following index tests were performed on Stratum IIb soils, with results as noted.

|  | No. of Tests | Min. Value | Max. Value | Average Value |
| --- | --- | --- | --- | --- |
| Water Content (WC)(%) | 67 | 26 | 88 | 34 |
| Liquid Limit (LL)(%) | 67 | Non-Plastic (NP) | 78 | 46 |
| Plastic Limit (PL)(%) | 67 | NP | 52 | 24 |
| Plasticity Index (PI) | 67 | NP | 43 | 22 |
| Fines Content (%) | 115 | 3 | 71 | 24 |
| Unit Weight (pcf) | 16 | 115 | 124 | 118 |

The test results are summarized in Table 2.5-32.  The water content and Atterberg limits are presented versus elevation in Figure 2.5-114.  They are also shown on the plasticity chart in Figure 2.5-115.  Grain size analyses indicated that Stratum IIb soils are primarily medium-fine sands.  The USCS designations were silty sand, poorly-graded sand to silty sand, clayey sand, silt, silt of high plasticity, clay of high plasticity, clay, and organic clay.  The predominant classifications, however, were silty sand, clayey sand, and poorly-graded sand to silty sand (SM, SC, and SP-SM).  Three samples were classified as organic clay or organic silt, although evidence of high organic content was not present during the field exploration.  The organic designation was based on laboratory (liquid limit) testing.  Follow up organic content testing on one sample indicated an organic content of 3.2 percent.  Despite the presence of organic matter in this sample, Stratum IIb soils are not considered organic soils since organic materials are virtually absent in these soils.  The plastic and fine-grained soil classifications are generally from the clayey/silty interbeds within this stratum.  For engineering analysis purposes, and given the predominance of granular proportions, Stratum IIb soils were characterized, on average, as sands with low plasticity, and with an average fines content of 20 percent.  Based on laboratory test results, an average unit weight of 120 pcf was also adopted for engineering purposes.

The shear strength of Stratum IIb soils was evaluated based upon laboratory testing and correlations with SPT N-values and CPT results.  Initially, the angle of shearing resistance of the soils was estimated from an empirical correlation with SPT N-values (Bowles, 1966).  Using the SPT N-value adjusted for hammer efficiency, a $\phi'$ of about 50 degrees is obtained for N = 45 blows/ft for sands.  A value of $\phi' = 40$ degrees was conservatively considered.  Friction angle values were also obtained from the CPT results, despite limited success penetrating these soils in entirety with the CPT. Estimates of friction angle using the method recommended in EPRI EL-6800 (EPRI, 1990) are presented versus elevation in Figure 2.5-116.  The estimated values range from 28 degrees to 49 degrees, with an average value of 39 degrees.  Three direct shear tests were performed on samples of Stratum IIb soils designated as organic silt and clayey sand by the USCS classification, resulting in average $\phi' = 31$ degrees and $c' = 0.4$ tsf.  The laboratory strength results are given in Table 2.5-33.  Strength parameters from three CIU-bar tests classified as organic clay, poorly-graded sand to silty sand, and silty sand, indicated average (effective) $\phi' = 31$ degrees and $c' = 0.5$ tsf and average (total) $\phi = 16$ degrees and $c = 1.7$ tsf. From the above results, the following is a summary of strength parameters for Stratum IIb soils based on various data and interpretation.

|  | SPT | CPT | Direct Shear | CIU-bar |
| --- | --- | --- | --- | --- |
| $\phi'$ (degrees) | 40 | 39 | 31 | 31 |
| c' (tsf) | 0 | 0 | 0.4 | 0.5 |
| $\phi$ (degrees) | --- | --- | --- | 16 |
| c (tsf) | --- | --- | --- | 1.7 |

The direct shear and CIU-bar results are comparable, as are values interpreted from the SPT and CPT data. Based on the above, $\phi' = 34$ degrees and $c' = 0$ is adopted for Stratum IIb soils.

Consolidation properties and stress history of Stratum IIb soils were evaluated via laboratory testing and evaluation of the CPT data. A summary of the laboratory consolidation test results is presented in Table 2.5-34. The laboratory results are also plotted versus elevation and shown in Figure 2.5-117. Results indicate that, on average, these soils are preconsolidated to 9 tsf, with an OCR of at least 5. OCR data were derived from the CPT results and are shown in Figure 2.5-118. The results are scattered over a large range, from OCR = 0.8 to OCR = 10, with no unique trend. At best, an average OCR may be discerned from the CPT data in Figure 2.5-118, or an approximate OCR of 7. A summary of OCR values from CPT data is shown in Table 2.5-34. An OCR = 3 and a preconsolidation pressure of 8 tsf were conservatively adopted for Stratum IIb soils.

The elastic modulus, E, of Stratum IIb soils was evaluated using the relationship in Davie (Davie, 1988), and Eq. 2.5.4-1. Using the previously established N-value of 45 blows/ft, an elastic modulus of 810 tsf is estimated for these soils. Also, an elastic modulus was estimated based on shear wave velocity for sandy soils (Senapathy, 2001), and Eqs. 2.5.4-2 through 2.5.4-4. Using an average Vs = 1530 ft/sec obtained from the measurements at the site (refer to Section 2.5.4.4 for discussions on this topic), $\gamma = 120$ pcf, and assuming $\mu = 0.3$ for sand, a modulus of elasticity of 1,134 tsf is estimated from Eq. 2.5.4-2. Using an average of the two estimates from SPT and shear wave velocity, an elastic modulus of 972 tsf is estimated. A value of 970 tsf was adopted for Stratum IIb soils. The values are shown in Table 2.5-35.

The static shear modulus, G, was estimated using Eq. 2.5.4-5. Using a Poisson's ratio of 0.3 for sandy soils, a shear modulus of 373 tsf is estimated for these soils. A value of 436 tsf was estimated using Eq. 2.5.4-3. Using an average of the two estimates, a value of 400 tsf was adopted for Stratum IIb soils. The values are shown in Table 2.5-35.

The coefficient of subgrade reaction for 1-ft wide or 1-ft square footings, $k_1$, was obtained from Terzaghi (Terzaghi, 1955). Based on material characterization for Stratum IIb soils, $k_1 = 300$ tcf was estimated and adopted.

Active, passive, and at rest static earth pressure coefficients, $K_a$, $K_p$, and $K_0$, respectively, were estimated assuming frictionless vertical walls and horizontal backfill using Rankine's Theory (Lambe, 1969), Eqs. 2.5.4-6 through 2.5.4-8, and the adopted $\phi' = 34$ degrees for Stratum IIb soils. The estimated earth pressure coefficients are $K_a = 0.28$, $K_p = 3.5$, and $K_0 = 0.44$. Values adopted for engineering purposes are $K_a = 0.3$, $K_p = 3.5$, and $K_0 = 0.5$.

The sliding coefficient, tangent $\delta$, for Stratum IIb soils in contact with concrete was estimated based on data in "Foundations and Earth Structures" (NFEC, 1986). Tangent $\delta = 0.45$ was adopted for Stratum IIb soils.

All of the material properties adopted for engineering purposes for Stratum IIb soils, as well as other useful information, are summarized in Table 2.5-36.

**Stratum IIc – Chesapeake Clay/Silt**

Underlying the cemented soils, another Chesapeake Clay/Silt stratum was encountered, although distinctly different from the one above the cemented soils. This stratum was encountered in all borings that were sufficiently deep to encounter these soils within the CCNPP Unit 3 powerblock and CLA1 areas. Although primarily gray to greenish gray clay/silt soils, they contain interbedded layers of sandy silt, silty sand, and cemented sands with varying

amounts of shell fragments.  The greenish tone is the result of glauconite in these soils. Glauconite is a silicate mineral of greenish color with relatively high iron content (about 20 percent).  Galuconite oxidizes on contact with air, producing a dark color tone.  It is normally found as sand-size, dark green nodules.  It can precipitate directly from marine waters or develop as a result of decaying of organic matter in animal shells or bottom-dwellers.

The thickness of Stratum IIc soils was estimated from the boring logs.  Only two borings, B-301 and B-401, were sufficiently deep to completely penetrate this stratum.  Based on borings B-301 and B-401, the thickness of this stratum is estimated as 190 ft, as shown in Table 2.5-26.

The stratum thickness was based on estimating the termination elevations encountered for the layer at the boring locations.  In Unit 3 area, the termination elevation of Stratum IIc soils was estimated at elevation -208 ft, whereas in CLA1 area it was estimated at elevation -211 ft, or an average elevation -209 ft, as shown in Table 2.5-27.  An elevation of -200 ft was adopted for simplicity.

Soil samples were obtained from the borings via SPT and tube samples.  SPT N-values were measured during the sampling and recorded on the boring logs.  In the CCNPP Unit 3 area, the SPT N-values ranged from 12 to greater than 100 blows/ft, with an average N-value of 23 blows/ft. In the adjacent CLA1 area, the SPT N-values ranged from 10 to 39 blows/ft, with an average N-value of 20 blows/ft.  The combined average SPT N-value is 21 blows/ft. Based on SPT N-values, Stratum IIc soils are considered very stiff on average.  Additional SPT information on this layer is presented in Table 2.5-28.  The measured N-values versus elevation are presented in Figure 2.5-112.  They indicate a relatively uniform trend in SPT N-value with depth in the upper half and an increasing trend in the lower half of the profile.  It also indicates lateral uniformity in SPT N-values across the CCNPP Unit 3 and CLA1 areas to be within a narrow range, as also evident from the average values in the two areas.  Evidences of intermittent cementation, or otherwise hardened zones, are also indicated by increasing SPT N-values at intermittent elevations, e.g., near elevation -40, elevation -110, and elevation -170 ft.

The SPT N-values were adjusted for hammer energy; the adjusted average field-measured N-value for Stratum IIc soils is 29 blows/ft.  A value of 25 blows/ft was conservatively adopted for engineering purposes, as shown in Table 2.5-30.

CPT soundings were attempted in Stratum IIc soils, following several attempts to penetrate these soils due to persistent refusal in overlying soils.  A profile of $q_c$ versus elevation is shown in Figure 2.5-113.  The results suggest relative uniformity in $q_c$ values with depth and lateral extent, as well as evidence of cemented (or hardened zones) near elevation -40 ft which was similarly reflected in the SPT N-value profile in Figure 2.5-112.  The $q_c$ values range from about 50 to 100 tsf, with an average of about 75 tsf.

Index tests and testing for determination of engineering properties were performed on selected samples from Stratum IIc soils.  Sample selection for testing was primarily based on the observed soil uniformity from the field classification, or conversely, the variation in material description based on logging in the field, in order to obtain a quantitative measure of the uniformity, or the variation, respectively.  The following index tests were performed on Stratum IIc soils, with results as noted.

|  | No. of Tests | Min. Value | Max. Value | Average Value |
|---|---|---|---|---|
| Water Content (WC) (%) | 88 | 26 | 123 | 54 |
| Liquid Limit (LL) (%) | 88 | 39 | 218 | 94 |
| Plastic Limit (PL) (%) | 88 | 30 | 100 | 50 |

|                          | No. of Tests | Min. Value | Max. Value | Average Value |
|--------------------------|--------------|------------|------------|---------------|
| Plasticity Index (PI)    | 88           | 9          | 118        | 44            |
| Fines Content (%)        | 82           | 18         | 100        | 54            |
| Unit Weight (pcf)        | 19           | 86         | 117        | 107           |

The test results are summarized in Table 2.5-32.  The water content and Atterberg limits are presented versus elevation in Figure 2.5-114.  They are also shown on the plasticity chart in Figure 2.5-115.  For engineering analysis purposes, Stratum IIc soils were characterized, on average, as high plasticity clay and silt, with an average PI = 45.  Their predominant USCS designation was clay of high plasticity and silt of high plasticity (CH and MH), however, sometimes with silty sand, clay, and organic clay classifications indicated.  Based on field observations during sampling, the organic designation based on laboratory (Liquid Limit) testing is not representative of these soils, and therefore, they are not considered organic soils. The organic designation (based on Liquid Limit tests) may be impacted by the glauconite content in the soils.  Based on laboratory testing, an average unit weight of 110 pcf was also adopted for Stratum IIc soils for engineering purposes.

The shear strength of Stratum IIc soils was evaluated based on laboratory testing, and using correlations with SPT N-values and the CPT results.  The results are summarized in Table 2.5-37.

The undrained shear strength, $s_u$, was estimated from Eq. 2.5.4-9 based on SPT N-values. Substituting the previously established N-value for Stratum IIc soils (SPT N-value = 25), $s_u$ = 1.6 tsf is estimated for these soils. Undrained shear strength was also estimated using the CPT data, following a CPT-$s_u$ correlation from Robertson (Robertson, 1988), using a cone factor $N_{kt}$ = 15. The shear strength values obtained from the CPT data are shown versus elevation in Figure 2.5-120, indicating an average $s_u$ = 4.7 tsf as summarized in Table 2.5-37.  A number of laboratory unconsolidated undrained (UU) triaxial and unconfined compression (UC) tests were performed on selected undisturbed samples. Laboratory test results on 10 samples resulted in an average $s_u$ = 2.2 tsf.  The laboratory shear strength test results are shown versus elevation in Figure 2.5-119.  Based on these results, an average undrained shear strength of 2.0 tsf was conservatively adopted for Stratum IIc soils.

The angle of shearing resistance of these soils was evaluated from laboratory test results.  The results are shown in Table 2.5-33.  Four direct shear tests were performed on samples of Stratum IIc soils, designated as clay, clay of high plasticity, and clayey sand by the USCS soil classification system, resulting in an average $\phi'$ = 25 degrees and $c'$ = 1.6 tsf.  Strength parameters from one CIU-bar test, indicated effective stress $\phi'$ = 29.1 degrees, $c'$ = 1.0 tsf, and total stress $\phi$ = 15.4 degrees, and c = 1.5 tsf. From the above, the following is a summary of average $\phi'$ values for the Stratum IIc soils based on various data and interpretation.

|                  | Direct Shear | CIU-bar |
|------------------|--------------|---------|
| $\phi'$ (degrees) | 25           | 29.1    |
| $c'$ (tsf)        | 1.6          | 1.0     |
| $\phi$ (degrees)  | ---          | 15.4    |
| c (tsf)           | ---          | 1.5     |

Based on the above, $\phi'$ = 27 degrees and $c'$ = 1.0 tsf is adopted for Stratum IIc soils.

Consolidation properties and stress history of Stratum IIc soils were evaluated via laboratory testing and evaluation of the CPT data.  A summary of the laboratory consolidation test results is presented in Table 2.5-34.  The laboratory results are also plotted versus elevation and shown in Figure 2.5-117.  Results indicate that, on average, these soils are preconsolidated to about 15 tsf, with an OCR of at least 3.  OCR data derived from CPT results are shown in Figure 2.5-118.

The CPT-derived results are scattered over a large range, from about OCR = 1.2 to OCR = 10, with no unique trend, although most values are in the range of about 5 to 10. An average OCR from the CPT data would be approximately 9. A summary of OCR values from CPT data is shown in Table 2.5-34. An OCR = 3 and preconsolidation pressure of 14 tsf were conservatively adopted for Stratum IIc soils. It is noted that this preconsolidation pressure is equivalent to about 200 to 300 ft of preloading by sediments that once covered these soils during prehistoric times. This is consistent with a study on the depositional history of Miocene-age soils in Maryland (Rosen, 1986) that estimated the burial depth of these soils in Western Maryland, e.g., Calvert County, at "much less" than 590 ft, which would be equivalent to about 200 to 300 ft assuming one-third to one-half of the referenced burial depth.

Static modulus of elasticity for Stratum IIc was evaluated using Eq. 2.5.4-12. For the adopted $s_u$ = 2 tsf, an elastic modulus of 900 tsf is estimated. Also, elastic modulus was estimated based on shear wave velocity from Eqs. 2.5.4-13 and 2.5.4-14. Using an average Vs = 1,250 ft/sec obtained from the measurements at the site (refer to Section 2.5.4.4 for discussions on this topic), unit weight of 110 pcf, and assuming Poisson's ratio 0.45 for clayey soils, a modulus of elasticity of 2,477 tsf is estimated from Eq. 2.5.4-13. Using $s_u$ = 2.0 tsf, an elastic modulus of 1,160 tsf is estimated from Eq. 2.5.4-14. Of the preceding estimates, the value based on PI appears high. Therefore, the PI-based value is conservatively omitted when estimating an average elastic modulus for Stratum IIc soils. Using an average of the estimated values from undrained strength and shear wave velocity, an elastic modulus of 1,030 tsf is estimated and adopted for Stratum IIc soils, as shown in Table 2.5-35.

The static shear modulus, G, was estimated using Eq. 2.5.4-5. Using $\mu$ = 0.45 for clay soils, a shear modulus of 355 tsf is estimated for these soils. Values of 853 and 400 tsf were estimated using Eqs. 2.5.4-13 and 2.5.4.-14. The higher value was ignored for conservatism. An average of the two other values, 370 tsf, was conservatively adopted for Stratum IIc soils, as shown in Table 2.5-35.

The coefficient of subgrade reaction for 1-ft wide or 1-ft square footings, $k_1$, was obtained from Terzaghi (Terzaghi, 1955). Based on material characterization for Stratum IIc soils, $k_1$ = 150 tcf was estimated and adopted.

Active, passive, and at rest static earth pressure coefficients, $K_a$, $K_p$, and $K_0$, respectively, were estimated assuming frictionless vertical walls and horizontal backfill using Rankine's Theory, Eqs. 2.5.4-6 through 2.5.4-8, and the adopted $\phi'$ = 27 degrees for Stratum IIc soils, the following earth pressures coefficients are estimated; $K_a$ = 0.4, $K_p$ = 2.6, and $K_0$ = 0.55. Given the overconsolidated nature of the soils, the $K_0$ value was increased. The adopted values for engineering purposes are $K_a$ = 0.4, K = 2.6, and $K_0$ = 0.7.

The sliding coefficient, tangent $\delta$, of 0.40 was adopted for Stratum IIc soils in contact with concrete (NFEC, 1986).

All of the material properties adopted for engineering purposes for Stratum IIc soils, as well as other useful information, are summarized in Table 2.5-36.

### 2.5.4.2.1.3    Stratum III – Nanjemoy Sand

Underlying the Chesapeake Clay/Silt stratum are the Nanjemoy soils (Stratum III). Stratum III was encountered in deep borings B-301 and B-401. This stratum consists primarily of dark, greenish-gray glauconitic sand, however, it contains interbedded layers of silt, clay, and cemented sands with varying amounts of shell fragments and varying degrees of cementation. The glauconite in these soils could vary from less than 10 percent to as much as 50 percent.

The thickness of Stratum III soils cannot be estimated from the information obtained from the CCNPP Unit 3 subsurface investigation (boring logs B-301 and B-401), as these borings did not penetrate these soils in their entirety, although they penetrated them by about 100 ft. The Nanjemoy soils are about 200 ft thick at the site (Hansen, 1996), consisting of primarily sandy soils in the upper 100 ft and clayey soils in the lower 100 ft. On this basis, the termination (bottom) of the upper sandy portion can be estimated at about elevation -315 ft and the termination of the lower clayey portion can be estimated at about elevation -415 ft. Information from borings B-301 and B-401 sufficiently characterizes the upper half of this geologic unit, as these borings were terminated at elevation -308 ft and elevation -329 ft, respectively.

Soil samples were collected from the borings via SPT sampling. Only one tube sample was collected in these soils, however, despite several attempts, given the depth and penetration difficulties involved. SPT N-values were measured during the sampling and recorded on the boring logs. In the CCNPP Unit 3 area, the SPT N-values ranged from 34 blows/ft to greater than 100 blows/ft, with an average N-value of 64 blows/ft. In the adjacent CLA1 area, the SPT N-values ranged from 28 blows/ft to greater than 100 blows/ft, with an average N-value of 56 blows/ft. The combined average SPT N-value is 61 blows/ft. Based on SPT N-values, Stratum III soils are considered very dense on average. The SPT information is presented in Table 2.5-28 The measured N-values versus elevation are presented in Figure 2.5-112. They indicate a generally increasing trend in SPT N-value with depth, although SPT N-values begin to decline near the bottom of the explored depth, a possible indication of nearing the underlying clay soils. Limited SPT values are available from this stratum to judge its lateral uniformity, however, most available data appear to fall in a relatively narrow range, except for intermittent "peak" values. The peak SPT N-values are likely due to the presence of cemented or otherwise hardened zones. CPT sounding could not reach these soils due to refusal in overlying soils.

The SPT N-values were adjusted for hammer energy; the adjusted average field-measured N-value for Stratum III soils is 72 blows/ft. A value of 70 blows/ft was conservatively adopted for engineering purposes, as shown in Table 2.5-30.

Index tests were performed on several samples from Stratum III soils. Sample selection for testing was primarily based on the observed soil uniformity from the field classification, or conversely, the variation in material description based on logging in the field, in order to obtain a quantitative measure of the uniformity, or the variation, respectively. Due to the limited quantity of available samples, the testing was limited. The following index tests were performed on selected samples of Stratum III soils, with the results as noted.

|                        | No. of Tests | Min. Value | Max. Value | Average Value |
|------------------------|--------------|------------|------------|---------------|
| Water Content (WC) (%) | 7            | 23         | 37         | 30            |
| Liquid Limit (LL)(%)   | 7            | 47         | 76         | 59            |
| Plastic Limit (PL)(%)  | 7            | 32         | 40         | 32            |
| Plasticity Index (PI)  | 7            | 15         | 36         | 27            |
| Fines Content (%)      | 10           | 12         | 29         | 19            |

The test results are summarized in Table 2.5-32. The water content and Atterberg limits are presented versus elevation in Figure 2.5-114. They are also shown on the plasticity chart in Figure 2.5-115. For engineering analysis purposes, Stratum III soils were characterized, on average, as sand of high plasticity, with an average PI = 30. Their predominant USCS designations were clayey sand and silty sand (SC and SM), although clay of high plasticity and silt of high plasticity were also indicated. Testing for unit weight was not performed since only

disturbed SPT samples could be obtained from this stratum; however, based on correlation with SPT N-values (Bowles, 1966), an average unit weight of 120 pcf was adopted for these soils.

The shear strength of Stratum III soils was evaluated using correlations with SPT N-values, assuming predominately granular behavior.  For an average SPT N-value = 70 blows/ft, an average $\phi'$ = 50 degrees is estimated (Bowles, 1966).  A $\phi'$ = 40 degrees was conservatively adopted.

Given the relatively high plasticity in these soils (LL = 60 and PI = 30 on average), their behavior could also be characterized using undrained parameters.  Although no laboratory strength tests were performed on these soils, their undrained shear strength, $s_u$, may be estimated from Eq. 2.5.4-9. For an average N-value = 70 blows/ft, $s_u$ = 4.4 tsf is estimated for these soils.  An undrained shear strength of 4.0 tsf may conservatively be assigned to Stratum III soils as summarized in Table 2.5-37.

Given the high SPT N-value, and associated strength, Stratum III soils are considered highly preconsolidated.  Although no consolidation or CPT tests were performed in these soils, their preconsolidation pressure is judged to be at least as high as the overlying soils (a preconsolidation pressure of 14 tsf was assigned to the overlying Stratum IIc soils).  The high degree of preconsolidation is evident by the indices that were measured, e.g., a profile of the water content versus elevation in Figure 2.5-114 clearly demonstrates the water contents to be consistently near the Plastic Limit, a strong indication of high preconsolidation in these soils.

Static modulus of elasticity for Stratum III soils was evaluated using Eq. 2.5.4-1.  For the adopted SPT N-value = 70 blows/ft, an elastic modulus of 1,260 tsf is estimated.  Similarly, Eqs. 2.5.4-12 through 2.5.4-14 were utilized, along with corresponding parameters previously noted, and elastic modulus values of 1,800, 1,879, and 2,080 tsf were estimated, as noted in Table 2.5-35.  A value of 1,750 tsf is estimated and adopted for Stratum III soils.

The static shear modulus, G, was estimated using Eq. 2.5.4-5.  Using $\mu$ = 0.3 for sandy soils, a shear modulus of 700 tsf is estimated and adopted for these soils, as shown in Table 2.5-35.

Foundations are not anticipated in Stratum III soils, therefore, estimating their coefficient of subgrade reaction, earth pressure, and sliding coefficient is unnecessary.

All of the material properties adopted for engineering purposes for Stratum III, as wells as other information, are summarized in Table 2.5-36.

### 2.5.4.2.1.4　　　Chemical Properties of Soils

Chemical laboratory tests were performed on selected soil and ground water samples. The ground water test results, and soil portions tested as part of the ground water characterization, are addressed in Section 2.4.13.  A brief summary of available information is evaluated and provided below.

### Chemical Testing for CCNPP Units 1 and 2

Chemical test results on soils are available in a report that was prepared as part of the design of an additional Diesel Generator Building (Bechtel, 1992) at the project site.  Three samples from each investigated stratum were tested, for pH, sulfate, and chloride.  A summary of the results is presented in Table 2.5-38.

**Chemical Testing on CCNPP Unit 3 Samples**

Field electrical resistivity tests were performed along four arrays, at locations shown in Figure 2.5-103 and Figure 2.5-104. The results are presented in Appendix 2.5-A, and summarized in Table 2.5-39. The results are approximately correlated with depth based on the array spacing, as shown in Table 2.5-39.

**Field Electrical Resistivity Testing for COL Investigation**

Field electrical resistivity tests were performed along four arrays, at locations shown in Figure 2.5-103 and Figure 2.5-104. The results are presented in Appendix 2.5-A, and summarized in Table 2.5-39. The results are approximately correlated with depth based on the array spacing, as shown in Table 2.5-39.

**Evaluation of Chemical Data**

Guidelines for interpretation of chemical test results are provided in Table 2.5-40, based on the following consensus standards, API Recommended Practice 651 (API, 2007), Reinforced Soil Structures (FHWA, 1990), Standard Specification for Portland Cement (ASTM C150), Manual of Concrete Practice (ACI, 1994), and Standard Specification for Blended Hydraulic Cement (ASTM, C595). From the average values of available results shown in Table 2.5-38 and Table 2.5-39, and guidelines in Table 2.5-40, the following conclusions were developed.

Attack on Steel (Corrosiveness): The resistivity test results indicate that all soils are "little corrosive," except for Stratum IIc Chesapeake Clay/Silt that may be "little to mildly corrosive." Based on the chloride contents being typically below 10 ppm, all soils are essentially non-corrosive. The pH results, however, indicate that all soils are "corrosive to very corrosive," except for Stratum IIc Chesapeake Clay/Silt that may be "mildly corrosive." It is noted that few chemical test results are available from Stratum IIc; however, that should be of no special importance because no Category I structure (or piping) is anticipated within these soils. The pH data dominate the corrosive characterization of the soils. Nevertheless, all natural soils at the site will be considered corrosive to metals, requiring protection if placed within these soils. Protection of steel against corrosion may include cathodic protection, or other measures, which will be determined during the detailed design phase of the project. It should be noted that additional pH testing on ground water samples obtained from the observation wells (refer to Section 2.4.13) indicate pH values of average 5.5, 6.8, and 7.1 for wells screened in Stratum I, Stratum IIa, and Stratum IIb soils, respectively. Except for values obtained in ground water associated with Stratum I soils indicating "corrosive" conditions, remaining pH data from other strata only indicate "mildly corrosive" conditions.

Attack on Concrete (Aggressiveness): The sulfate test results in all tested soils indicate a "severe" potential for attack on concrete, except for Stratum IIc Chesapeake Clay/Silt that may cause a "moderate" attack. As noted above, few chemical test results are available for Stratum IIc; however, that should be of no special importance because no Category I structure (or piping) is anticipated within these soils. Nevertheless, all natural soils at the site will be considered aggressive to concrete, requiring protection if placed within these soils. Protection of concrete is discussed in Sections 3.8.4 and 3.8.5.

**2.5.4.2.1.5     Subsurface Materials Below 400 Feet**

As indicated earlier, the field exploration for the CCNPP Unit 3 extended to a maximum depth of about 400 ft below ground. Coastal Plain sediments, however, are known to extend below this depth, to a depth of approximately 2,500 ft, or to top of bedrock (BGE, 1982). The subsurface conditions below 400 ft were addressed through reference to existing literature and

work that had been done by others, primarily for the purpose of seismic site characterization. The subsurface conditions below 400 ft are addressed in Sections 2.5.4.7 and 2.5.2.5.

### 2.5.4.2.1.6      Field Investigation Program

The planning of the field investigation referred to the guidance provided in NRC Regulatory Guide 1.132, "Site Investigations for Foundations of Nuclear Power Plants" (NRC, 2003). References to the industry standards used for field tests completed for the CCNPP Unit 3 subsurface investigation are shown in Table 2.5-25. The details and results of the field investigation are provided in Geotechnical Subsurface Investigation Data Report (Schnabel, 2007a) and included as Appendix 2.5-A.  The work was performed under the Bechtel QA program with work procedures developed specifically for the CCNPP Unit 3 subsurface investigation, including a subsurface investigation plan developed by Bechtel  The locations of borings in Figure 2.5-103 and Figure 2.5-104, although in agreement with the guidance in Regulatory Guide 1.132 (NRC, 2003a) at the time of developing the subsurface investigation plan, do not agree with the guidance of Regulatory Guide 1.132 (NRC, 2003a), for the current CCNPP Unit 3 layout since the layout has evolved over time and the locations of some of the structures have shifted.  This has resulted in borings or CPT soundings being outside the outline of some structures.  Although differing soil conditions are not expected, due to the observed lateral stratigraphic uniformity at the site, a complementary investigation will be performed as part of the detailed design of the project, with reference to guidance in Regulatory Guide 1.132 (NRC, 2003a) to verify subsurface uniformity at these locations.  If this additional investigation yields nonconservative results that impact the conclusions of this section, an update to the COL application will be made.

### 2.5.4.2.1.7      Laboratory Testing Program

The laboratory investigations of soils and rock was performed with in accordance with the guidance outlined in Regulatory Guide 1.138, Laboratory Investigations of Soils for Engineering Analysis and Design of Nuclear Power Plants (NRC, 2003b).  Deviations are identified, alternatives and/or basis for deviation are provided.

A summary, as well as detailed results, of all laboratory tests performed as part of the subsurface investigation is provided in Geotechnical Subsurface Investigation Data Report (Schnabel, 2007a)(Schnabel, 2007b), included as Appendix 2.5-A and Appendix 2.5-B.

The laboratory work was performed under the Bechtel QA program with work procedures developed specifically for the CCNPP Unit 3 subsurface investigation.

Soil samples were shipped under chain-of-custody protection from the on-site storage to the testing laboratories.  ASTM D4220 (ASTM, 2000a) provides guidance on standard practices for preserving and transporting soil samples.  This guidance was referenced in preparing technical specifications for the CCNPP Unit 3 subsurface investigation, addressing sample preservation and transportation, as well as other subsurface investigation and geotechnical requirements.

Laboratory testing consisted of testing soils and ground water samples obtained from the investigation program.  Testing of ground water samples is addressed is Section 2.4.13. Laboratory testing of soil samples consisted of index and engineering property tests on selected SPT, undisturbed, and bulk samples.  The SPT and undisturbed samples were recovered from the borings and the bulk samples were obtained from the test pits.  Soil laboratory tests included the following: water content, grain size (sieve and hydrometer), Atterberg limits, organic content, chemical analysis (pH, chloride, and sulfate), unit weight, specific gravity, moisture-density, consolidation, unconfined compression (UC),

unconsolidated-undrained triaxial compression (UU), consolidated-undrained triaxial compression (CIU-bar), direct shear (DS), and resonant column torsional shear (RCTS) testing.

Regulatory Guide 1.138 (NRC, 2003b) provides guidance for laboratory testing procedures for certain specific tests, including related references. Some of these references are not in common practice in the U.S. or are out-of-date. Laboratory testing of samples for the CCNPP Unit 3 subsurface investigation used commonly accepted, and updated practices such as more recent ASTM and EPA standards which are equivalent to the testing procedures referenced in the Regulatory Guide. Laboratory testing of samples for the CCNPP Unit 3 subsurface investigation did not rely upon non-U.S. or out-of-date versions of practices or standards provided in the Regulatory Guide. References to the industry standards used for this laboratory investigation, standards delineated in Regulatory Guide 1.138 (NRC, 2003b), and quantity of test are shown in Table 2.5-31.

All laboratories have completed their testing, with the results contained in Geotechnical Subsurface Investigation Data Report and associated Addendum No. 3 (Schnabel, 2007a) (Schnabel, 2007b), included as Appendix 2.5-A and Appendix 2.5-B.

The soil and rock laboratory tests listed in Regulatory Guide 1.138 (NRC, 2003b) are common tests performed in most well-equipped soil and rock testing laboratories, and they are covered by ASTM standards. Additional test that are not covered in regulatory guidance were also performed for the CCNPP Unit 3 subsurface investigation (e.g., CBR tests to assess suitability of subgrade or fill materials for pavement, and RCTS tests, which were used in lieu of the resonant column test alone to obtain shear modulus and damping ratio values for a wide range of strains). Appendix 2.5-B describes the test procedures used to perform RCTS testing. Results of Cation Exchange Capacity tests are addressed with the ground water chemistry data in Section 2.4.13.

### 2.5.4.2.1.8      Investigations

**Previous Subsurface Investigations**

Based on limited information available from the CCNPP Units 1 and 2 UFSAR (BGE, 1982), the original subsurface investigations for the CCNPP Units 1 and 2 performed in 1967 consisted of a total of 10 exploratory borings, ranging in depth from 146 to 332 ft, with soil samples obtained at various intervals for soil identification and testing. Seven piezometers were also installed for ground water observation and monitoring. The 1967 investigation included other field investigations (two seismic survey lines using Microtremor) and laboratory testing (moisture content, density, particle size, permeability, cation exchange, and x-ray diffraction). Supplemental investigations in support of detailed design were performed in July 1967 (5 borings), August 1967 (23 borings), December 1968 (18 borings), and 1969 (5 borings). Additional investigations were performed in 1980/1981 (borings, CPT soundings, and observation wells) in order to site a "generic Category I structure," and in 1992 additional investigations (borings, dilatometer soundings, crosshole seismic survey, field resistivity) were performed for an additional Diesel Generator Building. Various laboratory testing was also performed on selected portions of the recovered soils.

Geological descriptions in CCNPP Units 1 and 2 UFSAR (BGE, 1982) indicate the surficial deposits to be Pleistocene Age soils extending from the ground surface to about elevation 70 ft. These soils were estimated to extend to an average elevation 60 ft based on the CCNPP subsurface investigation. CCNPP Units 1 and 2 UFSAR (BGE, 1982) indicates that Chesapeake Group soils were encountered in the 1967 investigation between elevation 70 ft and elevation -200 ft. These soils were estimated to extend to approximately elevation -200 ft based on the

COL investigation.  CCNPP Units 1 and 2 UFSAR (BGE, 1982) indicates that Eocene deposits lie below elevation -200 ft and consist of glauconitic sands.  Comparable observations were made on these, and the overlying deposits, from the CCNPP subsurface investigation borings.  CCNPP Units 1 and 2 UFSAR (BGE, 1982) remarked that "good correlation of subsurface stratigraphy was obtained between the borings."  This remark is corroborated by the results obtained from the CCNPP subsurface investigation.

It is noted that the CCNPP Unit subsurface investigation involved a significantly larger quantity of testing than performed for the original CCNPP Units 1 and 2.  Given the reasonably parallel geologic conditions between CCNPP Units 1 and 2 and the CCNPP Unit 3 site, and the greater intensity in exploration and testing at the CCNPP Unit 3 site which should result in enhanced characterization of the subsurface conditions, findings from previous investigations are not discussed further, unless a differing condition is reported from the previous investigations.

### CCNPP Unit 3 Subsurface Investigation

The subsurface investigation program was performed with in accordance with the guidance outlined in Regulatory Guide 1.132 (NRC, 2003a).  Deviations are identified at point of use, alternatives and/or basis for deviation are provided.  The fieldwork was performed under the contractors QA program and work procedures developed specifically for the CCNPP Unit 3 subsurface investigation.

Regulatory Guide 1.132 (NRC, 2003a) provides guidance on spacing and depth of borings, sampling procedures, in-situ testing, geophysical investigations, etc.  This guidance was used in preparing a technical specification, addressing the basis for the CCNPP Unit 3 subsurface investigation.  The quantity of borings and CPTs for Category I structures was based on a minimum of one boring per structure and the one boring per 10,000-square ft criterion.  The maximum depths of the borings for Category I structures were based on a foundation to overburden stress ratio criterion of 10 percent.  The sampling intervals typically exceeded the guidance document by shortening the sample spacing in the upper 15 ft and maintaining 5-ft sampling intervals at depths greater than 50 ft, except for the case of 400-ft borings.  Continuous sampling was also performed, and will be described later.

Regulatory Guide 1.132 (NRC, 2003a) provides guidance in selecting the boring depth, $d_{max}$, based on a foundation to overburden stress ratio of 10 percent.  Using this criterion, a boring depth of approximately 350 ft was determined for the most heavily loaded structures supported on the Common Basemat.  Regulatory Guide 1.132 (NRC, 2003a), also indicates that at least one-fourth of the principal borings should penetrate to a depth equal to $d_{max}$.  Given the previously available knowledge of subsurface conditions as documented in the CCNPP Units 1 and 2 UFSAR (BGE, 1982) indicating stable, geologically old deposits at the site which would not adversely impact foundation stability, it was determined that one boring should be extended to about 400 ft, 4 borings extended to about 200 ft, and 4 borings extended to about 150 ft for the Common Basemat.  (The consistency across the site of the Miocene-age Chesapeake Group clays and silts that exist below about 100 ft depth and the underlying Nanjemoy Formation sands that start at around 300 ft depth is aptly demonstrated by the similarity of the shear wave velocity profiles obtained in boreholes almost 1,000 ft apart (Figure 2.5-124)).  Also included were 3 CPT soundings.  Borings associated with the Common Basemat extended at least 33 ft below the foundation level.  Additional boring are to be taken to meet the Regulatory Guide 1.132 guidance during detailed design.

As noted in section 2.5.4.2.1.6, the current quantity and locations of tests, shown in Figure 2.5-103 and Figure 2.5-104, do not necessarily coincide with the footprint of structures, for the current CCNPP Unit 3 layout has evolved since the investigation, as well as the need

during the field work to relocate the tests to locations that avoided wetlands, reduced cutting trees, and were accessible to the drilling equipment.  Although a differing subsurface condition is not anticipated due to the observed soil uniformity at the site, a complementary investigation will be performed during the detailed design stage to verify subsurface uniformity at these locations.

A team consisting of a geologist, a geotechnical engineer, and a member of the project management performed a site reconnaissance prior to start of the field investigation.  The focus of this task was to observe the site and access conditions, locations of borings and wells, and identify potential test relocation areas.  Information on site geology and geotechnical conditions, used as a basis for developing the soils investigation plan for the CCNPP subsurface investigation was obtained from the information contained in the CCNPP Units 1 and 2 UFSAR (BGE, 1982).

Regulatory Guide 1.132, (NRC, 2003a) provides that boreholes with depths greater than about 100 ft (30.5 m) should be surveyed for deviation.  In lieu of surveying for deviation in boreholes greater than 100 ft (30.5 m), deviation surveys, were used in the 10 suspension P-S velocity logging boreholes to depths ranging from about 200 to 400 ft.  The results indicated minimum, maximum, and average deviation of 0.6, 1.6, and 1.0 percent, respectively.  The information collected the necessary data for proper characterization of the CCNPP Unit 3 subsurface materials.

Regulatory Guide 1.132, (NRC, 2003a) provides guidance for color photographs of all cores to be taken soon after removal from the borehole to document the condition of the soils at the time of drilling.  For soil samples, undisturbed samples are sealed in steel tubes, and cannot be photographed.  SPT samples are disturbed, and by definition they do not resemble the condition of the material in-situ.  Sample photography is a practice typically limited to rock core samples, not soils, therefore, it was not used.  X-ray imaging, however, was performed on tube samples selected for RCTS testing.

The CCNPP Unit 3 subsurface field exploration was performed from April through August 2006.  This work consisted of an extensive investigation to define the subsurface conditions at the project area.  The exploration locations are shown in Figure 2.5-103 through Figure 2.5-105.  The scope of work and investigation methods were determined to be as follows:

♦ Surveying to establish the horizontal and vertical locations of exploration points.

♦ Evaluating the potential presence of underground utilities at exploration points.

♦ Drilling 145 test borings with SPT sampling and collecting in excess of 200 undisturbed samples (using Shelby push tubes, Osterberg sampler, and Pitcher sampler) to a maximum depth of 403 ft, including 4 borings with continuous SPT samples (B-305, B-409, B-324, and B-417), with the first two borings being 150 ft deep each and the last two borings being 100 ft deep each.  Note that "continuous sampling" was defined as one SPT sample for every 2.5-ft interval with one ft distance between each SPT sample.

♦ Installing and developing 40 ground water observation wells to a maximum depth of 122 ft, including Slug testing in each well.

♦ Excavating 20 test pits to a maximum depth of 10 ft and collecting bulk soil samples.

♦ Performing 63 CPT soundings, including off-set soundings that required pre-drilling to overcome CPT refusal, to a maximum depth of 142 ft, as well as seismic CPT and pore pressure dissipation measurements.

♦ Conducting 2-dimensional field electrical resistivity testing along four arrays.

♦ Performing borehole geophysical logging, consisting of suspension P-S velocity logging, natural gamma, long- and short-term resistivity, spontaneous potential, 3-arm caliper, and directional survey in 10 boreholes.

♦ Conducting SPT hammer-rod combination energy measurements on 5 drilling rigs.

♦ Performing laboratory testing of soils, consisting of natural water content, unit weight, specific gravity, sieve and hydrometer analysis, Atterberg limits, organic content, moisture-density, CBR, unconfined compression, consolidated and unconsolidated undrained triaxial compression, direct shear, consolidation, chemical analysis (pH, sulfate, and chloride), and RCTS testing.  RCTS testing is further discussed in Section 2.5.4.7.3.

♦ Performing laboratory testing on ground water samples obtained from the observation wells, consisting of pH, conductivity, dissolved oxygen, alkalinity, ammonia nitrogen, bromide, chloride, dissolved solids, fluoride, nitrate as N, nitrite as N, sulfate, and sulfide, including cation exchange testing on soils in the well screen area.  These results are discussed in Section 2.4.13.

The location of each exploration point was investigated for the presence of underground utilities prior to commencing exploration at that location.  Locations of several exploration points had to be adjusted due to proximity to utilities, inaccessibility due to terrain conditions, or proximity to wetlands.  Access had to be created to most exploration locations, via clearing roads and creating temporary roads, due to heavy brush and forestation.  These areas were restored subsequent to completion of the field investigation.

An on-site storage facility for soil samples was established before the exploration program commenced.  Each sample was logged into an inventory system.  Samples removed from the facility were noted in the inventory logbook.  A chain-of-custody form was also completed for all samples removed from the facility.  Material storage handling was in accordance with ASTM D4220 (ASTM, 2000a).

Complete results of the investigation are in Appendix 2.5-A and Appendix 2.5-B.  Laboratory test results are discussed and summarized in Section 2.5.4.2 and Appendix 2.5-C.  Geophysical test results are discussed and summarized in Section 2.5.4.4.  Further details pertaining to field activities related to borings, CPTs, Slug tests, geophysical surveys, and other activities are summarized below.

**Test Boring and Sampling**

Soils were sampled using the SPT sampler in accordance with ASTM D1586 (ASTM, 1999).  The soils were sampled at continuous intervals (one sample every 2.5-ft) to 15 ft depth. Subsequent SPT sampling was performed at regular 5 ft intervals. At boring B-401, with a total depth of 401.5 ft, SPT sampling was performed at about 10 ft intervals below a depth of 300 ft. The recovered soil samples were visually described and classified by the engineer or geologist in accordance with ASTM D2488 (ASTM, 2006d)).  A representative portion of the soil sample was placed in a glass jar with a moisture-preserving lid.  The sample jars were labeled, placed in

boxes, and transported to the on-site storage facility. Table 2.5-41 provides a summary of all test borings performed.  The boring locations are shown in Figure 2.5-103 and Figure 2.5-104. The boring logs are included in Appendix 2.5-A.  At boring completion, the boreholes were tremie-grouted using cement-bentonite grout.

Undisturbed samples were obtained in accordance with ASTM D1587 (ASTM, 2000c) using the push Shelby tubes, Osterberg sampler, and rotary Pitcher sampler.  Upon sample retrieval, the disturbed portions at both ends of the tube were removed, both ends were trimmed square to establish an effective seal, and pocket penetrometer (PP) tests were performed on the trimmed lower end of the samples.  Both ends of the sample were then sealed with hot wax, covered with plastic caps, and sealed once again using electrician tape and wax.  The tubes were labeled and transported to the on-site storage area. Table 2.5-42 provides a summary of undisturbed sampling performed during the subsurface investigation.  Undisturbed samples are also identified on the boring logs included in Appendix 2.5-A.

Energy measurements were made on the hammer-rod system on each of the five drilling rigs used in the subsurface investigation.  A Pile Driving Analyzer (PDA) was used to acquire and process the data.  A summary of measured energies is provided in Table 2.5-29.  Energy measurements were made at sampling intervals of 15 ft, with the total number of measurements made per boring ranging from 6 (at boring B-744) to 26 (at boring B-401), depending on boring depth.  Energy transfer to the gage locations was estimated using the Case Method, in accordance with ASTM D4633 (ASTM, 2005a).  The resultant energy transfer efficiency measurements ranged from 78 to 87 percent, with an average energy transfer efficiency of 83 percent.  Detailed results are presented in Appendix 2.5-A.

**Cone Penetration Testing**

CPT soundings were performed using an electronic seismic piezocone compression model, with a 15 cm$^2$ tip area and a 225 cm$^2$ friction sleeve area. CPT soundings were performed in accordance with ASTM D5778 (ASTM, 2000e)), except that tolerances for wear of the cone tip were in accordance with report SGF 1:93E, Recommended Standard for Cone Penetration Tests, (SGS, 1993) which are comparable to ASTM.  It is noted that for the 10-cm$^2$ base cone, the ASTM D5778 (ASTM, 2000e) specified dimensions for "base diameter," "cone height," and "extension" are minimum 34.7 mm, 24 mm, and 2 mm, respectively, compared to the report SGF 1:93E (SGS, 1993) recommended tolerances of minimum 34.8 mm, 24 mm, and 2 mm, for the same cone. The 2-mm SGF Report (SGS, 1993) value accounts for a constant 5-mm porous filter.  Pore pressures were measured in the soundings.  The equipment was mounted on a track-operated rig dedicated only to the CPT work.  Cone tip resistance, sleeve friction, and dynamic pore pressure were recorded every 5 cm (approximately every 2 in) as the cone was advanced into the ground.  Seismic shear wave velocity tests were also performed using a geophone mounted in the cone, a digital oscilloscope, and a beam, which was struck on the ground surface with a sledge hammer.  Pore pressure dissipation data were also obtained, with the data recorded at 5-sec intervals.

A total of 63 CPT soundings were performed, including additional off-set soundings due to persistent refusal in dense/hard or cemented soils.  At selected sounding locations, the soils causing refusal were pre-augered so that deeper CPT penetration could be obtained at the sounding location.  Pre-augering was performed at six locations, but often several times at the same sounding.  The sounding depths ranged from about 12 ft to 142 ft. Seismic CPT was performed at eight sounding locations.  Pore pressure dissipation tests were performed in 20 soundings, at 26 different depths. Table 2.5-43 provides a summary of CPT locations and details.  The locations are shown in Figure 2.5-103 and Figure 2.5-104.  The CPT logs, shear wave velocity, and pore pressure dissipation results are contained in Appendix 2.5-A.

**Observation Wells and Slug Testing**

A total of 40 observation wells were installed to a maximum depth of 122 ft during the CCNPP Unit 3 subsurface investigation under the full-time supervision of geotechnical engineers or geologists. Wells were installed either in SPT boreholes or at an off-set location, in accordance with ASTM D5092 (ASTM, 2004a). Wells installed in SPT boreholes were grouted to the bottom of the well, and the portion above was reamed to a diameter of at least 6 in using rotary methods and biodegradable drilling fluid. Off-set wells were installed using either 6¼-in ID hollow-stem augers or 6-in diameter holes using the rotary method and biodegradable drilling fluid. Each well was developed by pumping and/or flushing with clean water. Table 2.5-44 provides a summary of the observation well locations and details. The locations are shown in Figure 2.5-103 and Figure 2.5-104. Complete observation well details are provided in Section 2.4.12.

Slug testing, for the purposes of measuring the in-situ hydraulic conductivity of the soils, was performed in all 40 wells. The tests were conducted using the falling head method, in accordance with Section 8 of ASTM D4044 (ASTM, 2002b). Slug testing included establishing the static water level, lowering a solid cylinder (slug) into the well to cause an increase in water level in the well, and monitoring the time rate for the well water to return to the pre-test static level. Electronic transducers and data loggers were used to measure the water levels and times during the test. Table 2.5-45 provides a summary of the hydraulic conductivity values. Details on testing are provided in Section 2.4.12.

Appendix 2.5-A contains the details of well installation records, boring logs for observation wells, and the hydraulic conductivity test results.

**Test Pits**

A total of 20 test pits were excavated to a maximum depth of 10 ft each using a mechanical excavator. Bulk samples were collected at selected soil horizons in some of the test pits for laboratory testing. Table 2.5-46 provides a summary of the test pit locations. The locations are shown in Figure 2.5-105. Appendix 2.5-A contains the test pit records.

**Field Electrical Resistivity Testing**

A total of four field electrical resistivity (ER) tests were performed to obtain apparent resistivity values for the site soils. Table 2.5-47 provides a summary of the ER test locations. ER testing was conducted using an Advanced Geosciences, Inc., Sting resistivity meter, a Wenner four-electrode array, and "a" spacings of 1.5 ft, 3 ft, 5 ft, 7.5 ft, 10 ft, 15 ft, 20 ft, 30 ft, 40 ft, 50 ft, 100 ft, 200 ft, and 300 ft in accordance with ASTM G57 (ASTM, 2001a) and IEEE 81 (IEEE, 1983), except as noted below. The arrays were centered on each of the staked locations R-1 and R-2, R-3, and R-4, and are shown in Figure 2.5-103 and Figure 2.5-104. The electrodes were located using a 300-ft measuring tape along the appropriate bearings using a Brunton compass.

ASTM G57 (ASTM, 2001a) states that electrodes not be driven more than 5% of the electrode separation, which is about 0.9 in for the smallest "a" spacing of 1.5 ft used. Electrodes, however, were driven about 2.25 in (or about 12%) at locations where leaves and vegetation were present on the ground, to ensure adequate contact with the soils. ASTM G57 (ASTM, 2001a) states that a decade box be used to check the accuracy of the resistance meter. This verification, however, was conducted using a resistor supplied by the equipment manufacturer in compliance with the manufacturer's recommendations. ASTM G57 (ASTM, 2001a) states that measurement alignments be chosen along uniform topography. Given the topography at the site, however, the array alignments along R-1 and R-2 (shown in Figure 2.5-103) contained topographic variation. Finally, IEEE 81 (IEEE, 1983) states that electrodes not be driven into the ground more than 10% of the "a" spacing. As discussed above, at some locations electrodes

were driven about 2.25 in (or about 12%) into the ground.  Despite the noted deviations, the collected resistivity values are considered valid and suitable for use.

The raw field data are considered "apparent" resistivity values.  The data were modeled in an attempt to remove the geometric and sampling influences and develop vertical profiles that estimate "true" subsurface resistivity values.  The values, shown in Table 2.5-39, provide a summary of the field resistivity results, as well as "true" resistivity values with depth.  For developing vertical profiles, depth values were taken as 1/3 of the a-spacing in the Geotechnical Subsurface Investigation Data Report (Schnabel, 2007a).  The raw data are provided in Appendix 2.5-A.

### Suspension P-S Velocity Logging Survey

Borehole geophysical logging was performed in a total of 10 boreholes.  The geophysical survey consisted of natural gamma, long- and short-normal resistivity, spontaneous potential, three-arm caliper, direction survey, and suspension P-S velocity logging.  Geotechnical engineers or geologists provided full-time field inspection of borehole geophysical logging activities.  Detailed results are provided in Appendix 2.5-A.  The P-S logging results are discussed in detail in Section 2.5.4.4.

### Subsurface and Excavation Profiles

Subsurface profiles depicting the inferred subsurface stratigraphy are presented in Figure 2.5-107 through Figure 2.5-111. Profiles depicting excavation geometries and locations of Category I structures, as well as the relationship between their foundations with the subsurface materials, are addressed in Section 2.5.4.5.}

### 2.5.4.3      Foundation Interfaces

The U.S. EPR FSAR includes the following COL Item in Section 2.5.4.3:

Foundation interfaces with underlying materials are site specific and will be addressed by the COL applicant.  The COL applicant will confirm that the site soils have (1) sliding coefficient of friction equal to at least 0.7, (2) adequate shear strength to provide adequate static and dynamic bearing capacity, (3) adequate elastic and consolidation properties to satisfy the limits on settlement described in Section 2.5.4.10.2, and (4) adequate dynamic properties (i.e., shear wave velocity and strain-dependent modulus-reduction and hysteretic damping properties) to support the Seismic Category 1 structures of the U.S. EPR under earthquake loading.

This COL Item is addressed as follows:

{Foundation interfaces are discussed as an integral part of Sections 2.5.4.5 and 2.5.4.10.

The logs of test pits that were dug are included in the subsurface investigation report (Schnabel, 2007a).  Based on the information obtained during the review of information from the CCNPP Units 1 and 2 UFSAR (BGE, 1982) and the observations of the soil samples being taken for the CCNPP Unit 3 subsurface investigation, it was determined that exploratory trenches were not necessary in order to characterize the soils at the CCNPP Unit 3 site.}

### 2.5.4.4      Geophysical Surveys

The U.S. EPR FSAR includes the following COL Item in Section 2.5.4.4:

Geophysical surveys are site specific and will be addressed by the COL applicant.

This COL Item is addressed as follows:

{This section provides a summary of the geophysical survey undertaken for CCNPP Unit 3. Section 2.5.4.4.1 summarizes previous geophysical surveys performed at the CCNPP Units 1 and 2 areas. Section 2.5.4.4.2 summarizes those completed during the CCNPP Unit 3 subsurface investigation.

Sections 2.5.4.4.1 and 2.5.4.4.2 are added as a supplement to the U.S. EPR FSAR.

### 2.5.4.4.1      Previous Geophysical Survey for CCNPP Units 1 and 2

Various geophysical techniques were employed during the original site investigation for CCNPP Units 1 and 2 in 1967. These investigations are addressed in detail in the UFSAR (BGE, 1982). A brief summary of the investigations, reproduced from this reference, is as follows.

### 2.5.4.4.1.1      Seismic Refraction Survey

Refraction surveys were performed along two lines, 2,000 ft and 2,100 ft in length, for the purpose of obtaining compressional wave velocity data. The data indicated compressional wave velocities in the upper (approximately 40 ft) Pleistocene soils of about 2,200 ft/sec and in the lower (thickness undefined in the UFSAR) Miocene soils of about 5,500 ft/sec to 5,900 ft/sec. Data for deeper deposits, including bedrock, were obtained from measurements at a location several miles south of the site. The results are provided in a summary table, reproduced and shown in Table 2.5-48.

### 2.5.4.4.1.2      Uphole Seismic Velocity Survey

An uphole seismic survey was performed in the plant area for the purpose of correlating the results with those from the seismic refraction survey. The uphole survey was performed in a borehole (DM-4), about 148 ft deep. The results indicated a compressional wave velocity of 2,000 ft/sec in the upper approximately 40 ft and 5,500 ft/sec below, to the maximum depth of about 148 ft. The results are reproduced and shown in Figure 2.5-121.

### 2.5.4.4.1.3      Shear Wave Velocity Measurements

Shear wave propagation was evaluated from surface waves using a Sprengnether velocity meter. The measurements indicated that the shear wave velocity of the Miocene soils is about 1,600 ft/sec. Measurements for other deposits are not reported.

### 2.5.4.4.1.4      Micromotion Measurements

Micromotion measurements were made at three locations at the site using Microtremor equipment. The results indicated a predominant period of background vibration of about 0.5 sec to 0.75 sec. These measurements were reported to be consistent with results for reasonably dense soils. Based on these observations it was concluded that no special problems could arise in designing the facility at the site.

### 2.5.4.4.1.5      Laboratory Shockscope Tests

Several samples of the site soils were tested in the laboratory using the Shockscope to obtain compressional wave velocity measurements for correlation with the field measurements. The test results indicated compressional wave velocity measurements ranging from 1,000 ft/sec to 3,200 ft/sec for confining pressures of 0 to 6,000 psf, respectively. The results are reproduced herein and shown in Table 2.5-49.

#### 2.5.4.4.1.6    Velocity Profile for CCNPP Units 1 and 2

Based on results of the refraction survey, uphole survey, shear wave velocity measurements, micromotion data, and laboratory shockscope, as well as measurements made in 1943 that extended to greater depth, including bedrock, at locations several miles south of the site, a compressional and shear wave velocity model was prepared for the site, using estimated Poisson's ratios.  The results are reproduced herein and shown in Figure 2.5-122.

### 2.5.4.4.2    Geophysical Survey for CCNPP Unit 3

Suspension P-S velocity logging and down-hole seismic CPT tests were performed at 10 boreholes and 8 soundings, respectively, during the CCNPP subsurface investigation.  The results are discussed below.

#### 2.5.4.4.2.1    Suspension P-S Velocity Logging

Suspension P-S velocity logging was performed in borings B-301, B-304, B-307, B-318, B-323, B-401, B-404, B-407, B-418, and B-423.  The boreholes were uncased and filled with drilling fluid. Boreholes B-301 and B-401 were approximately 400 ft deep each, while the remaining boreholes were approximately 200 ft deep each.  The OYO/Robertson Model 3403 unit and the OYO Model 170 suspension logging recorder and probe were used to obtain the measurements.  Details of the equipment are described in Ohya (Ohya, 1986).  The velocity measurement techniques used for the project are described in Electric Power Research Institute (EPRI) Report TR-102293, Guidelines for Determining Design Basis Ground Motions, (EPRI, 1993).  The results are provided as tables and graphs in Appendix 2.5-A.

At this time, an ASTM standard is not available for the suspension P-S velocity logging method, therefore, a brief description follows.  Suspension P-S velocity logging uses a 23-ft (7-m) probe containing a source near the bottom, and two geophone receivers spaced 3.3 ft (1 m) apart, suspended by a cable.  The probe is lowered into the borehole to a specified depth where the source generates a pressure wave in the borehole fluid (drilling mud).  The pressure wave is converted to seismic waves (P-wave and S-wave) at the borehole wall.  At each receiver location, the P- and S-waves are converted to pressure waves in the fluid and received by the geophones mounted in the probe, which in turn send the data to a recorder on the surface.  At each measurement depth, two opposite horizontal records and one vertical record are obtained.  This procedure is typically repeated every 1.65 ft (0.5 m) or 3.3 ft (1 m) as the probe is moved from the bottom of the borehole toward the ground.  The elapsed time between arrivals of the waves at the geophone receivers is used to determine the average velocity of a 3.3-ft (1-m) high column of soil around the borehole.  For quality assurance, analysis is also performed on source-to-receiver data.

Compressional wave velocity (Vp) and shear wave velocity (Vs) results obtained during the CCNPP Unit 3 subsurface investigation are summarized in Figure 2.5-123 and Figure 2.5-124 and are discussed herein.  Ignoring the measurements above elevation 85 ft (approximate planned finished grade), Vp measurements in Stratum I Terrace Sand ranged from about 850 ft/sec to 5,560 ft/sec, with an increasing trend with depth. Vp measurements in Stratum IIa Chesapeake Clay/Silt ranged from about 3,120 ft/sec to 5,750 ft/sec, with typically decreasing trend with depth.  Vp measurements in Stratum IIb Chesapeake Cemented Sand ranged from about 2,350 ft/sec to 8,130 ft/sec, with initially increasing trend with depth, however, with fairly uniform values after a few feet of penetration, except at intermittent cemented zones with peak Vp values.  Vp measurements in Stratum IIc Chesapeake Clay/Silt ranged from about 4,800 ft/sec to 5,600 ft/sec, with relatively uniform values throughout the entire thickness, except for occasional minor peaks at intermittent depths.  Vp measurements in Stratum III Nanjemoy Sand ranged from about 5,420 ft/sec to 7,330 ft/sec, with relatively uniform values,

except for occasional minor peaks at intermittent depths. Results are relatively consistent with those reported from CCNPP Units 1 and 2 (Table 2.5-48 and Figure 2.5-121) for similar soils. It is noted that Vp values below about elevation 80 ft are typically at or above 5,000 ft/sec; these measurements reflect the saturated condition of the soils below the referenced elevation.

Ignoring the measurements above elevation 85 ft, Vs measurements in Stratum I Terrace Sand ranged from about 400 ft/sec to 1,150 ft/sec, with a relatively uniform trend with depth. Vs measurements in Stratum IIa Chesapeake Clay/Silt ranged from about 590 ft/sec to 1,430 ft/sec, with typically increasing trend with depth. Vs measurements in Stratum IIb Chesapeake Cemented Sand ranged from about 560 ft/sec to 3,970 ft/sec, with significant variation with depth owing to significant changes in density and cementation. Vs measurements in Stratum IIc Chesapeake Clay/Silt ranged from about 1,030 ft/sec to 1,700 ft/sec, with relatively uniform trend in values throughout the entire thickness, except for occasional minor peaks at intermittent depths. Vs measurements in Stratum III Nanjemoy Sand ranged from about 1,690 ft/sec to 3,060 ft/sec, with initially increasing trend in depth, however, relatively uniform at greater depth, except for occasional minor peaks at intermittent depths. Results are relatively consistent with those reported from CCNPP Units 1 and 2 (Figure 2.5-122). Based on all 10 suspension P-S velocity measurements, an average Vs profile was estimated for the upper 400 ft, as shown in Figure 2.5-125. The measurements from the two deepest boreholes (B-301 and B-401) are also shown for comparison purposes.

Poisson's ratio values were determined based on the Vp and Vs measurements, and are shown in Figure 2.5-126. Ignoring the values above elevation 85 ft, Poisson's ratio measurements in Stratum I Terrace Sand ranged from about 0.27 to 0.50. Poisson's ratio measurements in Stratum IIa Chesapeake Clay/Silt ranged from about 0.4 to 0.49, with typically decreasing trend with depth. Poisson's ratio measurements in Stratum IIb Chesapeake Cemented Sand ranged from about 0.26 to 0.49. Poisson's ratio measurements in Stratum IIc Chesapeake Clay/Silt ranged from about 0.45 to 0.48, with a relatively uniform trend in values throughout the entire thickness. Poisson's ratio measurements in Stratum III Nanjemoy Sand ranged from about 0.39 to 0.46, with initially a decreasing trend in depth, however, becoming relatively uniform at greater depth, except for occasional minor peaks at intermittent depths. Based on all 10 borehole measurements, an average Poisson's ratio profile was estimated for the upper 400 ft, which is shown in Figure 2.5-127. The values obtained based on velocity measurements from the two deepest boreholes (B-301 and B-401) are also shown for comparison purposes.

It is noted that the above Vp, Vs, and Poisson's ratio measurements reflect the conditions for the approximately upper 400 ft of the site, or to about elevation -317 ft. Information on deeper soils, as well as bedrock, was obtained from the available literature; it is discussed in Section 2.5.4.7.

### 2.5.4.4.2.2    CPT Seismic Measurements

Shear wave velocity measurements were made using a seismic cone at eight soundings (C-301, C-304, C-307, C-308, C-401, C-404, C-407, and C-408). The measurements were made at 5-ft intervals. At several locations, the soils required pre-drilling to advance the cone, particularly in the cemented zones. Although the deepest CPT sounding was about 142 ft, the combined measurements provided information for the upper approximately 200 ft of the site soils, extending to about elevation -80 ft. Further penetration was not possible due to continued cone refusal. An average of the seismic CPT results is compared with the suspension P-S velocity logging results and shown in Figure 2.5-128. The CPT results are found to be relatively consistent with the suspension P-S velocity logging results. The variations in different soils that were observed in the suspension P-S velocity logging data are readily duplicated by the CPT

results, including the peaks associated with cemented or hard zones.  Further details on testing and the results are provided, in tables and graphs, in Appendix 2.5-A.

### 2.5.4.4.2.3       Shear Wave Velocity Profile Selection

Given the similarity between the suspension P-S velocity logging and the seismic CPT results, and that the CPT results only extend to limited depth, the suspension P-S velocity logging results were used as the basis for determination of shear wave velocity profile for the site.  The overall recommended velocity profile for the site soils is addressed in Section 2.5.4.7, including the velocity profile for soils below 400 ft depth and bedrock.}

### 2.5.4.5       Excavation and Backfill

The U.S. EPR FSAR includes the following COL Item in Section 2.5.4.5:

Excavations and backfill are site specific and will be addressed by the COL applicant.

This COL Item is addressed as follows:

{Sections 2.5.4.5.1 through 2.5.4.5.4 are added as a supplement to the U.S. EPR FSAR.

### 2.5.4.5.1       Source and Quantity of Backfill and Borrow

A significant amount of earthwork is anticipated in order to establish the final site grade and to provide for the final embedment of the structures.  It is estimated that approximately 3.5 million cubic yards (cyd) of materials will be moved during earthworks to establish the site grade.

The materials excavated as part of the site grading are primarily the surficial soils belonging to the Stratum I Terrace Sand.  To evaluate these soils for construction purposes, 20 test pits were excavated at the site, as shown in Figure 2.5-105.  The maximum depth of the test pits was limited to 10 ft.  Results of laboratory testing on the bulk samples collected from the test pits for moisture-density and other indices are summarized in Table 2.5-50, with the details included in Appendix 2.5-A.  The results clearly indicate that there are both plastic and non-plastic soils included in Stratum I soils, including material designated as fill.  These fill soils are predominantly non-plastic.  A similar observation was made from the borings that extended deeper than the test pits.  Their composition consists of a wide variety of soils, including poorly-graded sand to silty sand, well graded sand to silty sand, clayey sand, silty sand, clay, clay of high plasticity, and silt of high plasticity, based on the USCS.  The highly plastic or clay portion of these soils will not be suitable for use as structural fill, given the high percentage of fines (average 59 percent) and the average natural moisture content nearly twice the optimum value of 10 percent.  The remaining sand or sandy portion will be suitable; however, these materials are typically fine (sometimes medium to fine) sand in gradation, and likely moisture-sensitive that may require moisture-conditioning.  Additionally, the suitable portions of the excavated soils are used for site grading purposes, with very little, if any, remaining to be used as structural fill.  It is estimated that about 2 million cyd of structural backfill are needed.  Therefore, structural fill shall be obtained from off-site borrow sources.  The structural fill for CCNPP Unit 3 shall be sound, durable, well-graded sand or sand and gravel, with maximum 25 percent fines content, and free of organic matter, trash, and deleterious materials.  Once the potential sources of structural fill have been identified, the material(s) are sampled and tested in the laboratory to establish their static and dynamic properties.  Chemical tests are also performed on the candidate backfill materials.  The results are evaluated to verify that the candidate backfill materials meet the design requirements for structural fill.

## 2.5.4.5.2    Extent of Excavations, Fills, and Slopes

In the area of planned CCNPP Unit 3, the current ground elevations range from approximately elevation 50 ft to elevation 120 ft, with an approximate average elevation 88 ft, as shown in Figure 2.5-103.  The planned finished grade in CCNPP Unit 3 powerblock area ranges from about elevation 75 ft to elevation 85 ft; with the centerline of Unit 3 planned at approximately Elevation 85 ft.  Earthwork operations are performed to achieve the planned site grades, as shown on the grading plan in Figure 2.5-129.  All safety-related structures are contained within the outline of CCNPP Unit 3, except for the water intake structures that are located near the existing intake basin, also shown in Figure 2.5-129.  A listing of the Category I structures with relevant foundation information is as follows (note that foundation elevations may be subject to minor change at this time).

|                                              | Foundation elevation (ft) |
|----------------------------------------------|:-------------------------:|
| Reactor Building                             | 44                        |
| Safeguards Buildings                         | 44                        |
| Fuel Building                                | 44                        |
| Emergency Power Generating Building          | 79                        |
| ESWS Cooling Towers                          | 63                        |
| Ultimate Heat Sink Makeup Water Intake Structure | -25                   |

Foundation excavations result in removing about 2 million cyd of materials.  The extent of all excavations, backfilling, and slopes for Category I structures are shown in Figure 2.5-130 through Figure 2.5-134.  These sections are taken at locations identified in Figure 2.5-103 and Figure 2.5-104.  These figures illustrate that excavations for foundations of Category I structures will result in removing Stratum I Terrace Sand and Stratum IIa Chesapeake Clay/Silt in their entirety, and will extend to the top of Stratum IIb Chesapeake Cemented Sand, except in the Ultimate Heat Sink Makeup Water Intake Structure area.  In the Ultimate Heat Sink Makeup Water Intake Structure area, the foundations are supported on Stratum IIc soils, given the interface proximity of Strata IIb and IIc.

The depth of excavations to reach Stratum IIb is approximately 40 ft to 45 ft below the final site grade in the Powerblock area.  Since foundations derive support from these soils, variations in the top of this stratum were evaluated, reflected as elevation contours for top of Stratum IIb in CCNPP Unit 3 and in CLA1 areas, as shown in Figure 2.5-135.  ThisFigure shows that the variation in top elevation of these soils is very little, approximately 4 ft or less (about 1 percent) across each major foundation area.  The extent of excavations to final subgrade, however, is determined during construction based on observation of the actual soil conditions encountered and verification of their suitability for foundation support.  Once subgrade suitability in Stratum IIb Cemented soils is confirmed, the excavations are backfilled with compacted structural fill to the foundation level of structures.  Subsequent to foundation construction, the structural fill is extended to the final site grade, or near the final site grade, depending on the details of the final civil design for the project.  Compaction and quality control/quality assurance programs for backfilling are addressed in Section 2.5.4.5.3.

Permanent excavation and fill slopes, created due to site grading, are addressed in Section 2.5.5.  Temporary excavation slopes, such as those for foundation excavation, are graded on an inclination not steeper than 2:1 horizontal:vertical (H:V) or even extended to inclination 3:1 H:V, if found necessary, and having a factor of safety for stability of at least 1.30 for static conditions.  These slopes are currently shown as 3:1 H:V in Figure 2.5-130 through Figure 2.5-133.

Excavation for the Ultimate Heat Sink Makeup Water Intake Structure is different than that for other CCNPP Unit 3 structures, as shown in Figure 2.5-134.  Given the proximity of this

excavation to the Chesapeake Bay, this excavation is made by installing a sheetpile cofferdam that not only provides excavation support but also aids with the dewatering needs. This is addressed further in Section 2.5.4.5.4.

### 2.5.4.5.3    Compaction Specifications

Once structural fill sources are identified, as discussed in Section 2.5.4.5.1, several samples of the materials are obtained and tested for indices and engineering properties, including moisture-density relationships. For foundation support and backfill against walls, structural fill is compacted to minimum 95 percent of its maximum dry density, as determined based on the Modified Proctor compaction test procedure (ASTM, 2002c). The fill is compacted to within 3 percent of its optimum moisture content.

Fill placement and compaction control procedures are addressed in a technical specification prepared during the detailed design stage of the project. It includes requirements for suitable fill, sufficient testing to address potential material variations, and in-place density and moisture content testing frequency, e.g., a minimum of one test per 10,000 square ft of fill placed. The technical specification also includes requirements for an on-site testing laboratory for quality control, especially material gradation and plasticity characteristics, the achievement of specified moisture-density criteria, fill placement/compaction, and other requirements to ensure that the fill operations conform to the earthwork specification for CCNPP Unit 3. The soil testing firm is required to be independent of the earthwork contractor and to have an approved quality program. A sufficient number of laboratory tests are required to be performed to ensure that variations in the fill material are accounted for. A trial fill program is normally conducted for the purposes of determining an optimum number of compactor coverages (passes), the maximum loose lift thickness, and other relevant data for optimum achievement of the specified moisture-density (compaction) criteria.

### 2.5.4.5.4    Dewatering and Excavation Methods

Ground Water control is required during construction. Ground Water conditions and dewatering are addressed in Sections 2.4.12.5 and 2.5.4.6.

Given the soil conditions, excavations are performed using conventional earth-moving equipment, likely using self-propelled scrapers with push dozers, excavators and dump trucks. Most excavations should not present any major difficulties. Blasting is not anticipated. The more difficult excavations would have been in Stratum IIb Cemented Sand, due to the cemented nature and proximity to ground water, but the cemented portions are not planned to be excavated, except where minor excavations are needed due to localized conditions or due to deeper foundation elevations such as at the Ultimate Heat Sink Makeup Water Intake Structure area. Excavations in localized, intermittent cemented soils may require greater excavating effort, such as utilizing hoe-rams or other ripping tools; however, these zones are very limited in thickness, with probably only occasional need for expending additional efforts. Excavations for the CCNPP Unit 3 powerblock foundations are planned as open cut. Upon reaching the final excavation levels, all excavations are cleaned of any loose materials, by either removal or compaction in place. All final subgrades are inspected and approved prior to being covered by backfill or concrete. The inspection and approval procedures are addressed in the foundation and earthworks specifications developed during the detailed design stage of the project. These specifications include measures, such as proof-rolling, excavation and replacement of unsuitable soils, and protection of surfaces from deterioration.

As discussed in Section 2.5.4.5.2, excavation for the Ultimate Heat Sink Makeup Water Intake Structure requires the installation of a sheetpile cofferdam. The sheetpile structure extends

from the ground surface to a depth of about 50 ft. The full scope of the sheetpile cofferdam is developed during the detailed design stage of the project. Excavation of soils in this area should not present any major difficulties given their compactness.

Foundation rebound (or heave) is monitored in excavations for selected Category I structures. Rebound estimates are addressed in Section 2.5.4.10. Monitoring program specifications are developed during the detailed design stage of the project. The specification document addresses issues, such as the installation of a sufficient quantity of instruments in the excavation zone, monitoring and recording frequency, and evaluation of the magnitude of rebound and settlement during excavation, dewatering, and foundation construction. }

### 2.5.4.6      Ground Water Conditions

The U.S. EPR FSAR includes the following COL Item in Section 2.5.4.6:

     The COL applicant will address site-specific ground water conditions.

This COL Item is addressed as follows:

{Sections 2.5.4.6.1 through 2.5.4.6.5 are added as a supplement to U.S. EPR FSAR.

### 2.5.4.6.1      Ground Water Conditions

The ground water data collection and monitoring program is still in progress, subsequent to the installation of observation wells during the CCNPP subsurface investigation. Details of available ground water conditions at the site are given in Section 2.4.12. Based on available information, through June 2007, the shallow (surficial) ground water level in CCNPP Unit 3 and CLA1 areas ranges from approximately elevation 73 to elevation 85.7 ft, or an average elevation of 80 ft. This elevation was used as the design ground water elevation in the geotechnical calculations, as opposed to the design ground water elevation of 73 ft as discussed in Section 2.4.12. The value used in the geotechnical calculations is bounded by the U.S. EPR FSAR value. Similarly, the ground water level associated with the deeper hydrostatic surface was found to range from approximately elevation 34 ft to elevation 42 ft, with an average elevation of 39 ft. The shallow ground water should have little to no impact on the stability of foundations, as the site grading and excavation plans will implement measures to divert these flows away from excavations, e.g., through runoff prevention measures and/or ditches. There are no Category I foundations planned within the upper water-bearing soils. The deeper ground water condition, within the cemented sands, could adversely impact foundation soil stability during construction if not properly controlled, resulting in loss of density, bearing, and equipment trafficability.

### 2.5.4.6.2      Dewatering During Construction

Temporary deatering is required for ground water managment during construction. Analysis of the ground water conditions at the site is presented in Section 2.4.12. On the basis of defined ground water conditions, ground water control/construction dewatering is needed at the site during excavations for CCNPP Unit 3 foundations. Ground water associated with seepage in the shallow (upper) zones (Surficial aquifer) is controlled through site grading and/or a system of drains and ditches, as previously discussed. This may also consist of more positive control, including a series of sumps and pumps strategically located in the excavation area to effectively collect and discharge the seepage that enters the excavation, in addition to ditches, drains, or other conveyance systems.

The drainage ditches are installed below grade level, at the peripheries, as the excavation progresses. These ditches are oriented in approximately north-south and east-west directions, e.g., at excavation corners or more frequently as warranted during construction. Once at the final subgrade, stone-filled drains are installed in the excavation interior for control of upward seepage, if any. These drains are in turn connected to exterior ditches and sumps. Each sump is equipped with a pump of sufficient capacity for efficient ground water removal. Based on the estimated lateral ground water flow rate of 44 to 64 gpm (167 to 242 lpm) derived in section 2.4.12.5, a total of four pumps with capacity of 100 gpm (379 lpm) each are used for the dewatering.

Temporary dewatering is required for the excavation of the Ultimate Heat Sink Makeup Water Intake Structure. A sheetpile cofferdam is designed to aid with dewatering needs to be extending it into low permeability soils; however, some level of ground water control is still required to maintain a relatively "dry" excavation during construction. As a minimum, sumps are installed to control and/or lower the ground water level inside the cofferdam. Given the limited excavation size, one 100 gpm (379 lpm) pump is sufficient for control of ground water in this excavation.

Additional auxiliary pumps are available for removal of water from excavations during periods of unexpected storm events. The ground water level in excavations shall be maintained a minimum of 3 ft (.09 m) below the final excavation level.

### 2.5.4.6.3    Analysis and Interpretation of Seepage

Analysis of the ground water conditions at the site is ongoing at this time, given continued ground water monitoring that is still in progress, as addressed in Section 2.4.12. A ground water model, based on information currently available, has been prepared for the overall ground water conditions at the site and is addressed in detail in Section 2.4.15. The ground water program and milestones are provided in Section 2.4.12.

### 2.5.4.6.4    Permeability Testing

Testing for permeability of the site soils was performed using Slug tests, as discussed in Section 2.5.4.3. A detailed description of the tests and the results is provided in Section 2.4.12. A summary of the hydraulic conductivity values is presented in Table 2.5-45.

### 2.5.4.6.5    History of Ground Water Fluctuations

A detailed treatment of the ground water conditions is provided in Section 2.4.12.}

### 2.5.4.7    Response of Soil and Rock to Dynamic Loading

The U.S. EPR FSAR includes the following COL Item in Section 2.5.4.7:

The COL applicant will address site-specific response of soil and rock to dynamic loading, including the determination of strain-dependent modulus-reduction and hysteretic damping properties.

This COL Item is addressed as follows:

{The SSE spectra and its specific location at a free ground surface reflect the seismic hazard in terms of PSHA and geologic characteristics of the site and represent the site-specific ground motion response spectrum. These spectra would be expected to be modified as appropriate to

develop ground motion for design considerations.  Detailed descriptions on response of site soils and rocks to dynamic loading are addressed in Section 2.5.2.

Sections 2.5.4.7.1 through 2.5.4.7.5 are added as a supplement to the U.S. EPR FSAR.

### 2.5.4.7.1      Site Seismic History

The seismic history of the area and the site, including any prior history of seismicity, evidence of liquefaction or boils, is addressed in Sections 2.5.1.1.4.4.5 and 2.5.1.2.6.4.

### 2.5.4.7.2      P- and S-Wave Velocity Profiles

Given the depth to bedrock of about 2,500 ft and the depth of velocity measurements during the CCNPP Unit 3 subsurface investigation, additional studies were performed to complete the soil column profile for the CCNPP Unit 3 site.

#### 2.5.4.7.2.1      Subsurface Conditions in the Upper 400 Feet

Geophysical measurements in the upper 400 ft were made during the CCNPP Unit 3 subsurface investigation and are addressed in Section 2.5.4.4.2.  The average shear wave velocity and Poisson's ratio profiles for the upper approximately 400 ft of the site, as obtained from the CCNPP Unit 3 subsurface investigation, are shown in Figure 2.5-125 andFigure 2.5-127, respectively.

#### 2.5.4.7.2.2      Subsurface Conditions Below 400 Feet

It is known that sediments at the site extend below the maximum depth of the CCNPP Unit 3 subsurface investigation.  With the maximum depth of the subsurface exploration at 400 ft, additional subsurface information was sought to characterize the site conditions below this depth, including bedrock.

**Soil Shear Wave Velocity Profile**

In seeking available resources, various geologic records were reviewed and communication made with staff at the Maryland Geological Survey, the United States Geological Survey, and the Triassic-Jurassic Study Group of Lamont-Doherty Earth Observatory, Columbia University.  The results of this work, and associated references, are addressed in Section 2.5.1.  In summary, a soil column profile was prepared, extending from the ground surface to the top of rock, as shown in Figure 2.5-136.  Soils below 400 ft consist of Coastal Plain sediments of Eocene, Paleocene, and Cretaceous eras, extending to an estimated depth of about 2,500 ft below the ground surface.  These soils contain sequences of sand, silt, and clay.  Given their geologic age, they are expected to be competent soils, consolidated to at least the weight of the overlying soils.

Several available geologic records were also reviewed in order to obtain information on both the depth to bedrock and the bedrock type, as addressed in Section 2.5.1.  Accordingly, the estimated depth to bedrock in the proximity of the site is about 2,555 ft, which is consistent with the depth of 2,500 ft reported in the CCNPP Units 1 and 2 UFSAR (BGE, 1982) and as shown in Figure 2.5-122.  Top of rock elevation at the CCNPP site is estimated, and adopted, at approximately elevation -2,446 ft which corresponds to a depth of about 2,531 feet.  Regional geologic data were also researched for information on bedrock type.  This revealed various rock types in the region, including Triassic red beds and Jurassic diabase, granite, schist, and gneiss.  However, only granitoid rocks (metamorphic gneiss, schist, or igneous granitic rocks), similar to those exposed in the Piedmont, could be discerned as the potential regional rock underlying

the CCNPP Unit 3 site.  For the purpose of rock response to dynamic loading, granitoid was considered as the predominant rock type at the CCNPP site.

With the geology established below a depth of 400 ft, velocity profiles also needed to be established.  The velocity data were found through a research of available geologic information for the area.  From the Maryland Geological Survey data, two sonic profiles were discovered for wells in the area that penetrated the bedrock, one at Chester, MD (about 38 miles north the site, (USGS, 1983) and another at Lexington Park, MD (about 13 miles south of the site, (USGS, 1984); their locations relative to the site are shown in Figure 2.5-136.  These two sonic profiles were digitized and converted to shear wave velocity, based on a range of Poisson's ratios for the soil and the rock.  The two Vs profiles for Chester and Lexington Park are plotted versus elevation, with the superimposed measured velocity profile from the upper 400 ft at the CCNPP site, as shown in Figure 2.5-137 and Figure 2.5-138.

The bottom of the measured Vs profile in the upper 400 ft fits well with the Chester data for which a soil's Poisson's ratio = 0.4 was used (Figure 2.5-137), whereas, in the case of Lexington Park data (Figure 2.5-138), the bottom of the measured data in the upper 400 ft fits well with the profile for which the soil's Poisson's ratio = 0.45 was used.  Geologically, the soils at the two sites are quite comparable (refer to Section 2.5.1 for more details on site geology).  The reason(s) for the different "fits" is not clear.  However, based on actual Poisson's ratio measurement at another deep Coastal Plain site (SNOC, 2006), where suspension P-S velocity logging measurements extended to a depth of over 1,000 ft, a Poisson's ratio of 0.4 was adopted to represent the soil conditions at the CCNPP site, given the geologic similarity of the soils at both sites.

If a Poisson's ratio of 0.4 is used to convert the Chester sonic log to a shear wave velocity log, this shear wave velocity log fits well with the bottom of the site Vs profile measured with suspension logging at comparable elevations (Figure 2.5-137).  A similarly good fit is obtained for the Lexington Park data when a Poisson's ratio of 0.45 is used (Figure 2.5-138).  Although geologically the soils at the Chester and Lexington Park sites are quite comparable (refer to Section 2.5.1 for more details on site geology), there are reasons why the soils at the elevation of the bottom of the site profile could have slightly different Poisson's ratio values, e.g., the Lexington Park soils may be more cohesive than the Chester soils.  Nevertheless, a single Poisson's ratio value was needed for below the bottom of the measured profile for the CCNPP site.  Based on actual Poisson's ratio measurements at another deep Coastal Plain site (SNOC, 2006), where suspension P-S velocity logging measurements extended to a depth of over 1,000 ft, a Poisson's ratio of 0.4 was adopted to represent the soil conditions at the CCNPP site, given the geologic similarity of the soils at CCNPP site and the other Coastal Plain site.

Both profiles (particularly the Chester profile) include significant "peaks," giving a visual impression that the difference in the two profiles may be large.  To further look at the variation in these two profiles based on the adopted Poisson's ratio of 0.4, both profiles were averaged over 100-ft intervals along the entire depth to "smooth" the peaks.  The original profiles for the two sites (based on a Poisson's ratio of 0.4) and the 100-ft interval average for the two measurements are shown in Figure 2.5-139.  A comparison of the two 100-ft interval averages show that once the effect of the "peaks" are removed, the two profiles are relatively similar for the same Poisson's ratio of 0.4.  Finally, an average of the 100-ft interval data for both sites was taken, as also shown in Figure 2.5-139.  This latter profile was compared with an available measured profile in deep Coastal Plain soils (SNOC, 2006); its similarity to the measured profile is indicative of its appropriateness for the geologic setting, as shown in Figure 2.5-140.  Accordingly, based on measured data in the upper 400 ft and data obtained from available literature in areas surrounding the CCNPP site, the recommended shear wave velocity profile in

soils at the CCNPP Unit 3 site is shown in Figure 2.5-141. This profile is later compared to the profile used for CCNPP Units 1 and 2.

**Bedrock Shear Wave Velocity Profile**

Similar to the soil profiles addressed above, two velocity profiles were also available for bedrock, based on the sonic data from Chester (USGS, 1983) and Lexington Park (USGS, 1984) sites. Rock was encountered at different depths at these two sites; however, the elevation difference in top of rock is only 11 ft between the two sites. The bottom portions of Figure 2.5-137 and Figure 2.5-138 (near the soil-rock interface) are enlarged for clarity and are shown in Figure 2.5-142 and Figure 2.5-143 for the Poisson's ratios shown.

A comparison of the Vs profiles in bedrock for the two sites reveals different velocity responses, regardless of the Poisson's ratio values considered. The Chester profile is somewhat transitional and does not approach 9,200 ft/sec at termination of measurements. The Lexington Park profile is rather abrupt, and is in excess of 9,200 ft/sec. The difference in these two responses is found in the geologic description of the bedrock at the two sites. At Chester, the bedrock is described as more the typical, regional metamorphic rock (granitic, schist, or gneiss). At Lexington Park, the bedrock is described as an intrusive diabase. Based on further evaluation of regional bedrocks, as addressed in Section 2.5.1, the following description was established for the CCNPP Unit 3 site: bedrock is probably granitoid rock, less likely to be sandstone or shale, even less likely to be diabase. Accordingly, the Lexington Park profile (that is for diabase rock) was excluded from further consideration.

Closer examination of the Chester bedrock velocity results reveal that the velocities are rather "insensitive" to the assumption of Poisson's ratio, as is evident in Figure 2.5-142. For all practical purposes, the assumption of Poisson's ratio of 0.2, 0.25, or 0.3 for the bedrock renders identical velocity profiles. The responses also follow a particular velocity gradient. For a Poisson's ratio of 0.3 for the rock, one could assume a bedrock velocity starting at some value at the soil-rock interface, transitioning to the 9,200 ft/sec at some depth. This approach was followed, as shown in Figure 2.5-144, showing the Vs profile versus elevation in bedrock. From this figure, starting at Vs of 5,000 ft/sec at the soil-rock interface, the 9,200 ft/sec velocity is reached within about 20 ft depth into rock. Many variations were tried (varying the starting velocity at soil-rock interface, varying the slope of transitioning velocity profile, transition in "slope" or in "step," different Poisson's ratios, etc.); the end result appeared relatively unchanged, i.e., the 9,200 ft/sec velocity is achieved within a short distance of penetrating the rock. On this basis, the "stepped" velocity gradient shown in Figure 2.5-144 was adopted to define the velocity profile for the rock. The recommended velocity profile for bedrock begins with Vs = 5,000 ft/sec at the soil-rock interface, as indicated from the sonic data and also shown in Figure 2.5-144, transitioning to 9,200 ft/sec in steps shown in Figure 2.5-144.

Both the soil and bedrock velocity profile are reflected in an overall site velocity profile for the CCNPP site, as shown in Figure 2.5-145. It should be noted that the top of rock elevation shown in Figure 2.5-145 was adjusted to conform to the estimated rock elevation for the CCNPP Unit 3 site, or elevation -2,446 ft (refer to Section 2.5.1). Figure 2.5-145 is considered the design shear wave velocity profile for the CCNPP Unit 3 site. A companionFigure shows the Poisson's ratios that were measured in the upper 400 ft and those estimated below 400 ft in Figure 2.5-146. The numerical values of velocity steps for the entire profile are given in Table 2.5-51.

A comparison was made of the adopted Vs and Poisson's ratio profiles described above (Figure 2.5-145 and Figure 2.5-146) with those used for the original design of CCNPP Units 1 and 2 (as shown inFigure 2.5-122). The average values for both CCNPP Units 1 and 2 and from the CCNPP Unit 3 investigation are summarized below, after being "weighted" with respect to a

common depth.  The weighting included obtaining an average value for each parameter over a particular depth (in this case 1,000 ft) for comparison purposes.

| | Average CCNPP Units 1 and 2 | | Average CCNPP Unit 3 | |
|---|---|---|---|---|
| | Vs (ft/sec) | μ | Vs (ft/sec) | μ |
| Upper ≈1,000 ft | 1,500 | 0.44 | 1,900 | 0.44 |
| Below ≈1,000 ft to Bedrock | 3,400 | 0.35 | 2,500 | 0.40 |
| Bedrock | 10,000 | 0.15 | 9,200 | 0.30 |

The average Vs (weighted) values in the upper 1,000 ft for the CCNPP Units 1 and 2 is about 1,500 ft/sec, compared to a weighted average Vs adopted for the CCNPP Unit 3 of 1,900 ft/sec over the same depth.  For the soils below 1,000 ft, the CCNPP Units 1 and 2 Vs is reported as 3,400 ft/sec, compared to a weighted average Vs adopted for the CCNPP Unit 3 of about 2,500 ft/sec over the same depth.  For bedrock, the CCNPP Units 1 and 2 used Vs = 10,000 ft/sec at the top of bedrock, compared to a "transitional" Vs adopted for the CCNPP Unit 3, starting at 5,000 ft/sec, transitioning to 9,200 ft/sec with depth.

The differences between the CCNPP Units 1 and 2 UFSAR (BGE, 1982) and CCNPP Unit 3 subsurface investigation values may be attributed to a variety of factors, including measurement techniques and available technology at the time of measurement, assumptions in data reduction, and available geologic references at the time, among many others.  It should be noted that the original 1967 investigation relied primarily on refraction survey and results of a 1943 geophysical survey several miles south of the site to define the soil-rock column profile (reference to both the 1967 and 1943 work are contained in the CCNPP Units 1 and 2 UFSAR (BGE, 1982)); only one measurement in a boring at the site to a depth of about 148 ft provided uphole measurements.  Conversely, the CCNPP Unit 3 subsurface investigation used 10 suspension P-S velocity logging sets of measurements at the site, a more advanced technology for velocity measurements than 1960s technology, extending to depths of about 400 ft, including deriving the deeper velocities from actual borehole sonic measurements as close as 13 miles from the site.  Similarly, the Poisson's ratios adopted in the CCNPP Unit 3 subsurface investigation derivation of velocity profiles below 400 ft were based on actual suspension P-S velocity logging measurements by others in similar Coastal Plain geology.  Equally, the geologic references adopted for estimation of the CCNPP Unit 3 subsurface investigation shear wave velocity profile are recent, building on prior decades of geologic knowledge in the area.  On these bases, the shear wave velocity profile adopted for the CCNPP Unit 3 subsurface investigation phase is considered a closer reflection of the site dynamic characterization.

### 2.5.4.7.3    Dynamic and Static Laboratory Testing

Dynamic laboratory testing, consisting of RCTS tests, to obtain data on shear modulus and damping characteristics of the soils has been completed.  A total of 13 undisturbed soil samples, from depths of about 15 feet to about 400 feet below the existing ground surface, were assigned for RCTS testing.  Results from the RCTS tests are provided in Appendix 2.5-B.  Initially, in the absence of RCTS test results, shear modulus degradation and damping ratio curves that were adopted from available literature were used for the material characterization.  The RCTS results were then evaluated by comparing them to the adopted literature values.  The results of this comparison are discussed in Appendix 2.5-C.  Evaluation of the impact of the RCTS test results on the seismic soil characterization calculations, and the acceptability of use of literature values for shear modulus degradation and damping ratio curves in these calculations, is provided in the report "Reconciliation of EPRI and RCTS Results, Calvert Cliffs Nuclear Power Plant Unit 3" (Bechtel, 2007), and is included as Appendix 2.5-C.  Descriptions of

shear modulus degradation parameters adopted for seismic soil characterization are presented below.

### 2.5.4.7.3.1    Shear Modulus Degradation and Damping Ratio Curves for Soils

In absence of actual data for the site soils, generic EPRI curves were adopted from EPRI TR-102293 (EPRI, 1993).  EPRI "sand" curves were used for predominately granular soils and "clay" curves were used for predominately clay soils based on estimated PI values.  The EPRI "sand" curves cover a depth range up to 1,000 ft.  Since soils at the CCNPP site extend beyond 1,000 ft, similar curves were extrapolated from the EPRI curves, extending beyond the 1,000-ft depth, to characterize the deeper soils.  For instance, the "1,000-2,000 ft" curve was extrapolated by "off-setting" this curve by the amount shown between the "250-500 ft" and "500-1,000 ft" curves in EPRI TR-102293 (EPRI, 1993).  EPRI curve selection for the upper 400 ft of the site soils was based on available soil characterization data from the site investigation.  Below 400 ft, the geologic profile that was prepared (Figure 2.5-136) was used as a basis for the soil profiles, including engineering judgment to arrive at the selected EPRI curves.  The developed EPRI (shear modulus and damping ratio) curves for the CCNPP Unit 3 site are shown in Figure 2.5-147.  These curves are shown being extended beyond the 1-percent shear strain provided in EPRI TR-102293 (EPRI, 1993), only to aid with the randomization process.  In reality, the extended portions will not be used in the final analyses due to the very low strain levels.  It should be noted that the damping ratio curves will be truncated at 15 percent, consistent with the maximum damping values that will be used for the site response analysis.  Tabulated values of shear modulus reduction and damping ratios are presented in Table 2.5-52.

### 2.5.4.7.3.2    Shear Modulus Degradation Curves for Rock

The two velocity profiles for the Chester and Lexington Park sites (Figure 2.5-142 and Figure 2.5-143), indicate that "hard" rock (identified with Vs = 9,200 ft/sec) is present at these two site.  Hard rocks typically exhibit an elastic response to loading, with little, if any, change is stiffness properties.  For the range of shear strains anticipated in the analysis ($10^{-4}$ to 1 percent range), essentially no shear modulus reduction is expected; therefore, for rocks at the site, the estimated shear moduli should remain unaffected, given the relatively high velocity observed from the area rocks.

Hard rocks are considered to have damping, but it is not strain dependent.  A damping ratio of 1 percent has been used for bedrock at other sites, e.g., for the Vogtle Early Site Permit application (SNOC, 2006) in order to obtain compatibility with soils above bedrock.  Experience on similar work has indicated that using damping ratios of 0.5 percent, 1 percent, 2 percent, and 5 percent produces essentially identical results (Dominion, 2006).  Therefore, for the CCNPP Unit 3, a damping ratio of 1 percent was adopted for the bedrock.  Bedrock shear modulus was considered to remain constant, i.e., no degradation, in the shear strain range of $10^{-4}$ percent to 1 percent.  The ground water level of elevation 80 ft was also adopted for the analyses.

Other material parameters that were used for dynamic analysis included material density and soil Plasticity Index.  The soil unit weights for the upper 400 ft were obtained from the laboratory test results and site characterization.  Those below a depth of 400 ft were estimated based on an approximate correlation of available laboratory data with Gamma-Gamma density measurements available from USGS (USGS, 1983).  The values are shown in Table 2.5-53.  The rock unit weight was estimated from the available literature (Deere, 1966)), as 162 pcf.  The Plasticity Index values were used for the selection of appropriate shear modulus and damping ratio curves for the clay soils.  Indices for soils in the upper 400 ft of the site were selected and

based on available laboratory data.  For deeper soils, they were estimated and based on descriptions of the soils in the available literature (USGS, 1983) (USGS, 1984).

### 2.5.4.7.3.3    Dynamic Properties of Structural Fill

As stated in Section 2.5.4.5.2, all Category I structures will be supported on structural fill, which is in turn supported on Stratum IIb Chesapeake Cemented Sand.  Material parameters, static or dynamic, are not available at this time, because the backfill source has yet to be determined.  In absence of this information, it is assumed that material parameters for the structural backfill will be similar to parameters for Stratum I Terrace Sand, and therefore, measurements available for Terrace Sand soils were adopted to represent the fill and used in the analyses.  Once the structural fill is identified and tested for characterization, a comparison will be made between the assumed parameters and actual data to verify that it meets the project requirements.  Should the results prove to be substantially different, such that they are likely to alter the seismic characterization of the site, a new set of data will be adopted based on the test results, and the calculations will be repeated.

### 2.5.4.7.4    Shear Modulus Estimation

With shear wave velocity and other parameters established, the low strain soil and rock shear modulus values can be estimated from the following equation (Bowles, 1966):

$$Gmax = \gamma \cdot (Vs)^2 / g \qquad \qquad \text{Eq. 2.5.4-15}$$

where, $\gamma$ = total unit weight, Vs = shear wave velocity, and g = acceleration of gravity.  The shear wave velocity data are given in Table 2.5-51.  The unit weight data are given in Table 2.5-53.  Strain compatible shear modulus values are estimated during the analysis using Eq. 2.5.4-15.

### 2.5.4.7.5    Acceleration Time History for Soil-Structure Interaction Analysis

A spectrum-compatible acceleration-time history was developed for use with the velocity profile described in Section 2.5.4.7.2.  This acceleration-time history was chosen based on the probabilistic seismic hazard deaggregation information described in Section 2.5.2.

The development of the single horizontal component spectrum-compatible time history is based on the mean $10^{-4}$ uniform hazard target spectrum described in Section 2.5.2.  The spectrum compatible time history was developed for the frequency range of 100 Hz to 0.5 Hz.

Using the site-specific soil column extended to the ground surface and the amplification factor, and the performance-based hazard methodology utilized to develop the SSE (refer to Sections 2.5.2.5 and 2.5.2.6), a zero depth peak ground acceleration of 0.084g associated with a magnitude M5.5 earthquake was computed.  These parameters apply to analysis of liquefaction and seismic stability of the soils.

For reconciliation of site specific design parameters affecting the SSE analysis results, refer to Sections 3.7.1 and 3.7.2.}

### 2.5.4.8    Liquefaction Potential

The U.S. EPR FSAR includes the following COL Item in Section 2.5.4.8:

The COL applicant will address site-specific liquefaction potential.  As stated in Section 2.5.2, the evaluation of liquefaction is performed for the seismic level of the site specific SSE.

---

This COL Item is addressed as follows:

{The potential for soil liquefaction at the CCNPP Unit 3 site was evaluated following NRC Regulatory Guide 1.198 (NRC, 2003c).  The soil properties and profiles utilized are those described in Section 2.5.4.2.

Sections 2.5.4.8.1 through 2.5.4.8.6 are added as a supplement to the U.S. EPR FSAR.

### 2.5.4.8.1    Previous Liquefaction Studies

Two liquefaction studies are cited in the CCNPP Units 1 and 2 UFSAR (BGE, 1982), as follows. The same reference cites a horizontal ground acceleration of 0.08 g and a Richter magnitude of 4 to 5 for the OBE case, and a horizontal ground acceleration of 0.15 g and a Richter magnitude of 5 to 5.5 for the SSE case.

### 2.5.4.8.1.1    Liquefaction Potential of Units 1 and 2

CCNPP Units 1 and 2 UFSAR (BGE, 1982) reports that the liquefaction potential at the site was evaluated using data from standard penetration test borings, laboratory test results, in-place density determinations, and geologic origin of the site soils.  The results showed that the site soils did not possess the potential to liquefy.  Quantitative values for the factor of safety against liquefaction were not given.

### 2.5.4.8.1.2    Liquefaction Potential of Diesel Generator Building

CCNPP Units 1 and 2 UFSAR (BGE, 1982) also reports on results of a liquefaction study for the siting of the Diesel Generator Building in the North Parking area as a part of CCNPP Units 1 and 2 development.  This liquefaction evaluation was performed on data from standard penetration test borings, resulting in computed factors of safety from 1.3 to 2.4, with a median value of 1.8.  On this basis, it was determined that the site of the Diesel Generator Building had adequate factor of safety against liquefaction (Bechtel, 1992).

### 2.5.4.8.2    Soil and Seismic Conditions for CCNPP Unit 3 Liquefaction Analysis

Preliminary assessments of liquefaction for the CCNPP Unit 3 soils were based on observations and conclusions contained within CCNPP Units 1 and 2 UFSAR (BGE, 1982).  The site soils that were investigated for the design and construction of CCNPP Units 1 and 2 did not possess the potential to liquefy.  Given the relative uniformity in geologic conditions between existing and planned units, the soils at CCNPP Unit 3 were preliminarily assessed as not being potentially liquefiable for similar ground motions, and were further evaluated for confirmation, as will be described later in this subsection.  Based on this assessment, it was determined that aerial photography as outlined in Regulatory Guide 1.198 (NRC, 2003c) would not add additional information to the planning and conduct of the subsurface investigation; therefore, was not conducted.

Given the relative uniformity in top and bottom elevations of various soil strata at the site, as indicated in the subsurface profiles in Figure 2.5-107 through Figure 2.5-111, a common stratigraphy was adopted for the purpose of establishing soil boundaries for liquefaction evaluation.  The adopted stratigraphy was that shown in Figure 2.5-108 for its location relative to Category I structures and including the deepest borings located on this profile.  Only soils in the upper 400 ft of the site were evaluated for liquefaction, based on available results from the CCNPP Unit 3 subsurface investigation.  Soils below a depth of 400 ft are considered geologically old and sufficiently consolidated.  These soils are not expected to liquefy, as will be further discussed in Section 2.5.4.8.4.

As described in Section 2.5.4.7.5, the resulting peak ground acceleration for the site was found to be 0.084g associated with a magnitude M5.5 earthquake. For conservatism, a peak ground acceleration of 0.125g and an earthquake magnitude of 6.0 were adopted and used for the liquefaction analysis.

### 2.5.4.8.3      Liquefaction Evaluation Methodology

Liquefaction is defined as the transformation of a granular material from a solid to a liquefied state as a consequence of increased pore water pressure and reduced effective stress (Youd, 2001). The prerequisite for soil liquefaction occurrence (or lack thereof) are the state of soil saturation, density, gradation and plasticity, and earthquake intensity. The present liquefaction analysis employs state-of-the-art methods provided in Youd (Youd, 2001) for evaluating the liquefaction potential of soils at the CCNPP Unit 3 site. Given the adequacy of these methods in assessing liquefaction of the site soils, and the resulting factors of safety which will be discussed later in this subsection, probabilistic methods were not used.

In brief, the present state-of-the-art method considers evaluation of data from SPT, Vs, and CPT data. Initially, a measure of stress imparted to the soils by the ground motion is calculated, referred to as the cyclic stress ratio (CSR). Then, a measure of resistance of soils to the ground motion is calculated, referred to as the cyclic resistance ratio (CRR). And finally, a factor of safety (FOS) against liquefaction is calculated as a ratio of cyclic resistance ratio and cyclic stress ratio. Details of the liquefaction methodology and the relationships for calculating CSR, CRR, FOS, and other intermediate parameters such as the stress reduction coefficient, magnitude scaling factor, accounting for non-linearity in stress increase, and a host of other correction factors, can be found in Youd (Youd, 2001). A magnitude scaling factor (MSF) of 1.97 was used in the calculations based on the adopted earthquake magnitude and guidelines in Youd (Youd, 2001). Below are examples of liquefaction resistance calculations using the available SPT, Vs, and CPT data in the powerblock area of CCNPP Unit 3 and the adjoining CLA1 area. Calculations were performed mainly using spreadsheets, supported by spot hand-calculations for verification.

### 2.5.4.8.3.1      FOS Against Liquefaction Based on SPT Data

The equivalent clean-sand $CRR_{7.5}$ value, based on SPT measurements, was calculated following recommendations in Youd (Youd, 2001), based on corrected SPT N-values $(N_1)_{60}$, as recommended in Youd (Youd, 2001), including corrections based on hammer-rod combination energy measurements at the site. It is noted that soils at CCNPP site include $(N_1)_{60}$30; Youd (Youd, 2001) indicates that clean granular soils with $(N_1)_{60}$30 are considered too dense to liquefy and are classified as non-liquefiable. Similarly, corrections were made for the soils fines contents, based on average fines contents provided in Table 2.5-36 and the procedure recommended in Youd (Youd, 2001).

The collected raw (uncorrected) SPT N-values are shown in Figure 2.5-148. SPT data from 41 borings located in Unit 3 power block area and in CLA1 are shown in thisFigure and were used for the liquefaction FOS calculations, or over 2,000 SPT N-value data points. An example of a FOS calculation for a SPT N-value = 8 from Boring B-330 at elevation 25.5 ft was hand-calculated for verification and found to conform to the spreadsheet calculations. The SPT value for this sample calculation is identified in Figure 2.5-148.

For completeness, all data points, including data for clay soils and data above the ground water level, were included in the FOS calculation, despite their known high resistance to liquefaction. The SPT N-values shown in Figure 2.5-148 were mostly taken at 5-ft intervals. SPT in the deepest borings (B-301 and B-401) extended to about 400 ft below the ground surface. The calculated FOS associated with each of the SPT values in Figure 2.5-148 is shown in

Figure 2.5-149.  Also, the FOS = 2.25 hand calculated for the SPT value in Boring B-330 at elevation 25.5 ft is shown. Figure 2.5-149 additionally shows a demarcation line for FOS = 1.1 (FOS = 1.1 is discussed at the end of this subsection).

Of the over 2,000 SPT N-value data points for which FOS values were calculated, all but 7 points resulted in FOS>1.1.  The 7 points with FOS<1.1 amount to less than 0.5 percent of all the data points evaluated; in other words, over 99.5 percent of the calculated FOS values exceeded 1.1. The FOS<1.1 are highlighted within a "dotted" inset in Figure 2.5-149 and are re-plotted for clarity to a higher scale in Figure 2.5-150. They range from 0.80 to 1.09.  An examination of each FOS is as follows.

| Boring | Ground Elevation (ft) | El of FOS < 1.1 | Value of FOS < 1.1 | Overlying Structure | Structure BOF Elevation (ft) | Disposition of Soils in the Area with FOS < 1.1 | |
|--------|------------|-----------|----------|------------|-----------|------------------------------|---|
| B-305 | 72.0 | 63.0 | 0.93 | Safeguard Bldg. | 43.6 | Soils will be removed to elevation 38± ft during excavation for Safeguard Bldg. | c) |
| B-314 | 52.8 | 50.9 | 0.80 | RadWaste Bldg. | 47.1 | Soils will be removed to at least elevation 47± ft during excavation for RadWaste Bldg | c) |
| B-331 | 68.3 | 66.1 | 0.94 | Turbine Bldg. | 45.0 | Soils will be removed to at least elevation 45 ft during excavation for Turbine Bldg. foundation | c) |
| B-404 | 67.9 | 27.9 | 0.82 | CLA1 | N.A. | No structures planned | |
| B-419 | 55.3 | 53.1, 48.8 & 30.3 | 1.06, 0.81 & 1.09 | CLA1 | N.A. | No structures planned | |

For c), see comments below.          N.A. = Not Applicable

From the above list, it is noted that all soils indicating FOS<1.1 are either at elevations that will eventually be lowered during construction which would result in the removal of these soils (as indicated by c), or are at locations where no structures are planned. Hence, the low FOSs should not be a concern for these samples.

### 2.5.4.8.3.2    FOS Against Liquefaction Based on Vs Data

Similar to the FOS calculations for the SPT values, equivalent clean-sand $CRR_{7.5}$ values, based on Vs measurements, were calculated following recommendations in Youd (Youd, 2001).  Similarly, corrections were made for the soils fines contents, based on average fines contents provided in Table 2.5-36 and the procedure recommended in ASCE (ASCE, 2000).  It is noted that soils at CCNPP site include soils with normalized shear wave velocity ($V_{s1}$) exceeding a value of 215 m/sec.  Clean granular soils with $V_{s1} \geq 15$ m/sec are considered too dense to liquefy and are classified as non-liquefiable (Youd, 2001).  The limiting upper value of $V_{s1}$ for liquefaction resistance is referred to as $V_{s1}^*$; the latter varies with fines content and is 215 m/sec and 200 m/sec for fines contents of $\leq 5$ percent and $\geq 35$ percent, respectively.  As such, when values of $V_{s1} \geq V_{s1}^*$, the soils were considered too dense to liquefy, and therefore, the maximum CRR value of 0.5 was used in the FOS calculations.

Shear wave velocity data from the P-S logging measurements were used for the FOS calculations.  The collected raw (uncorrected) $V_s$ data are shown in Figure 2.5-151, which is from all the 10 suspension P-S velocity logging boreholes in CCNPP Unit 3 and in CLA1 areas. Suspension P-S velocity logging measurements were made at 0.5-m intervals (~1.6-ft).  The two

deepest measurements (at borings B-301 and B-401) extended to about 400 ft below the ground surface.  Approximately 1,400 Vs data points were used for the FOS calculations.  An example of a FOS calculation for Vs = 590 ft/sec from Boring B-423 at elevation 80.6 ft was hand-calculated for confirmation.  This Vs value is identified in Figure 2.5-151.

For completeness, all data points, including data for clay soils, were included in the calculation, despite their known high resistance to liquefaction.  The calculated FOS associated with each of the Vs values shown in Figure 2.5-151 is shown in Figure 2.5-152.  Also, the FOS = 2.2 hand calculated for the Vs value in Boring B-423 at elevation 80.6 ft is shown. Figure 2.5-152 additionally shows a demarcation line for FOS = 1.1.

The results show that all calculated FOSs exceeded 1.1; almost all are at least 4.0, with a few scattered values at about 2.0.  The high calculated FOS values are the result of $V_{s1}$ values typically exceeding the limiting $V_{s1}^*$ values, indicating no potential for liquefaction, and therefore, a maximum CRR = 0.5 was used in the calculations.  The effect of CRR = 0.5, as applicable to $V_{s1} \geq V_{s1}^*$ cases, is observed in the rather consistent FOS values shown in Figure 2.5-152.

### 2.5.4.8.3.3    FOS Against Liquefaction Based on CPT Data

The CPT testing at the CCNPP Unit 3 site included the measurement of both commonly measured cone parameters (tip resistance, friction, and pore pressure) and shear wave velocity.  The evaluation of liquefaction based on both the commonly measured parameters and shear wave velocity is addressed herein.  The CCNPP Unit 3 site CPT data was reviewed and correlated with the applicable SPT data and compared with guidelines in Robertson (Robertson, 1988).  As discussed in subsections 2.5.4.2.1.1 through 2.5.4.2.1.3, this review process verified the CPT data by correlation to the CCNPP Unit 3 site-determined SPT values and data published for relevant soil parameters.

The equivalent clean-sand CRR7.5 value, based on CPT tip measurements, was calculated following recommendations in Youd (Youd, 2001), based on normalized clean sand cone penetration resistance (qc1N)cs and other parameters such as the soil behavior type index, Ic.

Cone tip resistance values, $q_c$, from all 27 CPT soundings in CCNPP Unit 3 powerblock and CLA1 areas are shown in Figure 2.5-153 and Figure 2.5-154.  The CPT soundings encountered repeated refusal in the cemented sand layer, and could only be advanced deeper after pre-drilling through these soils, indicative of their high level of resistance to liquefaction.  The deepest CPT sounding (C-407) penetrated 142 ft below the ground surface, encountering refusal at that depth, terminating at approximately elevation -80 ft.  Tip resistance measurements were made at 5-cm intervals (~2-in).  Approximately 5,200 tip resistance measurements were made in the soundings in CCNPP Unit 3 powerblock and CLA1 areas, and were used for the FOS calculations.  An example of a FOS calculation for a tip resistance value of 36.8 tsf in C-408 at elevation 76.4 ft was hand-calculated for confirmation.  This value is identified in Figure 2.5-154.

For completeness, all data points, including data for clay soils, were included in the calculation, despite their known high resistance to liquefaction.  The calculated FOS associated with each of the tip resistance values shown in Figure 2.5-154 are shown in Figure 2.5-155.  Also, the FOS = 1.52 hand-calculated for the tip resistance value of 36.8 tsf in CPT C-408 at elevation 76.4 ft is shown. Figure 2.5-155 additionally shows a demarcation line for FOS = 1.1.

Of the over 5,000 data points for which FOSs were calculated, about 100 points indicated FOS<1.1, or approximately 2 percent; in other words, 98 percent of the data points resulted in

FOS>1.1.  The points with FOS<1.1 are highlighted within a "dotted' inset on Figure 2.5-155 and are re-plotted for clarity to a higher scale in Figure 2.5-156.  An examination of each of these FOSs is as follows.

| Boring | Ground Elevation (ft) | El range of FOS<1.1 | Range of FOS<1.1 | Overlying Structure | Structure BOF Elevation (ft) | Disposition of Soils in the Area with FOS<1.1 | |
|---|---|---|---|---|---|---|---|
| C-304 | 60.9 | 60.1 – 60.0 | 0.93–1.04 | Emergency Power Generating Bldg. | 78.6 | Soils will be removed to elevation 40± ft* in excavation for Emergency Power Generating Building. | c) |
| C-308 | 84.3 | 61.4 | 1.03 | ESWS Cooling Towers | 62.6 | Soils will be removed to elevation 38± ft* in excavation for ESWS Cooling Towers | c) |
| C-314 | 80.1 | 78.1 – 64.7 | 0.82–1.08 | Transformers | N.K. | Soils will be removed to elevation 45± ft in excavation for Turbine Bldg. | c) |
| C-311 | 73.9 | 72.8– 70.5 | 1.05 | Turbine Bldg. | 45.0 | Soils will be removed to elevation 45 ft* in excavation for Turbine Bldg. foundations | c) |
| C-313 | 79.9 | 78.8 – 67.5 | 1.05–1.07 | Transformers | N.K. | Soils will be removed to elevation 65± ft in excavation for Turbine Bldg. | c) |
| C-402 | 73.1 | 72.5 – 70.8 | 0.81–1.05 | CLA1 | N.A. | No structures planned | |
| C-406 | 43.9 | 41.9 – 29.0 | 0.72–1.08 | CLA1 | N.A. | No structures planned | |

For c) and *  see comments below.      N.K. = Not Known      N.A. = Not Applicable

From the above list, it is noted that all soils that indicated FOS<1.1 are either within elevations that will eventually be lowered during construction which will result in the removal of these soils (as indicated by c) or are at locations where no structures are planned.  Excavation for the Emergency Power Generating Building, the ESWS Cooling Towers, and the Turbine Building (as indicated by *) will extend to the noted elevations for deriving support for their foundations from the Chesapeake Cemented Sand.  Nevertheless, it is noted that the CPT-based CRR relationship was intended to be conservative, not necessarily to encompass every data point; therefore, the presence of a few data points beyond the CRR base curve is acceptable (Youd, 2001).

Shear wave velocity measurements were made in 7 of the CPT soundings in Unit 3 and CLA1 areas at the locations shown in Figure 2.5-104.  As noted earlier, the CPT soundings encountered repeated refusal in the cemented sand layer, and they could only be advanced deeper after pre-drilling through these soils.  Shear wave velocity measurements from the seismic cone were compared to similar measurements using the P-S logging method.  The average results are shown in Figure 2.5-128.  By observation, the two independent measurements are comparable.  Given that Vs data from the suspension P-S velocity logging method resulted in high values of FOS against liquefaction, as described in this subsection, similar results are expected from the seismic CPT data, and therefore, separate calculations were not made for the CPT Vs results.

### 2.5.4.8.4    Liquefaction Resistance of Soils Deeper Than 400 Feet

Liquefaction evaluation of soils at the CCNPP Unit 3 site was focused on soils in the upper 400 ft.  The site soils, however, are much deeper, extending to approximately 2,500 ft below the ground surface.  Geologic information on soils below a depth of 400 ft was gathered from the available literature, indicating that these soils are from about 50 to over 100 million years old, as shown in Figure 2.5-136.  Liquefaction resistance increases markedly with geologic age, therefore, the deeper soils are geologically too old to be prone to liquefaction.  Additionally, their compactness and strength are only anticipated to increase with depth, compared with the overlying soils.  The Pleistocene soils have more resistance than Recent or Holocene soils and pre-Pleistocene sediments are generally immune to liquefaction (Youd, 2001).  Additionally, liquefaction analyses using shear wave velocity values of about 2,000 ft/sec near the 400-ft depth did not indicate any potential liquefaction at that depth, with the FOSs exceeding 4.0.  With shear wave velocities increasing below the 400-ft depth, in the range of about 2,200 ft/sec to 2,800 ft/sec as indicated in Figure 2.5-141, high resistance to liquefaction would be expected from these deeper soils.  On this basis, liquefaction of soils at the CCNPP Unit 3 site below a depth of 400 ft is not considered possible.

### 2.5.4.8.5    Concluding Remarks

A liquefaction analysis was performed using procedures outlined in Youd (Youd, 2001).  Over 2,000 SPT data points were analyzed from 41 test borings, from which 99.5 percent of the calculated FOSs exceeded 1.1.  Over 1,400 Vs data points from 10 suspension P-S velocity logging boreholes were analyzed; the calculated FOS for the overwhelming majority exceeded 4.0, with few values in the 2.0 range.  All values exceeded 1.1.  Finally, over 5,000 CPT data points from CPT soundings were evaluated.  Approximately 98 percent of the calculated FOSs exceeded 1.1.  An examination of the remaining 2 percent with FOS<1.1 revealed that the affected soils will either be removed during construction or are at locations where no structures are planned.

It is evident, from the collective results, that soils at the CCNPP Unit 3 site are so consolidated, geologically old, and sometimes even cemented that they are not susceptible to liquefaction due to acceleration levels from the anticipated earthquakes.  A very limited portion of the data at isolated locations indicated potentially liquefiable soils, however, this indication cannot be supported by the overwhelming percentage of the data that represent these soils.  Moreover, the state-of-the-art methodology used for the liquefaction evaluation was intended to be conservative, not necessarily to encompass every data point; therefore, the presence of a few data points beyond the CRR base curve is acceptable (Youd, 2001).  Additionally, in the liquefaction evaluation, the effects of age, overconsolidation, and cementation were ignored, which tend to increase resistance to liquefaction.  Finally, the earthquake acceleration and magnitude levels adopted for the liquefaction analysis are conservative.  More importantly, there is no documented liquefaction case for soils in the State of Maryland (USGS, 2000).  Therefore, liquefaction should not be a concern.  A similar conclusion was arrived at for the original CCNPP Units 1 and 2 (BGE, 1982).

A significant level of site grading is anticipated at the CCNPP Unit 3 site during construction.  This primarily results in the removal of geologically younger materials (the upper soils) from the higher elevations, and the placement of dense compacted fill in lower elevations, further improving the liquefaction resistance of soils at the site.

It is noted that limited man-made fill may be present at the CCNPP Unit 3 site at isolated locations.  These soils will be removed during construction, further improving the liquefaction resistance of soils at the site.

### 2.5.4.8.6     Regulatory Guide 1.198

Before and during the foregoing evaluation, guidance contained in NRC Regulatory Guide 1.198 (NRC, 2003c) was used.  The liquefaction evaluation conforms closely to the NRC Regulatory Guide 1.198 guidelines.

Under "Screening Techniques for Evaluation of Liquefaction Potential," NRC Regulatory Guide 1.198 (NRC, 2003c) lists the most commonly observed liquefiable soils as fluvial-alluvial deposits, eolian sands and silts, beach sands, reclaimed land, and uncompacted hydraulic fills.  The geology at the CCNPP site includes fluvial soils and man-made fill at isolated locations.  The liquefaction evaluation included all soils at the CCNPP site.  The man-made fill, which is suspected only at isolated locations, will be removed during the site grading operations.  In the same section, NRC Regulatory Guide 1.198 (NRC, 2003c) indicates that clay to silt, silty clay to clayey sand, or silty gravel to clayey gravel soils can be considered potentially liquefiable.  This calculation treated all soils at the CCNPP Unit 3 site as potentially liquefiable, including the fine-grained soils.  The finer-grained soils at the CCNPP Unit 3 site contain large percentages of fines and/or are plastic and are, therefore, considered non-liquefiable, as also indicated by the calculated FOSs for these soils.  In fact, all soils at the CCNPP Unit 3 site contain some percentage of fines and exhibit some plasticity, which tends to increase their liquefaction resistance.  The same section of NRC Regulatory Guide 1.198 (NRC, 2003c) confirms that potentially liquefiable soils that are currently above the ground water table, are above the historic high ground water table, and cannot reasonably be expected to become saturated, pose no potential liquefaction hazard.  In the liquefaction analyses, the ground water level was taken at elevation 80 ft.  This water level may be a "perched" condition, situated above Stratum IIa Chesapeake Clay/Silt, with the actual ground water level near the bottom of the same stratum in the Chesapeake Cemented Sand, or at about an average elevation 39 ft.  Despite the adopted higher ground water level (a higher piezometric head of more than 40 ft), the calculated FOS overwhelmingly exceeded 1.1.  The site historic ground water level is not known, however, it is postulated that the ground water level at the site has experienced some fluctuation due to pumping from wells in the area and climatic changes.  Ground Water levels at the site are not expected to rise in the future given the relief and topography of the site, promoting drainage.  Similarly, NRC Regulatory Guide 1.198 (NRC, 2003c) indicates that potentially liquefiable soils may not pose a liquefaction risk to the facility if they are insufficiently thick and of limited lateral extent.  At the CCNPP Unit 3 site, the soil layers are reasonably thick and uniformly extend across the site, except where they have been eroded, yet the FOSs overwhelmingly exceeded 1.1.  Soils identified as having FOS<1.1, regardless of the thickness, will be removed during grading operations or are located where no structures are planned.

Under "Factor of Safety Against Liquefaction," NRC Regulatory Guide 1.198 (NRC, 2003c) indicates that FOS≤1.1 is considered low, FOS≈1.1 to 1.4 is considered moderate, and FOS ≥ 1.4 is considered high.  A FOS = 1.1 appears to be the lowest acceptable value.  On the same issue, the Committee on Earthquake Engineering of the National Research Council (CEE, 1985) states that "There is no general agreement on the appropriate margin (factor) of safety, primarily because the degree of conservatism thought desirable at this point depends upon the extent of the conservatism already introduced in assigning the design earthquake.  If the design earthquake ground motion is regarded as reasonable, a safety factor of 1.33 to 1.35 ... is suggested as adequate.  However, when the design ground motion is excessively conservative, engineers are content with a safety factor only slightly in excess of unity."  This, and a minimum FOS = 1.1 in NRC Regulatory Guide 1.198 (NRC, 2003c), are consistent with the FOS = 1.1 adopted for the assessment of FOSs for the CCNPP Unit 3 site soils, considering the conservatism adopted in ignoring the cementation, age, and overconsolidation of the deposits, as well as the seismic acceleration and magnitude levels.  Such level of conservatism in the

evaluation, in conjunction with ignoring the geologic factors discussed above, justifies the use of FOS = 1.1 for liquefaction assessment of the CCNPP site soils.}

### 2.5.4.9    Earthquake Site Characteristics

The U.S. EPR FSAR includes the following COL Item in Section 2.5.4.9:

Site-specific earthquake site characteristics will be described by the COL applicant.

This COL Item is addressed as follows:

{Section 2.5.2.6 describes the development of the horizontal Safe Shutdown Earthquake (SSE) ground motion for the CCNPP Unit 3 site.  The selected SSE ground motion is based on the risk-consistent/performance-based approach of NRC Regulatory Guide 1.208, "A Performance-Based Approach to Define the Site-Specific Earthquake Ground Motion" with reference to NUREG/CR-6728 and ASCE/SEI 43-05 (refer to Section 2.5.2.6 for references).  Any deviation from the guidance provided in Regulatory Guide 1.208 is discussed in Section 2.5.2. Horizontal ground motion amplification factors are developed in Section 2.5.2.5 using site-specific data and estimates of near-surface soil and rock properties presented in Section 2.5.4.  These amplification factors are then used to scale the hard rock spectra, presented in Section 2.5.2.4, to develop Uniform Hazard Spectra (UHS), accounting for site-specific conditions using Approach 2A of NUREG/CR-6769.  Horizontal SSE spectra are developed from these soil UHS, using the performance-based approach of ASCE/SEI 43-05, accepted by Regulatory Guide 1.208.  The SSE motion is defined at the free ground surface of a hypothetical outcrop at the base of the foundation.  Section 2.5.2.6 also describes vertical SSE ground motion, which was developed by scaling the horizontal SSE by a frequency-dependent vertical-to-horizontal (V:H) factor, presented in Section 2.5.2.6.}

### 2.5.4.10    Static Stability

{The area of planned Unit 3 is graded to establish the final site elevation, which is to be at about elevation 85 ft at the center of the unit.  The Reactor, Safeguard, and Fuel Buildings are seismic Category I structures and are supported on a common basemat.  The common basemat has an irregular shape, estimated to be approximately 64,400 square ft, or about 322 ft x 200 ft in plan dimensions if a rectangular configuration is considered.  All Category I structures' size and depth ranges are summarized below.

| Category I Structure | Estimated Foundation Elevation (ft) | Estimated Final Site Grade Elevation (ft) | Estimated Foundation Depth (ft)* | Estimated Footing Size (ft x ft) |
|---|---|---|---|---|
| Reactor | 44 | 85 | 41 | 322 x 200 |
| ESWS Cooling Towers | 63 | 81–82 | 18–19 | 147 x 96 |
| Emergency Power Generating Building | 79 | 82 | 3 | 131 x 93 |
| Ultimate Heat Sink Makeup Water Intake Structure | -25 | 10 | 35 | 78 x 47 |

* below respective final site grade

Structures locations and designations are shown in Figure 2.5-104.  Other major structures in the power block area include the Nuclear Auxiliary Building, Access Building, RadWaste Building, and the Turbine Building, which are not Category I structures.

Construction of the Reactor basemat requires an excavation of about 41 ft (from approximately elevation 85 ft). The resulting rebound (heave) in the ground due to the removal of the soils is expected to primarily take place in Stratum IIc Chesapeake Clay/Silt soils. A rebound of about 2 in is estimated due to excavation for the Reactor basemat, and is expected to take place concurrent with the excavation. Ground rebound is monitored during excavation. The heave estimate was made based on the elastic properties of the CCNPP site soils and the response to the unloading of the ground by about 41 ft of excavation. The magnitude and rate of ground heave is a function of, among other factors, excavation speed and duration that the excavation remains open. Other factors remaining unchanged, shorter durations culminate in smaller values of ground heave. The excavation shall remain open for a period sufficiently long such that ground heave fully develops.}

### 2.5.4.10.1    Bearing Capacity

The U.S. EPR FSAR includes the following COL Item in Section 2.5.4.10.1:

> A COL applicant that references the U.S. EPR design certification will verify that site-specific foundation soils beneath the foundation basemats of Seismic Category I structures have the capacity to support the bearing pressure with a factor of safety of 3.0 under static conditions.

This COL Item is addressed as follows:

{Sections 2.5.4.10.1.1 and 2.5.4.10.1.2 are added as a supplement to the U.S. EPR FSAR.

### 2.5.4.10.1.1    Bearing Condition of Units 1 and 2 Soils

CCNPP Units 1 and 1 UFSAR (BGE, 1982) provides an evaluation of the site soils for bearing purposes for CCNPP Units 1 and 2. It indicates that the upper (Pleistocene Age) soils are capable of supporting light loads, on the order of 2 to 3 kips per square foot (ksf) for a small amount of settlement. The lower (Miocene Age) soils are described as being capable of supporting heavy loads, on the order of 15 ksf to 20 ksf with slight consolidation.

The CCNPP Units 1 and 2 Turbine Building, Nuclear Auxiliary Building, Containments, Turbine Generators, and Circulating Water Systems are supported on mat foundations on the Miocene soils. Site grading prior to foundation construction resulted in significant ground unloading. The following is a summary of pertinent information (BGE, 1982).

| Structure | Contact Pressure (ksf) | Foundation Elevation (ft) | Average Ground Elevation (ft) | Average Excavation Unloading (ksf) |
|---|---|---|---|---|
| Nuclear Containment Structure Mat | 8 | -1 | 60 to 75 | 6.6 to 8.4 |
| Auxiliary Building Mat | 8 | -14 to -19 | 70 | 8.3 to 8.85 |
| Turbine Pedestal Mat | 5 | --- | --- | --- |
| Turbine Building Column Footings | 5 | -11 | 40 to 60 | 4.9 to 7.3 |
| Intake & Discharge Structure Mat | 2.5 | -27 to -30 | 20 to 80 | 4.05 to 10.8 |

It is also reported in CCNPP Units 1 and 1 UFSAR (BGE, 1982) that elastic expansion of the soils occurred as a result of the excavations, producing "slight upward movement." No magnitude, however, is given. Reference is also made to downward movement of the soils as the foundation load was applied, resulting in a "small" movement and "was complete when construction was completed." No magnitude, however, is given.

### 2.5.4.10.1.2    Bearing Capacity of CCNPP Unit 3 Structures

The ultimate (gross) bearing capacity of a footing, $q_{ult}$, supported on homogeneous soils can be estimated by (Vesic, 1975):

$$q_{ult} = cN_c\zeta_c + \gamma'D_fN_q\zeta_q + 0.5\gamma BN_\gamma\zeta_\gamma \qquad\qquad \text{Eq. 2.5.4-16}$$

where,  c = undrained shear strength for clay material ($c_u$) or cohesion intercept for (c, $\phi$) material,

$\gamma'D_f$ = effective overburden pressure at base of foundation,

$\gamma'$  = effective unit weight of soil,

$D_f$ = depth from ground surface to base of foundation,

B  = width of foundation,

$N_c$, $N_q$, and $N_\gamma$ are bearing capacity factors (defined in Vesic, 1975), and

$\zeta_c$, $\zeta_q$, and $\zeta_\gamma$ are shape factors (defined in Vesic, 1975).

The ultimate bearing capacity, $q_u$, of a footing supported on a strong sandy layer underlain by weaker soil (a 2-layer system) can be estimated by Meyerhof (Meyerhof, 1978):

$$q_u = q_b + \gamma_1H^2\left(1 + \frac{B}{L}\right)\left(1 + \frac{2D_f}{H}\right)\left(\frac{K_s\tan\phi_1}{B}\right) - \gamma_1H \le q_t \qquad \text{Eq. 2.5.4-17}$$

where, $q_b = c_2 N_{c2}\zeta_{c2} + \gamma_1(D_f + H)N_{q2}\zeta_{q2} + 0.5\gamma_2BN_{\gamma2}\zeta_{\gamma2}$          Eq. 2.5.4-18A

$q_t = c_1 N_{c1}\zeta_{c1} + \gamma_1D_fN_{q1}\zeta_{q1} + 0.5\gamma_1BN_{\gamma1}\zeta_{\gamma1}$               Eq. 2.5.4-18B

$K_s$ = punching shear coefficient, defined in Meyerhof (Meyerhof, 1978)

H = depth to the lower layer

The factors in Eqs. 2.5.4-18A and 2.5.4-18B, are defined as follows:

| Layer | Effective Unit Weight | Soil Friction | Shear Strength | Bearing Capacity Factors | Shape Factors |
|---|---|---|---|---|---|
| Top (strong layer) | $\gamma_1$ | $\phi_1$ | $c_1$ | $N_{c1}$, $N_{q1}$, $N_{\gamma1}$ | $\zeta_{c1}$, $\zeta_{q1}$, $\zeta_{\gamma1}$ |
| Bottom (weak layer) | $\gamma_2$ | $\phi_2$ | $c_2$ | $N_{c2}$, $N_{q2}$, $N_{\gamma2}$ | $\zeta_{c2}$, $\zeta_{q2}$, $\zeta_{\gamma2}$ |

For each of the Category I structures under consideration, the bearing capacity of the foundations was estimated using two methods, i.e., (1) considering a layered system (Meyerhof, 1978), assuming a strong layer (Stratum IIb Chesapeake Cemented Sand) over a "weak" layer (Stratum IIc Chesapeake Clay/Silt), and (2) considering homogenous soils (Vesic, 1975), assuming Stratum IIc Chesapeake Clay/Silt soils are present under the foundation in entirety. This assumption provides a lower-bound estimate of the bearing capacity.

It is noted that the Reactor, Safeguard, and Fuel Buildings, which are on a common basemat, will essentially derive support from Stratum IIb Chesapeake Cemented Sand. All other structures, except the Ultimate Heat Sink Makeup Water Intake Structure, are supported on compacted structural fill resting on Stratum IIb Chesapeake Cemented Sand.  The Ultimate Heat Sink Makeup Water Intake Structure derives support from Stratum IIc Chesapeake Clay/Silt

soils.  No Category I structure is supported on Stratum I Terrace Sand or Stratum IIa Chesapeake Clay/Silt.

The subsurface conditions and material properties were described in Section 2.5.4.2.  Material properties, conservatively designated for the various strata, were used for foundation evaluation, as shown in Table 2.5-36.  The specific parameter values used in the bearing capacity evaluations are provided in Table 2.5-54.  The following bounding property values for compacted fill were used in the analyses: a unit weight of 120 pcf, an angle of internal friction of 32 degrees, and a modulus of elasticity of 500 tsf. Compacted fill is verified to meet the design requirements during construction. Location of structures, relative to the subsurface conditions, are shown in Figure 2.5-130 through Figure 2.5-134.  An average ground water level at elevation 80 ft was used for foundation evaluation.  For the case of the UHS Makeup Water Intake Structure where the ground surface was below elevation 80 ft, the ground water elevation was considered to be at the ground surface.

A summary of the estimated allowable bearing pressures, using both the layered and the homogeneous soils assumptions, including recommended values, are as follows.  A factor of safety of 3.0 was applied to obtain the allowable values.

| Category I Structure | Allowable Bearing Pressure (Layered System) (ksf) | Lower-Bound Allowable Bearing Pressure (ksf) | Recommended Max. Bearing Pressure (ksf) |
|---|---|---|---|
| Essential Service Water System (ESWS) Cooling Tower (Ultimate Heat Sink) | 13 - 14 | 8.0 | 13 |
| Emergency Power Generating Building (EDGB) | 14 - 15 | 7.8 | 13 |
| Common Basemat | 24 | 8.3 | 22 |
| Ultimate Heat Sink Makeup Water Intake Structure | --- | 8.0 | 8 |

Design values of foundation pressures for the Category I structures were estimated based on project knowledge and typical loading for similar structures.  The design values were adopted for comparison with the allowable values above and are as follows.

| | |
|---|---|
| ESWS Cooling Tower (Ultimate Heat Sink) | 7 |
| EDGB | 5 |
| Common Basemat | 15 |
| Ultimate Heat Sink Makeup Water Intake Structure | 6 |

The recommended maximum bearing pressures exceed the estimated design foundation pressures.  Traditionally, a factor of safety of 3.0 has been found acceptable for foundation design, although lower factors of safety (1.7 to 2.5) have been suggested for mat foundations (Bowles, 1996).  A factor of safety of 3.0 was used in the bearing capacity evaluations.  A comparison of the recommended maximum bearing pressures with the estimated foundation pressures suggest that the final factor of safety is even higher than 3.0.  Additionally, the recommended bearing pressures are comparable with estimates of bearing capacity identified in the CCNPP Units 1 and 2 UFSAR (BGE, 1982); the notable difference is between the estimate of design foundation pressure of 15 ksf for the Common Basemat and the "contact pressure" of 8 ksf for the Containment Structure Mat of CCNPP Units 1 and 2.

Table 5.0-1 of the U.S. EPR FSAR identifies the soil bearing capacity as a required parameter to be enveloped, defined as "Minimum bearing capacity (static) 22 ksf in localized areas at the

bottom of the Nuclear Island basemat and 15 ksf on average across the total area of the bottom of the Nuclear Island basemat."

For static loading conditions, and based on a factor of safety of 3.0, the calculated allowable bearing pressure for the NI basemat is 24 ksf (as shown above).  On this basis, the available bearing capacity for the actual site specific condition meets the minimum 22 ksf and the average 15 ksf values identified in the U.S. EPR FSAR.}

### 2.5.4.10.2    Settlement

The U.S. EPR FSAR includes the following COL Item in Section 2.5.4.10.2:

> A COL applicant that references the U.S. EPR design certification will verify that the differential settlement value of ½ inch per 50 ft in any direction across the foundation basemat of a Seismic Category I structure is not exceeded.  Settlement values larger than this may be demonstrated acceptable by performing additional site specific evaluations.

This COL Item is addressed as follows:

{This COL Item is addressed in the following section {and in Section 3.8.5.}

{The pseudo-elastic method of analysis was used for settlement estimates.  This approach is suitable for the overconsolidated soils at the site.  The analysis is based on a stress-strain model that computes settlement of discrete layers:

$$\delta = \Sigma(\Delta p_i \times \Delta h_i)/E_i \qquad\qquad \text{Eq. 2.5.4-19}$$

where,

$\delta$ = settlement

$i$ = 1 to n, where n is the number of soil layers

$p_i$ = vertical applied pressure at center of layer i

$h_i$ = thickness of layer i

$E_i$ = elastic modulus of layer i

The stress distribution below the rectangular foundations is based on a Boussinesq-type distribution for flexible foundations (Poulos, 1974).  The computation extends to a depth where the increase in vertical stress ($\Delta p$) due to the applied load is equal to or less than 10 percent of the applied foundation pressure.  The Boussinesq-type vertical pressure under a rectangular footing, $\sigma_z$, is as follows (Poulos, 1974):

$$\sigma_z = (p/2\pi)(\tan^{-1}(lb/(zR_3)) + (lbz/R_3)(1/R_1^2 + 1/R_2^2)) \qquad\qquad \text{Eq. 2.5.4-20}$$

where,

$l$ = length of footing

$b$ = width of footing

$z$ = depth below footing at which pressure is computed

$R_1 = (l^2 + z^2)^{0.5}$

$R_2 = (b^2 + z^2)^{0.5}$

$R_3 = (l^2 + b^2 + z^2)^{0.5}$

Settlement estimates were made following the preceding relationships and using available soils properties given in Table 2.5-36.  To estimate settlement values, a subsurface profile in the foundation area of interest was adopted, as shown in Figure 2.5-130 through Figure 2.5-134.  The soil layers were further subdivided into sublayers for refined estimates.  From the stress distribution in Eq. 2.5.4-20, sublayer thickness, and elastic modulus for the particular soil, values for settlement were estimated using Eq. 2.5.4-19.  The final settlement is the sum of the estimated values for all of the sublayers combined.  Significant to estimating settlement values is the value of elastic modulus, E.  This parameter was selected from the available summary of soil engineering properties, as shown in Table 2.5-36, complimented with estimates of elastic moduli, reduced for strain magnitude, based on the average shear wave velocity values shown in Table 2.5-36.  Settlement estimates were made for all Category I structures, for the estimated design foundation pressures given in this subsection.  They are as follows.

| Category I Structure | Est. Design Foundation Pressure (ksf) | Est. Foundation Settlement (in.) | | |
|---|---|---|---|---|
| | | Center | Edge | Average |
| ESWS Cooling Tower (Ultimate Heat Sink) | 7 | 5 | 3 | 4 |
| EDGB | 5 | 4 | 2 | 3 |
| Common Basemat | 15 | 10 | 6 | 8 |
| Ultimate Heat Sink Makeup Water Intake Structure | 6 | 2 | 1 | 1.5 |

The settlement magnitudes are discussed later.

The planned site grading results in removing as much as 23 ft of soil from the area of the Emergency Power Generating Building-South (1UBP and 2UBP, shown in Figure 2.5-104) and in adding as much as 17 ft of fill to the Emergency Power Generating Building-North (3 UBP and 4 UBP shown in Figure 2.5-104).  Additionally, foundations rest as much as 3 ft to 41 ft below the final site grade for the Emergency Power Generating Building and the Common Basemat, respectively, resulting in further changes in the net foundation loading.  Net foundation pressures were estimated, based on available grading information, as follows.

| Category I Structure[1] | Average Existing Site Grade Elevation (ft) | Final Grade Elevation (ft) | Foundation Elevation (ft) | Est. Design Foundation Pressure (ksf) | Est. Net Foundation Pressure (ksf) |
|---|---|---|---|---|---|
| ESWS Cooling Tower North(URB3&4) | 60 - 95 (80) | 81 | 63 | 7 | 6 |
| ESWS Cooling Tower-South(URB1&2) | 90 - 120 (100) | 82 | 63 | 7 | 4 |
| EDGB-North(UBP3&4) | 55 - 70 (65) | 82 | 79 | 5 | 7 |
| EDGB-South(UBP1&2) | 105 – 115 (105) | 82 | 79 | 5 | 2 |
| Common Basemat | 70 – 110 (90) | 85 | 44 | 15 | 11 |
| Ultimate Heat Sink Makeup Water Intake Str. | 10 (10) | 10 | -25 | 6 | 4 |

(1) Refer to Figure 2.5-104 for locations

Estimated settlements corresponding to the net foundation pressures are given below. It is noted, however, that the magnitude of estimated settlements are generally not significantly changed, given the typically small change in foundation pressures.

| Category I Structure | Est. Net Foundation Pressure (ksf) | Est. Foundation Settlement (in) | | |
|---|---|---|---|---|
| | | Center | Edge | Average |
| ESWS Cooling Tower-North | 6 | 5 | 3 | 4 |
| ESWS Cooling Tower-South | 4 | 3 | 2 | 2 |
| EDGB-North | 7 | 5 | 3 | 4 |
| EDGB-South | 2 | 2 | 1 | 1 |
| Common Basemat | 11 | 7 | 5 | 6 |
| Ultimate Heat Sink Makeup Water Intake Structure. | 4 | 1 | 1 | 1 |

The average total settlement estimates above are in the range of about 1 to 4 in except for the Common Basemat which is about 6 in for the 11 ksf loading case and about 8 in for the 15 ksf loading case. The maximum total settlement (at center of common basemat) is estimated to be about 10 in resulting from the 15 ksf loading. Generally acceptable total and differential settlements for mat foundations supported on clays are typically in the range of 2.5 in and 1.5 in, respectively, although tolerable total settlements as high as 4 in have been suggested for mat foundations (Bowles, 1966). Higher total settlements are accommodated by delaying critical connections to adjacent structures, utilities, and pavements until as late in the construction schedule as practicable. Differential settlement, however, is more critical than total settlement. Acceptable tilt for foundations is on the order of 1/300 (Bowles, 1966), although values as low as 1/750 have been stated for foundations that support machinery sensitive to settlement (Das, 1990).

From the above estimates, average foundation settlement for the Ultimate Heat Sink Makeup Water Intake Structure is within the acceptable range of 2.5 in to 4 in  Similarly average settlement estimates for the Emergency Power Generating Building and the ESWS Cooling Towers are within the acceptable range of 2.5 in to 4 in  For the Common Basemat, an average settlement of about 8 in was estimated for the 15 ksf loading. This estimated total settlement is largely the result of the extreme foundation size and loading as well as the depth of influence of the large mat.

Differential settlements were estimated as the difference in settlement values at the center and edge of foundations. The estimated values are as follows: 1 in to 2 in for the ESWS Cooling Towers, 1 in to 2 in for the Emergency Power Generating Building, 2 in to 4 in for the Common Basemat, and practically zero for the Ultimate Heat Sink Makeup Water Intake Structure. From these values, tilt was estimated at about 1/600 for the ESWS Cooling Towers, 1/550 for the EDGB, and in the range of 1/600 to 1/1,200 for the Common Basemat foundations. Estimates of tilt for all structures, including the Common Basemat, are well within the acceptable limit of 1/300, however, they exceed the 1/750 for the special case of sensitive machinery, although the difference is not substantial. It is noted that the tabulated settlement estimates are based on the assumption of a flexible foundation; they do not take into account the effects of a thick, highly reinforced foundation mat which tends to mitigate differential settlements.

Foundation settlements largely take place concurrent with construction; therefore, a majority (i.e., more than half) of the settlements will have taken place prior to placing the equipment, piping, and the final finishes. Hence, post-construction total and differential settlements are expected to be lower than the values noted herein, particularly after accounting for foundation mat rigidity.

To verify that foundations perform according to estimates, and to provide an ability to make corrections, if needed, major structure foundations are monitored for rate of movement during and after construction.

In general, the estimated foundation settlements are larger than those indicated for CCNPP Units 1 and 2, although no estimates or measured values are available for Units 1 and 2, as discussed in Section 2.5.4.10.1. The difference in settlement between the two areas is not due to differing soil conditions, as the soils are comparable. Rather, they are largely due to the difference in magnitude of net loading imposed by these structures on the soils, and foundation size. The influence of the larger and heavier Common base mat for Unit 3 extends deeper, thereby influencing a larger volume of soils.

However, all foundations are designed to safely tolerate the anticipated total and differential settlements. Additionally, engineering measures are incorporated into design for control of differential movements between adjacent structures, piping, and appurtenances sensitive to movement, consistent with settlement estimates. This includes the development and implementation of a monitoring plan that supplies and requires evaluation of information throughout construction and post-construction on ground heave, settlement, pore water pressure, foundation pressure, building tilt, and other necessary data. This information provides a basis for comparison with design conditions and for projections of future performance.

These estimated differential settlements, except for those associated with the Ultimate Heat Sink Makeup Water Intake Structure represent departures from the U.S. EPR FSAR requirements. Additional discussion of the acceptability of these estimated differential settlements is provided in Section 3.8.5.

Sections 2.5.4.10.2.1 through 2.5.4.10.2.2 are added as a supplement to the U.S. EPR FSAR.

### 2.5.4.10.2.1    Earth Pressures

Static and seismic lateral earth pressures are addressed for plant below-ground walls. Seismic earth pressure diagrams are structure-specific and are, therefore, only addressed generically herein. Specific earth pressure diagrams are developed for specific structures based upon each structure's final configuration. Passive earth pressures are not addressed; they are ignored for conservatism for general purpose applications. The following soil properties were assumed for the backfill; an angle of shearing resistance of 30 degrees and a total unit weight of 120 pcf. Structural backfill material is verified to meet the design requirements prior to use during construction. A surcharge pressure of 500 psf was assumed as well. The validity of this assumption will be confirmed during detailed design. Lateral pressures due to compaction are not included; these pressures are controlled by compacting backfill with light equipment near structures.

Earthquake-induced horizontal ground accelerations are addressed by the application of $k_h \cdot g$. Vertical ground accelerations ($k_v \cdot g$) are considered negligible and were ignored (Lambe, 1969). A seismic acceleration of 0.125g was adopted for developing the generic earth pressure diagrams. Backgrounds on seismic accelerations are discussed in Section 2.5.4.8.2.

### 2.5.4.10.2.1.1 Static Lateral Earth Pressures

The static active earth pressure, pAS, is estimated using (Lambe, 1969):

$$p_{AS} = K_{AS} \cdot \gamma \cdot z$$                                        Eq. 2.5.4-21

where $K_{AS}$ = Rankine coefficient of static active lateral earth pressure

$\gamma$ = unit weight of backfill

z = depth below ground surface

The Rankine coefficient, $K_{AS}$, is calculated from

$$K_{AS} = \tan^2 (45 - \phi'/2)$$                   Eq. 2.5.4-22

where, $\phi'$ = angle of shearing resistance of the backfill, in degrees.

The static at-rest earth pressure, $p_{0S}$, is estimated using (Lambe, 1969):

$$p_{0S} = K_{0S} \cdot \gamma \cdot z$$                   Eq. 2.5.4-23

where, $K_{0S}$ = coefficient of at-rest static lateral earth pressure and is given by

$$K_{0S} = 1 - \sin \phi'$$                   Eq. 2.5.4-24

Hydrostatic ground water conditions are considered for active and at-rest static conditions. The lateral hydrostatic pressure is calculated by:

$$p_W = \gamma_W \cdot z_w$$                   Eq. 2.5.4-25

where, $p_w$ = hydrostatic lateral earth pressure

$z_w$ = depth below ground water table

$\gamma_W$ = 62.4 pcf

### 2.5.4.10.2.1.2 Seismic Lateral Earth Pressures

The active seismic pressure, $p_{AE}$, is given by the Mononobe-Okabe equation (Whitman, 1991), represented by

$$p_{AE} = K_{AE} \cdot \gamma \cdot (H-z)$$                   Eq. 2.5.4-26

where,

$\Delta K_{AE}$ = coefficient of active seismic earth pressure = $K_{AE} - K_{AS}$

$K_{AE}$ = Mononobe-Okabe coefficient of active seismic earth thrust                   Eq. 2.5.4-27

$\gamma$ = unit weight of backfill at depth z

z = depth below the top of the backfill

H = below-grade height of wall

$K_{AE} = \cos^2(\phi'-\theta)/(\cos^2\theta(1+(\sin\phi' \sin(\phi'-\theta)/\cos(\theta))^{0.5})^2)$                   Eq. 2.5.4-28

$\theta = \tan^{-1}(k_h)$

$K_{AE}$ may be estimated as $3/4 \cdot k_h$ for $k_h$ values less than about 0.25g, regardless of the angle of shearing resistance of the backfill.

The at-rest seismic conditions are reported to be two times as large as the active earth pressures calculated by the Mononobe-Okabe equation (Whitman, 1991). Given that most below-grade walls actually yield to some extent, the actual "at rest" seismic pressures may not

---

be as high as previously indicated (Whitman, 1991). Thus the "at rest" seismic earth pressures will be taken as twice the active values, or, $\Delta K_{0E} = 2 \, \Delta K_{AE}$.

For well-drained backfills, seismic ground water pressures need not be considered (Ostadan, 2004). Since granular backfill <u>is</u> used for the project, only hydrostatic pressures are taken into consideration, as given in Eq. 2.5.4-25. It is noted that seismic ground water thrust greater than 35 percent of the hydrostatic thrust can develop for cases when $k_h>0.3g$ (Whitman, 1990). Given the relatively low seismicity at the CCNPP Unit 3 site ($k_h<0.3g$), seismic ground water considerations can be ignored.

### 2.5.4.10.2.1.3 Lateral Earth Pressures Due to Surcharge

Lateral earth pressures as a result of surcharge applied at the ground surface at the top of wall, $p_{sur}$, are calculated as follows:

$$p_{sur} = K \cdot q \qquad\qquad \text{Eq. 2.5.4-29}$$

where, K = earth pressure coefficient; $K_{AS}$ for active; $K_0$ for at-rest; $K_{AE}$ or $K_{oE}$ for seismic loading depending on the nature of loading, and q = uniform surcharge pressure.

### 2.5.4.10.2.1.4 Sample Earth Pressure Diagrams

Using the relationship outlined above and assumed backfill properties, sample earth pressures were estimated. Sample earth pressure diagrams are provided in Figure 2.5-157 and Figure 2.5-158 for a wall height of 41 ft, level ground surface, and with ground water level at 5 ft below the surface. The backfill is taken as granular soils, with $\phi' = 30$ degrees and $\gamma = 120$ pcf. The horizontal ground acceleration is taken as 0.125g. A permanent uniform surcharge load of 500 psf is also included. The validity of assumptions regarding surcharge loads, backfill properties, and structural configurations is confirmed during the detailed design stage. Actual earth pressure evaluations are performed at that time for the design of below-grade walls, based on actual project conditions. The results of these earth pressure evaluations shall be included in an update to the FSAR at that time.

### 2.5.4.10.2.2    Selected Design Parameters

The field and laboratory test results are discussed in Section 2.5.4.2. The parameters employed for the bearing capacity, settlement, and earth pressure evaluations are based on the material characterization addressed in Section 2.5.4.2, and as summarized in Table 2.5-36. The parameters reflected in this table were conservatively chosen, as discussed in Section 2.5.4-2. The ground water level was chosen at elevation 80 ft, whereas this could be a "perched" condition only. The factor of safety utilized for bearing capacity of soils typically exceeds 3.0, whereas a value of 3.0 is commonly used. An angle of shearing resistance of 30 degrees was used for characterization of a structural backfill for earth pressure evaluations, which is considered conservative for granular fill compacted to 95 percent Modified Proctor compaction. Similarly, a seismic acceleration of 0.125g and a magnitude 6.0 earthquake were used in the evaluations, which are higher than the 0.084g zero depth peak ground acceleration and 5.5 magnitude indicated by the seismic analyses, therefore resulting in conservative estimates.}

### 2.5.4.10.3    Uniformity and Variability of Foundation Support Media

The U.S. EPR FSAR includes the following COL Item in Section 2.5.4.10.3:

A COL applicant that references the U.S. EPR design certification will investigate and determine the uniformity of the underlying layers of site specific soil conditions beneath

the foundation basemats.  The classification of uniformity or non-uniformity will be established by a geotechnical engineer.

~~These~~This COL Item is addressed as follows:

{Three criteria are identified in the U.S. EPR FSAR for establishing uniformity in foundation support media, namely, 1) presence of soil and rock, 2) dip angle of soil layers, and 3) shear wave velocity.  Each is addressed below:

1.  Foundations of all Seismic Category I structures at the CCNPP Unit 3 site are supported on compacted structural fill which is in turn supported on natural soils.  Bedrock at the site is very deep, at about 2,500 ft below ground surface.  Given the considerable depth to bedrock, non-uniform foundation conditions resulting from combined soil-rock support are not applicable to foundations at the CCNPP Unit 3 site.

2.  Detailed subsurface information is presented in Section 2.5.4.  Stratigraphic profiles (presented in Figure 2.5-130 through Figure 2.5-134 of the referenced section) indicate that the stratigraphic lines delineating various soil units have gentle slopes, mostly sloping about 1 to 2 degrees.  This is consistent with the regional dip of 1 to 2 degrees in Coastal Plain deposits (refer to Section 2.5.1 for more details).  However, at isolated CCNPP Unit 3 locations, stratigraphic units dip steeper, up to about 10 degrees (shown in Figure 2.5-130 through Figure 2.5-134 of the referenced section) which may be due to inherent assumptions in developing the stratigraphic lines or paleochannels and/or irregular erosional surfaces.  Regardless, these steeper angles are less than the dip angle of 20 degrees from the horizontal identified in the U.S. EPR FSAR as the criterion for determining levelness of layers.  On this basis, the soil layers at the CCNPP site are considered horizontal.

3.  Classification of uniformity (or non-uniformity) in foundation support media resides with the geotechnical engineer, per the U.S. EPR FSAR.  Shear wave velocity (Vs) measurements are used for this determination because they are a) in-situ measurements reflecting the natural ground conditions and b) important input to the safety evaluation of structures such as in soil-structure interaction and seismic analyses.  The Vs values were evaluated to a depth of 344 ft below the Nuclear Island (NI) foundation basemat, corresponding to El. -300 ft.  The 344 ft value was selected based on the three U.S. EPR FSAR criteria of: 1) 1.5 times an equivalent radius of foundation basemat, 2) 1.0 times the maximum foundation basemat dimension, or 3) no less than 200 ft below the bottom of the foundation basemat; with criterion (2) selected as the governing condition for the CCNPP Unit 3 NI basemat for its greater dimension.  It is noted that minor appendages and protrusions in the irregularly-shaped U.S. EPR NI foundation were ignored in selecting the 344 ft value.

Detailed Vs data are presented in Section 2.5.4, Figure 2.5-124, Figure 2.5-125, and Figure 2.5-128, with results discussed in detail in Section 2.5.4.4.2.  An evaluation of Vs values to 344 ft below the NI foundation basemat (from El. 44 ft to El. -300 ft) is as follows.

|  | Stratum IIb | Stratum IIc | Stratum III |
| --- | --- | --- | --- |
| Stratum Name | Ches, Cem. Sand | Ches. Clay/Silt | Nanjemoy Sand |
| Approx. Stratum Thickness (ft) | 60 | 185 | 100 |
| Range of Vs (ft/sec) | 560 - 3,790 | 1,030 - 1,700 | 1,690 - 1,980 |

|                              | Stratum IIb | Stratum IIc | Stratum III |
|------------------------------|-------------|-------------|-------------|
| Average Vs (ft/sec)*         | 1,530       | 1,250       | 1,980       |
| Average Vs Std. Dev. (ft/sec)* | 480       | 64          | 98          |
| Average Vs Coef. Of Var. (%) | 30          | 5           | 5           |

weighted average, with respect to sub-layer thickness

|                        | Weighted Average Values for Entire 344 ft Soil Column |
|------------------------|-------------------------------------------------------|
| Vs (ft/sec)            | 1,510                                                 |
| Vs Std. Dev. (ft/sec)  | 146                                                   |
| Vs Coef. Of Var. (5)   | 9                                                     |

From the above values, the lowest standard deviations and coefficients of variation (therefore, the lowest variability - or the highest uniformity) are noted for Strata IIc and III. These two strata combined make up over 80% of the 344 ft soil column, for which very high uniformity (coefficients of variation of 5%) is indicated.

Larger variations are noted in Stratum IIb soils. These soils make up less than 20% of the 355 ft soil column. Stratum IIb soils are interbedded layers of silty/clayey sands, sandy silts, and low to high plasticity clays, with varying amounts of shell fragments and with varying degrees of cementation (detailed description is give in Section 2.5.4.2.1.2). Cemented soils are a special class of soils with characteristics distinctly different from other natural soils. Therefore, they are expected to have properties that vary, particularly when interbedded.

These naturally-occurring variations were confirmed from the site investigation results via two different measurement techniques for shear wave velocity (by suspension P-S velocity logging and seismic CPT), both indicating similar velocity profiles, as shown in Figure 2.5-128 of the referenced FSAR section. The variations observed in the suspension P-S velocity logging data are shown to be readily duplicated by the CPT results, including the peaks associated with cemented or hard zones, indicative of the random, isolated variations in these natural soils. Such variations in Vs are not of major significance when considered over the entire 344 ft for they do not have a defining control over the characteristics of the 344 ft soil column, as indicated by a standard deviation of 146 ft/sec and a coefficient of variation of 9% Vs for the CCNPP soils are recognized through delineating the Vs values into thinner sub-strata (shown in Figure 2.5-125) which were used as input for the project seismic evaluation. Therefore, they have been accounted for in developing the site-specific horizontal and vertical ground motion response spectra (GMRS) shown in Figure 2.5-145. The GMRS are defined at a depth of 41 ft which is the foundation level for the U.S. EPR Nuclear Island (NI) as shown in Figure 2.5-144. Therefore, the GMRS coincide with the foundation input response spectra (FIRS) for the NI. Since the GMRS (FIRS for the NI) are enveloped by the certified seismic design response spectra (CSDRS) for the NI, the noted natural variations in Vs, minor as they are relative to the overall 344 ft soil column, are accounted for in the development of the site-specific input motion.}

### 2.5.4.10.4    Site Investigation for Uniform Sites

No departures or supplements.

### 2.5.4.10.5    Site Investigation for Non-uniform Sites

No departures or supplements.

### 2.5.4.11    Design Criteria

{No departures or supplements.}

### 2.5.4.12    Techniques to Improve Subsurface Conditions

The U.S. EPR FSAR includes the following COL Items in Section 2.5.4.12:

Techniques used for improving subsurface conditions are site specific and will be addressed by the COL applicant.

This COL Item is addressed as follows:

{Major structures derive support from the very dense cemented soils or compacted structural backfill.  Given the planned foundation depths and soil conditions at these depths, as shown in Figure 2.5-130 through Figure 2.5-134, no special ground improvement measures are warranted.  Ground improvement is limited to excavation of unsuitable soils, such as existing fill or loose/soft soils, and their replacement with structural backfill.  It also includes proof-rolling of foundation subgrade for the purpose of identifying any unsuitable soils for further excavation and replacement, which further densifies the upper portions of the subgrade.  In absence of subsurface conditions at the site that require ground improvement, ground control, i.e., maintaining the integrity of existing dense or stiff foundation soils, is the primary focus of earthworks during foundation preparation.  These measures include ground water control, use of appropriate measures and equipment for excavation and compaction, subgrade protection, and other similar measures.

### 2.5.4.13    References

This section is added as a supplement to the U.S. EPR FASAR.

**ACI, 1994.**  Manual of Concrete Practice, Part 1, Materials and General Properties of Concrete, American Concrete Institute, 1994.

**API, 2007.**  Cathodic Protection of Aboveground Petroleum Storage Tanks, API Recommended Practice Number 651, American Petroleum Institute, 2007

**ASCE, 1978.**  Definition of Terms Related to Liquefaction, ASCE Journal of Geotechnical and Environmental Engineering, W. Marcusson III, Volume 104, Number 9, 1978.

**ASCE, 2000.**  Liquefaction Resistance of Soils from Shear Wave Velocity, ASCE Journal of Geotechnical and Environmental Engineering, R. Andrus and K. Stokoe, November 2000.

**ASTM, 1999**.  Standard Test Method for Penetration Test and Split-Barrel Sampling of Soils, American Society for Testing and Materials, ASTM D1586-99,1999.

**ASTM, 2000a**.  Standard Practices for Preserving and Transporting Soil Samples, American Society for Testing and Materials, ASTM D4220-95(2000), 2000.

**ASTM, 2000c**.  Standard Practice for Thin-Walled Tube Sampling of Soils for Geotechnical Purposes, American Society for Testing and Materials, ASTM D1587-00, 2000.

**ASTM, 2000d**.  Standard Test Method for Moisture, Ash, and Organic Matter of Peat and Other Organic Soils, American Society for Testing and Materials, ASTM D2974-00, 2000.

**ASTM, 2000e**. Standard Test Method for Performing Electronic Friction Cone and Piezocone Penetration Testing of Soils, American Society for Testing and Materials, ASTM D5778-95 (reapproved 2000), 2000.

**ASTM, 2001a**. Standard Test Method for Field Measurement of Soil Resistivity Using the Wenner Four-Electrode Method, American Society for Testing and Materials, ASTM G57-95 (reapproved 2001), 2001

**ASTM, 2001b**. Standard Test Method for pH of Soils, American Society for Testing and Materials, ASTM D4972, 2001.

**ASTM, 2002a**. Standard Test Method for Particle Size Analysis of Soils, American Society for Testing and Materials, ASTM D422-63 (reapproved 2002) 2002.

**ASTM, 2002b**. Standard Test Method (Field Procedure) for Instantaneous Change in Head (Slug) Tests for Determining Hydraulic Properties of Aquifers, American Society for Testing and Materials, ASTM D4044-96 (reapproved 2002), 2002.

**ASTM, 2002c.** Standard Test Methods for Laboratory Compaction Characteristics of Soil Using Modified Effort (56,000 ft-lbf/ft3 (2,700 kN-m/m3)), American Society for Testing and Materials, ASTM D1557-02, 2002.

**ASTM, 2003**. Standard Test Method for Unconsolidated Undrained Triaxial Compression Test on Cohesive Soils, American Society for Testing and Materials, ASTM D2850-03, 2003.

**ASTM, 2004a**. Standard Practice for Design and Installation of Ground Water Monitoring Wells, American Society for Testing and Materials, ASTM D5092-04, 2004.

**ASTM, 2004b**. Standard Test Method for Particle Size Distribution (Gradation) of Soils Using Sieve Analysis, American Society for Testing and Materials, ASTM D6913-04, 2004.

**ASTM, 2004c**. Standard Test Method for Consolidated Undrained Triaxial Compression Test for Cohesive Soils, American Society for Testing and Materials, ASTM D4767-04, 2004.

**ASTM, 2004d**. Standard Test Method for Direct Shear Test of Soil Under Consolidated Drained Conditions, American Society for Testing and Materials, ASTM D3080-04, 2004.

**ASTM, 2004e**. Standard Test Method for One-Dimensional Consolidation Properties of Soils Using Incremental Loading, American Society for Testing and Materials, ASTM D2435-04, 2004.

**ASTM, 2004f**. Standard Practice for Determining the Normalized Penetration Resistance of Sands for Evaluation of Liquefaction Potential, American Society for Testing and Materials, ASTM D6066-96 (reapproved 2004), 2004.

**ASTM, 2005a**. Standard Test Method for Energy Measurement for Dynamic Penetrometers, American Society for Testing and Materials, ASTM D4633-05, 2005.

**ASTM, 2005b**. Standard Test Method for Liquid Limit, Plastic Limit, and Plasticity Index of Soils, American Society for Testing and Materials, ASTM D4318-05, 2005.

**ASTM, 2005c**. Standard Test Method for Laboratory Determination of Water (Moisture) Content of Soil and Rock by Mass, American Society for Testing and Materials, ASTM D2216-05, 2005.

**ASTM, 2005d**. Standard Test Method for CBR (California Bearing Ratio) of Laboratory-Compacted Soils, American Society for Testing and Materials, ASTM D1883-05, 2005.

**ASTM, 2005e.** Standard Specification for Portland Cement, American Society for Testing and Materials, ASTM C150-05, 2005.

**ASTM, 2006a.** Standard Test Method for Classification of Soils for Engineering Purposes (unified Soil Classification System), American Society for Testing and Materials, ASTM D2487-06, 2006.

**ASTM, 2006b**. Test Method for Specific Gravity of Soil Solids by Water Pycnometer, American Society for Testing and Materials, ASTM D854-06, 2006.

**ASTM, 2006c**. Standard Test Method for Unconfined Compressive Strength of Cohesive Soils, American Society for Testing and Materials, ASTM D2166-06, 2006.

**ASTM, 2006d**. Standard Practice for Description and Identification of Soils (Visual-Manual Procedure), American Society for Testing and Materials, ASTM D2488-06, 2006.

**ASTM, 2007a**. Standard Specification for Blended Hydraulic Cements, American Society for Testing and Materials, ASTM C595-07, 2007.

**Bechtel, 1992**. Subsurface Investigation and Foundation Report for Calvert Cliffs Nuclear Plant Diesel Generator Project, Prepared for Baltimore Gas and Electric Company, Bechtel Power Corporation, June 1992.

**Bechtel, 2007**. Reconciliation of EPRI and RCTS Results, Calvert Cliffs Nuclear Power Plant Unit 3, Bechtel Power Corporation, December 2007.

**BGE, 1982** Updated Final Safety Analysis Report, Calvert Cliffs Nuclear Power Plant (Units 1 and 2), Docket 50-317 and 50-318, Calvert County, Maryland, Baltimore Gas and Electric Company, Baltimore, Maryland, 1982.

**Bowles, 1966**. Foundation Analysis and Design, J. Bowles, 5th Edition, McGraw-Hill Book Company, 1996.

**CEE, 1985**. Liquefaction of Soils During Earthquakes, National Research Council, Committee on Earthquake Engineering, National Academy Press, 1985.

**Das, 1990**. Principles of Foundation Engineering, 2nd Edition, B. Das, PWS-Kent, 1990.

**Davie, 1988**. Settlement of Two Tall Chimney Foundations, J. Davie and M. Lewis, Proceedings 2nd International Conference on Case Histories in Geotechnical Engineering, pp 1309-1313, 1988.

**Dominion, 2006.** North Anna Early Site Permit Application, Revision 9 Docket Number. 05200008, Dominion Nuclear North Anna LLC, September 2006.

**Deere, 1966**. Engineering Classification and Index Properties of Intact Rock, University of Illinois, Prepared for Air Force Weapons Laboratory, Technical Report Number AFWL-TR-65-116, D. Deere and R. Miller, December 1966.

**ECL, 2007**. Standard Operating Procedure, Cation Exchange Capacity, Enviro-Chem Laboratories, Inc., ECL-SOP-313, 2007.

**EPA, 1993**. EPA 300.0, Method for the Determination of Inorganic Substances in Environmental Samples, United States Environmental Protection Agency, Report Number EPA/600/R-93/100, 1993.

**EPRI, 1990.** Manual on Estimating Soil Properties for Foundation Design, F. Kulhawy and P. Mayne, Electric Power Research Institute, Report EL-6800, 1990.

**EPRI, 1993**. Guidelines for Determining Design Basis Ground Motions, Electric Power Research Institute, Report Number TR-102293, 1993.

**FHWA, 1990**. Reinforced Soil Structures, Vol. 1, Design and Construction Guidelines, Federal Highway Administration, Federal Highway Administration Report Number FHWA-RD-89-043,1990.

**IEEE, 1983**. Guide for Measuring Earth Resistivity, Ground Impedance, and Earth Surface Potentials of a Ground System Part 1: Normal Measurements, Institute of Electrical and Electronics Engineers, IEEE 81, 1983.

**Hansen, 1996**. Hydrostratigraphic Framework of the Piney Point-Nanjemoy Aquifer and Aquia Aquifer in Calvert and St. Mary's Counties, Maryland, H. Hansen, Maryland Geological Survey, Open-File Report No. 96-02-8, 1996.

**Lambe, 1969.** Soil Mechanics, T. Lambe and R. Whitman, John Wiley and Sons Inc, New York, p 553, 1969.

**Lowe, 1975.** Subsurface Explorations and Sampling, Chapter 1 in Foundation Engineering Handbook, J. Lowe III, and P. Zaccheo, edited by H. Winterkorn and H. Fang, pp 1-66, Van Nostrand Reinhold Co, 1975.

**Meyerhof, 1978**. Ultimate Bearing Capacity of Foundation on Layered Soil Under Inclined Load, G. Meyerhof and A. Hanna, Canadian Geotechnical Journal, Volume 15, Number 4, pp 565-572, 1978.

**NFEC, 1986.** Foundations and Earth Structures, Design Manual 7.02, Naval Facilities Engineering Command, pp 7.02-63, Table 1, 1986.

**NRC, 2003a**. Site Investigations for Foundations of Nuclear Power Plants, Regulatory Guide 1.132, U.S. Nuclear Regulatory Commission, 2003

**NRC, 2003b**. Laboratory Investigations of Soils for Engineering Analysis and Design of Nuclear Power Plants, Regulatory Guide 1.138, Revision 2, U.S. Nuclear Regulatory Commission, 2003.

**NRC, 2003c.** Procedures and Criteria for Assessing Seismic Soil Liquefaction at Nuclear Power Plant Sites, Regulatory Guide 1.198, U.S. Nuclear Regulatory Commission, 2003.

**NRC, 2007.** Combined License Applications For Nuclear Power Plants (LWR Edition), Regulatory Guide 1.206, U.S. Nuclear Regulatory Commission, 2007.

**Ohya, 1986**. In Situ P and S Wave Velocity Measurement, Proceedings of In Situ '86, American Society of Civil Engineers, 1986.

**Ostadan, 2004**. Seismic Soil Pressure for Building Walls-An Updated Approach, F. Ostadan, 11th International Conference on Soil Dynamics and Earthquake Engineering and 3rd International Conference on Earthquake Geotechnical Engineering, University of California, Berkeley, January 2004.

**Poulos, 1974**. Elastic Solutions for Soil and Rock Mechanics, H. Poulos and E. Davis, John Wiley, New York, 1974.

**Robertson, 1988**. Guidelines for Geotechnical Design Using CPT and CPTU, P. K. Robertson, and R. G. Campanella, Soil Mechanics Series No. 120, University of British Columbia, 1988.

**Rosen, 1986**. Origin of Dolomite Cement in Chesapeake Group (Miocene) Siliciclastic Sediments: An Alternative Model to Burial Dolomatization, M. Rosen and G. Holdren, Journal of Sedimentary Petrology, Volume 56, Number 6, pp 788-798, November 1986.

**Schnabel, 2007a**. Geotechnical Subsurface Investigation Data Report (Revision No. 1), CGG Combined Operating License Application (COLA) Project, Calvert Cliffs Nuclear Power Plant (CCNPP), Calvert County, Maryland, Report by Schnabel Engineering North, LLC, April 2007.

**Schnabel, 2007b**. Geotechnical Subsurface Investigation Data Report Addendum No. 3 (RCTS Test Results), Revision 2, CGG Combined Operating License Application (COLA) Project, Calvert Cliffs Nuclear Power Plant (CCNPP), Calvert County, Maryland, Report by Schnabel Engineering North, LLC, December 2007.

**Seed, 1988**. Design of Earth Retaining Structures for Dynamic Loads, Proc. Specialty Conference on Lateral Stresses in the Ground and Design of Earth-Retaining Structures, H. Seed and R. Whitman, ASCE, NY, pp 103-147, 1988.

**Senapathy, 2001.** Estimating Dynamic Shear Modulus in Cohesive Soils, H. Senapathy, J. Clemente, and J. Davie, XVth International Conference on Soil Mechanics and Geotechnical Engineering, August 2001.

**SGS, 1993**. Swedish Geotechnical Society, Recommended Standard for Cone Penetration Tests, Report SGF 1:93E, Stockholm, Sweden, 1993

**SNOC, 2006.** Vogtle Early Site Permit Application, Revision 1, Docket No. 052011, Southern Nuclear Operating Company, Inc., November 2006.

**Terzaghi, 1955.** Evaluation of Coefficient of Subgrade Reaction, Geotechnique, K. Terzaghi, Volume 5, pp 297-326, Tables 1 and 2, 1955.

**USGS, 1983**. Preliminary Analysis of Geohydrologic Data from Test Wells Drilled Near Chester, on Kent Island, Queen Anne's County, Maryland, U.S. Geological Survey, Open File Report 82-854, Maryland Geological Survey, F. Mack, 1983.

**USGS, 1984**. Summary of Hydrogeologic Data from a Deep (2,678 ft) Well at Lexington Park, St. Mary's County, Maryland, U.S. Geological Survey, Open File Report 84-02-1, Maryland Geological Survey, H. Hansen and J. Wilson, 1984

**USGS, 2000**. Data for Quaternary Faults, Liquefaction Features, and Possible Tectonic Features in the Central and Eastern United States, East of the Rocky Mountain Front, U.S. Geological Survey, Open File Report 00-260, J. Crone and R. Wheeler, 2000.

**Vesic, 1975**. Bearing Capacity of Shallow Foundations, Foundation Engineering Handbook, A. Vesic, H. Winterkorn and H. Fang, Editors, Van Nostrand Reinhold Co, 1975.

**Whitman, 1990**. Seismic Design and Behavior of Gravity Walls, Proceedings, Specialty Conference on Design and Performance of Earth-Retaining Structures, R. Whitman, ASCE, NY, pp 817-842, 1990.

**Whitman, 1991**. Seismic Design of Earth Retaining Structures, R. Whitman, Proceedings 2$^{nd}$ International Conference on Recent Advances in Geotechnical Earthquake Engineering and Soil Dynamics, pp 1767-1778, 1991.

**Youd, 2001**. Liquefaction Resistance of Soils: Summary Report from the 1996 NCEER and 1998 NCEER/NSF Workshops on Evaluation of Liquefaction of Soils, ASCE Journal of Geotechnical and Geoenvironmental Engineering, T. Youd et al., Volume 127, Number 10, pp 817-833, October 2001.}

## 2.5.5      STABILITY OF SLOPES

The U.S. EPR FSAR includes the following COL Item for Section 2.5.5:

> A COL applicant that references the U.S. EPR design certification will evaluate site-specific information concerning the stability of earth and rock slopes, both natural and manmade (e.g., cuts, fill, embankments, dams, etc.), of which failure could adversely affect the safety of the plant.

This COL Item is addressed as follows:

{This section addresses the stability of constructed and natural slopes. It was prepared based on the guidance in relevant Section of NRC Regulatory Guide 1.206, "Combined License Applications for Nuclear Power Plants (LWR Edition)," (NRC, 2007). Constructed slopes evolve as part of the overall site development.

{The site of the Calvert Cliffs Nuclear Power Plant (CCNPP) Unit 3 is comprised of rolling topography. The site is planned to be graded in order to establish the final grade for the project, resulting in cuts and fills, as well as slopes. The stability of these slopes and their potential impact on safety-related structures are evaluated herein. Natural slopes at the site consist of the Calvert Cliffs. They are steep slopes, undergoing continuous erosion. The impact of naturally-occurring erosion on these cliffs and their potential impact on safety-related structures are also evaluated.

Sections 2.5.5.1 through 2.5.5.5 are added as a supplement to the U.S. EPR FSAR.

### 2.5.5.1      Slope Characteristics

The characteristics of constructed and natural slopes are described below.

### 2.5.5.1.1    Characteristics of Constructed Slopes

Natural ground surface elevations at the CCNPP Unit 3 site area range approximately from Elevation 50 ft (15.2 m) to Elevation 120 ft (36.5 m), as shown in Figure 2.5-103.  It is noted that all elevations referenced in this Section are based on NGVD 29.  Site grading for CCNPP Unit 3 structures will include such areas as the power block, switchyard, cooling tower, and Ultimate Heat Sink (UHS) / Circulating Water Supply System (CWS) makeup intake structures.  The power block includes the Reactor Building, Fuel Building, Safeguards Building, Emergency Power Generating Building, Nuclear Auxiliary Building, Access Building, Radioactive Waste Building, Turbine Building, and Ultimate Heat Sink.  The centerline of the CCNPP Unit 3 power block is planned to be graded to approximately Elevation 85 ft (25.9 m).  The finished grade in the area of each major structure will be approximately:

♦   Power block: Elevation 75 ft (22.9 m) to 85 ft (25.9 m)

♦   Switchyard: Elevation 90 ft (27.4 m) to 98 ft (29.9 m)

♦   Cooling Tower: Elevation 94 to 101 ft (28.6 m to 30.8 m)

♦   UHS/CWS Makeup Water Intake Structures: Elevation 10 ft (3 m)

Locations of these structures, and a schematic of the overall grading configuration, are shown in Figure 2.5-159.  The site grading will require both cut and fill, currently estimated at approximately 40 ft (12.1 m) and 45 ft (13.7 m) maximum depth, respectively, except in the area near the UHS/CWS makeup water intake structures where a maximum cut of about 70 ft (21.3 m) is estimated.  The cut/fill operations will result in permanent slopes in and around the power block and around Category I structures outside the immediate power block area.  The maximum height of new slopes in the area of CCNPP Unit 3 power block is approximately 50 ft (15.2 m), located on the eastern side of the power block area.  The maximum height of new slopes in the area of UHS/CWS makeup water intake structures is approximately 92 ft (28 m), located on the western side of UHS/CWS makeup water intake structures.  All permanent slopes, whether cut or fill, will have an inclination of approximately 3:1 (Horizontal:Vertical).  Earthworks for slope construction, including fill control, compaction, testing, etc. are addressed in Section 2.5.4.5.

Seven cross-sections (Cross-Sections A through G) that represent the typical site grading configuration were selected for evaluation based on location (e.g., proximity to major structures), slope geometry (e.g., height), and soil conditions.  These cross-sections, and their locations, are shown in Figure 2.5-159 through Figure 2.5-161.  Slope stability calculations were made for these cross-sections; the results are discussed in Section 2.5.5.2.

### 2.5.5.1.2    Characteristics of Natural Calvert Cliffs

The CCNPP Unit 3 site area is located about 1,000 ft (305 m) west of the steep cliffs known as the Calvert Cliffs, as shown in Figure 2.5-159.  These cliffs make up the Chesapeake Bay shoreline and reach elevations as high as 100 ft (30.5 m) at their closest point to the CCNPP Unit 3 power block area.  A profile of the Calvert Cliffs is shown in Figure 2.5-162 (BGE, 1992) for illustration purposes.  Stability of the Calvert Cliffs is discussed in Section 2.5.5.2.

### 2.5.5.1.3    Exploration Program and Geotechnical Conditions

The soil exploration program, ground water conditions, sampling, materials and properties, liquefaction potential, and other details are addressed in Section 2.5.4.  A summary relevant to the slope stability evaluation is presented below.

Two (shallow and deep) ground water regimes, with two different elevations (average about Elevation 80 ft (24.4 m) and Elevation 39 ft (11.9 m)), are presently identified at the CCNPP site based on on-going ground water level measurements, as discussed in Section 2.5.4.6. The average ground water level of Elevation 80 ft (24.4 m) was chosen for slope stability evaluation, for conservatism. In naturally low-lying areas, i.e., in areas with ground surface elevations lower than the Elevation 80 ft (24.4 m) (taken as the ground water level), the ground may be saturated. These areas will be inspected during construction for ground water condition. Should these areas appear saturated and if they are to receive fill during construction, a layer of highly permeable drainage material, such as crushed stone with associated filter protection, will be placed between the natural soils and the fill to preclude saturation of the fill and to maintain the ground water level near the bottom of the fill.

As presented in detail in Section 2.5.4, the subsurface stratigraphy at this site is relatively uniform. Based on this uniformity, a typical soil profile at the site may be adopted for the purpose of slope stability evaluation. This profile is shown in Figure 2.5-163. The profile parameters are based on material properties derived from the data collected during the preconstruction exploration program, as presented in Table 2.5-36. The two soil layers referred to as Clay/Silt IIa and Clay/Silt IIc are the fine-grained portions of Chesapeake soils and are below the adopted ground water level; therefore, their total stress properties, i.e., undrained shear strength, were used for stability analysis. The Terrace Sand and Cemented Sand are predominately granular soils; therefore, their effective stress properties were used for stability analysis. Also, since fill material for site grading purposes will be obtained from excavated portions of the Terrace Sand stratum, soil properties for the fill were adopted based on properties assigned to Terrace Sand. This is a conservative assumption given that these materials will be placed and compacted to a higher density than their current compactness level. The properties of natural Terrace Sand are given in Table 2.5-36. A criterion of 95% modified Proctor will be assigned to compacting these soils during construction, which is equivalent to a very dense condition, compared to their current (natural) condition which is medium dense on average.

### 2.5.5.2    Design Criteria and Analysis

The stability of constructed slopes was assessed using limit equilibrium methods, which generally consider moment or force equilibrium of a potential sliding mass by discretizing the mass into vertical slices, as shown in Figure 2.5-164. This approach results in a Factor Of Safety (FOS) that can be defined as (Duncan, 1996):

$$FOS = \frac{Shear\ Strength\ of\ Soil}{Shear\ Stress\ Required\ for\ Equilibrium} \qquad \text{(Eq. 2.5.5-1)}$$

Various limit equilibrium methods are available for slope stability evaluation, including the Ordinary method (Fellenius, 1936), Bishop's simplified method (Bishop, 1955), Janbu's simplified method (Janbu, 1968), and the Morgenstern-Price method (Morgenstern, 1965), among others. These methods were selected for evaluation of slopes for they are routinely used, and their limitations, and advantages, are well documented. The main differences are:

1.  Equations of statics that are included and satisfied.

2.  Interslice forces that are included in the analysis.

3.  Assumed relationship between the interslice shear and normal forces.

The Ordinary (Fellenius, 1936) method is one of the earliest methods developed. It ignores all interslice forces and satisfies only moment equilibrium. Both Bishop's (Bishop, 1955) simplified method and Janbu's (Janbu, 1968) simplified method include the interslice normal force, E, but ignore the interslice shear force, X, shown in Figure 2.5-164. Bishop's (Bishop, 1955) and Janbu's (Janbu, 1968) simplified methods satisfy only moment equilibrium and horizontal force equilibrium, respectively. The Morgenstern-Price (Morgenstern, 1965) method, however, considers both shear and normal interslice forces, and it satisfies both moment and force equilibrium. These four methods were used to calculate FOSs for constructed slopes at the CCNPP Unit 3 site area.

Dynamic analysis of the slopes can be performed using a pseudo-static approach, which represents the effects of seismic shaking by accelerations that create inertial forces. These forces act in the horizontal and vertical directions at the centroid of each slice, and are defined as:

$$F_h = (a_h / g)W = k_h W \qquad\qquad (\text{Eq. 2.5.5-2})$$

$$F_v = (a_v / g)W = k_v W \qquad\qquad (\text{Eq. 2.5.5-3})$$

Where $a_h$ and $a_v$ are horizontal and vertical ground accelerations, respectively, W is the slice weight, and g is the gravitational acceleration constant. The inertial effect is specified by $k_h$ and $k_v$ coefficients, based on site seismic considerations.

Typical minimum acceptable values of FOS are 1.5 for normal long-term loading conditions and 1.0 to 1.2 for infrequent loading conditions (Duncan, 1996), e.g., during earthquakes.

### 2.5.5.2.1    Stability of Constructed Slopes

The software Slope/W (Slope/W, 2004) was used for the stability analysis. This software has been independently validated by Bechtel (Slope/W, 2005). The software searches for a critical slip surface by attempting several hundred combinations of surfaces of different shapes. Both static and pseudo-static analyses were performed for the selected cross-sections, allowing the program to search for the critical surface.

A computer analysis was made for expediting computations and to examine several hundred potential slip surfaces. The computer program Slope/W (Slope/W, 2004) was used for the stability analysis. Slope/W is an interactive program with a large number of options to suit the modeling needs of the user. In brief, the initial code for Slope/W was developed by Professor D.G. Fredlund at the University of Saskatchewan in Canada. The PC version became available in the 1980s. Slope/W contains formulation for 10 different methods for evaluating the stability of slopes, each with various assumptions in its development of the respective mathematical model, some of which were described earlier in Section 2.5.5.2, with the main difference being in the treatment of interslice forces. Slope/W contains a variety of options for the shape of trial surfaces, e.g., circular, planar, composite, or block type, and locates the critical surface with the lowest possible FOS. The reasonableness of the surface, however, should be determined by the user as Slope/W, or other similar applications, cannot be expected to make these judgments. Slope/W also allows for the incorporation of forces due to water, as well as negative pore water (suction) and externally applied forces, when needed. Material properties may simply be

defined in terms of friction and/or cohesion, or made a function of other parameters, e.g., change with stress. Slope/W has two options for evaluating slopes subjected to rapid loading; namely, pseudostatically or using results from other dynamic analyses such as a companion program that obtains dynamic stresses and pore water pressure. Slope/W offers many other computational options. A complete description of Slope/W and slope stability formulations is given in Slope/W user Manual (SlopeW, 2004) and Krahn (Krahn, 2004).

The effect of surcharge loading was excluded from the analyses. Planned structures are sufficiently set back from edges of slopes so that they do not impose surcharge loading on the slopes, as evident in Figure 2.5-160 and Figure 2.5-161. The site soils are not considered liquefiable for the seismic conditions of the site; therefore, liquefaction is not applicable to stability of slopes at the site. Liquefaction potential is addressed in detail in Section 2.5.4.8.

For the pseudo-static analysis, the inertial effect coefficient $k_h = 0.125$ was used, based on $a_h = 0.125g$, as discussed in Section 2.5.4.7. The vertical component, $k_v$, was chosen as 0.063.

Results of the static and pseudo-static slope stability analyses for critical surfaces, i.e., surfaces with the lowest FOS, are shown in Figure 2.5-165 through Figure 2.5-171. The computed FOSs shown on these figures are based on the Morgenstern-Price (Morgenstern, 1965) method. This method was chosen for its complete consideration of interslice forces as well as force and moment equilibrium. In addition to the Morgenstern-Price (Morgenstern, 1965) method, FOSs were also estimated using the Ordinary (Fellenius, 1936) method, Bishop's (Bishop, 1955) simplified method, and Janbu's (Janbu, 1968) simplified method for comparison, which are all implemented in Slope/W. These FOSs are summarized in Table 2.5-55. An examination of the FOSs in Table 2.5-55 indicates that for a particular slope, there is no appreciable difference among the FOSs computed by the different methods. The FOSs, based on the Morgenstern-Price (Morgenstern, 1965) method, range from about 1.4 to 1.9 from the static analysis and from about 1.0 to 1.4 from the pseudo-static analysis. The FOSs are further explained below, referencing results obtained from the Morgenstern-Price (Morgenstern, 1965) method.

In the power block and adjacent areas (Cross-sections A through F in Figure 2.5-160), all slopes show FOSs greater than 1.8 for the static case and greater than 1.3 for the pseudo-static case. Additionally, in this area, all slopes indicated that the critical sliding surface is very limited and surficial, except for cross-Section B. The static FOS for cross-Section B exceeds 1.8, despite the deep-seated surface indicated. Since all cross-sections analyzed, except cross-Section B, resulted in shallow, sloughing-type slip surfaces, additional analyses were made to evaluate FOSs associated with potential deeper slip surfaces. The deeper slip surfaces were arbitrarily chosen, but forced into deeper soils to encompass a larger volume of the soil mass. The analyses were repeated for all sections that showed shallow slip surfaces in the initial trial. The estimated FOSs for the deeper (forced) surfaces are shown in Table 2.5-56; location of deeper surfaces are shown in Figure 2.5-172 through Figure 2.5-176. As would be expected, these FOSs are higher than those previously estimated, and they are at least 2.0 for the static case and at least 1.4 for the pseudo-static case, based on the Morgenstern-Price method. These FOSs are consistent with the simple formulation of stability, based on the ratio of the tangent of soil friction to tangent of slope inclination, or a FOS of about 1.9 for $\phi = 32$ degrees and slope inclination of 18.4 degrees (3H:1V).

In the UHS/CWS makeup intake structures area, at cross-Section G shown in Figure 2.5-161, a static FOS of 1.42 and a pseudo-static FOS of 1.02 were estimated with the Morgenstern-Price (Morgenstern, 1965) method, as shown in Figure 2.5-171. The slope at this cross-Section is 3:1 H:V, and is approximately 91 ft (27.7 m) high. The preconstruction site exploration did not

specifically include borings or other tests in this area for the purpose of evaluating the stability of this slope.  The stability evaluation, however, was performed due to a recent design modification that placed the UHS makeup water intake structure and the CWS makeup water intake structure near the shoreline of the Chesapeake Bay.  Only the UHS makeup water intake structure is considered a Category I structure.  In absence of data specific to the slope in this area, the average soil model (thickness, elevations, properties, etc.), as obtained from the investigation in the power block area, shown in Figure 2.5-163, was applied to this slope, including the adopted Elevation 80 ft (24.4 m) for ground water level, resulting in the referenced FOSs.

As stated previously, typical minimum acceptable values of FOS are 1.5 for normal long-term loading conditions and 1.0 to 1.2 for infrequent loading conditions.  In and around the power block area, the calculated FOSs for all slopes exceed 1.8 for the static case and 1.3 for the dynamic case.  Accordingly, the slopes in the power block area have sufficient static and dynamic stability.  This conclusion is consistent with conditions at the site for the relatively flat slope geometry of 3:1 H:V, ground water level below the ground surface, and relatively dense/stiff soil conditions.  For the slope adjoining the UHS/CWS makeup intake structures, the static FOS is near 1.4 and the dynamic FOS is near 1.0.  The FOSs are slightly lower than those typically applied to similar slopes.  The lower values are very likely the result of the assumed model for this slope in absence of actual data, such as stratigraphy, ground water level, etc.  Based on expected performance from similar slopes, a 3:1 slope in dense/stiff soils such as those at the site, is expected to result in slightly higher FOSs.  It is noted that the horizontal distance between the toe of slope G and the UHS makeup water intake structure is about 160 ft (48.8).  Assuming the dynamic FOS is realistic, should this slope fail during a seismic event, and should the soils from the failure have enough energy to reach the UHS makeup water intake structure (a distance of about 160 ft (48.8 m)), the volume of soils reaching this structure could result in loading the adjacent wall of the structure by an equivalent soil height of about 1 ft (0.3 m).  The magnitude of this loading is considered small relative to other dynamic loads that this structure is expected to be designed for, such as earthquakes, hurricanes, or tsunamis.  Nonetheless, this slope will be the subject of an evaluation once again during the detailed design phase of the project.  To obtain refined FOSs for this slope, borings and other tests will be performed in this area, and the slope conditions re-evaluated during detailed design.  Should the results at that time indicate unacceptable FOSs, additional measures will be taken to mitigate its impact on the Category I, UHS makeup intake structure, such as by further flattening of the slope, further set back from structures, or other engineering measures.

Results of stability analyses are presented in Table 2.5-55 and Table 2.5-56.  The strength parameters for materials are shown in Figure 2.5-163.  Forces acting on the slope (slices) are shown in Figure 2.5-164.  There are no external forces, i.e., surcharge, acting on the slopes.  Pore pressures acting within the slope are represented by the ground water condition adopted at Elevation 80 ft (24.4 m), as shown in Figure 2.5-163.  The types of failure surfaces are shown on the final stability results in Figure 2.5-165 through Figure 2.5-171.  Units for soil properties shown on these figures are consistent with those shown in Figure 2.5-163.

The critical surfaces are shown graphically in Figure 2.5-165 through Figure 2.5-171.  The FOSs associated with these surfaces are identified in Table 2.5-55 and Table 2.5-56.  Locations of sections are shown in Figure 2.5-160 and Figure 2.5-161.

Dams and embankments, including descriptions of any adverse conditions such as high water levels attributable to the Probable Maximum Flood (PMF), sudden drawdown, or steady seepage at various levels are addressed in Section 2.5.6.

### 2.5.5.2.2    Stability of Natural Calvert Cliffs

The Calvert Cliffs are steep, near-vertical slopes, formed by erosion processes over the last several thousand years.  These processes are addressed in more detail in Section 2.4.9.  The on-going erosion results in the cliffs failing along irregular, near-vertical surfaces. The failures are the result of shoreline erosion undermining the cliffs at the beach line.  With sufficient undermining, the weight of the overlying deposits that make up the cliffs exceeds their shear strength, resulting in the undermined portion falling to the shoreline.  Long-term and short-term processes, e.g., waves, tidal fluctuations, and extreme weather conditions, affect the Calvert Cliffs.  The cliffs are estimated to undergo erosion near the CCNPP Unit 3 site area of about 2 ft (0.6 m) to 4 (1.2 m) ft per year, as described in Section 2.4.9.

In the proximity of CCNPP Unit 3, the cliffs rise to elevations in the range of about Elevation 30 ft (9.1 m) to Elevation 100 ft (30.5 m), with a major portion maintaining about Elevation 90 ft (27.4 m), as shown in Figure 2.5-159.  Given the past performance of the high cliffs, there is no reason to expect their future performance would appreciably differ; therefore, these cliffs are anticipated to continue to be globally stable, owing to the relatively high strength of the soil deposits that make up the cliffs (refer to Section 2.5.4.2 for strength data for these soils).  Consistent with the results of the preconstruction exploration, all soils that make up the cliffs also include some level of plasticity, as well as a moderate amount of fines (refer to Table 2.5-32 for data), resulting in moderate capillary forces and, therefore, enhanced stability and resistance to erosion.

The easternmost boundary of the CCNPP Unit 3 power block is set back a distance of about 1,000 ft (305 m) from the cliffs, with at least 1,200 ft (365.8 m) to the nearest Category I structure, as shown in Figure 2.5-159.  This set back area will be free from any major construction, surcharge, re-grading, or other activities that could modify the ground or the loading conditions which would adversely impact the cliffs or their stability.  Therefore, they are anticipated to remain unaffected by construction factors.

Although not expected, should the global stability of the cliffs, due to unforeseen conditions, be adversely impacted such that a major cliff failure could ensue, hypothesized failure scenarios may be in the form of (1) a wedge (or a plane) portion of the cliffs sliding into the Chesapeake Bay at an inclined angle, or (2) a portion of the cliffs separate and topple into the Chesapeake Bay.  For the wedge-shaped hypothesis, conservatively assuming that an inclined angle of 45 degrees from the base of the cliffs could form a wedge that daylights at the top of the cliffs, only an area of approximately 100 ft (30.5 m) from the cliffs' edge would be impacted by such an unexpected scenario, and the remaining 900-plus ft (274-plus m) setback area would still be intact to provide sufficient global stability to CCNPP Unit 3.  For the toppling hypothesis, except for cases associated with erosion that will be discussed below, the hydrogeologic conditions that are prerequisite to this failure situation are not known to exist at the site, such as fractured bedrock or soils with planes of weakness due to fissures, slickensides, faults, or discontinuities; excessive seepage forces that could promote such failures; or prior failure history of the type hypothesized.  Therefore, massive toppling failure of the Calvert Cliffs that could have an immediate, adverse impact on CCNPP Unit 3 is not kinematically possible.

The Calvert Cliffs, however, are expected to continue to erode, as they have in the past.  Based on the estimated rate of erosion of 2 ft (0.6 m) to 4 ft (1.2 m) annually, at a constant rate, it will take approximately 25 to 50 years to erode about 100 ft (30.5 m) of the cliffs.  Or, it would take approximately 125 to 250 years for the cliffs to erode to within a distance of 500 ft (152.4 m) from CCNPP Unit 3 outline (or 700 ft (213.4 m) from any Category I structure).  The estimated periods of 125 to 250 years are appreciably more than the anticipated operating life of CCNPP

Unit 3; therefore, stability of Calvert Cliffs due to erosion should not pose any immediate risk to the stability of soils supporting CCNPP Unit 3 in its lifetime.

### 2.5.5.2.3    Concluding Remarks

Based on analyses provided in this Section, it is concluded that the constructed and natural slopes at the site are sufficiently stable and present no failure potential that would adversely affect the safety of the proposed CCNPP Unit 3.  If final geotechnical results for the area of the UHS makeup water intake structure indicate than any potential slope failure could adversely affect the safety of the proposed CCNPP Unit 3, corrective actions will be taken to preclude this potential slope failure.

### 2.5.5.3    Logs of Borings

Logs of borings, and associated references, are provided in Appendix 2.5-A.

### 2.5.5.4    Compacted Fill

Compacted fill, and associated references, are addressed in Section 2.5.4.5.

### 2.5.5.5    References

**BGE, 1992.**  Updated Final Safety Analysis Report, Calvert Cliffs Nuclear Power Plant (Units 1 and 2), Calvert County, Maryland, Docket Numbers 50-317 and 50-318, Baltimore Gas and Electric Company, 1992.

**Bishop, 1955.**  The Use of the Slip Circle in the Stability Analysis of Slopes, A. W. Bishop, Geotechnique, Vol. 5 (1), 7-17, 1955.

**Duncan, 1996.**  State of the art: Limit equilibrium and finite-element analysis of slopes, J. M. Duncan, Journal of Geotechnical Engineering, ASCE, Vol. 122 (7), 577-596, 1996.

**Fellenius, 1936.**  Calculation of Stability of Dams, W. Fellenius, Second Congress on Large Dams Transactions, Vol. 4, 445-462, 1936.

**Janbu, 1968.**  Slope Stability Computations. N. Janbu, Soil Mechanics and Foundation Engineering, The Technical University of Norway, 1968.

**Krahn, 2004.**  Stability Modeling for SLOPE/W, An Engineering Methodology, First Edition, Revision 1, J. Krahn, Geo-Slope/W International, 2004.

**Morgenstern, 1965.** The Analysis of the Stability of General Slip Surfaces, N.R. Morgenstern and V. E. Price, Geotechnique, Vol. 15(1), 79-93, 1965.

**NRC, 2007.**  Combined License Applications for Nuclear Power Plants (LWR Edition), Regulatory Guide 1.206, Revision 0, U.S. Nuclear Regulatory Commission, March 2007.

**Slope/W, 2004.**  Slope/W User's Manual, Geo-Slope International, v. 6.13, 2004.

**Slope/W, 2005.**  Validation Manual for GE262, SLOPE/W Version 6.13, A Computer Program for Slope Stability Analysis, Revision 1, 2005.}

## 2.5.6    REFERENCES

No departures or supplements.

**Table 2.5-1—{Definitions of Classes Used in the Compilation of Quaternary Faults, Liquefaction Features, and Deformation in the Central and Eastern United States}**

| Class Category | Definition |
|---|---|
| Class A | Geologic evidence demonstrates the existence of a Quaternary fault of tectonic origin, whether the fault is exposed for mapping or inferred from liquefaction to other deformational features. |
| Class B | Geologic evidence demonstrates the existence of a fault or suggests Quaternary deformation, but either (1) the fault might not extend deeply enough to be a potential source of significant earthquakes, or (2) the currently available geologic evidence is too strong to confidently assign the feature to Class C but not strong enough to assign it to Class A. |
| Class C | Geologic evidence is insufficient to demonstrate (1) the existence of tectonic fault, or (2) Quaternary slip or deformation associated with the feature. |
| Class D | Geologic evidence demonstrates that the feature is not a tectonic fault or feature; this category includes features such as demonstrated joints or joint zones, landslides, erosional or fluvial scarps, or landforms resembling fault scarps, but of demonstrable non-tectonic origin. |

**Table 2.5-2—{Earthquakes 1985–2005, Update to the EPRI (NP-4726-A 1988)
Seismicity Catalog with Emb ≥ 2.8, Within a 35° to 43° N, 71° to 89° W
Latitude-Longitude Window, Incorporating the 200 mi (320 km) Radius Site Region}**
(Page 1 of 3)

| Catalog reference | Year | Month | Day | Hour | Minute | Second | Lat °N | Lon °W | Depth (km) | Dist. (km) [1] | Int | Emb |
|---|---|---|---|---|---|---|---|---|---|---|---|---|
| Canada | 1985 | 4 | 14 | 3 | 44 | 39.00 | 42.950 | 80.040 | 18 | 584 | | 3.10 |
| Canada | 1985 | 4 | 14 | 11 | 39 | 54.00 | 41.580 | 80.400 | 18 | 484 | | 3.20 |
| SEUSSN | 1985 | 6 | 10 | 12 | 22 | 38.30 | 37.248 | 80.485 | 11.1 | 378 | 4 | 3.30 |
| ANSS | 1985 | 10 | 15 | 20 | 0 | 39.30 | 42.493 | 71.502 | 2 | 612 | | 2.97 |
| ANSS | 1985 | 10 | 19 | 10 | 7 | 40.30 | 40.980 | 73.830 | 6 | 359 | | 3.90 |
| ANSS | 1985 | 10 | 21 | 10 | 37 | 15.00 | 40.990 | 73.840 | 5 | 359 | | 3.30 |
| ANSS | 1986 | 1 | 31 | 16 | 46 | 43.33 | 41.650 | 81.162 | 10 | 536. | | 5.00 |
| SEUSSN | 1986 | 3 | 26 | 16 | 36 | 23.90 | 37.245 | 80.494 | 11.9 | 379 | 4 | 3.30 |
| SEUSSN | 1986 | 12 | 3 | 9 | 44 | 21.20 | 37.580 | 77.458 | 1.6 | 129 | 4 | 3.30 |
| SEUSSN | 1986 | 12 | 10 | 11 | 30 | 6.10 | 37.585 | 77.468 | 1.2 | 130 | 5 | 3.50 |
| SEUSSN | 1986 | 12 | 24 | 17 | 58 | 38.30 | 37.583 | 77.458 | 1 | 129 | 4 | 3.30 |
| SEUSSN | 1987 | 1 | 13 | 14 | 50 | 40.90 | 37.584 | 77.465 | 2.5 | 129 | 4 | 3.30 |
| ANSS | 1987 | 7 | 13 | 5 | 49 | 17.43 | 41.896 | 80.767 | 5 | 530 | | 3.80 |
| ANSS | 1987 | 7 | 13 | 7 | 52 | 12.00 | 41.900 | 80.800 | 5 | 533 | | 3.00 |
| ANSS | 1987 | 7 | 13 | 13 | 5 | 22.00 | 41.900 | 80.800 | 5 | 533 | | 2.90 |
| Ohio | 1987 | 7 | 13 | 18 | 25 | 11.98 | 41.880 | 80.750 | 0 | 528 | | 2.80 |
| ANSS | 1987 | 7 | 14 | 14 | 51 | 10.00 | 41.900 | 80.800 | 5 | 533 | | 2.80 |
| Canada | 1987 | 8 | 13 | 7 | 52 | 13.00 | 41.930 | 80.710 | 5 | 530 | | 3.30 |
| SEUSSN | 1988 | 2 | 16 | 15 | 26 | 54.80 | 36.595 | 82.274 | 4 | 552 | 4 | 3.30 |
| Ohio | 1988 | 3 | 31 | 16 | 30 | 3.87 | 41.313 | 81.046 | 0 | 505 | | 2.80 |
| ANSS | 1988 | 4 | 14 | 23 | 37 | 31.10 | 37.238 | 81.987 | 0 | 503 | | 4.10 |
| ANSS | 1988 | 5 | 28 | 16 | 18 | 28.12 | 39.753 | 81.613 | 0 | 469 | | 3.40 |
| SEUSSN | 1988 | 8 | 27 | 16 | 52 | 29.50 | 37.718 | 77.775 | 14.3 | 141 | 4 | 3.30 |
| Canada | 1988 | 12 | 28 | 23 | 28 | 24.00 | 41.640 | 81.170 | 5 | 536 | | 2.80 |
| ANSS | 1989 | 4 | 10 | 18 | 12 | 16.00 | 37.136 | 82.068 | 0 | 514 | | 4.30 |
| SEUSSN | 1989 | 6 | 4 | 9 | 49 | 28.20 | 37.224 | 78.293 | 8.8 | 210 | 3 | 2.80 |
| Ohio | 1989 | 8 | 1 | 16 | 12 | 48.75 | 41.898 | 80.758 | 0 | 530 | | 2.80 |
| Ohio | 1989 | 8 | 1 | 16 | 50 | 30.74 | 41.893 | 80.752 | 0 | 529 | | 2.90 |
| SEUSSN | 1990 | 1 | 13 | 20 | 47 | 56.20 | 39.366 | 76.851 | 4.1 | 110 | 5 | 3.50 |
| ANSS | 1990 | 5 | 5 | 20 | 48 | 56.18 | 36.035 | 71.674 | 10 | 497 | | 3.70 |
| ANSS | 1990 | 10 | 23 | 1 | 34 | 48.27 | 39.512 | 75.506 | 10 | 144 | | 3.16 |
| Canada | 1990 | 12 | 14 | 19 | 38 | 7.00 | 41.840 | 77.480 | 18 | 387 | | 3.00 |
| ANSS | 1991 | 1 | 26 | 3 | 21 | 22.61 | 41.536 | 81.453 | 5 | 547 | | 3.40 |
| Ohio | 1991 | 1 | 27 | 3 | 21 | 24.23 | 41.610 | 81.594 | 9.7 | 561 | | 3.50 |
| SEUSSN | 1991 | 3 | 15 | 6 | 54 | 8.30 | 37.746 | 77.909 | 15.5 | 149 | 5 | 3.80 |
| SEUSSN | 1991 | 4 | 22 | 1 | 1 | 20.20 | 37.942 | 80.205 | 14.8 | 333 | 4 | 3.50 |
| ANSS | 1991 | 6 | 17 | 8 | 53 | 16.74 | 42.630 | 74.678 | 5 | 488 | | 4.10 |
| SEUSSN | 1991 | 6 | 28 | 18 | 34 | 55.50 | 38.231 | 81.335 | 7 | 427 | | 3.00 |
| ANSS | 1991 | 8 | 15 | 7 | 16 | 7.15 | 40.786 | 77.657 | 1 | 281 | | 3.00 |
| ANSS | 1991 | 10 | 28 | 20 | 58 | 26.10 | 41.070 | 73.578 | 10 | 380 | | 3.00 |
| ANSS | 1992 | 1 | 9 | 8 | 50 | 45.22 | 40.363 | 74.341 | 7.9 | 279 | | 3.06 |
| ANSS | 1992 | 3 | 10 | 23 | 50 | 46.90 | 40.991 | 72.086 | 10 | 467 | | 2.80 |
| ANSS | 1992 | 3 | 15 | 6 | 13 | 55.22 | 41.911 | 81.245 | 5 | 560 | | 3.50 |
| Canada | 1992 | 3 | 26 | 3 | 43 | 20.00 | 42.110 | 80.850 | 2 | 552 | | 2.90 |
| Canada | 1992 | 3 | 28 | 8 | 22 | 46.00 | 41.920 | 80.810 | 5 | 535 | | 3.10 |
| Canada | 1992 | 3 | 31 | 1 | 54 | 55.00 | 42.010 | 80.790 | 18 | 541 | | 2.80 |

**Table 2.5-2—{Earthquakes 1985–2005, Update to the EPRI (NP-4726-A 1988)
Seismicity Catalog with Emb ≥ 2.8, Within a 35° to 43° N, 71° to 89° W
Latitude-Longitude Window, Incorporating the 200 mi (320 km) Radius Site Region}**
(Page 2 of 3)

| Catalog reference | Year | Month | Day | Hour | Minute | Second | Lat °N | Lon °W | Depth (km) | Dist. (km)[1] | Int | Emb |
|---|---|---|---|---|---|---|---|---|---|---|---|---|
| SEUSSN | 1993 | 1 | 1 | 5 | 8 | 5.20 | 35.878 | 82.086 | 2.3 | 573 | | 2.97 |
| SEUSSN | 1993 | 3 | 10 | 14 | 32 | 21.60 | 39.233 | 76.882 | 5 | 97 | 4 | 3.30 |
| SEUSSN | 1993 | 3 | 15 | 4 | 29 | 54.70 | 39.197 | 76.870 | 0.9 | 93 | 5 | 3.50 |
| ANSS | 1993 | 5 | 10 | 9 | 15 | 8.60 | 40.347 | 76.018 | 5 | 215 | | 2.80 |
| SEUSSN | 1993 | 7 | 12 | 4 | 48 | 20.80 | 36.035 | 79.823 | 5 | 399 | 4 | 3.30 |
| ANSS | 1993 | 10 | 16 | 6 | 30 | 5.32 | 41.698 | 81.012 | 5 | 530 | | 3.60 |
| SEUSSN | 1993 | 10 | 28 | 6 | 0 | 0.00 | 39.250 | 76.770 | 0 | 95 | 4 | 3.30 |
| SEUSSN | 1993 | 10 | 28 | 6 | 1 | 0.00 | 39.250 | 76.770 | 0 | 95 | 4 | 3.30 |
| Canada | 1993 | 11 | 1 | 0 | 14 | 16.00 | 42.690 | 81.170 | 8.5 | 617 | | 2.80 |
| ANSS | 1994 | 1 | 16 | 0 | 42 | 43.20 | 40.327 | 76.007 | 5 | 213 | | 4.20 |
| ANSS | 1994 | 1 | 16 | 1 | 49 | 16.21 | 40.330 | 76.037 | 5 | 213 | | 4.60 |
| ANSS | 1994 | 1 | 16 | 5 | 14 | 32.30 | 40.321 | 76.007 | 5 | 212 | | 2.90 |
| ANSS | 1994 | 2 | 12 | 2 | 40 | 24.50 | 36.800 | 82.000 | 5 | 521 | | 3.42 |
| ANSS | 1994 | 3 | 12 | 10 | 43 | 15.74 | 42.782 | 77.876 | 1 | 496 | | 3.60 |
| SEUSSN | 1994 | 8 | 6 | 19 | 54 | 11.80 | 35.101 | 76.786 | 0 | 369 | 5 | 3.70 |
| ANSS | 1994 | 10 | 2 | 11 | 27 | 22.58 | 42.347 | 72.277 | 10 | 558 | | 3.70 |
| ANSS | 1994 | 10 | 2 | 14 | 36 | 36.73 | 42.360 | 72.218 | 10 | 562 | | 3.30 |
| Ohio | 1995 | 1 | 12 | 21 | 25 | 51.00 | 40.800 | 82.680 | 0 | 594 | | 3.30 |
| SEUSSN | 1995 | 1 | 22 | 8 | 24 | 48.80 | 37.050 | 80.789 | 9.3 | 411 | 4 | 2.90 |
| ANSS | 1995 | 2 | 23 | 9 | 32 | 13.00 | 41.870 | 80.830 | 5 | 532 | | 2.90 |
| ANSS | 1995 | 5 | 25 | 14 | 22 | 32.69 | 42.995 | 78.831 | 5 | 543 | | 3.00 |
| SEUSSN | 1995 | 6 | 26 | 0 | 36 | 17.10 | 36.752 | 81.481 | 1.8 | 480 | 5 | 3.40 |
| SEUSSN | 1995 | 7 | 7 | 21 | 1 | 3.00 | 36.493 | 81.833 | 10 | 521 | 4 | 3.06 |
| SEUSSN | 1995 | 8 | 3 | 13 | 7 | 5.60 | 37.393 | 76.693 | 1 | 116 | 4 | 2.90 |
| Canada | 1995 | 10 | 21 | 17 | 4 | 24.00 | 42.800 | 77.880 | 1 | 498 | | 2.90 |
| ANSS | 1996 | 3 | 22 | 20 | 22 | 12.58 | 41.690 | 71.242 | 11.9 | 569 | | 3.17 |
| Canada | 1996 | 6 | 8 | 20 | 14 | 0.00 | 42.940 | 74.050 | 10.4 | 538 | | 2.80 |
| ANSS | 1996 | 6 | 29 | 19 | 30 | 42.67 | 37.187 | 81.950 | 1 | 502 | | 4.10 |
| ANSS | 1997 | 4 | 3 | 18 | 32 | 15.39 | 42.922 | 75.708 | 10.53 | 501 | | 3.43 |
| ANSS | 1997 | 10 | 28 | 10 | 36 | 46.56 | 37.162 | 82.025 | 1 | 509 | | 3.42 |
| SEUSSN | 1997 | 11 | 14 | 3 | 44 | 11.70 | 40.741 | 76.549 | 0 | 256 | | 2.97 |
| Canada | 1998 | 1 | 27 | 0 | 38 | 30.00 | 42.030 | 80.990 | 18 | 554 | | 3.00 |
| SEUSSN | 1998 | 4 | 21 | 23 | 28 | 26.60 | 38.171 | 78.569 | 2 | 188 | 3 | 2.80 |
| SEUSSN | 1998 | 6 | 5 | 2 | 31 | 3.90 | 35.554 | 80.785 | 9.4 | 499 | | 3.34 |
| ANSS | 1998 | 9 | 25 | 19 | 52 | 52.07 | 41.495 | 80.388 | 5 | 477 | | 5.20 |
| SEUSSN | 1998 | 10 | 21 | 5 | 56 | 46.90 | 37.422 | 78.439 | 12.6 | 207 | 3 | 3.80 |
| ANSS | 1998 | 11 | 25 | 2 | 55 | 6.07 | 41.071 | 82.405 | 5 | 586 | | 2.85 |
| Canada | 1998 | 12 | 25 | 21 | 22 | 3.00 | 41.120 | 81.750 | 18 | 542 | | 2.80 |
| ANSS | 1999 | 1 | 25 | 20 | 12 | 30.00 | 42.730 | 77.850 | 3 | 490 | | 2.85 |
| ANSS | 1999 | 9 | 22 | 10 | 2 | 22.29 | 41.826 | 81.476 | 18 | 569 | | 2.93 |
| ANSS | 2000 | 1 | 27 | 14 | 49 | 40.00 | 43.000 | 71.180 | 1.4 | 671 | | 3.09 |
| ANSS | 2000 | 6 | 16 | 4 | 2 | 53.00 | 42.100 | 72.820 | 9.8 | 508 | | 3.33 |
| ANSS | 2000 | 8 | 7 | 2 | 2 | 30.40 | 40.958 | 81.151 | 5 | 490 | | 3.01 |
| ANSS | 2001 | 1 | 26 | 3 | 3 | 20.06 | 41.942 | 80.802 | 5 | 536 | | 4.23 |
| Canada | 2001 | 1 | 26 | 5 | 36 | 53.00 | 41.980 | 80.700 | 5 | 533 | | 3.20 |
| ANSS | 2001 | 2 | 3 | 20 | 15 | 15.00 | 42.345 | 77.394 | 0 | 440 | | 3.25 |

**Table 2.5-2—{Earthquakes 1985–2005, Update to the EPRI (NP-4726-A 1988)
Seismicity Catalog with Emb ≥ 2.8, Within a 35° to 43° N, 71° to 89° W
Latitude-Longitude Window, Incorporating the 200 mi (320 km) Radius Site Region}**
(Page 3 of 3)

| Catalog reference | Year | Month | Day | Hour | Minute | Second | Lat °N | Lon °W | Depth (km) | Dist. (km)[1] | Int | Emb |
|---|---|---|---|---|---|---|---|---|---|---|---|---|
| ANSS | 2001 | 6 | 3 | 22 | 36 | 46.46 | 41.905 | 80.767 | 5 | 531 | | 3.42 |
| Canada | 2001 | 7 | 26 | 10 | 46 | 55.00 | 41.200 | 82.510 | 5 | 601 | | 3.10 |
| SEUSSN | 2001 | 9 | 22 | 16 | 1 | 20.60 | 38.026 | 78.396 | 0.4 | 176 | 3 | 3.20 |
| SEUSSN | 2001 | 12 | 4 | 21 | 15 | 13.90 | 37.726 | 80.752 | 8.5 | 384 | | 3.10 |
| ANSS | 2002 | 4 | 28 | 0 | 7 | 20.90 | 41.850 | 81.370 | 5 | 564 | | 2.85 |
| ANSS | 2002 | 7 | 11 | 21 | 53 | 45.96 | 40.386 | 71.332 | 0 | 488 | | 3.07 |
| ANSS | 2002 | 9 | 28 | 23 | 47 | 27.00 | 42.870 | 71.730 | 5 | 631 | | 2.93 |
| SEUSSN | 2003 | 5 | 5 | 16 | 32 | 33.90 | 37.655 | 78.055 | 2.8 | 165 | 5 | 3.90 |
| ANSS | 2003 | 6 | 30 | 19 | 21 | 17.20 | 41.800 | 81.200 | 4.6 | 549 | | 3.58 |
| ANSS | 2003 | 8 | 26 | 18 | 24 | 18.40 | 40.606 | 75.106 | 3 | 266 | | 3.74 |
| ANSS | 2003 | 11 | 4 | 13 | 37 | 31.80 | 40.251 | 75.877 | 1 | 207 | | 2.85 |
| SEUSSN | 2003 | 12 | 9 | 20 | 59 | 18.70 | 37.774 | 78.100 | 10 | 162 | 6 | 4.50 |
| Canada | 2004 | 6 | 16 | 6 | 31 | 26.00 | 42.790 | 79.010 | 7 | 529 | | 3.10 |
| ANSS | 2004 | 6 | 30 | 4 | 3 | 14.58 | 41.780 | 81.080 | 5 | 541 | | 3.33 |
| ANSS | 2005 | 2 | 8 | 11 | 42 | 53.00 | 37.220 | 81.930 | 9.4 | 499 | | 2.85 |
| ANSS | 2005 | 2 | 15 | 2 | 36 | 55.00 | 37.190 | 81.920 | 11.2 | 499 | | 2.93 |
| ANSS | 2005 | 8 | 25 | 3 | 9 | 42.00 | 35.880 | 82.800 | 7.9 | 629 | | 3.66 |
| ANSS | 2005 | 12 | 7 | 19 | 29 | 45.83 | 35.862 | 82.380 | 5 | 597 | | 2.93 |
| ANSS | 2006 | 3 | 7 | 10 | 28 | 2.00 | 35.910 | 82.340 | 3.7 | 591 | | 2.93 |
| ANSS | 2006 | 3 | 11 | 12 | 27 | 15.60 | 41.780 | 81.390 | 5 | 560 | | 3.17 |
| ANSS | 2006 | 6 | 20 | 20 | 11 | 18.54 | 41.840 | 81.230 | 5 | 554 | | 3.80 |

Note:  Information included in Int column when reference material provided the information.

## Table 2.5-3—{Conversion Between Body-Wave (m_b) and Moment (M) Magnitudes}

| Convert | To | Convert | To |
|---|---|---|---|
| m_b | M | M | m_b |
| 4.00 | 3.77 | 4.00 | 4.28 |
| 4.10 | 3.84 | 4.10 | 4.41 |
| 4.20 | 3.92 | 4.20 | 4.54 |
| 4.30 | 4.00 | 4.30 | 4.66 |
| 4.40 | 4.08 | 4.40 | 4.78 |
| 4.50 | 4.16 | 4.50 | 4.90 |
| 4.60 | 4.24 | 4.60 | 5.01 |
| 4.70 | 4.33 | 4.70 | 5.12 |
| 4.80 | 4.42 | 4.80 | 5.23 |
| 4.90 | 4.50 | 4.90 | 5.33 |
| 5.00 | 4.59 | 5.00 | 5.43 |
| 5.10 | 4.69 | 5.10 | 5.52 |
| 5.20 | 4.78 | 5.20 | 5.61 |
| 5.30 | 4.88 | 5.30 | 5.70 |
| 5.40 | 4.97 | 5.40 | 5.78 |
| 5.50 | 5.08 | 5.50 | 5.87 |
| 5.60 | 5.19 | 5.60 | 5.95 |
| 5.70 | 5.31 | 5.70 | 6.03 |
| 5.80 | 5.42 | 5.80 | 6.11 |
| 5.90 | 5.54 | 5.90 | 6.18 |
| 6.00 | 5.66 | 6.00 | 6.26 |
| 6.10 | 5.79 | 6.10 | 6.33 |
| 6.20 | 5.92 | 6.20 | 6.40 |
| 6.30 | 6.06 | 6.30 | 6.47 |
| 6.40 | 6.20 | 6.40 | 6.53 |
| 6.50 | 6.34 | 6.50 | 6.60 |
| 6.60 | 6.49 | 6.60 | 6.66 |
| 6.70 | 6.65 | 6.70 | 6.73 |
| 6.80 | 6.82 | 6.80 | 6.79 |
| 6.90 | 6.98 | 6.90 | 6.85 |
| 7.00 | 7.16 | 7.00 | 6.91 |
| 7.10 | 7.33 | 7.10 | 6.97 |
| 7.20 | 7.51 | 7.20 | 7.03 |
| 7.30 | 7.69 | 7.30 | 7.09 |
| 7.40 | 7.87 | 7.40 | 7.15 |
| 7.50 | 8.04 | 7.50 | 7.20 |
|  |  | 7.60 | 7.26 |
|  |  | 7.70 | 7.32 |
|  |  | 7.80 | 7.37 |
|  |  | 7.90 | 7.43 |
|  |  | 8.00 | 7.49 |

**Table 2.5-4—{Summary of Bechtel Group Seismic Sources}**

| Source | Description | Distance[1] (km) | (mi) | Pa [2] | M$_{max}$ (m$_b$) and Wts[3] | Smoothing Options and Wts[4] | Contributed to 99% of EPRI Hazard[5] | Geometry?[6] | M$_{max}$?[7] | RI?[8] |
|---|---|---|---|---|---|---|---|---|---|---|
| | | | | | | | | New Information to Suggest Change in Source: | | |
| **Sources within 200 mi (320 km)** | | | | | | | | | | |
| BZ5 | S. Appalachians | 0 | 0 | 1.00 | 5.7 (0.10) 6.0 (0.40) 6.3 (0.40) 6.6 (0.10) | 1 (0.33) 2 (0.34) 3 (0.33) | Yes | No | No | No |
| E | Central Virginia | 79 | 49 | 0.35 | 5.4 (0.10) 5.7 (0.40) 6.0 (0.40) 6.6 (0.10) | 1 (0.33) 2 (0.34) 4 (0.33) | Yes | No | No | No |
| BZ4 | Atlantic Coastal Region | 104 | 65 | 1.00 | 6.6 (0.10) 6.8 (0.10) 7.1 (0.40) 7.4 (0.40) | 1 (0.33) 2 (0.34) 3 (0.33) | Yes | No | No | No |
| 17 | Stafford fault zone | 70 | 43 | 0.10 | 5.4 (0.10) 5.7 (0.40) 6.0 (0.40) 6.6 (0.10) | 1 (0.33) 2 (0.34) 4 (0.33) | No | No | No | No |
| 13 | Eastern Mesozoic Basins | 99 | 62 | 0.10 | 5.4 (0.10) 5.7 (0.40) 6.0 (0.40) 6.6 (0.10) | 1 (0.33) 2 (0.34) 4 (0.33) | No | No | No | No |
| 24 | Bristol Trends | 135 | 84 | 0.25 | 5.7 (0.10) 6.0 (0.40) 6.3 (0.40) 6.6 (0.10) | 1 (0.33) 2 (0.34) 4 (0.33) | No | No | No | No |
| 23 | Lebanon Trend | 177 | 110 | 0.05 | 5.4 (0.10) 5.7 (0.40) 6.0 (0.40) 6.6 (0.10) | 1 (0.33) 2 (0.34) 4 (0.33) | No | No | No | No |
| 25 | NY-Alabama Lineament | 240 | 149 | 0.30 | 5.4 (0.10) 5.7 (0.40) 6.0 (0.40) 6.6 (0.10) | 1 (0.33) 2 (0.34) 4 (0.33) | No | No | No | No |

Notes:
1. Closest Distance between site and source measured in WLA GIS system using EPRI source files
2. Pa = probability of activity
3. Maximum Magnitude (M$_{max}$) and weights (wts.)
4. Smoothing options are defined as follows:
   1 = constant a, constant b (no prior b)
   2 = low smoothing on a, high smoothing on b (no prior b)
   3 = low smoothing on a, low smoothing on b (no prior b)
   4 = low smoothing on a, low smoothing on b (weak prior of 1.05)
   Weights on magnitude intervals are (1.0, 1.0, 1.0, 1.0, 1.0, 1.0, 1.0)
5. Did the source contribute to 99% of EPRI hazard calculated at CCNPP?
6. No, unless new geometry proposed in literature
7. No, unless EPRI M$_{max}$ exceeded in literature
8. RI = recurrence interval; assumed no change if no new paleoseismic data or rate of seismicity has not significantly changed.

## Table 2.5-5—{Summary of Dames & Moore Seismic Sources}
### (Page 1 of 2)

| Source | Description | Distance[1] (km) | Distance[1] (mi) | Pa[2] | $M_{max}$ ($m_b$) and Wts.[3] | Smoothing Options and Wts.[4] | Contributed to 99% of EPRI Hazard[5] | New Information to Suggest Change in Source: Geometry?[6] | $M_{max}$?[7] | RI?[8] |
|---|---|---|---|---|---|---|---|---|---|---|
| **Sources within 200 mi (320 km)** | | | | | | | | | | |
| 47 | Connecticut Basin | 0 | 0 | 0.28 | 6.0 (0.75) 7.2 (0.25) | 3 (0.75) 4 (0.25) | Yes | No | No | No |
| 53 | S. Appalachian Mobile Belt (Default Zone) | 0 | 0 | 0.26 | 5.6 (0.80) 7.2 (0.20) | 1 (0.75) 2 (0.25) | Yes | No | No | No |
| 41 | S. Cratonic Margin (Default Zone) | 65 | 40 | 0.12 | 6.1 (0.80) 7.2 (0.20) | 1 (0.75) 2 (0.25) | Yes | No | No | No |
| 42 | Newark-Gettysburg Basin | 92 | 57 | 0.40 | 6.3 (0.75) 7.2 (0.25) | 3 (0.75) 4 (0.25) | Yes | No | No | No |
| 40 | Central VA Seismic Zone | 110 | 68 | 1.00 | 6.6 (0.80) 7.2 (0.20) | 1 (0.75) 2 (0.25) | Yes | No | No | No |
| 4 | Appalachian Fold Belts | 138 | 86 | 0.35 | 6.0 (0.80) 7.2 (0.20) | 1 (0.75) 2 (0.25) | Yes | No | No | No |
| 4A | Kink in Fold Belts | 669 | 416 | 0.65 | 6.8 (0.75) 7.2 (0.25) | 3 (0.75) 4 (0.25) | Yes | No[9] | No | No |
| 44 | Stafford Fault Zone | 64 | 40 | 1.00 | 5.0 (0.80) 7.2 (0.20) | 1 (0.69) 2 (0.23) 3 (0.06) 4 (0.02) | No | No | No | No |
| C01 | Combination zone 4-4A-4B-4C-4D | 138 | 86 | NA | 6.0 (0.80) 7.2 (0.20) | 1 (0.75) 2 (0.25) | No | No | No | No |
| 4C | Kink in Fold Belt | 164 | 102 | 0.65 | 5.0 (0.75) 7.2 (0.25) | 3 (0.75) 4 (0.25) | No | No | No | No |
| 45 | Hopewell Fault Zone | 181 | 112 | 1.00 | 5.0 (0.80) 7.2 (0.20) | 1 (0.69) 2 (0.23) 3 (0.06) 4 (0.02) | No | No | No | No |
| 48 | Buried Triassic Basins | 197 | 122 | 0.28 | 6.0 (0.75) 7.2 (0.25) | 3 (0.75) 4 (0.25) | No | No | No | No |
| 46 | Dan River Basin | 241 | 150 | 0.28 | 6.0 (0.75) 7.2 (0.25) | 3 (0.75) 4 (0.25) | No | No | No | No |
| 8 | E. Marginal Basin | 272 | 169 | 0.08 | 5.6 (0.80) 7.2 (0.20) | 1 (0.75) 2 (0.25) | No | No | No | No |

**Table 2.5-5—{Summary of Dames & Moore Seismic Sources}**
(Page 2 of 2)

| Source | Description | Distance[1] (km) | Distance[1] (mi) | Pa[2] | $M_{max}$ ($m_b$) and Wts.[3] | Smoothing Options and Wts.[4] | Contributed to 99% of EPRI Hazard[5] | New Information to Suggest Change in Source: Geometry?[6] | New Information to Suggest Change in Source: $M_{max}$?[7] | New Information to Suggest Change in Source: RI?[8] |
|---|---|---|---|---|---|---|---|---|---|---|
| **Sources within 200 mi (320 km)** | | | | | | | | | | |
| C02 | Combination zone    8-9 | 272 | 169 | NA | 5.6 (0.80) 7.2 (0.20) | 1 (0.75) 2 (0.25) | No | No | No | No |
| 4B | Kink in Fold Belt    (Giles Co. Area) | 273 | 170 | 0.65 | 6.2 (0.75) 7.2 (0.25) | 3 (0.75) 4 (0.25) | No | No | No | No |
| 4D | Kink in Fold Belt | 279 | 173 | 0.65 | 5.6 (0.75) 7.2 (0.25) | 3 (0.75) 4 (0.25) | No | No | No | No |
| 49 | Jonesboro Basin | 302 | 188 | 0.28 | 6.0 (0.75) 7.2 (0.25) | 3 (0.75) 4 (0.25) | No | No | No | No |
| 43 | Ramapo Fault | 319 | 198 | 0.20 | 6.1 (0.75) 7.2 ( 0.25) | 3 (0.75) 4 (0.25) | No | No | No | No |

1. Closest Distance between site and source measured in WLA GIS system using EPRI source files
2. Pa = probability of activity
3. Maximum Magnitude ($M_{max}$) and weights (wts.)
4. Smoothing options are defined as follows:
1 =  No smoothing on a, no smoothing on b (strong prior of 1.04)
2 =  No smoothing on a, no smoothing on b (weak prior of 1.04)
3 =  Constant a, constant b (strong prior of 1.04)
4 =  Constant a, constant b (weak prior of 1.04)
Weights on magnitude intervals are (0.1, 0.2, 0.4, 1.0, 1.0, 1.0, 1.0)
5. Did the source contribute to 99% of EPRI hazard calculated at CCNPP?
6. No, unless new geometry proposed in literature
7. No, unless EPRI $M_{max}$ exceeded in literature
8. RI = recurrence interval; assumed no change if no new paleoseismic data or rate of seismicity has not significantly changed.
9. This source zone falls outside the project area and was not covered by the post-EPRI earthquake catalog  discussed in 2.5.2.1.

2‑1256

Rev. 4

Geology, Seismology, and Geotechnical Engineering

**Table 2.5-6—{Summary of Law Engineering Seismic Sources}**

(Page 1 of 2)

| Source | Description | Distance[1] (km) | (mi) | Pa[2] | $M_{max}$ ($m_b$) and Wts.[3] | Smoothing Options and Wts.[4] | Contributed to 99% of EPRI Hazard[5] | New Information to Suggest Change in Source: Geometry?[6] | $M_{max}$?[7] | RI?[8] |
|---|---|---|---|---|---|---|---|---|---|---|
| **Sources within 200 mi (320 km)** | | | | | | | | | | |
| C11 | Combination Zone 22-35 | 0 | 0 | NA | 6.8 (1.00) | 2a (1.00) | Yes | No | No | No |
| 22 | Reactivated E. Seaboard Normal | 0 | 0 | 0.27 | 6.8 (1.00) | 2a (1.00) | Yes | No | No | No |
| C10 | Combination Zone 8-35 | 7.5 | 5 | NA | 6.8 (1.00) | 2a (1.00) | Yes | No | No | No |
| C09 | Mesozoic Basins (8-bridged) | 7.5 | 5 | NA | 6.8 (1.00) | 2a (1.00) | Yes | No | No | No |
| 107 | Eastern Piedmont | 8 | 5 | 1.00 | 4.9 (0.30) 5.5 (0.40) 5.7 (0.30) | 1a (1.00) | Yes | No | No | No |
| 17 | Eastern Basement | 71 | 44 | 0.62 | 5.7 (0.20) 6.8 (0.80) | 1b (1.00) | Yes | No | No | No |
| M21 | Mafic Pluton | 83 | 52 | 0.43 | 6.8 (1.00) | 5 (1.00) (a = 0.65, b = 0.99) | Yes | No | No | No |
| M20 | Mafic Pluton | 90 | 56 | 0.43 | 6.8 (1.00) | 5 (1.00) (a = 0.57, b = 0.99) | Yes | No | No | No |
| M19 | Mafic Pluton | 100 | 62 | 0.43 | 6.8 (1.00) | 5 (1.00) (a = 0.35, b = 0.99) | Yes | No | No | No |
| M18 | Mafic Pluton | 128 | 80 | 0.43 | 6.8 (1.00) | 5 (1.00) (a = 0.22, b = 1.04) | Yes | No | No | No |
| M17 | Mafic Pluton | 169 | 105 | 0.43 | 6.8 (1.00) | 5 (1.00) (a = 0.5, b = 1.04) | Yes | No | No | No |
| M16 | Mafic Pluton | 186 | 116 | 0.43 | 6.8 (1.00) | 5 (1.00) (a = 0.87, b = 1.04) | Yes | No | No | No |
| C13 | Combination Zone 22 - 24 - 35 | 0 | 0 | NA | 6.8 (1.00) | 2a (1.00) | No | No | No | No |
| 8-16 | Mesozoic Basins – 16 | 7.5 | 5 | 0.27 | 6.8 (1.00) | a and b values calculated for C09 | No | No | No | No |
| 217 | Eastern Basement Background | 71 | 44 | 1.00 | 4.9 (0.50) 5.7 (0.50) | 1b (1.00) | No | No | No | No |
| M25 | Mafic Pluton | 124 | 77 | 0.43 | 6.8 (1.00) | 5 (1.00) (a = -0.48, b = 1.05) | No | No | No | No |
| M22 | Mafic Pluton | 148 | 92 | 0.43 | 6.8 (1.00) | 5 (1.00) (a = 0.66, b = 0.99) | No | No | No | No |
| M26 | Mafic Pluton | 158 | 98 | 0.43 | 6.8 (1.00) | 5 (1.00) (a = -0.32, b = 1.05) | No | No | No | No |

# Table 2.5-6—{Summary of Law Engineering Seismic Sources}

(Page 2 of 2)

| Source | Description | Distance[1] | | | $M_{max}$ | Smoothing | Contributed to 99% of EPRI | New Information to Suggest Change in Source: | | |
|---|---|---|---|---|---|---|---|---|---|---|
| | | (km) | (mi) | Pa[2] | ($m_b$) and Wts.[3] | Options and Wts.[4] | Hazard[5] | Geometry?[6] | $M_{max}$?[7] | RI?[8] |
| **Sources within 200 mi (320 km)** | | | | | | | | | | |
| M23 | Mafic Pluton | 198 | 123 | 0.43 | 6.8 (1.00) | 5 (1.00)<br>(a = 1.26, b = 0.99) | No | No | No | No |
| M24 | Mafic Pluton | 204 | 127 | 0.43 | 6.8 (1.00) | 5 (1.00)<br>(a = 1.27, b = 0.99) | No | No | No | No |
| 8-12 | Mesozoic Basins – 12 | 207 | 129 | 0.27 | 6.8 (1.00) | a and b values calculated for C09 | No | No | No | No |
| 101 | Western New England | 214 | 133 | 1.00 | 4.5 (0.15)<br>5.5 (0.85) | 1c (1.00) | No | No | No | No |
| M30 | Mafic Pluton | 243 | 151 | 0.43 | 6.8 (1.00) | 5 (1.00)<br>(a = -1.23, b = 1.05) | No | No | No | No |
| M29 | Mafic Pluton | 257 | 160 | 0.43 | 6.8 (1.00) | 5 (1.00)<br>(a = -0.38, b = 1.05) | No | No | No | No |
| M27 | Mafic Pluton | 259 | 161 | 0.43 | 6.8 (1.00) | 5 (1.00)<br>(a = 0.41, b = 1.04) | No | No | No | No |
| 112 | Ohio-Pennsylvania Block | 269 | 167 | 1.00 | 4.6 (0.20)<br>5.1 (0.50)<br>5.5 (0.30) | 1a (1.00) | No | No | No | No |
| M28 | Mafic Pluton | 273 | 170 | 0.43 | 6.8 (1.00) | 5 (1.00)<br>(a = 0.38, b = 1.04) | No | No | No | No |

1. Closest Distance between site and source measured in WLA GIS system using EPRI source files
2. Pa = probability of activity
3. Maximum Magnitude ($M_{max}$) and weights (wts.)
4. Smoothing options are defined as follows:
   - 1a = High smoothing on a, constant b (strong prior of 1.05)
   - 1b = High smoothing on b, constant b (strong prior of 1.00)
   - 1c = High smoothing on a, constant b (strong prior of 0.95)
   - 2a = Constant a, constant b (strong prior of 1.05)
   - 5 = a,b values as listed above, with weights shown
5. Did the source contribute to 99% of EPRI hazard calculated at CCNPP?
6. No, unless new geometry proposed in literature
7. No, unless EPRI $M_{max}$ exceeded in literature
8. RI = recurrence interval; assumed no change if no new paleoseismic data or rate of seismicity has not significantly changed.

**Table 2.5-7—{Summary of Rondout Seismic Sources}**
(Page 1 of 2)

| Source | Description | Distance[1] (km) | Distance[1] (mi) | Pa[2] | $M_{max}$ ($m_b$) and Wts.[3] | Smoothing Options and Wts.[4] | Contributed to 99% of EPRI Hazard[5] | Geometry?[6] | $M_{max}$?[7] | RI?[8] |
|---|---|---|---|---|---|---|---|---|---|---|
| **Sources within 200 mi (320 km)** | | | | | | | | | | |
| C01 | Background 49 | 0 | 0 | NA | 4.8 (0.20) 5.5 (0.60) 5.8 (0.20) | 3 (1.00) | Yes | No | No | No |
| 30 | Shenandoah | 21 | 13 | 0.96 | 5.2 (0.30) 6.3 (0.55) 6.5 (0.15) | 1 (1.00)  (a = -1.710, b = 1.010) | Yes | No | No | No |
| 29 | Central VA | 88 | 55 | 1.00 | 6.6 (0.30) 6.8 (0.60) 7.0 (0.10) | 1 (1.00)  (a = -0.900, b = 0.930) | Yes | No | No | No |
| 31 | Quakers | 112 | 70 | 1.00 | 5.8 (0.15) 6.5 (0.60) 6.8 (0.25) | 1 (1.00)  (a = -1.200, b = 0.960) | Yes | No | No | No |
| C09 | 49+32 | 0 | 0 | NA | 4.8 (0.20) 5.5 (0.60) 5.8 (0.20) | 3 (1.00) | No | No | No | No |
| 49-03 | Appalachian Basement 3 | 0 | 0 | 1.00 | 4.8 (0.20) 5.5 (0.60) 5.8 (0.20) | 2 (1.00) | No | No | No | No |
| 32 | Norfolk Fracture Zone | 116 | 72 | 0.67 | 5.8 (0.15) 6.5 (0.60) 6.8 (0.25) | 1 (1.00)  (a = -2.110, b = 1.040) | No | No | No | No |
| 49-04 | Appalachian Basement 4 | 198 | 123 | 1.00 | 4.8 (0.20) 5.5 (0.60) 5.8 (0.20) | 2 (1.00) | No | No | No | No |
| C07 | 50 (02) + 12 | 213 | 132 | NA | 4.8 (0.20) 5.5 (0.60) 5.8 (0.20) | 3 (1.00) | No | No | No | No |

## Table 2.5-7—{Summary of Rondout Seismic Sources}
(Page 2 of 2)

| Source | Description | Distance[1] (km) | (mi) | Pa[2] | $M_{max}$ ($m_b$) and Wts.[3] | Smoothing Options and Wts.[4] | Contributed to 99% of EPRI Hazard[5] | New Information to Suggest Change in Source: Geometry?[6] | $M_{max}$?[7] | RI?[8] |
|---|---|---|---|---|---|---|---|---|---|---|
| **Sources within 200 mi (320 km)** | | | | | | | | | | |
| 50-02 | Grenville Province 2 | 213 | 132 | 1.00 | 4.8 (0.20) 5.5 (0.60) 5.8 (0.20) | 2 (1.00) | No | No | No | No |
| 28 | Giles County | 316 | 196 | 1.00 | 6.6 (0.30) 6.8 (0.60) 7.0 (0.10) | 1 (1.00)   (a = -1.130, b = 0.900) | No | No | No | No |

1. Closest Distance between site and source measured in WLA GIS system using EPRI source files
2. Pa = probability of activity;
3. Maximum Magnitude ($M_{max}$) and weights (wts.)
4. Smoothing options are defined as follows:
1, 6, 7, 8 = a, b values as listed above, with weights shown
2 = Not listed in EQHAZARD Primer
3 = Low smoothing on a, constant b (strong prior of 1.0)
5 = a, b values as listed above, with weights shown
5. Did the source contribute to 99% of EPRI hazard calculated at CCNPP?
6. No, unless new geometry proposed in literature
7. No, unless EPRI $M_{max}$ exceeded in literature
8. RI = recurrence interval; assumed no change if no new paleoseismic data or rate of seismicity has not significantly changed.

**Table 2.5-8—{Summary of Weston Seismic Sources}**

(Page 1 of 3)

| Source | Description | Distance[1] (km) | Distance[1] (mi) | Pa[2] | $M_{max}$ ($m_b$) and Wts.[3] | Smoothing Options and Wts.[4] | Contributed to 99% of EPRI Hazard[5] | New Information to Suggest Change in Source: Geometry?[6] | $M_{max}$?[7] | RI?[8] |
|---|---|---|---|---|---|---|---|---|---|---|
| **Sources within 200 mi (320 km)** | | | | | | | | | | |
| C21 | Combination Zone 104-25 | 0 | 0 | NA | 5.4 (0.24) 6.0 (0.61) 6.6 (0.15) | 1a (0.30) 2a (0.70) | Yes | No | No | No |
| C23 | Combination Zone 104-22-26 | 0 | 0 | NA | 5.4 (0.80) 6.0 (0.14) 6.6 (0.06) | 1a (0.50) 2a (0.50) | Yes | No | No | No |
| C24 | Combination Zone 104-22-25 | 0 | 0 | NA | 5.4 (0.80) 6.0 (0.14) 6.6 (0.06) | 1a (0.50) 2a (0.50) | Yes | No | No | No |
| C27 | Combination Zone 104-28BCDE-22-25 | 0 | 0 | NA | 5.4 (0.30) 6.0 (0.70) | 1a (0.70) 2a (0.30) | Yes | No | No | No |
| C28 | Combination Zone 104-28BCDE-22-26 | 0 | 0 | NA | 5.4 (0.30) 6.0 (0.70) | 1a (0.70) 2a (0.30) | Yes | No | No | No |
| C34 | Combination Zone 104-28BE-26 | 0 | 0 | NA | 5.4 (0.24) 6.0 (0.61) 6.6 (0.15) | 1a (0.20) 1b (0.80) | Yes | No | No | No |
| C35 | Combination Zone 104-28BE-25 | 0 | 0 | NA | 5.4 (0.24) 6.0 (0.61) 6.6 (0.15) | 1a (0.20) 1b (0.80) | Yes | No | No | No |
| 28E | Zone of Mesozoic Basin | 7 | 4 | 0.26 | 5.4 (0.65) 6.0 (0.25) 6.6 (0.10) | 1b (1.00) | Yes | No | No | No |
| 22 | Central VA Seismic Zone | 72 | 45 | 0.82 | 5.4 (0.19) 6.0 (0.65) 6.6 (0.16) | 1b (1.00) | Yes | No | No | No |
| C19 | Combination Zone 103-23-24 | 118 | 73 | NA | 5.4 (0.26) 6.0 (0.58) 6.6 (0.16) | 1a (1.00) | Yes | No | No | No |
| C07 | Combination Zone 21-19 | 182 | 113 | NA | 5.4 (0.62) 6.0 (0.29) 6.6 (0.09) | 1b (0.70) 2b (0.30) | Yes | No | No | No |
| C22 | Combination Zone 104-26 | 0 | 0 | NA | 5.4 (0.24) 6.0 (0.61) 6.6 (0.15) | 1a (0.30) 1b (0.70) | No | No | No | No |

## Table 2.5-8—{Summary of Weston Seismic Sources}

(Page 2 of 3)

| Source | Description | Distance[1] (km) | (mi) | Pa[2] | $M_{max}$ ($m_b$) and Wts.[3] | Smoothing Options and Wts.[4] | Contributed to 99% of EPRI Hazard[5] | New Information to Suggest Change in Source: Geometry?[6] | $M_{max}$?[7] | RI?[8] |
|---|---|---|---|---|---|---|---|---|---|---|
| **Sources within 200 mi (320 km)** | | | | | | | | | | |
| C25 | Combination Zone 104-28BCDE | 0 | 0 | NA | 5.4 (0.24) 6.0 (0.61) 6.6 (0.15) | 1a (0.30) 2a (0.70) | No | No | No | No |
| C26 | Combination Zone 104-28BCDE-22 | 0 | 0 | NA | 5.4 (0.24) 6.0 (0.61) 6.6 (0.15) | 1a (0.30) 2a (0.70) | No | No | No | No |
| 104 | Southern Coastal Plain | 0 | 0 | 1.00 | 5.4 (0.24) 6.0 (0.61) 6.6 (0.15) | 1a (0.20) 2a (0.80) | No | No | No | No |
| C01 | Combination Zone 28A thru E | 7 | 4 | NA | 5.4 (0.65) 6.0 (0.25) 6.6 (0.10) | 1b (1.00) | No | No | No | No |
| 28B | Zone of Mesozoic Basin | 92 | 57 | 0.26 | 5.4 (0.65) 6.0 (0.25) 6.6 (0.10) | 1b (1.00) | No | No | No | No |
| 103 | Southern Appalachians | 118 | 73 | 1.00 | 5.4 (0.26) 6.0 (0.58) 6.6 (0.16) | 1a (0.20)   2a (0.80) | No | No | No | No |
| C17 | Combination Zone 103-23 | 118 | 73 | NA | 5.4 (0.26) 6.0 (0.58) 6.6 (0.16) | 1a (0.70) 2a (0.30) | No | No | No | No |
| C18 | Combination Zone 103-24 | 118 | 73 | NA | 5.4 (0.26) 6.0 (0.58) 6.6 (0.16) | 1a (0.70) 1b (0.30) | No | No | No | No |
| 21 | New York Nexus | 182 | 113 | 1.00 | 5.4 (0.62) 6.0 (0.29) 6.6 (0.09) | 1b (1.00) | No | No | No | No |
| C08 | Combination Zone 21-19-10A | 182 | 113 | NA | 5.4 (0.62) 6.0 (0.29) 6.6 (0.09) | 1b (0.70) 2b (0.30) | No | No | No | No |
| 28A | Mesozoic Basin (or Intersection of sources 28 and 21) | 182 | 113 | 0.26 | 5.4 (0.65) 6.0 (0.25) 6.6 (0.10) | 1b (1.00) | No | No | No | No |

## Table 2.5-8—{Summary of Weston Seismic Sources}
(Page 3 of 3)

| Source | Description | Distance[1] (km) | (mi) | Pa[2] | M$_{max}$ (m$_b$) and Wts.[3] | Smoothing Options and Wts.[4] | Contributed to 99% of EPRI Hazard[5] | New Information to Suggest Change in Source: Geometry?[6] | M$_{max}$?[7] | RI?[8] |
|---|---|---|---|---|---|---|---|---|---|---|
| **Sources within 200 mi (320 km)** | | | | | | | | | | |
| 28D | Zone of Mesozoic Basin | 205 | 127 | 0.26 | 5.4 (0.65) 6.0 (0.25) 6.6 (0.10) | 1b (1.00) | No | No | No | No |
| C09 | Combination Zone 21-19-10A-28A | 213 | 132 | NA | 5.4 (0.62) 6.0 (0.29) 6.6 (0.09) | 1b (1.00) | No | No | No | No |
| C10 | Combination Zone 21-19-28A | 213 | 132 | NA | 5.4 (0.62) 6.0 (0.29) 6.6 (0.09) | 1b (1.00) | No | No | No | No |
| 28C | Zone of Mesozoic Basin | 263 | 163 | 0.26 | 5.4 (0.65) 6.0 (0.25) 6.6 (0.10) | 1b (1.00) | No | No | No | No |
| 102 | Appalachian Plateau | 290 | 180 | 1.00 | 5.4 (0.62) 6.0 (0.29) 6.6 (0.09) | 1a (0.20) 2a (0.80) | No | No | No | No |

1. Closest Distance between site and source measured in WLA GIS system using EPRI source files
2. Pa = probability of activity
3. Maximum Magnitude (M$_{max}$) and weights (wts.)
4. Smoothing options are defined as follows:
1a = Constant a, constant b (medium prior of 1.0)
1b = Constant a, constant b (medium prior of 0.9)
2a = Medium smoothing on a, medium smoothing on b (medium prior of 1.0)
2b = Medium smoothing on a, medium smoothing on b (medium prior of 0.9)
5. Did the source contribute to 99% of EPRI hazard calculated at CCNPP?
6. No, unless new geometry proposed in literature
7. No, unless EPRI M$_{max}$ exceeded in literature
8. RI = recurrence interval; assumed no change if no new paleoseismic data or rate of seismicity has not significantly changed.

## Table 2.5-9—{Summary of Woodward-Clyde Seismic Sources}
(Page 1 of 2)

| Source | Description | Distance[1] (km) | Distance[1] (mi) | Pa[2] | $M_{max}$ ($m_b$) and Wts.[3] | Smoothing Options and Wts.[4] | Contributed to 99% of EPRI Hazard[5] | New Information to Suggest Change in Source: Geometry?[6] | $M_{max}$?[7] | RI?[8] |
|---|---|---|---|---|---|---|---|---|---|---|
| **Sources within 200 mi (320 km)** | | | | | | | | | | |
| B20 | Calvert Cliffs Background | 0 | 0 | NA | 5.8 (0.33) 6.2 (0.34) 6.6 (0.33) | 1 (0.25) 6 (0.25) 7 (0.25) 8 (0.25) | Yes | No | No | No |
| 61 | Tyrone-Mt. Union Lineament | 0 | 0 | 0.048 | 5.4 (0.33) 6.5 (0.34) 7.1 (0.33) | 3 (0.33) 4 (0.34) 5 (0.33) | Yes | No | No | No |
| 21 | New Jersey Isostatic Gravity Saddle | 77 | 48 | 0.135 | 5.3 (0.33) 6.5 (0.34) 6.9 (0.33) | 2 (0.10) 3 (0.10) 4 (0.10) 5 (0.10) 9 (0.60) (a = -1.406, b = 1.020) | Yes | No | No | No |
| 63 | Pittsburg-Washington Lineament | 84 | 52 | 0.050 | 5.4 (0.33) 6.3 (0.34) 7.1 (0.33) | 3 (0.33) 4 (0.34) 5 (0.33) | Yes | No | No | No |
| 26 | Central VA Gravity Saddle | 108 | 67 | 0.434 | 5.4 (0.33) 6.5 (0.34) 7.0 (0.33) | 2 (0.25) 3 (0.25) 4 (0.25) 5 (0.25) | Yes | No | No | No |
| 27 | State Farm Complex | 111 | 69 | 0.474 | 5.6 (0.33) 6.3 (0.34) 6.9 (0.33) | 2 (0.25) 3 (0.25) 4 (0.25) 5 (0.25) | Yes | No | No | No |
| 23 | Newark Basin Perimeter | 166 | 103 | 0.374 | 5.5 (0.33) 6.3 (0.34) 6.8 (0.33) | 2 (0.10) 3 (0.10) 4 (0.10) 5 (0.10) 9 (0.60) (a = 1.415, b = 0.900) | Yes | No | No | No |
| 21A | New Jersey Isostatic Gravity Saddle No. 2 (Combo C2) | 77 | 48 | 0.045 | 5.5 (0.33) 6.3 (0.34) 7.1 (0.33) | 2 (0.10) 3 (0.10) 4 (0.10) 5 (0.10) 9 (0.60) (a = -1.406, b = 1.020) | No | No | No | No |
| 28 | Richmond Basin | 135 | 84 | 0.092 | 5.3 (0.33) 6.0 (0.34) 7.2 (0.33) | 3 (0.33) 4 (0.34) 5 (0.33) | No | No | No | No |
| 02 | Cont. Shelf Int | 147 | 91 | 0.129 | 5.3 (0.33) 6.5 (0.34) 6.8 (0.33) | 3 (0.33) 4 (0.34) 5 (0.33) | No | No | No | No |
| 53 | SE NY/NJ/PA NOTA Zone | 154 | 96 | 0.100 | 5.5 (0.33) 6.3 (0.34) 6.8 (0.33) | 2 (0.10) 3 (0.10) 4 (0.10) 5 (0.10) 9 (0.60) (a = -1.406, b = 1.020) | No | No | No | No |

**Table 2.5-9—{Summary of Woodward-Clyde Seismic Sources}**
(Page 2 of 2)

| Source | Description | Distance[1] (km) | (mi) | Pa[2] | $M_{max}$ ($m_b$) and Wts.[3] | Smoothing Options and Wts.[4] | Contributed to 99% of EPRI Hazard[5] | New Information to Suggest Change in Source: Geometry?[6] | $M_{max}$?[7] | RI?[8] |
|---|---|---|---|---|---|---|---|---|---|---|
| **Sources within 200 mi (320 km)** | | | | | | | | | | |
| 01 | Cont. Shelf | 171 | 106 | 0.158 | 5.4 (0.33)<br>5.5 (0.34)<br>7.0 (0.33) | 3 (0.33)<br>4 (0.34)<br>5 (0.33) | No | No | No | No |
| 22 | Newark Basin | 194 | 121 | 0.078 | 5.5 (0.33)<br>6.5 (0.34)<br>7.1 (0.33) | 2 (0.10)<br>3 (0.10)<br>4 (0.10)<br>5 (0.10)<br>9 (0.60)<br>(a = -1.503, b = 0.776) | No | No | No | No |
| 24 | Ramapo Fault | 315 | 196 | 0.128 | 5.8 (0.33)<br>6.8 (0.34)<br>7.1 (0.33) | 3 (0.33)<br>4 (0.34)<br>5 (0.33) | No | No | No | No |
| 25 | Hudson Valley | 315 | 196 | 0.140 | 5.5 (0.33)<br>6.3 (0.34)<br>6.8 (0.33) | 2 (0.20)<br>3 (0.20)<br>4 (0.20)<br>5 (0.20)<br>9 (0.20)<br>(a = -0.929, b = 0.857) | No | No | No | No |

1. Closest Distance between site and source measured in WLA GIS system using EPRI source files
2. Pa = probability of activity
3. Maximum Magnitude ($M_{max}$) and weights (wts.)
4. Smoothing options are defined as follows:

    1 = Low smoothing on a, high smoothing on b (no prior)
    2 = High smoothing on a, high smoothing on b (no prior)
    3 = High smoothing on a, high smoothing on b (moderate prior of 1.0)
    4 = High smoothing on a, high smoothing on b (moderate prior of 0.9)
    5 = High smoothing on a, high smoothing on b (moderate prior of 0.8)
    6 = Low smoothing on a, high smoothing on b (moderate prior of 1.0)
    7 = Low smoothing on a, high smoothing on b (moderate prior of 0.9)
    8 = Low smoothing on a, high smoothing on b (moderate prior of 0.8)
    Weights on magnitude intervals are all 1.0
    9 = a and b values as listed

5. Did the source contribute to 99% of EPRI hazard calculated at CCNPP?
6. No, unless new geometry proposed in literature
7. No, unless EPRI $M_{max}$ exceeded in literature.
8. RI = recurrence interval; assumed no change if no new paleoseismic data or rate of seismicity has not significantly changed.

**Table 2.5-10—{Comparison of EPRI Characterizations of the Central Virginia Seismic Zone}**

| EPRI Team | Source | Description | Distance[1] (km) | Distance[1] (mi) | Pa[2] | $M_{max}$ ($m_b$) and Wts.[3] | Largest $M_{max}$ Value Considered by EPRI Team (mb) | Largest $M_{max}$ Value Considered by EPRI Team (Mw[4]) | Contributed to 99% of EPRI Hazard[5] |
|---|---|---|---|---|---|---|---|---|---|
| Bechtel Group | E | Central Virginia | 79 | 49 | 0.35 | 5.4 (0.10) 5.7 (0.40) 6.0 (0.40) 6.6 (0.10) | 6.6 | 6.49 | Yes |
| Dames & Moore | 40 | Central VA Seismic Zone | 110 | 68 | 1.00 | 6.6 (0.80) 7.2 (0.20) | 7.2 | 7.51 | Yes |
| Law Engineering[6] | na | na | na | na | na | na | na | na | na |
| Rondout | 29 | Central VA | 85 | 55 | 1.00 | 6.6 (0.30) 6.8 (0.60) 7.0 (0.10) | 7.0 | 7.16 | Yes |
| Weston | 22 | Central VA Seismic Zone | 72 | 45 | 0.82 | 5.4 (0.19) 6.0 (0.65) 6.6 (0.16) | 6.6 | 6.49 | Yes |
| Woodward-Clyde Consultants | 26 | Central VA Gravity Saddle | 108 | 67 | 0.434 | 5.4 (0.33) 6.5 (0.34) 7.0 (0.33) | 7.0 | 7.16 | Yes |
| Range of Largest $M_{max}$ Value Considered by EPRI Teams = | | | | | | $m_b$ 6.6 - 7.2 **M 6.5 - 7.5** | | | |
| Average of Largest $M_{max}$ Values for 5 EPRI Teams ($m_b$) = | | | | | | 6.9 | | | |
| Average of Largest $M_{max}$ Values for 5 EPRI Teams (**M**) = | | | | | | 7.0 | | | |

1. Closest distance between site and source measured in WLA GIS system using EPRI source files
2. Pa = probability of activity
3. Maximum Magnitude ($M_{max}$) and weights (wts.)
4. mb converted from Mw using relations as presented in Microsoft Excel spreadsheet and included in Table 2.5-3
5. Source contribution to 99% of EPRI hazard at Calvert Cliffs
6. Law Engineering team did not define a Central VA seismic zone, but did define several mafic pluton sources in the central Virginia area. The seismicity parameters for the pluton sources were calculated from a large region surrounding each pluton, which effectively captured a majority of seismicity from the CVSZ

**Table 2.5-11—{Bollinger (1992) Seismic Source Zone Parameters}**

| Source | Description | Approx. Distance[1] | | a | b | $M_{max}$ mbLg[2] | Ms[2] | Mw[3] | Focal Depth Distribution (km) | |
|---|---|---|---|---|---|---|---|---|---|---|
| | | (km) | (mi) | | | | | | Upper Bound ($D_U$) 10% Quantile | Lower Bound ($D_L$) 90% Quantile |
| RZ6 | Central VA | 80 | 50 | 1.18 | 0.64 | 6.40 | 7.10 | 6.20 | 4.5 | 13.4 |
| RZ3 | Giles County, VA | 356 | 221 | 1.07 | 0.64 | 6.30 | 6.80 | 6.06 | 4.4 | 15.1 |
| CZ1 | Complementary (Background) | 0 | 0 | 2.70 | 0.84 | 5.75 | 5.80 | 5.36 | 3.3 | 18.5 |
| LZ1 | Charleston, SC | 665 | 413 | 1.69 | 0.77 | 6.90 | 8.10 | 6.98 | 5.0 | 10.2 |
| RZ4A | Eastern TN | 613 | 380 | 2.72 | 0.90 | 7.35 | 8.75 | 7.78 | 7.6 | 20.8 |
| RZ4 | Eastern TN | 613 | 380 | 2.72 | 0.90 | 6.45 | 7.15 | 6.27 | 7.6 | 20.8 |
| RZ5 | NW S.C. and SW N.C. | 534 | 331 | 2.14 | 0.82 | 6.00 | 6.20 | 5.66 | 2.3 | 11.2 |
| LZ3 | South Carolina Piedmont and Coastal Plain | 520 | 323 | 1.86 | 0.80 | 6.00 | 6.20 | 5.66 | 0.8 | 7.4 |
| LZ4 | SC Fall Line | 779 | 484 | 1.58 | 0.81 | 6.25 | 6.50 | 5.99 | 0.9 | 6.1 |
| LZ2 | Bowman, S.C. | 654 | 406 | 1.34 | 0.78 | 6.00 | 6.20 | 5.66 | 2.4 | 5.8 |
| LZ5 | Area of LZ3 minus Area of LZ4 | 534 | 331 | 1.70 | 0.80 | 6.00 | 6.20 | 5.66 | 0.9 | 6.5 |
| LZ6 | Savannah River Site | 715 | 444 | 1.34 | 0.80 | 6.50 | 7.20 | 6.34 | 0.8 | 7.4 |
| RZ1 | New Madrid, MO (small) | 1129 | 701 | 3.32 | 0.91 | 7.35 | 8.75 | 7.78 | 3.0 | 11.6 |
| RZ2 | New Madrid, MO (large) | 988 | 613 | 3.43 | 0.88 | 6.70 | 7.65 | 6.65 | 2.8 | 12.4 |

Note:

1　Closest Distance between site and source estimated (approximately)

2　$m_b$ and Ms values presented in Bollinger (1992).

3　**M** converted from mbLg using average relations as presented in Table 2.5-3

### Table 2.5-12—{Chapman Seismic Source Zone Parameters}

| Source | Description | Approx. Distance[1] (km) | (mi) | Area (sq. km ) | Reference [3] | $M_{max}$ [4, 5] (mbLg) | $M_{max}$ [6] ($M_w$) | $M_{max}$ [6] ($m_b$) |
|---|---|---|---|---|---|---|---|---|
| 1 | Giles County, VA | 350 | 217 | $5.1 \times 10^3$ | A | 7.25 | 7.53 | 7.22 |
| 2 | Central VA | 73 | 45 | $2.0 \times 10^4$ | A | 7.25 | 7.53 | 7.22 |
| 3 | Eastern TN | 660 | 410 | $3.7 \times 10^4$ | A | 7.25 | 7.53 | 7.22 |
| 4 | Southern Appalachians (VA, NC, SC, TN) | 290 | 180 | $7.6 \times 10^4$ | C | 7.25 | 7.53 | 7.22 |
| 5 | Northern VA, MD | 40 | 25 | $4.3 \times 10^4$ | C | 7.25 | 7.53 | 7.22 |
| 6 | Central Appalachians (PA, NJ, NY) | 100 | 60 | $6.8 \times 10^4$ | C | 7.25 | 7.53 | 7.22 |
| 7 | Piedmont - Coastal Plain | 0 | 0 | $4.4 \times 10^5$ | C | 7.25 | 7.53 | 7.22 |
| 8 | Charleston, SC | 680 | 420 | $1.2 \times 10^3$ | A | 7.25 | 7.53 | 7.22 |
| 9 | Appalachian Foreland (TN, KY, OH, WVA, PA) | 100 | 60 | $6.5 \times 10^5$ | A | 7.25 | 7.53 | 7.22 |
| 10 | New Madrid, MO | 1165 | 725 | $6.1 \times 10^3$ | B | 7.70 | 8.28 | 7.32 |

Notes:

| | | | | | | | | |
|---|---|---|---|---|---|---|---|---|
| 1 | Closest Distance between site and source estimated (approximately) fromFigure 1 in Chapman (Chapman, 1994). | | | | | | | |
| 3 | Reference cited: | | | A | Bollinger (Bollinger, 1989) | | | |
| | | | | B | Johnston (Johnson, 1985) | | | |
| | | | | C | Chapman  (Chapman, 1994) | | | |
| 4 | Values listed in Chapman (Chapman, 1994).  With the exception of New Madrid, they assumed all sources would have the same $M_{max}$ as the largest EQ to have occurred in the southeastern U.S. region, the 1886 Charleston, SC event. The Johnston (1992) Mw 7.5 was used and converted to mbLg by Chapman  (Chapman, 1994) using Atkinson (Atkinson, 1987) relation. | | | | | | | |
| 5 | Note that more recent estimates of Charleston EQ magnitude are lower than Mw 7.53 of Johnston (1992): | | | | | | | |
| | | | Mw  =  7.3 +0.26/-0.26 (Johnston, 1996) | | | | | |
| | | | Mw  = 6.8 +0.3/-0.4 (Bakun, 2004) | | | | | |
| 6 | mb to Mw conversion done using average of  relations as presented in Microsoft Excel spreadsheet and in Table 2.5-3. | | | | | | | |

## Table 2.5-13—{Summary of Selected USGS Seismic Sources}

| Source | Description | $M_{max}$ ($M_w$) and Wts. | Largest $M_{max}$ Value Considered by USGS | |
|---|---|---|---|---|
| | | | $M_w$ | $m_b$ [1] |
| Sources within 200 mi (320 km) | | | | |
| | Extended Margin Background | 7.5 (1.00) | 7.5 | 7.20 |
| Selected Sources Beyond 200 mi (320km) | | | | |
| | Charleston | 6.8 (0.20) 7.1 (0.20) 7.3 (0.45) 7.5 (0.15) | 7.5 | 7.20 |
| | Stable Craton Background | 7.0 (1.00) | 7.0 | 6.91 |
| | | | | |

Note:
(1)   mb converted from **M** using average relations, as presented in Table 2.5-3.

## Table 2.5-14—{Chapman and Talwani (2002) Seismic Source Zone Parameters}

| Charleston Characteristic Sources | Mean Recurrence | $M_{max}$ [2] mbLg | M |
|---|---|---|---|
| Charleston Area Source | 550 years | nr | 7.1 (.2)<br>7.3 (.6)<br>7.5 (.2) |
| ZRA Fault Source (Zone of River Anomalies) | 550 years | nr | 7.1 (.2)<br>7.3 (.6)<br>7.5 (.2) |
| Ashley River-Woodstock Fault Source (modeled as 3 parallel faults) | 550 years | nr | 7.1 (.2)<br>7.3 (.6)<br>7.5 (.2) |

| Non-Characteristic Background Sources | | $a$ [1] | $b$ [1] | mbLg | M |
|---|---|---|---|---|---|
| 1. | Zone1 | 0.242 | 0.84 | 6.84 | 7.00 |
| 2. | Zone2 | -0.270 | 0.84 | 6.84 | 7.00 |
| 3. | Central Virginia | 1.184 | 0.64 | 6.84 | 7.00 |
| 4. | Zone4 | 0.319 | 0.84 | 6.84 | 7.00 |
| 5. | Zone5 | 0.596 | 0.84 | 6.84 | 7.00 |
| 6. | Piedmont and Coastal Plain | 1.537 | 0.84 | 6.84 | 7.00 |
| 6a. | Pied&CP NE | 0.604 | 0.84 | 6.84 | 7.00 |
| 6b. | Pied&CP SW | 1.312 | 0.84 | 6.84 | 7.00 |
| 7. | South Carolina Piedmont | 2.220 | 0.84 | 6.84 | 7.00 |
| 8. | Middleton Place | 1.690 | 0.77 | 6.84 | 7.00 |
| 9. | Florida and continental margin | 1.371 | 0.84 | 6.84 | 7.00 |
| 10. | Alabama | 1.800 | 0.84 | 6.84 | 7.00 |
| 11. | Eastern Tennessee | 2.720 | 0.90 | 6.84 | 7.00 |
| 12. | Southern Appalachian | 2.420 | 0.84 | 6.84 | 7.00 |
| 12a. | Southern Appalachian North | 2.185 | 0.84 | 6.84 | 7.00 |
| 13. | Giles County, VA | 1.070 | 0.84 | 6.84 | 7.00 |
| 14. | Central Appalachians | 1.630 | 0.84 | 6.84 | 7.00 |
| 15. | Western Tennessee | 2.431 | 1.00 | 6.84 | 7.00 |
| 16. | Central Tennessee | 2.273 | 1.00 | 6.84 | 7.00 |
| 17. | Ohio-Kentucky | 2.726 | 1.00 | 6.84 | 7.00 |
| 18. | West VA-Pennsylvania | 2.491 | 1.00 | 6.84 | 7.00 |
| 19. | USGS (1996) gridded seismicity rates and b value | nr [3] | 0.95 | 6.84 | 7.00 |

Notes:

1　a and b values in terms of mbLg magnitude

2　$M_{max}$ range for characteristic events was designed to "represent the range of magnitude estimates of the 1886 Charleston shock. Square brackets indicate weights assigned to characteristic magnitudes. For non-characteristic background events, a truncated form of the exponential probability density function was used.

3　nr = not reported

**Table 2.5-15—{Summary of Charleston Seismic Sources Changed in New UCSS Model (Bechtel, 2006)}**

(Page 1 of 2)

| ESTs | Source | Description | Distance (km) | Distance (mi) | Pa[1] | $M_{max}$ ($m_b$) and Wts.[2] | Smoothing Options and Wts.[3] | Interdependencies[4] | New Information to Suggest Change in Source: Geometry?[5] | $M_{max}$?[6] | RI?[7] |
|---|---|---|---|---|---|---|---|---|---|---|---|
| Bechtel Group | H | Charleston Area | 644 | 400 | 0.50 | 6.8 (0.20) 7.1 (0.40) 7.4 (0.40) | 1 (0.33) 2 (0.34) 4 (0.33) | P(H\|N3) = 0.15 | Yes[8] | Yes[8] | Yes[8] |
| Bechtel Group | N3 | Charleston Faults | 673 | 418 | 0.53 | 6.8 (0.20) 7.1 (0.40) 7.4 (0.40) | 1 (0.33) 2 (0.34) 4 (0.33) | P(N3\|H) = 0.16 | Yes[8] | Yes[8] | Yes[8] |
| Dames & Moore | 54 | Charleston Seismic Zone | 637 | 395 | 1.00 | 6.6 (0.75) 7.2 (0.25) | 1 (0.22) 2 (0.08) 3 (0.52) 4 (0.18) | none | Yes[8] | Yes[8] | Yes[8] |
| Law Engineering | 35 | Charleston Seismic Zone | 648 | 403 | 0.45 | 6.8 (1.00) | 2a (1.00) | Overlaps 8 and 22 | Yes[8] | Yes[8] | Yes[8] |
| Rondout | 24 | Charleston | 631 | 392 | 1.00 | 6.6 (0.20) 6.8 (0.60) 7.0 (0.20) | 1 (1.00) (a = -0.710, b = 1.020) | none | Yes[8] | Yes[8] | Yes[8] |
| Weston | 25 | Charleston Seismic Zone | 619 | 384 | 0.99 | 6.6 (0.90) 7.2 (0.10) | 1b (1.00) | none | Yes[8] | Yes[8] | Yes[8] |
| Woodward-Clyde | 30 | Charleston (includes NOTA) | 646 | 401 | 0.573 | 6.8 (0.33) 7.3 (0.34) 7.5 (0.33) | 2 (0.10) 3 (0.10) 4 (0.10) 5 (0.10) 9 (0.60) (a = -1.005, b = 0.852) | ME with 29, 29A | Yes[8] | Yes[8] | Yes[8] |
| Woodward- Clyde | 29 | S. Carolina Gravity Saddle (Extended) | 534 | 332 | 0.122 | 6.7 (0.33) 7.0 (0.34) 7.4 (0.33) | 2 (0.25) 3 (0.25) 4 (0.25) 5 (0.25) | ME with 29A, 29B, and 30 | Yes[8] | Yes[8] | Yes[8] |

**Table 2.5-15—{Summary of Charleston Seismic Sources Changed in New UCSS Model (Bechtel, 2006)}**

(Page 2 of 2)

| ESTs | Source | Description | Distance (km) | Distance (mi) | Pa[1] | M$_{max}$ (m$_b$) and Wts.[2] | Smoothing Options and Wts.[3] | Interdependencies[4] | New Information to Suggest Change in Source: Geometry?[5] | New Information to Suggest Change in Source: M$_{max}$?[6] | New Information to Suggest Change in Source: RI?[7] |
|---|---|---|---|---|---|---|---|---|---|---|---|
| Woodward- Clyde | 29A | SC Gravity Saddle No. 2 (Combo C3) | 577 | 359 | 0.305 | 6.7 (0.33) 7.0 (0.34) 7.4 (0.33) | 2 (0.25) 3 (0.25) 4 (0.25) 5 (0.25) | ME with 29, 29B, and 30 | Yes[8] | Yes[8] | Yes[8] |
| Notes: | | | | | | | | | | | |
| 1 | Pa = probability of activity | | | | | | | | | | |
| 2 | Maximum Magnitude (M$_{max}$) and weights (wts.) | | | | | | | | | | |
| 3 | Smoothing options are defined as follows:  SeeTable 2.5-3 thru Table 2.5-8 for details. | | | | | | | | | | |
| 4 | ME = mutually exclusive; PD = perfectly dependent; | | | | | | | | | | |
| 5 | No, unless (1) new geometry proposed in literature or (2) new seismicity pattern | | | | | | | | | | |

**Table 2.5-16—{Geographic Coordinates (Latitude and Longitude) of Corner Points of Updated Charleston Seismic Source (UCSS) Geometries (Bechtel, 2006)}**

| Source Geometry | Longitude, West (decimal degrees) | Latitude, North (decimal degrees) |
|---|---|---|
| A | 80.707 | 32.811 |
| A | 79.840 | 33.354 |
| A | 79.527 | 32.997 |
| A | 80.392 | 32.455 |
| | | |
| B | 81.216 | 32.485 |
| B | 78.965 | 33.891 |
| B | 78.3432 | 33.168 |
| B | 80.587 | 31.775 |
| | | |
| B' | 78.965 | 33.891 |
| B' | 78.654 | 33.531 |
| B' | 80.900 | 32.131 |
| B' | 81.216 | 32.485 |
| | | |
| C | 80.397 | 32.687 |
| C | 79.776 | 34.425 |
| C | 79.483 | 34.351 |
| C | 80.109 | 32.614 |

### Table 2.5-17—{Local Charleston-Area Tectonic Features}

| Name of Feature | Evidence | Key References |
|---|---|---|
| **Adams Run fault** | **subsurface stratigraphy** | **(Weems, 2007)** |
| Ashley River fault | microseismicity | Talwani (1982, 2000) **(Weems, 2007)** |
| Appalachian detachment (decollement) | gravity & magnetic data seismic reflection & refraction | Cook (1979, 1981) Behrendt (1981, 1983) (Seeber, 1981) |
| Blake Spur fracture zone | oceanic transform postulated to extend westward to Charleston area | (Fletcher, 1978) (Sykes, 1978) (Seeber, 1981) |
| Bowman seismic zone | microseismicity | Smith and Talwani (1985) |
| Charleston fault | subsurface stratigraphy | (Lennon, 1986) (Talwani, 2000) **(Weems, 2007)** |
| Cooke fault | seismic reflection | Behrendt (1981, 1983) (USGS, 1983a) (USGS, 1983c) Behrendt and Yuan (1987) |
| Drayton fault | seismic reflection | (USGS, 1983a) (Behrendt, 1983) (Behrendt, 1987) |
| East Coast fault system/ Zone of river anomalies (ZRA) | geomorphology seismic reflection microseismicity | (Marple ,1993) Marple (2000, 2004) |
| Gants fault | seismic reflection | (Hamilton, 1983) (Behrendt, 1987) |
| Helena Banks fault zone | seismic reflection | Behrendt (1981, 1983) (Behrendt, 1987) |
| Middleton Place-Summerville seismic zone | microseismicity | (SSA, 1981) (SSA, 1993) |
| **Sawmill Branch fault** | **microseimicity** | **(Talwani, 2004)** |
| **Summerville fault** | **microseimicity** | **USGS, 1997** |
| Woodstock fault | geomorphology microseismicity | Talwani (1982, 1999, 2000) Marple (1990, 2000) |

Note: Those tectonic features identified following publication of the EPRI teams' reports (post-1986) are highlighted by **bold-face** type.

**Table 2.5-18—{Comparison of Post-EPRI NP-6395-D 1989 Magnitude Estimates for the 1886 Charleston Earthquake}**

| Study | Magnitude Estimation Method | Reported Magnitude Estimate | Assigned Weights | Mean Magnitude (M) |
|---|---|---|---|---|
| EPRI (1994) | worldwide survey of passive-margin, extended-crust earthquakes | **M 7.56 ± 0.35** | -- | 7.56 |
| Martin (1994) | geotechnical assessment of 1886 liquefaction data | **M 7 - 7.5** | -- | 7.25 |
| Johnston (1996) | isoseismal area regression, accounting for eastern North America anelastic attenuation | **M 7.3 ± 0.26** | -- | 7.3 |
| Chapman (2002) (South Carolina Department of Transportation) | consideration of available magnitude estimates | **M 7.1** <br> **M 7.3** <br> **M 7.5** | 0.2 <br> 0.6 <br> 0.2 | 7.3 |
| Frankel et al. (2002) (USGS National seismic hazard mapping project) | consideration of available magnitude estimates | **M 6.8** <br> **M 7.1** <br> **M 7.3** <br> **M 7.5** | 0.20 <br> 0.20 <br> 0.45 <br> 0.15 | 7.2 |
| Bakun (2004) | isoseismal area regression, including empirical site corrections | MI 6.4 - 7.2 | -- | 6.9 |
| Note: | | | | |

95% confidence interval estimate; MI (intensity magnitude) is considered equivalent to **M** (Bakun and Hopper 2004).

**Table 2.5-19—{Comparison of Talwani and Schaeffer (2001) and UCSS Age Constraints on Charleston-Area Paleoliquefaction Events}**

| Liquefaction Event | Event Age (YBP) [2] | Talwani (2001) [1] | | | | | (Bechtel 2006) |
| | | Scenario 1 | | Scenario 2 | | | Event Age (YBP) [2, 3, 4] |
| | | Source | M | Source | M | | |
| 1886 A.D. | 64 | Charleston | 7.3 | Charleston | 7.3 | | 64 |
| A | 546 ± 17 | Charleston | 7+ | Charleston | 7+ | | 600 ± 70 |
| B | 1,021 ± 30 | Charleston | 7+ | Charleston | 7+ | | 1,025 ± 25 |
| C | 1,648 ± 74 | Northern | 6+ | -- | -- | | -- |
| C' | 1,683 ± 70 | -- | -- | Charleston | 7+ | | 1,695 ± 175 |
| D | 1,966 ± 212 | Southern | 6+ | -- | -- | | -- |
| E | 3,548 ± 66 | Charleston | 7+ | Charleston | 7+ | | 3,585 ± 115 |
| F | 5,038 ± 166 | Northern | 6+ | Charleston | 7+ | | -- |
| F' | -- | -- | -- | -- | -- | | 5,075 ± 215 |
| G | 5,800 ± 500 | Charleston | 7+ | Charleston | 7+ | | -- |

Notes:

1  Modified after Talwani, 2001 Table 2.

2  Years before present, relative to 1950 A.D.

3  Event ages based upon recalibration of radiocarbon (to 2-sigma using OxCal 3.8 (Bronk Ramsey, 1995; 2001) data presented in Talwani 2001 Table 2.

4 See Table B-1 for recalibrated 2-sigma sample ages and Table B-2 for 2-sigma age constraints on paleoliquefaction events.

**Table 2.5-20—{Comparison of EPRI-SOG Seismic Hazard Results and Replication Calculated in 2006, for PGA, 10 Hz, and 1 Hz Spectral Velocity}**

| PGA Comparison | | | |
|---|---|---|---|
| Ampl, cm/s^2 | 2006 mean | EPRI-SOG mean | % difference |
| 50 | 4.57E-04 | 4.30E-04 | 6.3% |
| 100 | 1.12E-04 | 1.03E-04 | 8.4% |
| 250 | 1.25E-05 | 1.13E-05 | 10.4% |
| 500 | 1.54E-06 | 1.37E-06 | 12.4% |
| **10 Hz comparison** | | | |
| Ampl, cm/s | 2006 mean | EPRI-SOG mean | % difference |
| 1 | 8.11E-04 | 7.74E-04 | 4.8% |
| 5 | 2.52E-05 | 2.32E-05 | 8.7% |
| 10 | 3.67E-06 | 3.33E-06 | 10.3% |
| **1 Hz comparison** | | | |
| Ampl, cm/s | 2006 mean | EPRI-SOG mean | % difference |
| 1 | 1.61E-03 | 1.56E-03 | 3.3% |
| 5 | 1.38E-04 | 1.33E-04 | 3.9% |
| 10 | 3.77E-05 | 3.58E-05 | 5.2% |

**Table 2.5-21—{Mean Magnitudes and Distances from Deaggregations}**

| Struct. frequency | Annual Freq. Exceed. | Overall hazard | | Hazard from R<100 km | | Hazard from R>100 km | |
|---|---|---|---|---|---|---|---|
| | | M | R, km | M | R, km | M | R, km |
| 1 & 2.5 Hz | 1E-4 | 6.3 | 300 | 5.6 | 39 | 6.8 | 430 |
| 5 & 10 Hz | 1E-4 | 5.5 | 97 | 5.5 | 35 | 6.2 | 220 |
| 1 & 2.5 Hz | 1E-5 | 6.3 | 220 | 5.8 | 27 | 6.9 | 450 |
| 5 & 10 Hz | 1E-5 | 5.5 | 35 | 5.5 | 18 | 6.5 | 193 |

**Table 2.5-22—{Recommended Horizontal and Vertical SSE and OBE Amplitudes and Common V/H Ratios}**

| Freq | Horizontal SSE (g) | Vertical SSE (g) | Horizontal OBE (g) | Vertical OBE (g) | V/H |
|------|--------------------|------------------|--------------------|------------------|------|
| 0.1 | 2.67E-03 | 2.00E-03 | 8.91E-04 | 6.68E-04 | 0.75 |
| 0.125 | 4.69E-03 | 3.52E-03 | 1.56E-03 | 1.17E-03 | 0.75 |
| 0.15 | 7.84E-03 | 5.88E-03 | 2.61E-03 | 1.96E-03 | 0.75 |
| 0.2 | 1.79E-02 | 1.34E-02 | 5.97E-03 | 4.48E-03 | 0.75 |
| 0.3 | 2.66E-02 | 1.99E-02 | 8.86E-03 | 6.64E-03 | 0.75 |
| 0.4 | 3.35E-02 | 2.51E-02 | 1.12E-02 | 8.38E-03 | 0.75 |
| 0.5 | 4.49E-02 | 3.37E-02 | 1.50E-02 | 1.12E-02 | 0.75 |
| 0.6 | 6.66E-02 | 5.00E-02 | 2.22E-02 | 1.67E-02 | 0.75 |
| 0.7 | 7.63E-02 | 5.72E-02 | 2.54E-02 | 1.91E-02 | 0.75 |
| 0.8 | 7.92E-02 | 5.94E-02 | 2.64E-02 | 1.98E-02 | 0.75 |
| 0.9 | 8.42E-02 | 6.32E-02 | 2.81E-02 | 2.11E-02 | 0.75 |
| 1. | 8.79E-02 | 6.59E-02 | 2.93E-02 | 2.20E-02 | 0.75 |
| 1.25 | 9.53E-02 | 7.15E-02 | 3.18E-02 | 2.38E-02 | 0.75 |
| 1.5 | 9.98E-02 | 7.48E-02 | 3.33E-02 | 2.49E-02 | 0.75 |
| 2. | 1.05E-01 | 7.88E-02 | 3.50E-02 | 2.63E-02 | 0.75 |
| 2.5 | 1.16E-01 | 8.67E-02 | 3.85E-02 | 2.89E-02 | 0.75 |
| 3. | 1.32E-01 | 9.93E-02 | 4.41E-02 | 3.31E-02 | 0.75 |
| 4. | 1.44E-01 | 1.08E-01 | 4.79E-02 | 3.59E-02 | 0.75 |
| 5. | 1.60E-01 | 1.20E-01 | 5.32E-02 | 3.99E-02 | 0.75 |
| 6. | 1.65E-01 | 1.28E-01 | 5.50E-02 | 4.28E-02 | 0.778 |
| 7. | 1.65E-01 | 1.33E-01 | 5.51E-02 | 4.42E-02 | 0.802 |
| 8. | 1.59E-01 | 1.31E-01 | 5.29E-02 | 4.36E-02 | 0.823 |
| 9. | 1.51E-01 | 1.27E-01 | 5.03E-02 | 4.23E-02 | 0.841 |
| 10. | 1.45E-01 | 1.24E-01 | 4.82E-02 | 4.13E-02 | 0.858 |
| 12.5 | 1.32E-01 | 1.18E-01 | 4.40E-02 | 3.93E-02 | 0.892 |
| 15. | 1.19E-01 | 1.10E-01 | 3.98E-02 | 3.67E-02 | 0.921 |
| 20. | 9.62E-02 | 9.29E-02 | 3.21E-02 | 3.10E-02 | 0.965 |
| 25. | 8.39E-02 | 8.39E-02 | 2.80E-02 | 2.80E-02 | 1 |
| 30. | 7.65E-02 | 7.65E-02 | 2.55E-02 | 2.55E-02 | 1 |
| 35. | 7.26E-02 | 7.26E-02 | 2.42E-02 | 2.42E-02 | 1 |
| 40. | 7.03E-02 | 7.03E-02 | 2.34E-02 | 2.34E-02 | 1 |
| 45. | 6.90E-02 | 6.90E-02 | 2.30E-02 | 2.30E-02 | 1 |
| 50. | 6.83E-02 | 6.83E-02 | 2.28E-02 | 2.28E-02 | 1 |
| 60. | 6.76E-02 | 6.76E-02 | 2.25E-02 | 2.25E-02 | 1 |
| 70. | 6.73E-02 | 6.73E-02 | 2.24E-02 | 2.24E-02 | 1 |
| 80. | 6.71E-02 | 6.71E-02 | 2.24E-02 | 2.24E-02 | 1 |
| 90. | 6.70E-02 | 6.70E-02 | 2.23E-02 | 2.23E-02 | 1 |
| 100. | 6.70E-02 | 6.70E-02 | 2.23E-02 | 2.23E-02 | 1 |

**Table 2.5-23—{Calvert Cliffs Site} Amplification Factors for $10^{-4}$ and $10^{-5}$ Input Motions and HF and LF Rock Spectra}**

| Freq. (Hz) | $10^{-4}$ HF | $10^{-4}$ LF | $10^{-5}$ HF | $10^{-5}$ LF |
|---|---|---|---|---|
| 0.1 | 2.09 | 1.43 | 2.19 | 1.44 |
| 0.125 | 2.01 | 1.64 | 2.05 | 1.68 |
| 0.15 | 2.15 | 1.98 | 2.17 | 2.05 |
| 0.2 | 2.86 | 2.88 | 2.82 | 2.89 |
| 0.3 | 2.45 | 2.42 | 2.39 | 2.29 |
| 0.4 | 1.77 | 1.71 | 1.78 | 1.67 |
| 0.5 | 1.98 | 1.89 | 2.04 | 1.91 |
| 0.6 | 2.59 | 2.51 | 2.61 | 2.47 |
| 0.7 | 2.70 | 2.64 | 2.67 | 2.54 |
| 0.8 | 2.60 | 2.56 | 2.56 | 2.44 |
| 0.9 | 2.62 | 2.56 | 2.56 | 2.45 |
| 1 | 2.67 | 2.61 | 2.55 | 2.44 |
| 1.25 | 2.47 | 2.41 | 2.29 | 2.15 |
| 1.5 | 2.03 | 1.99 | 1.88 | 1.78 |
| 2 | 1.63 | 1.60 | 1.53 | 1.45 |
| 2.5 | 1.62 | 1.57 | 1.48 | 1.38 |
| 3 | 1.66 | 1.59 | 1.45 | 1.34 |
| 4 | 1.33 | 1.28 | 1.14 | 1.04 |
| 5 | 1.24 | 1.18 | 1.04 | 0.93 |
| 6 | 1.17 | 1.09 | 0.93 | 0.83 |
| 7 | 1.08 | 1.01 | 0.84 | 0.74 |
| 8 | 0.98 | 0.91 | 0.73 | 0.65 |
| 9 | 0.88 | 0.82 | 0.65 | 0.57 |
| 10 | 0.81 | 0.75 | 0.58 | 0.52 |
| 12.5 | 0.67 | 0.63 | 0.45 | 0.42 |
| 15 | 0.56 | 0.54 | 0.36 | 0.37 |
| 20 | 0.40 | 0.42 | 0.26 | 0.31 |
| 25 | 0.33 | 0.38 | 0.21 | 0.28 |
| 30 | 0.29 | 0.35 | 0.20 | 0.27 |
| 35 | 0.28 | 0.34 | 0.19 | 0.27 |
| 40 | 0.28 | 0.34 | 0.20 | 0.28 |
| 45 | 0.29 | 0.35 | 0.21 | 0.28 |
| 50 | 0.30 | 0.36 | 0.22 | 0.30 |
| 60 | 0.36 | 0.41 | 0.26 | 0.34 |
| 70 | 0.44 | 0.49 | 0.32 | 0.41 |
| 80 | 0.53 | 0.58 | 0.38 | 0.48 |
| 90 | 0.62 | 0.66 | 0.45 | 0.55 |
| 100 | 0.69 | 0.72 | 0.50 | 0.60 |

**Table 2.5-24—{Values of UHS (Hard Rock Conditions)}**

| Frequency, Hz | $10^{-4}$ SA, g | $10^{-4}$ SA, g | $10^{-5}$ SA, g | $10^{-5}$ SA, g | $10^{-6}$ SA, g | $10^{-6}$ SA, g |
|---|---|---|---|---|---|---|
| | Mean | Median | Mean | Median | Mean | Median |
| 100 | 0.0766 | 0.0579 | 0.271 | 0.198 | 0.845 | 0.546 |
| 25 | 0.228 | 0.155 | 0.767 | 0.529 | 2.39 | 1.46 |
| 10 | 0.149 | 0.121 | 0.493 | 0.389 | 1.42 | 1.04 |
| 5 | 0.102 | 0.0839 | 0.309 | 0.246 | 0.846 | 0.599 |
| 2.5 | 0.0577 | 0.0459 | 0.158 | 0.123 | 0.402 | 0.274 |
| 1 | 0.0269 | 0.0191 | 0.0722 | 0.0450 | 0.166 | 0.0989 |
| 0.5 | 0.0164 | 0.00938 | 0.0488 | 0.0224 | 0.114 | 0.0476 |

**Table 2.5-25—{Summary of Field Testing Quantities}**

| Field Test | Standard | Quantity |
|---|:---:|:---:|
| Test Borings | ASTM D1586/1587 | 145 |
| Observation Wells | ASTM D5092 | 40 |
| CPT Soundings | ASTM D5778 | 50* |
| Suspension P-S Velocity Logging | EPRI TR-102293 | 10 |
| Test Pits | N/A | 20 |
| Field Electrical Resistivity Arrays | ASTM G57/IEEE 81 | 4 |
| SPT Hammer Energy Measurements | ASTM D4633 | 5 |

Note:

\* Not including additional off-set soundings performed

### Table 2.5-26—{Summary Thickness of Various Soil Strata}

| Stratum I Terrace Sand | | | Chesapeake | | | Nanjemoy |
|---|---|---|---|---|---|---|
| From Existing Ground Surface (ft) | | Below elevation 85 (ft) | Stratum IIa Clay/Silt (ft) | Stratum IIb Cemented Sand (ft) | Stratum IIc Clay/Silt (ft) | Stratum III Sand (ft) |
| **CCNPP Unit 3** | | | | | | |
| Maximum | 51 | 20 | 35 | 73 | 190* | >101* |
| Minimum | 2 | 0 | 4 | 57 | 190* | >101* |
| Average | 21 | 14 | 20 | 66 | 190* | >101* |
| **Construction Laydown Area 1 (CLA1)** | | | | | | |
| Maximum | 59 | 27 | 26 | 65 | 190* | >119* |
| Minimum | 2 | 11 | 8 | 24 | 190* | >119* |
| Average | 34 | 18 | 20 | 58 | 190* | >119* |
| **CCNPP Unit 3 and CLA1 Combined** | | | | | | |
| Maximum | 59 | 27 | 35 | 73 | 190 | >119 |
| Minimum | 2 | 0 | 4 | 24 | 190 | >101 |
| Average | 27 | 16 | 20 | 55 | 190 | >110 |
| **Cooling Tower Area** | | | | | | |
| Maximum | 69 | 38 | 31 | 65 | >13* | --- |
| Minimum | 2 | 5 | 5 | >1 | >13* | --- |
| Average | 30 | 25 | 19 | >30 | >13* | --- |
| **Switchyard Area** | | | | | | |
| Maximum | 53 | 27 | 36 | >63 | --- | --- |
| Minimum | 7 | 14 | 4 | >8 | --- | --- |
| Average | 30 | 21 | 22 | >31 | --- | --- |
| **Entire Site** | | | | | | |
| Maximum | 69 | 38 | 36 | 73 | 190 | >119 |
| Minimum | 2 | 0 | 4 | 28 | 190 | >101 |
| Average | 28 | 19 | 20 | 60 | 190 | >110 |

Note:

\* Data based on a single boring

### Table 2.5-27—{Summary Termination Elevation of Various Soil Strata}

| | Stratum I Terrace Sand (ft) | Chesapeake | | | Nanjemoy |
| | | Stratum IIa Clay/Silt (ft) | Stratum IIb Cemented Sand (ft) | Stratum IIc Clay/Silt (ft) | Stratum III Sand (ft) |
|---|---|---|---|---|---|
| **CCNPP Unit 3** | | | | | |
| Maximum | 80 | 56 | 3 | -208* | --- |
| Minimum | 47 | 38 | -31 | -208* | --- |
| Average | 66 | 47 | -19 | -208* | --- |
| **Construction Laydown Area 1 (CLA1)** | | | | | |
| Maximum | 74 | 50 | -8 | -211* | --- |
| Minimum | 35 | 27 | -23 | -211* | --- |
| Average | 63 | 45 | -14 | -211* | --- |
| **CCNPP Unit 3 and CLA1 Combined** | | | | | |
| Maximum | 80 | 56 | 3 | -208 | --- |
| Minimum | 35 | 27 | -31 | -211 | --- |
| Average | 65 | 46 | -17 | -209 | --- |
| **Cooling Tower Area** | | | | | |
| Maximum | 66 | 46 | -24 | --- | --- |
| Minimum | 46 | 26 | -24 | --- | --- |
| Average | 56 | 36 | -24 | --- | --- |
| **Switchyard Area** | | | | | |
| Maximum | 71 | 67 | --- | --- | --- |
| Minimum | 58 | 30 | --- | --- | --- |
| Average | 64 | 42 | --- | --- | --- |
| **Entire Site** | | | | | |
| Maximum | 80 | 72 | -8 | -208 | --- |
| Minimum | 7 | 21 | -31 | -211 | --- |
| Average | 61 | 42 | -18 | -209 | --- |

\* Data based on a single boring
Note: Only data from borings that fully penetrated each stratum was considered for determination of the maximum, minimum, and average termination elevations shown.  For instance, a termination elevation for Stratum III is not provided since no boring reached the bottom of this stratum, as indicated by "---" .

**Table 2.5-28—{Summary of Measured (Uncorrected) SPT N-Values for Various Soil Strata}**

| | | | | Chesapeake | | Nanjemoy |
| --- | --- | --- | --- | --- | --- | --- |
| | | **Stratum I Terrace Sand (blows/ft)** | **Stratum IIa Clay/Silt (blows/ft)** | **Stratum IIb Cemented Sand (blows/ft)** | **Stratum IIc Clay/Silt (blows/ft)** | **Stratum III Sand (blows/ft)** |
| **CCNPP Unit 3** | Maximum | 70 | 46 | 100 | 100 | 100 |
| | Minimum | 0 | 1 | 4 | 12 | 34 |
| | Average | 10 | 9 | 45 | 23 | 64 |
| **CLA1** | Maximum | 43 | 45 | 100 | 39 | 100 |
| | Minimum | 0 | 1 | 0 | 10 | 28 |
| | Average | 12 | 9 | 45 | 20 | 56 |
| **CCNPP Unit 3 and CLA1 Combined** | Maximum | 70 | 46 | 100 | 100 | 100 |
| | Minimum | 0 | 1 | 0 | 10 | 28 |
| | Average | 11 | 9 | 45 | 21 | 61 |
| **Switchyard Area** | Maximum | 27 | 19 | 100 | --- | --- |
| | Minimum | 2 | 4 | 7 | --- | --- |
| | Average | 9 | 10 | 35 | --- | --- |
| **Cooling Tower Area** | Maximum | 49 | 26 | 100 | 25 | --- |
| | Minimum | 0 | 1 | 9 | 19 | --- |
| | Average | 12 | 10 | 38 | 23 | --- |
| **Entire Site** | Maximum | 70 | 46 | 100 | 100 | 100 |
| | Minimum | 0 | 1 | 0 | 10 | 28 |
| | Average | 11 | 10 | 41 | 22 | 61 |

Note: A cut off SPT N-value of 100 blows/ft is shown whenever SPT refusal (50 blows/6 in or less) was measured or the linearly extrapolated N-value exceeded 100 blows/ft.

**Table 2.5-29—{Summary of Hammer-Rod Energy Measurements}**

| Drill Rig | Measurement in Boring No. | ETR range (%) | Average ETR (%) | Energy Adjustment (ETR% / 60%) |
|---|---|---|---|---|
| Failing 1500 | B-401 | 67-88 | 78 | 1.30 |
| CME 550X ATV | B-403 | 73-92 | 84 | 1.40 |
| CME 750 ATV | B-404 | 78-90 | 87 | 1.45 |
| CME 75 Truck | B-409 | 69-90 | 84 | 1.40 |
| Deidrich D50 ATV | B-744 | 73-84 | 81 | 1.35 |

Note:

ETR = Percentage of theoretical hammer energy measured in the field

**Table 2.5-30—{Summary of Adjusted SPT N-Values Based on Energy Measurements}**

| Stratum | Adjusted Minimum N-value (blows/ft) | Adjusted Maximum N-value (blows/ft) | Adjusted Average N-value (blows/ft) | Adopted N-value for Engineering Purposes (blows/ft) |
|---|---|---|---|---|
| I – Terrace Sand | 0 | 91 | 16 | 15 |
| IIa – Ches. Clay/Silt | 1 | 64 | 13 | 10 |
| IIb – Ches. Cemented sand | 0 | 100 | 48 | 45 |
| IIc – Ches. Clay/Silt | 14 | 100 | 29 | 25 |
| III – Nanjemoy Sand | 36 | 100 | 72 | 70 |

Note: Adjusted values are for "Entire Site" shown in Table 2.5-28.

**Table 2.5-31—{Summary of Laboratory Tests and Quantities}**

| Identification and Index Testing | | Quantity | Standard/Method Used | Regulatory Guide 1.138 Recommended |
|---|---|---|---|---|
| | Unified Soil Classification System (USCS) | NA | ASTM D2487 (ASTM, 2006a) ASTM D2488 (ASTM, 2006d) | ASTM D2487-00 |
| | Sieve and Hydrometer Analysis | 398 | ASTM D422 (ASTM, 2002a) ASTM D6913 (ASTM, 2004b) | ASTM D422-63(98) |
| | Atterberg Limits | 330 | ASTM D4318 (ASTM, 2005b) | ASTM D4318--00 |
| | Natural Moisture Content | 812 | ASTM D2216 (ASTM, 2005c) | ASTM D2216-98 |
| | Specific Gravity | 77 | ASTM D854 (ASTM, 2006b) | ASTM D854-00 |
| | Organic Content | 9 | ASTM D2974 (ASTM, 2000d) | ASTM D2974-00 |
| Compaction and Strength Tests | | | | |
| | Moisture-Density Relationship | | ASTM D1557 (ASTM, 2002c) | ASTM D1557-00 |
| | California Bearing Ratio | 12 | ASTM D1883 (ASTM, 2005d) | |
| | Unconfined Compression | 22 | ASTM D2166 (ASTM, 2006c) | ASTM D2166-98 |
| | Unconsolidated-Undrained Triaxial Compression | 38 | ASTM D2850 (ASTM, 2003) | ASTM D2850-95 (99) |
| | Consolidated-Undrained Triaxial compression | 10 | ASTM D4767 (ASTM, 2004c) | ASTM D4767-95 |
| | Direct Shear | 19 | ASTM D3080 (ASTM, 2004d) | ASTM D3080-98 |
| Compressibility Tests | Consolidation | 50 | ASTM D2435 (ASTM, 2004e) | ASTM D2435--96 |
| Chemical Testing – Soils | | | | |
| | pH | 77 | ASTM D4972 (ASTM, 2001b) | * |
| | Chloride | 77 | EPA 300.0 (EPA, 1993) | * |
| | Sulfate | 77 | EPA 300.0 (EPA, 1993) | * |
| | Cation Exchange Capacity | NA | (ECL, 2007) | Not Specified |
| Proctor Compaction | | 28 | ASTM D1587 | Not Specified |
| Unit Weight | | 78 | Not specified | Not specified |
| Resonant Column Torsional Shear (RCTS) | | 13 | Not specified | Not specified |

* Regulatory Guide 1.138 states that Manual of Soil Laboratory Testing Volume 1, 1992 information on the most widely used clinical test for soils and ground water.

Results of Cation Exchange Capacity tests are addressed with the ground water chemistry data in Subsection 2.4.13.

## Table 2.5-32—{Summary Average Values of Laboratory Index Properties}

**Atterberg Limits**

| Stratum | No. of Tests | Average LL (%) | Average PI (%) | Average WC (%) | USCS Classification | Adopted PI for Engineering Purposes (%) |
|---|---|---|---|---|---|---|
| I - Terrace Sand | 31 | NP | NP | 15 | SP-SM, SC, SM, CL, SW-SM, CH, ML, MH | NP |
| IIa- Chesapeake Clay/Silt | 67 | 57 | 35 | 32 | CH, MH, CL, SM, SC-SM, OH | 35 |
| IIb- Chesapeake Cemented Sand | 67 | 46 | 22 | 34 | SM, ML, MH, CH, CL, SP-SM, SC, OH | 20 |
| IIc- Chesapeake Clay/Silt | 88 | 94 | 44 | 54 | MH, CH, SM, CL, OH | 45 |
| III- Nanjemoy Sand | 7 | 59 | 27 | 30 | SC, SM, CH, MH | 30 |

**Fines Content (% Passing No. 200 Sieve)**

| Stratum | No. of Tests | Average Fines Content (%) | Adopted Value for Engineering Purposes (%) |
|---|---|---|---|
| I -Terrace Sand | 85 | 19 | 20 |
| IIa - Chesapeake Clay/Silt | 72 | 77 | 75 |
| IIb - Chesapeake Cemented Sand | 115 | 24 | 25 |
| IIc - Chesapeake Clay/Silt | 82 | 54 | 50 |
| III - Nanjemoy Sand | 10 | 19 | 20 |

**Unit Weight**

| Stratum | No. of Tests | Average Unit Weight (pcf) | Adopted Value for Engineering Purposes (pcf) |
|---|---|---|---|
| I - Terrace Sand | 3 | 120 | 120 |
| IIa - Chesapeake Clay/Silt | 40 | 116 | 115 |
| IIb - Chesapeake Cemented Sand | 16 | 118 | 120 |
| IIc - Chesapeake Clay/Silt | 19 | 107 | 110 |
| III – Nanjemoy Sand | 0 | N.A. | 120* |

Notes:
N.A. – Not Available
* – Estimated

| Group Symbols | Typical Names |
|---|---|
| SW | Well graded sands, gravelly sands, little or no fines |
| SP | Poorly graded sands, gravelly sands, little or no fines |
| SM | Silty sands, poorly graded sand-silt mixtures |
| SC | Clayey sands, poorly graded sand-clay mixtures |
| ML | Inorganic silts and very find sands, rock flour, silty or clayey fine sands with slight plasticity |
| CL | Inorganic clays of low to medium plasticity, gravelly clays, sandy clays, silty clays, lean clays |
| MH | Inorganic silts, micaceous or diatomaceous fine sandy or silty soils, elastic silts |
| CH | Inorganic clays of high plasticity, fat clays |
| OH | Organic clays of medium to high plasticity |

### Table 2.5-33—{Summary Laboratory Strength Results}

**Summary – Direct Shear Test Results**

| Boring | elevation (ft) | USCS | $\phi'$ (deg.) | c' (tsf) | Boring | elevation (ft) | USCS | $\phi'$ (deg.) | c' (tsf) |
|---|---|---|---|---|---|---|---|---|---|
| **Stratum I – Terrace Sand** | | | | | **Stratum IIb – Chesapeake Cemented Sand** | | | | |
| B-743 | 78.1 | CL | 29.2 | 0.3 | B-724 | 21.5 | OL | 27.5 | 0.6 |
| **Stratum IIa – Chesapeake Clay/Silt** | | | | | B-440 | 3.3 | SC | 30.3 | 0.4 |
| B-319 | 67.4 | CL | 24.9 | 0.4 | B-420 | -2.9 | SC | 34 | 0.2 |
| B-320 | 65.9 | SC | 26 | 0.2 | | | **Maximum** | 34 | 0.6 |
| B-735 | 61.2 | CH | 27.2 | 0.4 | | | **Minimum** | 27.5 | 0.2 |
| B-319 | 57.7 | CH | 20.8 | 0.7 | | | **Average** | 31 | 0.4 |
| B-326 | 57.6 | OH | 19 | 0.4 | **Stratum IIc – Chesapeake Clay/Silt** | | | | |
| B-433 | 57.0 | CH | 20.2 | 0.7 | B-313 | -44.0 | CL | 29 | 0.8 |
| B-320 | 56.4 | CH | 21.6 | 0.7 | B-307 | -61.1 | SC | 35 | 0 |
| B-316 | 52.6 | CL | 30.1 | 0.3 | B-423 | -78.9 | MH | 18.5 | 1.7 |
| B-427 | 50.8 | OH | 29.2 | 0.4 | B-401 | -102.3 | CH | 18.9 | 2.3 |
| B-737 | 51.0 | CH | 22.7 | 0.4 | | | **Maximum** | 35 | 2.3 |
| B-413 | 47.9 | CH | 31.4 | 0.5 | | | **Minimum** | 18.5 | 0 |
| | | **Maximum** | 31.4 | 0.7 | | | **Average** | 25 | 1.6 |
| | | **Minimum** | 19 | 0.2 | **Stratum IIb – Chesapeake Cemented Sand** | | | | |
| | | **Average** | 25 | 0.5 | B-724 | 21.5 | OL | 27.5 | 0.6 |

**Summary – CIU-bar Test Results**

| Boring | elevation (ft) | USCS | Effective | | Total | |
|---|---|---|---|---|---|---|
| | | | $\phi'$ (deg.) | c' (tsf) | $\phi$ (deg.) | c (tsf) |
| **Stratum IIa – Chesapeake Clay/Silt** | | | | | | |
| B-320 | 65.9 | SC | 27.9 | 0.3 | 13.3 | 0.6 |
| B-317 | 63.9 | CL | 31 | 0.2 | 17 | 0.4 |
| B-316 | 52.6 | CL | 32.1 | 0.5 | 12.5 | 1.0 |
| B-414 | 51.2 | CH | 20 | 0.7 | 10.4 | 1.0 |
| B-433 | 47 | CH/CL | 19.3 | 0.3 | 8.3 | 0.4 |
| B-317 | 43.9 | CL | 33.5 | 0.3 | 19.5 | 0.6 |
| | | **Maximum** | 33.5 | 0.7 | 19.5 | 1.0 |
| | | **Minimum** | 19.3 | 0.2 | 8.3 | 0.4 |
| | | **Average** | 27 | 0.4 | 14 | 0.7 |
| **Stratum IIb – Chesapeake Cemented Sand** | | | | | | |
| B-328 | 10.8 | OH | 34.6 | 0.0 | 13.4 | 1.7 |
| B-423 | 6.6 | SP-SC | 27 | 0.8 | 14.1 | 2.3 |
| B-321 | -4.8 | SM | 30 | 0.5 | 20 | 1.0 |
| | | **Maximum** | 34.6 | 0.8 | 20 | 2.3 |
| | | **Minimum** | 27 | 0.5 | 13.4 | 1.0 |
| | | **Average** | 31 | 0.5 | 16 | 1.7 |
| **Stratum IIc – Chesapeake Clay/Silt** | | | | | | |
| B-420 | -65.9 | OH | 29.1 | 1.0 | 15.4 | 1.5 |

**Table 2.5-34—{Summary Consolidation Properties}**

**Laboratory Testing**

| Stratum | No. of Tests | | $C_r$ [1] | $C_c$ [1] | $e_o$ | Pp' (tsf) | OCR |
|---|---|---|---|---|---|---|---|
| Stratum I – Terrace Sand | 2 | Maximum | 0.018 | 0.146 | 0.82 | 6 | 4.5 |
| | | Minimum | 0.018 | 0.071 | 0.78 | 4 | 3.7 |
| | | Average | 0.018 | 0.108 | 0.80 | 5 | 4.1 |
| Stratum IIa – Ches. Clay/Silt | 25 | Maximum | 0.126 | 0.915 | 1.95 | 18.5 | 12.5 |
| | | Minimum | 0.018 | 0.071 | 0.78 | 4 | 1.2 |
| | | Average | 0.054 | 0.526 | 1.09 | 9.1 | 5.6 |
| Stratum IIb – Ches. Cemented Sand | 9 | Maximum | 0.137 | 1.092 | 1.73 | 14.2 | 11.6 |
| | | Minimum | 0.005 | 0.109 | 0.70 | 1.1 | 0.4 |
| | | Average | 0.033 | 0.396 | 1.05 | 9 | 5.2 |
| Stratum IIc Ches. Clay/Silt | 14 | Maximum | 0.152 | 2.052 | 2.80 | 23 | 5.9 |
| | | Minimum | 0.004 | 0.276 | 0.93 | 7 | 1.2 |
| | | Average | 0.041 | 0.905 | 1.53 | 15.5 | Boring |

**CPT Data Interpretation**

| Stratum | Min. OCR | Max. OCR | Average OCR |
|---|---|---|---|
| Stratum I - Terrace Sand | 0.6 | 10 | 5.3 |
| Stratum IIa – Ches. Clay/Silt | 0.6 | 10 | 5.9 |
| Stratum IIb – Ches. Cemented Sand | 0.8 | 10 | 7.1 |
| Stratum IIc Ches. Clay/Silt | 1.2 | 10 | 9.2 |

**Average Values Adopted for Engineering Purposes**

| Stratum | OCR | Pp' (tsf) |
|---|---|---|
| Stratum I - Terrace Sand | 4 | 4 |
| Stratum IIa – Ches. Clay/Silt | 4 | 6 |
| Stratum IIb – Ches. Cemented Sand | 3 | 8 |
| Stratum IIc Ches. Clay/Silt | 3 | 14 |

Notes:

$C_r$ = recompression index

$C_c$ = compression index

$e_o$ = void ratio

Pp' = preconsolidation pressure

OCR = overconsolidation ratio

(1) values are void ratio-based

**Table 2.5-35—{High Strain Elastic and Shear Moduli Estimation}**

## High Strain Elastic Modulus (E)

| | | Chesapeake | | | Nanjemoy |
|---|---|---|---|---|---|
| **Relationship** | **Stratum I Terrace Sand (tsf)** | **Stratum IIa Clay/Silt (tsf)** | **Stratum IIb Cemented Sand (tsf)** | **Stratum IIc Clay/Silt (tsf)** | **Stratum III Sand (tsf)** |
| $E = 18\,N$ | 270 | --- | 810 | --- | 1,260 |
| $E_u = 450\,s_u$ | --- | 450 | --- | 900 | 1,800 |
| $E_{.375\%} = f(V_s)$ | 302 | --- | 1,134 | --- | 1,879 |
| $E_{.375\%} = f(PI)$ | --- | 1,766 | --- | 2,477 | --- |
| $E_{.375\%} = f(s_u)$ | --- | 580 | --- | 1,160 | 2,080 |

### Adopted E-Values for Engineering Purposes

| | | | | | |
|---|---|---|---|---|---|
| E (tsf) | 280 | 510 | 970 | 1,030 | 1,750 |

## High Strain Shear Modulus (G)

| | | Chesapeake | | | Nanjemoy |
|---|---|---|---|---|---|
| **Relationship** | **Stratum I Terrace Sand (tsf)** | **Stratum IIa Clay/Silt (tsf)** | **Stratum IIb Cemented Sand (tsf)** | **Stratum IIc Clay/Silt (tsf)** | **Stratum III Sand (tsf)** |
| $G_{.375\%} = f(V_s)$ | 116 | --- | 436 | --- | 723 |
| $G_{.375\%} = f(PI)$ | --- | 609 | --- | 853 | --- |
| $G_{.375\%} = f(s_u)$ | --- | 200 | --- | 400 | --- |
| $G_{.375\%} = E/(2(1+\mu))$ | 108 | 176 | 373 | 355 | 673 |

### Adopted G-Values for Engineering Purposes

| | | | | | |
|---|---|---|---|---|---|
| G (tsf) | 110 | 180 | 400 | 370 | 700 |

**Table 2.5-36—{Summary Average Soils Engineering Properties[1]}**

| | Stratum | | | | |
|---|---|---|---|---|---|
| **Parameter** | **I<br>Terrace<br>Sand** | **IIa<br>Chesapeake<br>Clay/Silt** | **IIb<br>Chesapeake<br>Cemented<br>Sand** | **IIc<br>Chesapeake<br>Clay/Silt** | **III<br>Nanjemoy<br>Sand** |
| Average thickness, feet | 20 | 20 | 60 | 190 | >110 |
| USCS symbol (Predominant class. underlined) | SP-SM, SM, SP, SC | CH, MH, CL, SM, SC-SM, OH | SM, SC, SP-SM, SP , OH | MH, CH, SM, CL, OH | SC, SM, MH, CH |
| Natural water content (WC), % | 15 | 32 | 34 | 54 | 30 |
| Moist unit weight $\gamma_{moist}$), pcf | 120 | 115 | 120 | 110 | 120 |
| Fines content , % | 20 | 75 | 20 | 50 | 20 |
| Liquid limit (LL), % | NP | 57 | 46 | 94 | 60 |
| Plasticity index (PI), % | NP | 35 | 20 | 45 | 30 |
| Measured SPT N-value, bpf | 11 | 10 | 41 | 22 | 61 |
| Adjusted SPT $N_{60}$-value, bpf | 15 | 10 | 45 | 25 | 70 |
| Shear Wave Velocity, ft/sec | 790 | 1,100 | 1,530 | 1,250 | 1,970 |
| Undrained shear strength ($s_u$), tsf | N/A[2] | 1.0 | N/A[2] | 2.0 | 4.0 |
| Friction angle (Ø'), degree<br>Cohesion (c'), tsf | 32<br>0 | 26<br>0.4 | 34<br>0 | 27<br>1.0 | 40<br>0 |
| Elastic modulus (high strain) ($E_s$), tsf | 280 | 510 | 970 | 1,030 | 1,750 |
| Shear modulus (high strain) ($G_s$), tsf | 110 | 180 | 400 | 370 | 700 |
| Coefficient of Subgrade Reaction ($k_1$), tcf (for 1-ft. sq. area) | 75 | 75 | 300 | 150 | N/A[2] |
| Earth Pressure Coefficients | | | | | |
|    Active ($K_a$) | 0.3 | 0.4 | 0.3 | 0.4 | N/A[2] |
|    Passive ($K_p$) | 3.3 | 2.6 | 3.5 | 2.6 | N/A[2] |
|    At Rest ($K_0$) | 0.5 | 0.8 | 0.5 | 0.7 | N/A[2] |
| Coefficient of Sliding | 0.40 | 0.35 | 0.45 | 0.40 | N/A[2] |
| Consolidation Properties | | | | | |
| $C_c$ ($C_r$) (void ratio-based) | 0.108 (0.018) | 0.526 (0.054) | 0.396 (0.033) | 0.905 (0.041) | N/A[2] |
| Void Ratio, e | 0.80 | 1.09 | 1.05 | 1.53 | N/A[2] |
| $P_p'$, tsf ( OCR ) | 4 ( 4 ) | 6 ( 4 ) | 8 ( 3 ) | 14 ( 3 ) | N/A[2] |

Notes:

[1]The values tabulated below are designated for the various strata.  Reference should be made to specific boring and CPT logs and laboratory test results for appropriate modifications at specific locations and for specific calculations.

[2]N/A indicates that the properties were either not measured or are not applicable.

**Table 2.5-37—{Summary Undrained Shear Strength for Cohesive Soils}**

| From Correlation with SPT N-Values | | |
|---|---|---|
| Stratum | SPT N-Value (blows/ft) | $S_u$ (tsf) |
| Stratum IIa – Ches. Clay/Silt | 10 | 0.63 |
| Stratum IIc – Ches. Clay/Silt | 25 | 1.6 |
| Stratum III – Nanjemoy Clayey Sand | 70 | 4.4* |

### From Laboratory UU and UC Tests

| Stratum | Max. $S_u$ (tsf) | Min. $S_u$ (tsf) | Average $S_u$ (tsf) |
|---|---|---|---|
| Stratum IIa – Ches. Clay/Silt | 2.4 | 0.3 | 1.1 |
| Stratum IIc – Ches. Clay/Silt | 5.2 | 0.2 | 2.2 |

### From Correlation with CPT Results

| Stratum | Max. $S_u$ (tsf) | Min. $S_u$ (tsf) | Average $S_u$ (tsf) |
|---|---|---|---|
| Stratum IIa – Ches. Clay/Silt | 9.3 | 0.7 | 1.6 |
| Stratum IIc – Ches. Clay/Silt | 9.6 | 1.4 | 4.7 |

### Adopted Values for Engineering Purposes

| Stratum | $S_u$ (tsf) |
|---|---|
| Stratum IIa – Ches. Clay/Silt | 1.0 |
| Stratum IIc – Ches. Clay/Silt | 2.0 |
| Stratum III – Nanjemoy Clayey Sand | 4.0* |

Note:

* Assuming "undrained" behavior

### Table 2.5-38—{Summary Soils Chemical Test Results}

**From CCNPP Unit 1 and 2 Exploration**

|  | Stratum IIa Chesapeake Clay/Silt | Stratum IIb Chesapeake Cemented Sand |
|---|---|---|
| pH (unit) | | |
| min. value | 6.2 | 7.1 |
| max. value | 7.1 | 8.0 |
| average value | 6.7 | 7.5 |
| Sulfate (ppm) | | |
| min. value | 1,800 | 600 |
| max. value | 2,000 | 600 |
| average value | 1,900 | 600 |
| Chloride (ppm) | | |
| min. value | 20 | 10 |
| max. value | 110 | 60 |
| average | 60 | 57 |

**From CCNPP Subsurface Investigation**

|  | No. of Tests |  | pH (CaCl) | pH (H$_2$O) | Sulfate (%) | Chloride (ppm) |
|---|---|---|---|---|---|---|
| Stratum I Terrace Sand | 21 | Maximum | 6.7 | 7.6 | 2.570 | 48.6 |
|  |  | Minimum | 2.6 | 2.7 | 0.001 | <10 |
|  |  | Average | 4.6 | 5.5 | 0.236 | <12 |
| Stratum IIa Ches. Clay/Silt | 18 | Maximum | 4.9 | 5.8 | 2.590 | 10.7 |
|  |  | Minimum | 2.6 | 2.5 | 0.006 | <10 |
|  |  | Average | 3.1 | 3.5 | 0.914 | <10 |
| Stratum IIb Ches. Cemented Sand | 37 | Maximum | 7.4 | 8 | 3.130 | 145 |
|  |  | Minimum | 2.4 | 2.5 | 0.010 | <10 |
|  |  | Average | 5.7 | 5.8 | 0.567 | <22 |
| Stratum IIc Ches. Clay/Silt | 1 |  | 6.6 | 7 | 0.196 | <10 |

**Table 2.5-39—{Summary Field Electrical Resistivity Test Results Measured Data ("apparent" values)}**

| Location | | R-1 | R-2 | R-3 | R-4 | Values in Ohm-m | | |
|---|---|---|---|---|---|---|---|---|
| Ground Surface El. (ft) | | 85.5 | 85.5 | 89.1 | 99.4 | Min. | Max. | Average |
| Array Spacing | 1.5 ft | 1,210 | 1,520 | 3,070 | 471 | 471 | 3,070 | 1,568 |
| | 3 ft | 2,480 | 2,410 | 3,750 | 640 | 640 | 3,750 | 2,320 |
| | 5 ft | 3,220 | 2,780 | 4,550 | 660 | 660 | 4,550 | 2,803 |
| | 7.5 ft | 3,110 | 2,890 | 5,440 | 806 | 806 | 5,440 | 3,062 |
| | 10 ft | 2,490 | 2,700 | 6,240 | 1,130 | 1,130 | 6,240 | 3,140 |
| | 15 ft | 1,870 | 2,780 | 5,370 | 1,340 | 1,340 | 5,370 | 2,840 |
| | 20 ft | 1,570 | 1,960 | 4,100 | 1,790 | 1,570 | 4,100 | 2,355 |
| | 30 ft | 1,310 | 2,060 | 1,960 | 1,640 | 1,310 | 2,060 | 1,743 |
| | 40 ft | 739 | 1,590 | 1,010 | 1,280 | 739 | 1,590 | 1,155 |
| | 50 ft | 314 | 1,080 | 415 | 975 | 314 | 1,080 | 696 |
| | 100 ft | 45 | 487 | 69 | 463 | 45 | 487 | 266 |
| | 200 ft | 37 | 116 | 38 | 57 | 37 | 116 | 62 |
| | 300 ft | 48 | 76 | 31 | 41 | 31 | 76 | 49 |

**Modeled Data ("true" values)**

| Location | Depth of Layer (ft) | Resistivity (Ohm-m) |
|---|---|---|
| R-1 | 0.5 | 428 |
| | 2.2 | 12,318 |
| | 6.3 | 966 |
| | 15 | 3,114 |
| | 43.1 | 51 |
| | 119.4 | 17 |
| | N/A | 94 |
| R-2 | 0.5 | 639 |
| | 7.6 | 3,648 |
| | 17.9 | 2,247 |
| | 62.9 | 1,184 |
| | N/A | 68 |
| R-3 | 2.4 | 2,952 |
| | 10.6 | 11,930 |
| | 59.8 | 128 |
| | N/A | 30 |
| R-4 | 4.6 | 494 |
| | 13.8 | 5,040 |
| | 39.9 | 891 |
| | 53.2 | 375 |
| | N/A | 36 |

**An Approximate Correlation with Depth**

| Stratum | | Depth Range (ft) | |
|---|---|---|---|
| I. Terrace Sand | | upper 20 ft | |
| IIa. Ches. Clay/Silt | | 20 - 40 ft | |
| IIb. Ches. Cem. Sand | | 40 - 100 ft | |
| IIc. Ches. Clay/Silt | | below 100 ft | |

## Table 2.5-40—{Guidelines for Soil Chemistry Evaluation}

### Soil Corrosiveness

| | Range for Steel Corrosiveness | | | | |
|---|---|---|---|---|---|
| | Little Corrosive | Mildly Corrosive | Moderately Corrosive | Corrosive | Very Corrosive |
| Resistivity (ohm-m) | >100 | 20-100<br>50-100<br>>30 | 10-20<br>20-50 | 5-10<br>7-20 | <5<br><7 |
| pH | | >5.0 and <10 | | 5.0-6.5 | <5.0 |
| Chlorides (ppm) | | <200 | | 300-1,000 | >1,000 |

### Soil Aggressiveness

| | Recommendations for Normal Weight Concrete Subject to Sulfate Attack | | |
|---|---|---|---|
| Concrete Exposure | Water Soluble Sulfate (SO$_4$) in Soil, Percent | Cement Type | Water Cement Ratio (Maximum) |
| Mild | 0.00-0.10 | --- | --- |
| Moderate | 0.10-0.20 | II, IP(MS), IS(MS) | 0.5 |
| Severe | 0.20-2.0 | V[1] | 0.45 |
| Very Severe | Over 2.0 | V with pozzolan | 0.45 |

Note:

[1] Or a blend of Type II cement and a ground granulated blast furnace slag or a pozzolan that gives equivalent sulfate resistance.

**Table 2.5-41—{Summary As-Conducted Boring Information}**

(Page 1 of 4)

| Location | Depth (ft) | Termination (bottom) Elevation (ft) | Coordinates (ft), Maryland State Plane (NAD 1927) | | Ground Surface Elevation (ft) (NGVD 1929) | Date of As Built Survey |
|---|---|---|---|---|---|---|
| | | | North | East | | |
| B-301 | 403.0 | -308.5 | 217024.06 | 960815.05 | 94.51 | 9/15/2006 |
| B-302 | 200.0 | -123.6 | 217122.24 | 960766.98 | 76.41 | 9/15/2006 |
| B-303 | 200.0 | -112.6 | 217016.91 | 960867.69 | 87.40 | 9/15/2006 |
| B-304 | 200.0 | -132.0 | 217188.61 | 960896.88 | 68.00 | 9/15/2006 |
| B-305 | 151.5 | -79.5 | 217166.25 | 960686.74 | 72.01 | 9/15/2006 |
| B-306 | 150.0 | -31.4 | 217024.31 | 960681.82 | 118.58 | 9/15/2006 |
| B-307 | 201.5 | -82.2 | 216955.27 | 960690.13 | 119.28 | 9/15/2006 |
| B-308 | 150.0 | -42.9 | 216906.69 | 960771.28 | 107.10 | 9/15/2006 |
| B-309 | 150.0 | -49.9 | 216949.24 | 960890.70 | 100.06 | 9/15/2006 |
| B-310 | 100.0 | -8.4 | 217081.40 | 960616.60 | 91.62 | 5/15/2006 |
| B-311 | 150.0 | -91.6 | 217268.61 | 960771.76 | 58.43 | 9/15/2006 |
| B-312 | 99.5 | -44.2 | 217293.00 | 960740.00 | 55.27 | 5/15/2006 |
| B-313 | 150.0 | -99.3 | 217372.34 | 960713.67 | 50.73 | 9/15/2006 |
| B-314 | 100.0 | -47.2 | 217321.89 | 960654.50 | 52.78 | 9/15/2006 |
| B-315 | 100.0 | -34.5 | 217184.68 | 960559.43 | 65.54 | 9/15/2006 |
| B-316 | 100.0 | 8.1 | 216767.16 | 960864.35 | 108.07 | 9/15/2006 |
| B-317 | 100.0 | -5.6 | 217094.70 | 961249.20 | 94.42 | 5/15/2007 |
| B-318 | 200.0 | -102.2 | 217019.30 | 961227.20 | 97.82 | 5/15/2006 |
| B-319 | 100.0 | 2.9 | 216963.62 | 961123.01 | 102.87 | 9/15/2006 |
| B-320 | 150.0 | -43.6 | 216943.50 | 961044.10 | 106.43 | 5/15/2006 |
| B-321 | 150.0 | -79.3 | 217152.50 | 960333.20 | 70.66 | 5/25/2006 |
| B-322 | 100.0 | -10.1 | 217170.03 | 960202.65 | 89.87 | 9/15/2006 |
| B-323 | 200.0 | -92.5 | 217027.97 | 960060.86 | 107.48 | 9/15/2006 |
| B-324 | 101.5 | 3.7 | 216906.40 | 960114.44 | 105.20 | 9/15/2006 |
| B-325 | 100.0 | -15.0 | 216948.98 | 960549.73 | 84.97 | 9/15/2006 |
| B-326 | 100.0 | 3.1 | 216859.22 | 960652.25 | 103.11 | 9/15/2006 |
| B-327 | 150.0 | -63.1 | 216865.70 | 960573.37 | 86.92 | 9/15/2006 |
| B-328 | 150.0 | -73.7 | 216828.86 | 960493.21 | 76.29 | 9/19/2006 |
| B-329 | 100.0 | -25.2 | 216800.38 | 960379.43 | 74.83 | 9/19/2006 |
| B-330 | 100.0 | -14.5 | 216715.40 | 960523.70 | 85.46 | 9/15/2006 |
| B-331 | 100.0 | -31.7 | 216970.57 | 960481.79 | 68.32 | 9/15/2006 |
| B-332 | 100.0 | -34.6 | 217127.42 | 960400.52 | 65.40 | 9/15/2006 |
| B-333 | 98.8 | -9.3 | 216657.04 | 960386.24 | 89.49 | 9/15/2006 |
| B-334 | 100.0 | -13.3 | 216515.53 | 960556.61 | 86.75 | 9/15/2006 |
| B-335 | 100.0 | -0.5 | 216732.70 | 960703.30 | 99.47 | 5/15/2006 |
| B-336 | 100.0 | -3.1 | 216632.91 | 960750.27 | 96.87 | 9/15/2006 |
| B-337 | 100.0 | -28.2 | 217257.88 | 960264.41 | 71.77 | 9/15/2006 |
| B-338 | 99.6 | -1.6 | 217121.10 | 960150.10 | 97.97 | 5/25/2006 |
| B-339 | 100.0 | -8.0 | 217095.21 | 960211.99 | 91.96 | 9/15/2006 |
| B-340 | 100.0 | -15.4 | 217171.34 | 961225.22 | 84.57 | 9/15/2006 |
| B-341 | 100.5 | -2.3 | 217036.40 | 961104.48 | 98.16 | 9/15/2006 |
| B-401 | 401.5 | -329.4 | 216344.12 | 961516.81 | 72.06 | 9/15/2006 |
| B-402 | 200.0 | -117.8 | 216405.10 | 961463.50 | 82.22 | 5/15/2006 |
| B-403 | 200.0 | -136.6 | 216305.80 | 961562.90 | 63.41 | 5/15/2006 |
| B-404 | 200.0 | -132.1 | 216441.34 | 961596.49 | 67.90 | 9/21/2006 |
| B-405 | 150.0 | -28.0 | 216487.38 | 961408.73 | 122.00 | 9/15/2006 |

**Table 2.5-41—{Summary As-Conducted Boring Information}**
(Page 2 of 4)

| Location | Depth (ft) | Termination (bottom) Elevation (ft) | Coordinates (ft), Maryland State Plane (NAD 1927) | | Ground Surface Elevation (ft) (NGVD 1929) | Date of As Built Survey |
|---|---|---|---|---|---|---|
| | | | North | East | | |
| B-406 | 150.0 | -31.6 | 216315.62 | 961352.01 | 118.36 | 9/15/2006 |
| B-407 | 200.0 | -118.4 | 216238.96 | 961412.45 | 81.63 | 9/15/2006 |
| B-408 | 150.0 | -81.6 | 216261.74 | 961482.04 | 68.41 | 9/15/2006 |
| B-409 | 150.0 | -88.5 | 216253.80 | 961614.80 | 61.55 | 4/20/2006 |
| B-410 | 55.0 | 64.1 | 216374.30 | 961323.70 | 119.05 | 4/20/2006 |
| B-410A* | 98.7 | 20.4 | 216381.30 | 961323.70 | 119.05 | 4/20/2006 |
| B-411 | 150.0 | -68.6 | 216556.31 | 961517.19 | 81.45 | 9/15/2006 |
| B-412 | 98.9 | -6.7 | 216589.24 | 961495.42 | 92.17 | 9/15/2006 |
| B-413 | 150.0 | -27.1 | 216694.88 | 961413.25 | 122.90 | 9/15/2006 |
| B-414 | 100.0 | 21.2 | 216630.18 | 961354.48 | 121.20 | 9/15/2006 |
| B-415 | 98.7 | 20.6 | 216480.90 | 961264.20 | 119.26 | 4/20/2006 |
| B-416 | 100.0 | -13.8 | 216084.50 | 961596.34 | 86.22 | 9/15/2006 |
| B-417 | 101.5 | -52.3 | 216435.75 | 961901.11 | 49.23 | 9/15/2006 |
| B-418 | 200.0 | -156.3 | 216340.25 | 961976.71 | 43.67 | 9/22/2006 |
| B-419 | 100.0 | -44.7 | 216267.83 | 961895.60 | 55.29 | 9/21/2006 |
| B-420 | 150.0 | -87.4 | 216213.53 | 961670.44 | 62.57 | 9/15/2006 |
| B-421 | 150.0 | -34.4 | 216497.56 | 961019.77 | 115.58 | 9/15/2006 |
| B-422 | 100.0 | 4.0 | 216478.23 | 960915.01 | 104.02 | 9/15/2006 |
| B-423 | 201.5 | -91.4 | 216331.76 | 960850.21 | 110.14 | 9/15/2006 |
| B-424 | 100.0 | 18.9 | 216263.30 | 960818.60 | 118.92 | 4/26/2006 |
| B-425 | 101.5 | 16.9 | 216247.50 | 961274.70 | 118.43 | 4/20/2006 |
| B-426 | 100.0 | -16.3 | 216193.04 | 961386.57 | 83.73 | 9/21/2006 |
| B-427 | 150.0 | -33.7 | 216164.05 | 961272.73 | 116.27 | 9/19/2006 |
| B-428 | 150.0 | -35.9 | 216109.19 | 961210.06 | 114.11 | 9/19/2006 |
| B-429 | 100.0 | 3.7 | 216087.85 | 961119.27 | 103.66 | 9/19/2006 |
| B-430 | 100.0 | 2.5 | 216006.88 | 961193.12 | 102.48 | 9/19/2006 |
| B-431 | 101.5 | 16.9 | 216271.10 | 961177.30 | 118.43 | 4/20/2006 |
| B-432 | 100.0 | 18.6 | 216399.00 | 961139.10 | 118.62 | 4/20/2006 |
| B-433 | 100.0 | -2.5 | 215963.80 | 961107.50 | 97.49 | 4/27/2006 |
| B-434 | 100.0 | 5.2 | 215827.10 | 961244.30 | 105.15 | 5/2/2006 |
| B-435 | 100.0 | 7.7 | 216020.06 | 961404.74 | 107.71 | 9/15/2006 |
| B-436 | 100.0 | 8.3 | 215923.92 | 961441.55 | 108.29 | 9/22/2006 |
| B-437 | 100.5 | 10.1 | 216521.76 | 960968.80 | 110.63 | 9/15/2006 |
| B-438 | 6.5 | 99.5 | 216414.91 | 960848.90 | 105.95 | 9/28/2006 |
| B-438A | 100.0 | 6.6 | 216411.98 | 960867.31 | 106.59 | 9/28/2006 |
| B-439 | 100.0 | 13.8 | 216340.49 | 960948.68 | 113.80 | 9/15/2006 |
| B-440 | 100.0 | -43.7 | 216349.47 | 961813.66 | 56.34 | 9/21/2006 |
| B-701 | 75.0 | -66.3 | 219485.54 | 960507.60 | 8.66 | 9/21/2006 |
| B-702* | 50.0 | -39.7 | 218980.62 | 961183.23 | 10.33 | 9/21/2006 |
| B-703 | 100.0 | -54.6 | 218171.00 | 960957.01 | 45.42 | 9/21/2006 |
| B-704 | 50.0 | -10.4 | 217991.06 | 960926.05 | 39.58 | 9/21/2006 |
| B-705 | 50.0 | -3.3 | 217581.30 | 960917.90 | 46.75 | 4/19/2006 |
| B-706 | 50.0 | 27.4 | 217140.14 | 961339.74 | 77.42 | 9/21/2006 |
| B-707 | 50.0 | 17.4 | 217396.98 | 961481.84 | 67.38 | 9/21/2006 |
| B-708 | 100.0 | -62.7 | 217585.84 | 961810.64 | 37.35 | 9/28/2006 |
| B-709 | 50.0 | -18.8 | 217642.82 | 961978.18 | 31.25 | 9/28/2006 |
| B-710 | 75.0 | -27.0 | 217542.51 | 962136.88 | 47.96 | 9/28/2006 |

**Table 2.5-41—{Summary As-Conducted Boring Information}**
(Page 3 of 4)

| Location | Depth (ft) | Termination (bottom) Elevation (ft) | Coordinates (ft), Maryland State Plane (NAD 1927) | | Ground Surface Elevation (ft) (NGVD 1929) | Date of As Built Survey |
|---|---|---|---|---|---|---|
| | | | North | East | | |
| B-711 | 50.0 | 3.0 | 216755.70 | 961743.50 | 53.01 | 4/19/2006 |
| B-712 | 50.0 | -7.6 | 216506.16 | 961997.56 | 42.41 | 9/22/2006 |
| B-713 | 50.0 | 8.0 | 216117.68 | 962283.16 | 57.99 | 9/28/2006 |
| B-714 | 50.0 | 66.0 | 215705.73 | 962034.37 | 116.02 | 10/16/2006 |
| B-715 | 50.0 | 36.3 | 214951.76 | 962639.59 | 86.29 | 10/17/2006 |
| B-716 | 49.5 | 32.9 | 215003.21 | 961364.57 | 82.35 | 10/16/2006 |
| B-717 | 50.0 | 40.7 | 214302.45 | 962349.27 | 90.72 | 10/17/2006 |
| B-718 | 50.0 | 67.5 | 214130.52 | 961929.05 | 117.47 | 10/18/2006 |
| B-719 | 49.4 | 25.8 | 213978.69 | 961500.20 | 75.23 | 10/18/2006 |
| B-720 | 75.0 | -1.5 | 215674.48 | 962378.47 | 73.47 | 9/28/2006 |
| B-721 | 100.0 | 1.3 | 215545.80 | 962462.10 | 101.30 | 5/4/2006 |
| B-722 | 73.9 | 25.9 | 215386.10 | 962467.00 | 99.78 | 5/4/2006 |
| B-723 | 75.0 | 15.0 | 215108.00 | 963000.80 | 90.02 | 4/28/2006 |
| B-724 | 100.0 | -3.0 | 214780.00 | 963106.20 | 96.97 | 4/28/2006 |
| B-725 | 75.0 | -16.0 | 214664.30 | 963219.40 | 59.02 | 4/28/2006 |
| B-726 | 75.0 | 3.3 | 215564.67 | 961709.57 | 78.33 | 10/16/2006 |
| B-727 | 100.0 | 4.9 | 215300.85 | 961884.98 | 104.88 | 10/16/2006 |
| B-728 | 75.0 | 37.3 | 215163.63 | 961910.05 | 112.30 | 10/16/2006 |
| B-729 | 75.0 | 42.3 | 214861.87 | 962454.60 | 117.28 | 10/17/2006 |
| B-730 | 75.0 | 40.4 | 214728.50 | 962523.84 | 115.36 | 10/17/2006 |
| B-731 | 99.3 | 16.4 | 214546.48 | 962547.88 | 115.67 | 10/17/2006 |
| B-732 | 75.0 | 15.7 | 215034.10 | 961594.70 | 90.72 | 5/11/2006 |
| B-733 | 100.0 | -12.1 | 214866.80 | 961697.70 | 87.92 | 5/11/2006 |
| B-734 | 75.0 | 30.7 | 214589.60 | 961812.50 | 105.73 | 5/9/2006 |
| B-735 | 75.0 | 16.2 | 214805.48 | 961021.83 | 91.20 | 10/16/2006 |
| B-736 | 75.0 | 23.3 | 214681.67 | 961154.26 | 98.29 | 10/16/2006 |
| B-737 | 100.0 | -36.5 | 214511.91 | 961147.40 | 63.47 | 10/16/2006 |
| B-738 | 75.0 | 12.3 | 213826.30 | 961679.62 | 87.29 | 10/19/2006 |
| B-739 | 99.8 | 0.5 | 213719.60 | 961793.32 | 100.35 | 10/19/2006 |
| B-740 | 75.0 | -0.7 | 213605.13 | 961781.13 | 74.29 | 10/19/2006 |
| B-741 | 75.0 | 6.4 | 213760.48 | 961029.82 | 81.38 | 10/18/2006 |
| B-742 | 100.0 | 2.4 | 213472.84 | 961217.19 | 102.39 | 10/18/2006 |
| B-743 | 75.0 | 28.6 | 213315.70 | 961232.00 | 103.60 | 5/9/2006 |
| B-744 | 100.0 | 13.3 | 216377.30 | 959963.38 | 113.28 | 9/29/2006 |
| B-745 | 75.0 | 36.7 | 215971.20 | 960529.02 | 111.71 | 9/29/2006 |
| B-746 | 75.0 | 7.8 | 215743.35 | 960721.36 | 82.79 | 9/29/2006 |
| B-747 | 75.0 | 15.3 | 216176.28 | 959944.95 | 90.34 | 9/29/2006 |
| B-748 | 100.0 | -17.6 | 216039.74 | 960288.74 | 82.40 | 9/29/2006 |
| B-749 | 75.0 | 27.5 | 215775.08 | 960332.24 | 102.53 | 9/29/2006 |
| B-750 | 73.9 | -1.6 | 215849.16 | 959930.06 | 72.35 | 9/29/2006 |
| B-751 | 73.9 | 18.3 | 215588.86 | 960146.20 | 92.23 | 9/29/2006 |
| B-752 | 100.0 | -4.2 | 215489.21 | 960257.57 | 95.79 | 9/29/2006 |
| B-753 | 40.0 | 8.8 | 217831.20 | 960648.86 | 48.81 | 9/21/2006 |
| B-754 | 50.0 | 17.0 | 217369.78 | 960290.37 | 67.00 | 9/21/2006 |
| B-755 | 40.0 | 55.0 | 215923.66 | 961637.86 | 94.98 | 9/22/2006 |
| B-756 | 50.0 | 56.9 | 215504.60 | 961215.10 | 106.85 | 4/21/2006 |
| B-757 | 40.0 | 66.9 | 215135.13 | 960760.60 | 106.86 | 10/16/2006 |

### Table 2.5-41—{Summary As-Conducted Boring Information}
(Page 4 of 4)

| Location | Depth (ft) | Termination (bottom) Elevation (ft) | Coordinates (ft), Maryland State Plane (NAD 1927) | | Ground Surface Elevation (ft) (NGVD 1929) | Date of As Built Survey |
|---|---|---|---|---|---|---|
| | | | North | East | | |
| B-758 | 40.0 | 42.6 | 215133.29 | 960332.67 | 82.63 | 10/16/2006 |
| B-759 | 100.0 | -1.7 | 214526.25 | 960025.32 | 98.35 | 10/19/2006 |
| B-765 | 102.0 | -4.6 | 216424.51 | 959701.22 | 97.37 | 9/29/2006 |
| B-766 | 50.0 | 58.9 | 216932.89 | 959791.50 | 108.89 | 9/19/2006 |
| B-768 | 100.0 | -51.6 | 217116.03 | 962242.98 | 48.39 | 9/28/2006 |
| B-769 | 50.0 | 4.2 | 216589.75 | 962559.47 | 54.23 | 9/28/2006 |
| B-770 | 50.0 | 71.6 | 215466.60 | 962826.95 | 121.59 | 10/18/2006 |

Note:

(1) Location and elevation approximated based on offset observed in the field and recorded on Field Checklist.

**Table 2.5-42—{Summary Undisturbed Tube Sample}**
(Page 1 of 5)

| Boring | Drill Rig | Date | Sample No. | Depth (ft) | Rec (in.) | Field Remarks |
|---|---|---|---|---|---|---|
| B-301 | U. TRUCK | 5/25/2006 | UD-1 | 33.5 - 35.5 | 24 | MH |
| | | | UD-2 | 43.5 - 45.3 | 21 | MH |
| | | | UD-3 | 88.5 - 90.5 | 0 | |
| | | | UD-4 | 98.5 - 99.8 | 6 | SM |
| | | | UD-5 | 138.5 - 140.5 | 4 | SC / SM |
| | | 5/30/2006 | UD-6 | 158.5 - 159.6 | 13 | 13" push, CL with fine sand |
| | | | UD-7 | 168.5 - 170.5 | 9 | CL / MH |
| | | | UD-8 | 183.5 - 184.3 | 10 | MH |
| B-302 | C. ATV | 5/30/2006 | UD-1 | 83.5 - 84.9 | 16 | 16" push, SM with fine sand, shell |
| | | | UD-2 | 128.5 - 130.5 | 12 | MH |
| B-303 | U. TRUCK | 5/9/2006 | UD-1 | 28 - 30 | 24 | CL |
| | | | | 38 - 39.6 | 19 | 19" push, SC |
| B-304 | U. ATV | 5/30/2006 | UD-1 | 73.5 - 75.5 | 22 | SM |
| | | | UD-2 | 98.5 - 99.5 | 12 | 12" push, SC |
| | | | UD-3 | 138.5 - 139.3 | 10 | MH |
| B-305 | C.ATV | 7/17/2006 | UD-1 | 12.5 - 14.3 | 22 | CH |
| | | | UD-2 | 19.5 - 21.2 | 16 | MH |
| | | | P-3 | 35 - 37 | 5 | pitcher, cemented sand |
| | | | P-4 | 39.5 - 41.5 | 22 | pitcher, SM |
| | | | UD-5 | 52.5 - 53.5 | 7 | f. sandy silt, shell |
| | | | P-6 | 89.5 - 91.5 | 8 | pitcher, sand |
| B-306 | U. TRUCK | 5/5/2006 | UD-1 | 58 - 60 | 24 | CL |
| | | 5/5/2006 | UD-2 | 68 - 70 | 24 | CL |
| B-307 | U. TRUCK | 5/15/2006 | UD-1 | 123.5 - 124.7 | 14 | SM |
| | | | UD-2 | 178.5 - 180.4 | 23 | MH |
| B-308 | U. TRUCK | 5/3/2006 | UD-1 | 43 - 45 | 24 | CL |
| | | 5/4/2006 | UD-2 | 53 - 55 | 16 | CL |
| | | 5/4/2006 | UD-3 | 63 - 65 | 0 | sand |
| B-309 | C. TRUCK | 5/11/2006 | UD-1 | 33.5 - 35.5 | 23 | CL |
| | | 5/11/2006 | UD-2 | 43.5 - 45.5 | 24 | CL |
| | | 5/11/2006 | UD-3 | 53.5 - 55.5 | 23 | SC |
| B-310 | C. ATV | 6/15/2006 | UD-1 | 78.5 - 79.8 | 15 | SC |
| B-312 | C. ATV | 5/18/2006 | UD-1 | 10.5 - 12.3 | 17 | 21" push, CH |
| | | 5/18/2006 | UD-2 | 38.5 - 38.6 | 0 | 0.5" push |
| | | 5/18/2006 | UD-3 | 98.5 - 99.5 | 12 | 12" push, MH |
| B-313 | U. ATV | 5/22/2006 | UD-1 | 93.5 - 94.7 | | CL |
| | | | UD-2 | 123.5 - 124.3 | | ML |
| B-314 | | | UD-1 | 13.5 - 15.5 | 12 | CH |
| B-315 | C. ATV | 5/22/2006 | UD-1 | 23.5 - 25.5 | 14 | CH |
| B-316 | C. TRUCK | 5/4/2006 | UD-1 | 43.5 - 45.5 | 24 | CL |
| | | 5/4/2006 | UD-2 | 53.5 - 55.5 | 24 | CL |
| B-317 | C. TRUCK | 5/5/2006 | UD-1 | 28.5 - 30.5 | 24 | CL |
| | | 5/5/2006 | UD-2 | 38.5 - 40.5 | 24 | CH |
| | | 5/5/2006 | UD-3 | 48.5 - 50.3 | 21 | SC |
| B-318 | U. ATV | 6/3/2006 | UD-1 | 148.5 - 149.1 | 3 | 7" push, f. sandy SILT |
| B-319 | U. ATV | 5/5/2006 | UD-1 | 33.5 - 35.5 | 24 | MH |
| | | 5/5/2006 | UD-2 | 43.5 - 45.5 | 27 | MH |
| | | 5/5/2006 | UD-3 | 53.5 - 54.3 | 10 | MH |

**Table 2.5-42—{Summary Undisturbed Tube Sample}**
(Page 2 of 5)

| Boring | Drill Rig | Date | Sample No. | Depth (ft) | Rec (in.) | Field Remarks |
|--------|-----------|------|------------|------------|-----------|---------------|
| B-320 | C. TRUCK | 5/8/2006 | UD-1 | 38.5 - 40.5 | 24 | MH |
| | | 5/9/2006 | UD-2 | 48.5 -50 | 18 | 18" push, clayey sand |
| B-321 | C. ATV | 6/5/2006 | UD-1 | 23.5 - 25 | 18 | CH |
| | | 6/6/2006 | UD-2 | 73.5 - 75.5 | 24 | SM |
| B-322 | U. ATV | 5/18/2006 | UD-1 | 28.5 - 30.5 | 28 | CL |
| | | | UD-2 | 38.5 - 39.9 | 27 | SM |
| | | | UD-3 | 48.5 - 49.3 | 9 | SC |
| B-323 | U. ATV | 6/7/2006 | UD-1 | 83.5 - 84.8 | 15 | MH |
| | | | UD-2 | 178.5 - 179.1 | 0 | MH |
| B-324 | | | UD-1 | 60 - 62 | 24 | CH |
| | | | P-2 | 69 - 71 | 22 | SM |
| | | | P-3 | 85.5 - 87.5 | 5 | SM |
| B-326 | U. ATV | 5/4/2006 | UD-1 | 33.5 - 35.5 | 28 | CL |
| | | 5/4/2006 | UD-2 | 43.5 - 45.5 | 28 | MH |
| | | 5/4/2006 | UD-3 | 53.5 - 55.5 | 27 | bottom 2" bent, sandy lean clay |
| B-327 | C. ATV | 5/25/2006 | UD-1 | 113.5 - 114.2 | 9 | ML |
| | | | UD-2 | 138.5 - 140.5 | 10 | SM |
| B-328 | C.ATV | 6/19/2006 | UD-1 | 63.5 - 65.5 | 24 | SM |
| | | | UD-2 | 93.5 - 94.6 | 12 | SC |
| | | | UD-3 | 123.5 - 124.4 | 11 | ML, shell |
| B-329 | C.ATV | 6/13/2006 | UD-1 | 63.5 - 65.3 | 22 | SM |
| | | | UD-2 | 73.5 - 75.5 | 24 | SM |
| B-330 | U. ATV | 5/25/2006 | UD-1 | 28.5 - 29.2 | 0 | |
| B-331 | C. ATV | 5/24/2006 | UD-1 | 18.5 - 20.5 | 24 | MH |
| B-332 | C. ATV | 6/2/2006 | UD-1 | 73.5 - 74.6 | 13 | SM |
| B-333 | U. ATV | 5/17/2006 | UD-1 | 28.5 - 30.5 | 24 | MH |
| | | | UD-2 | 38.5 - 40.5 | 24 | CL |
| | | | UD-3 | 48.5 - 48.8 | 4 | SM |
| B-334 | U. TRUCK | 5/24/2006 | UD-1 | 23 - 25 | 24 | CL |
| | | | UD-2 | 33 - 35 | 13 | CL |
| B-335 | U. ATV | 5/3/2006 | UD-1 | 31 - 33 | 24 | CL |
| | | | UD-2 | 38.5 - 40.5 | 24 | CH |
| | | | UD-3 | 48.5 - 50.5 | 24 | CL |
| | | | UD-4 | 58.5 - 58.8 | 3 | tube deformed, SPT @ bottom, sand with shell |
| B-336 | U. ATV | 5/15/2006 | UD-1 | 33.5 - 35.5 | 24 | CH |
| | | | UD-2 | 43.5 - 45.5 | 24 | CH |
| | | | UD-3 | 53.5 - 55.5 | 15 | SC |
| B-337 | C. ATV | 6/7/2006 | UD-1 | 53.5 - 54.6 | 13 | ML |
| B-338 | C.ATV | 6/13/2006 | UD-1 | 48.5 - 50.5 | 24 | MH / ML |
| | | | | 94.5 - 95.0 | ? | not on boring log |
| | | | | 95 - 97 | ? | not on boring log |
| | | | UD-4 | 98.5 - 99.6 | 7 | SM |
| B-340 | C.TRACK | 8/4/2006 | P-1 | 66 - 68 | 12 | SC, cemented |
| B-341 | | | UD-1 | 88.5 - 90.5 | 24 | SM |
| | | | UD-2 | 98.5 - 100.5 | 24 | SP-SM |
| B-401 | U.TRUCK | 6/20/2006 | UD-1 | 68.5 - 70.5 | 23 | SM |
| | | | UD-2 | 98.5 - 99.8 | 15 | ML |

## Table 2.5-42—{Summary Undisturbed Tube Sample}
(Page 3 of 5)

| Boring | Drill Rig | Date | Sample No. | Depth (ft) | Rec (in.) | Field Remarks |
|--------|-----------|------|------------|------------|-----------|---------------|
| | | | UD-3 | 123.5 - 124.8 | 16 | CL |
| | | | UD-4 | 138.5 - 140.5 | 23 | MH |
| | | 6/21/2006 | UD-5 | 158.5 -159.3 | 10 | MH |
| | | 6/21/2006 | UD-6 | 173.5 - 174.4 | 11 | MH |
| | | 6/22/2006 | UD-7 | 198.5 - 200.5 | 21 | ML |
| | | 6/22/2006 | UD-8 | 213.5 - 214.6 | 13 | ML |
| | | | UD-9 | 228.5 - 229.6 | 13 | ML |
| | | | UD-10 | 243.5 - 244.4 | 8 | ML |
| | | | UD-11 | 348.5 - 350.5 | 7 | |
| B-403 | C.ATV | 6/21/2006 | UD-1 | 63.5 - 64.9 | 20 | SM |
| | | | UD-2 | 98.5 - 99.5 | 12 | ML |
| | | | UD-3 | 123.5 - 124.5 | 12 | ML |
| B-404 | U.ATV | 6/23/2006 | UD-1 | 52 - 53.6 | 18 | SP-SM |
| | | | UD-2 | 66 - 67.5 | 18 | SC |
| | | | UD-3 | 83.5 - 85.1 | 17 | SC |
| B-405 | C. TRUCK | 5/16/2006 | UD-1 | 58.5 - 60.5 | 22 | CL |
| | | | UD-2 | 68.5 - 70.5 | 24 | CL |
| B-406 | U. TRUCK | 5/17/2006 | UD-1 | 63.5 - 65.5 | 24 | CH |
| | | | UD-2 | 73.5 - 75.2 | 12 | 21" push, SC |
| B-407 | U. ATV | 5/14/2006 | UD-1 | 53.5 - 54.5 | 11 | 12" push, SM with shell |
| | | 5/15/2006 | UD-2 | 78.5 - 79 | 4 | tube bent, SM |
| | | 5/15/2006 | UD-3 | 128.5 - 129 | 6 | ML with sand |
| | | 5/15/2006 | UD-4 | 153.5 - 153.9 | 5 | tube bent, MH |
| B-409 | C.TRUCK | 6/22/2006 | P-1 | 35 | 13 | Pitcher, SP |
| | | | UD-2 | 17.5 - 19 | 24 | SC |
| | | | UD-3 | 50 - 52 | 24 | SM |
| | | | UD-4 | 62.5 - 64.5 | 24 | SM |
| | | | UD-5 | 95 -96.6 | 19 | ML, sandy SILT |
| | | 6/27/2006 | UD-6 | 137.5 - 139 | 18 | MH |
| B-410 | C. TRUCK | 5/1/2006 | UD-1 | 53.5 - 55.5 | 0 | shelby tube lost in hole, not accepted |
| | | 5/1/2006 | UD-2 | 60.5 - 62.5 | 15.5 | remnant tube recovered, not accepted |
| B-410A | C. TRUCK | 5/1/2006 | | 53.5 - 55.5 | 24 | CH, not on log |
| | | 5/1/2006 | UD-2 | 63.5 - 65.5 | 7 | CH |
| | | 5/2/2006 | UD-3 | 73.5 - 75 | 18 | CH, f. sand at bottom |
| B-411 | C.ATV | 7/26/2006 | UD-1 | 23 - 25 | 16 | CH |
| B-413 | U. TRUCK | 5/15/2006 | UD-1 | 73 - 75 | 24 | CL |
| B-414 | U. TRUCK | 5/11/2006 | UD-1 | 58 - 60 | 24 | CL |
| | | 5/11/2006 | UD-2 | 68 - 70 | 24 | CL |
| B-418 | U.ATV | 6/28/2006 | UD-1 | ? | 0 | |
| B-420 | U. TRUCK | 6/6/2006 | UD-1 | 63.5 - 65.5 | 24 | SM |
| | | 6/7/2006 | UD-2 | 128.5 - 130.3 | 22 | CL |
| B-421 | C. TRUCK | 5/10/2006 | UD-1 | 48.5 - 50.5 | 24 | ML |
| | | 5/10/2006 | UD-2 | 58.5 - 60.5 | 24 | CL |
| B-422 | C. ATV | 5/4/2006 | UD-1 | 38.5 - 40.5 | 24 | CL |
| | | 5/4/2006 | UD-2 | 48.5 - 50.5 | 23 | CH |
| | | 5/4/2006 | UD-3 | 58.5 - 59.3 | 8 | CH / SC |
| B-423 | | | UD-1 | 103.5 - 105.3 | 21 | SM |

**Table 2.5-42—{Summary Undisturbed Tube Sample}**
(Page 4 of 5)

| Boring | Drill Rig | Date | Sample No. | Depth (ft) | Rec (in.) | Field Remarks |
|--------|-----------|------|-----------|-----------|-----------|---------------|
| | | | UD- | 113.5 - 113.8 | 0 | |
| | | | UD-2 | 158.5 - 160.1 | 19 | CL |
| | | | UD-3 | 178.5 - 179.8 | 16 | MH |
| | | | UD-4 | 188.5 - 189.2 | 8 | MH |
| B-425 | U. TRUCK | 5/1/2006 | UD-1 | 57 - 59 | 24 | CH |
| | | 5/1/2006 | UD-2 | 65 - 67 | 24 | CH |
| | | 5/1/2006 | UD-3 | 75 - 77 | 24 | CH |
| B-427 | C. TRUCK | 5/2/2006 | UD-1 | 63.5 - 65.5 | 24 | CH |
| | | 5/2/2006 | UD-2 | 73.5 - 74.8 | 15 | SC |
| B-428 | U. TRUCK | 5/2/2006 | UD-1 | 57 - 59 | 21 | CH, bottom 10" bent |
| | | 5/2/2006 | UD-2 | 60 - 62 | 24 | CL, bent |
| | | 5/2/2006 | UD-3 | 63 - 65 | 20 | CL, bottom 10" bent |
| | | 5/2/2006 | UD-4 | 66 - 68 | 24 | CL, bottom 5" bent |
| | | 5/2/2006 | UD-5 | 69 - 71 | 7 | CL, bottom 3" bent |
| B-429 | U. ATV | 5/1/2006 | UD-1 | 45 - 47 | 24 | CH |
| | | 5/1/2006 | UD-2 | 53.5 - 55.5 | 0 | |
| | | 5/1/2006 | UD-3 | 58.5 - 60 | 18 | SC |
| B-430 | C. ATV | 5/1/2006 | UD-1 | 30 - 32 | 10 | ML |
| | | 5/1/2006 | UD-2 | 38.5 - 39.2 | 5 | SC |
| | | 5/1/2006 | UD-3 | 48.5 - 50.1 | 18 | MH |
| | | 5/1/2006 | UD-4 | 58.5 - 59.3 | 18 | ML |
| B-433 | C. TRUCK | 5/17/2006 | | 28.5 - 30.5 | 24 | not on log |
| | | 5/17/2006 | UD-2 | 38.5 - 40.5 | 24 | CL |
| | | 5/17/2006 | UD-3 | 48.5 - 48.8 | 4 | CL from log |
| B-434 | C. ATV | 5/9/2006 | UD-1 | 43.5 - 45.5 | 6.5 | CL |
| | | 5/9/2006 | UD-2 | 53.5 - 55 | 18 | CH |
| | | 5/10/2006 | UD-3 | 63.5 - 64.3 | 14 | CH |
| B-436 | C. ATV | 5/9/2006 | UD-1 | 48.5 - 50.5 | 18 | CL |
| B-437 | U.TRUCK | 7/10/2006 | UD-1 | 13.5 - 15.5 | 23 | SM |
| | | | UD-2 | 98.5 - 100.5 | 22 | SM |
| B-438a | | | UD-1 | 93.5 - 95.5 | 14 | SM |
| B-440 | U. ATV | 6/6/2006 | UD-1 | 51 - 53 | 24 | SM |
| | | | UD-2 | 58.5 - 58.6 | 0 | |
| B-701 | C.TRUCK | 6/28/2006 | UD-1 | 43.5 - 44.9 | 17 | ML |
| B-703 | | | UD-1 | 18.5 - 20.5 | 19 | CH |
| | | | UD-2 | 73.5 - 75.5 | 10 | SM |
| B-708 | U. ATV | 5/9/2006 | UD-1 | 78.5 - 79.5 | 12 | 12" push, sand |
| B-714 | | | UD-1 | 48 - 50 | 24 | SC |
| B-722 | U.ATV | 7/18/2006 | UD-1 | 13 - 15 | 24 | SM |
| B-723 | C.TRACK | 6/1/2006 | UD-1 | 28.5 - 30.2 | 20 | SP-SC |
| | | | UD-2 | 38.5 - 40.5 | 24 | CL |
| B-724 | C. TRACK | 6/5/2006 | UD-1 | 73.5 - 75.5 | 21 | SM |
| B-725 | C. TRACK | 6/6/2006 | UD-1 | 63.5 - 65.5 | 24 | SM |
| B-726 | C.TRACK | 8/1/2006 | UD-1 | 10.5 - 12.5 | 0 | No Recovery |
| | | 8/1/2006 | UD-2 | 23.5 - 25.5 | 19.5 | CH |
| B-727 | C. ATV | 5/10/2006 | UD-1 | 48.5 - 50.5 | 22 | |
| | | 5/11/2006 | UD-2 | 63.5 - 65.5 | 20 | 24" push |
| B-728 | C. ATV | 5/11/2006 | UD-1 | 53.5 - 55.5 | 23 | CH |
| B-729 | C. TRUCK | 5/19/2006 | UD-1 | 68.5 - 70.5 | 24 | CH |

**Table 2.5-42—{Summary Undisturbed Tube Sample}**
(Page 5 of 5)

| Boring | Drill Rig | Date | Sample No. | Depth (ft) | Rec (in.) | Field Remarks |
|---|---|---|---|---|---|---|
| B-730 | C. TRUCK | 5/18/2006 | UD-1 | 53.5 - 55.5 | 0 | No Recovery |
| | | | UD-2 | 68.5 - 70.5 | 24 | CH |
| B-731 | C. TRACK | 5/31/2006 | UD-1 | 58.5 - 60.5 | 24 | SM |
| B-732 | C.TRACK | 6/8/2006 | UD-1 | 15 - 17 | 24 | SM |
| B-733 | C. TRACK | 6/8/2006 | UD-1 | 23.5 - 25.5 | 24 | CL |
| | | | UD-2 | 88.5 - 90.5 | | CH/MH |
| B-734 | C. TRACK | 6/7/2006 | UD-1 | 48.5 - 50.5 | 24 | CL |
| B-735 | C.TRACK | 6/28/2006 | UD-1 | 28 - 30 | 24 | sand |
| B-737 | C.TRACK | 7/19/2006 | UD-1 | 10.5 - 12.5 | 24 | SC / CL |
| B-739 | | 6/15/2006 | UD-1 | 51- 52 | 12 | SC |
| | | | UD-2 | 83.5 - 84 | 5 | CL |
| | | | UD-3 | 96 - 96.8 | 9 | SP-SM |
| B-742 | | | UD-1 | 78.5 - 78.6 | 0 | |
| | | | UD-2 | 88.5 - 88.8 | 3 | SM, sample placed in jar |
| B-743 | U.ATV | 7/10/2006 | UD-1 | 23.5 - 25.5 | 21 | SM |
| | | | UD-2 | 38 - 40 | 0 | |
| B-746 | C. TRACK | 7/18/2006 | UD-1 | 13.5 -15.5 | 24 | SM |
| B-748 | C.TRACK | 7/17/2006 | UD-1 | 13.5 - 15.5 | 24 | ML |
| B-749 | C. TRUCK | 5/23/2006 | UD-1 | 43.5 - 45.5 | | |
| B-750 | C.TRACK | 7/10/2006 | UD-1 | 28.5 - 30.5 | 0 | |
| | | | UD-2 | 48.5 - 49.5 | 11 | clayey sand, shells |
| B-751 | C. TRUCK | 5/22/2006 | UD-1 | 33.5 - 35.5 | | |
| | | | UD-2 | 43.5 - 45.5 | | |
| B-752 | C.TRACK | 7/5/2006 | UD-1 | 58 - 59.5 | 18 | clay |
| B-759 | | | UD-1 | 56.5 - 57 | 0 | |
| | | | UD-2 | 66 - 68 | 24 | CH |
| | | | UD-3 | 98 - 98.5 | 5 | SC, tube bent |
| B-765 | C. TRACK | 7/12/2006 | P- | 70 - 72 | 8 | cemented fine sandy silt, trace clay, trace shells |
| | | | P- | 100 - 102 | 20 | clayey fine sandy silt |
| B-768 | C.TRUCK | 6/20/2006 | UD-1 | 43.5 - 45.3 | 20 | SM |
| | | | UD-2 | 73.5 - 75.5 | 24 | SM |

Total Tubes Attempted:  217

### Table 2.5-43—{Summary As-Conducted CPT Information}
(Page 1 of 2)

| Location | Depth (ft) | Termination (bottom) Elevation (ft) | Coordinates (ft), Maryland State Plane (NAD 1927) North | East | Ground Surface Elevation (ft) (NGVD 1929) | Date of As Built Survey | Remarks Pre-Drill | | Seismic | Dissipation |
|---|---|---|---|---|---|---|---|---|---|---|
| C-301 | 52.3 | 42.5 | 217041.78 | 960820.13 | 94.84 | 9/15/2006 | | | ✓ | |
| C-302 | 61.7 | 29.3 | 217088.90 | 960833.77 | 90.94 | 9/15/2006 | | | | ✓ |
| C-302-2* | 55.3 | 39.2 | 217026.56 | 960817.55 | 94.51 | 7/26/2006 | | | | |
| C-302-2a* | 138.0 | -43.5 | 217026.56 | 960817.55 | 94.51 | 7/26/2006 | ✓ | 85 ft | | ✓ |
| C-303 | 25.4 | 36.2 | 217230.60 | 960804.00 | 61.58 | 4/24/2006 | | | | |
| C-303a* | 47.1 | 14.5 | 217230.60 | 960804.00 | 61.58 | 7/25/2006 | ✓ | 45 ft | | |
| C-303a-1* | 71.4 | -9.8 | 217230.60 | 960804.00 | 61.58 | 7/25/2006 | ✓ | 50 ft | | |
| C-303b* | 123.4 | -61.8 | 217230.60 | 960804.00 | 61.58 | 7/25/2006 | ✓ | 80 ft | | ✓ |
| C-304 | 26.7 | 34.2 | 217235.29 | 960606.73 | 60.95 | 9/15/2006 | | | ✓ | ✓ |
| C-305 | 74.3 | 41.6 | 216876.50 | 960961.50 | 115.91 | 4/24/2006 | | | | |
| C-306 | 56.9 | 40.4 | 217042.12 | 961184.89 | 97.31 | 9/15/2006 | | | | ✓ |
| C-306a* | 102.5 | -5.2 | 217038.92 | 961181.69 | 97.31 | 7/27/2006 | ✓ | 80 ft | | |
| C-307 | 75.3 | 42.4 | 216853.68 | 961079.64 | 117.64 | 9/15/2006 | | | ✓ | |
| C-308 | 48.2 | 36.1 | 217129.90 | 960263.70 | 84.33 | 5/1/2006 | | | ✓ | |
| C-309 | 70.1 | 36.0 | 217045.62 | 960110.76 | 106.04 | 9/15/2006 | | | | ✓ |
| C-311 | 34.9 | 39.0 | 216869.75 | 960488.16 | 73.97 | 9/15/2006 | | | | |
| C-312 | 56.4 | 43.3 | 216799.20 | 960596.36 | 99.75 | 9/15/2006 | | | | |
| C-313 | 37.2 | 42.7 | 216757.92 | 960336.75 | 79.93 | 9/15/2006 | | | | |
| C-314 | 39.5 | 40.6 | 216531.40 | 960493.83 | 80.09 | 9/15/2006 | | | | |
| C-401 | 28.1 | 39.4 | 216384.26 | 961574.09 | 67.46 | 9/15/2006 | | | ✓ | |
| C-401-2a* | 81.9 | -14.4 | 216381.06 | 961570.89 | 67.46 | 7/27/2006 | ✓ | 55 ft | ✓ | |
| C-401-2b* | 131.2 | -63.8 | 216381.06 | 961570.89 | 67.46 | 7/27/2006 | ✓ | 85 ft | ✓ | ✓ |
| C-402 | 34.5 | 38.7 | 216333.85 | 961494.18 | 73.13 | 9/15/2006 | | | | ✓ |
| C-403 | 43.8 | 39.2 | 216517.33 | 961511.47 | 82.96 | 9/15/2006 | | | | |
| C-404 | 80.1 | 39.2 | 216524.30 | 961308.90 | 119.21 | 4/20/2006 | | | ✓ | ✓ |
| C-405 | 40.0 | 35.5 | 216163.49 | 961666.32 | 75.54 | 9/15/2006 | | | | |
| C-406 | 15.6 | 28.3 | 216380.92 | 961901.51 | 43.89 | 9/28/2006 | | | | ✓ |
| C-407 | 32.3 | 30.9 | 216159.20 | 961732.20 | 63.23 | 6/22/2006 | | | ✓ | ✓ |
| C-407-2a* | 96.3 | -33.1 | 216161.50 | 961726.70 | 63.23 | 7/28/2006 | ✓ | 50 ft | ✓ | ✓ |
| C-407-b* | 142.4 | -79.2 | 216161.50 | 961726.70 | 63.23 | 7/31/2006 | ✓ | 95 ft | ✓ | ✓ |
| C-408 | 77.4 | 40.8 | 216396.64 | 961001.81 | 118.18 | 9/15/2006 | | | ✓ | |
| C-408a* | 98.3 | 19.9 | 216398.76 | 960999.69 | 118.18 | 7/24/2006 | ✓ | 98 ft | | |
| C-408-2a* | 123.7 | -5.5 | 216393.81 | 961004.64 | 118.18 | 7/31/2006 | ✓ | 105 ft | ✓ | |
| C-409 | 80.5 | 38.6 | 216288.45 | 960760.56 | 119.12 | 9/15/2006 | | | | ✓ |
| C-411 | 80.4 | 36.2 | 216178.94 | 961178.21 | 116.60 | 9/19/2006 | | | | ✓ |
| C-412 | 76.8 | 37.5 | 216093.75 | 961306.66 | 114.31 | 9/28/2006 | | | | |
| C-413 | 13.6 | 86.3 | 216045.53 | 961037.78 | 99.90 | 9/28/2006 | | | | |
| C-414 | 62.5 | 39.9 | 215893.42 | 961201.10 | 102.36 | 9/28/2006 | | | | ✓ |
| C-415 | 20.0 | 36.6 | 216305.70 | 961857.40 | 56.63 | 5/26/2006 | | | | |
| C-701 | 29.5 | -18.6 | 219262.19 | 960933.61 | 10.95 | 9/21/2006 | | | | ✓ |
| C-701a* | 28.1 | -17.1 | 219265.39 | 960936.81 | 10.95 | 7/21/2006 | | | | |
| C-702 | 20.3 | -9.0 | 218720.05 | 961033.95 | 11.34 | 9/21/2006 | | | | |

**Table 2.5-43—{Summary As-Conducted CPT Information}**
(Page 2 of 2)

| Location | Depth (ft) | Termination (bottom) Elevation (ft) | Coordinates (ft), Maryland State Plane (NAD 1927) North | East | Ground Surface Elevation (ft) (NGVD 1929) | Date of As Built Survey | Remarks Pre-Drill | Seismic | Dissipation |
|---|---|---|---|---|---|---|---|---|---|
| C-703 | 32.6 | 35.2 | 217361.27 | 961165.03 | 67.82 | 10/17/2006 | | | |
| C-704 | 48.2 | -2.9 | 217500.74 | 961710.02 | 45.36 | 9/28/2006 | | | |
| C-705 | 34.0 | -2.9 | 217637.26 | 961983.10 | 31.08 | 9/28/2006 | | | |
| C-706 | 50.0 | 55.2 | 216958.95 | 961494.86 | 105.28 | 9/21/2006 | | | |
| C-707 | 19.5 | 20.8 | 216308.12 | 962079.42 | 40.35 | 9/22/2006 | | | |
| C-708 | 50.0 | 62.9 | 215658.28 | 961962.86 | 112.97 | 10/16/2006 | | | |
| C-709 | 50.0 | 61.7 | 215027.59 | 962824.89 | 111.73 | 10/18/2006 | | | |
| C-710 | 21.2 | 85.0 | 214875.83 | 961187.31 | 106.15 | 10/16/2006 | | | |
| C-711 | 34.9 | 65.6 | 214222.13 | 962176.75 | 100.54 | 10/17/2006 | | | |
| C-712 | 29.7 | 29.4 | 213909.83 | 961370.06 | 59.05 | 10/18/2006 | | | ✓ |
| C-713 | 41.8 | 21.3 | 215855.86 | 962296.57 | 63.11 | 9/28/2006 | | | |
| C-714 | 85.1 | 24.2 | 214920.30 | 963057.62 | 109.32 | 10/18/2006 | | | ✓ |
| C-715 | 57.3 | 33.6 | 215445.62 | 961798.99 | 90.85 | 10/16/2006 | | | |
| C-716 | 20.5 | 75.7 | 214432.49 | 962659.44 | 96.21 | 10.17/2006 | | | |
| C-717 | 66.6 | 35.8 | 214698.14 | 961692.58 | 102.35 | 10/16/2006 | | | ✓ |
| C-718 | 34.1 | 33.6 | 214343.71 | 961205.59 | 67.67 | 10/16/2006 | | | |
| C-719 | 12.0 | 78.2 | 214025.30 | 961636.90 | 90.21 | 10/18/2006 | | | |
| C-720 | 70.7 | 28.0 | 213593.77 | 961134.09 | 98.66 | 10/18/2006 | | | ✓ |
| C-721 | 52.0 | 35.6 | 216157.88 | 960330.47 | 87.62 | 9/29/2006 | | | |
| C-722 | 38.4 | 36.1 | 215478.76 | 960648.26 | 74.52 | 10/16/2006 | | | |
| C-723 | 68.7 | 28.9 | 215988.18 | 959760.36 | 97.60 | 9/29/2006 | | | ✓ |

* Location and elevation approximated based on offset observed in the field and recorded on Field Checklist

**Table 2.5-44—{Summary As-Conducted Observation Well Information}**

| Location | Depth (ft) | Termination (bottom) Elevation (ft) | Coordinates (ft), Maryland State Plane (NAD 1927) | | Ground Surface Elevation (ft) (NGVD 1929) | Elevation (ft), Top of Concrete at Base of Well Head Protector | Elevation (ft), Ground Water Level Measuring Point (V-Notch) | Date of As Built Survey |
|---|---|---|---|---|---|---|---|---|
| | | | North | East | | | | |
| OW-301 | 80.0 | 14.5 | 217048.02 | 960814.47 | 94.51 | 94.78 | 96.27 | 9/15/2006 |
| OW-313A | 57.5 | -6.5 | 217367.31 | 960705.30 | 51.03 | 51.31 | 53.20 | 9/15/2006 |
| OW-313B | 110.0 | -59.3 | 217372.34 | 960713.67 | 50.73 | 51.16 | 53.54 | 9/15/2006 |
| OW-319A | 35.0 | 68.1 | 216962.56 | 961116.12 | 103.13 | 103.31 | 104.91 | 9/15/2006 |
| OW-319B | 85.0 | 18.5 | 216957.32 | 961125.02 | 103.53 | 103.85 | 105.35 | 9/19/2006 |
| OW-323 | 43.5 | 63.5 | 217034.46 | 960057.07 | 106.96 | 107.55 | 109.69 | 9/19/2006 |
| OW-328 | 72.0 | 4.3 | 216828.86 | 960493.21 | 76.29 | 76.55 | 77.85 | 9/19/2006 |
| OW-336 | 74.0 | 23.1 | 216643.18 | 960746.61 | 97.11 | 97.50 | 99.07 | 9/16/2006 |
| OW-401 | 77.5 | -6.1 | 216348.86 | 961530.99 | 71.38 | 71.91 | 73.49 | 9/21/2006 |
| OW-413A | 50.0 | 73.2 | 216703.14 | 961418.81 | 123.15 | 123.51 | 125.04 | 9/15/2006 |
| OW-413B | 125.0 | -2.1 | 216694.88 | 961413.25 | 122.90 | 123.25 | 124.85 | 9/15/2006 |
| OW-418A | 40.0 | 3.7 | 216340.41 | 961966.46 | 43.66 | 44.31 | 45.83 | 9/22/2006 |
| OW-418B | 92.0 | -48.3 | 216340.25 | 961976.71 | 43.67 | 44.13 | 45.77 | 9/22/2006 |
| OW-423 | 43.0 | 68.1 | 216339.99 | 960882.24 | 111.12 | 111.67 | 113.16 | 9/15/2006 |
| OW-428 | 50.0 | 63.9 | 216105.21 | 961212.38 | 113.92 | 114.32 | 115.92 | 9/19/2006 |
| OW-436 | 50.0 | 58.1 | 215922.47 | 961446.87 | 108.13 | 108.53 | 110.39 | 9/22/2006 |
| OW-703A | 49.0 | -5.0 | 218171.23 | 960967.72 | 44.02 | 44.44 | 45.65 | 9/21/2006 |
| OW-703B | 80.0 | -34.4 | 218171.67 | 960958.91 | 45.57 | 45.97 | 47.53 | 9/21/2006 |
| OW-705 | 52.0 | -4.3 | 217566.62 | 960917.18 | 47.71 | 47.77 | 50.22 | 9/15/2006 |
| OW-708A | 34.0 | 3.4 | 217586.23 | 961803.52 | 37.44 | 37.82 | 39.61 | 9/28/2006 |
| OW-711 | 50.0 | 2.9 | 216748.48 | 961741.61 | 52.92 | 53.26 | 55.31 | 9/22/2006 |
| OW-714 | 50.0 | 66.0 | 215705.73 | 962034.37 | 116.02 | 116.32 | 117.98 | 10/16/2006 |
| OW-718 | 43.0 | 75.5 | 214133.58 | 961924.87 | 118.53 | 118.96 | 120.41 | 10/18/2006 |
| OW-725 | 60.0 | -2.0 | 214649.30 | 963212.73 | 58.04 | 58.38 | 59.94 | 10/18/2006 |
| OW-729 | 42.0 | 76.9 | 214872.58 | 962445.93 | 118.88 | 119.44 | 121.11 | 10/17/2006 |
| OW-735 | 72.0 | 19.2 | 214805.48 | 961021.83 | 91.20 | 91.81 | 93.44 | 10/16/2006 |
| OW-743 | 55.0 | 48.7 | 213320.62 | 961234.01 | 103.65 | 104.05 | 105.89 | 10/18/2006 |
| OW-744 | 50.0 | 47.5 | 216405.37 | 960089.41 | 97.50 | 97.96 | 99.81 | 9/29/2006 |
| OW-752A | 37.0 | 58.3 | 215482.18 | 960250.12 | 95.30 | 95.73 | 97.00 | 9/29/2006 |
| OW-752B | 97.0 | -1.2 | 215489.21 | 960257.57 | 95.79 | 96.09 | 97.41 | 9/29/2006 |
| OW-754 | 44.0 | 23.0 | 217369.78 | 960290.37 | 67.00 | 67.21 | 68.85 | 9/15/2006 |
| OW-756 | 42.0 | 64.6 | 215497.07 | 961212.39 | 106.56 | 107.07 | 108.77 | 10/16/2006 |
| OW-759A | 35.0 | 62.8 | 214536.47 | 960055.02 | 97.78 | 98.05 | 99.69 | 10/19/2006 |
| OW-759B | 90.0 | 8.3 | 214526.25 | 960056.32 | 98.35 | 98.72 | 100.14 | 10/19/2006 |
| OW-765A | 29.0 | 68.4 | 216424.51 | 959701.22 | 97.37 | 97.92 | 99.60 | 9/29/2006 |
| OW-765B | 102.0 | -5.2 | 216420.42 | 959693.64 | 96.82 | 97.19 | 98.47 | 9/29/2006 |
| OW-766 | 50.0 | 58.9 | 216932.89 | 959791.50 | 108.89 | 109.32 | 110.72 | 9/19/2006 |
| OW-768A | 42.0 | 6.5 | 217106.06 | 962238.98 | 48.48 | 48.96 | 49.84 | 9/28/2006 |
| OW-769 | 42.0 | 12.2 | 216589.75 | 962559.47 | 54.23 | 54.39 | 56.43 | 9/28/2006 |
| OW-770 | 42.0 | 79.6 | 215466.60 | 962826.95 | 121.59 | 121.79 | 123.08 | 10/18/2006 |

**Table 2.5-45—{In-Situ Hydraulic Conductivity (Slug) Test Results}**

| Location | Screened Interval Depth (ft) | USCS Soil Classification | Hydraulic Conductivity (feet/sec) |
|---|---|---|---|
| OW-301 | 65 – 75 | SP | $1.58 \times 10^{-4}$ |
| OW-313A | 40 – 50 | SM, ML | $7.50 \times 10^{-6}$ |
| OW-313B | 95 – 105 | CL, ML, MH | $2.74 \times 10^{-7}$ |
| OW-319A | 20 – 30 | SP-SM, SC, CH, CL | $2.89 \times 10^{-6}$ |
| OW-319B | 70 – 80 | SM | $3.42 \times 10^{-5}$ |
| OW-323 | 30 – 40 | SP, SP-SM | $6.24 \times 10^{-5}$ |
| OW-328 | 60 – 70 | SM, OH | $3.79 \times 10^{-6}$ |
| OW-336 | 60 – 70 | SP-SM, SM | $2.10 \times 10^{-5}$ |
| OW-401 | 63 – 73 | SM | $6.77 \times 10^{-6}$ |
| OW-413A | 35 – 45 | SP-SM | $1.21 \times 10^{-5}$ |
| OW-413B | 110 – 120 | SP-SM, SM | $2.78 \times 10^{-6}$ |
| OW-418A | 25 – 35 | SP-SM | $4.41 \times 10^{-6}$ |
| OW-418B | 75 – 85 | SC, SM | $2.16 \times 10^{-7}$ |
| OW-423 | 28 – 38 | SP-SM, SM, SC | $6.86 \times 10^{-5}$ |
| OW-428 | 35 – 45 | SM, SC | $1.19 \times 10^{-5}$ |
| OW-436 | 29 – 39 | SC, SM | $2.80 \times 10^{-6}$ |
| OW-703A | 35 – 45 | SM | $1.34 \times 10^{-5}$ |
| OW-703B | 68 – 78 | SM, ML | $1.08 \times 10^{-6}$ |
| OW-705 | 40 – 50 | SC, SM | $4.99 \times 10^{-6}$ |
| OW-708 | 22 – 32 | SM | $2.56 \times 10^{-5}$ |
| OW-711 | 35 – 45 | SM | $6.04 \times 10^{-6}$ |
| OW-714 | 38 – 48 | SP-SM, SC | $2.81 \times 10^{-6}$ |
| OW-718 | 30 – 40 | SP-SM | $4.44 \times 10^{-6}$ |
| OW-725 | 48 – 58 | SM | $7.54 \times 10^{-6}$ |
| OW-735 | 60 – 70 | SP-SM, SM | $5.48 \times 10^{-5}$ |
| OW-743 | 40 – 50 | SP-SM, SM | $6.23 \times 10^{-7}$ |
| OW-744 | 38 – 48 | CL, SC, SM | $1.07 \times 10^{-6}$ |
| OW-752A | 25 – 35 | CH, SM | $7.03 \times 10^{-5}$ |
| OW-752B | 85 – 95 | SP-SM | $3.35 \times 10^{-6}$ |
| OW-754 | 32 – 42 | CL, SM | $5.29 \times 10^{-6}$ |
| OW-756 | 30 – 40 | SP-SM, SP-SC | $2.01 \times 10^{-4}$ |
| OW-759A | 20 – 30 | SM, SC, MH | $4.64 \times 10^{-7}$ |
| OW-759B | 75 – 85 | SM, SP, SP-SM | $1.17 \times 10^{-6}$ |
| OW-765A | 17 – 27 | SP-SM | $1.00 \times 10^{-5}$ |
| OW-765B | 82 – 92 | SM | $1.36 \times 10^{-6}$ |
| OW-766 | 20 – 30 | SP-SM | $1.10 \times 10^{-6}$ |
| OW-768 | 30 – 40 | SM | $5.29 \times 10^{-6}$ |
| OW-769 | 32 – 42 | SM, SC | $1.74 \times 10^{-6}$ |

**Table 2.5-46—{Summary As-Conducted Test Pit Information}**

| Location | Depth (ft) | Termination (bottom) Elevation (ft) | Coordinates (ft), Maryland State Plane (NAD 1927) | | Ground Surface Elevation (ft) (NGVD 1929) | Date of As Built Survey |
| --- | --- | --- | --- | --- | --- | --- |
| | | | North | East | | |
| TP-B307 | 6.7 | 112.7 | 216957.53 | 960690.62 | 119.35 | 9/19/2006 |
| TP-B314 | 9.0 | 43.8 | 217320.35 | 960658.25 | 52.78 | 9/15/2006 |
| TP-B315 | 8.5 | 57.3 | 217182.50 | 960563.12 | 65.80 | 9/15/2006 |
| TP-B334 | 10.0 | 77.0 | 216515.64 | 960560.94 | 87.03 | 9/19/2006 |
| TP-B335 | 8.0 | 91.6 | 216730.79 | 960706.97 | 99.64 | 9/19/2006 |
| TP-B407 | 7.0 | 74.3 | 216391.76 | 961465.02 | 81.25 | 9/21/2006 |
| TP-B414 | 6.5 | 114.3 | 216631.18 | 961530.95 | 120.83 | 9/15/2006 |
| TP-B415 | 6.5 | 112.4 | 216490.91 | 961298.37 | 118.92 | 9/15/2006 |
| TP-B423 | 8.0 | 97.9 | 216414.95 | 960849.03 | 105.86 | 9/19/2006 |
| TP-B434 | 8.5 | 96.7 | 215825.90 | 961244.18 | 105.24 | 9/22/2006 |
| TP-B435 | 10.0 | 97.7 | 216020.06 | 961404.74 | 107.71 | 9/19/2006 |
| TP-B715 | 8.5 | 79.7 | 214964.18 | 962637.77 | 88.16 | 10/17/2006 |
| TP-B716 | 8.8 | 88.3 | 214983.83 | 961289.79 | 97.13 | 10/16/2006 |
| TP-B717 | 8.0 | 82.5 | 214297.68 | 962346.36 | 90.53 | 10/17/2006 |
| TP-B719 | 8.0 | 64.3 | 213966.93 | 961493.94 | 72.28 | 10/18/2006 |
| TP-B727 | 7.0 | 97.3 | 215299.14 | 961883.13 | 104.33 | 10/16/2006 |
| TP-B744 | 6.5 | 106.8 | 316377.30 | 959963.38 | 113.28 | 9/29/2006 |
| TP-B758 | 9.0 | 73.6 | 215133.29 | 960332.67 | 82.63 | 10/16/2006 |
| TP-C309 | 8.0 | 100.5 | 217020.05 | 960105.24 | 108.45 | 9/19/2006 |
| TP-C723 | 7.0 | 89.8 | 215989.07 | 959754.78 | 96.75 | 9/29/2006 |

**Table 2.5-47—{Summary Field Electrical Resistivity Information}**

| Location | Coordinates (ft), Maryland State Plane (NAD 1927) | | Ground Surface Elevation (ft) (NGVD 1929) | Date of As Built Survey |
|---|---|---|---|---|
| | North | East | | |
| R-1 | 215837.30 | 960255.80 | 85.45 | 5/3/2006 |
| R-2 | 215837.30 | 960255.80 | 85.45 | 5/3/2006 |
| R-3 | 216622.50 | 960406.80 | 89.12 | 5/2/2006 |
| R-4 | 215915.40 | 961114.00 | 99.40 | 4/27/2006 |

## Table 2.5-48—{Geophysical Data from CCNPP Units 1 and 2 UFSAR}

| STATION | SURFICIAL SEDIMENTS (PLEISTOCENE) COMPRESSIONAL | | UNCONSOLIDATED SEDIMENTS (TERTIARY) COMPRESSIONAL | | INTERMEDIATE SEDIMENTS (CRETACEOUS)[a] COMPRESSIONAL | | BASEMENT ROCK COMPRESSIONAL | |
|---|---|---|---|---|---|---|---|---|
| | WAVE VELOCITY (fps) | THICKNESS (ft) | WAVE VELOCITY (fps) | THICKNESS (ft) | WAVE VELOCITY (fps) | THICKNESS (ft) | WAVE VELOCITY (fps) | THICKNESS (ft) |
| Solomons Shoal[b] | – | – | 5900 | 3080 | – | – | 15,170 | 3130 |
| Solomons Deed[b] | – | – | 6080 | 1070 | 6980 | 1900 | 18,100 | 3080 |
| Site[c] | 2200 | 40 | 5500 | – | – | – | – | – |
| Site[c] | – | – | 5900 | – | – | – | – | – |

Notes:

(a) These measurements refer to a "masked" arrival and the results are questionable.

(b) Adapted from Ewing and Worzel.

(c) Measurements by Dames & Moore.

**Table 2.5-49—{Shockscope Data from CCNPP Units 1 and 2 UFSAR}**

| BORING | DEPTH (ft) | CONFINING PRESSURE (lbs/ft²) | COMPRESSIONAL WAVE VELOCITY (fps) |
|---|---|---|---|
| DM-2 | 5 | 0 | 1,000 |
| | | 2000 | 1,200 |
| | | 4000 | 1,400 |
| | | 6000 | 1,700 |
| DM-9 | 15 | 0 | 1,200 |
| | | 2000 | 1,300 |
| | | 4000 | 1,500 |
| | | 6000 | 1,700 |
| DM-1 | 30 | 0 | 1,400 |
| | | 2000 | 1,500 |
| | | 4000 | 1,800 |
| | | 6000 | 2,100 |
| DM-10 | 68 | 0 | 2,600 |
| | | 2000 | 2,600 |
| | | 4000 | 3,200 |
| | | 6000 | 3,200 |
| DM-10 | 111 | 0 | 2,600 |
| | | 2000 | 2,600 |
| | | 4000 | 3,000 |
| | | 6000 | 3,000 |
| DM-10 | 156 | 0 | 1,800 |
| | | 2000 | 1,800 |
| | | 4000 | 1,900 |
| | | 6000 | 1,900 |
| DM-10 | 211 | 0 | 1,600 |
| | | 2000 | 1,700 |
| | | 4000 | 1,700 |
| | | 6000 | 1,700 |
| DM-10 | 256 | 0 | 2,100 |
| | | 2000 | 2,100 |
| | | 4000 | 2,200 |
| | | 6000 | 2,200 |
| DM-10 | 271 | 0 | 2,000 |
| | | 2000 | 2,200 |
| | | 4000 | 2,300 |
| | | 6000 | 2,600 |

### Table 2.5-50—{Summary Laboratory Test Results on Bulk Soil Samples}

**Non-Plastic Soils**

| Location | Depth (ft) | USCS | WC (%) | % Material Passing #4 | % Material Passing #200 | Mod. Proctor Compaction Max dry density (pcf) | Mod. Proctor Compaction Opt. WC (%) | CBR Unsoaked | CBR Soaked |
|---|---|---|---|---|---|---|---|---|---|
| TP-B307 | 4.5 | SP-SM | 2.3 | 100 | 5.8 | 109.3 | 10.5 | 14.8 | 4.4 |
| TP-B315 | 6.0 | SP-SM | 5.4 | 99.8 | 9.7 | 114.9 | 11.4 | 11.6 | 18.9 |
| TP-B334 | 3.0 | SM | 7.4 | 100 | 13.9 | 116.3 | 9.3 | | |
| TP-B334 | 6.0 | SM | 14.5 | 100 | 13.2 | 129.8 | 8.0 | | |
| TP-B335 | 5.0 | SM | 8.9 | 100 | 24.6 | 130.5 | 7.6 | 36.2 | 18.0 |
| TP-B407 | 4.5 | SW-SM | 7.1 | 97.8 | 9.0 | 118.9 | 8.8 | 14.8 | 17.0 |
| TP-B414 | 6.0 | SP-SM | 6.0 | 100 | 6.4 | 105.4 | 11.9 | | |
| TP-B415 | 3.0 | SP | 10.2 | 99.8 | 3.5 | 116.7 | 9.8 | 11.1 | 4.7 |
| TP-B435 | 5.0 | SM | 6.0 | 100 | 13.2 | 119.1 | 8.9 | | |
| TP-B435 | 7.0 | SP-SM | 4.6 | 99.2 | 8.3 | 123.9 | 8.9 | 26.8 | 33.7 |
| TP-B715 | 5.5 | SP-SM | 4.8 | 99.1 | 11.0 | 110.7 | 11.8 | | |
| TP-B716 | 6.0 | SP-SM | 3.8 | 99.0 | 6.0 | 116.3 | 9.4 | | |
| TP-B717 | 7.0 | SP-SM | 3.4 | 97.4 | 6.4 | 123.8 | 10.2 | 17.2 | 23.1 |
| TP-B719 | 7.0 | SM | 26.7 | 100 | 44.3 | 119.6 | 10.0 | 41.3 | 29.0 |
| TP-B727 | 6.0 | SM | 10.3 | 100 | 30.1 | 130.5 | 6.8 | | |
| TP-B758 | 2.0 | SP-SM | 6.0 | 99.2 | 8.4 | 121.0 | 8.8 | | |
| TP-B758 | 7.5 | SM | 11.8 | 97.4 | 31.1 | 127.3 | 8.9 | 11.3 | 4.4 |
| TP-C309 | 2.0 | SP | 4.3 | 98.8 | 3.7 | 111.2 | 13.9 | | |
| TP-C309 | 7.0 | SP-SM | 8.7 | 100 | 7.8 | 112.3 | 9.8 | | |
| TP-C723 | 6.0 | SP-SM | 4.6 | 98.8 | 7.5 | 113.8 | 6.8 | | |
| Min. | 2 | | 2.3 | 97.4 | 3.5 | 105.4 | 6.8 | 11.1 | 4.4 |
| Max. | 7.5 | | 26.7 | 100 | 44.3 | 130.5 | 13.9 | 41.3 | 33.7 |
| **Average:** | **5** | | **8** | **99** | **13** | **119** | **10** | **21** | **17** |

**Plastic Soils**

| Location | Depth (ft) | USCS | WC (%) | LL | PL | PI | % Material Passing #4 | % Material Passing #200 | Mod. Proctor Compaction Max Dry density (pcf) | Mod. Proctor Compaction Opt. WC (%) | CBR Unsoaked | CBR Soaked |
|---|---|---|---|---|---|---|---|---|---|---|---|---|
| TP-B314 | 4.0 | CH | 37.0 | 71 | 24 | 47 | 100 | 93.1 | 114.6 | 15.5 | | |
| TP-B335 | 3.0 | CL | 19.0 | 30 | 20 | 10 | 100 | 65.3 | 128.8 | 9.9 | | |
| TP-B423 | 5.0 | CL | 16.0 | 24 | 16 | 8 | 100 | 51.1 | 123.4 | 10.8 | | |
| TP-B434 | 2.0 | CL | 21.0 | 25 | 18 | 7 | 99.8 | 59.8 | 127.1 | 10.1 | 9.3 | 3.2 |
| TP-B435 | 9.0 | SC | 6.7 | 34 | 17 | 17 | 100 | 14.1 | 130.2 | 7.3 | 34.4 | 41.8 |
| TP-B719 | 0.5 | CL | 23.9 | 35 | 22 | 13 | 100 | 84.5 | 118.4 | 13.5 | | |
| TP-B744 | 1.5 | CL | 18.0 | 25 | 17 | 8 | 100 | 64.2 | 131.2 | 8.0 | | |
| TP-C723 | 2.5 | SC | 12.0 | 30 | 15 | 15 | 100 | 39.5 | 132.8 | 7.3 | 26.8 | 17.2 |
| Min. | 0.5 | | 6.7 | 24 | 15 | 7 | 99.8 | 14.1 | 114.6 | 7.3 | 9.3 | 3.2 |
| Max. | 9 | | 37 | 71 | 24 | 47 | 100 | 93.1 | 132.8 | 15.5 | 34.4 | 41.8 |
| **Average:** | **3** | | **19** | **34** | **19** | **16** | **100** | **59** | **126** | **10** | **24** | **21** |

**Table 2.5-51—{Design Vs Profile for CCNPP Unit 3 Subsurface Seismic Evaluation}**

| Unit | Soil | Depth Range (ft) | | El Range (ft) | | Vs (feet/sec) |
|------|------|------|------|------|------|------|
| I | Terrace SAND | 0 | 25 | +85 | +60 | 790 |
| II-a | Chesapeake CLAY/SILT | 25 | 40 | +60 | +45 | 1,100 |
| II-b-1 | Chesapeake Cemented SAND | 40 | 55 | +45 | +30 | 1,450 |
| II-b-2 | Chesapeake Cemented SAND | 55 | 70 | +30 | +15 | 1,800 |
| II-b-3 | Chesapeake Cemented SAND | 70 | 85 | +15 | 0 | 1,130 |
| II-b-4 | Chesapeake Cemented SAND | 85 | 100 | 0 | -15 | 1,740 |
| II-c-1 | Chesapeake CLAY/SILT | 100 | 135 | -15 | -50 | 1,250 |
| II-c-2 | Chesapeake CLAY/SILT | 135 | 285 | -50 | -200 | 1,250 |
| III-a-1 | Nanjemoy SAND | 285 | 305 | -200 | -220 | 1,790 |
| III-a-2 | Nanjemoy SAND | 305 | 315 | -220 | -230 | 2,330 |
| III-a-3 | Nanjemoy SAND | 315 | 355 | -230 | -270 | 2,030 |
| III-a-4 | Nanjemoy SAND | 355 | 400 | -270 | -315 | 1,930 |
| III-b | Nanjemoy CLAY/SILT * | 400 | 500 | -315 | -415 | 2,200 |
| IV | Aquia-Brightseat SAND | 500 | 631 | -415 | -546 | 2,200 |
| V-1 | Patapsco SAND | 631 | 1,085 | -546 | -1,000 | 2,200 |
| V-2 | Patapsco SAND | 1,085 | 1,585 | -1,000 | -1,500 | 2,330 |
| V-3 | Patapsco SAND | 1,585 | 1,731 | -1,500 | -1,646 | 2,550 |
| VI-1 | Patuxent/Arundel CLAY | 1,731 | 2,085 | -1,646 | -2,000 | 2,550 |
| VI-2 | Patuxent/Arundel CLAY | 2,085 | 2,531 | -2,000 | -2,446 | 2,800 |
| VII-1 | Granitoid Bedrock | 2,531 | 2,531 | -2,446 | -2,446 | 5,000 |
| VII-2 | Granitoid Bedrock | 2,531 | 2,541 | -2,446 | 2,456 | 7,000 |
| VII-3 | Granitoid Bedrock | 2,541 | 2,551 | -2,456 | -2,466 | 9,200 |
| VII-4 | Granitoid Bedrock | 2,551 | 3,085 | -2,466 | -3,000 | 9,200 |

*May include the Marlboro Clay

**Table 2.5-52—{Summary Shear Modulus and Damping Ratios for the CCNPP Unit 3 Seismic Evaluation}**

| Depth 0-25 ft (Terrace Sand) | | | Depth 25-40 ft (Chesapeake Clay/Silt) | | | Depth 40-100 ft (Ches. Cemented Sand) | | | Depth 100-285 ft (Ches. Clay/Silt) | | | Depth 285-355 ft (Nanjemoy Cemented Clay/Silt) | | |
|---|---|---|---|---|---|---|---|---|---|---|---|---|---|---|
| Cyclic Shear Strain (%) | $G/G_{max}$ | $D/D_{max}$ | Cyclic Shear Strain (%) | $G/G_{max}$ | $D/D_{max}$ | Cyclic Shear Strain (%) | $G/G_{max}$ | $D/D_{max}$ | Cyclic Shear Strain (%) | $G/G_{max}$ | $D/D_{max}$ | Cyclic Shear Strain (%) | $G/G_{max}$ | $D/D_{max}$ |
| 1.E-04 | 1 | 1.4 | 1.E-04 | 1 | 1.5 | 1.E-04 | 1 | 1 | 1.E-04 | 1 | 2 | 1.E-04 | 1 | 1.5 |
| 3.E-04 | 1 | 1.5 | 3.E-04 | 1 | 1.5 | 3.E-04 | 1 | 1 | 3.E-04 | 1 | 2 | 3.E-04 | 1 | 1.5 |
| 1.E-03 | 0.98 | 1.8 | 1.E-03 | 1 | 1.6 | 1.E-03 | 1 | 1.2 | 1.E-03 | 1 | 2 | 1.E-03 | 1 | 1.6 |
| 3.E-03 | 0.914 | 2.8 | 3.E-03 | 0.97 | 2.05 | 3.E-03 | 0.97 | 1.64 | 3.E-03 | 0.995 | 2.13 | 3.E-03 | 0.97 | 2.05 |
| 1.E-02 | 0.75 | 5 | 1.E-02 | 0.878 | 3.21 | 1.E-02 | 0.87 | 2.8 | 1.E-02 | 0.955 | 2.75 | 1.E-02 | 0.878 | 3.21 |
| 3.E-02 | 0.509 | 9.3 | 3.E-02 | 0.685 | 5.77 | 3.E-02 | 0.68 | 5.49 | 3.E-02 | 0.832 | 4.38 | 3.E-02 | 0.685 | 5.77 |
| 1.E-01 | 0.27 | 15.3 | 1.E-01 | 0.413 | 10.64 | 1.E-01 | 0.43 | 10.2 | 1.E-01 | 0.59 | 8 | 1.E-01 | 0.413 | 10.64 |
| 3.E-01 | 0.116 | 21.9 | 3.E-01 | 0.208 | 16.22 | 3.E-01 | 0.22 | 16.5 | 3.E-01 | 0.34 | 13.16 | 3.E-01 | 0.208 | 16.22 |
| 1.E+00 | 0.04 | 27 | 6.E-01 | 0.115 | 18.65 | 1.E+00 | 0.09 | 22.9 | 6.E-01 | 0.22 | 16.15 | 6.E-01 | 0.115 | 18.65 |
| 3.E+00 | 0.02 | 30 | 1.E+00 | 0.075 | 19 | 3.E+00 | 0.05 | 27 | 1.E+00 | 0.15 | 17.56 | 1.E+00 | 0.075 | 19 |
| 1.E-04 | 1 | 0.7 | 1.E-04 | 1 | 1.5 | 1.E-04 | 1 | 0.6 | 1.E-04 | 1 | 0.55 | 1.E-04 | 1 | 1.5 |
| 3.E-04 | 1 | 0.8 | 3.E-04 | 1 | 1.5 | 3.E-04 | 1 | 0.6 | 3.E-04 | 1 | 0.55 | 3.E-04 | 1 | 1.5 |
| 1.E-03 | 1 | 0.8 | 1.E-03 | 1 | 1.6 | 1.E-03 | 1 | 0.6 | 1.E-03 | 1 | 0.55 | 1.E-03 | 1 | 1.6 |
| 3.E-03 | 0.988 | 1.12 | 3.E-03 | 0.97 | 2.05 | 3.E-03 | 0.99 | 0.81 | 3.E-03 | 1 | 0.77 | 3.E-03 | 0.97 | 2.05 |
| 1.E-02 | 0.93 | 1.8 | 1.E-02 | 0.878 | 3.21 | 1.E-02 | 0.95 | 1.2 | 1.E-02 | 0.96 | 1.15 | 1.E-02 | 0.878 | 3.21 |
| 3.E-02 | 0.791 | 3.53 | 3.E-02 | 0.685 | 5.77 | 3.E-02 | 0.852 | 2.5 | 3.E-02 | 0.88 | 2.1 | 3.E-02 | 0.685 | 5.77 |
| 1.E-01 | 0.57 | 7.1 | 1.E-01 | 0.413 | 10.64 | 1.E-01 | 0.65 | 5.3 | 1.E-01 | 0.71 | 4.2 | 1.E-01 | 0.413 | 10.64 |
| 3.E-01 | 0.321 | 12.78 | 3.E-01 | 0.208 | 16.22 | 3.E-01 | 0.41 | 10.27 | 3.E-01 | 0.47 | 8.45 | 3.E-01 | 0.208 | 16.22 |
| 1.E+00 | 0.15 | 19.3 | 6.E-01 | 0.115 | 18.65 | 1.E+00 | 0.2 | 16.7 | 1.E+00 | 0.265 | 14.5 | 6.E-01 | 0.115 | 18.65 |
| 3.E+00 | 0.09 | 23 | 1.E+00 | 0.075 | 19 | 3.E+00 | 0.1 | 20.1 | 3.E+00 | 0.16 | 17.4 | 1.E+00 | 0.075 | 19 |

**Table 2.5-53—{Material Density and PI Adopted for the CCNPP Unit 3 Seismic Evaluation}**

| Unit | Soil | Est. Total Unit Weight (pcf) | Est. PI |
|------|------|------------------------------|---------|
| I | Terrace SAND | 120 | NP |
| II-a | Chesapeake CLAY/SILT | 115 | 35 |
| II-b | Chesapeake Cemented SAND | 120 | 20 |
| II-c | Chesapeake CLAY/SILT | 110 | 45 |
| III-a | Nanjemoy SAND | 120 | 30 |
| III-b | Nanjemoy CLAY/SILT * | 120 | N/A |
| IV | Aquia/Brightseat SAND | 115 | N/A |
| V | Patapsco SAND | 115 | N/A |
| VI | Patuxent/Arundel CLAY | 115 | N/A |

NP  =  Non-Plastic

PI  =  Plasticity Index

N/A  =  not available

* may include the Marlboro Clay

## Table 2.5-54—{Bearing Capacity Evaluation Parameters}

| Structure | Embedment, D (ft) | Length, L (ft) | Width, B (ft) | B/L | Soil Layer | c (ksf) | $\phi$ (deg) | $N_c$ | $N_q$ | $N_\gamma$ | $\zeta_c$ | $\zeta_q$ | $z_q$ |
|---|---|---|---|---|---|---|---|---|---|---|---|---|---|
| ESWS Cooling Towers | 13.7–22.7 | 147 | 96 | 0.65 | Stratum II-b | 0 | 34 | 42.16 | 29.44 | 41.06 | 1.46 | 1.44 | 0.74 |
| | | | | | Stratum II-c | 4 | 0 | 5.14 | 1 | 0 | 1.13 | 1 | 0.74 |
| Emergency Power Generating Buildings | 3 - 6 | 131 | 93 | 0.71 | Stratum II-b | 0 | 32 | 35.49 | 23.18 | 30.22 | 1.46 | 1.44 | 0.72 |
| | | | | | Stratum II-c | 4 | 0 | 5.14 | 1 | 0 | 1.14 | 1 | 0.72 |
| Reactor (Common Basemat) | 41 | 322 | 200 | 0.62 | Stratum II-b | 0 | 34 | 42.16 | 29.44 | 41.06 | 1.43 | 1.42 | 0.75 |
| | | | | | Stratum II-c, III | 2.3 | 16 | 11.63 | 4.34 | 3.06 | 1.23 | 1.18 | 0.75 |
| UHS Makeup Water Intake Structure | 30.5 | 78 | 47 | 0.60 | Stratum II-c | 4 | 0 | 5.14 | 1 | 0 | 1.12 | 1 | --- |

### Table 2.5-55—{Computed Factors of Safety (FOS) for the Critical Slip Surface}

| Slope Section | Static Analysis | | | | Pseudo-Static Analysis | | | |
|---|---|---|---|---|---|---|---|---|
| | Ordinary | Bishop | Janbu | M-P | Ordinary | Bishop | Janbu | M-P |
| A | 1.89 | 1.89 | 1.89 | 1.89 | 1.34 | 1.34 | 1.34 | 1.34 |
| B | 1.77 | 1.84 | 1.82 | 1.85 | 1.26 | 1.36 | 1.31 | 1.41 |
| C | 1.89 | 1.89 | 1.88 | 1.89 | 1.35 | 1.35 | 1.34 | 1.35 |
| D | 1.88 | 1.88 | 1.88 | 1.88 | 1.33 | 1.34 | 1.33 | 1.33 |
| E | 1.88 | 1.88 | 1.88 | 1.88 | 1.33 | 1.34 | 1.33 | 1.33 |
| F | 1.96 | 1.96 | 1.96 | 1.96 | 1.38 | 1.38 | 1.38 | 1.38 |
| G | 1.30 | 1.41 | 1.35 | 1.42 | 0.97 | 1.01 | 0.98 | 1.02 |

Notes:

Ordinary = Ordinary method

Bishop = Bishop's simplified method

Janbu = Janbu's simplified method

M-P = Morgenstern-Price method

**Table 2.5-56—{Computed Factors of Safety (FOS) for (Forced) Deeper Slip Surfaces}**

| Slope Section | Static Analysis | | | | Pseudo-Static Analysis | | | |
|---|---|---|---|---|---|---|---|---|
| | Ordinary | Bishop | Janbu | M-P | Ordinary | Bishop | Janbu | M-P |
| A | 1.79 | 1.98 | 1.86 | 2.00 | 1.37 | 1.40 | 1.37 | 1.41 |
| B | --- | --- | --- | --- | --- | --- | --- | --- |
| C | 2.10 | 2.16 | 2.10 | 2.16 | 1.46 | 1.51 | 1.47 | 1.51 |
| D | 1.94 | 1.99 | 1.94 | 1.99 | 1.38 | 1.42 | 1.38 | 1.42 |
| E | 1.98 | 2.03 | 1.98 | 2.03 | 1.40 | 1.44 | 1.40 | 1.44 |
| F | 1.98 | 2.03 | 1.98 | 2.03 | 1.40 | 1.44 | 1.40 | 1.44 |
| G | --- | --- | --- | --- | --- | --- | --- | --- |

Notes:

Ordinary = Ordinary method

Bishop = Bishop's simplified method

Janbu = Janbu's simplified method

M-P = Morgenstern-Price method

--- indicates no computation

**Figure 2.5-1—{Map of Physiographic Province}**
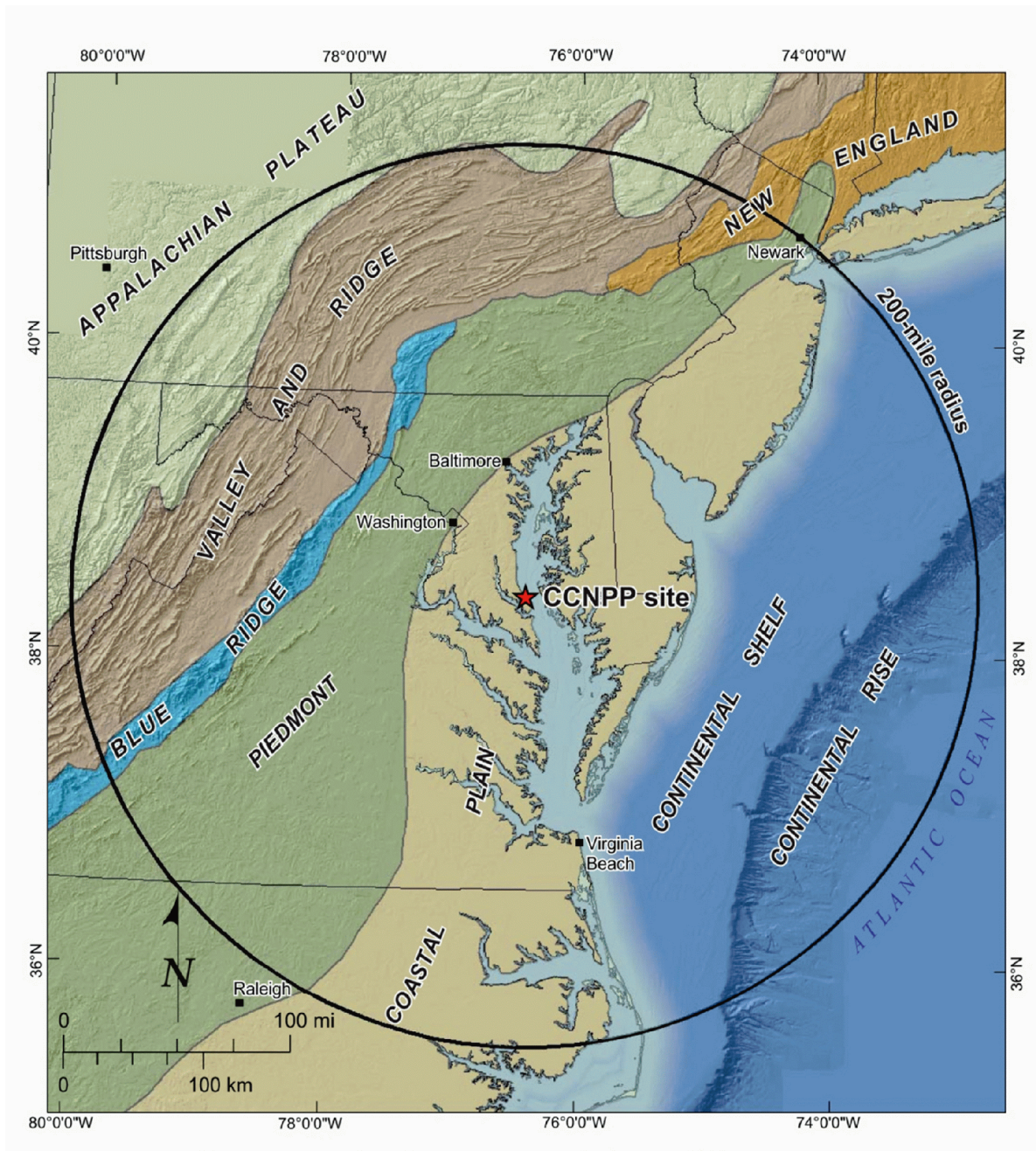
# Figure 2.5-2—{Site Vicinity Topographic Map 25-Mile (40-Km) Radius}

Index of USGS 1:100,000 maps

Washington East | Seaford
Leonardtown | Salisbury

25-mile radius

CCNPP Unit 3

Patuxent River

Chesapeake Bay

Potomac River

N

0   5   10 mi
0   5   10 km
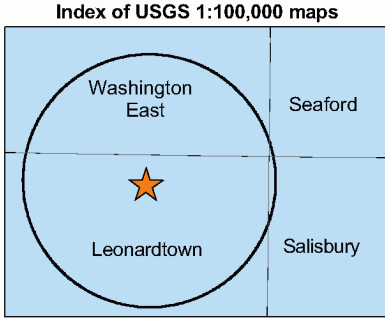
**Figure 2.5-3—{Site Area Topographic Map 5-Mile (8-Km) Radius}**



Base map: Leonardtown 30' x 60'  U.S. Geological Survey Topographic Map

# Figure 2.5-4—{Site Topographic Map 0.6-Mile (1-Km) Radius}
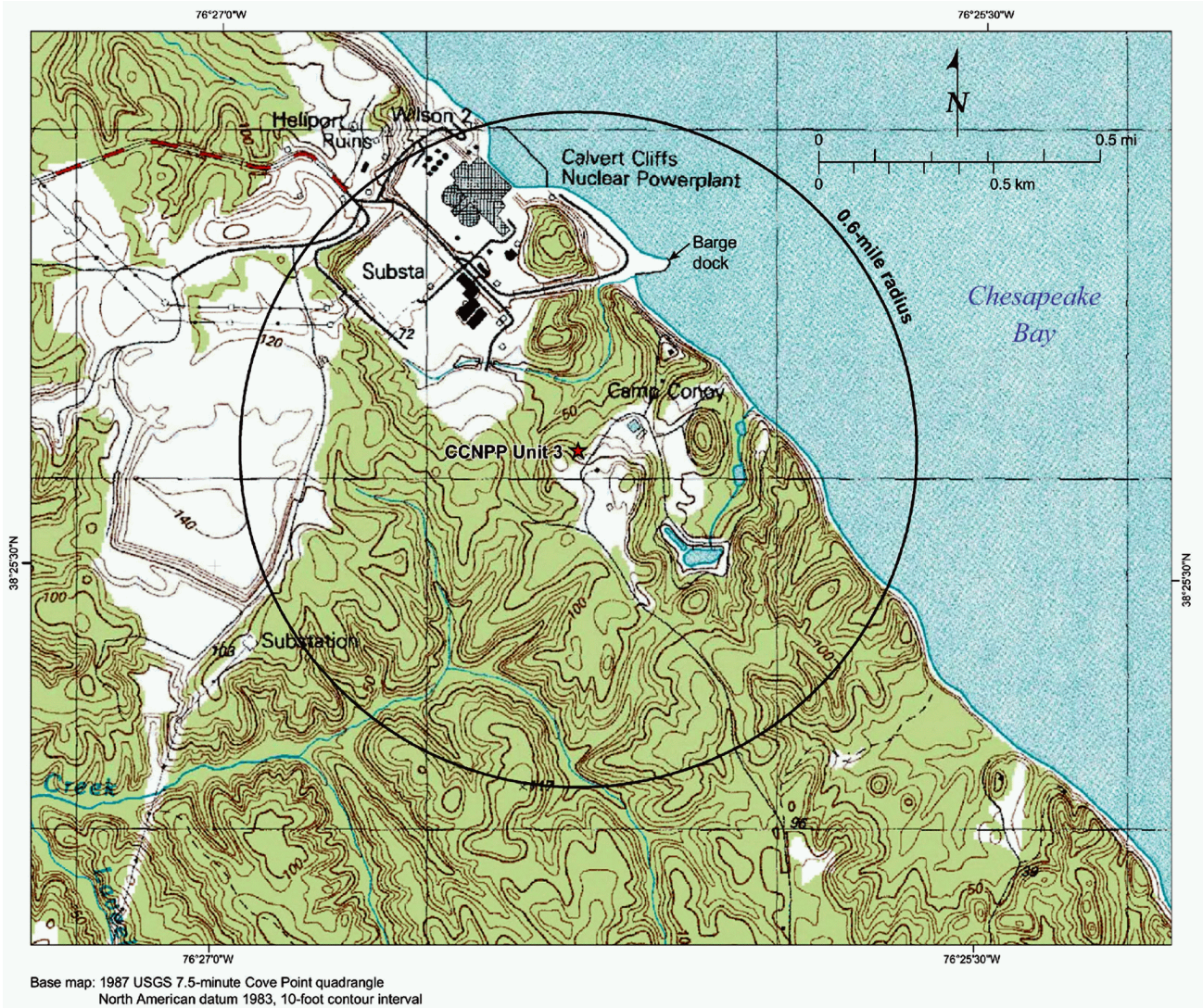
**Figure 2.5-5—{Regional Geologic Map 200-Mile (320-Km) Radius}**

Explanation

- - - Fault

⬡ Chesapeake impact crater (red)

– – Pre-Wisconsin glacial limit

– – Wisconsin glacial limit

Notes: 1. Modified after King and Beikman (1974) as digitized by Schruben et al. (1994).
2. See Figure 2.5-6 for explanation of map units.

CCNPP site

200-mile radius

ATLANTIC OCEAN

Inner and outer crater rim

N

| 0 | 50 | 100 mi |
| 0 | 50 | 100 km |
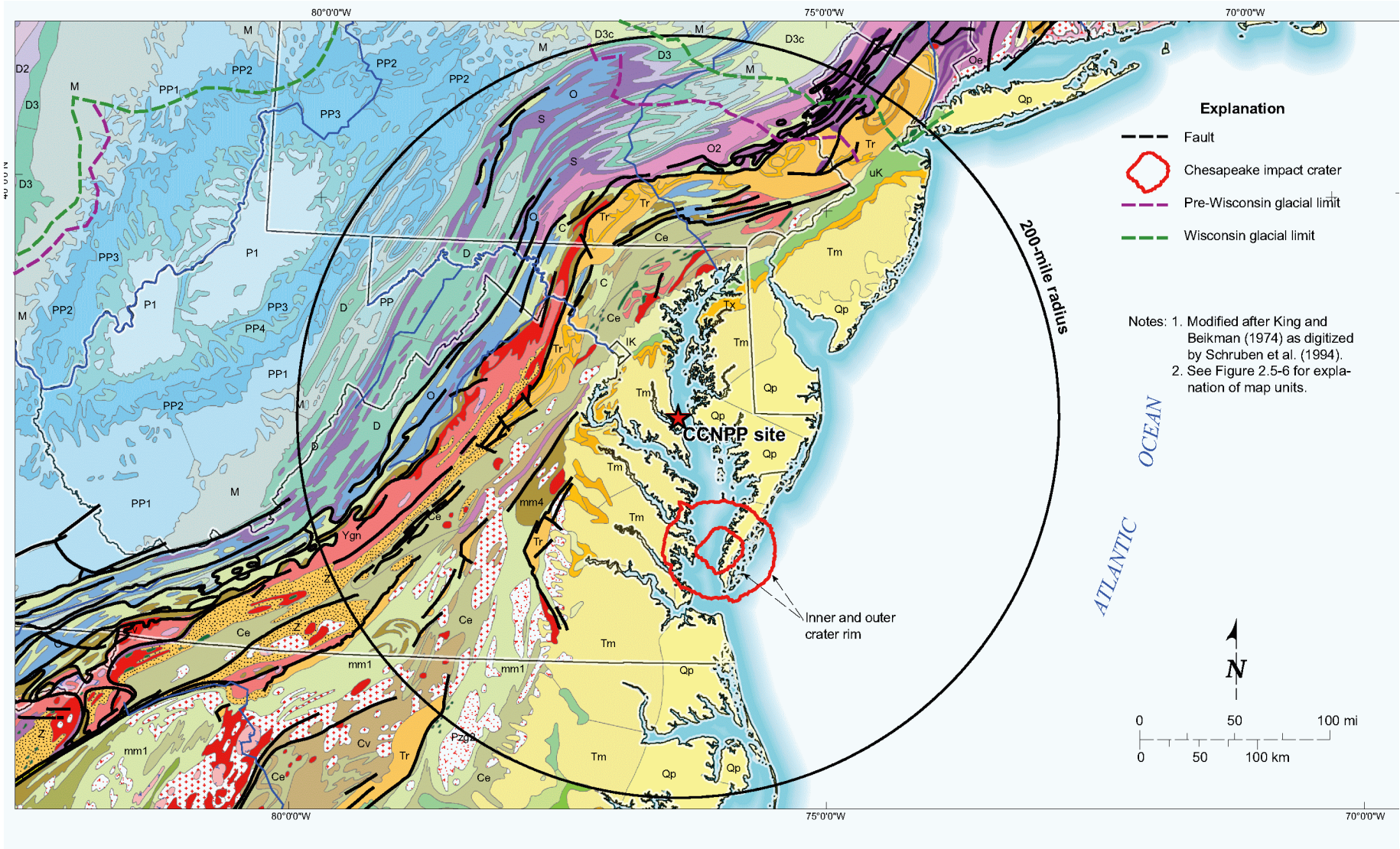
## Figure 2.5-6—{Regional Geologic Map 200-Mile (320-Km) Radius Explanation}

**Explanation**

*CCNPP 200-mile Geology*
*King and Beikman (1974) Unit Descriptions*

| | | | | |
|---|---|---|---|---|
| Qp | Pleistocene | | D3 | Upper Devonian |
| Tm | Miocene | | D3c | Upper Devonian continental |
| Te | Eocene | | Pzg2 | Middle Paleozoic granitic rocks |
| Tx | Paleocene | | D2 | Middle Devonian |
| uK4 | Navarro Group | | D | Devonian |
| uK | Upper Cretaceous | | De | Devonian eugeosynclinal |
| uK1 | Woodbine and Tuscaloosa Groups | | D1 | Lower Devonian |
| lK3 | Washita Group | | DS | Devonian and Silurian |
| lK | Lower Cretaceous | | S3 | Upper Silurian (Cayugan) |
| Trv | Mafic Lava interbedded in Triassic Newark Group | | S | Silurian |
| Tri | Triassic mafic intrusives | | lPz | Lower Paleozoic |
| Tr | Triassic | | O2 | Middle Ordovician (Mohawkian) |
| um | Ultramafic rocks | | O | Ordovician |
| P1 | Wolfcampian series | | Oe | Ordovician eugeosynclinal |
| cal c | Catacalastic rocks | | Ov | Ordovician volcanic rocks |
| PP4 | Virgilian Series | | Pzg1 | Lower Paleozoic granitic rocks |
| Pzg3 | Upper Paleozoic granitic rocks | | O1 | Lower Ordovician (Canadian) |
| PP3 | Missourian series | | OC | Lower Ordovician and Cambrian carbonate rocks |
| PP2 | Des Moinesian series | | C | Cambrian |
| PP | Pennsylvanian | | Ce | Cambrian eugeosynclinal |
| PP1 | Atokan and Morrowan series | | Cv | Cambrian volcanics |
| mm1 | Felsic paragneiss and schist | | Cq | Basal Lower Cambrian clastic rocks |
| mm2 | Mafic paragneiss (= hornblendite, amphibolite) | | Z | Z sedimentary rocks |
| mm3 | Migmatite | | Zg | Z granitic rocks |
| Pzmi | Paleozoic mafic intrusives | | Zv | Z volcanic rocks |
| mm4 | Felsic orthogneiss (= granite gneiss) | | Ym | Paragneiss and schist |
| M | Mississippian | | Ya | Anorthosite |
| | | | Ygn | Orthogneiss |

# Figure 2.5-7—{Physiographic Map of Maryland}

Appalachian Plateaus Province

Ridge and Valley Province

Blue Ridge Province

Piedmont Plateau Province

Allegheny Mountain Section

Folded Appalachian Mountains Section

Great Valley Section

Lowland Section

Upland Section

Western Shore Lowlands Region

**Physiographic Provinces and Their Subdivisions in Maryland**

Western Shore Uplands Region

Chesapeake Estuary Region

Delmarva Peninsula Region

Atlantic Continental Shelf Province

miles

0        50

Province Boundary

Subdivision Boundary

Maryland Geological Survey
January, 2001
http://www.mgs.md.gov

Calvert Cliffs Site

**Coastal Plain Province**
Embayed Section

**Figure 2.5-8—{Evolution of the Applachian Orogen}**
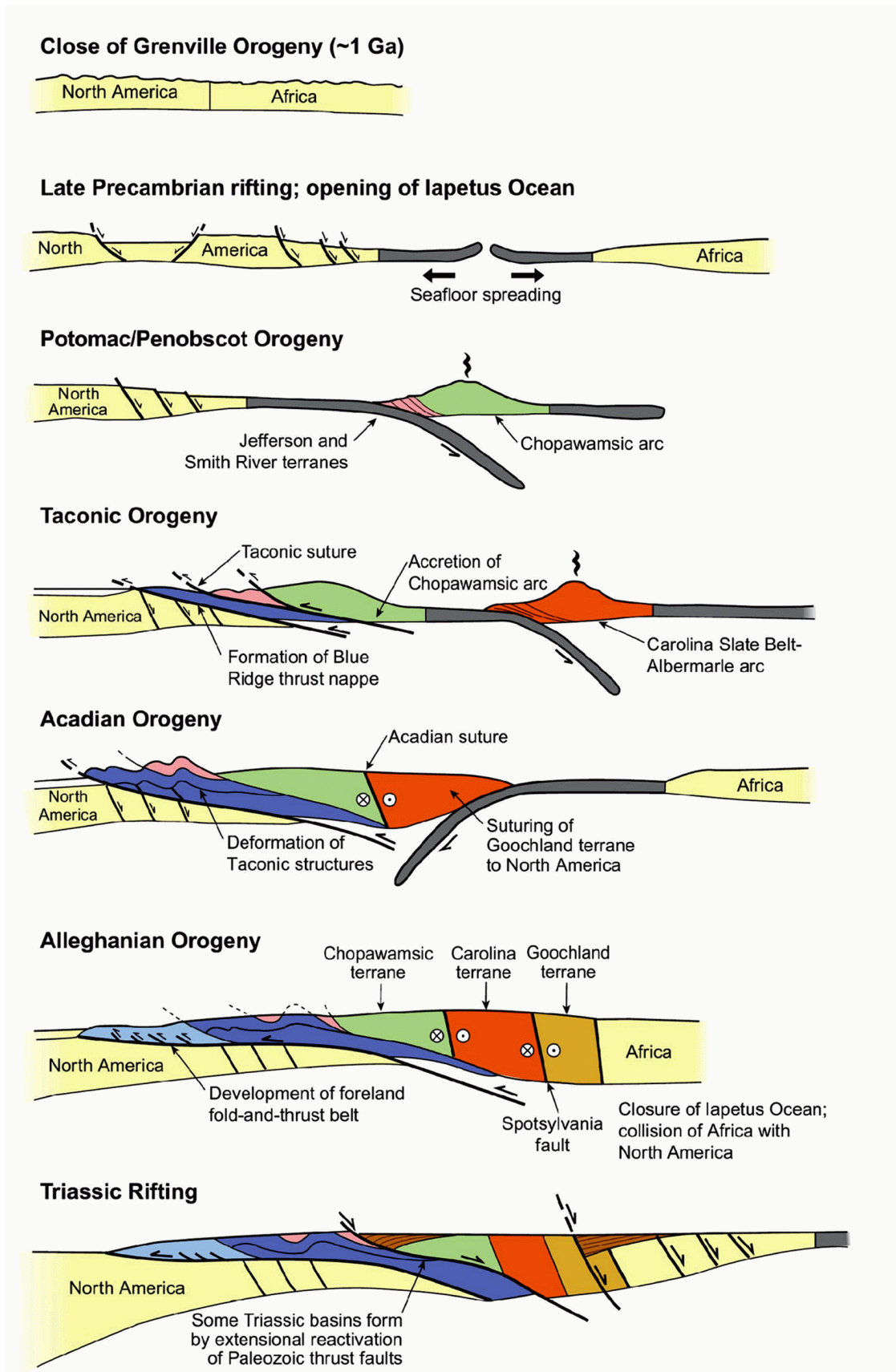
**Figure 2.5-9—{Lithotectonic Belts of the Piedmont Province}**



Source: Bledsoe and Marine, 1980; and
Fichter and Baedke, 2000
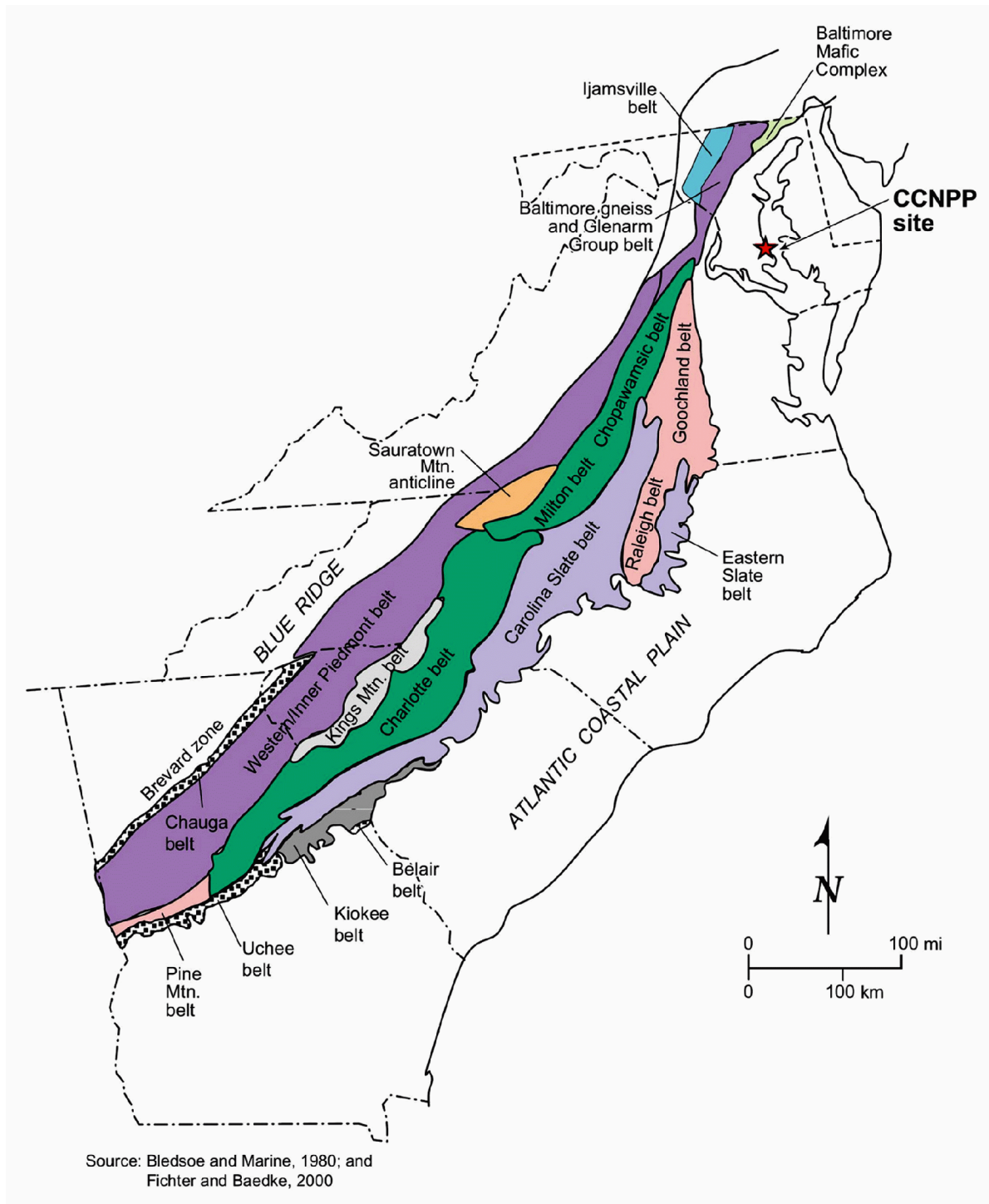
# Figure 2.5-10—{Map of Mesozoic Basins}
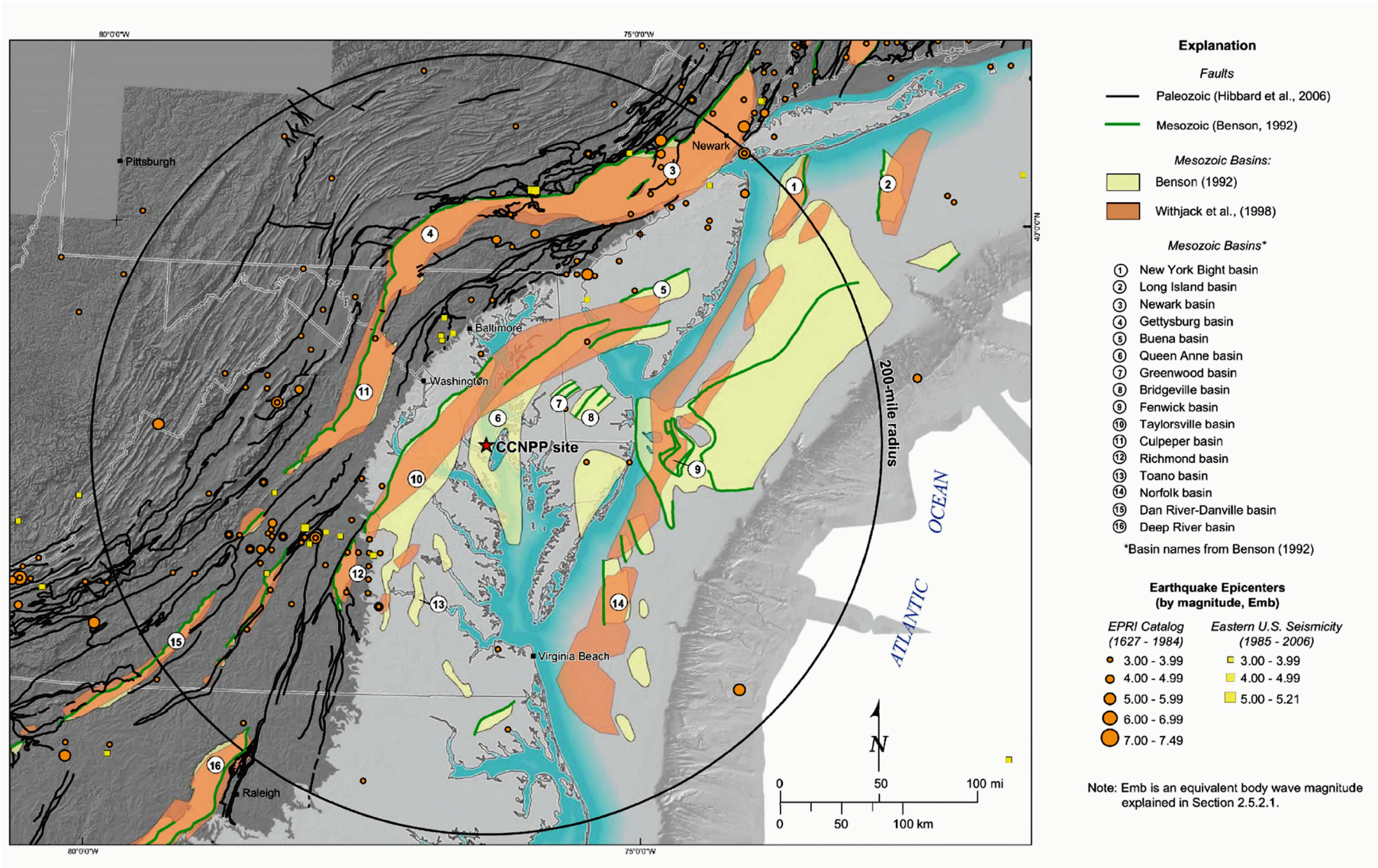
## Figure 2.5-11—{Lithologies of Basement Rocks from Coastal Plain Wells}
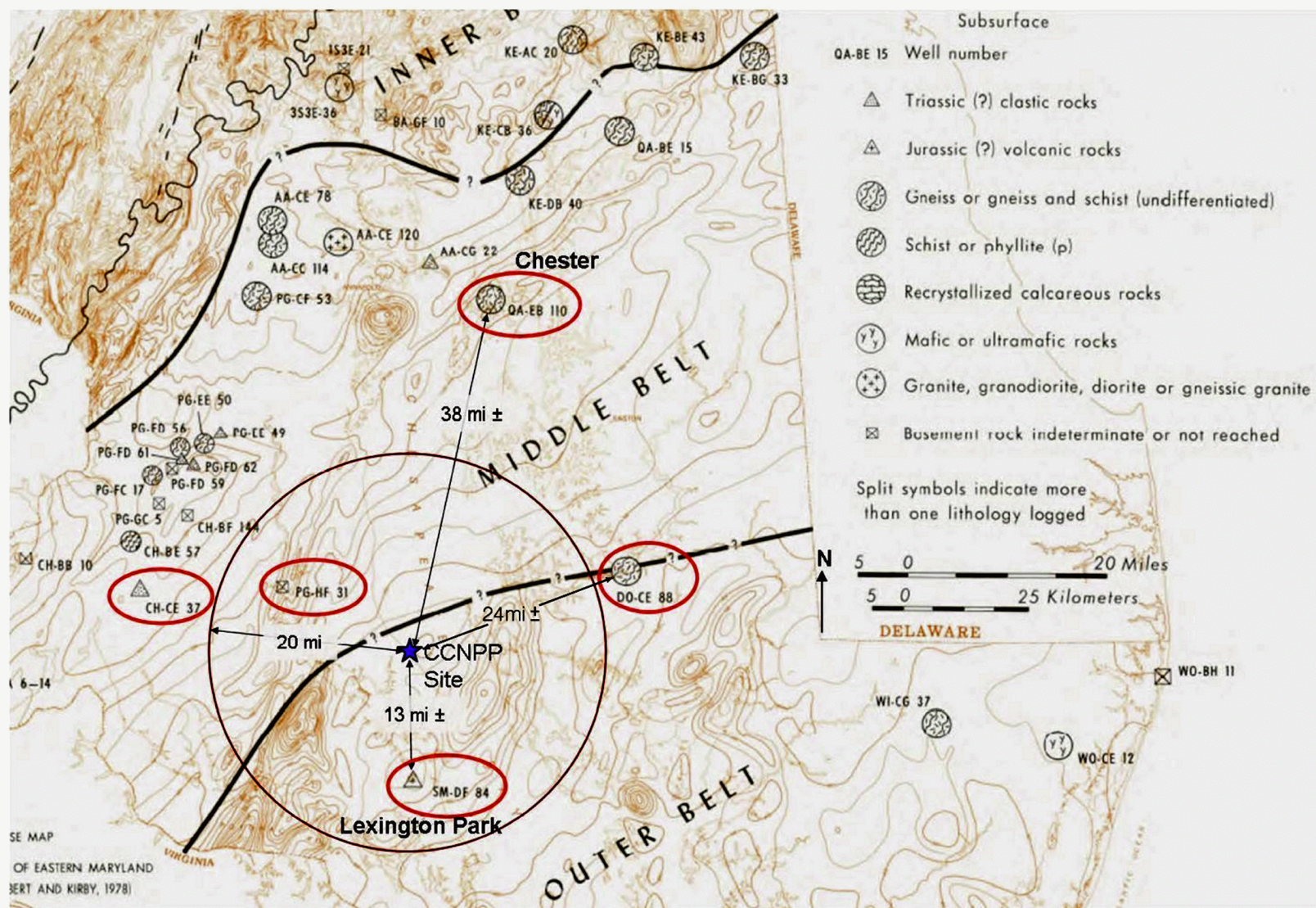
**Figure 2.5-12—{Tectonic Features of the Mid-Atlantic Passive Margin}**



Modified from Klitgord et al. (1995)
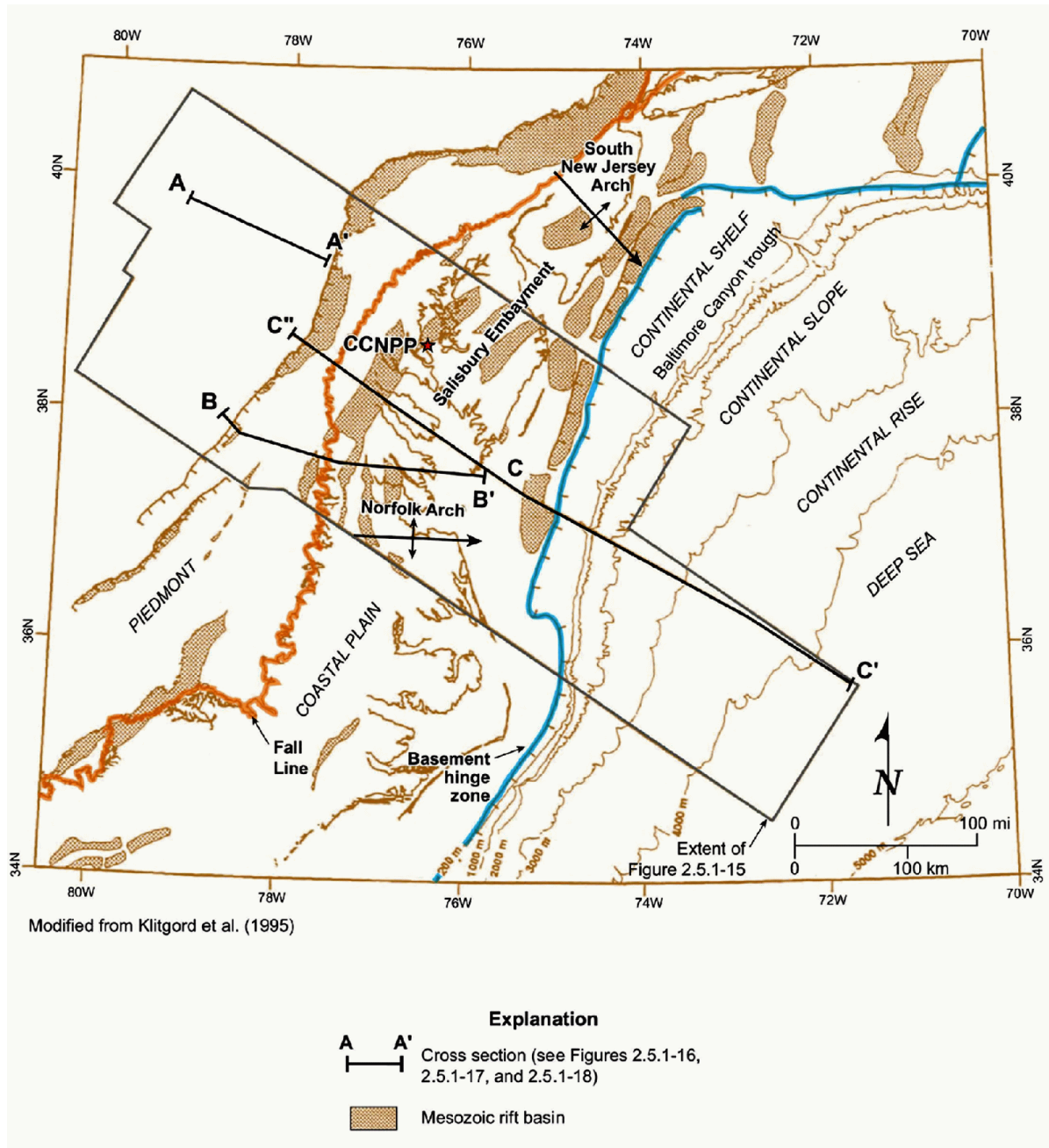
THE CCNPP SITE IS REPRESENTED
BY THE WELLS CA-Ed 45 AND 22.
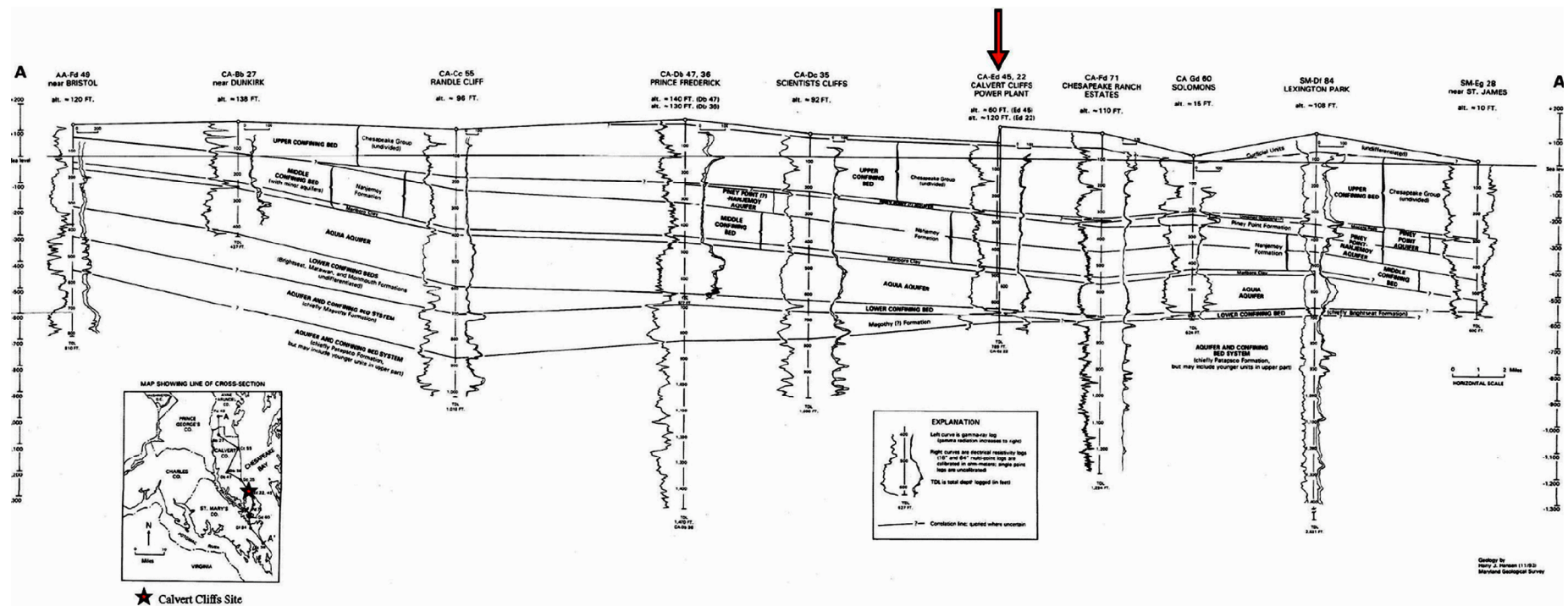
**Figure 2.5-14—{Structure-Contour Map of the Top of the Piney Point-Nanjemoy Aquifer}**
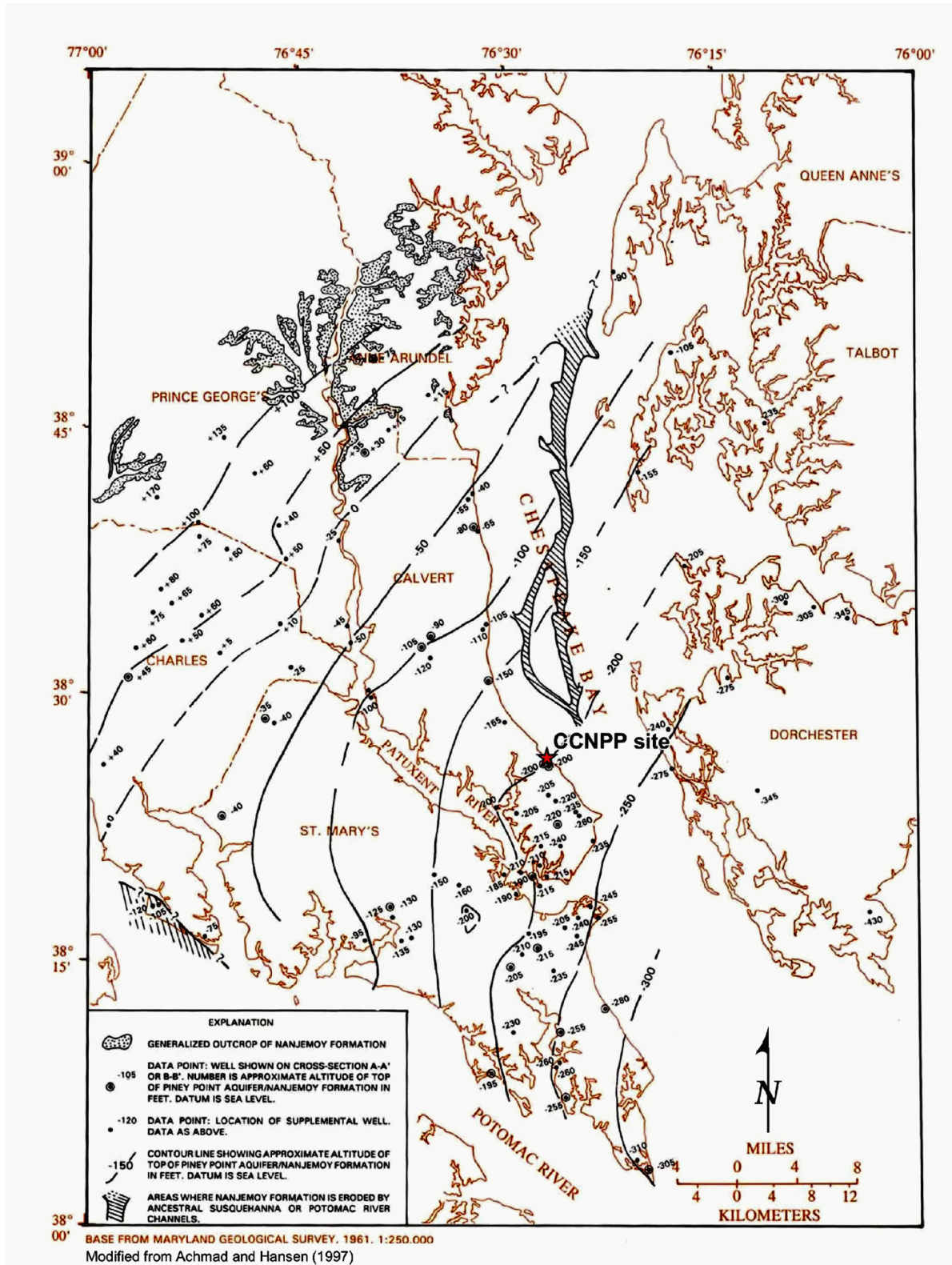
**Figure 2.5-15—{Crusted Ages}**
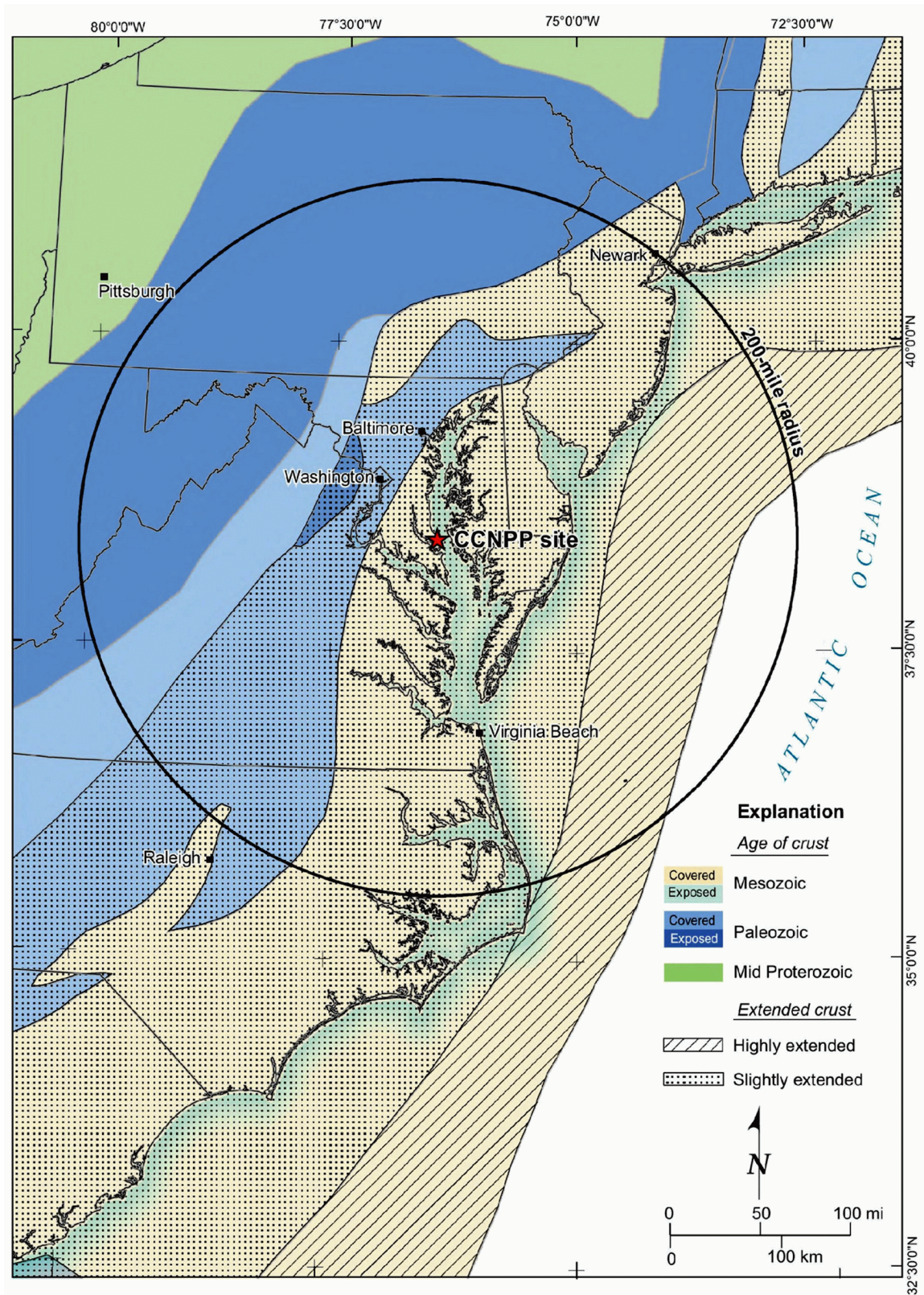
**Figure 2.5-16—{Regional Strip Maps Showing Tectonostratigraphic Divisions and Regional Cross-Section Lines}**
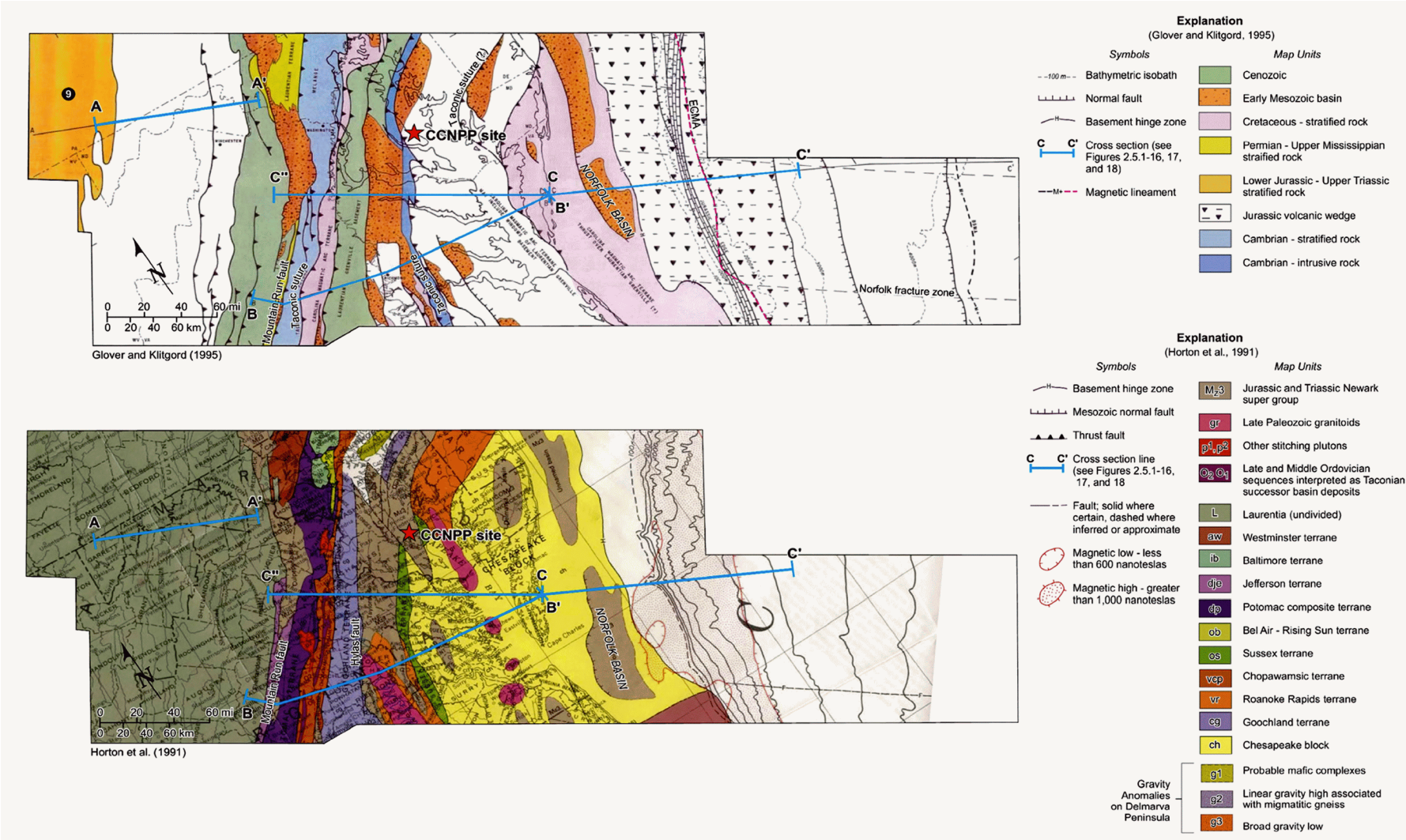
**Figure 2.5-17—{Crustal-Scale Cross Section Through the Appalachian Orogen and Coastal Plain}**
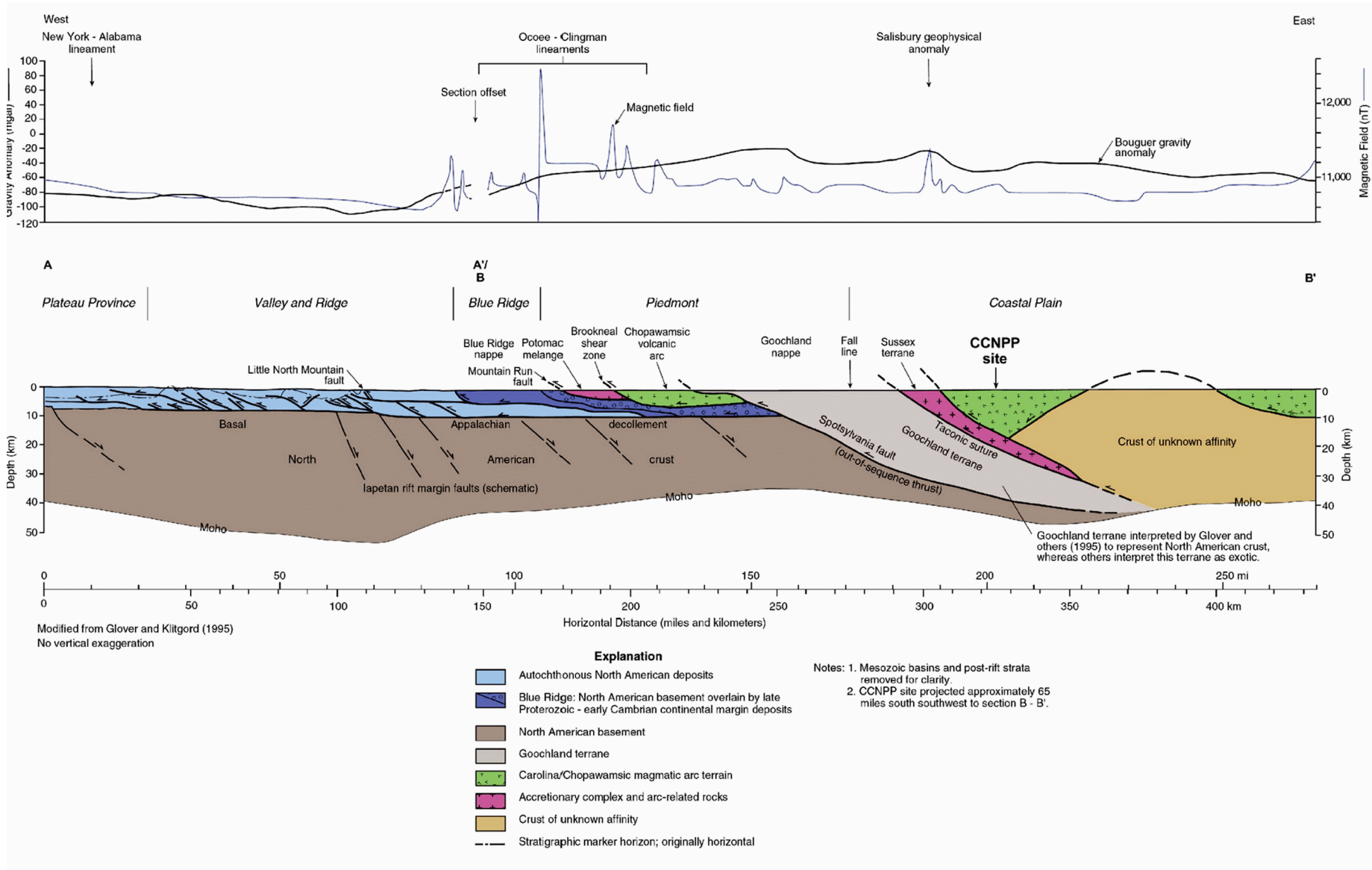
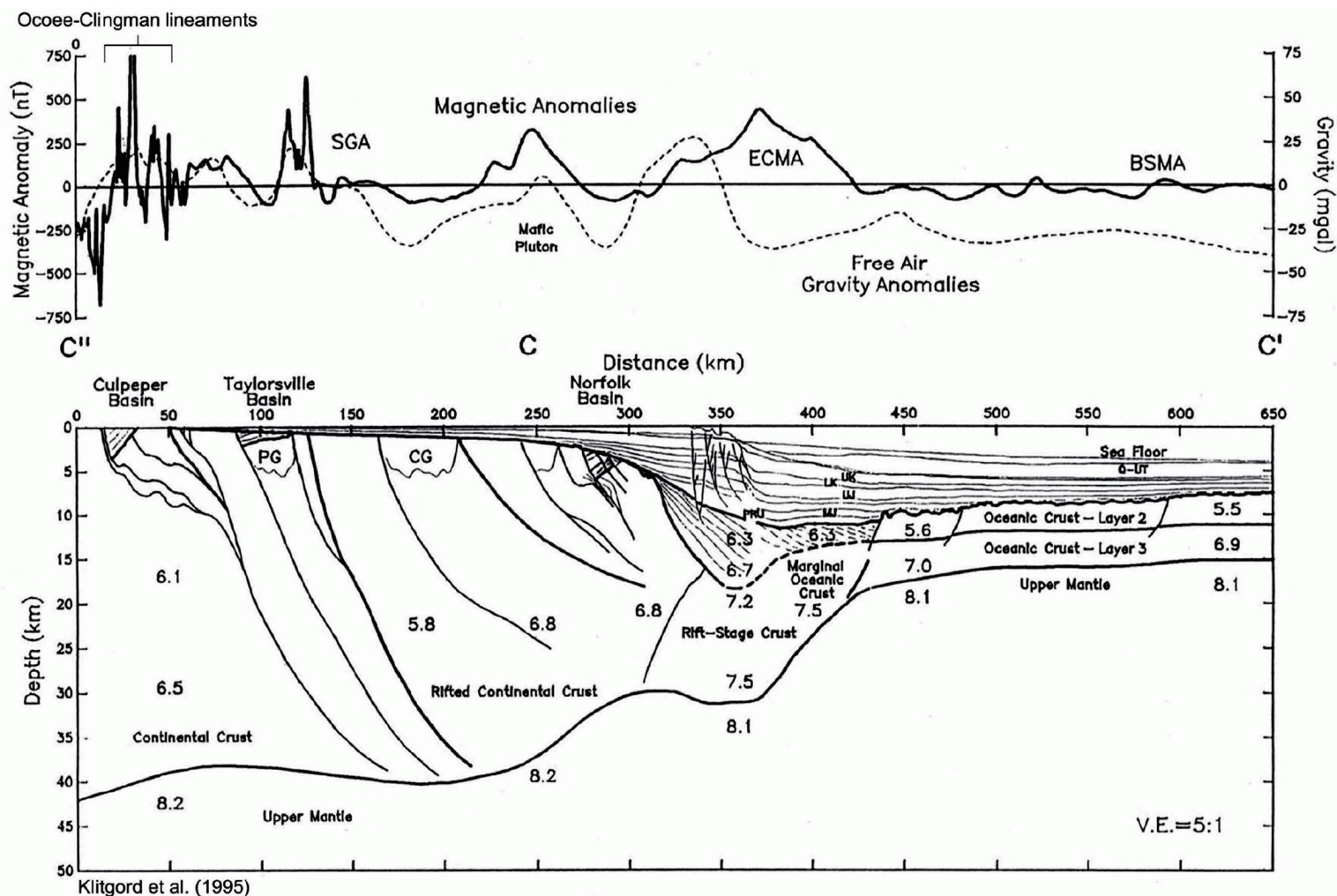**Figure 2.5-18—{Crustal-Scale Cross Section Across the Mid-Atlantic Continental Shelf, Slope and Rise}**



Modified from Glover and Klitgord (1995)
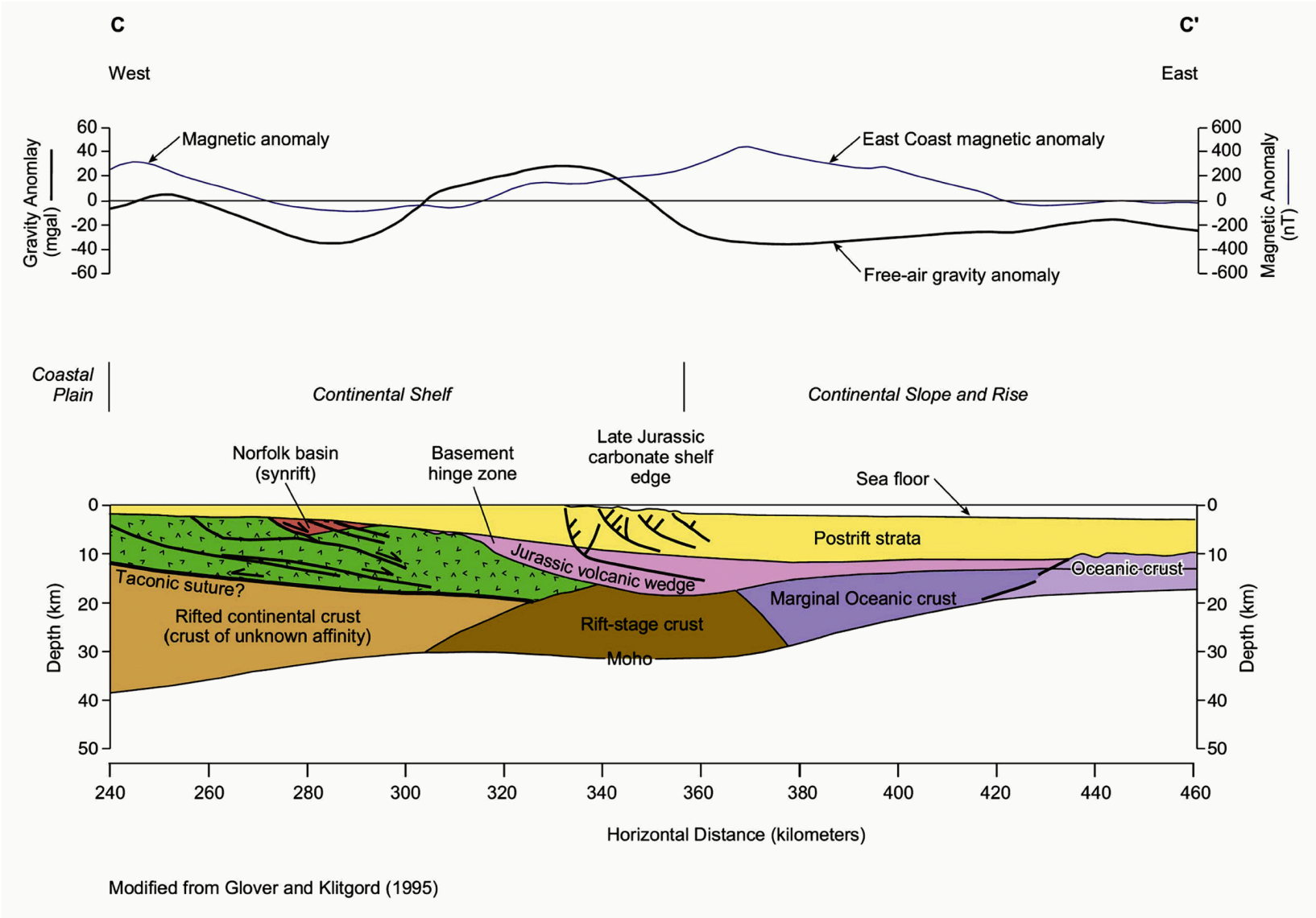
**Figure 2.5-19—{Crustal-Scale Cross Section of the Mid-Atlantic Passive Margin}**



Cross section along line C" - C - C' displaying selected crustal fractures. Surface features along segment C" - C are taken directly from the geologic map panel. Subsurface features have been projected northward onto the profile from cross section B - B'. Magnetic and gravity anomaly profiles along the section and selected refraction velocity values (in km/sec) are shown. Major sub-horizontal crustal boundaries are indicated by heavy lines. Sedimentary strata are indicated by the light lines above the upper heavy line. SGA - Salisbury geophysical anomaly; ECMA = East Coast magnetic anomaly; BSMA = Blake Spur magnetic anomaly; PG = Petersburg Granite; CG = Chesapeake Granite. See Figure 2.5.1-15 for section location. C- C' is the same as Figure 2.5.1-17, but represents an alternative interpretation.
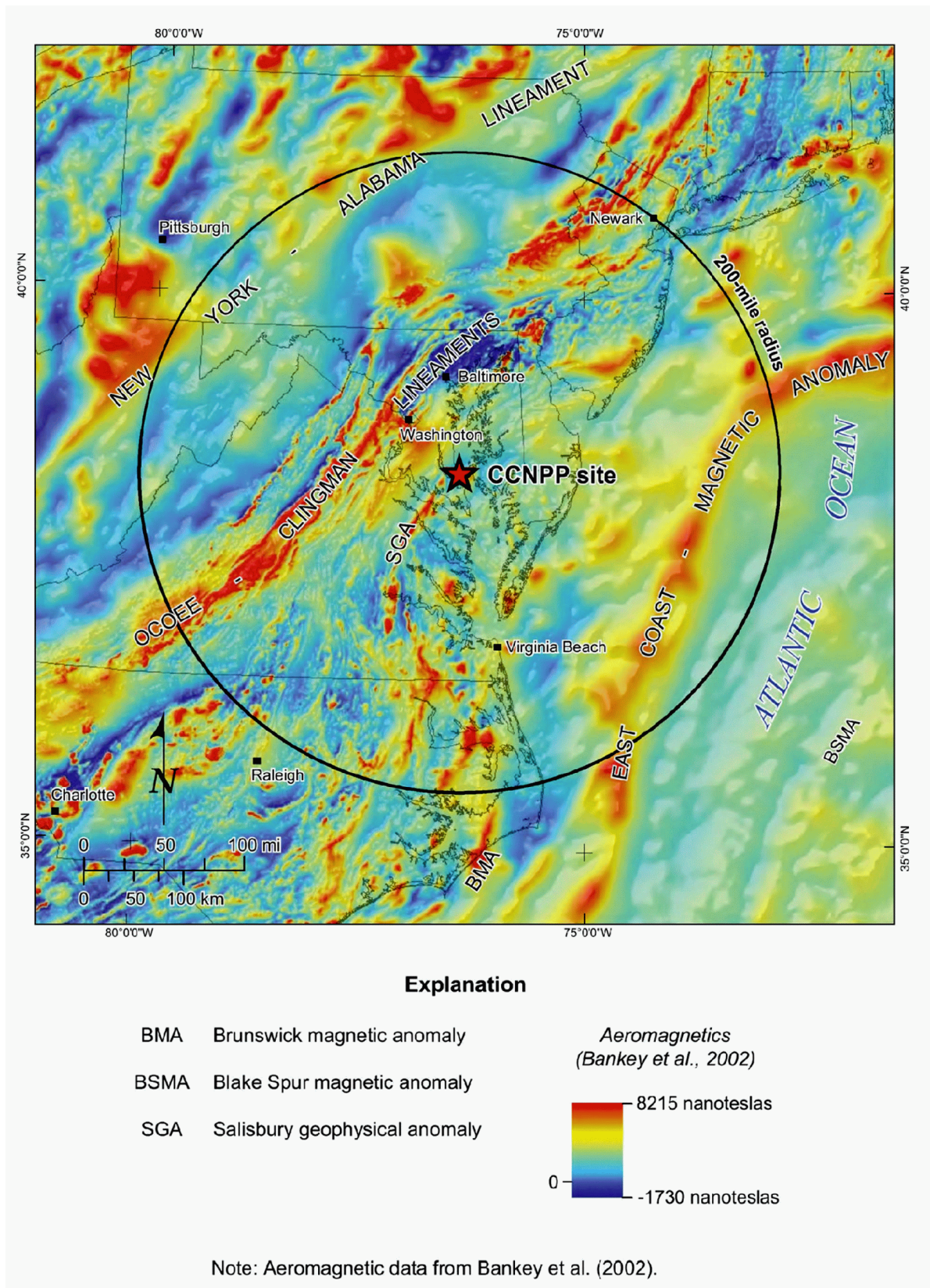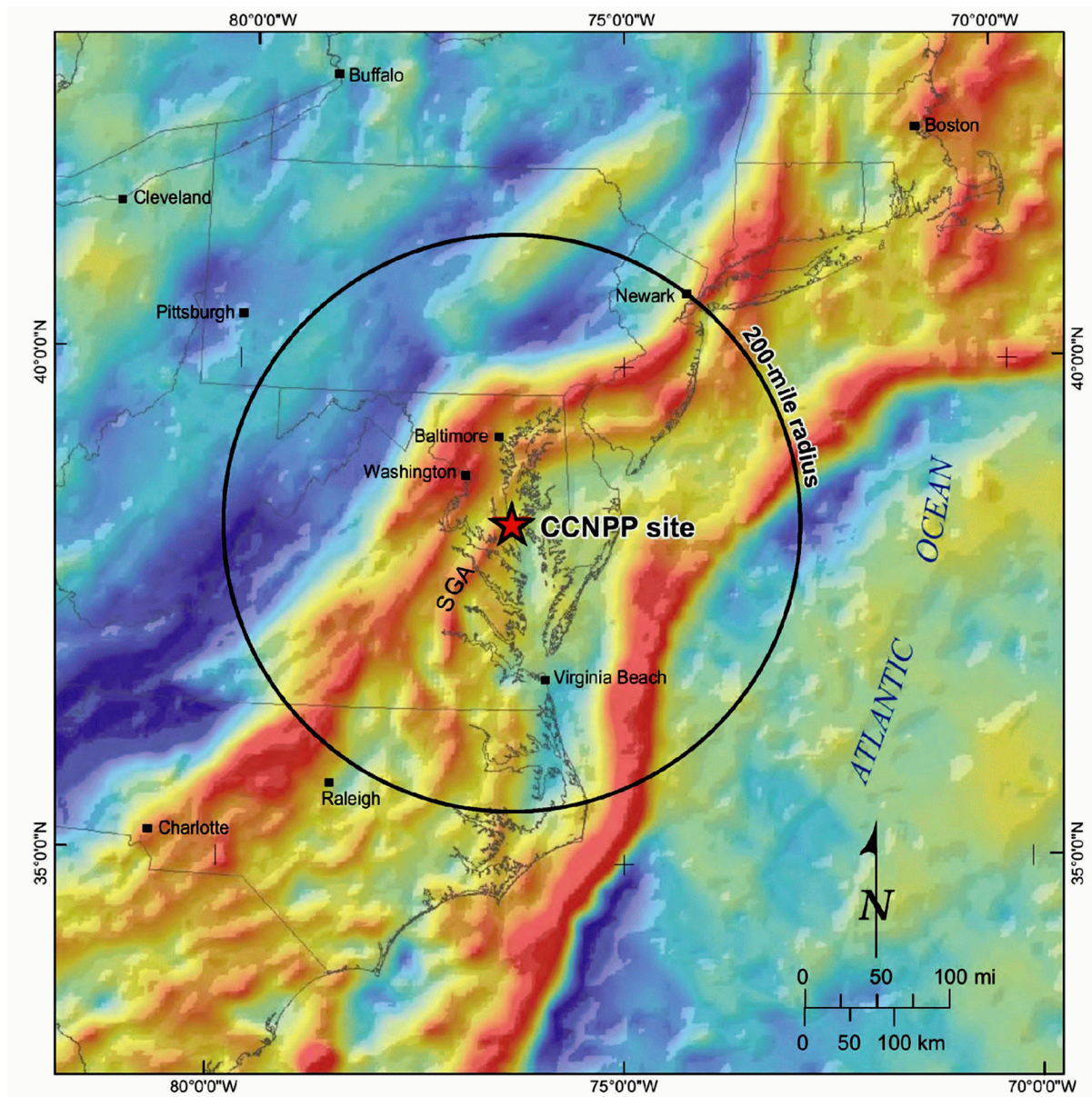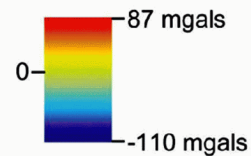
**Figure 2.5-20—{Regional Magnetic Anomaly Map}**



**Explanation**

BMA     Brunswick magnetic anomaly

BSMA    Blake Spur magnetic anomaly

SGA     Salisbury geophysical anomaly

*Aeromagnetics*
*(Bankey et al., 2002)*

8215 nanoteslas

0

-1730 nanoteslas

Note: Aeromagnetic data from Bankey et al. (2002).

## Figure 2.5-21—{Regional Gravity Anomaly Map}



**Explanation**

SGA    Salisbury geophysical anomaly

*Gravity Anomaly*

Notes: 1. Gravity data from Hittelman et al. (1994).
2. Gravity measurements over land are Bouger gravity anomalies.
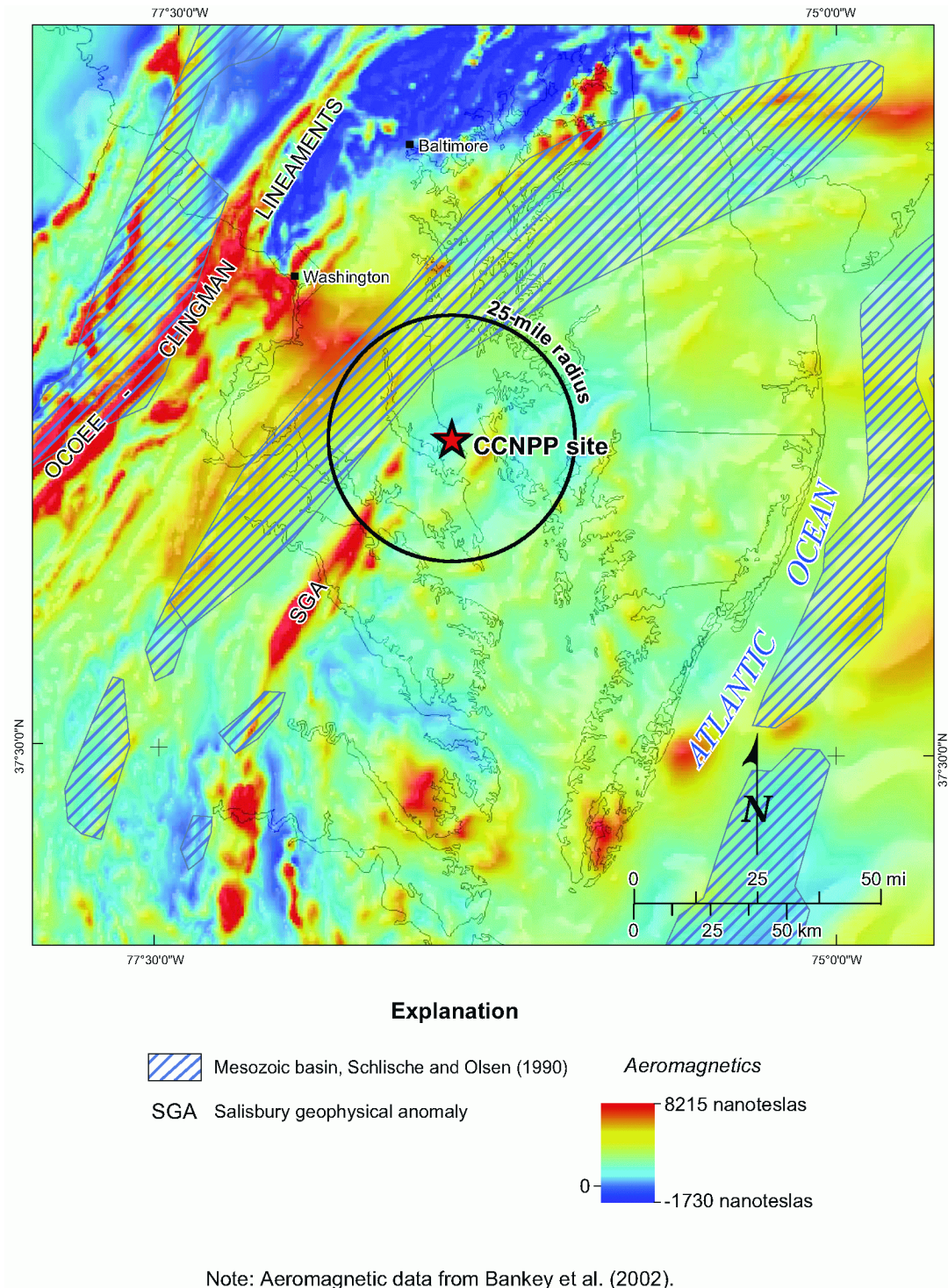3. Gravity measurements over water are free-air anomalies.

**Figure 2.5-22—{Chesapeake Bay Region Magnetic Anomalies with Mesozoic Basins}**



**Explanation**

Mesozoic basin, Schlische and Olsen (1990)

SGA    Salisbury geophysical anomaly

*Aeromagnetics*

8215 nanoteslas

0

-1730 nanoteslas

Note: Aeromagnetic data from Bankey et al. (2002).

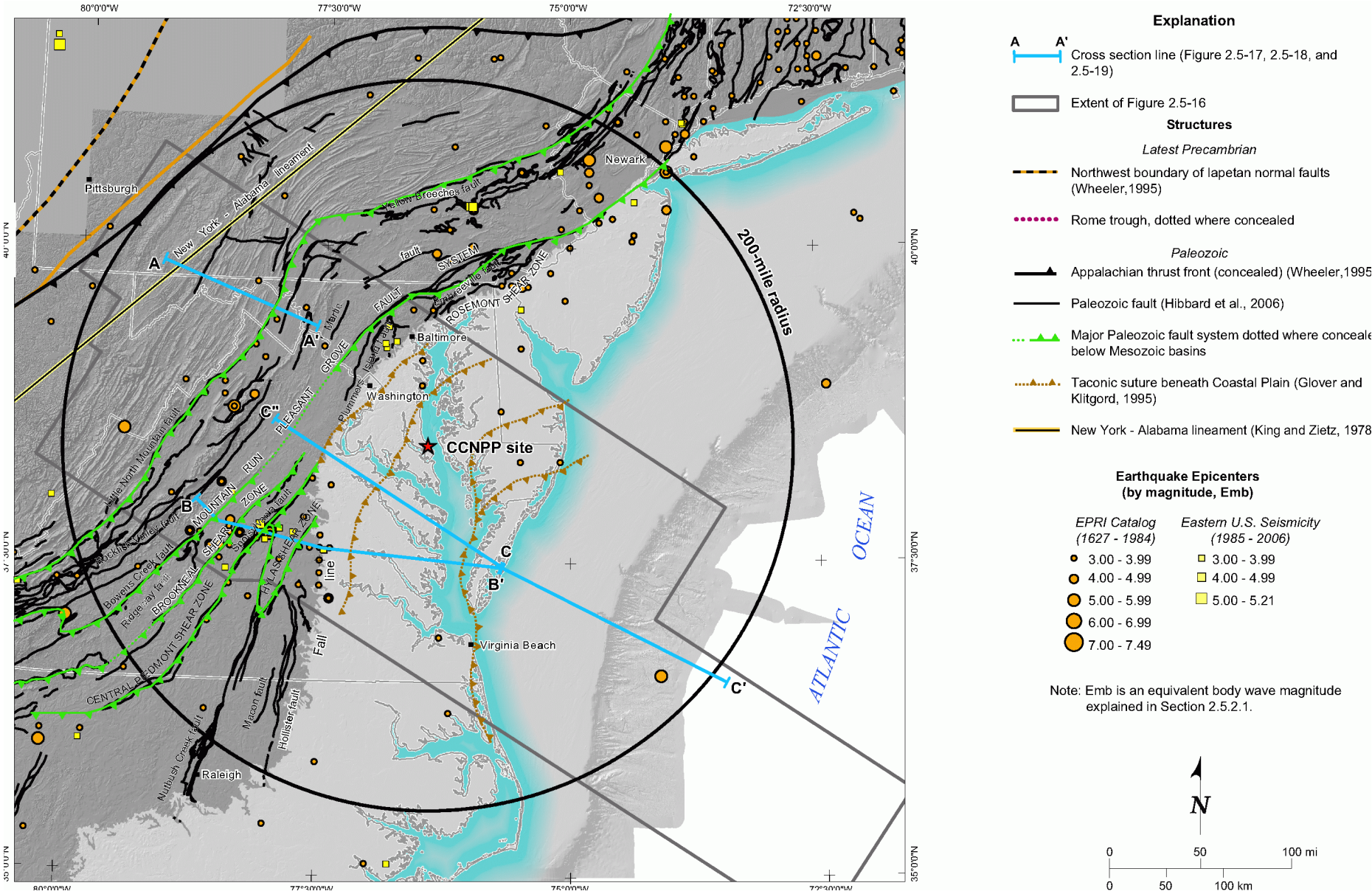**Figure 2.5-23—{Late Proterozoic and Paleozoic Tectonic Features}**

## Figure 2.5-24—{Seismic Zones and Seismicity in CEUS}